HANDBOOK ON

NONDESTRUCTIVE TESTING OF CONCRETE

SECOND EDITION

Edited by
V.M. MALHOTRA and N.J. CARINO

CRC PRESS

Boca Raton London New York Washington, D.C.

Library of Congress Cataloging-in-Publication Data

Catalog record is available from the Library of Congress

Visit the CRC Press Web site at www.crcpress.com

ASTM International, 100 Barr Harbor Drive, West Conshohocken, PA 19428
Tel.: 1-610-832-9500
www.astm.org
ISBN 0-8031-2099-0

No claim to original U.S. Government works
International Standard Book Number 0-8493-1485-2
Printed in the United States of America 1 2 3 4 5 6 7 8 9 0
Printed on acid-free paper

Foreword

ASTM International is pleased to join CRC Press to co-publish *Handbook on Nondestructive Testing of Concrete, Second Edition*. ASTM distributes many publications including standards, adjuncts, journals, special technical publications, manuals, data series, monographs, and reference radiographs. ASTM is proud to include this book in its publications series.

ASTM International has 130 technical committees including Committee C09 on Concrete and Concrete Aggregates. This committee was formed in 1914 and currently has over 700 members. The committee has jurisdiction of 152 standards. It meets in June and December.

ASTM Committee C09 on Concrete and Concrete Aggregate's scope is (1) the assembling and study of data pertaining to the properties of hydraulic-cement concrete and its constituent materials, including the study of the effect of characteristics of materials and mixtures on the properties of concrete; and (2) the development of standards for concrete and for the constituent materials of concrete (except cement), as well as for certain related materials, such as materials used in curing.

The scope of the Committee does not include the field of design and construction of concrete structures except insofar as references need to be made to construction methods in special case of concrete as "over-the-counter" material.

For additional information on ASTM International, 100 Barr Harbor Drive, West Conshohocken, PA 19428, visit www.astm.org, e-mail: service@astm.org, phone: +1.610.832-9500.

Preface

In the inspection of metals, nondestructive testing is an accepted practice. For example, radiographic and ultrasonic techniques are routinely used to identify anomalies in steel pipelines, and there are recognized national and international standards on their use. In the inspection of concrete, however, the use of nondestructive testing is relatively new. The slow development of nondestructive testing techniques for concrete is because, unlike steel, concrete is a highly nonhomogeneous composite material with varying composition and different raw materials. Apart from precast concrete units that, like steel products, are fabricated at a plant, most concrete is produced in relatively small ready-mixed concrete plants and delivered to the construction site. The placing, consolidation, and curing of concrete takes place in the field using labor that is relatively unskilled. The resulting product is, by its very nature and construction method, highly variable and does not lend itself to testing by traditional nondestructive methods as easily as steel products.

Despite the above drawbacks, there has been progress in the development of nondestructive methods for testing concrete, and several methods have been standardized by the American Society for Testing and Materials (ASTM), the Canadian Standards Association (CSA), the International Standards Organization (ISO), the British Standards Institute (BSI), and others. The direct determination of mechanical and other properties requires that concrete specimens taken from the structure be tested destructively; therefore, nondestructive methods cannot yield absolute values of these properties. Methods have been developed to measure other properties of concrete from which estimates of mechanical properties or other characteristics related to performance can be inferred.

Broadly speaking, there are two classes of nondestructive test methods for concrete. The first class consists of those methods that are used to estimate strength. The surface hardness, penetration resistance, pullout, break-off, pull-off, and maturity techniques belong to this category. Some of these methods are not truly nondestructive because they cause some surface damage, which is, however, minor compared with that produced by drilling a core. The second class includes those methods that measure other characteristics of concrete such as moisture content, density, thickness, resistivity, and permeability. Also included in the second class are such methods as stress wave propagation, ground probing radar, and infrared thermography techniques, which are used to locate delaminations, voids, and cracks in concrete. In addition, there are methods to provide information on steel reinforcement such as bar location, bar size, and whether the bars are corroding.

This second edition provides comprehensive treatment of nondestructive test methods that are used to evaluate concrete structures. The opening chapter deals with surface hardness test methods, followed by chapters on penetration resistance, pullout, break-off, maturity, pull-off, permeation, resonant frequency, and pulse velocity techniques. These chapters are followed by a chapter on the combined methods, in which more than one technique are used to estimate strength of concrete. The remaining chapters deal with magnetic, electrical, radioactive, nuclear, radar, stress wave propagation, infrared thermography, and acoustic emission techniques.

This handbook is written primarily for practicing engineers engaged in quality control or investigations of hardened concrete. The chapter authors are recognized specialists in the subject areas, and are, or have been, active participants in technical committees on nondestructive testing of concrete. Each chapter discusses the basic principles of the methods and provides practical information for their use. In-depth mathematical treatment and derivations have been kept to a minimum. Those interested in more detailed information about the development of these methods are referred to the original papers cited at the end of each chapter.

Some of the test methods described in this handbook are based on fairly simple principles and are easy to carry out, whereas others are based on complex principles and require sophisticated equipment and trained personnel to perform the tests. Regardless of which test is used, it is strongly recommended that interpretation of test results be performed by persons who are thoroughly familiar with the principles and limitations of the method. Interpretation should not be delegated to unqualified field technicians.

It is hoped that this second edition of the handbook will meet the growing needs of practicing engineers and technologists in the area of nondestructive testing of concrete. Graduate students in concrete technology should also find this handbook useful as a comprehensive state-of-the-art document, and as a source of reference material on the subject.

V. Mohan Malhotra

Nicholas J. Carino

The Editors

V. Mohan Malhotra, P.Eng., DDL (Hon), D.Eng. (Hon), internationally known researcher, author, and speaker, is Scientist Emeritus, CANMET, Department of Natural Resources, Ottawa, Canada. Dr. Malhotra received his B.Sc. degree in 1951 from Delhi University, India and his B.E. (Civil) in 1957 from the University of Western Australia, Perth. In 1984, he was awarded the honorary degree of Doctor of Laws (DDL) by the University of Dundee, Dundee, Scotland, and in 1999 he was awarded the honorary degree of Doctor of Engineering by the University de Nuevo Leon, Monterrey, Mexico.

Dr. Malhotra has been actively engaged in research in all aspects of concrete technology, including nondestructive testing, for the past 35 years. From 1975 to 1990 he was Chair of ASTM subcommittee C09 02.05 on Nondestructive Testing of Concrete. Dr. Malhotra is an Honorary Member and a Charter Fellow of the American Concrete Institute, Fellow of the American Society for Testing and Materials (ASTM), a Fellow of the Canadian Society for Civil Engineering, a Fellow of the Engineering Institute of Canada, an Honorary Member of the Concrete Society, U.K., and an Honorary Fellow of the Institute of Concrete Technology, U.K. He has received numerous awards and honors from the American Concrete Institute (ACI) and ASTM.

Dr. Malhotra is on the editorial board of several international journals on concrete technology. He has published more than 150 technical papers on concrete technology including nondestructive testing. He is the author or co-author of several books, including *Condensed Silica Fume*, published by CRC Press in 1988. He has edited numerous special publications for the American Concrete Institute and CANMET. His book, *High Performance, High Volume, Fly Ash Concrete*, was published in 2002. Dr. Malhotra has organized and chaired numerous international conferences on concrete technology throughout the world. In 1984, he organized and chaired the CANMET/ACI International Conference on In-situ/Non-destructive Testing of Concrete in Ottawa, Canada.

Nicholas J. Carino, Ph.D., is a research structural engineer in the Materials and Construction Research Division of the National Institute of Standards and Technology (formerly National Bureau of Standards) in Gaithersburg, Maryland. Dr. Carino received his undergraduate and graduate education at Cornell University (B.S., 1969; M.S., 1971; and Ph.D., 1974). Upon receiving his Ph.D., Dr. Carino accepted a teaching position at The University of Texas at Austin, where he received several awards for teaching excellence.

In 1979, Dr. Carino accepted a research position at the National Bureau of Standards. His research has dealt with methods for in-place testing of concrete for strength, with nondestructive methods for flaw detection in concrete, and with testing high-strength concrete. His work on the maturity method gained national and international recognition for which he received a U.S. Department of Commerce Bronze Medal in 1983. In 1996 he was co-recipient of the ACI Wason Medal for Materials Research for a paper dealing with the effects of cementitious materials on maturity functions. He was co-developer

with Dr. Mary Sansalone of the impact-echo method, and in 1996 they received the ACI Wason Medal for their paper describing the application of the impact-echo method for delamination detection.

In addition to research, Dr. Carino has been involved in structural investigations. In 1987, he was project leader in the structural assessment of the new office building of the U.S. Embassy in Moscow. He participated in the investigation of the 1981 condominium collapse in Cocoa Beach, Florida; the 1982 highway ramp failure in East Chicago, Indiana; and conducted damage assessments after the 1989 Loma Prieta earthquake and the 1994 Northridge earthquake.

Dr. Carino is a Fellow of the ACI, a Fellow of the ASTM, and a member of the American Society of Civil Engineers. He serves as Chair of ASTM Committee C09 on Concrete and Concrete Aggregates. He has held numerous other technical committee leadership positions including Chair of the ACI Committee on Nondestructive Testing for Concrete and the ASTM Subcommittee on Nondestructive and In-Place Testing. He also served on the ACI Board of Direction and the ACI Technical Activities Committee.

Contributors

P.A. Muhammed Basheer
Professor and Chair of Structural Materials
School of Civil Engineering
The Queen's University of Belfast
Northern Ireland
United Kingdom

Georges G. Carette[1]
CANMET
Department of Natural Resources Canada
Ottawa, Ontario
Canada

Nicholas J. Carino
Research Structural Engineer
Building and Fire Research Laboratory
National Institute of Standards and Technology
Gaithersburg, Maryland

Gerardo G. Clemeña
Principal Research Scientist
Virginia Transportation Research Council
Charlottesville, Virginia

Graeme D. Henderson
Dr. Doran and Partners
Belfast
Northern Ireland
United Kingdom

[1]Deceased

Kenneth R. Lauer
Professor Emeritus
Department of Civil Engineering and Geological Sciences
University of Notre Dame
Notre Dame, Indiana

Adrian E. Long
Professor
School of Civil Engineering
The Queen's University of Belfast
Northern Ireland
United Kingdom

V. Mohan Malhotra
Scientist Emeritus
CANMET
Department of Natural Resources Canada
Ottawa, Ontario
Canada

Sidney Mindess
Professor, Civil Engineering
University of British Columbia
Vancouver, British Columbia
Canada

Terry M. Mitchell
Materials Research Engineer
Turner-Fairbank Highway Research Center
Federal Highway Administration
U.S. Department of Transportation
McLean, Virginia

Tarun R. Naik
Director, Center for By-Products Utilization
Professor, Civil Engineering
College of Engineering and Applied Science
The University of Wisconsin–Milwaukee
Milwaukee, Wisconsin

John S. Popovics
Assistant Professor
Department of Civil and Environmental Engineering
University of Illinois at Urbana-Champaign
Urbana, Illinois

Aleksander Samarin
Consultant
Rhodes, New South Wales
Australia

Vasanthy Sivasundaram
Research Engineer
CANMET
Department of Natural Resources Canada
Ottawa, Ontario
Canada

Gary J. Weil
President
EnTech Engineering, Inc.
St. Louis, Missouri

Contents

1 Surface Hardness Methods *V. Mohan Malhotra*
- 1.1 Introduction
- 1.2 Indentation Methods
- 1.3 Rebound Method
- 1.4 Limitations
- 1.5 Rebound Number and Estimation of Compressive Strength
- 1.6 Rebound Number and Flexural Strength
- 1.7 Rebound Number and Modulus of Elasticity
- 1.8 North American Survey on the Use of the Rebound Hammer
- 1.9 Standardization of Surface Hardness Methods
- 1.10 Limitations and Usefulness

2 Penetration Resistance Methods *V. Mohan Malhotra, Georges G. Carette*
- 2.1 Introduction
- 2.2 Probe Penetration Test System
- 2.3 Evaluation of the Probe Penetration Test
- 2.4 Pin Penetration Test
- 2.5 Standardization of Penetration Resistance Techniques
- 2.6 Limitations and Usefulness of Penetration Resistance Methods

3 Pullout Test *Nicholas J. Carino*
- 3.1 Introduction
- 3.2 Historical Background
- 3.3 Failure Mechanism
- 3.4 Statistical Characteristics
- 3.5 Applications
- 3.6 Concluding Remarks

4 The Break-Off Test Method *Tarun R. Naik*
- 4.1 Introduction
- 4.2 Theoretical Considerations
- 4.3 BO Test Equipment
- 4.4 Historical Background
- 4.5 Test Procedure
- 4.6 Evaluation of Test Specimens
- 4.7 Applications

4.8 Advantages and Limitations
4.9 Standardization of the B.O. Method

5 The Maturity Method *Nicholas J. Carino*
5.1 Introduction
5.2 Historical Background
5.3 Theoretical Basis
5.4 Application of Maturity Method
5.5 Standard Practice
5.6 Conclusion

6 Pull-Off Test and Permeation Tests *Graeme D. Henderson, P.A. Muhammed Basheer, Adrian E. Long*
6.1 Introduction
6.2 In Situ Strength Assessment
6.3 Measuring Concrete Permeation Properties
6.4 Description of Test Methods
6.5 Concluding Remarks

7 Resonant Frequency Methods *V. Mohan Malhotra, Vasanthy Sivasundaram*
7.1 Introduction
7.2 Resonant Frequency Method
7.3 Other Methods of Resonant Frequent Testing
7.4 Factors Affecting Resonant Frequency and Dynamic Modulus of Elasticity
7.5 Resonant Frequency and Durability of Concrete
7.6 Reproducibility of Test Results
7.7 Correlation between Dynamic Modulus of Elasticity and Strength Properties of Concrete
7.8 Comparison of Moduli of Elasticity Determined from Longitudinal and Transverse Frequencies
7.9 Comparison of Dynamic and Static Moduli of Elasticity
7.10 Specialized Applications of Resonance Tests
7.11 Damping Properties of Concrete
7.12 Standardization of Resonant Frequency Methods
7.13 Limitations and Usefulness of Resonant Frequency Methods

8 The Ultrasonic Pulse Velocity Method *Tarun R. Naik, V. Mohan Malhotra, John S. Popovics*
8.1 Historical Background
8.2 Theory of Wave Propagation
8.3 Pulse Velocity Test Instrument
8.4 The Pulse Velocity Method
8.5 Factors Affecting Pulse Velocity
8.6 Standardization of the Pulse Velocity Method
8.7 Applications
8.8 Advantages and Limitations

9 Combined Methods *Aleksander Samarin*
9.1 Introduction
9.2 Historical Development
9.3 Combined Ultrasonic Pulse Velocity and Hardness Measurement Techniques
9.4 Conclusions

10 Magnetic/Electrical Methods *Kenneth R. Lauer*
10.1 Introduction
10.2 Magnetic Methods
10.3 Electrical Methods

11 Methods to Evaluate Corrosion of Reinforcement *Nicholas J. Carino*
11.1 Introduction
11.2 Principles of Corrosion
11.3 Corrosion of Steel in Concrete
11.4 Half-Cell Potential Method
11.5 Concrete Resistivity
11.6 Polarization Resistance
11.7 Summary

12 Radioactive/Nuclear Methods *Terry M. Mitchell*
12.1 Introduction
12.2 General Principles
12.3 Radiometry
12.4 Radiography
12.5 Neutron-Gamma Techniques

13 Short-Pulse Radar Methods *Gerardo G. Clemeña*
13.1 Introduction
13.2 Principle of Short-Pulse Radar
13.3 Instrumentation
13.4 Applications
13.5 Standardization of Short-Pulse Radar Methods
13.6 Conclusions

14 Stress Wave Propagation Methods *Nicholas J. Carino*
14.1 Introduction
14.2 Basic Principles
14.3 Test Methods
14.4 Summary

15 Infrared Thermographic Techniques *Gary J. Weil*
15.1 Introduction
15.2 Historical Background
15.3 Theoretical Considerations

15.4 Testing Equipment
15.5 Testing Procedures
15.6 Case Histories
15.7 Advantages and Limitations
15.8 Summary

16 Acoustic Emission Methods *Sidney Mindess*
16.1 Introduction
16.2 Historical Background
16.3 Theoretical Considerations
16.4 Evaluation of Acoustic Emission Signals
16.5 Instrumentation and Test Procedures
16.6 Parameters Affecting Acoustic Emissions from Concrete
16.7 Laboratory Studies of Acoustic Emission
16.8 Field Studies of Acoustic Emission
16.9 Conclusions

1

Surface Hardness Methods*

1.1 Introduction
1.2 Indentation Methods
Testing Pistol by Williams · Spring Hammer by Frank · Pendulum Hammer by Einbeck
1.3 Rebound Method
Rebound Hammer by Schmidt
1.4 Limitations
Smoothness of Surface under Test · Size, Shape, and Rigidity of Test Specimens · Age of Test Specimen · Surface and Internal Moisture Condition of the Concrete · Type of Coarse Aggregate · Type of Cement · Type of Mold · Carbonation of Concrete Surface
1.5 Rebound Number and Estimation of Compressive Strength
1.6 Rebound Number and Flexural Strength
1.7 Rebound Number and Modulus of Elasticity
1.8 North American Survey on the Use of the Rebound Hammer
1.9 Standardization of Surface Hardness Methods
1.10 Limitations and Usefulness

V. Mohan Malhotra
Department of Natural Resources Canada, Ottawa

The chapter deals with surface hardness methods for nondestructive testing of concrete. These methods consist of the indentation type and those based on the rebound principle. The rebound method is described in detail, and a procedure is given for the preparation of correlation curves between compressive strength and rebound number. The advantages and limitations of the surface hardness methods are discussed. it is concluded that these methods must be regarded as substitutes for standard compression tests, but as a means for determining the uniformity of concrete in a structure and comparing one concrete against another.

1.1 Introduction

The increase in the hardness of concrete with age and strength has led to the development of test methods to measure this property. These methods consist of the indentation type and those based on the rebound principle. The indentation methods consist principally of impacting the surface of concrete by means of a given mass having a given kinetic energy and measuring the width and or depth of the resulting

* ©Minister of Supply and Services Canada, 1989.

indentation. The methods based on the rebound principle consist of measuring the rebound of a spring-driven hammer mass after its impact with concrete.

1.2 Indentation Methods

According to Jones,[1] the indentation methods originated in Germany in 1934 and were incorporated in the German standards in 1935.[2,3] The use of these methods has also been reported in the U.K.[4] and the USSR.[5] There is little apparent theoretical relationship between the strength of concrete and its surface hardness. However, several researchers have published empirical correlations between the strength properties of concrete and its surface hardness as measured by the indentation methods.

The three known historical methods based on the indentation principle are:

- Testing Pistol by Williams
- Spring Hammer by Frank
- Pendulum Hammer by Einbeck

1.2.1 Testing Pistol by Williams

In 1936 Williams[4] reported the development of a testing pistol that uses a ball as an indenter. The diameter of the impression made by the ball is measured by a graduated magnifying lens or other means. The impression is usually quite sharp and well defined, particularly with concrete of medium and high strength. The depth of indentation is only about 1.5 mm for concrete with compressive strengths as low as 7 MPa.

The utility of the method according to Williams[4] depends on the approximate relationship found to exist between the compressive strength of concrete and the resistance of its surface to indentation during impact.

Skramtaev and Leshchinszy[5] have also reported the use of a pistol in the testing of concrete in the USSR.

1.2.2 Spring Hammer by Frank

The device developed by Frank consists of a spring-controlled mechanism housed in a tubular frame. The tip of the hammer can be fitted with balls having different diameters, and impact is achieved by placing the hammer against the surface under test and manipulating the spring mechanism. Generally about 20 impact readings are taken at short distances from one another and the mean of the results is considered as one test value. The diameter and/or depth of the indentation is measured, and this, in turn, is correlated with the compressive strength of concrete.[6] The spring mechanism can be adjusted to provide an energy of 50 kg/cm or of 12.5 kg/cm so that the indentation on the concrete surface is within 0.3 to 0.7 times the diameter of the steel ball.

1.2.3 Pendulum Hammer by Einbeck

A line diagram of the pendulum hammer developed by Einbeck is given in Figure 1.1.[6] The hammer consists of horizontal leg, at the end of which is pivoted an arm with a pendulum head with a mass of 2.26 kg. The indentation is made by holding the horizontal leg against the concrete surface under test and allowing the pendulum head to strike the concrete. The height of fall of the pendulum head can be varied from full impact (180°) to half impact (90°). The diameter and depth of indentation are measured, and these are correlated with the compressive strength of concrete.

The biggest drawback to this hammer is that it can be used only on vertical surfaces and is, therefore, less versatile than the spring hammer by Frank.

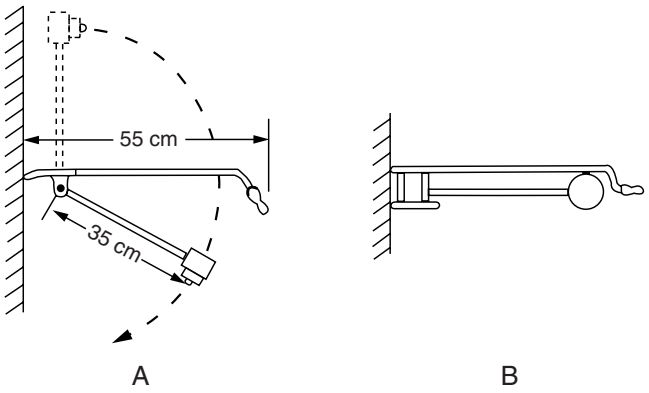

FIGURE 1.1 Vertical elevation and plan of Einbeck pendulum hammer. (Adapted from Reference 6.)

1.3 Rebound Method

1.3.1 Rebound Hammer by Schmidt

In 1948 a Swiss engineer, Ernst Schmidt,[7–9] developed a test hammer for measuring the hardness of concrete by the rebound principle. Results of his work were presented to the Swiss Federal Materials Testing and Experimental Institute of Zurich, where the hammer was constructed and extensively tested. About 50,000 Schmidt rebound hammers had been sold by 1986 on a worldwide basis.

Principle — The Schmidt rebound hammer is principally a surface hardness tester with little apparent theoretical relationship between the strength of concrete and the rebound number of the hammer. However, within limits, empirical correlations have been established between strength properties and the rebound number. Further, Kolek[10] has attempted to establish a correlation between the hammer rebound number and the hardness as measured by the Brinell method.

Description — The Schmidt rebound hammer is shown in Figure 1.2. The hammer weighs about 1.8 kg and is suitable for use both in a laboratory and in the field. A schematic cutaway view of the rebound hammer is shown in Figure 1.3. The main components include the outer body, the plunger, the hammer mass, and the main spring. Other features include a latching mechanism that locks the hammer mass to the plunger rod and a sliding rider to measure the rebound of the hammer mass. The rebound distance is measured on an arbitrary scale marked from 10 to 100. The rebound distance is recorded as a "rebound number" corresponding to the position of the rider on the scale.

Method of Testing — To prepare the instrument for a test, release the plunger from its locked position by pushing the plunger against the concrete and slowly moving the body away from the concrete. This causes the plunger to extend from the body and the latch engages the hammer mass to the plunger rod (Figure 1.3A). Hold the plunger perpendicular to the concrete surface and slowly push the body toward

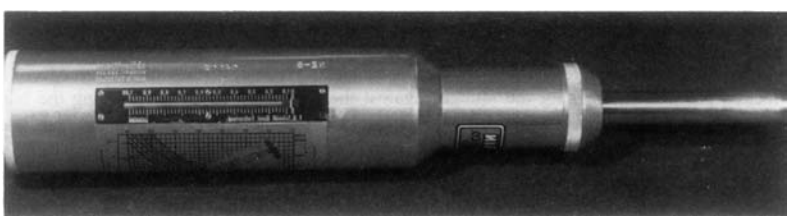

FIGURE 1.2 Schmidt rebound hammer.

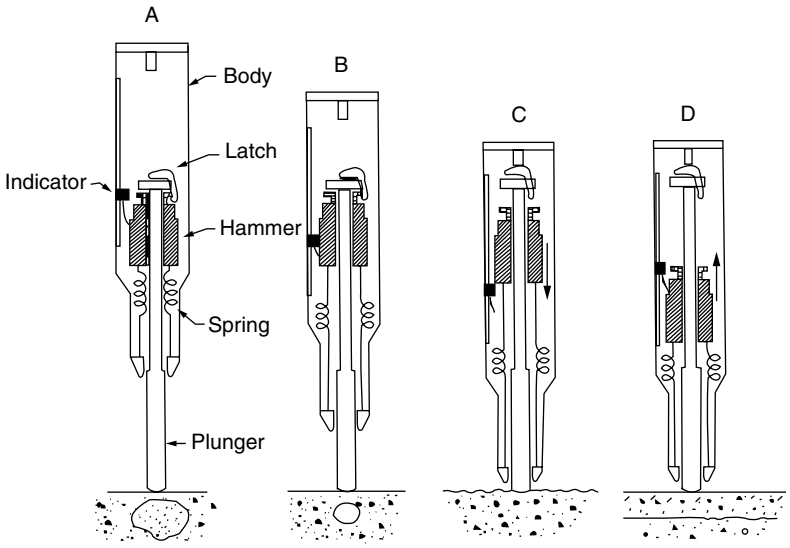

FIGURE 1.3 A cutaway schematic view of the Schmidt rebound hammer.

the test object. As the body is pushed, the main spring connecting the hammer mass to the body is stretched (Figure 1.3B). When the body is pushed to the limit, the latch is automatically released, and the energy stored in the spring propels the hammer mass toward the plunger tip (Figure 1.3C). The mass impacts the shoulder of the plunger rod and rebounds. During rebound, the slide indicator travels with the hammer mass and records the rebound distance (Figure 1.3D). A button on the side of the body is pushed to lock the plunger in the retracted position, and the rebound number is read from the scale.

The test can be conducted horizontally, vertically upward or downward, or at any intermediate angle. Due to different effects of gravity on the rebound as the test angle is changed, the rebound number will be different for the same concrete and will require separate calibration or correction charts.

Correlation Procedure — Each hammer is furnished with correlation curves developed by the manufacturer using standard cube specimens. However, the use of these curves is not recommended because material and testing conditions may not be similar to those in effect when the calibration of the instrument was performed. A typical correlation procedure is given below.

1. Prepare a number of 150 × 300-mm cylinders* covering the strength range to be encountered on the job site. Use the same cement and aggregates that are to be used on the job. Cure the cylinders under standard moist-curing room conditions,** keeping the curing period the same as the specified control age in the field.
2. After capping, place the cylinders in a compression-testing machine under an initial load of approximately 15% of the ultimate load to restrain the specimen. Ensure that cylinders are in a saturated surface-dry condition.
3. Make 15 hammer rebound readings, 5 on each of 3 vertical lines 120° apart, against the side surface in the middle two thirds of each cylinder. Avoid testing the same spot twice. For cubes, take five readings on each of the four molded faces without testing the same spot twice.
4. Average the readings and call this the rebound number for the cylinder under test.***
5. Repeat this procedure for all the cylinders.

*In countries where a cube is the standard specimen, use 150-mm cube specimens.

**Temperature 73.4 ± 3°F (23 ± 1.7°C) and 100% relative humidity.

***Some erratic rebound readings may occur when a test is performed directly over an aggregate particle or an air void. Accordingly, the outliers should be discarded and ASTM C 805 has a procedure for discarding these test results.

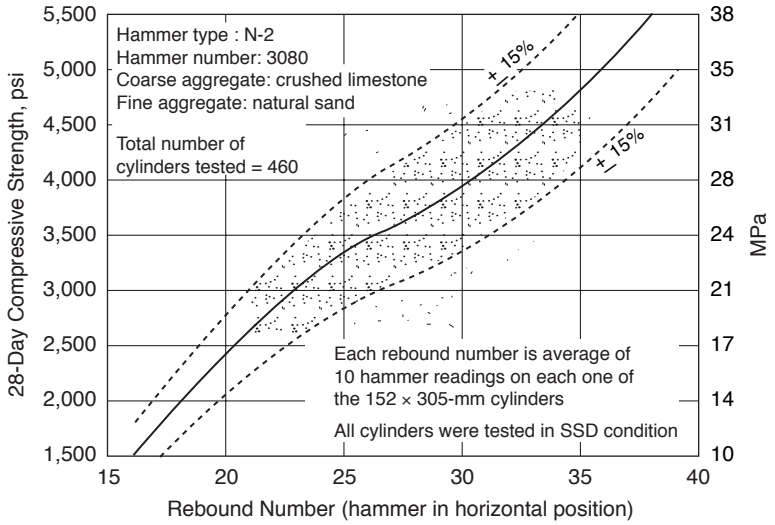

FIGURE 1.4 Relationship between 28-day compressive strength and rebound number for limestone aggregate concrete obtained with Type N-2 hammer. (Adapted from Reference 13.)

6. Test the cylinders to failure in compression and plot the rebound numbers against the compressive strengths on a graph.
7. Fit a curve or a line by the method of least squares.

A typical curve established by Zoldners[11] for limestone aggregate concrete is shown in Figure 1.4. This curve was based on tests performed at 28 days using different concrete mixtures.

Figure 1.5 shows four calibration curves obtained by research workers in four different countries.[10] It is important to note that some of the curves deviate considerably from the curve supplied with the hammer.

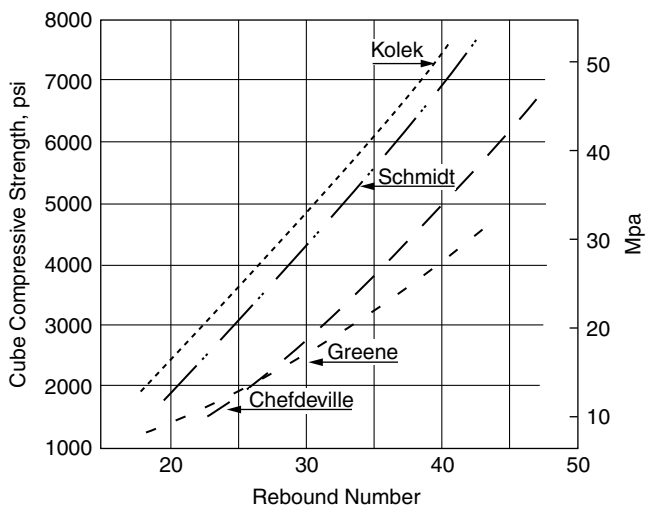

FIGURE 1.5 Correlation curves obtained by different investigators with a Schmidt rebound hammer Type N-2. Curve by Greene was obtained with Type N. (Adapted from Reference 5.)

To gain a basic understanding of the complex phenomena involved in the rebound test, Akashi and Amasaki[12] have studied the stress waves in the plunger of a rebound hammer at the time of impact. Using a specially designed plunger instrumented with strain gauges, the authors showed that the impact of the hammer mass produces a large compressive wave σi and large reflected stress wave σr at the center of the plunger. The ratio σr/σi of the amplitudes of these waves and the time T between their appearance was found to depend upon the surface hardness of hardened concrete. The rebound number was found to be approximately proportional to the ratio of the two stresses, and was not significantly affected by the moisture condition of the concrete. A schematic diagram of the equipment used for observing stress waves is shown in Figure 1.6, and Figure 1.7 is an oscilloscope trace of the impact stresses in the plunger showing the initial and reflected waves. From their research, the authors concluded that to correctly measure the rebound number of hardened concrete, the Schmidt hammer should be calibrated by testing a material with a constant hardness and measuring the resulting impact stress waves. Thus, by measuring the impact waves in the plunger, the surface hardness of concrete can be measured with a higher accuracy. A typical relationship between the rebound number R and stress σr/σi is shown in Figure 1.8.

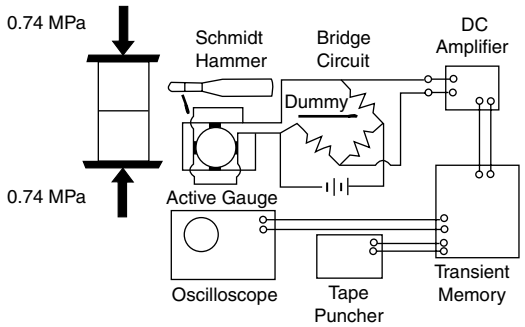

FIGURE 1.6 Schematic diagram of the equipment used for observing stress waves. (Adapted from Reference 12.)

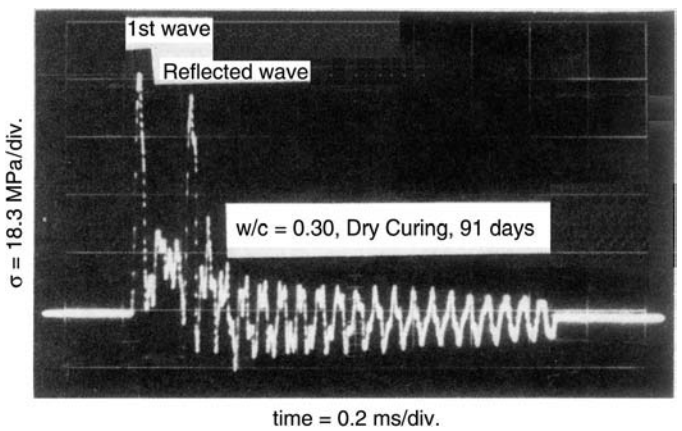

FIGURE 1.7 Oscilloscope trace of stress waves in the test plunger when testing concrete. (Adapted from Reference 12.)

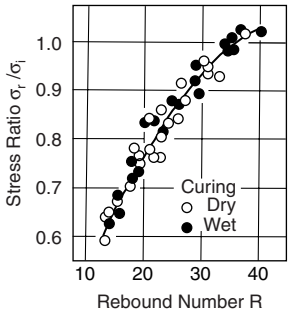

FIGURE 1.8 Stress ratio vs. rebound number. (Adapted from Reference 12.)

1.4 Limitations

Although the rebound hammer provides a quick, inexpensive means of checking the uniformity of concrete, it has serious limitations and these must be recognized. The results of the Schmidt rebound hammer are affected by:

1. Smoothness of test surface
2. Size, shape, and rigidity of the specimens
3. Age of test specimens
4. Surface and internal moisture conditions of the concrete
5. Type of coarse aggregate
6. Type of cement
7. Type of mold
8. Carbonation of the concrete surface

These limitations are discussed in the foregoing order.

1.4.1 Smoothness of Surface under Test

Surface texture has an important effect on the accuracy of the test results. When a test is performed on a rough textured surface, the plunger tip causes excessive crushing and a reduced rebound number is measured. More accurate results can be obtained by grinding a rough surface to uniform smoothness with a carborundum stone. it has been shown by Kolek[10] and Greene[13] that trowelled surfaces or surfaces made against metal forms yield rebound numbers 5 to 25% higher than surfaces made against wooden forms. This implies that if such surfaces are to be used, a special correlation curve or correction chart must be developed. Further, trowelled surfaces will give a higher scatter of individual results and, therefore, a lower confidence in estimated strength.

1.4.2 Size, Shape, and Rigidity of Test Specimens

If the concrete section or test specimen is small, such as a thin beam, wall, 152-mm cube, or 150 × 300-mm cylinder, any movement under the impact will lower the rebound readings. In such cases the member has to be rigidly held or backed up by a heavy mass.

It has been shown by Mitchell and Hoagland[14] that the restraining load for test specimens at which the rebound number remains constant appears to vary with the individual specimen. However, the effective restraining load for consistent results appears to be about 15% of the ultimate strength of 152 × 305-mm cylinders (Figure 1.9). Zoldners,[11] Greene,[13] and Grieb[15] have indicated effective stresses of 1,

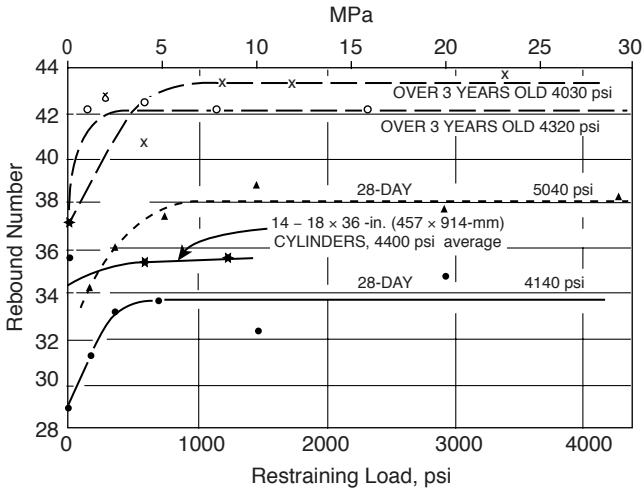

FIGURE 1.9 Restraining load vs. rebound readings for 6 × 12-in. (152 × 305-mm) cylinders. (Adapted from Reference 14.)

1.7, and 2.0 MPa, respectively, and these are considerably lower than the 15% value obtained by Mitchell and Hoagland.

1.4.3 Age of Test Specimen

Kolek[10] has indicated that the rate of gain of surface hardness of concrete is rapid up to the age of 7 days, following which there is little or no gain in the surface hardness; however, for a properly cured concrete, there is significant strength gain beyond 7 days. It has been confirmed by Zoldners[14] and Victor[16] that for equal strength, higher rebound values are obtained on 7-day-old concrete than on 28-day-old concrete. It is emphasized that when old concrete is to be tested, direct correlations are necessary between the rebound numbers taken on the structure and the compressive strength of cores taken from the structure.

The use of the Schmidt hammer for testing low-strength concrete at early ages, or where concrete strength is less than 7 MPa, is not recommended because rebound numbers are too low for accurate reading and the test hammer badly damages the concrete surface.[14] Figure 1.10 shows blemishes caused by rebound tests on surfaces of 8-h-old and 3-day-old concrete cylinders.

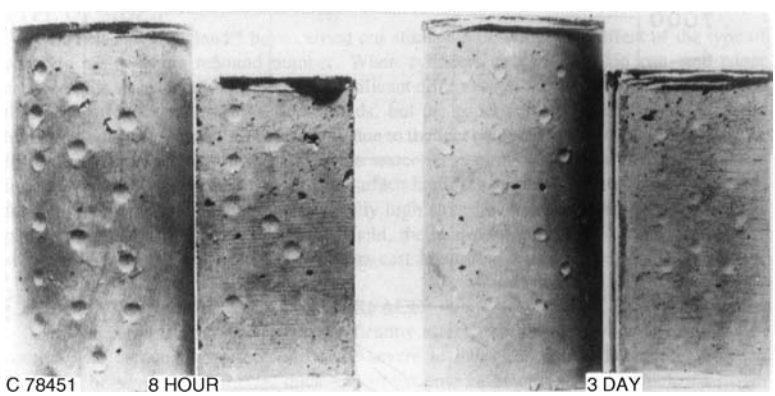

FIGURE 1.10 Eight-hour-old (left) and the three-day-old (right) specimens showing surface blemishes after Schmidt hammer impact. (Adapted from Reference 14.)

1.4.4 Surface and Internal Moisture Condition of the Concrete

The degree of saturation of the concrete and the presence of surface moisture have a decisive effect on the evaluation of test hammer results.[11,16,17] Zoldners[13] has demonstrated that well-cured, air-dried specimens, when soaked in water and tested in the saturated surface-dried condition, show rebound readings 5 points lower than when tested dry. When the same specimens were left in a room at 70°F (21.1°C) and air dried, they recovered 3 points in 3 days and 5 points in 7 days. Klieger et al.[18] have shown that for a 3-year-old concrete differences up to 10 to 12 points in rebound numbers existed between specimens stored in a wet condition and laboratory-dry samples. This difference in rebound numbers represents approximately 14 MPa difference in compressive strength.

It is suggested that, whenever the actual condition of the field concrete or specimens is not known, it would be desirable to presaturate the surface several hours prior to testing and use the correlation for tests on saturated surface-dried specimens.

1.4.5 Type of Coarse Aggregate

It is generally agreed that the rebound number is affected by the type of aggregate used. According to Klieger et al.,[18] for equal compressive strengths, concretes made with crushed limestone coarse aggregate show rebound numbers approximately 7 points lower than those for concretes made with gravel coarse aggregate, representing approximately 7 MPa difference in compressive strength.

Grieb[15] has shown that, even though the type of coarse aggregate used is the same, if it is obtained from different sources different correlation curves would be needed. Figure 1.11 shows results of one such study where four different gravels were used to make the concrete cylinders tested. At equal rebound numbers, the spread in compressive strength among the correlation curves varied from 1.7 to 3.9 MPa.

Greene[13] found that the use of the test hammer on specimens and structures made of lightweight concrete showed widely differing results. For example, lightweight concrete made with expanded shale aggregate yielded, at equal compressive strengths, different rebound numbers from concrete made with pumice aggregate. But for any given type of lightweight aggregate concrete, the rebound numbers proved to be proportional to the compressive strength.

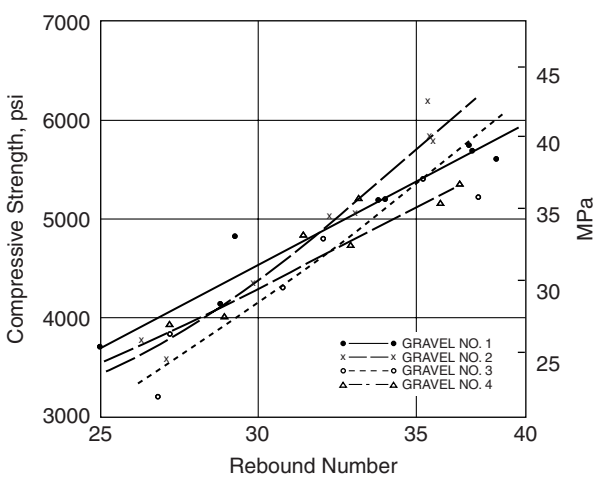

FIGURE 1.11 Effect of gravel from different sources on rebound numbers of concrete cylinders. (Adapted from Reference 15.)

1.4.6 Type of Cement

According to Kolek,[19] the type of concrete significantly affects the rebound number readings. High-alumina cement concrete can have actual strengths 100% higher than those obtained using a correlation curve based on concrete made with ordinary portland cement. Also, supersulfated cement concrete can have 50% lower strength than obtained from the ordinary portland cement concrete correlation curves.

1.4.7 Type of Mold

Mitchell and Hoagland[14] have carried out studies to determine the effect of the type of concrete mold on the rebound number. When cylinders cast in steel, tin can, and paper carton molds were tested, there was no significant difference in the rebound readings between those cased in steel molds and tin can molds, but the paper carton-molded specimens gave higher rebound numbers. This is probably due to the fact that paper molds withdraw moisture from the fresh concrete, thus lowering the water-cement ratio at the surface and resulting in a higher strength. As the hammer is a surface hardness tester, it is possible in such cases for the hammer to indicate an unrealistically high strength. It is therefore suggested that if paper carton molds are being used in the field, the hammer should be correlated against the strength results obtained from test cylinders cast in similar molds.

1.4.8 Carbonation of Concrete Surface

Surface carbonation of concrete significantly affects the Schmidt rebound hammer test results. The carbonation effects are more severe in older concretes when the carbonated layer can be several millimeters thick and in extreme cases up to 20 mm thick.[19] In such cases, the rebound numbers can be up to 50% higher than those obtained on an uncarbonated concrete surface. Suitable correction factors should be established in such cases, otherwise overestimation of concrete strength will result.

1.5 Rebound Number and Estimation of Compressive Strength

According to Kolek[10] and Malhotra[20,21] there is a general correlation between compressive strength of concrete and the hammer rebound number. However, there is a wide degree of disagreement among various researchers concerning the accuracy of the estimation of strength from the rebound readings and the correlation relationship. Coefficients of variation for compressive strength for a wide variety of specimens averaged 18.8% and exceeded 30% for some groups of specimens.[7] The large deviations in strength can be narrowed down considerably by developing a proper correlation curve for the hammer, which allows for various variables discussed earlier. By consensus, the accuracy of estimation of compressive strength of test specimens cast, cured, and tested under laboratory conditions by a properly calibrated hammer lies between ±15 and ±20%. However, the probable accuracy of estimation of concrete strength in a structure is ±25%.

Carette and Malhotra[22] have investigated the within-test variability of the rebound hammer test at test ages of 1 to 3 days and to the ability of the test to determine early-age strength development of concrete for formwork removal purposes. The rebound tests were performed at 1, 2, and 3 days on plain concrete slabs 300 × 1270 × 1220 mm in size. Also, companion cylinders and cores taken from the slabs were tested in compression. The mixture proportioning data, and within-test variation for the rebound hammer test and compression strength tests are shown in Tables 1.1 to 1.5. Boundy and Hondros[23] have suggested the use of the rebound hammer in conjunction with some method of accelerated curing to provide a rapid and convenient method for estimating the expected strength and quality of concrete test specimens. For *in situ* applications, Facaoaru[24] has suggested combined methods based on rebound number and pulse velocity measurements (see Chapter 5).

From the analyses of the test data, the authors concluded that because of the large within-test variation, the rebound hammer test was not a satisfactory method for predicting strength development of concrete at early ages.

TABLE 1.1 Properties of Fresh and Hardened Concrete[a]

Mix No.	Nominal Cement Content, (kg/m³)	Properties of Fresh Concrete: Density (kg/m³)	Slump (mm)	Air Content (%)	Properties of Hardened Concrete: Compressive Strength (MPa)[b] 1 Day	2 Days	3 Days	28 Days
1	250	2345	75	5.5	10.4	17.2	19.2	26.5
2	300	2390	100	4.4	15.3	21.6	24.6	33.3
3	350	2410	145	3.3	20.1	24.8	26.1	34.5
4	350	2410	75	3.8	20.1	25.0	26.3	35.1

[a] Determined on 150 × 300-mm cylinders.
[b] From Reference 22.

TABLE 1.2 Summary of Compressive Strength[a] and Rebound Hammer Test Results at Ages 1, 2, and 3 Days (Mixture No. 1)

Test	n[b]	Average 1 Day	Average 2 Days	Average 3 Days	Standard Deviation 1 Day	Standard Deviation 2 Days	Standard Deviation 3 Days	Coefficient of Variation (%) 1 Day	Coefficient of Variation (%) 2 Days	Coefficient of Variation (%) 3 Days
Compressive strength of cylinders										
150 × 300-mm cylinders, MPa	3	10.4	17.2	19.2	0.39	0.25	0.14	3.80	1.48	0.73
100 × 200-mm cylinders, MPa	5	9.5	16.0	18.4	0.53	0.83	0.40	5.58	5.19	2.17
Compressive strength of cores										
100 × 200-mm cores, MPa	3	11.1	16.9	18.3	0.57	0.36	0.17	3.21	3.38	0.92
Rebound hammer										
Rebound number	20	15.1	20.5	22.2	2.49	1.93	2.60	16.49	9.43	11.74

[a] From Reference 22.
[b] Number of test determinations.

TABLE 1.3 Summary of Compressive Strength[a] and Rebound Hammer Test Results at Ages 1, 2, and 3 Days (Mixture No. 2)

Test	n[b]	Average 1 Day	Average 2 Days	Average 3 Days	Standard Deviation 1 Day	Standard Deviation 2 Days	Standard Deviation 3 Days	Coefficient of Variation (%) 1 Day	Coefficient of Variation (%) 2 Days	Coefficient of Variation (%) 3 Days
Compressive strength of cylinders										
150 × 300-mm cylinders, MPa	3	15.3	21.6	24.6	0.57	0.21	0.25	3.71	0.98	1.03
100 × 200-mm cylinders, MPa	5	14.2	20.8	24.1	0.46	0.71	0.61	3.24	3.41	2.54
Compressive strength of cores										
100 × 200-mm cores, MPa	3	15.9	18.1	18.7	0	0	0.42	0	0	2.24
Rebound hammer										
Rebound number	20	18.9	21.9	21.5	1.89	3.18	2.24	9.99	14.51	10.40

[a] From Reference 22.
[b] Number of test determinations.

1.6 Rebound Number and Flexural Strength

Greene[13] and Klieger et al.[18] have established correlation relationships between the flexural strength of concrete and the hammer rebound number. They have found that the relationships are similar to those obtained for compressive strength, except that the scatter of the results is greater. Further, they found that the rebound numbers for tests conducted on the top of finished surface of a beam were 5 to 15% lower than those conducted on the sides of the same beam.

The effects of moisture condition and aggregate type on the flexural strength are similar to those found for the compressive strength.

TABLE 1.4 Summary of Compressive Strength[a] and Rebound Hammer Test Results at Ages 1, 2, and 3 Days (Mixture No. 3)

Test	n[b]	Average			Standard Deviation			Coefficient of Variation (%)		
		1 Day	2 Days	3 Days	1 Day	2 Days	3 Days	1 Day	2 Days	3 Days
Compressive strength of cylinders										
150 × 300-mm cylinders, MPa	3	20.1	24.8	26.1	0.81	0.31	0.19	4.04	1.24	0.71
100 × 200-mm cylinders, MPa	5	18.8	25.8	28.1	0.50	1.03	0.60	2.65	3.98	2.14
Compressive strength of cores										
100 × 200-mm cores, MPa	3	19.1	24.7	24.5	0.13	0.27	0.32	0.66	1.11	1.29
Rebound hammer										
Rebound number	20	19.8	21.2	22.0	2.61	2.17	3.46	13.17	10.23	15.75

[a] From Reference 22.
[b] Number of test determinations.

TABLE 1.5 Summary of Compressive Strength[a] and Rebound Hammer Test Results at Ages 1, 2, and 3 Days (Mixture No. 4)

Test	n[b]	Average			Standard Deviation			Coefficient of Variation (%)		
		1 Day	2 Days	3 Days	1 Day	2 Days	3 Days	1 Day	2 Days	3 Days
Compressive strength of cylinders										
150 × 300-mm cylinders, MPa	3	20.1	25.0	26.3	0.53	0.58	0.31	2.64	2.31	1.17
100 × 200-mm cylinders, MPa	5	19.8	25.8	27.5	0.94	1.24	1.52	4.74	4.80	2.94
Compressive strength of cores										
100 × 200-mm cores, MPa	3	19.7	20.6	21.6	0.16	0.82	0.63	0.81	4.00	2.94
Rebound hammer										
Rebound number	20	19.9	21.3	20.2	2.46	1.79	1.87	12.37	8.36	9.29

[a] From Reference 22.
[b] Number of test determinations.

1.7 Rebound Number and Modulus of Elasticity

Mitchell and Hoagland[14] have attempted to correlate hammer rebound number with the modulus of elasticity of the concrete specimens. The concluded that no generally valid correlation could be made between the rebound number and the static modulus of elasticity; however, a satisfactory relationship between the two might be possible if the hammer were to be calibrated for each individual type of concrete.

Petersen and Stoll[25] and Klieger[26] have established an empirical relationship between dynamic* modulus of elasticity and rebound number. They have shown that the relationships are affected by both moisture condition and aggregate type in the same manner as for compressive and flexural strengths.

1.8 North American Survey on the Use of the Rebound Hammer

In the early 1980s, a survey of concrete testing laboratories in Canada and the United States revealed that despite its limitations, the rebound hammer was the most often used nondestructive test method by those surveyed.[27]

*Modulus of elasticity obtained by flexural vibration of a cylindrical or prismatic specimen.

1.9 Standardization of Surface Hardness Methods

The indentation methods, although once included in the German Standards, are no longer used in the industry, and no major international standardization organization has issued any standards on the subject. In contrast, the rebound method has won considerable acceptance, and standards have been issued both by the ASTM and ISO and by several other countries for determining the rebound number of concrete.

ASTM Standard C 805 "Standard Test Method for Rebound Number of Hardened Concrete" was first issued as a tentative test method in 1975 and adopted as a standard test method in 1979. The test method has been revised periodically; the significance and use statement of the 2002 version of the standard is as follows:[28]

5.1 This test method is applicable to assess the in-place uniformity of concrete, to delineate regions in a structure of poor quality or deteriorated concrete, and to estimate in-place strength development.

5.2 To use this test method to estimate strength requires establishing a relationship between strength and rebound number. The relationship shall be established for a given concrete mixture and given apparatus. The relationship shall be established over the range of concrete strength that is of interest. To estimate strength during construction, establish the relationship by performing rebound number tests on molded specimens and measuring the strength of the same or companion molded specimens. To estimate strength in an existing structure, establish the relationship by correlating rebound numbers measured on the structure with the strengths of cores taken from corresponding locations. See ACI 228.1R for additional information on developing the relationship and on using the relationship to estimate in-place strength.

5.3 For a given concrete mixture, the rebound number is affected by factors such as moisture content of the test surface, the method used to obtain the test surface (type of form material or type of finishing), and the depth of carbonation. These factors need to be considered in preparing the strength relationship and interpreting test results.

5.4 Different hammers of the same nominal design may give rebound numbers differing from 1 to 3 units. Therefore, tests should be made with the same hammer in order to compare results. If more than one hammer is to be used, perform tests on a range of typical concrete surfaces so as to determine the magnitude of the differences to be expected.

5.5 This test method is not intended as the basis for acceptance or rejection of concrete because of the inherent uncertainty in the estimated strength.

1.10 Limitations and Usefulness

The rebound hammer developed by Schmidt provides an inexpensive and quick method for nondestructive testing of concrete in the laboratory and in the field.

The limitations of the Schmidt hammer should be recognized and taken into account when using the hammer. It cannot be overstressed that the hammer must not be regarded as a substitute for standard compression tests but rather as a method for determining the uniformity of concrete in the structures, and comparing one concrete against another. Estimation of strength of concrete by the rebound hammer within an accuracy of ±15 to ±20% may be possible only for specimens cast, cured, and tested under conditions similar to those from which the correlation curves are established.

References

1. Jones, R., A review of the non-destructive testing of concrete, *Proc. Symp. Non-destructive Testing of Concrete and Timber*, Institution of Civil Engineers, London, June 1969, 1.
2. Ball Impact Test for Normal Concrete (Kugelschlagprüfung von Beton mit dichtem Gefüge), Standard Code DIN 4240, No. 6, German Committee for Reinforced Concrete, 1966, 311.

3. Ball Test for Cellular Concrete (Kugelschlagprüfung von Gas- und Schaumbeton), Draft Code of Practice (June 1955, *Beton Stahlbetonbau (Berlin)*, 50(8), 224, 1955.
4. Williams, J.F., A method for the estimation of compressive strength of concrete in the field, *Struct. Eng. (London)*, 14(7), 321, 1936.
5. Skramtaev, B.G. and Leshchinszy, M.Yu, Complex methods of non-destructive tests of concrete in construction and structural works, *RILEM Bull. (Paris)*, New Series No. 30, 99, 1966.
6. Gaede, K., Ball Impact Testing for Concrete (Die Kugelschlagprüfung von Beton), Bull. No. 107, Deutscher Ausschuss für Stahlbeton, Berlin, 1952, 15.
7. Schmidt, E., The concrete test hammer (Der Beton-Prüfhammer), *Schweiz. Bauz. (Zurich)*, 68(28), 378, 1950.
8. Schmidt, E., Investigations with the new concrete test hammer for estimating the quality of concrete (Versuche mit den neuen Beton Prüfhammer zur Qualitätsbestimmung des Beton), *Schweiz. Archiv angew. Wiss. Tech. (Solothurn)*, 17(5), 139, 1951.
9. Schmidt, E., The concrete sclerometer, *Proc. Int. Symp. Non-destructive Testing on Materials and Structures*, Vol. 2, RILEM, Paris, 1954, 310.
10. Kolek, J., An appreciation of the Schmidt rebound hammer, *Mag. Concr. Res. (London)*, 10(28), 27, 1958.
11. Zoldners, N.G., Calibration and use of impact test hammer, *ACI J. Proc.*, 54(2), 161, 1957.
12. Akashi, T. and Amasaki, S., Study of the Stress Waves in the Plunger of a Rebound Hammer at the Time of Impact, Malhotra, V.M., Ed., American Concrete Institute Special Publication SP-82, 1984, 17.
13. Greene, G.W., Test hammer provides new method of evaluating hardened concrete, *ACI J. Proc.*, 51(3), 249, 1954.
14. Mitchell, L.J. and Hoagland, G.G., Investigation of the Impact Tube Concrete Test Hammer, Bull. No. 305, Highway Research Board, 1961, 14.
15. Grieb, W.E., Use of Swiss hammer for establishing the compressive strength of hardened concrete, *Public Roads*, 30(2), 45, 1958.
16. Victor, D.J., Evaluation of hardened field concrete with rebound hammer, *Indian Conc. J. (Bombay)*, 37(11), 407, 1963.
17. Willets, C.H., Investigation of the Schmidt Concrete Test Hammer, Miscellaneous Paper No. 6-627, U.S. Army Engineer Waterways Experiment Station, Vicksburg, MS, June 1958.
18. Klieger, P., Anderson, A.R., Bloem, D.L., Howard, E.L., and Schlintz, H., Discussion of "Test Hammer Provides New Method of Evaluating Hardened Concrete" by Gordon W. Greene, *ACI J. Proc.*, 51(3), 256-1, 1954.
19. Kolek, J., Non-destructive testing of concrete by hardness methods, *Proc. Symp. on Non-destructive Testing of Concrete and Timber*, Institution of Civil Engineers, London, June 1969, 15.
20. Malhotra, V.M., Non-destructive Methods for Testing Concrete, Mines Branch Monogr. No. 875, Department of Energy Mines and Resources, Ottawa, 1968.
21. Malhotra, V.M., Testing of hardened concrete: non-destructive methods, ACI Monogr. No. 9, 1976, 188.
22. Carette, G.G. and Malhotra, V.M., In-situ tests: variability and strength prediction of concrete at early ages, Malhotra, V.M., Ed., American Concrete Institute, Special Publication SP-82, 111.
23. Boundy, C.A.P. and Hondros, G., Rapid field assessment of strength of concrete by accelerated curing and Schmidt rebound hammer, *ACI J. Proc.*, 61(9), 1185, 1964.
24. Facaoaru, I., Report on RILEM Technical Committee on Non-destructive Testing of Concrete, Materials and Structure/Research and Testing (Paris), 2(10), 251, 1969.
25. Petersen, H. and Stoll, U.W., Relation of rebound hammer test results to sonic modulus and compressive strength data, *Proc. Highway Res. Board*, 34, 387, 1955.
26. Klieger, P., Discussion of "Relation of Rebound Hammer Test Results to Sonic Modulus and Compressive Strength Data" by Perry H. Petersen and Ulrich W. Stoll, *Proc. Highway Res. Board*, 34, 392, 1955.

27. ACI 228 Committee Report, In-place methods for determination of strength of concrete, *ACI J. Mater.*, September/October 1988.
28. ASTM C 805-02, Standard Test Method for Rebound Number of Hardened Concrete, *Annual Book of ASTM Standards*, Vol. 04.02, ASTM, West Conshohocken, PA, 2003.

2

Penetration Resistance Methods*

2.1 Introduction

2.2 Probe Penetration Test System
Principle · Description · Method of Testing · Correlation Pocedure

2.3 Evaluation of the Probe Penetration Test
Mechanism of Concrete Failure · Correlations between Probe Test Results and Compressive Strength · Variability of the Probe Penetration Test · Variations in the Estimated Strength Values · Nondestructive Nature of the Probe Penetration Test · Use of the Probe Penetration Test for Early Form Removal · Probe Penetration Test vs. Core Testing · Probe Penetration Test vs. Rebound Hammer Test · North American Survey on the Use of the Probe Penetration Test · Advantages and Disadvantages of the Probe Penetration Test

2.4 Pin Penetration Test

2.5 Standardization of Penetration Resistance Techniques

2.6 Limitations and Usefulness of Penetration Resistance Methods

V. Mohan Malhotra
Department of Natural Resources Canada, Ottawa

Georges G. Carette**
Department of Natural Resources Canada, Ottawa

This chapter reviews the development of penetration resistance methods for testing concrete nondestructively. These are being increasingly used for quality control and strength estimation of *in situ* concrete. Among the penetration techniques presently available, the most well known and widely used is the Windsor probe test. The principle of this method, the test equipment and procedures, and the preparation of calibration charts are described in detail. Factors affecting the variability of the test are discussed. Correlations that have been developed between the Windsor probe test results and the compressive strength of concrete are presented. A pin penetration test was developed in Canada for the purpose of determining safe form removal times. The advantages, limitations, and applications of the penetration methods are outlined. The chapter concludes with a list of pertinent references.

2.1 Introduction

Penetration resistance methods are based on the determination of the depth of penetration of probes (steel rods or pins) into concrete. This provides a measure of the hardness or penetration resistance of the material that can be related to its strength.

*©Minister of Supply and Services Canada, 1989.

**Deceased.

The measurement of concrete hardness by probing techniques was reported by Voellmy[1] in 1954. Two techniques were used. In one case, a hammer known as Simbi was used to perforate concrete, and the depth of the borehole was correlated to the compressive strength of concrete cubes. In the other technique, the probing of concrete was achieved by Spit pins, and the depth of penetration of the pins was correlated with the compressive strength of concrete

Apart from the data reported by Voellmy, there is little other published work available on these tests, and they appear to have received little acceptance in Europe or elsewhere. Perhaps the introduction of the rebound method around 1950 was one of the reasons for the failure of the above tests to achieve general acceptance.

In the 1960s, the Windsor probe test system was introduced in the United States and this was followed by the pin penetration test in Canada in the 1980s.

2.2 Probe Penetration Test System

Between 1964 and 1966. a device known as the Windsor probe was advanced for penetration testing of concrete in the laboratory as well as *in situ*. The device was meant to estimate the quality and compressive strength of *in situ* concrete by measuring the depth of penetration of probes driven into the concrete by means of a powder-actuated driver. The development of this technique was the joint undertaking of the Port of New York Authority, New York, and the Windsor Machinery Co., Connecticut. This development was closely related to studies reported by Kopf.[2] Results of the investigations carried out by the Port of New York Authority were presented by Cantor[3] in 1970. Meanwhile, a number of other organizations had initiated exploratory studies of this technique,[4–8] and a few years later, Arni[9,10] reported the results of a detailed investigation on the evaluation of the Windsor probe, while Malhotra[11–13] reported the results of his investigations on both 150 × 300-mm cylinders and 610 × 610 × 200-mm concrete slabs.

In 1972, Klotz[14] stated that extensive application of the Windsor probe test system had been made in investigations of in-place compressive strength of concrete and in determinations of concrete quality. The Windsor probe had been used to test reinforced concrete pipes, highway bridge piers, abutments, pavements, and concrete damaged by fire. In the 1970s, several U.S. federal agencies and state highway departments reported investigations on the assessment of the Windsor probe for *in situ* testing of hardened concrete.[15–19] In 1984 Swamy and Al-Hamed[20] in the U.K. published results of a study on the use of the Windsor probe system to estimate the *in situ* strength of both lightweight and normal weight concretes.

2.2.1 Principle

The Windsor probe, like the rebound hammer, is a hardness tester, and its inventors claim that the penetration of the probe reflects the precise compressive strength in a localized area is not strictly true.[21] However, the probe penetration relates to some property of the concrete below the surface, and, within limits, it has been possible to develop empirical correlations between strength properties and the penetration of the probe.

2.2.2 Description

The Windsor probe consists of a powder-actuated gun or driver (Figure 2.1), hardened alloy-steel probes, loaded cartridges, a depth gauge for measuring the penetration of probes, and other related equipment. The probes have a tip diameter of 6.3 mm, a length of 79.5 mm, and a conical point (Figure 2.2). Probes of 7.9 mm diameter are also available for the testing of concretes made with lightweight aggregates. The rear of the probe is threaded and screws into a probe-driving head, which is 12.7 mm in diameter and fits snugly into the bore of the driver. The probe is driven into the concrete by the firing of a precision powder charge that develops an energy of 79.5 m-kg. For the testing of relatively low-strength concrete, the powder level can be reduced by pushing the driver head further into the barrel.

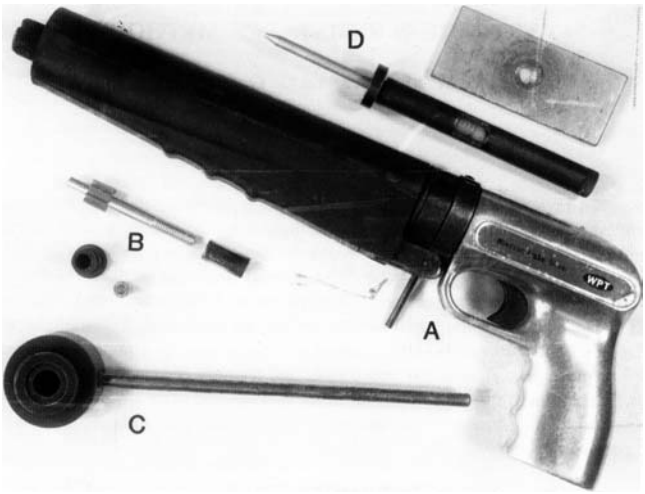

FIGURE 2.1 A view of the Windsor probe equipment. (A) Driver unit. (B) Probe for normal-weight concrete. (C) Single probe template. (D) Calibrated depth gauge. (Adapted from Reference 11.)

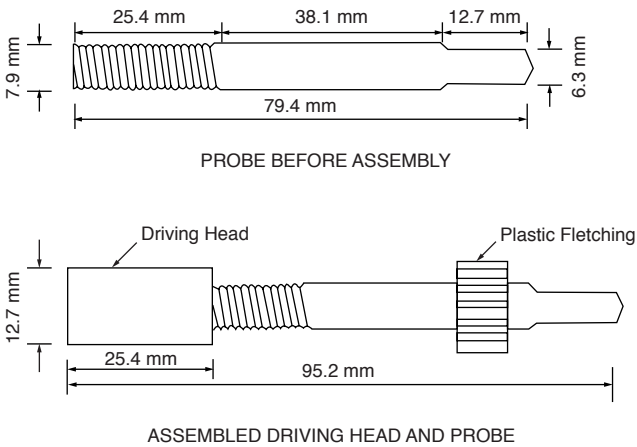

FIGURE 2.2 A view of probe for normal-weight concrete before and after assembly. (Adapted from Reference 11.)

2.2.3 Method of Testing

The method of testing is relatively simple and is given in the manual supplied by the manufacturer. The area to be tested must have a brush finish or a smooth surface. To test structures with coarse finishes, the surface first must be ground smooth in the area of the test. Briefly, the powder-actuated driver is used to drive a probe into concrete. If flat surfaces are to be tested, a suitable locating template to provide 178-mm equilateral triangular pattern is used, and three probes are driven into the concrete, one at each corner. The exposed lengths of the individual probes are measured by a depth gauge. The manufacturer also supplies a mechanical averaging device for measuring the average exposed length of the three probes fired in a triangular pattern. The mechanical averaging device consists of two triangular plates. The reference plate with three legs slips over the three probes and rests on the surface of the concrete. The other triangular plate rests against the tops of the three probes. The distance between the two plates, giving the mechanical average of exposed lengths of the three probes, is measured by a depth gauge inserted through a hole in the center of the top plate. For testing structures with curved surfaces, three

probes are driven individually using the single probe locating template. In either case, the measured average value of exposed probe length may then be used to estimate the compressive strength of concrete by means of appropriate correlation data.

2.2.4 Correlation Procedure

The manufacturer of the Windsor probe test system has published tables relating exposed length of the probe with compressive strength of concrete. For each exposed length value, different values for compressive strength are given, depending on the hardness of the aggregate as measured by the Mohs scale of hardness. The tables provided by the manufacturer are based on empirical relationships established in his laboratory. However, investigations carried out by Gaynor,[7] Arni,[9] Malhotra,[11–13] and several others[8,16,22–24] indicate that the manufacturer's tables do not always give satisfactory results. Sometimes they considerably overestimate the actual strength[11,20–22] and in other instances they underestimate the strength. It is, therefore, imperative for each user of the probe to correlate probe test results with the type of concrete being used. Although the penetration resistance technique has been standardized, the standard does not provide a procedure for developing a correlation. A practical procedure for developing such a relationship is outlined below.

1. Prepare a number of 150 × 300-mm cylinders, or 150-mm cubes, and companion 600 × 600 × 200-mm concrete slabs covering a strength range that is to be encountered on a job site. Use the same cement and the same type and size of aggregates as those to be used on the job. Cure the specimens under standard moist-curing conditions, keeping the curing period the same as the specified control age in the field.
2. Test three specimens in compression at the age specified, using standard testing procedure. Then fire three probes into the top surface of the slab at least 150 mm apart and at least 150 mm from the edges (Figure 2.3). If any of the three probes fails to properly penetrate the slab, remove it and fire another. Make sure that at least three valid probe results are available, measure the exposed probe lengths, and average the three results.
3. Repeat the above procedure for all test specimens.
4. Plot the exposed probe length against the compressive strength, and fit a curve or line by the method of least squares. The 95% confidence limits for individual results may also be drawn on the graph. These limits will describe the interval within which the probability of a test result falling is 95%.

A typical correlation curve is shown in Figure 2.4, together with the 95% confidence limits for individual values. The correlation published by several investigators for concretes made with limestone gravel, chert, and traprock aggregates are shown in Figure 2.5. Note that different relationships have been obtained for concretes with aggregates having similar Mohs hardness numbers.

2.3 Evaluation of the Probe Penetration Test

2.3.1 Mechanism of Concrete Failure

There is no rigorous theoretical analysis of the probe penetration test available. Such analysis may, in fact, not be easy to achieve in view of the complex combinations of dynamic stresses developed during penetration of the probe, and the heterogeneous nature of concrete. The test involves a given initial amount of kinetic energy of the probe, which is absorbed during penetration, in large part through crushing and fracturing of the concrete, and in lesser part through friction between the probe and the concrete.

Penetration of the probe causes the concrete to fracture within a cone-shaped zone below the surface with cracks propagating up to the surface (Figure 2.6). Further penetration below this zone is, in large part, resisted by the compression of the adjacent material, and it has been claimed[25] that the Windsor

FIGURE 2.3 A view of the Windsor probe in operation: a 600 × 600 × 200-mm slab under test for correlation purposes. (Adapted from Reference 21.)

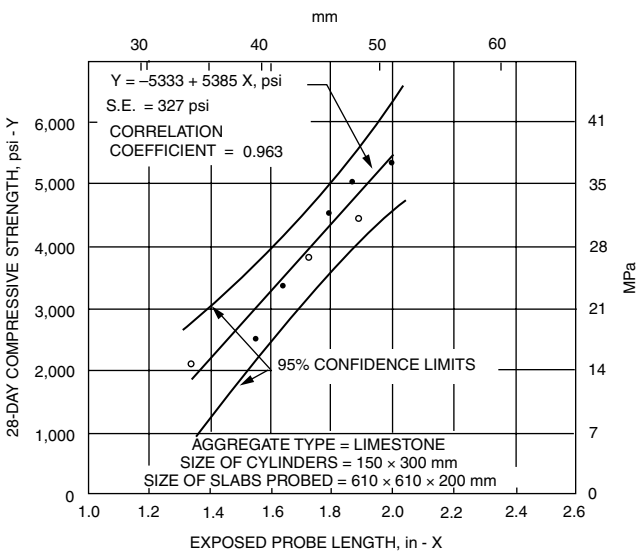

FIGURE 2.4 Relationship between exposed probe length and 28-day compressive strength of concrete. (Adapted from Reference 12.)

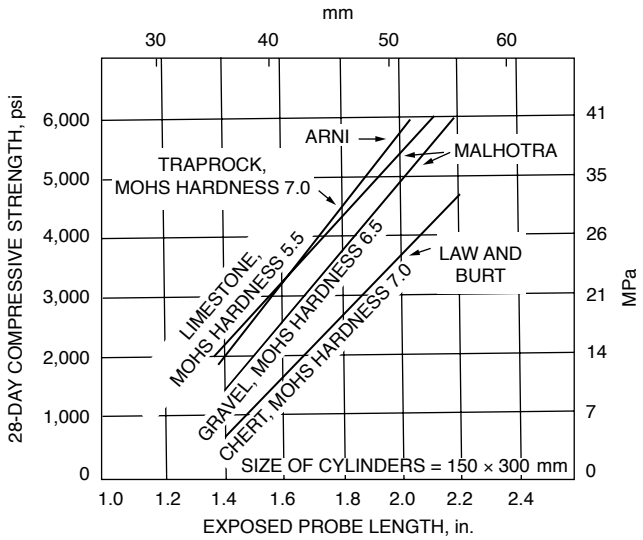

FIGURE 2.5 Relationship between exposed probe length and 28-day compressive strength of concrete as obtained by different investigators. (Adapted from References 8, 9, and 12.)

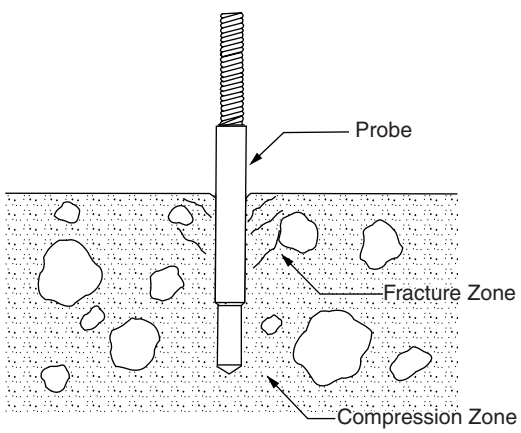

FIGURE 2.6 Typical failure of mature concrete during probe penetration.

probe test measures the compressibility of a localized area of concrete by creating a subsurface compaction bulb. Further, it has been claimed that the energy required to break pieces of aggregate is a low percentage of the total energy of the driven probe, and the depth of penetration is not significantly affected. However, these claims have never been proven.

Notwithstanding the extent to which the above claims may be true, it nevertheless appears clear that the probe penetrations do relate to some strength parameter of the concrete below the surface, which makes it possible to establish useful empirical relationships between the depth of penetration and compressive strength.

2.3.2 Correlations between Probe Test Results and Compressive Strength

The usefulness of the probe penetration test lies primarily upon its being able to establish sufficiently accurate relationships between probe penetration and compressive strength. A factor, long recognized, that affects

this relationship is the hardness of the coarse aggregate, and this is taken into account in the correlation tables provided by the equipment manufacturer. However, as previously mentioned, the use of the manufacturer's tables has been found by several investigators not to be satisfactory. This is probably because factors other than aggregate hardness, which also affect probe penetration, have not been considered.

There appears to have been no systematic attempts to determine the relative influences of these factors that could affect the probe penetration test results. However, it is generally agreed that the largest influence comes from the coarse aggregate. Apart from its hardness, the type and size of coarse aggregate used have been reported to have a significant effect on probe penetration.[9,20,23] The considerable differences shown in Figure 2.5 between correlations obtained by various investigators tend to support the important influence of the aggregate type. However, other parameters such as mixture proportions, moisture content, curing engine, and surface conditions are likely to have affected these correlations to some extent, and could explain some of the observed differences.

Other significant parameters that may also affect the accuracy of the probe penetration-strength relationships include the degree of carbonation and the age of concrete.[4,20,21] Carbonation may change the physical and chemical characteristics of concrete through a substantial depth below the surface, and can clearly have an important influence on the depth of penetration of the probe. On the other hand, the age of concrete has been found[20] to considerably affect the accuracy of strength prediction in some instances. In particular, for very old concrete, the probe test may indicate higher strength than actually exists in the structure. It has been suggested that the higher values may be related to microcracking between the aggregates and the paste, which affects compressive strength but not probe penetration.[26] Similarly, the stress history of concrete has been identified as a potential factor influencing the relationship between probe penetration and *in situ* strength.[27] This is due to the cracking from service loading again affecting the cylinder strength test, but not affecting the probe penetration test.

In view of the above, when the probe penetration test is to be used for strength estimation, it is advisable to prepare a correlation curve based on the particular type of concrete to be investigated. Further, any other factors that may limit the accuracy of the correlation, such as factors related to particular testing conditions, would need to be recognized and taken into account in the use of these correlation curves.

2.3.3 Variability of the Probe Penetration Test

The within-batch variability in the probe test results as obtained by various investigators is shown in Table 2.1. Variability is reported in terms of standard deviations and coefficients of variation with values in the latter case being calculated from the exposed probe readings, although more correctly, they should be based on the embedded lengths of the probe. These data show that for concrete with a maximum size of aggregate of 19 mm, a typical value for the within-test coefficient of variation (based on depth of penetration) is about 5%.[28] Statistically, for such concrete, the minimum number of individual penetration tests required to ensure that the average penetration is known with the same degree of confidence as the average standard cylinder strength (assuming a coefficient of variation of 4% based on two cylinders) would be three. This number, however, would not ensure that the *in situ* strength is known with the same degree of confidence, since, obviously, the above within-test coefficient of variation for the probe penetration test does not take into account the uncertainty of the correlation relationship, which also affects the reliability of the estimated strength.

In general, the within-batch variability of probe penetration tests can be attributed partly to operator and equipment errors, and partly to the heterogeneous nature of concrete. In the former case, the operator error has been reported to be generally minimal, and the variations come rather from the test equipment. For example, the variations may be due to the degree of precision achieved in measuring the length of the exposed portion of the probe. In this regard, it has been suggested that the development of more accurate devices for measuring exposed probe length could possibly reduce the within-test variations.[29] On the other hand, the heterogeneous nature of concrete, which on a macro-scale can be regarded as the result of phases such as coarse aggregate and air-voids distributed in the mortar matrix, is likely the

TABLE 2.1 Within-Batch Standard Deviation and Coefficient of Variation of Probe Penetration Measurements

Investigation Reported by	Type of Aggregate Used	Maximum Aggregate Size (mm)	Type of Specimens Tested	Total Number of Probes	Number of Probes per Test	Age of Test (days)	Average Standard Deviation (mm)	Average Coefficient of Variation (%)[a]
Arni (Ref. 9)	Gravel, limestone, trap rock	50	410 × 510 × 200-mm slabs	136	9	3, 7, 14, and 28	3.62	7.1
		25	410 × 510 × 200-mm slabs	198	9	3, 7, 14, and 28	2.66	5.4
Malhotra (Ref. 11)	Limestone	19	152 × 305-mm cylinders	20	2	7 and 28	3.14	7.7
		19	610 × 610 × 200-mm slabs	48	3	7 and 28	1.37	3.4
	Gravel	19	150 × 150 × 1690-mm prisms	28	2	35	1.57	3.4
		19	610 × 610 × 200-mm slabs	48	3	7 and 28	2.21	5.5
Gaynor (Ref. 7)	Quartz	25	150 × 580 × 1210-mm walls	384	16	3 and 91	4.05	—
	Semi-lightweight expanded shale as coarse aggregate	25	150 × 580 × 1210-mm walls	256	9	3 and 91	4.30	—
Carette, Malhotra (Ref. 29)	Limestone	19	300 × 1220 × 1220-mm slabs	72	6	1, 2, and 3	2.52	8.3 (5.4)
Keiller (Ref. 22)	Limestone, gravel	19	250 × 300 × 1500-mm prisms	45	3	7 and 28	1.91	3.5

[a] Based on exposed length of the probe, except for the value in parentheses, which is based on depth of penetration.

major contributor to variations in the probe test results. In particular, the random distribution of larger size aggregates tends to magnify the effect of heterogeneity over the relatively small area affected by the test, and it has indeed been shown that the variability of the probe penetration test increases with an increase in the maximum size of aggregates.[9] As already mentioned, the effect of the aggregate hardness on the probe penetration is generally well recognized. However, its effect on the variability of the results has not been made clear. Some investigations have indicated a possible increase of variability with harder aggregates.[22] In their investigations, Swamy and Al-Hamed[20] have observed a slightly higher variability of the exposed probe length readings for normal weight aggregate concrete than for lightweight aggregate concrete.

2.3.4 Variations in the Estimated Strength Values

Although the variability of the probe penetration test provides a useful index of precision for the test, it is however the magnitude of variation in the strength values estimated from the probe readings which provides a basis for the interpretation of the probe test results. The uncertainty in the estimated strength is a function of both the variability of the penetration measurements, and the degree of sensitivity of the penetration test in detecting small changes in strength. There is relatively little information concerning the variability of the estimated strength, though there has been mention of its being relatively large.[3,30] It can nevertheless be readily demonstrated from typical correlations developed by various investigators (Figure 2.5) that variations in probe readings of the order shown in Table 2.1 would correspond to variabilities in strength significantly larger than those normally observed with the standard cylinder test. For the proper interpretation of the probe test results, it is, therefore, necessary to make use of statistical

procedures that do take into account the variability of the penetration readings, and the uncertainty of the correlation relationship.[28]

2.3.5 Nondestructive Nature of the Probe Penetration Test

The probe penetration test is generally considered as nondestructive in nature; however, this is not exactly true. The probe leaves a minor disturbance on a very small area with an 8-mm hole in the concrete for the depth of penetration of the probe. In the case of mature concrete, there is also around the probe a cone-shaped region where the concrete may be heavily fractured, and which may extend to the depth of probe penetration.

This damage would be of little consequence if testing were being carried out on the side of a wall that is to be backfilled or on a foundation slab that is to be covered. However, on an exposed face the damage would be unsightly. The probes would have to be removed and the surface patched at added cost. The test may be considered nondestructive to the extent that concrete can be tested *in situ*, and the strength of structural members is not affected significantly by the test.

2.3.6 Use of the Probe Penetration Test for Early Form Removal

An increasingly important area of the application of nondestructive techniques is in the estimation of early-age strength of concrete for the determination of safe form removal times.

Relatively little information has been published in regard to the performance of the probe penetration test at early ages. However, by the late 1970s, it had been reported that the probe penetration test was probably the most widely used nondestructive method for the determination of safe stripping times.[18] One main advantage cited was the great simplicity of the test: "One simply fires the probes into the concrete and compares penetration to previously established criteria. If the probes penetrate too far, the contractor knows the concrete is not yet strong enough."

Carette and Malhotra[29] have investigated in the laboratory the within-test variability at the ages of 1 to 3 days of the probe penetration test, and the ability of the test to indicate the early-age strength development of concrete for formwork removal purposes. The penetration tests were performed at 1, 2, and 3 days on plain concrete slabs of 300 × 1220 × 1220 mm, along with compression tests on standard cylinders and cores taken from the slabs. The mixture proportioning data along with the probe penetration and strength results are shown in Tables 2.2 to 2.6. Excellent correlations between compressive strength and probe penetration were observed at these ages for each concrete. From the analysis of the test data, the authors concluded that unlike the rebound method, the probe penetration test can estimate the early-age strength development of concrete within a reasonable degree of accuracy, and thus can be applied to determine safe stripping times for the removal of formwork in concrete constructions.

TABLE 2.2 Properties of Fresh and Hardened Concrete[a]

		Properties of Fresh Concrete			Properties of Hardened Concrete Compressive Strength[a] (MPa)			
Mixture No.	Nominal Cement Content (kg/m^3)	Density (kg/m^3)	Slump (mm)	Air Content (%)	1 Day	2 Days	3 Days	28 Days
1	250	2345	75	5.5	10.4	17.2	19.2	26.5
2	300	2390	100	4.4	15.3	21.6	24.6	33.3
3	350	2410	145	3.3	20.1	24.8	26.1	34.5
4	350	2410	75	3.8	20.1	25.0	26.3	35.1

[a] Determined on 150 × 300-mm cylinders.
Source: Reference 29.

TABLE 2.3 Summary of Compressive Strength and Windsor Probe Test Results at Ages 1, 2, and 3 Days (Mixture No. 1)

Test	n[a]	Average			Standard Deviation			Coefficient of Variation (%)		
		1 Day	2 Days	3 Days	1 Day	2 Days	3 Days	1 Day	2 Days	3 Days
Compressive strength of cylinders										
150 × 300-mm cylinders, MPa	3	10.4	17.2	19.2	0.29	0.25	0.14	3.80	1.48	0.73
100 × 200-mm cylinders, MPa	5	9.5	16.0	18.4	0.53	0.83	0.40	5.58	5.19	2.17
Compressive strength of cores										
100 × 200-mm cores, MPa	3	11.1	16.9	18.3	0.36	0.57	0.17	3.21	3.38	0.92
Penetration resistance (Windsor probe)										
Exposed length of probe, mm	6	17.9	29.0	33.1	2.12	3.69	2.20	11.84	12.72	6.65
Embedded length of probe, mm		61.5	50.4	46.3	2.12	3.69	2.20	3.45	7.32	4.76

[a] Number of test determinations.
Source: Reference 29.

2.3.7 Probe Penetration Test vs. Core Testing

The determination of the strength of concrete in a structure may become necessary when standard cylinder strength test results fail to comply with specified values, or the quality of the concrete is being questioned because of inadequate placing or curing procedures. It may also be required in the case of older structures where changes in the quality of the concrete are being investigated. In these instances, the most direct and common method of determining the strength of concrete is through drilled core testing; however, some nondestructive techniques such as the probe penetration test have been gaining acceptance as a means to estimate the *in situ* strength of concrete.[18,31]

TABLE 2.4 Summary of Compressive Strength and Windsor Probe Test Results at Ages 1, 2, and 3 Days (Mixture No. 2)

Test	n[a]	Average			Standard Deviation			Coefficient of Variation (%)		
		1 Day	2 Days	3 Days	1 Day	2 Days	3 Days	1 Day	2 Days	3 Days
Compressive strength of cylinders										
150 × 300-mm cylinders, MPa	3	15.3	21.6	24.6	0.57	0.21	0.25	3.71	0.98	1.03
100 × 200-mm cylinders, MPa	5	14.2	20.8	24.1	0.46	0.71	0.61	3.24	3.41	2.54
Compressive strength of cores										
100 × 200-mm cores, MPa	3	15.9	18.1	18.7	0	0	0.42	0	0	2.24
Penetration resistance (Windsor probe)										
Exposed length of probe, mm	6	29.1	33.2	38.0	2.21	2.05	2.78	7.59	6.17	7.32
Embedded length of probe, mm		50.3	46.2	41.4	2.21	2.85	2.78	4.39	4.44	6.71

[a] Number of test determinations.
Source: Reference 29.

TABLE 2.5 Summary of Compressive Strength and Windsor Probe Test Results at Ages 1, 2, and 3 Days (Mixture No. 3)

Test	n[a]	Average			Standard Deviation			Coefficient of Variation (%)		
		1 Day	2 Days	3 Days	1 Day	2 Days	3 Days	1 Day	2 Days	3 Days
Compressive strength of cylinders										
150 × 300-mm cylinders, MPa	3	20.1	24.8	26.1	0.81	0.31	0.19	4.04	1.24	0.71
100 × 200-mm cylinders, MPa	5	18.8	25.8	28.1	0.50	1.03	0.60	2.65	3.98	2.14
Compressive strength of cores										
100 × 200-mm cores, MPa	3	19.1	24.7	24.5	0.13	0.27	0.32	0.66	1.11	1.29
Penetration resistance (Windsor probe)										
Exposed length of probe, mm	6	23.2	34.1	36.3	2.64	1.78	2.48	11.38	5.22	6.83
Embedded length of probe, mm		56.2	45.3	43.1	2.64	1.78	2.48	4.70	3.93	5.76

[a] Number of test determinations.
Source: Reference 29.

TABLE 2.6 Summary of Compressive Strength and Windsor Probe Test Results at Ages 1, 2, and 3 Days (Mixture No. 4)

Test	n[a]	Average			Standard Deviation			Coefficient of Variation (%)		
		1 Day	2 Days	3 Days	1 Day	2 Days	3 Days	1 Day	2 Days	3 Days
Compressive strength of cylinders										
150 × 300-mm cylinders, MPa	3	20.1	25.0	26.3	0.53	0.58	0.31	2.64	2.31	1.17
100 × 200-mm cylinders, MPa	5	19.8	25.8	27.5	0.94	1.24	1.52	4.74	4.80	2.94
Compressive strength of cores										
100 × 200-mm cores, MPa	3	19.7	20.6	21.6	0.16	0.82	0.63	0.81	4.00	2.94
Penetration resistance (Windsor probe)										
Exposed length of probe, mm	6	31.8	36.5	38.3	3.43	3.28	1.64	10.79	8.99	4.28
Embedded length of probe, mm		47.6	42.9	41.1	3.43	3.28	1.64	7.21	7.65	3.99

[a] Number of test determinations.
Source: Reference 29.

It has been claimed that the probe penetration test is superior to core testing and should be considered as an alternative to the latter for estimating the compressive strength of concrete.[25] It is true that the probe test can be carried out in a matter of minutes, whereas cores, if from exposed areas and if they have to be tested in accordance with ASTM C 42-87, must be soaked for 40 h;[32] also, the cores may have to be transported to a testing laboratory, causing further delay in getting the results. However, the advantages of the probe penetration test should be judged against the precision of its test results, and the following statement by Gaynor[7] should be of interest in this regard:

> Based on these tests, the probe system does not supply the accuracy required if it is to replace conventional core tests. However, it will be useful in much the same manner that the rebound hammer

is useful. In these tests, neither the probe system nor the rebound hammer provides precise quantitative estimates of compressive strength of marginal concretes. Both should be used to locate areas of relatively low- or relatively high-strength concretes in structures.

On the other hand, it has been shown by Malhotra and Painter[12] that the standard error of estimate of 28 day compressive strength of concrete cylinders is of the same order for both the probe and the core tests. More recently, Swamy and Al-Hamed[20] have compared the results of the probe penetration test and core strength tests, and examined how these related to the results of the standard wet-cube strength test. Their work was carried out on slabs of 1800 × 890 × 125 mm, and on 50-mm cores and 100-mm cubes, and covered both normal-weight and lightweight concretes. One of their conclusions was that the probe system, as a general method of nondestructive testing, estimated the wet-cube strength better than the small diameter cores at ages up to 28 days while the cores estimated the strength of older concrete better, particularly in the lower range of strength.

Carette and Malhotra[29] have also observed that, at early ages, probe penetration test results showed better correlation with standard cylinder strengths than with core strengths. This was attributed by the investigators to the variations in the temperature history of the large test slabs used.

It must be stressed that in cases where standard cylinder or cube strength is strictly the parameter of interest because of the specifications being expressed primarily in these terms, the core test which provides a direct measure of compressive strength clearly remains the most reliable means of estimating *in situ* strength. In many situations, however, it has been found possible to establish, within certain limits of material composition and testing conditions, relationships between probe penetration and strength that are accurate enough so that the probe test can be used as a satisfactory substitute for the core test.[31]

2.3.8 Probe Penetration Test vs. Rebound Hammer Test

Both the probe penetration test and the rebound hammer test provide means of estimating the relative quality of concrete under investigation. Correlations between the rebound numbers and the exposed probe lengths as obtained by Malhotra and Painter[12] are shown in Figure 2.7. Because the probe can penetrate up to about 50 mm in concrete, the probe penetration results are more meaningful than the results of the rebound hammer, which is a surface hardness tester only. Because of the greater penetration in concrete, the probe test results are influenced to a lesser degree by surface moisture, texture, and carbonation effects.[4] However, size and distribution of coarse aggregate in the concrete affect the probe

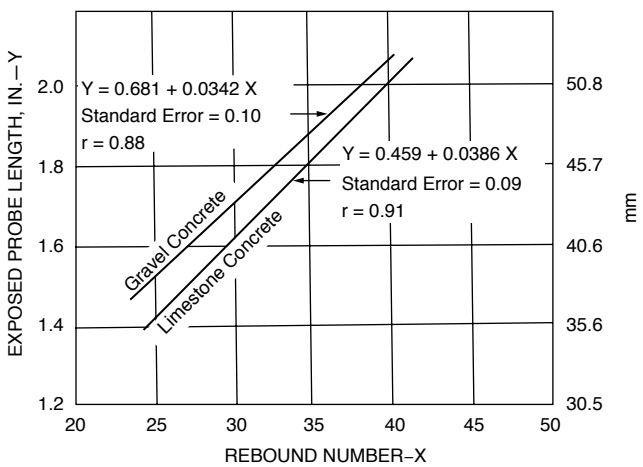

FIGURE 2.7 Relationship between rebound number and exposed length of probe. (Adapted from Reference 12.)

test results to a much greater degree than those obtained by the rebound hammer. Where cost is a critical factor, the above advantages of the probe penetration test may be offset by a higher initial cost of the equipment compared with the rebound hammer, and the recurring expenses for the probes. Both tests damage the concrete surface to varying degrees. The rebound hammer leaves surface blemishes on young concrete, whereas the probe leaves a hole 8 mm in diameter for the depth of the probe and may cause minor cracking.

2.3.9 North American Survey on the Use of the Probe Penetration Test

In the early 1980s, a survey of concrete testing laboratories in Canada and the United States indicated that the Windsor probe penetration technique was the second most often used method for *in situ* strength testing of concrete.[28] The survey included methods such as rebound hammer, probe penetration, pullout, pulse velocity, maturity, and cast-in-place cylinder. In terms of reliability, simplicity, accuracy, and economy, the probe test was given one of the best combined ratings.

2.3.10 Advantages and Disadvantages of the Probe Penetration Test

The probe penetration test system is simple to operate, rugged and needs little maintenance except for occasional cleaning of the gun barrel. The system has a number of built-in safety features that prevent accidental discharge of the probe from the gun. However, wearing of safety glasses is required. In the field, the probe penetration test offers the main advantages of speed and simplicity, and that of requiring only one surface for the test. Its correlation with concrete strength is affected by a relatively small number of variables which is an advantage over some other methods for *in situ* strength testing.

However, the probe test has limitations that must be recognized. These limitations include minimum size requirements for the concrete member to be tested. The minimum acceptable distance from a test location to any edges of the concrete member or between two given test locations is of the order of 150 to 200 mm, while the minimum thickness of the members is about three times the expected depth of penetration. Distance from reinforcement can also have an effect on depth of probe penetration especially when the distance is less than about 100 mm.[27]

As previously indicated, the uncertainty of the estimated strength value, in general, is relatively large and the test results may lack the degree of accuracy required for certain applications. The test is limited to a certain range of strength (<40 MPa), and the use of two different power levels to accommodate a larger range of concrete strength within a given investigation complicates the correlation procedures. Finally, as noted above, the test causes some minor damage to the surface, which generally needs to be repaired.

2.4 Pin Penetration Test

In the late 1980s, Nasser and Al-Manaseer[33,34] reported the development of a simple pin penetration test for the determination of early-stage strength of concrete for removal of concrete formwork. Briefly, this apparatus consists of a device that grips a pin having a length of 30.5 mm, a diameter of 3.56 mm and a tip machined at an angle of 22.5° (Figure 2.8). The pin is held within a shaft, which is encased within the main body of the tester. The pin is driven into the concrete by a spring, which is mechanically compressed when the device is prepared for a test. The spring is reported to have a stiffness of 49.7 N/mm and stores about 10.3 N · m of energy when compressed.

When ready for testing, the apparatus is held against the surface of concrete to be tested, and a triggering device is used to release the spring forcing the pin into the concrete. Following this, the apparatus is removed, and the small hole created in the concrete is cleared by means of an air blower. A dial gauge is then inserted in the pin hole to measure the penetration depth.

A typical correlation between the pin penetration (depth of the hole) and the compressive strength of concrete is shown in Figure 2.9.

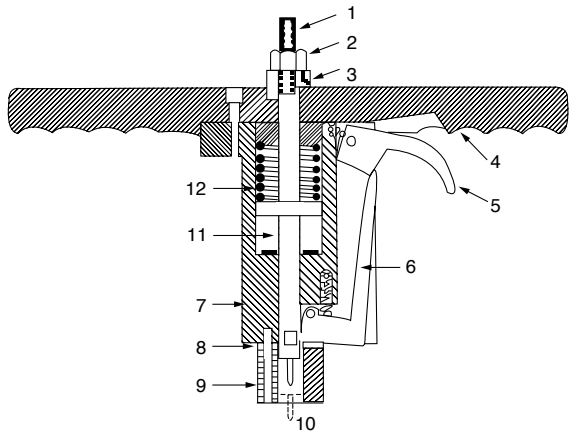

FIGURE 2.8 Diagram of pin penetration testing apparatus. (Adapted from Reference 33.)

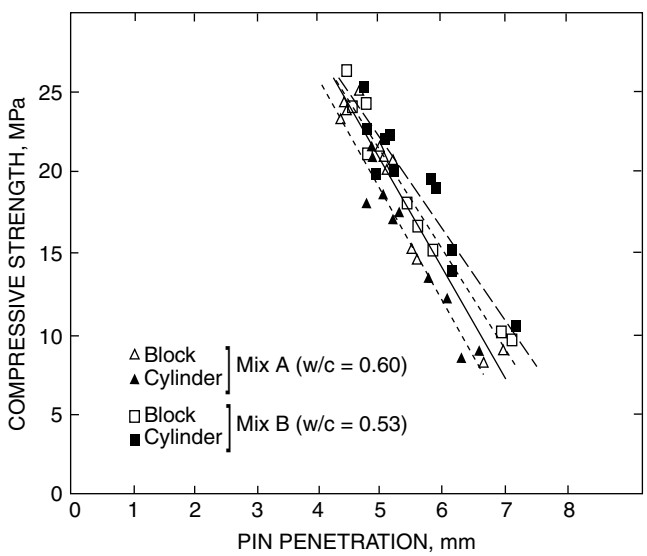

FIGURE 2.9 Relationship between pin penetration and compressive strength of concrete. (Adapted from Reference 33.)

The test, although simple in concept, has limitations. The pin penetrates only a small depth into the concrete, and therefore the results can be seriously affected by the conditions of the material at the surface. For a similar reason, the variability of the test, for which no documentation is yet available, is expected to be relatively large. The tests results are invalid when an aggregate particle is struck. The simplicity of the

test makes it possible to obtain as many readings as necessary at little extra cost, and this could somewhat overcome some of the variations in the test results. The equipment is rather heavy for field use, and because of the nature of the spring mechanism, cannot be used for concrete with strength greater than about 30 MPa. Calibration of the equipment is important and its frequent verification may be necessary.

2.5 Standardization of Penetration Resistance Techniques

ASTM Committee C-9 initiated the development of a standard for penetration resistance testing in 1972 and a tentative test method covering probe penetration was first issued in 1975. A standard test method designated ASTM C 803 "Penetration Resistance of Hardened Concrete" was later issued in 1982. In 1990, the method was revised by the addition of the pin penetration method.[33] The significance and use statement of the 2003 version of the test method is as follows:[35]

5.1 This test method is applicable to assess the uniformity of concrete and to delineate zones of poor quality or deteriorated concrete in structures.

5.2 This test method is applicable to estimate in-place strength, provided that a relationship has been experimentally established between penetration resistance and concrete strength. Such a relationship must be established for a given test apparatus (see also 9.1.5), using similar concrete materials and mixture proportions as in the structure. Use the procedures and statistical methods in ACI 228.1R for developing and using the strength relationship.

NOTE 1 — Since penetration results may be affected by the nature of the formed surfaces (for example, wooden forms versus steel forms), correlation testing should be performed on specimens with formed surfaces similar to those to be used during construction. Additional information on the factors affecting penetration test results and summaries of past research are available.

5.3 Steel probes are driven with a high-energy, powder-actuated driver, and probes may penetrate some aggregate particles. Probe penetration resistance is affected by concrete strength as well as the nature of the coarse aggregate. Steel pins are smaller in size than probes and are driven by a low energy, spring-actuated driver. Pins are intended to penetrate the mortar fraction only; therefore, a test in which a pin strikes a coarse aggregate particle is disregarded.

5.4 This test method results in surface damage to the concrete, which may require repair in exposed architectural finishes.

2.6 Limitations and Usefulness of Penetration Resistance Methods

Penetration resistance methods are basically hardness methods, and like other hardness methods, should not be expected to yield absolute values of strength of concrete in a structure. However, like surface hardness tests, penetration tests provide an excellent means of determining the relative strength of concrete in the same structure, or relative strengths in different structures without extensive correlation with specific concretes. The probe penetration test can also be used to estimate strength of concrete *in situ*, however this requires accurate correlations. The correlation curves provided by the test equipment manufacturer do not appear to be satisfactory. It is, therefore, recommended for each user of the probe equipment to prepare his own correlation curves for the type of concrete under investigation. The test is particularly sensitive to certain characteristics of the aggregate and with a change in source of aggregates, the establishment of new correlations become mandatory.

References

1. Voellmy, A., Examination of Concrete by Measurements of Superficial Hardness, *Proc. Int. Symp. on Nondestructive Testing of Materials and Structures, RILEM Paris*, 2, 323, 1954.

2. Kopf, R.J., Powder Actuated Fastening Tools for Use in the Concrete Industry, Mechanical Fasteners for Concrete, SP-22, American Concrete Institute, Detroit, 1969, 55.
3. Cantor, T.R., Status Report on the Windsor Probe Test System, presented to Highway Research Board Committee A2-03, Mechanical Properties of Concrete, 1970 Annual Meeting, Washington, D.C., January 1970.
4. Freedman, S., Field testing of concrete strength, *Modern Concr.*, 14(2), 31, 1969.
5. Arizona Aggregate Association, Report on Windsor Probe, Available from Portland Cement Association, Phoenix, AZ, 1969.
6. Probe quickly shows concrete strength, *Eng. News-Rec.*, 183, 43, 1969.
7. Gaynor, R.D., In-Place Strength of Concrete—A Comparison of Two Test Systems, presented at 39th Annual Convention of the National Ready Mixed Concrete Association (New York, January 28, 1969). Published with NRMCA Tech. Information Letter No. 272, November 4, 1969.
8. Law, S.M. and Burt, W.T., III, Concrete Probe Strength Study, Research Report No. 44, Research Project No. 68-2C(B), Louisiana HPR (7), Louisiana Department of Highways, December 1969.
9. Arni, H.T., Impact and penetration tests of portland cement concrete, *Highway Res. Rec.*, 378, 55, 1972.
10. Arni, H.T., Impact and Penetration Tests of Portland Cement Concrete, Federal Highway Administration Rep. No. FHWA-RD-73-5, 1973.
11. Malhotra, V.M., Preliminary Evaluation of Windsor Probe Equipment for Estimating the Compressive Strength of Concrete, Mines Branch Investigation Rep. IR 71-1, Department of Energy, Mines and Resources, Ottawa, December 1970.
12. Malhotra, V.M. and Painter, K.P., Evaluation of the Windsor Probe Test for Estimating Compressive strength of Concrete, Mines Branch Investigation Rep. IR 71-50, Ottawa, Canada, 1971.
13. Malhotra, V.M., Evaluation of the Windsor Probe Test for Estimating Compressive Strength of Concrete, RILEM Materials and Structures, Paris, 7:37:3-15, 1974.
14. Klotz, R.C., Field investigation of concrete quality using the Windsor probe test system, *Highway Res. Rec.*, 378, 50, 1972.
15. Keeton, J.R. and Hernandez, V., Calibration of Windsor Probe Test System for Evaluation of Concrete in Naval Structures, Technical Note N-1233, Naval Civil Engineering Laboratory, Port Hueneme, CA, 1972.
16. Clifton, J.R., Non-Destructive Tests to Determine Concrete Strength—A Status Report, NBSIR 75-729, National Bureau of Standards, Washington, D.C.
17. Bowers, D.G.G., "Assessment of Various Methods of Test for Concrete Strength," Connecticut Department of Transportation/Federal Highway Administration, December 1978 (available through National Technical Information Service, NTIS No. PB 296317, Springfield, VA).
18. Bartos, M.J., Testing concrete in place, Civil Engineering, *Am. Soc. Civ. Engrs.*, 1979, 66.
19. Strong, H., In-Place Testing of Hardened Concrete with the Use of the Windsor Probe, New Idaho Test Method T-128-79, Division of Highways, State of Idaho, 1979, 1.
20. Swamy, R.N. and Al-Hamed, A.H.M.S., Evaluation of the Windsor Probe Test to Assess In-Situ Concrete Strength, Proc. Inst. Civ. Eng., Part 2, June 1984, 167.
21. Malhotra, V.M., Testing Hardened Concrete: Non-destructive Methods, American Concrete Institute Monogr. No. 9, Iowa University Press/American Concrete Institute, Detroit, MI, 1976, 188.
22. Keiller, A.P., A Preliminary Investigation of Test Methods for the Assessment of Strength of In-Situ Concrete, Tech. Rep. No. 551, Cement and Concrete Association, Wexham Springs, September 1982.
23. Bungey, J.H., *The Testing of Concrete in Structures*, Chapman and Hall, New York, 1982.
24. Keiller, A.P., Assessing the strength of in-situ concrete, *Concr. Int.*, ACI, February 1985, 15.
25. Compressive Strength Testing of Concrete, Windsor Probe Test System, Inc., Elmwood, CT, 1970.
26. ACI 207-79, Practices for Evaluation of Concrete in Existing Massive Structures for Service Conditions, ACI Manual of Concrete Practice, American Concrete Institute, Detroit, MI, 1983.

27. Lee, S.L., Tam, C.T., Paramasivam, P., Ong, K.C.G., Swaddiwudhipong, S., and Tan, K.H., Structural Assessment in In-Situ Testing and Interpretation of Concrete Strength, Department of Civil Engineering, National University of Singapore, July 1988.
28. ACI Committee 228, In-place methods for determination of strength of concrete, *ACI Mater. J.*, 85(5), 446, 1988.
29. Carette, G.G. and Malhotra, V.M., In-Situ Tests: Variability and Strength Prediction of Concrete at Early Ages, Malhotra, V.M., Ed., American Concrete Institute, Spec. Publ. SP-82, 1984, 111.
30. Jenkins, R.S., Non-destructive testing — an evaluation tool, *Concr. Int.*, ACI, 1985, 22.
31. Kopf, R.J., Cooper, C.G., and Williams, F.W., In-Situ Strength Evaluation of Concrete Case Histories and Laboratory Investigations, *Concr. Int. Design and Construction*, ACI, March 1981, 66.
32. ASTM C 42/C 42 M-03, Standard Test Method for Obtaining and Testing Drilled Cores and Sawed Beams of Concrete, *Annual Book of ASTM Standards*, Vol. 04.02, ASTM, West Conshohocken, PA, 2003.
33. Nasser, K.W. and Al-Manaseer, A., New non-destructive test for removal of concrete forms, *Concr. Int. ACI*, 9(1), 41, 1987.
34. Nasser, K.W. and Al-Manaseer, A., Comparison of non-destructive testers of hardened concrete, *ACI J.*, 84(5), 374, 1987.
35. ASTM C 803-02, Standard Test Method for Penetration Resistance of Hardened Concrete, *Annual Book of ASTM Standards*, Vol. 04.02, ASTM, West Conshohocken, PA, 2003.

3

Pullout Test*

3.1 Introduction

3.2 Historical Background
Development in the former Soviet Union • Development in the United States • Danish Test (Lok-Strength) • U.S. Test by Richards • Modifications by Kaindl • Summary

3.3 Failure Mechanism
Qualitative Explanations • Analytical Studies • Experimental Studies • Summary

3.4 Statistical Characteristics
Repeatability • Strength Relationship • Summary

3.5 Applications
Standards • Strength Relationship • Interpretation of Results • Precision • Number of Tests • Post-Installed Tests • Summary

3.6 Concluding Remarks

Nicholas J. Carino
National Institute of Standards and Technology

The pullout test measures the force needed to extract an embedded insert from a concrete mass. By using a previously established relationship, the measured ultimate pullout load is used to estimate the in-place compressive strength of the concrete. This chapter reviews the history of the development of this test method, including the various analytical studies conducted to understand the underlying failure mechanism for the test. Statistical characteristics of the method, such as within-test variability and the nature of the correlation with compressive strength, are discussed. It is shown that the characteristics of the coarse aggregate play an important role in the statistical properties of the test. Some of the requirements of the ASTM standard on the pullout test are discussed, and recommendations for developing correlation relationships and interpreting tests results are presented. The chapter concludes with a review of test methods that can be performed on existing construction.

3.1 Introduction

The pullout test measures the force required to pull an embedded metal insert with an enlarged head from a concrete specimen or a structure. Figure 3.1 illustrates the configuration of a pullout test. The insert is pulled by a loading ram seated on a bearing ring that is concentric with the insert shaft. The bearing ring transmits the reaction force to the concrete. As the insert is pulled out, a conical-shaped fragment of concrete is extracted from the concrete mass. The idealized shape of the extracted conic frustum is shown in Figure 3.1. Frustum geometry is controlled by the inner diameter of the bearing ring (D), the diameter of the insert head (d), and the embedment depth (h). The apex angle (2α) of the idealized frustum is given by

$$2\alpha = 2\tan^{-1}\frac{D-d}{2h} \tag{3.1}$$

*Contribution of the National Institute of Standards and Technology and not subject to copyright in the United States.

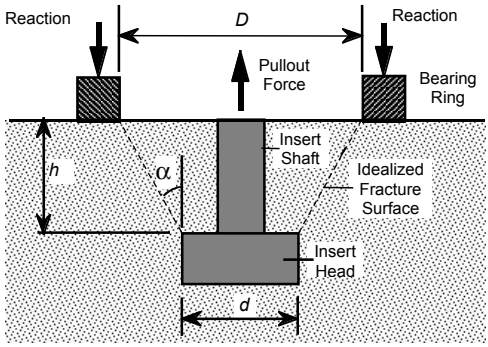

FIGURE 3.1 Schematic of the pullout test.

The pullout test is used during construction to estimate the in-place strength of concrete to help decide whether critical activities such as form removal, application of post-tensioning, or termination of cold weather protection can proceed. Because the compressive strength is usually required to evaluate structural safety, the ultimate pullout load measured during the in-place test is converted to an equivalent compressive strength by means of a previously established relationship.

Unlike some other tests used to estimate the in-place strength of concrete, the pullout test subjects the concrete to a slowly applied load and measures an actual strength property of the concrete. The concrete is subjected, however, to a complex three-dimensional state of stress, and the pullout strength is not likely to be related simply to uniaxial strength properties. Nevertheless, by use of a previously established correlation, the pullout test can be used to make reliable estimates of in-place strength.

The purpose of this chapter is to provide basic and practical information about the pullout test. The chapter begins with a brief historical review of the developments leading to the current test method. This is followed by discussions of the failure mechanism and the statistical characteristics of the test. The chapter concludes with a discussion of practical matters in the application of the test.

3.2 Historical Background

3.2.1 Development in the Former Soviet Union

The earliest known description of the pullout test method was reported by Skramtajew[1] of the Central Institute for Industrial Building Research in the former Soviet Union. His article reviewed a variety of proposed methods to measure the in-place strength of concrete. One of these methods involved embedding a rod with a spherical end into the fresh concrete and measuring the force required to extract the rod from the hardened concrete. The method was reportedly developed simultaneously by two engineers, Volf and Gershberg. Volf's insert was described as follows:[1]

> The rod is of steel, its overall length is 48 mm, of which 38 mm are embedded in concrete, its throat diameter is 8 mm, and the diameter of the spherical end — 12 mm.

Figure 3.2 shows the geometry of the rod based on this description and the sketches provided in Reference 1. The insert was attached to the formwork by a screw. At the time of test, the holding screw was removed, an eyebolt was screwed into the insert, a mechanical jack was attached, and the rod was extracted.

Skramtajew noted that when the rod was pulled, the concrete was subjected to tensile and shear stresses and failure occurred by pulling out a cone of concrete with an apex angle of approximately 90°. In this test the bearing plate of the jack was sufficiently large so that it did not interfere with concrete fracture during pullout of the cone. The large diameter of the extracted cone was reported to be between 100

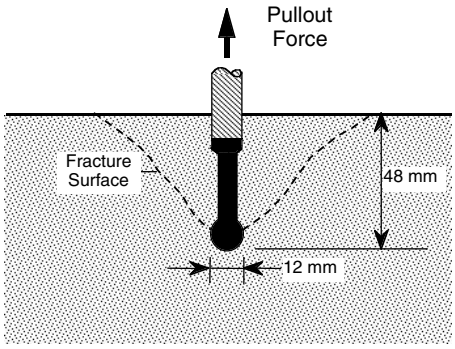

FIGURE 3.2 Configuration of first pullout test developed by Volf.[1]

and 120 mm. The exact geometries of the extracted cones were not described, but it is assumed that they were similar to that shown in Figure 3.2.

It was reported[1] that, for concrete strengths less than about 10 MPa (1500 psi), there was nearly a constant ratio between ultimate pullout load and the compressive strength of companion cubes. The ratios of ultimate pullout load to cube strength varied between ±9% of the average value. Skramtajew concluded that the pullout test had the advantages of simplicity, availability, and precision. The disadvantages included the need to attach the inserts to formwork at planned locations and the need to repair the holes created by the test. He concluded, however, that the advantages were so significant that the method should be used widely.

3.2.2 Development in the United States

Six years after the publication of Skramtajew's paper, Tremper[2] became the first American to report research results of pullout tests. To simplify fabrication of the inserts, a cylindrical head was used rather than a spherical head as in the Soviet design. Figure 3.3 shows the approximate dimensions of Tremper's insert. The shoulder of the enlarged head was machined at a 45° angle. The bearing ring had a diameter of 152 mm (6 in.). According to Tremper:[2]

> Failure occurred by the formation of a cone 4 to 6 in. in diameter extending to a point about midway in the length of the enlarged end.

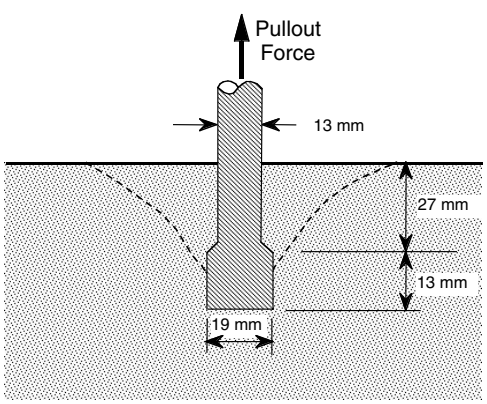

FIGURE 3.3 Configuration of pullout test developed by Tremper.[2]

The approximate shape of the failure cone, based on this description, is shown in Figure 3.3. Because of the large diameter, the bearing ring did not interfere with the failure cone. Hence, Tremper's test was similar to the earlier Soviet test.

Tremper did pullout tests on prisms and companion compression tests on cylinders. Six concrete mixtures were used, and the compressive strength varied between about 6 to 40 MPa (1000 to 6000 psi). Five mixtures were made with rounded gravel, and the sixth mixture was made with 50% crushed gravel and 50% rounded gravel. The nominal maximum aggregate size was 30 mm (1-1/4 in.).

At each test age, Tremper performed five replicate pullout tests and five replicate compression tests. Figure 3.4 shows the average test results. Over the complete range of concrete strength, the relationship between compressive strength and ultimate pullout load is not linear. The equation of the nonlinear relationship is shown in Figure 3.4. For concrete with a compressive strength below 20 MPa (3000 psi), Tremper used a straight line to approximate the relationship as shown in Figure 3.4. An important observation in Figure 3.4 is that the data for the five concrete mixtures made with gravel appear to obey the same relationship. The concrete with 50% crushed gravel appears, however, to have higher pullout strength for the same level of compressive strength. Thus, as early as 1944, there was evidence that the ultimate pullout load was influenced by the characteristics of the coarse aggregate.

Tremper found that the within-test coefficient of variation of the pullout tests was 9.6% while that for the cylinder tests was 8.4%.* Thus he concluded that the pullout strength could be measured with as much precision as the cylinder strength. A seen in Figure 3.4, data scatter about the correlation curve increased for compressive strength above 25 MPa (3500 psi). As a final conclusion, Tremper stated:[2]

> Data from laboratory tests indicate that the pull-out test can be applied to concrete in structures with less error in estimating actual compressive strengths that are not above about 3500 psi than is often obtained through the use of test cylinders.

Despite Tremper's encouraging results, the use of the pullout test did not gain acceptance. Only after the work of Kierkegaard-Hansen in Denmark and that of Richards in the United States did the pullout test become recognized as a useful field technique.

3.2.3 Danish Test (Lok-Strength)

In 1962, Kierkegaard-Hansen[3] initiated a research program to determine the optimum geometry for the pullout test so that it could be performed in the field with simple equipment and so that there would be a high correlation between ultimate pullout load and compressive strength. The results of his work led to the widely used test system known as the LOK-TEST. Kierkegaard-Hansen's work is reviewed in detail because it is useful to understand the reasoning used to establish the values of the embedment depth, insert head diameter, and bearing ring diameter for this test system.

According to Kierkegaard-Hansen, the embedment depth should be sufficient to assure that more than the outermost "skin" of the concrete is tested and that some coarse aggregates is included within the failure cone. This would favor deep embedment. With increasing embedment, however, the force required to pullout the insert would increase, leading to bulky testing equipment and increasing the damage to the structure. Based on these factors, an embedment depth of 25 mm (1 in.) was chosen arbitrarily.

Kierkegaard-Hansen performed a series of pilot tests to establish the optimum diameters for the insert head and bearing ring. Figure 3.5 shows the test configuration used in these pilot tests. Because a suitable tension loading system did not exist, a laboratory compression testing machine was used to apply the load. The insert was extracted by applying a compressive load to the bottom of the embedded disk, as shown in Figure 3.5. In this configuration, the pullout test can also be considered a punching-type test. The Danish word for punching is *lokning*. Hence, Kierkegaard-Hansen called the quantity measured by the test the "lok-strength" rather than the pullout strength.

*By today's standards, a coefficient of variation of 8.4% for the strength of laboratory-prepared cylinders would be considered unusually high.

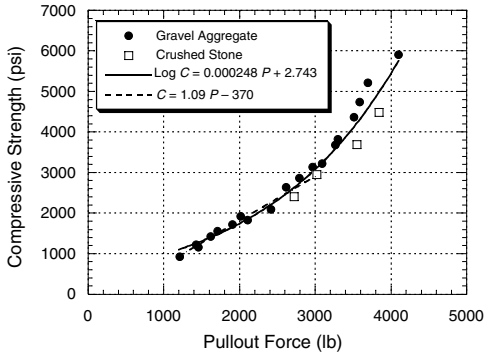

FIGURE 3.4 Compressive strength and pullout force results reported by Tremper.[2]

In the first series of tests, the head diameter was varied from 20 to 40 mm (0.79 to 1.57 in.). For these tests, a large-diameter bearing ring was used so that the failure cone formed within the ring. He observed that the failure surface was not the idealized conic frustum shown in Figure 3.1. Instead, the extracted fragment was "trumpet-shaped"; i.e., the inclination of the fracture surface, with respect to the load direction, increased with increasing distance from the insert. It was found that the pullout strength increased about 1% for each 1 mm increase in diameter. The insert head diameter was chosen arbitrarily to be 25 mm (1 in.).

The next series of pilot tests examined the relationship between compressive strength and ultimate pullout load. A bearing ring with a diameter of 130 mm (5.1 in.) was used. For this large diameter, failure occurred within the bearing ring, and the test was analogous to the earlier tests of Volf and Tremper. The compressive strength ranged from about 10 to 45 MPa (1500 to 6500 psi). In agreement with Tremper, Kierkegaard-Hansen found that the relationship between ultimate pullout load and compressive strength was nonlinear, and he stated:[3]

> It follows from this that the stress field in the rupture surface cannot be equal to the stress field occurring during crushing of cylinders.

The relationship had a shape similar to that of tensile strength vs. compressive strength. It was concluded that, for a large bearing ring, the pullout strength is likely to be related to the concrete tensile strength. Because of the nonlinear relationship, test sensitivity decreased with increasing strength of concrete; i.e., large changes in compressive strength resulted in small changes in pullout strength (see Figure 3.4). Thus, Kierkegaard-Hansen decided to examine the effects of reducing the bearing ring diameter. Here is where the modern pullout test improved upon the earlier tests of Volf and Tremper.

As the ring diameter decreases, the fracture surface area decreases. It was reasoned that the ultimate pullout load would also decrease unless the presence of the ring alters the state of stress, in which case it could increase. Hence, in the next series of pilot tests, Kierkegaard-Hansen examined the relationship between ring diameter and ultimate pullout load. The ring diameter was varied between 130 and 50 mm (5.1 and 2.0 in.). He found that the ultimate pullout load increased gradually as the diameter decreased from 130 mm (5.1 in.) to about 80 mm (3.1 in.). As the diameter was reduced further, the ultimate pullout load increased rapidly. After these pilot tests were completed, a loading apparatus was developed for applying a tensile load to the insert as depicted in Figure 3.1.

The new loading apparatus was used to examine further the relationship between bearing ring diameter and pullout strength. For the next series of tests, the pullout strength was expressed as a stress by dividing the ultimate pullout load by the area of the idealized conic frustum defined by the embedment depth,

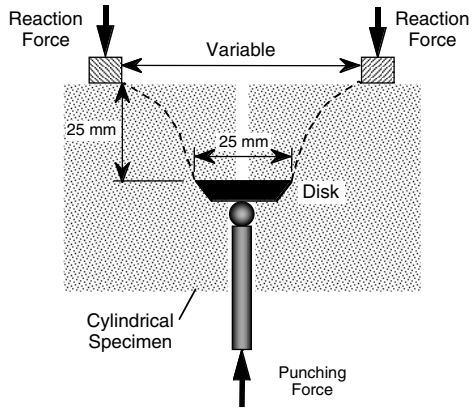

FIGURE 3.5 Testing configuration for pilot tests by Kierkegaard-Hansen. (Adapted from Reference 3.)

insert head diameter, and bearing ring diameter. For reasons not clearly stated, Kierkegaard-Hansen concluded that the optimum bearing ring diameter should be 55 mm (2.2 in.).*

After establishing the dimensions of the pullout test, Kierkegaard-Hansen studied the relationship between ultimate pullout load and compressive strength. The results of these studies are discussed in a subsequent section.

In 1970, Kierkegaard-Hansen obtained a U.S. patent** for "A Method for Testing the Strength of Cast Structures, Particularly Concrete Structures," which described a pullout testing device composed of an embedded disk (called a "piston" in the patent), a pull rod, and a bearing ring. Specific dimensions of the test system were not given except that the apex angle of the conic frustum should be "at least about 60°."

3.2.4 U.S. Test by Richards

In the early 1970s, Richards of the United States obtained a U.S. patent*** on a pullout test system similar to Kierkegaard-Hansen's. One of the differences was that Richards' insert (described as a "shank" in the patent) consisted of an enlarged head that was integral with the insert shaft (see Figure 3.1). The patent did not recommend an apex angle for the idealized conic frustum.

Rutenbeck[4] was the first to report the results of work based on Richards' ideas. In these early studies, the insert shaft was made from 19-mm (3/4 in.) threaded steel rod, and the insert head was formed by a steel washer brazed to a nut screwed onto the rod. The insert head diameter (d) was 57 mm (2.25 in.), the depth of embedment (h) was 53 mm (2.08 in.), and the bearing ring diameter (D) was 127 mm (5 in.). The apex angle for this configuration was 67°. A similar insert was used in evaluations by Malhotra.[5,6]

Richards' early test configuration produced a conic frustum with a surface area of about 18,320 mm^2 (28.4 in.^{2}), which is about five times greater than the surface area of Kierkegaard-Hansen's system. The author believes that Richards chose this size so that the conic surface area would be approximately equal to the cross-sectional area of a 152 × 305-mm (6 × 12-in.) cylinder. Because of the large dimensions, the test equipment was bulky and not suited for field applications.

*For a ring diameter of 55 mm, the correlation between ultimate pullout load and compressive strength was such that the pullout load expressed in kilonewtons was about the same number as the compressive strength of the concrete expressed in MPa. Thus, if the ultimate pullout load was 20 kN, the compressive strength would be about 20 MPa. (Note that in Figure 3.4 there is similar numerical relationship between pullout load (in lb) and compressive strength (in psi) at the lower strength range.)

**U.S. patent 3,541,845, November 24,1970.

***U.S. patent 3,595,072, July 27, 1971.

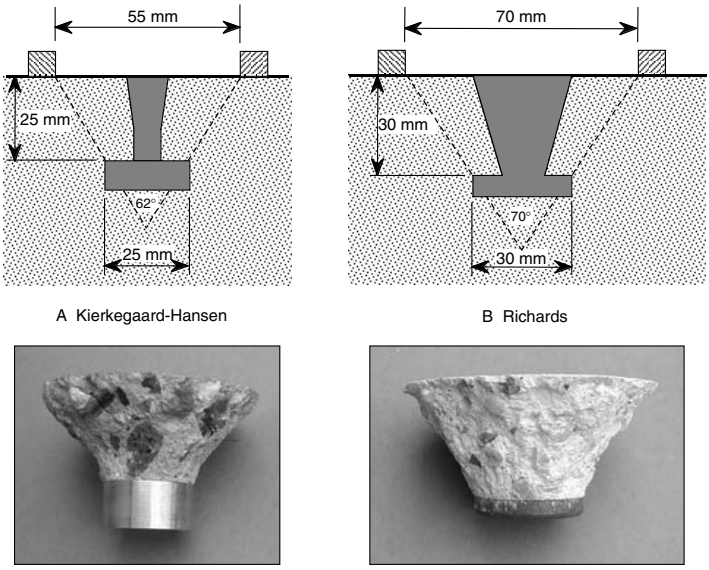

FIGURE 3.6 Comparison of pullout test configurations and examples of extracted conic frustums.

In 1977, Richards[7] reported on a smaller, machine-produced insert with a head diameter and embedment depth of 30 mm (1.18 in.). The bearing ring diameter was 70 mm (2.75 in.), thereby preserving a 67° apex angle. Richards' new configuration has a fracture surface that is about 50% greater than that of Kierkegaard-Hansen. These two pullout test configurations are compared in Figure 3.6. The shaft of Richards' insert is integral with the head. The pullout force is applied through a rod screwed into the shaft. On the other hand, Kierkegaard-Hansen's insert has a removable shaft, and a high strength pullrod is screwed into the head for load application.

3.2.5 Modifications by Kaindl

In 1975, Kaindl of Austria obtained a U.S. patent* (with Richards as assignee) describing an assortment of modifications to the basic pullout test system. Some of these included screens placed around the insert head to exclude coarse aggregates from the failure surface. The objective was to reduce test variability by excluding coarse aggregate from the failure zone. These screens have not found widespread application.

Other modifications included the use of compressible pads to permit pullout testing without removing forms or to permit testing deep within the structure. Figure 3.7 shows some of these modifications as used by Richards.[7] The configuration in Figure 3.7A would be used to perform a pullout test deep within a structural member. The plastic disk is used to define the large diameter of the conic frustum, and the compressible pad allows pullout of the conical fragment. The configuration in Figure 3.7B would be used to perform a pullout test without having to remove formwork. There is no bearing ring in these configurations. There are few data on the performance of these modified pullout tests.

3.2.6 Summary

The ideas for the modern pullout tests go back to a Soviet test described in 1938. This test, and the later test by Tremper, did not use a bearing ring, and the ultimate pullout load was believed to be controlled by the tensile strength of the concrete. As a result, the correlation between pullout strength and compressive strength was found to be nonlinear. In 1962, Kierkegaard-Hansen improved upon the original

*U.S. patent 3,861,201, January 21, 1975.

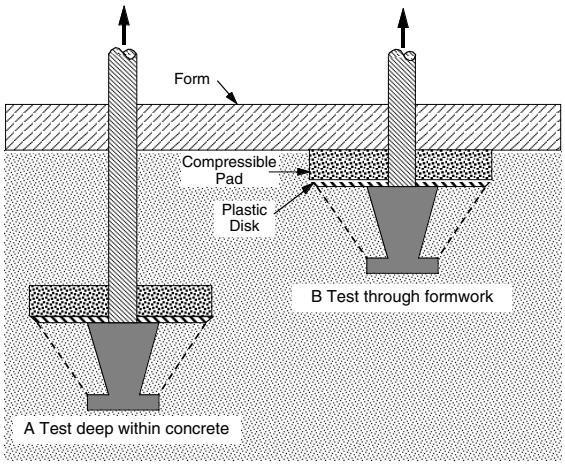

FIGURE 3.7 Techniques suggested by Richards for (A) performing a pullout test deep within a structure and (B) performing a surface pullout test without removing forms.

idea by introducing a bearing ring. This modification resulted in a failure cone with a well-defined geometry and he reported a linear correlation between pullout strength and compressive strength (over the strength range used). The apex angle in Kierkegaard-Hansen's test was 62°. Later, Richards introduced a similar pullout test to North America, but he suggested an apex angle of 67°.

3.3 Failure Mechanism

The pullout test subjects the concrete to static load. Therefore, it should be possible to calculate the internal stresses in the concrete and to predict the onset of cracking and the ultimate pullout load. This is desirable so that the ultimate pullout load could be related to the uniaxial strength properties of concrete. Unfortunately, the stress distribution is not easy to calculate, the state of stress is altered by the presence of coarse aggregate particles, and the fundamental failure criterion for concrete is not completely understood. This section reviews various theories about the failure mechanism for the pullout test. It will be shown that there is no consensus on this point.

3.3.1 Qualitative Explanations

In his paper, Skramtajew[1] noted:

> In this case concrete is simultaneously in tension and shear, the generating lines of the cone running approximately at an angle of 45 degrees to the vertical.

Thus, from the beginning it was recognized that the pullout test subjects the concrete to a complex state of stress. Figure 3.8 is a freebody diagram of the idealized conic frustum extracted during a pullout test. The pullout force (P) is resisted by normal (σ) and shearing stresses (τ) acting on the frustum surface. The normal stress acts perpendicular to the surface and is a tensile stress, while the shearing stress acts parallel to the surface in the direction shown. The vertical components of these stresses multiplied by the surface area (A) produce a vertical force to counteract the applied pullout force. Assuming that these stresses are uniformly distributed on the failure surface, one can show that

$$\sigma = \frac{P}{A}\sin\alpha \tag{3.2}$$

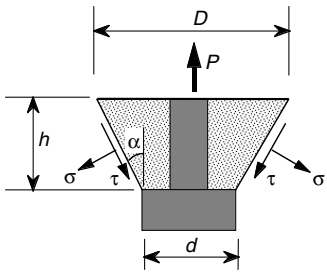

FIGURE 3.8 Freebody diagram showing normal and shearing stresses acting on failure surface of idealized frustum.

$$\tau = \frac{P}{A}\cos\beta \tag{3.3}$$

The surface area of the frustum is calculated as follows:

$$A = \frac{\pi(D+d)}{4}\sqrt{4h^2 + (D-d)^2} \tag{3.4}$$

where

D = bearing ring diameter
d = insert head diameter
h = embedment depth

In his patent disclosure, Kierkegaard-Hansen made the following statement about the failure cones:

> [T]he fracture faces attain substantially the same shape as one half of the well known hour-glass-shaped fracture faces, which are produced in compressive strength tests of cylindrical specimens.

This implies that the cones of the pullout test are related to the end cones typically observed during the testing of cylinders, and this was offered as an explanation for the correlation between pullout strength and compressive strength. This explanation is incorrect because the cones are formed due to entirely different factors. In the pullout test, the cone is extracted from the concrete mass under the action of the applied pullout force. In the compression test, the cones represent intact concrete that is prevented from failing due to triaxial compressive stresses introduced by friction between the cylinder and the solid loading platens.[8]

Malhotra and Carette[6] calculated a "pullout strength" by dividing the ultimate pullout load by the surface area of the idealized frustum. The pullout test geometry developed by Richards was used (apex angle = 67°). The ratio of this pullout strength to the compressive strength of companion cylinders or cores varied from 0.24 to 0.18, as the compressive strength varied from about 20 MPa (2900 psi) to 52 MPa (7500 psi). These ratios were similar to the reported ratios of shear strength to compressive strength obtained from triaxial tests.[9] Therefore, it was suggested that the pullout strength may be related to the direct shear strength of concrete. The criticism to this analysis is that the calculated "pullout strength" is not really a stress because the pullout force is inclined to the surface of the frustum. Dividing the pullout force by the surface area results in neither a normal stress nor a shearing stress. The author believes that the "pullout strength" was found to be approximately 20% of the compressive strength because of the particular value of the apex angle recommended by Richards, rather than because of an inherent relationship between shear strength and pullout strength. In addition, the so-called "direct shear" strengths in Reference 9 were obtained by assuming a straight line envelope to the Mohr's circles of failure stresses under triaxial loading.[10] These computed direct shear strengths are recognized as larger than the true shear strength of concrete.[9]

In summary, these qualitative explanations do not provide insight into the actual failure mechanism during a pullout test.

3.3.2 Analytical Studies

3.3.2.1 Rigid-Plastic Analysis

Jensen and Braestrup[11] presented the first analytical study that attempted to provide a theoretical basis for the existence of a linear relationship between ultimate pullout load and compressive strength. They assumed that concrete obeys the modified Mohr–Coulomb failure theory (sliding or separation possible) and that the extracted cone has the shape of the idealized conic frustum. The analysis assumed "rigid-plastic" behavior and that the normal and shearing stresses were distributed uniformly on the failure surface. It was concluded that, if the friction angle of the concrete equals one-half of the apex angle and if the tensile strength is a constant fraction of the compressive strength, there is a proportional relationship between the ultimate pullout load and compressive strength. The analysis has been criticized as not providing a true behavioral prediction because the conclusions are a direct result of the underlying assumptions rather than from a rigorous assessment of the true behavior during the test.[12–14]

3.3.2.2 Nonlinear Finite Element Analysis

In 1981, Ottosen was the first to use the finite-element method to analyze the state of stress and to attempt to determine the failure mechanism of the pullout test.[15] He used nonlinear material models, a three-dimensional failure criterion, and a smeared cracking approach to follow the progression of failure with increasing pullout load. The pullout test geometry developed by Kierkegaard-Hansen was used. The analysis considered the concrete a homogenous material, i.e., the presence of individual coarse aggregate particles was not modeled.

A significant finding of Ottosen's analysis was that, at about 65% of the ultimate load, a series of circumferential cracks had developed extending from the edge of the insert head to the bearing ring. Despite the circumferential cracks, additional load could be sustained by a highly stressed narrow band, or "strut," extending from the insert head to the bearing ring. Ultimate failure was attributed to "crushing," or compressive failure, of the concrete within this strut. Ottosen concluded that this was the reason for the good correlation between pullout strength and compressive strength.

Ottosen's analysis demonstrated that the pullout test subjects the concrete to a highly nonuniform, triaxial state of stress. Within the compression strut, Ottosen found that the state of stress was predominantly biaxial-compression "occasionally superposed by small tensile stresses."[15] Because of the tensile stresses, Ottosen concluded that the tensile strength of concrete had a secondary influence on the ultimate pullout load. He showed that, because the ratio of tensile strength to compressive strength decreases with increasing strength of concrete, the ratio of pullout strength to compressive strength would be expected to decrease for increasing concrete strength. This would explain the previous observations of Malhotra and Carette[6] and Richards.[7]

Yener and Vajarasathira[16] performed a plastic fracture analysis using the finite element method. Cracking was assumed to occur perpendicular to the direction of maximum tensile strain. "Crushing" failure was defined to occur if the maximum strain was compressive when an element cracked. It was noted that the high shearing stresses within the region between the insert head and bearing ring cause high tensile stresses, which result in circumferential cracking that defines the eventual failure surface. The analysis predicted that circumferential cracking began to form at the corner of the insert head at about 25% of the ultimate load. The circumferential crack propagated toward the bearing ring, but was arrested by high compressive stresses at about 50% of ultimate load. Another crack initiated at the corner of the insert head and propagated toward the bearing ring, so that at 70% of the ultimate load the trumpet-shaped frustum was completely formed. At this stage, the frustum was prevented from pulling out completely by frictional resistance due to high radial compressive stresses acting at the juncture of the frustum and the main body, just below the bearing ring perimeter. Additional load could be applied until crushing occurred around the perimeter of the frustum. Thus, while the crack patterns were similar to those in Ottosen's analysis, a different ultimate load carrying mechanism was hypothesized.

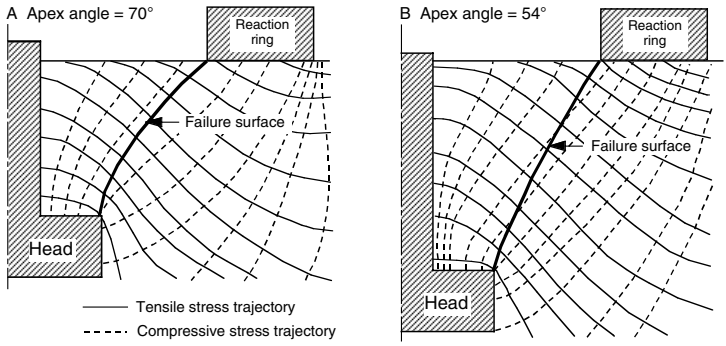

FIGURE 3.9 Tension and compression stress trajectories before formation of cracks and the approximate shape of the conic frustums after ultimate load.[17]

3.3.2.3 Linear-Elastic Finite Element Analysis

Stone and Carino[17] also performed finite-element analyses for pullout tests with apex angles of 54° and 70°. Because their analyses were linear-elastic, the results are applicable only until the formation of cracks. In agreement with Ottosen, Stone and Carino found that the pullout test subjects the concrete to a complex three-dimensional state of stress. High compressive stresses exist within the "strut" region between the bearing ring and insert head. Figure 3.9 shows the principal stress trajectories for the two test configurations that were analyzed (because of symmetry only one-half of the specimens are shown). For the 70° apex angle, there is close agreement between the compressive stress trajectories and the trumpet-shaped fracture surface observed in the companion test specimen.[12] Note that the principal tensile stresses act perpendicular to the compressive stress trajectories. For the 54° apex angle, the compressive stress trajectories and failure surface are less curved. The agreement between the directions of the stress trajectories and the shape of the failure surface led Stone and Carino to conclude that tensile strength is likely to play a greater role in the pullout test than was proposed by Ottosen.

The nonuniformity of the stresses along the idealized conic frustum is illustrated in Figure 3.10, which shows the variation of the principal stresses for the 70° apex angle at about 20% of the ultimate load.[17] There are very high tensile and compressive stresses at the edge of the insert head due to the stress concentration effect at the sharp corner. The tensile stresses decrease with distance from the insert head and become compressive near the bearing ring. The compressive stresses are high near the insert head and near the bearing ring, and they are nearly uniform in the middle region of the idealized frustum. Thus, in contrast to Ottosen's conclusion, the frustum is subjected to significant tensile stresses.

3.3.2.4 Fracture Mechanics Analysis

Another finite-element analysis used the principles of nonlinear fracture mechanics to gain an understanding of the failure mechanism.[18] This analysis used a discrete cracking model with special elements to represent the behavior of cracked concrete. The pullout test configuration had the following geometry: D = 61 mm (2.4 in.); $d = h$ = 25.4 mm (1 in.); and apex angle (2α) = 70°.

The nonlinear, fracture mechanics analysis revealed that two crack systems develop during the course of the pullout test. The first (primary) crack is a circumferential crack that initiates at the edge of the insert head and propagates into the concrete at angle of about 60° with the load axis. The first crack begins at a low pullout load because of the large tensile stress concentration at the insert head (Figure 3.10), and it is arrested as it penetrates a region of low tensile stress below the bearing ring. Tensile and shearing stresses continue to be carried across the first crack because of the small crack-opening displacement. According to the analysis, the formation of the first crack results in high tensile stresses in the region between the insert head and the bearing ring. Thus, a second (or secondary) crack initiates at a point between the insert head and bearing ring, and it propagates in two directions toward the ring and the insert head.

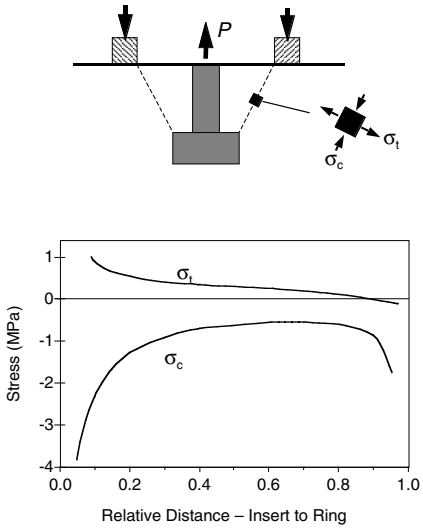

FIGURE 3.10 Variation of principal stresses along a line extending from insert head to bearing ring (70° apex angle).[17]

Figure 3.11 shows the deformed shape (highly exaggerated) of the finite-element model after the second crack has propagated toward the ring and insert head. It is apparent that the second crack defines the shape of the conical fragment that is eventually extracted from the concrete. The ultimate load could not be determined in the analysis because the computer program would not permit the formation of a crack at the highly compressed node at the corner of the bearing ring. It was postulated that the failure surface would be formed completely by cracking of the final ligament between the insert head and the secondary crack tip. This final crack propagation would be primarily a shear failure along a surface inclined at a small angle to the load axis.

The results of the analysis were compared with experimental crack patterns observed in sectioned pullout test specimens that had been loaded to various fractions of ultimate strength.[18] For example, Figure 3.12 shows the crack pattern in a specimen loaded to ultimate pullout load. The primary (first) and secondary (second) crack systems are clearly visible, and it is seen that the crack trajectory at the insert head is nearly parallel to the load axis. This figure also shows that the trumpet-shaped failure surface is completely formed; yet the conic frustum is not separated from the base concrete. The reason for this behavior is explained in the next section.

Ballarini et al.[19] reported on the results of a linear-elastic fracture analysis of a two-dimensional (as opposed to axisymmetric) pullout test. A perfectly elastic, brittle material was assumed. Some of the conclusions of their analysis are as follows:

- Cracking begins at the edge of the insert as a tensile crack (as opposed to shearing).
- Initial cracking begins at an angle of about 75° with respect to the load axis, and the initial cracking is stable.

With increasing load, the crack propagates toward the bearing ring at a decreasing angle with respect to the load axis.

Experiments using mortar specimens and different pullout configurations verified the analytical predictions. It was found that, by expressing ultimate load in terms of fracture toughness, differences between the correlations for various test configurations were greatly reduced. Although not directly applicable to actual pullout tests, this study provided some insight into the crack propagation process.

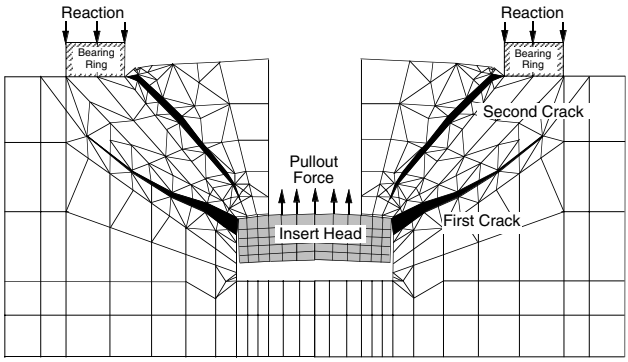

FIGURE 3.11 Deformed shape of finite element model showing the primary and secondary cracks. (Adapted from Reference 18.)

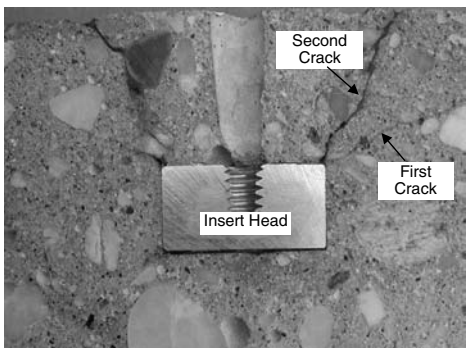

FIGURE 3.12 Internal cracking in pullout test loaded to ultimate load.

3.3.3 Experimental Studies

Compared with extensive experimental work to establish the nature of the correlation between pullout strength and compressive strength, there has been relatively little experimental work on the failure mechanism. Two of the notable studies were the large-scale tests performed at the National Bureau of Standards (NBS — in 1988, the name was changed to the National Institute of Standards and Technology, NIST), and the microcracking study at the Denmark Technical University.

3.3.3.1 Large-Scale Tests

Stone and Carino performed large-scale pullout tests to gain an understanding of the failure mechanism.[12,17] The pullout test geometry was scaled up from conventional tests by a factor of about 12 so that strain gauges could be embedded in the concrete to measure strain distributions during the test. Two specimens were tested having apex angles of 54° and 70°.

By analyzing the strain gauge readings as a function of pullout load, Stone and Carino concluded that the failure sequence comprised three phases:[12]

Phase I: Initiation of circumferential cracking at the edge of the insert head at about 1/3 of the ultimate load

Phase II: Completion of circumferential cracking, from the insert head to the bearing ring, at about 2/3 of the ultimate load

Phase III: Shear failure of the matrix (mortar) and degradation of aggregate interlock beginning at about 80% of the ultimate load

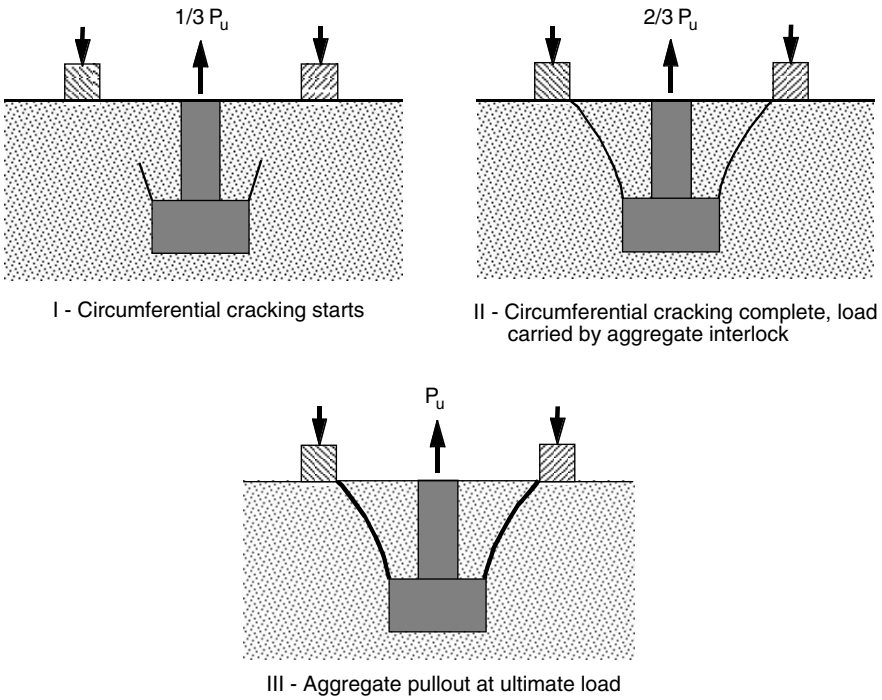

FIGURE 3.13 Failure sequence based on NBS large-scale pullout tests.[12]

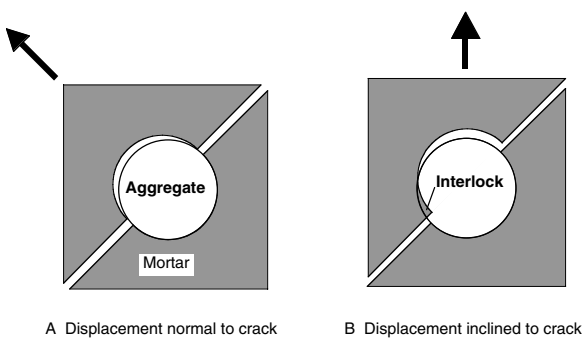

FIGURE 3.14 Model to illustrate aggregate interlock mechanism during pullout test.

These phases are illustrated in Figure 3.13. Thus, Stone and Carino proposed that aggregate interlock is the ultimate load-carrying mechanism and that the ultimate load is reached when the coarse aggregates bridging the failure surface are pulled out of the mortar.

Figure 3.14 is a simple model of concrete to illustrate how aggregate interlock permits load to be carried across a crack. The model consists of a round aggregate particle embedded in a matrix and a crack passing through the matrix and around the aggregate particle. In Figure 3.14A, the relative displacement of the two halves of the model is perpendicular to the crack. In this case, there is no interference between the matrix and the aggregate particle. Therefore, force cannot be transmitted across the crack.

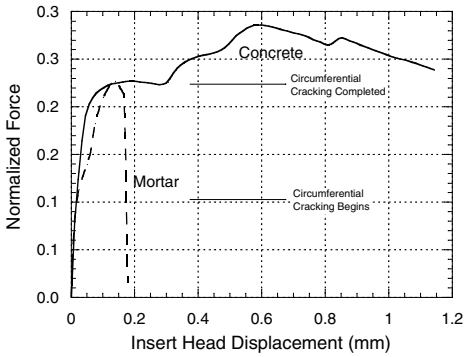

FIGURE 3.15 Load vs. insert head displacement for pullout tests in concrete and mortar specimens.[20]

In Figure 3.14B, the relative displacement of the two halves of the model is inclined to the crack. In this case, there is interference between the matrix and the aggregate, and a force can be transmitted across the crack. In the pullout test, the displacement condition is similar to Figure 3.14B. This model justifies Stone and Carino's assertion[12] that additional load can be applied to the insert even though there is a circumferential crack from the insert head to the bearing ring.

If the aggregate interlock mechanism were to govern the ultimate pullout load, Stone and Carino argued that for a homogenous matrix (no aggregate) the ultimate load would be reached when the circumferential crack extended from the insert head to the bearing ring. Verification of this hypothesis was provided by pullout tests in concrete and in mortar, in which the displacement of the insert head was measured as a function of the pullout load.[20] Figure 3.15 compares the load-displacement histories for pullout tests (apex angle = 62°) in concrete and in mortar. The pullout load has been normalized by dividing by the product of the compressive strength of companion cylindrical specimens and the area of the idealized conic frustum. At small loads, the load-displacement response is linear. At about 1/3 of the ultimate load, the response deviates from linearity as the circumferential crack propagates between the head and bearing ring. When the circumferential crack is formed completely, there is a marked difference between the responses of the concrete and mortar specimens. In the mortar, there is no aggregate interlock and the load drops abruptly. On the other hand, for the concrete there is a large increase in head displacement with no increase in load. Then the load begins to increase until the maximum load is reached. Beyond the ultimate load, the load decreases gradually with increasing head displacement. Thus, the pullout test in the concrete behaves in a more "ductile" manner than the test in the mortar. The behavior in Figure 3.15 is consistent with the aggregate interlock mechanism.

Ottosen[15] stated that the observed ductile failure mode of the pullout test was due to compressive failure of the concrete. The aggregate interlock mechanism provides an alternative explanation for this ductile behavior. Ottosen[15] noted that when a pullout cone is extracted, "crushed materials are observed, aggregates as well as cement paste." In addition, for low-strength concrete the failure surface of the cone consists of "fish scale layers." These observations were cited as further evidence that compressive failure occurs. These observations are, however, also consistent with the aggregate interlock mechanism. The "crushed material" could result from pullout of aggregate particles bridging the circumferential crack. The "fish scale" could be due to cracking of the matrix as the aggregate particles are pulled out, rather than due to parallel cracks associated with compressive failure.

3.3.3.2 Microcracking Analysis

Krenchel and Shah[21] loaded pullout inserts to predetermined fractions of the expected ultimate load. The specimens were unloaded, cut in half, and prepared for examination of microcracks. They also monitored acoustic emissions (AE) during the tests.

Based on the microcracking analysis, Krenchel and Shah concluded that the pullout test involves two circumferential crack systems. There is a stable primary crack that begins at the insert head at about 30% of the peak load and propagates to a point below the bearing ring at an apex angle between 140° and 160°. There is a secondary system that becomes fully developed after the peak load and defines the shape of the extracted cone. The existence of two crack systems agrees with the independent analytical results of Hellier et al.[18] There is disagreement, however, regarding when the secondary system develops. Hellier et al. claim that it develops before the peak load, while Krenchel and Shah state that it becomes fully developed after the peak load. Krenchel and Shah reported that specimens unloaded from the peak load showed no surface cracking at the bearing ring. This would support their claim. Some of the figures in Reference 21 appear, however, to show a fully developed secondary crack at loads less than the peak.

Krenchel and Shah observed that the start of AE activity coincided with the limit of proportionality of the load vs. insert displacement curve, and this was interpreted as the initiation of the first (primary) crack. AE activity increased gradually as the load approached the peak value and increased dramatically thereafter.

Upon review of the various analytical and experimental investigations that had been conducted, Krenchel and Bickley concluded that the failure mechanism of the pullout test involves the following stages[22] (Figure 3.16):

Stage 1 — At a load of about 30 to 40% of the ultimate, "tensile cracks" originate at the corner of the insert head and propagate into the concrete for a distance of 15 to 20 mm (0.6 to 0.8 in.) forming an apex angle between 100° and 135° (Figure 3.16A). This cracking concentrates subsequent straining of the concrete so that "all load is taken up in the truncated zone" between the insert head and the bottom of the bearing ring.

Stage 2 — A large number of stable microcracks develop in the truncated zone. These cracks run from the top of the insert head to the bottom of the bearing ring, forming an apex angle of about 84° (Figure 3.16B). This second stage cracking occurs as the load increases up to and just past the ultimate load. These stable microcracks are analogous to the vertical cracks observed during an ordinary uniaxial compression test of a cylinder or prism.

Stage 3 — Beyond the ultimate load, a circumferential "tensile/shear" crack develops that forms the final shape of the extracted cone (see Figure 3.16C).

Krenchel and Bickley emphasize that the progression of microcracking in Stage 2 is directly related to the ultimate load during the test, and that the fracture surface formed when the cone is completely extracted has little to do with the failure mechanism at ultimate load. As an analogy, they cite the case where a cylinder is compressed past the ultimate load point, and the resulting fracturing that is observed has little to do with the fracture mechanism at ultimate load.

3.3.4 Summary

A series of independent analytical and experimental studies have been performed to gain an understanding of the fundamental failure mechanism of the pullout test. It is understood that the pullout test subjects the concrete to a nonuniform, three-dimensional state of stress. It also has been demonstrated that there are at least two circumferential crack systems involved: a stable primary system, which initiates at the insert head at about 1/3 of the ultimate load and propagates into the concrete at a large apex angle, and a secondary system, which defines the shape of the extracted cone. There is not a consensus, however, on the failure mechanism at the ultimate load. Some believe that ultimate load occurs as a result of compressive failure of concrete along a line from the bottom of the bearing ring to the top face of the insert head. This could explain why good correlation exists between pullout strength and compressive strength. Others believe that the ultimate failure is governed by aggregate interlock across the secondary crack system, and the ultimate load is reached when sufficient aggregate particles have been pulled out of the matrix. In the latter case, it is argued that good correlation exists between pullout strength and compressive strength because both properties are controlled by the strength of the mortar.

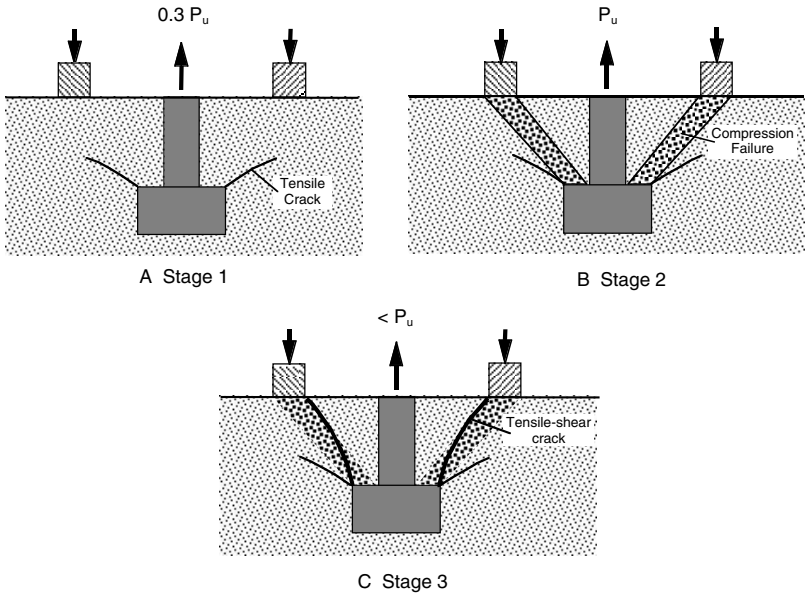

FIGURE 3.16 Failure mechanism of pullout tests according to Krenchel and Bickley.[22]

Despite the lack of agreement on the exact failure mechanism, it has been shown that pullout strength has good correlation with compressive strength of concrete and that the test has good repeatability. These aspects are discussed in the next section.

3.4 Statistical Characteristics

Two important statistical characteristics of tests for in-place concrete strength, such as the pullout test, are the within-test variability and the relationship (correlation) between the test results and compressive strength. Within-test variability, also called "repeatability," refers to the scatter of results when the test is repeated on identical concrete using the same test equipment, procedures, and personnel. For a given concrete, the repeatability of a test affects the number of tests required to establish, with a desired degree of certainty, the average value of the property being measured by the test.[23] The relationship is required to convert the test results to a compressive strength value. This section examines these two characteristics of the pullout test.

3.4.1 Repeatability

If pullout tests are repeated on the same concrete at the same maturity, the ultimate pullout loads would be expected to be normally distributed about the average value and the standard deviation would be the measure of repeatability. If replicate tests were performed on the same concrete but at different maturities, so that there would be different average pullout strengths, would the standard deviation be independent of the average pullout strength? If the standard deviation were found to be proportional to the average pullout strength, the coefficient of variation (standard deviation divided by the average) would be the correct measure of repeatability.

In a review of about 4300 field pullout tests, Bickley[24] concluded that the standard deviation of pullout strength was constant. Because average values were not given, it is not known whether this conclusion applies over a wide range of average pullout strength. The standard deviations reported by Carette and Malhotra[25] and by Keiller[26] offer some insight. Figure 3.17A shows the standard deviation of the ultimate pullout load plotted as a function of the average value. The same commercial test system (LOK-TEST)

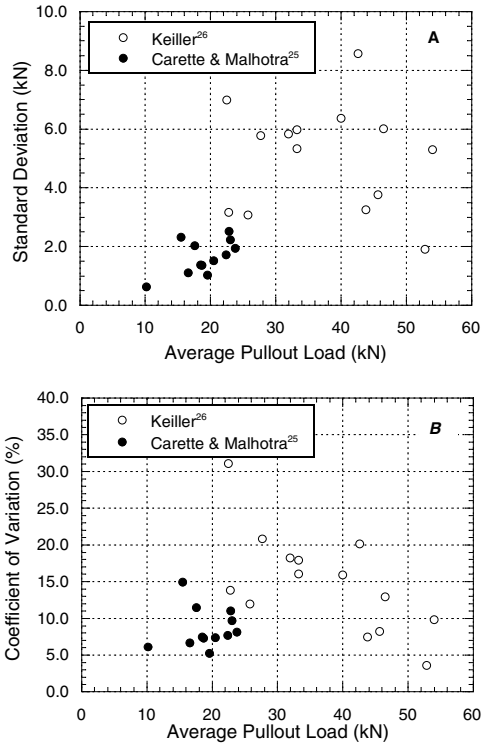

FIGURE 3.17 Repeatability of the pullout test as a function of average pullout strength:[25,26] (A) in terms of standard deviation and (B) in terms of coefficient of variation.

was used by the two research groups, but the number of replications differed. It is clear that the standard deviations reported by Carette and Malhotra are lower than those reported by Keiller, but so are the average ultimate pullout loads. For comparison, Figure 3.17B, shows the corresponding coefficients of variation as a function of average pullout load. The differences between the two groups of data are reduced and this suggests that the coefficient of variation may be the appropriate indicator of repeatability over a wide range of pullout load.

Additional evidence that the standard deviation depends on the level of pullout load is provided by the results of Stone et al.,[27] shown in Figure 3.18A. Three of the test series involved a pullout test configuration having a 70° apex angle and a 25-mm (1-in.) depth of embedment, but concretes with different types of coarse aggregate (river gravel, crushed limestone, and expanded shale) were used. The fourth series used a 54° apex angle and river gravel aggregate. Figure 3.18A shows that the standard deviation tends to increase with increasing average pullout load. In contrast, Figure 3.18B shows that the coefficient of variation appears to be independent of the average pullout load.

Based on the above discussion, it is concluded that the coefficient of variation is the better statistic for quantifying the repeatability of the pullout test. Table 3.1, which was prepared by the author and included in Reference 28, lists some of the reported values of the coefficient of variation for replicate pullout tests. The average values vary from about 4 to 15%. In a summary of the experiences with the LOK-TEST system, Krenchel and Peterson[31] also reported coefficients of variation ranging between 4 and 15%, with an average of about 8%.

The data in Table 3.1 are for different test configurations (apex angle and embedment depth), aggregate types, aggregate sizes, and sample sizes. Similarly, the results summarized by Krenchel and Peterson involved different types and sizes of aggregates as well as different sample sizes. The NBS performed a study to determine whether some of these variables have an effect on the repeatability of the pullout test.

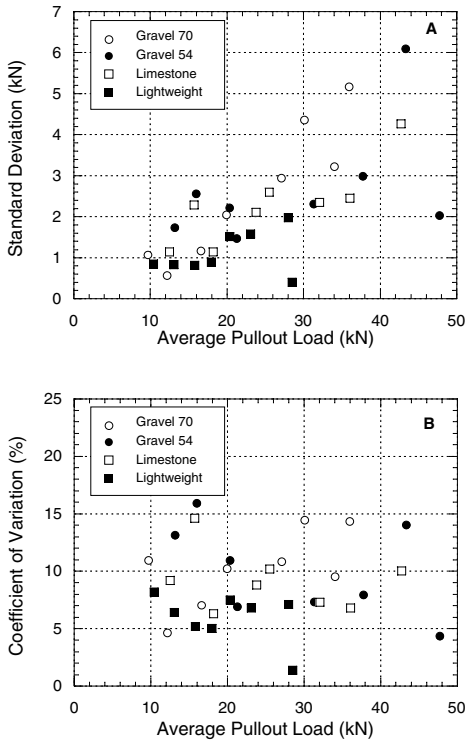

FIGURE 3.18 Repeatability of the pullout test for different test conditions: (A) in terms of standard deviation and (B) in terms of coefficient of variation.[27]

The following variables were considered: apex angle, embedment depth, maximum aggregate size, and aggregate type. The experimental details were reported by Stone and Giza.[20] Basically, 11 pullout inserts were embedded in 152 × 152 × 914 mm (6 × 6 × 36 in.) beam specimens. Mortar and concrete beams were cast, and the 11 inserts in each beam were extracted at a given test age. Concrete strength was not a variable, so the average companion cylinder strengths varied over a narrow range of 14 and 17 MPa (2000 to 2500 psi).

TABLE 3.1 Within-Test Coefficient of Variation of Pullout Tests

Ref.	Apex Angle (°)	Embedment Depth (mm)	Max. Agg. Size (mm)	Aggregate Type	Sample Size	Range of CV (%)	Average CV (%)
5	67	53	19	Limestone	3	2.3–6.3	3.9
6	67	53	25	River gravel	2	0.9–14.3	5.3
24	62	25	10	Unknown	8	3.2–5.3	4.1
29	70	25	20	Granite	6	1.9–12.3	6.9
25	67	53	19	Limestone	4	1.9–11.8	7.1
25	62	25	19	Limestone	10	5.2–14.9	8.5
26	62	25	20	Limestone	6	7.4–31	14.8
27	70	25	19	River gravel	11	4.6–14.4	10.2
27	70	25	19	Limestone	11	6.3–14.6	9.2
27	70	25	19	Lightweight	11	1.4–8.2	6.0
27	54	25	19	River gravel	11	4.3–15.9	10.0
30	67	30	12	Gravel	24	2.8–6.1	4.3

TABLE 3.2 Effects of Test Variables on Within-Test Coefficient of Variation of Pullout Tests

Test Series	Apex Angle (°)	Embedment Depth (mm)	Max. Agg. Size (mm)	Aggregate Type	No. of Data Sets[a]	Range of CV (%)	Average CV (%)
Apex angle	30	25	19	River gravel	2	9.1–11.4	10.3
			Mortar		1		4.6
	46	25	19	River gravel	4	5.6–13.3	8.9
			Mortar		2	4.5–6.5	5.5
	54	25	19	River gravel	2	6.3–6.7	6.5
			Mortar		1		4.3
	58	25	19	River gravel	2	7.3–8.6	8.0
			Mortar		1		4.9
	62	25	19	River gravel	2	7.5–9.6	8.6
			Mortar		1		4.1
	70	25	19	River gravel	4	8.0–10.1	8.8
			Mortar		6	4.0–6.9	5.6
	86	25	19	River gravel	2	7.5–9.0	8.3
			Mortar		1		2.8
Embedment depth	58	12	19	River gravel	1		12.9
			Mortar		1		5.3
	58	20	19	River gravel	2	7.7–10.9	9.3
			Mortar		1		6.4
	58	23	19	River gravel	2	6.5–6.7	6.6
			Mortar		1		4.7
	58	25	19	River gravel	2	7.3–8.6	8.0
			Mortar		1		4.9
	58	27	19	River gravel	2	8.0–8.8	8.4
			Mortar		1		2.8
	58	32	19	River gravel	2	8.1–9.1	8.6
			Mortar		1		3.1
	58	43	19	River gravel	2	7.9–9.4	8.7
			Mortar		1		4.1
Aggregate size	70	25	6	River gravel	2	4.1–7.0	5.6
	70	25	10	River gravel	5	3.5–6.5	4.9
	70	25	13	River gravel	4	3.3–10.6	5.5
	70	25	19	River gravel	4	8.0–10.1	8.8
Aggregate type	70	25	19	Lightweight	2	5.7	5.7
	70	25	19	River gravel	4	8.9–10.1	8.8
	70	25	19	Gneiss	2	7.2–7.5	7.4
	70	25	19	Porous limestone	2	7.7–10.9	9.3

[a] Number of data sets having various numbers of replicates after discarding outliers:

n =	11	10	9	8
Concrete	25	18	2	2
Mortar	10	5	4	

Source: Stone, W.C. and Giza, B.J., *Concr. Int.*, 7(2), 27, 1985.

The author has used the techniques in ASTM E 178[32] to remove outliers from the data reported by Stone and Giza.[20] Usually, an erratic low pullout load resulted because of abnormal cracking of the beam outside of the bearing ring, and an erratic high load resulted when a large aggregate particle was situated across the fracture surface of the conical fragment. Table 3.2 summarizes the testing variables and the resulting coefficients of variation. To visualize the results, the data are also plotted. Figure 3.19A shows the effect of the apex angle. For pullout tests in concrete, a variation of the apex angle from 30° to 86° does not appear to have a strong effect on the repeatability, but there is a tendency for more scatter at lower apex angles. The tests in mortar were less variable, and, likewise, there was no dependence on the apex angle. The effects of embedment depth are summarized in Figure 3.19B. Because of the few data points, it is not possible to conclude whether embedment depth has an effect. It appears, however, that

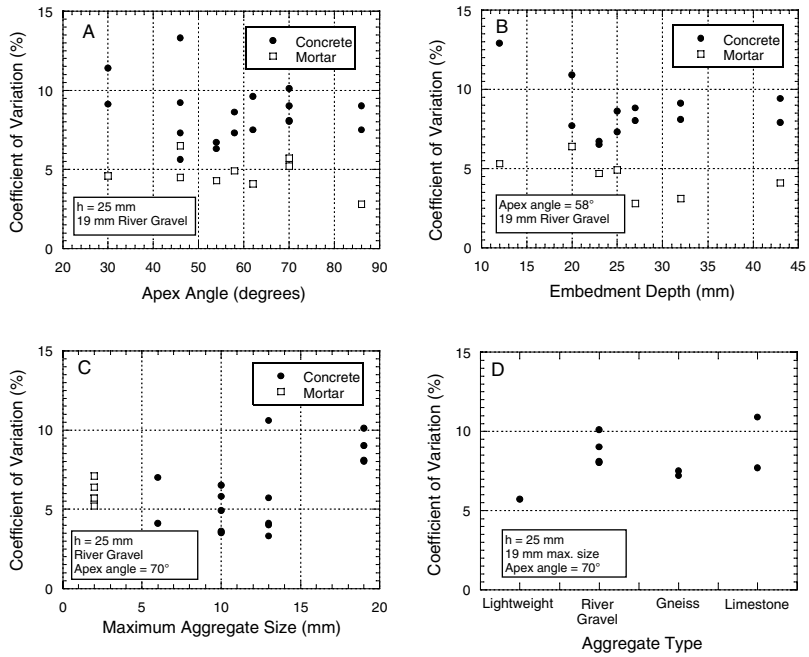

FIGURE 3.19 Coefficient of variation as a function of: (A) apex angle, (B) embedment depth, (C) maximum aggregate size, and (D) aggregate type. (Data from Reference 20.)

when the embedment was equal to or less than the maximum aggregate size, 19 mm (3/4 in.), there was a tendency for more variability. Again, pullout tests in mortar have less variability. The effects of aggregate size are shown in Figure 3.19C. For an embedment depth of 25 mm (1 in.), the 19-mm (3/4 in.) maximum aggregate size resulted in greater variability than the smaller aggregate sizes. In addition, there were no differences between the tests in mortar and those in concrete with the 6-, 10-, and 13-mm (1/4-, 3/8-, and 1/2-in.) aggregates. Finally, Figure 3.19D shows the effects of coarse aggregate type. The tests in concretes made with normal weight aggregates had about the same coefficient of variation. The tests in lightweight concrete, however, had a lower coefficient of variation of 5.7%, which is practically identical to the average value of 5.6% obtained from tests in mortar.

The NBS study showed that, for a 25-mm (1-in.) embedment depth, tests in concrete made with 19-mm (3/4-in.) aggregate had higher variability, and tests in concrete made with lightweight aggregate had lower variability. These observations support the notion that aggregate interlock controls the ultimate load during the test. Stone and Giza[20] also found that the average pullout loads in the mortar specimens where consistently lower than the strengths in concrete specimens, and the difference tended to be higher for smaller apex angles. They argued that, at smaller apex angles, aggregate interlock effects are greater, and more load is needed to extract the aggregates from the mortar matrix. They reasoned that tests in concrete had greater variability than tests in mortar because of the random manner in which coarse aggregate particles cross the eventual failure surface. They further observed that, for the tests in concrete with lightweight aggregate, the fracture surface went through the aggregate particles rather than around them, as was observed in concretes made with the normal weight aggregates. Thus, for the weak lightweight aggregates, interlock effects were not significant, and the repeatability was similar to tests in mortar.

In summary, the repeatability of the pullout test is characterized by the coefficient of variation. Reported values of the coefficient of variation, for different aggregate materials and test configurations, have ranged from about 4 to 15% with an average value of about 8%. The maximum size of the aggregate in relation to the embedment depth appears to be a significant factor. Tests on concrete made with coarse aggregate having a maximum size less than the embedment depth tend to have lower variability. The

type of coarse aggregate appears to be insignificant, except for lightweight aggregate that results in less variability.

3.4.2 Strength Relationship

The term *strength relationship* is used for the relationship between pullout strength and compressive strength of concrete that is obtained by regression analysis of test data. In the review of the early pullout test developed in the former Soviet Union, Skramtajew[1] reported that for concrete with cube strengths between 1.5 and 10.5 MPa (200 to 1500 psi) there was a constant ratio between pullout load and cube strength. On the other hand, Tremper[2] showed that, over a wide range of concrete strength, the relationship between pullout load and compressive strength was nonlinear and may be affected by the type of aggregate (Figure 3.4). Recall that these early tests did not involve a bearing ring.

To improve the correlation between pullout strength and compressive strength, Kierkegaard-Hansen[3] introduced a bearing ring and concluded from his tests that: "There is nothing to indicate that the relationship between the two strength measurements is nonlinear." Kierkegaard-Hansen found, however, that the relationship was linear but not proportional, i.e., the straight line had a nonzero intercept. In addition, he found that the relationship depended on the maximum size of the coarse aggregate. He suggested the following strength relationships for his lok-strength system:

$$P = 5.10 + 0.806C \text{ (16 mm maximum aggregate size)} \tag{3.5}$$

$$P = 9.48 + 0.829C \text{ (32 mm maximum aggregate size)} \tag{3.6}$$

where

P = ultimate pullout load (kN)
C = cylinder compressive strength of concrete (MPa)

Thus, for equal cylinder compressive strength, concrete with a larger coarse aggregate will have a greater ultimate pullout load.

The manufacturer[33] of the widely used LOK-TEST system originally proposed the following strength relationship for all concrete with aggregate sizes up to 32 mm (1 1/4 in.):

$$P = 5 + 0.8C \tag{3.7}$$

Bickley[24] reported, however, that correlation testing performed at six test sites, using the same LOK-TEST system, resulted in straight lines that differed from Equation 3.7. Table 3.3 summarizes the best-fit values of the slopes and intercepts obtained by Bickley. The table shows that there are positive and negative intercepts and that some of the slopes are significantly greater than the recommended value of 0.8 kN/MPa. It was shown that, in general, Equation 3.7 is a "conservative" relationship, i.e., for a given pullout load Equation 3.7 estimates a lower compressive strength than the straight lines in Table 3.3.

The lack of agreement among the strength relationships obtained with the same test system, and the illogical result of a nonzero intercept, has caused skepticism among potential users of the pullout test method. This section demonstrates that, for a given test system, there is not a unique strength relationship applicable to all concrete. Also, it is shown that the correlation for a particular combination of materials and test system is not necessarily linear. The discussion is limited to relationships between ultimate pullout load and cylinder compressive strength.

First, the shape of the strength relationship is investigated. Figure 3.20A shows correlation data obtained using concrete made with 19-mm (3/4 in.) crushed limestone.[27] The pullout test system had a 70° apex angle and a 25-mm (1 in.) embedment depth. Rather than using a linear relationship, consider a power function as follows:

TABLE 3.3 Linear Strength Relationships by Bickley[24] with LOK-TEST System ($P = a + bC$)

Strength Range (MPa)	Intercept a (kN)	Slope b (kN/MPa)
7.1–38.3	−0.9	0.88
12.7–28.8	−2.0	1.05
9.7–44.4	2.4	0.85
5.9–32.5	1.7	0.81
13.7–34.4	−2.0	1.06
8.8–25.2	2.7	0.89

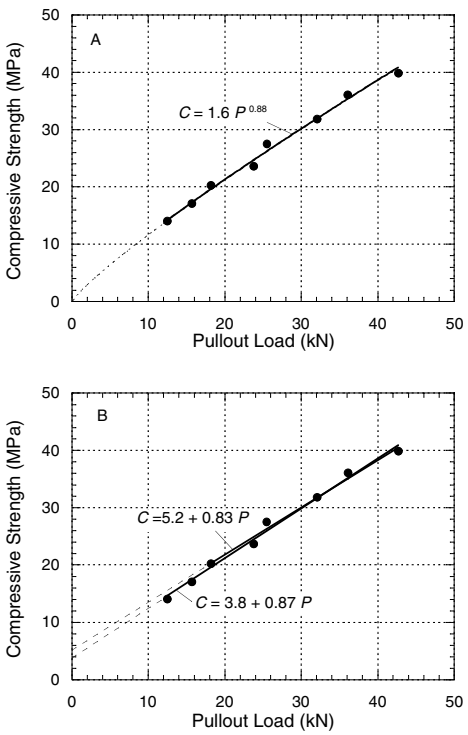

FIGURE 3.20 Strength relationships for concrete made with crushed limestone:[27] (A) power function relationship and (B) straight line relationships for different strength ranges.

$$C = \alpha P^{\beta} \tag{3.8}$$

By taking the logarithms of both sides, Equation 3.8 is transformed to

$$\log(C) = \log(\alpha) + \beta \log(P) \tag{3.9}$$

Thus, by plotting the logarithm of compressive strength vs. the logarithm of pullout load, the power function is transformed into a straight line. The best-fit values of α and can be obtained by linear regression analysis using the transformed data.* The best-fit power function for the data in Figure 3.20A is

*Linear regression analysis of the transformed data is preferred when the coefficient of variation of the dependent variable (concrete strength in this case) is constant.[27]

$$C = 1.6P^{0.86} \tag{3.10}$$

The power function fits the data quite well and the shape is nearly a straight line over the range covered by the data.

Now, examine what happens if a linear relationship is assumed having the equation:

$$C = a + bP \tag{3.11}$$

If all points are considered, the best-fit straight line is

$$C = 3.8 + 0.87P \tag{3.12}$$

If we consider only the six points for compressive strengths above 20 MPa (2900 psi), the best-fit straight line is

$$C = 5.2 + 0.83P \tag{3.13}$$

It is seen that the two straight lines in Figure 3.20C are practically the same for compressive strength above 20 MPa. The point of this exercise is to illustrate that, if the true strength relationship is nonlinear and it is approximated with a straight line, the slope and intercept of the straight line depend on the strength range covered by the correlation data.

Next, consider correlation data for the same test system but for concrete made with 19-mm (3/4 in.) river gravel.[27] The data are shown in Figure 3.21A and the best-fit power function is

$$C = 1.07P^{1.02} \tag{3.14}$$

The power function looks very much like a straight line. In this case, the exponent is greater than 1, and the curvature of the strength relationship is opposite to that shown in Figure 3.20A. Figure 3.21B shows the best-fit straight lines for all the data and for only the six data points above 20 MPa (2900 psi). Again, the equations of the straight lines are different but the strength relationships are similar for the data above 20 MPa. Also, note that because of the different curvature, the values of the intercepts are negative.

Thus, if the true strength relationship is slightly nonlinear and if the curvature can depend on the type of aggregate, one can explain why Bickley[24] reported different linear relationships for the same pullout test system.

The manufacturer[33] of the LOK-TEST system later proposed the following relationship, which differs from Equation 3.7, for concrete with compressive strengths between 3 and 25 MPa (400 and 3600 psi):

$$P = 1.0 + 0.96C \tag{3.15}$$

Because the strength relationship is used to estimate compressive strength based on the measured pullout load, it is preferable to treat compressive strength as the dependent variable. Thus, the relationships for the LOK-TEST system are as follows:

$$C = -1.0 + 1.04P \text{ (for 3 MPa} < C < \text{25 MPa)} \tag{3.16}$$

$$C = -6.3 + 1.25\,P \text{ (for } C \geq \text{25 MPa)} \tag{3.17}$$

These two straight lines are shown in Figure 3.22A. For purposes of illustration, eight evenly spaced points were chosen along this bilinear strength relationship, as shown in Figure 3.22B. A best-fit power function was fitted to the points, and the equation of the function is as follows:

$$C = 0.6P^{1.14} \tag{3.18}$$

It is seen that the power function is nearly identical to the bilinear function.

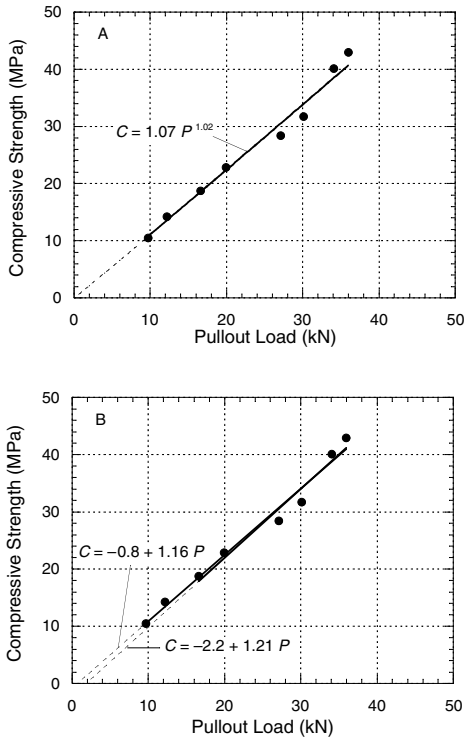

FIGURE 3.21 Strength relationships for concrete made with river gravel:[27] (A) power function and relationship (B) straight line relationships for different strength ranges.

Figure 3.23 shows correlation data reported by Khoo[29] for pullout tests and tests of corresponding cores. The pullout configuration had an apex angle of 70° and the embedment depth was 25 mm (1 in.). The concrete was made with 20-mm (0.8 in.) maximum size crushed granite, and the compressive strength ranged between 10 and 40 MPa (1500 and 5800 psi). The best-fit straight-line relationship for the data, as determined by this author, is

$$C = -1.11 + 1.19P \tag{3.19}$$

while the best-fit power function is

$$C = 1.12P^{1.00} \tag{3.20}$$

Because the exponent of the power function is equal to 1, the power function is actually a straight line passing through the origin. The intercept in Equation 3.19 is not statistically significant, and, for the range of strength considered, the compressive strength of the cores is proportional to the pullout load.

Finally, let us examine the effects of test geometry and aggregate type on the strength relationship. Figure 3.24A shows the reported[27] power-function relationships for two pullout test configurations: one had an apex angle of 54° and the other an angle of 70°. The embedment depth and insert head diameter were 25 mm (1 in.), and the concrete was made with 19-mm 3/4-in.) river gravel. The exponents for the two curves are close to 1 so both relationships are very close to linear. As shown in Table 3.1, the repeatability of the two test configurations was found to be similar. As was discussed by Stone and Giza,[20] because the slope of the relationship for the 54° pullout configuration is lower than for the 70°

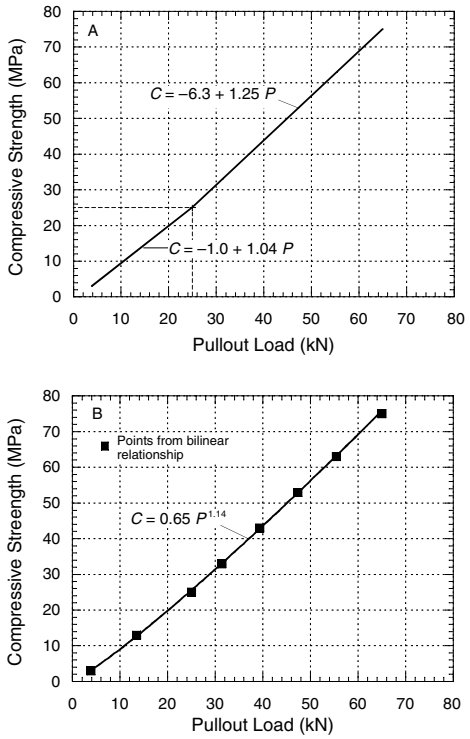

FIGURE 3.22 (A) Bilinear strength relationship proposed for LOK-TEST system.[33] (B) Power function approximation of the two lines.

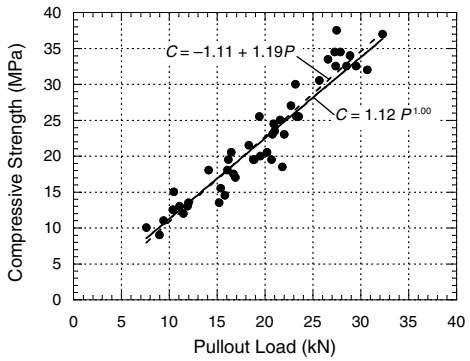

FIGURE 3.23 Correlation data by Khoo[29] and best fit linear and power function relationships.

configuration, the relationship for the 54° configuration would result in slightly less uncertainty in the estimated compressive strength.

Figure 3.24B compares power-function relationships for different types of aggregates using the 70° pullout test configuration.[27] The relationships were found to be statistically different. Note that for compressive strengths above 20 MPa (3000 psi), the concrete with crushed limestone resulted in much greater pullout loads. Thus, there is evidence that the aggregate type can affect the strength relationship.

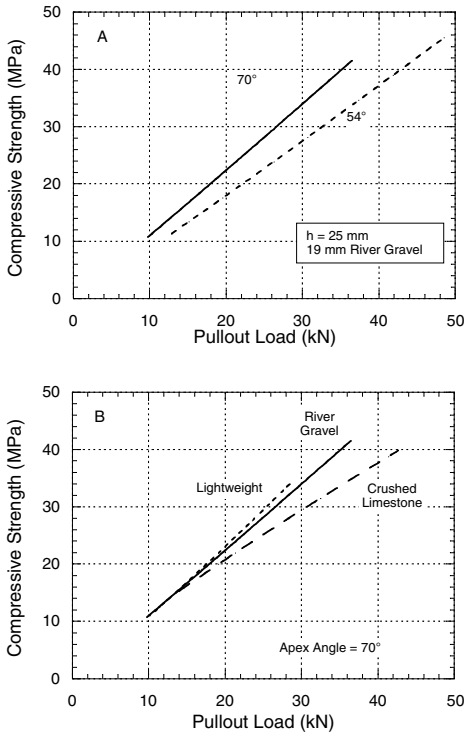

FIGURE 3.24 Strength relationships as affected by (A) apex angle and (B) aggregate type.[27]

3.4.3 Summary

This section has reviewed available information on the within-test variability (repeatability) and the strength relationship of the pullout test. Over a wide range of concrete strength, the standard deviation of the ultimate pullout loads, for repeated tests in the same concrete, increases with increasing strength. Hence the coefficient of variation is the appropriate statistic to describe repeatability. A significant amount of repeatability data have been published, and it appears that the average value of the coefficient of variation for the pullout test is about 8%. The size and type of the coarse aggregate, however, affect the coefficient of variation, and the repeatability for a given concrete mixture can be higher or lower than 8%.

Considerable correlation data have been published for the commercially available LOK-TEST system, which uses a 62° apex angle and a 25 mm embedment depth. The majority of the empirically determined relationships have been reported to be straight lines with nonzero intercepts. It has been explained that these linear relationships are approximations to inherently nonlinear relationships. For this reason, the slopes and intercepts depend on the strength ranges used in developing the correlation data. It has been proposed that a power function is a superior equation for analyzing correlation data. The coefficients of the power function are readily determined by linear regression analysis of the logarithms of pullout and compressive strength data. As demonstrated by examples, the power function can accommodate various degrees of nonlinearity.

Some of the early studies indicated that, for a given test system, the strength relationship is influenced by the maximum aggregate size. More recent results show that the type of aggregate also has an effect. Thus, for the most reliable estimates of in-place strength, a strength relationship should be developed for the specific concrete mixture to be used in construction.[28] The next section discusses methods for developing correlation data.

3.5 Applications

The pullout test has been adopted as a standard test method in many parts of the world, including North America, and its successful use on large construction projects has been reported.[24,34,35] This section reviews the evolution of the current ASTM (American Society for Testing and Materials) standard governing the pullout test, and discusses some of the practical aspects for implementing the method and interpreting test results.

3.5.1 Standards

The first standard for the pullout test was established in Denmark in 1977,[33] and the method is recognized for the acceptance of concrete in structures. In North America, ASTM adopted a tentative test method in 1978, which was subsequently revised and issued as a standard in 1982. The ASTM standard does not limit the test configuration to a specific geometry. The following compares some of the geometrical requirements in the 1978 tentative method with those in the 1982 ASTM standard:

	ASTM C 900-78T	ASTM C 900-82
Embedment depth	1.0*d* to 1.2*d*	1.0*d*
Bearing ring	2.0*d* to 2.4*d*	2.0*d* to 2.4*d*
Apex angle	45° to 70°	53° to 70°

The 1982 standard set the embedment depth equal to the insert head diameter, *d*, thereby limiting the range of possible apex angles from 53° to 70°. The 1987 revision of the ASTM standard made no changes to the allowable test configurations.[36]

The ASTM standard allows three procedures for placement of cast-in-place pullout inserts:

1. Attached to the surface of formwork prior to concrete placement
2. Attached to formwork with special hardware to enable testing deep within the concrete (refer to Figure 3.7A)
3. Placed into the surface of freshly placed concrete

In the third procedure, inserts are placed manually into the top surface of the fresh concrete. Special inserts with a "cup" or a plastic plate are used to provide a smooth surface for proper seating of the bearing ring. Manual placement requires care to assure that the concrete around the insert is properly consolidated and surface air voids are minimized. In general, manually placed inserts result in higher variability[24,37] and are not recommended unless absolutely necessary. In all cases, the clear spacing between the inserts and the edges of the member should be at least four times the insert head diameter. Also, each insert should be placed so that reinforcing steel does not interfere with the eventual fracture surface when the insert is pulled out.

The number of required pullout tests in the field was a controversial subject during the development of the ASTM standard. The 1978 tentative method had no requirement. The 1982 standard stated that a "minimum of three pullout tests shall comprise a test result," and Note 6 stated: "Often it will be desirable to provide more than three individual pullout inserts in a given placement." In 1987, the section on the number of tests was expanded to the following:

> When pullout test results are used to assess the in-place strength in order to allow the start of critical operations, such as formwork removal or application of post tensioning, at least five individual pullout tests shall be performed for a given placement for every 115 m^3 (150 yd^3), or fraction thereof, or for every 470 m^2 (5000 ft^2), or a fraction thereof, of the surface area of one face in the case of slabs or walls.

A note to this requirement stated: "Inserts shall be located in those portions of the structure that are critical in terms of exposure conditions and structural requirements." In addition, the following statement was also added to the 1987 standard:

> When planning pullout tests and analyzing test results, consideration should be given to the normally expected decrease of concrete strength with increasing height within a given concrete placement in a structural element.

This so-called top-to-bottom effect is well documented.[38–41] Standards and codes, however, have not addressed the significance of the effect; therefore, there are no guidelines on how to deal with such variability. The important point is that when high variability is obtained from pullout tests performed at different elevations within a structural element, it should not be interpreted to mean that the pullout test is unreliable. Engineering judgment is required in selecting the test locations and in interpreting the results.

The 1978 and 1982 versions of the ASTM test method allowed the option of reporting the pullout strength as a stress, obtained by dividing the ultimate pullout load by the area of the idealized conic frustum. There were criticisms that the calculation was not meaningful because the pullout force is inclined to the surface of the frustum. In 1987, the procedure was changed to allow the calculation of a nominal normal stress as given by the previous Equation 3.2. As was discussed, the normal stress distribution on the idealized conic frustum is nonuniform. Therefore, this calculated normal stress is fictitious and should be used only for comparing results of different pullout test configurations. In the 1999 revision of ASTM C 900, the equations for computing nominal stresses on the surface of the idealized frustum were moved to a nonmandatory appendix. The reason was that stress calculations are rarely used in practice and are not essential to the test method.

The ASTM standard has the following statement regarding the relationships between pullout strength and other strength tests:

> Such strength relationships depend on the configuration of the embedded insert, bearing ring dimensions, depth of embedment, and the level of strength development in that concrete. Prior to use, these relationships must be established for each system and new combination of concreting materials.

Aside from assuring a strength relationship that is applicable to the particular combinations of equipment and materials, this requirement also forces testing agencies to become familiar with the details of pullout testing procedures prior to using the test equipment at the project site.

Before 2001, ASTM C900 required that the pullout test be completed within 90 to 150 s. Most standard test methods that measure strength properties of concrete require loading at a specified stress rate. Thus, in 2001, the test method was revised so that the nominal normal stress on the assumed conic frustum (see Equation 3.2) was required to increases at a rate from 40 to 100 kPa/s (5.8 to 14.5 psi/s). To assist users of the most common testing configuration, a table was provided that showed the acceptable range of time to complete the test depending on the expected ultimate pullout load.

3.5.2 Strength Relationship

The development of the strength relationship applicable to the specific construction project is a critical step in implementing the pullout test. Unfortunately, no standard procedures exist to obtain correlation data, although American Concrete Institute (ACI) 228.1R provides recommendations.[28]

Historically, various techniques have been used to acquire companion pullout strength and compressive strength data. Kierkegaard-Hansen[3] placed pullout inserts in the bottoms of standard cylindrical specimens. A pullout test was performed on the cylinder, and then the same cylinder was capped and tested for compressive strength. If the pullout test was stopped just beyond the point of maximum load, the pullout cone was not extracted, and it was shown that the cylinder could be tested in compression without significant effect on the compressive strength. Bickley[24] also provided data showing negligible effects of this procedure on compressive strength. Such a procedure is possible because, during a standard compression test, the ends of the cylinder are subjected to confining stresses[8] that prevent premature failure of the cylinder due to the damage incurred during the pullout test. However, it was found that, as concrete strength increased, radial cracking occurred at the end of the cylinder outside of the bearing ring, and this reduced the ultimate pullout load.[3,24] Later studies confirmed that, for concrete with compressive

strengths above 40 MPa (5800 psi), pullout tests in 150-mm (6-in.) diameter cylinders resulted in lower strengths than pullout tests on larger specimens that did not experience radial cracking. For this reason and because there is a limit to the size of the pullout test configuration than can be used on the bottom of a cylinder, this approach is not recommended.

An alternative to placing inserts in standard cylinders is to place them in slabs and cast companion standard cylinders. At designated ages, replicate pullout tests are performed on the slab and replicate cylinders are tested in compression. A drawback to this approach is the need to assure that the pullout tests and compression tests are performed at the same maturity. Because of their different masses and shapes, the slab and cylinders are not likely to experience the same temperature history during the critical early ages, when strength changes rapidly with age and is strongly dependent on temperature history.[42] Failure to account for possible maturity differences can lead to inaccurate strength relationships. Either maturity meters should be used to ensure companion testing at equal maturities, or compression tests should be performed on cores drilled from the slab. Although the latter approach helps assure equal maturities, it is time-consuming.

For the commercially available pullout systems, having embedment depths of 30 mm (1.2 in.) or less and apex angles of 70° or less, the preferred approach is to place inserts on the side faces of 200-mm (8-in.) cubes and cast companion standard cylinders. Because of similar surface-to-volume ratios, the early-age temperature histories of the two types of specimens will be similar. The cubes and cylinders should be compacted similarly, and the use of an internal vibrator or a vibrating table is recommended.

Committee 228 of the American Concrete Institute (ACI) recommends performing eight replicate pullout tests and two cylinder compression tests at each test age.[28] These numbers of tests assure that the average pullout strength and average compressive strength are determined with about the same degree of certainty. By placing four inserts in each cube, this recommendation requires two cubes and two cylinders at each test age. The specimens should be moist-cured until time of testing.

The next question is how many sets of pullout and compression tests should be performed to establish the strength relationship. The chosen number should satisfy two needs: the tests should span as a wide range of strength as is possible, and there should be enough points to define the relationship with a reasonable degree of accuracy. Based on field experience, Bickley[24] suggested that the range of compressive strength should be at least 20 MPa (3000 psi) but preferably greater than this. ACI Committee 228[28] recommends performing companion tests at a minimum of six evenly spaced strength levels. Generally, if test ages are increased by a factor of 2, there will be about the same strength increase between successive tests. For example, tests at ages of 1, 2, 4, 8, 16, and 32 days should result in approximately evenly spaced test points. This of course assumes a constant temperature during the curing period. If the pullout test will be used to estimate in-place strengths at very low levels, the first test age should be reduced to 12 h. This will require care in handling the low-strength specimens.

Thus, the recommended correlation testing program involves casting at least 12 cubes, with 4 inserts per cube, and 12 cylinder specimens. The inserts in 2 cubes and 2 cylinders are tested at different ages to produce evenly spaced points when the correlation data are plotted. The average of the pullout strengths and compressive strengths are used in a least-squares fit analysis to develop the strength relationship.[27,43,44]

3.5.3 Interpretation of Results

To estimate in-place strength, pullout tests are performed on a particular part of the structure and the strength relationship is used to convert the test results to a compressive strength value. To judge whether sufficient strength has been attained, the estimated compressive strength is compared with the required strength in the project documents. However, to provide for a margin of safety, the pullout test results should be treated statistically rather than simply by comparing the average estimated in-place strength with the required strength.

In assessing the safety of a structure, the "specified" concrete strength is used in the design equations to calculate member resistances. The specified strength is the strength that is expected to be exceeded by

a large proportion of the concrete in the structure, and it is often called the "characteristic strength." In North American practice,[45] this proportion (or fraction) is about 90%. Alternatively, it is expected that 10% of the concrete in the structure will be weaker than the specified strength. Thus, in interpreting test results, the characteristic strength indicated by the pullout tests should be computed for comparison with the required strength.

One approach,[24,46] which was developed in Denmark and has been used in North America, uses the lower tolerance limit of the in-place strength as the characteristic strength. The lower tolerance limit is a statistical term that represents the value that is expected to be exceeded by a certain fraction of the population with certain degree of confidence (or probability level).[47] It is calculated by subtracting the product of the standard deviation and the appropriate tolerance factor from the average value. In applying this approach to pullout tests, the following procedure is used:

- Perform the pullout tests.
- Convert the test results to compressive strength values by means of the strength relationship.
- Compute the average and standard deviation of the compressive strength values.
- Compute the characteristic strength as follows:

$$C_{0.1} = C_a - KS \tag{3.21}$$

where

$C_{0.1}$ = the characteristic strength, i.e., the strength not expected to be exceeded by 10% of the concrete in the structure
C_a = average compressive strength based on the pullout test results
K = one-sided tolerance factor
S = the standard deviation of the compressive strength values

The tolerance factor value depends on the number of tests and the confidence level. Proponents of this approach usually use a confidence level of 0.75.[24,46] Table 3.4 lists the one-sided tolerance factors for an understrength fraction of 10% and a confidence level of 0.75.[47]

In a strict sense, the tolerance limit approach is not intended for application to values (compressive strength) estimated through the use of an empirical correlation. The approach has been criticized[27,43] because of the following assumptions implied in its use:

- The strength relationship has no error, i.e., the coefficients describing the relationship are known with absolute certainty.
- The standard deviation of the actual in-place compressive strength is assumed to equal the standard deviation of compressive strengths estimated from the correlation curve.

The first assumption can lead to unconservative estimates of the in-place strength. The second assumption is likely to be conservative because the variability of the in-place compressive strength is not expected to be as great as that of pullout strength. In addition to these assumptions, the strength relationships were determined using ordinary least-squares analysis, which is not strictly applicable when the independent variable (pullout strength in this case) has measurement error.

To overcome the deficiencies of the tolerance limit approach, the U.S. NBS developed a rigorous statistical procedure to establish the strength relationship and estimate the in-place characteristic strength to a desired confidence level.[43] Basically, the NBS procedure estimates the expected characteristic strength and its uncertainty. From these estimates, one determines the value the characteristic strength that is expected to be exceeded with a high level of confidence. The procedure is complex, but it is well suited for implementation on a personal computer. The NBS method assumes that the ratio of the standard deviation of cylinder strength to the standard deviation of pullout strength has the same value in the field as was obtained during the laboratory correlation testing. Characteristic strengths computed by using this rigorous approach were compared with the values computed using the tolerance limit method.[27] The comparison showed that the tolerance limit approach leads to overly conservative estimates of

TABLE 3.4 One-Sided Tolerance Factor for 10% Understrength and 0.75 Confidence Level for Normal Distribution

No. of Tests	*K*	No. of Tests	*K*
3	2.501	12	1.624
4	2.134	13	1.606
5	1.961	14	1.591
6	1.860	15	1.577
7	1.791	16	1.566
8	1.740	17	1.554
9	1.702	18	1.544
10	1.671	19	1.536
11	1.646	20	1.528

Source: Natrella, M., Experimental Statistics, Handbook 91, National Bureau of Standards, U.S. Government Printing Office, Washington, D.C., Oct. 1966.

in-place characteristic strength, especially when the variability of the pullout test results is high. Although this is acceptable for safety, it may lead to unnecessary delays in the construction schedule.

A simplified procedure was developed to interpret pullout test results and was implemented with spreadsheet software.[44] A spreadsheet template was prepared that contained the necessary equations to develop the strength relationship and analyze subsequent in-place test results. To use the template, the user enters the test data from the correlation testing program, and the strength relationship is automatically computed. The user then enters the in-place pullout test results, and the characteristic strength is automatically computed. A Windows™-based program has been developed that implements the simplified procedure.[48] The program stores correlation data in a database that can be reused when the same concrete is used on different projects.

In arriving at a reliable estimate of in-place characteristic strength, the simplified method[44,49] considers the following sources of variability or uncertainty:

- The variability of the in-place concrete strength
- The uncertainty in the average value of the in-place pullout strength
- The uncertainty in the strength relationship

Simulation studies[44] indicated that the simplified method and the rigorous approach resulted in similar estimates of in-place characteristic strength.

Consensus has not been reached in North America on the recommended approach for analyzing in-place test results. ACI 228.1R[28] discusses the above statistical methods, but leaves it to the user to decide which should be used for a specific project. The user is encouraged to study the cited references for additional guidance on the interpretation of pullout test results.

3.5.4 Precision

ASTM test methods require precision statements that indicate the expected variability of test results. These statements are based typically on round-robin testing. Because of the high costs that would be required to carry out a properly designed interlaboratory testing program for the pullout test, a precision statement on repeatability was developed on the basis of the data summarized in ACI 228.1R.[28] For cast-in-place tests with embedment depth of 25 mm (1 in.) and maximum aggregate size of 19 mm (3/4 in.), the single operator coefficient of variation is 8%. Therefore, the ranges of individual test results are not expected to exceed the following:

Number of Tests	Acceptable Range (Percent of Average)
5	31
7	34
10	36

A note to the precision statement discusses actions to consider if the variability in a set of results exceeds the above ranges.

3.5.5 Number of Tests

As was stated earlier, an issue of contention during the development of the 1987 ASTM standard was the number of pullout tests that should be performed in a given placement to have a reliable estimate of the in-place strength. Before discussing this issue, consider a statistical principle. Suppose there are two test methods with values of repeatability, as expressed by the coefficient of variation, equal to V_1 and V_2. If the respective material properties are to be measured with the same degree of certainty, the number of replicate tests, n_1 and n_2, for each method should obey the following relationship:[23]

$$\frac{n_1}{n_2} = \left(\frac{V_1}{V_2}\right)^2 \tag{3.22}$$

Thus, if the coefficient of variation of method 1 is twice the coefficient of variation of method 2, four times as many replicate measurements should be made with method 1. Of course, the degree of uncertainty in the average value decreases as the number of tests increases.

Now consider the sampling requirements in ACI 318[50] for acceptance of concrete. The current requirement is that two cylinders should be tested for every 115 m^3 (150 yd^3) of concrete, or in the case of slabs and walls for every 470 m^2 (5000 ft^2) of surface area (of one face). The coefficient of variation of the standard cylinder compression test is about 4%.[28] If the same sampling frequency were used for pullout tests and if the coefficient of variation of the pullout test is taken as 8%, at least eight pullout tests should be performed for the above quantities of concrete. Note that this only assures that the pullout strength is known with the same degree of certainty as the standard cylinder strength. The estimated in-place compressive strength will have greater uncertainty because of the additional uncertainties associated with the strength relationship.

Some have suggested that a minimum of ten pullout tests should be performed for a given concrete placement.[25,29,34] As a practical matter, Bickley[34] advocated the placement of 15 inserts per 100 m^3 (130 yd^3). When it is anticipated that the desired strength level has been reached, 5 inserts are randomly selected for testing. If the results indicate less than the required strength level, testing is discontinued and additional curing is provided. At a later age, the remaining 10 inserts are tested. This procedure provides for a reserve in the event that testing is begun too soon. Bickley and others[51] also advocate the use of a maturity meter to determine the appropriate time to perform the pullout tests (see Chapter 5 by Carino on the maturity method for additional information).

Thus, while the ASTM standard requires a minimum of five pullout tests for every 115 m^3 (150 yd^3) of concrete, or in the case of slabs or walls for every 470 m^2 (5000 ft^2) of the surface area of one face, a greater number of inserts is recommended for added reliability and as a safety measure in the event testing is begun too soon.[28]

3.5.6 Post-Installed Tests

A drawback of the cast-in-place pullout test is that the locations of the inserts have to be planned in advance of concrete placement and the inserts have to be fastened to the formwork. This limits the

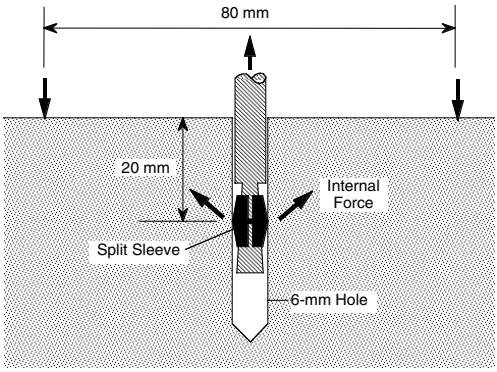

FIGURE 3.25 BRE internal fracture test.[52,53]

applicability of the method to new construction. In an effort to extend the application of pullout testing to existing structures, various "drilled in" or "post-installed" techniques have been investigated.

Spurred by the need to evaluate distress in structures made with high alumina cement, the Building Research Establishment (BRE)[52,53] developed a technique based on commercial anchor bolts with expanding sleeves, as shown in Figure 3.25. A 6-mm (1/4-in.) hole is drilled into the concrete, the hole is cleaned, and an anchor bolt is inserted into the hole so that the split-sleeve is at a depth of 20 mm (0.8 in.). After applying an initial load to expand and engage the sleeve, the bolt is loaded in tension and the maximum load during the extraction is recorded. Reaction is provided by three "feet" located along the perimeter of a ring 80 mm (3.1in) in diameter. The expanding sleeve applies to the concrete a force having vertical and horizontal components, as indicated by the inclined arrows in Figure 3.25. The concrete fracture differs from that in the standard pullout test, and the test is referred to an "internal fracture test" rather than a "pullout test." The reported strength relationship between ultimate load and compressive strength has a pronounced nonlinearity, indicating that the failure mechanism is probably related to the tensile strength of the concrete. The within-test variability was found to be greater than that of the standard pullout test, and the 95% confidence limits of the strength relationship were found to range between ±30% of the mean curve.

In the BRE test system, the pullout force is applied by turning a nut on the end of the anchor bolt and measuring the maximum torque achieved during the test. Bungey[54] developed a mechanical loading system with the aim of reducing the scatter of test results compared with using the torque loading system. Using the mechanical loading system, the 95% confidence intervals for the estimated compressive strength were estimated to be ±20%, which is a significant improvement. The comparatively low precision of the internal fracture test has been attributed to two principal causes:[54] (1) the variability in the hole drilling and preparation; and (2) the influence of aggregate particles on the load transfer mechanism and on the failure initiation load.

Mailhot et al.[55] investigated the feasibility of several drilled-in pullout tests. One of these used a split-sleeve and tapered bolt. In this case, the bolt assembly was placed in a 19-mm (3/4-in.) hole drilled into the concrete. As shown in Figure 3.26A, this technique differs from the BRE method because the reaction to the pulling force acts through a specially designed high-strength, split-sleeve assembly. Thus, the force transmitted to the concrete is predominantly a lateral load due to the expansion of the sleeve. The developers claimed that failure occurred by shear. The author, however, believes that failure is more likely to occur by splitting as in the standard splitting tension test of a cylinder. Similar to the BRE test, the variability of this test was reported to be rather high.[55] A second successful method involved epoxy-grouting a 16-mm (5/8-in.) threaded rod to a depth of 38 mm (1 1/2 in.) in a 19-mm (3/4-in.) diameter hole. After the epoxy had cured, the rod was pulled using a tension jack reacting against a bearing ring. This method was also reported to have high variability. The study concluded that these two methods

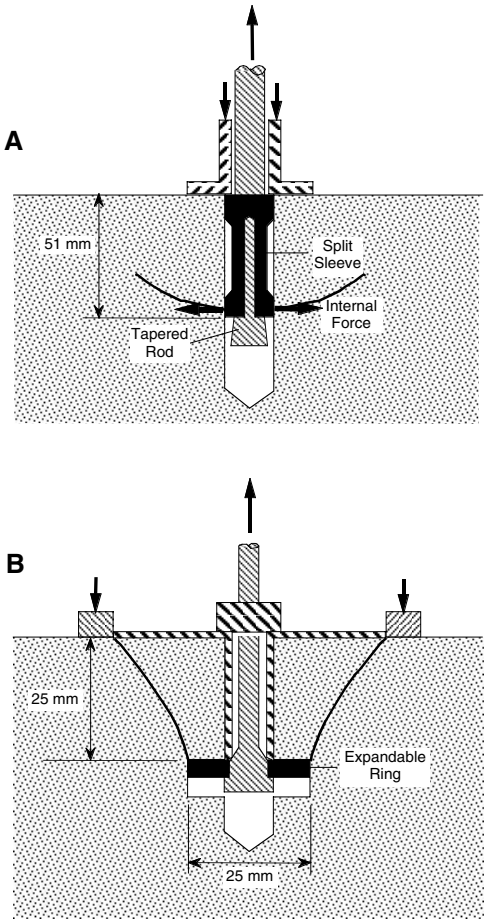

FIGURE 3.26 (A) Post-installed pullout test using spilt-sleeve and tapered bolt.[53] (B) The CAPO test by undercutting and using an expandable ring.[33]

have the potential for assessing the strength in existing construction. Additional research was recommended to enhance their reliability.

Domone and Castro[56] developed a technique similar to that shown in Figure 3.26A, except that the load was applied by a torque meter and the embedment was 20 mm (3/4 in.) as in the BRE method. Based on a limited number of comparative laboratory tests, it was concluded that the new method resulted in better correlations than the BRE method.

Another method was developed by the manufacturer of the LOK-TEST system and is referred to as the CAPO test (for *c*ut *a*nd *p*ull*o*ut).[33] The method involves drilling an 18-mm (0.7-in.) hole into the concrete and using a special milling tool to undercut a 25-mm (1-in.) diameter slot at a depth of 25 mm (1 in.). An expandable ring is placed into the hole, and the ring is expanded using special hardware. Figure 3.26B shows the ring after expansion. The entire assembly used to expand the ring is then pulled out of the concrete using the same loading system as for an ordinary pullout test. Thus, unlike the other methods discussed above, the CAPO test subjects the concrete to the same type of loading as the standard pullout test. The performance of the CAPO test in laboratory evaluations has been reported to be similar to the LOK-TEST.[33] In early field trials of the CAPO test, the variability of results was higher than for cast-in-place tests. This was attributed primarily to difficulties in obtaining a flat bearing surface perpendicular to the axis of the post-installed insert. With improvement in the hardware and technique, the

variability was reduced and results comparable to cast-in-place tests were reported.[57] In 1999, ASTM C 900 was revised to include pullout tests with post-installed inserts. The procedure calls for careful attention to surface preparation before testing.

3.5.7 Summary

This section has discussed some of the practical considerations in the application of the pullout test. Considerable information has been published on laboratory and field experience involving the method, and standard test procedures and recommended practices have been established.

Prior to using the pullout test to estimate in-place strength, a relationship between ultimate pullout load and compressive strength must be established for the particular test system and concrete materials. The maximum size and type of coarse aggregate can have a significant influence on the strength relationship. Although no standards currently exist, recommendations for establishing this relationship have been published. The preferred procedure is to perform the pullout tests on cube specimens. Correlation data should span as wide a strength range as is practicable, and the strength level that is expected to be measured in the field should fall within this range. At least six data sets should be used to develop the strength relationship.

In implementing pullout testing in the field, the number of pullout tests and statistical analysis of the results are critical. The number of tests should be chosen so that the average value and the variability of the pullout strength are established with a reasonable degree of confidence. Most practitioners use more than the minimum number required by the current ASTM standard. The inserts should be located in critical portions of the structure. Test results should be subjected to statistical analysis so that the estimated in-place strength will be exceeded by a large fraction of the concrete in the structure. Several statistical methods have been proposed, but there is no consensus on which should be used. Danish practice has promoted the tolerance limit approach, but there are more rigorous methods that can be implemented using a personal computer.

Finally, there has been a brief discussion of recent developments related to drilled-in tests that do not require the installation of inserts prior to concrete placement. Some of these methods load the concrete in a different manner compared with the standard pullout test, and higher within-test variability have been reported. One of these methods loads the concrete in a manner similar to the standard cast-in-place test, and comparable performance has been reported in laboratory and field evaluations. This post-installed pullout test is included in ASTM C 900.

3.6 Concluding Remarks

The pullout test measures the load required to extract a conical fragment of specified geometry from a concrete mass. The modern test is an outgrowth of earlier attempts that did not use a bearing ring to transmit the reaction of the tension load to the concrete mass. Danish research conducted in the late 1960s demonstrated that, by introducing the bearing ring, there was an approximately linear relationship between the ultimate pullout load and the compressive strength of concrete.

The pullout test subjects the concrete to a static load and, therefore, the test is amenable to theoretical analysis. Independent analytical and experimental investigations have been performed to gain an understanding of the failure mechanism. There has been agreement on some aspects of the failure process and divergent points of view on others. It is agreed that the concrete is subjected to highly nonuniform, triaxial stresses and that there is a stress concentration at the edge of the insert head. At about one third of the ultimate load, circumferential cracking begins in the highly stressed region. This first crack propagates at a greater apex angle than that defining the extracted conical fragment, and the first crack stabilizes at less than the ultimate load. A second circumferential crack forms that defines the eventual shape of the extracted fragment. At about 70% of the ultimate load, this second crack has extended from the insert head to the bearing ring. The ultimate load carrying mechanism is a point of contention. Some believe that there is a compression strut between the insert head and the bearing ring, and others believe

that additional load is carried by an aggregate interlock mechanism. Experimental evidence has been used to support both points of view. Despite the lack of agreement on the ultimate failure mechanisms, there is consensus that the ultimate pullout load is governed by the same strength properties that govern the compressive strength of concrete.

Some of the early proponents of the pullout test have claimed that the repeatability was similar to, and in some cases less than, the repeatability of standard compression tests. Consideration of a wide variety of published data, however, indicates that the within-test coefficient of variation of the pullout test is about twice that of the cylinder compression test. The size of the coarse aggregate in relation to the insert embedment appears to have the most significant effects on the scatter of pullout test results. In addition, the variability is lower in mortar and lightweight concrete than in normal weight concrete.

A relationship between pullout strength and compressive strength is needed to estimate in-place strength. Some claim that for a given test system there is a unique relationship. There is evidence that the nature of the coarse aggregate influences the relationship. Therefore, the recommended practice is to develop the strength relationship for the particular concrete to be used in construction. A large number of correlation studies have reported that compressive strength is a linear function of pullout strength. Research, however, suggests that the relationship may be nonlinear, and a power function is a more suitable equation for the strength relationship.

An important step in implementing the method is choosing the locations and number of pullout tests in a given placement of concrete. The inserts should be located in the most critical portions of the structure and there should be a sufficient number of tests to provide statistically significant results. Additional inserts are recommended in the event that testing begins too soon, and the concrete has not yet attained the required strength. The use of maturity meters along with pullout tests is encouraged to assist in selecting the correct testing times and in interpreting possible low-strength results.

In-place pullout data should be statistically analyzed so that there is a high confidence in the estimated strength. Although a standard analysis procedure has not been adopted, several methods are available. The more rigorous approaches are well suited for computer implementation.

Techniques have been developed that permit testing in existing construction by drilling a hole and inserting some type of expansion anchor. Some methods subject the concrete to different stress conditions and have different failure mechanisms than the standard cast-in-place pullout test; however, these methods have not found widespread acceptance because of their high variability. One method produces a failure surface that is similar to that of the cast-in-place test, and it has been included in the ASTM standard.

In summary, the pullout test has been standardized and is recognized as a reliable method for assessing the in-place strength of concrete during construction so that critical activities may be performed safely. As with other in-place tests, the active involvement of a qualified individual in all aspects of the testing program, from the correlation testing to the analysis of in-place data, is recommended to realize the potential benefits of the method.

References

1. Skramtajew, B.G., Determining concrete strength for control of concrete in structures, *J. Am. Concr. Inst.*, 34, 285, 1938.
2. Tremper, B., The measurement of concrete strength by embedded pull-out bars, *Proc. Am. Soc. Testing Mater.*, 44, 880, 1944.
3. Kierkegaard-Hansen, P., Lok-strength, *Nord. Betong*, 3, 19, 1975.
4. Rutenbeck, T., New developments in in-place testing of concrete, in *Use of Shotcrete for Underground Structural Support*, ACI SP-45, American Concrete Institute, Farmington Hills, MI, 1973, 246.
5. Malhotra, V.M., Evaluation of the pull-out test to determine strength of in-situ concrete, *Mater. Struct.* (RILEM), 8(43), 1975, 17.
6. Malhotra, V.M. and Carette, G.G., Comparison of pullout strength of concrete with compression strength of cylinders and cores, pulse velocity, and rebound number, *ACI J.*, 77(3), 17, 1980.

7. Richards, O., Pullout strength of concrete, *Reproducibility and Accuracy of Mechanical Tests*, ASTM SP 626, 1977, 32.
8. Ottosen, N.S., Evaluation of concrete cylinder tests using finite elements, *ASCE J. Eng. Mech.*, 110(3), 465, 1984.
9. Mass concrete, ACI 207.1R, Report of ACI Committee 207, *2002 Manual of Concrete Practice*, American Concrete Institute, Farmington Hills, MI, 2002.
10. Test method for determining the mechanical properties of hardened concrete under triaxial loads, ASTM C 801, *2002 Annual Book of ASTM Standards*, Vol. 04.02, ASTM International, West Conshohocken, PA, 2002.
11. Jensen, B.C. and Braestrup, M.W., Lok-tests determine the compressive strength of concrete, *Nord. Betong*, 2, 9, 1976.
12. Stone, W.C. and Carino, N.J., Deformation and failure in large-scale pullout tests, *ACI J.,* 80(6), 501, 1983.
13. Discussion of Reference 12, *ACI J.*, 81(5), 525, 1984.
14. Yener, M. and Chen, W. F., On in-place strength of concrete and pullout tests, *ASTM J. Cem. Concr. Aggregates*, Winter, 90, 1984.
15. Ottosen, N.S., Nonlinear finite element analysis of pullout test, *ASCE J. Struct. Div.*, 107(ST4), 591, 1981.
16. Yener, M. and Vajarasathira, K., Plastic-fracture finite element analysis of pullout tests, Preprints of the 22nd Annual Technical Meeting of the Society of Engineering Science, ESP22/8so38, Pennsylvania State University, Oct. 7–9, 1985.
17. Stone, W.C. and Carino, N.J., Comparison of analytical with experimental strain distribution for the pullout test, *ACI J.,* 81(1), 3, 1984.
18. Hellier, A.K., Sansalone, M., Carino, N.J., Stone, W.C., and Ingraffea, A.R., Finite-element analysis of the pullout test using a nonlinear discrete cracking approach, *ASTM J. Cem. Concr. Aggregates*, 9(1), 20, 1987.
19. Ballarini, R., Shah, S.P., and Keer, L.M., Failure characteristics of short anchor bolts embedded in a brittle material, *Proc. R. Soc. London*, A404, 35, 1986.
20. Stone, W.C. and Giza, B.J., The effect of geometry and aggregate on the reliability of the pullout test, *Concr. Int.*, 7(2), 27, 1985.
21. Krenchel, H. and Shah, S.P., Fracture analysis of the pullout test, *Mater. Struct.* (RILEM), 18(108), 439, 1985.
22. Krenchel, H. and Bickley, J.A., Pullout testing of concrete: historical background and scientific level today, *Nord. Betong,* 6, 155, 1987.
23. Practice for calculation of sample size to estimate, with a specified tolerable error, the average characteristic of a lot or process, ASTM E 122, *2002 Annual Book of ASTM Standards*, Vol. 14.02, ASTM International, West Conshohocken, PA, 2002.
24. Bickley, J.A., The variability of pullout tests and in-place concrete strength, *Concr. Int.*, 4(4), 44, 1982.
25. Carette, G.G. and Malhotra, V.M., In-situ tests: variability and strength prediction at early ages, in *In-Situ/Nondestructive Testing of Concrete*, ACI SP-82, V.M. Malhotra, Ed., American Concrete Institute, Farmington Hills, MI, 1984, 111.
26. Keiller, A.P., A preliminary investigation of test methods for the assessment of strength of in-situ concrete, Technical Report 42.551, Cement and Concrete Association, Wexam Springs, U.K., 1982.
27. Stone, W.C., Carino, N.J., and Reeve, C.P., Statistical methods for inplace strength prediction by the pullout test, *ACI J.*, 83(5), 745. 1986.
28. In-Place Methods to Estimate Concrete Strength, ACI 228.1R, Report of ACI Committee 228, *2002 Manual of Concrete Practice*, American Concrete Institute, Farmington Hills, MI, 2002.
29. Khoo, L.M., Pullout techniques — an additional tool for in-situ concrete strength determination, in *In-Situ/Nondestructive Testing of Concrete*, ACI SP-82, V.M. Malhotra, Ed., American Concrete Institute, Farmington Hills, MI, 1984, 143.

30. Bocca, P., The application of pull out test to high strength concrete strength estimation, *Mater. Struct.* (RILEM), 17(99), 1984, 211.
31. Krenchel, H. and Peterson, C.G., In-place testing with LOK-Test: Ten years' experience, paper presented at International Conference on in-Situ/Non-Destructive Testing of Concrete, Ottawa, Oct. 2–5, 1984.
32. Practice for dealing with outlying observations, ASTM E 178, *2002 Annual Book of ASTM Standards*, Vol.. 14.02, ASTM International, West Conshohocken, PA, 2002.
33. Peterson, C.G., LOK-test and CAPO-test development and their applications, *Proc. Inst. Civ. Eng.* I, 76, 539, 1984.
34. Bickley, J.A., Evaluation and acceptance of concrete quality by in-place testing, in *In-Situ/Nondestructive Testing of Concrete*, ACI SP-82, V.M. Malhotra, Ed., American Concrete Institute, Farmington Hills, MI, 1984, 95.
35. Bickley, J.A., Concrete optimization, *Concr. Int.*, 4(6), 38, 1982.
36. Test method for pullout strength of hardened concrete, ASTM C 900, *2002 Annual Book of ASTM Standards*, Vol.. 04.02, ASTM International, West Conshohocken, PA, 2002.
37. Vogt, W.L., Beizai, V., and Dilly, R.L., In-situ pullout strength of concrete with inserts embedded by "finger placing," in *In-Situ/Nondestructive Testing of Concrete*, ACI SP-82, V.M. Malhotra, Ed., American Concrete Institute, Farmington Hills, MI, 1984, 161.
38. Dilly, R.L. and Ledbetter, W.B., Concrete strength based on maturity and pullout, *ASCE J. of Struct. Eng.*, 110(2), 354, 1984.
39. Murphy, W.E., The interpretation of tests on the strength of concrete in structures, in *In-Situ/Nondestructive Testing of Concrete*, ACI SP-82, V.M. Malhotra, Ed., American Concrete Institute, Farmington Hills, MI, 1984, 377.
40. Munday, J.G.L. and Dhir, R.K., Assessment of in-situ concrete quality by core testing, in *In-Situ/Nondestructive Testing of Concrete*, ACI SP-82, V.M. Malhotra, Ed., American Concrete Institute, Farmington Hills, MI, 1984, 393.
41. Haque, M.N., Day, R.L., and Langan, B.W., Realistic strength of air-entrained concrete with and without fly ash, *ACI J.*, 85(4), 241, 1988.
42. Parsons, T.J. and Naik, T.R., Early age concrete strength determination by pullout testing and maturity, in *In-Situ/Nondestructive Testing of Concrete*, ACI SP-82, V.M. Malhotra, Ed., American Concrete Institute, Farmington Hills, MI, 1984, 177.
43. Stone, W.C. and Reeve, C.P., A new statistical method for prediction of concrete strength from in-place tests, *ASTM J. Cem. Concr. Aggregates*, 8(1), 3, 1986.
44. Carino, N.J. and Stone, W.C., Analysis of in-place test data with spreadsheet software, in *Computer Use of Statistical Analysis of Concrete Tests*, ACI SP-101, P. Balaguru and V. Ramakrishnan, Eds., American Concrete Institute, Farmington Hills, MI, 1987, 1.
45. Recommended practice for evaluation of strength test results of concrete, ACI 214, Report of ACI Committee 214, *2002 Manual of Concrete Practice*, American Concrete Institute, Farmington Hills, MI, 2002.
46. Hindo, K.R. and Bergstrom, W.R., Statistical evaluation of the in-place compressive strength of concrete, *Concr. Int.*, 7(2), 44, 1985.
47. Natrella, M., Experimental Statistics, Handbook 91, National Bureau of Standards, U.S. Government Printing Office, Washington, D.C., Oct. 1966.
48. Chang, L.M. and Carino, N.J., Analyzing in-place concrete tests by computer, *Concr. Int.*, 20(12), 34, 1998.
49. Carino, N.J., Statistical methods to evaluate in-place test results, *New Concrete Technology: Robert E. Philleo Symposium*, ACI SP-141, T.C. Liu and G.C. Hoff, Eds., American Concrete Institute, Farmington Hills, MI, 1993, 39.
50. Building code requirements for structural concrete (318-02) and commentary (ACI 318R-02), Report of ACI Committee 318, *2002 Manual of Concrete Practice*, American Concrete Institute, Farmington Hills, MI, 2002.

51. Peterson, C.G. and Hansen, A.J., Timing of loading determined by pull-out and maturity tests, in *RILEM International Conference on Concrete at Early Ages,* Paris, Vol. I, Ecole Nationale des Ponts et Chausses, 1982, 173.
52. Chabowski, A.J. and Bryden-Smith, D.W., A simple pull-out test to assess the strength of in-situ concrete, *Precast Concr.*, 8(5), 243, 1977.
53. Chabowski, A.J. and Bryden-Smith, D.W., Assessing the strength of concrete of in-situ portland cement concrete by internal fracture tests, *Mag. Concr. Res.*, 32(112), 164, 1980.
54. Bungey, J.H., Concrete strength determination by pull-out tests on wedge anchor bolts, *Proc. Inst. Civ. Eng* II, 71, 379, June 1981.
55. Mailhot, G., Bisaillon, G., Carette, G.G., and Malhotra, V.M., In-place concrete strength: new pullout methods, *ACI J.*, 76(12), 1267, 1979.
56. Domone, P.L. and Castro, P.F., An expanding sleeve test for in-situ concrete and mortar strength evaluation, in *Proceedings Structural Faults and Repairs 87*, Engineering Technics Press, Edinburgh, 1987, 149.
57. Peterson, C.G., LOK-TEST and CAPO-TEST pullout testing, twenty years experience, in *Proc Conf. on Non-Destructive Testing in Civil Eng.,* J.H. Bungey, Ed., British Institute of Non-Destructive Testing, 1997, 77.

4

The Break-Off Test Method

4.1 Introduction
4.2 Theoretical Considerations
4.3 BO Test Equipment
4.4 Historical Background
4.5 Test Procedure
Inserting Sleeves in Fresh Concrete · Preparation for Core Drilling from Hardened Concrete · Conducting the BO Test · The BO Tester Calibration Procedure · Developing a Correlation Curve
4.6 Evaluation of Test Specimens
4.7 Applications
4.8 Advantages and Limitations
4.9 Standardization of the BO Method

Tarun R. Naik
University of Wisconsin–Milwaukee

In-place concrete strength is not the same as cylinder concrete strength because the in-place concrete is placed, compacted, and cured in a different manner than the cylinder specimen concrete. Determination of accurate in-place strength is critical in form removal and prestress or post-tension force release operations. Fast construction techniques and construction failures emphasize the need for adopting methods for determining in-place concrete strength. Several such methods exist and a considerable amount of information is available. Out of many of these currently available nondestructive testing (NDT) methods, only the break-off (BO) and the pullout tests measure a direct strength parameter. The BO test consists of breaking off an in-place cylindrical concrete specimen at a failure plane parallel to the finished surface of the concrete element. The BO stress at failure can then be related to the compressive or flexural strength of the concrete using a predetermined relationship that relates the concrete strength to the BO strength for a particular source of concrete. The BO test was developed in Norway by Johansen in 1976, and it was then introduced in North America, initially by Malhotra in Canada and later by Naik in the United States.

This chapter provides complete and detailed information regarding the theory behind the BO method, factors affecting this method, and the practical use of this method for laboratory and site investigations. Selected case histories and lab investigations are also included.

4.1 Introduction

For many years questions have been raised regarding concrete quality assurance test methods based upon standard cylinder tests, which measure the potential strength of a concrete batch. In-place concrete strength is not the same as the cylinder concrete strength because the in-place concrete is placed, compacted, and cured in a different manner than the cylinder specimen concrete. Determination of accurate in-place strength is critical in form removal and prestress or post-tension force release operations.

Fast construction techniques and construction failures emphasize the need for adopting methods for determining in-place concrete strength. Several such methods exist and a considerable amount of information is available.[1–5] Out of many of these currently available NDT methods, only the BO and the pullout tests measure a direct strength parameter. The BO test consists of breaking off an in-place cylindrical concrete specimen at a failure plane parallel to the finished surface of the concrete element. The BO stress at failure can then be related to the compressive or flexural strength of the concrete using a predetermined relationship that relates the concrete strength to the BO strength for a particular source of concrete. The BO test was developed in Norway by Johansen in 1976.[6] The BO test is still not very widely used in North America. The primary factor that limited the widespread use of this method was the lack of necessary technical data and experience in North America. Initial work at CANMET in the early 1980s had indicated a lack of reproducibility in results of this test method.* Several papers were published in Europe about the BO method. This chapter provides complete and detailed information regarding the theory behind the BO method, factors affecting this method, and the practical use of this method for laboratory and site investigations. Selected case histories and lab investigations are also included.

4.2 Theoretical Considerations

The BO method is based upon breaking off a cylindrical specimen of in-place concrete. The test specimen has a 55 mm (2.17 in.) diameter and a 70 mm (2.76 in.) height. The test specimen is created in the concrete by means of a disposable tubular plastic sleeve, which is cast into the fresh concrete and then removed at the planned time of testing, or by drilling the hardened concrete at the time of the BO test. Figures 4.1 and 4.2 show tubular plastic sleeves and a drill bit, respectively. Both the sleeve and the drill bit are capable of producing a 9.5 mm ($^3/_8$ in.) wide groove (counter bore) at the top of the test specimen (see Figure 4.3) for seating the load cell (see Section 4.3). A force is applied through the load cell by means of a manual hydraulic pump. Figure 4.3 is a schematic of a BO concrete cylindrical specimen obtained by inserting a sleeve or drilling a core. The figure also shows location of the applied load at the top of the BO test specimen. In essence, the load configuration is the same as a cantilever beam with circular cross section, subjected to a concentrated load at its free end. The force required to break off a test specimen is measured by a mechanical manometer. The BO stress can then be calculated as:

$$f_{BO} = M/S$$

where

$M = P_{BO} \cdot h$
P_{BO} = BO force at the top
h = 65.3 mm
$S = (d)/32$
d = 55 mm

The BO method assumes that the ultimate flexural strength of the concrete is reached at the extreme outside fiber at the base of the BO test specimen. In this case, the circular cross-section area would restrict the ultimate fiber stress theoretically to a point, and a crack is initiated at this point. The exact location of the rupture is determined by the loading arrangement (see Figure 4.3) at a distance of 55 mm from the concrete surface. Away from the extreme outside fiber at the base, the stresses successively change in the direction of the neutral axis from tension to compression. The BO method is presently the only available test method for directly determining flexural strength of in-place concrete; there is a linear relationship between the BO flexural strength and modulus of rupture as determined by a beam test.[7–12] In the above simplified

*Personal communication from V.M. Malhotra, 1984.

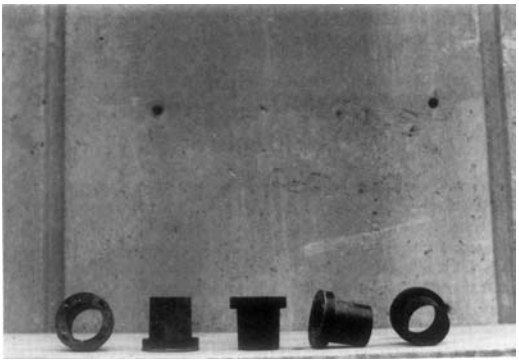

FIGURE 4.1 Tubular plastic sleeves for inserting in fresh concrete for the BO test.

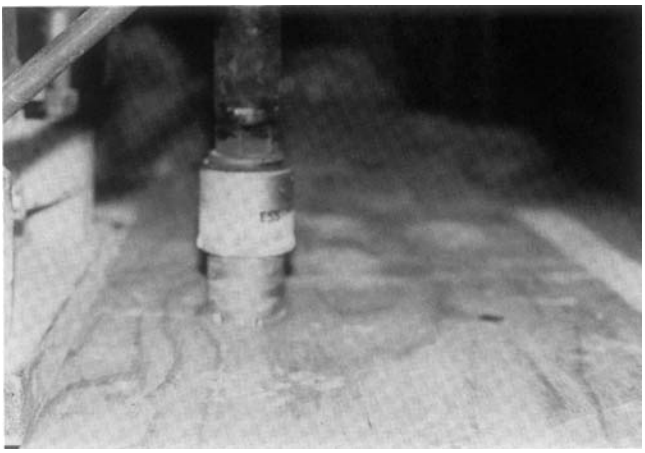

FIGURE 4.2 Core drill bit for drilling a core for BO testing of existing concrete element.

formula, the manufacturer uses the elementary theory of strength of materials and does not apply the concept of deep beam analysis even though the diameter to length ratio is 1:1.3. This point has been further explored.[13–15]

4.3 BO Test Equipment

The BO tester (see Figure 4.4), consists of a load cell, a manometer, and a manual hydraulic pump capable of breaking a cylindrical concrete specimen having the specified dimensions given in Section 4.2. The load cell has two measuring ranges: low range setting for low strength concrete up to approximately 20 MPa (3000 psi) and high range setting for higher strength concrete up to about 60 MPa (9000 psi) (see Figure 4.5). A tubular plastic sleeve, with internal diameter of 55 mm (2.17 in.) and geometry shown in Figure 4.1, is used for forming cylindrical specimen in fresh concrete. A sleeve remover (see Figure 4.6) is used for removing the plastic sleeve from the hardened concrete. A diamond tipped drilling bit is used for drilling cores for the BO test in hardened concrete (see Figure 4.2). The bit is capable of producing a cylindrical core, along with a reamed ring (counter bore) in the hardened concrete at the top with dimensions similar to that produced by using a plastic sleeve. The manufacturer also provides a calibrator for calibration and adjustment of the BO tester (see Figure 4.7). The procedure of calibrating a BO tester is discussed later.

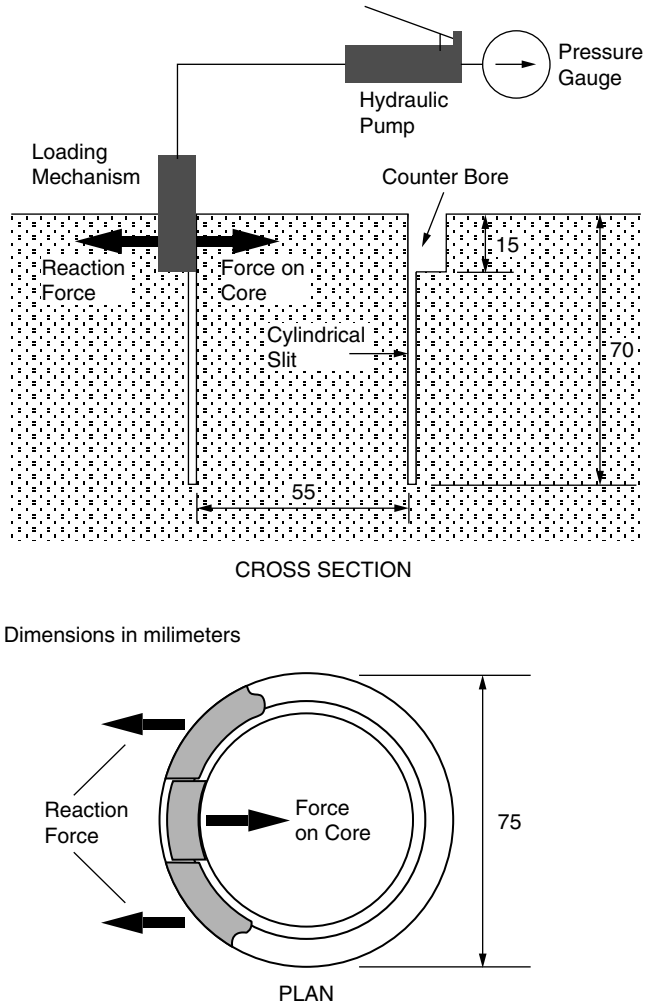

FIGURE 4.3 Schematic of concrete cylindrical specimen obtained by inserting a sleeve or drilling a core, and location of applied load.

4.4 Historical Background

The BO method is a relatively new NDT. The first paper was published by Johansen in 1976[6] and the research work was done at the Norwegian Technical University (NTH). In 1977 researchers at the NTH and the Research Institute for Cement & Concrete in Norway developed and patented the BO tester as a method for determination of compressive strength of in-place concrete.

Johansen,[6] in his first paper, indicated the main use of this method as a very efficient way of determining the in-place concrete strength for form removal. In 1984, Dahl-Jorgensen and Johansen[12] published a paper on the use of the BO method to detect variation in the concrete strength and curing conditions. In their research a comparison was made between the BO method and the pullout test method. The compressive strength of cores obtained from the BO tests and the standard cube compressive strength were also compared. They concluded that the pullout test method and the core compressive strength values obtained from the BO tests have a better ability to differentiate between concrete qualities than the cube test. On the other hand, the BO test results and the core compressive strength results

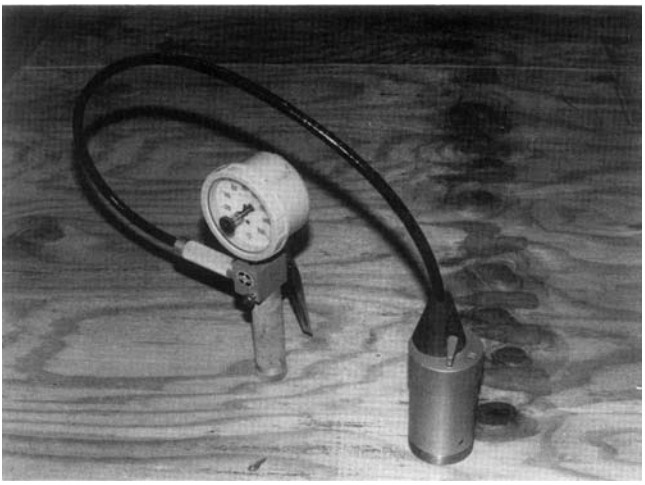

FIGURE 4.4 The BO test equipment: load cell, manometer, and hydraulic hand pump.

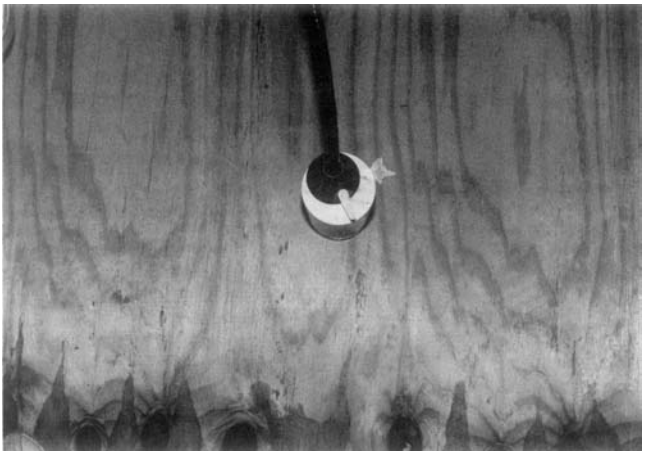

FIGURE 4.5 Low and high range settings of the BO tester load cell.

demonstrated their ability in detecting variation in curing conditions, while the pullout test method did not register some of the curing differences demonstrated by the BO and the core results.

In 1979, Johansen published another paper[9] on the use of the BO method, with a particular reference to its application to airport pavements made of vacuum concrete. The author concluded that the variation of the concrete strength detected by the BO method is of the same order of magnitude as the variation detected by conventional flexural beam test. Furthermore, the BO strength was about 30% higher than the conventional modulus of rupture because of deviations in the load configurations and geometric parameters between the two test methods. A high sensitivity of the BO method to sense the influence of the ambient air temperature on early strength was also indicated in this paper. A good relationship was obtained between BO test reading and the compressive strength of the concrete obtained by standard cube testing.

In 1980 Byfors tested concrete at early ages using the BO method.[7] In his research Byfors tested concretes with different water-to-cement ratios, and different aggregate sizes 8, 16, and 32 mm ($^5/_{16}$ in., $^5/_8$ in., and $1^1/_4$ in.). The conclusion was that the BO method is well suited to detecting low-strength concrete made with different sizes of coarse aggregates.

FIGURE 4.6 Sleeve remover.

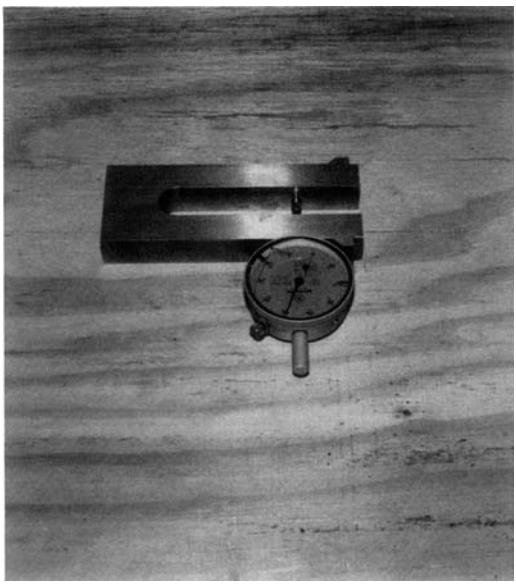

FIGURE 4.7 The BO tester calibrator.

After modifications to the BO tester, Dahl-Jorgensen published two reports on the use of the BO method.[12,16] In this study, he investigated the use of the new equipment in testing epoxy to concrete bond strength, and compared the results of the BO and the pullout methods. He concluded that the BO test provided results with smaller variations between individual tests than the pullout method. Also, fewer tests were rejected for the BO method compared to the pullout method.

Nishikawa published his work in 1983[10] after conducting very limited laboratory research on the use of the BO method for determining flexural strength of concrete. He concluded that the relationship between the BO test results and cylinder compressive strength tests was complex and of little practical value. Therefore, no attempt was made to correlate these two test results. This is, of course, contrary to all other published information about the BO method. He further concluded that the change in the shape

of the aggregates was not sensed by the BO method. These two conclusions are further discussed in Section 4.6. Nishikawa indicated a relatively high within test variation for the inserted sleeve BO tests as compared to cylinder and beam tests. With respect to other variables, he found that the BO test results were affected by water-cement ratio, age, curing conditions, and cement type.

In 1984 Carlsson et al. published a paper on field experiences with the use of the BO tester.[17] Six case histories were discussed. The authors concluded there was a trend toward greater acceptance of the BO test method in the field.

In 1987 another very limited exploratory investigation was done by Barker and Ramirez.[18] The Scancem version of the tester was used. They investigated the effects of the water to cement ratio, maximum aggregate size, and aggregate shape. They indicated a relatively low within test variation of the method of 6.1%, while that of the cylinder and beam tests were 7.6 and 4.6%, respectively. A regression analysis was performed between BO test results and the cylinder test results. Good correlation was obtained and a detailed statistical study was performed on the effects of different parameters on the BO compressive and flexural strengths relation. Also in 1987, Naik et al. conducted a comprehensive laboratory investigation at the University of Wisconsin-Milwaukee.[13–15] They were the first to study the effects of the method of obtaining the BO test specimen, either by inserting a plastic sleeve in fresh concrete or by drilling a core after the concrete had hardened. Furthermore, they investigated the applicability of the BO test for high-strength concrete. The strengths investigated were 45 and 55 MPa (6000 and 8000 psi), along with 30 MPa (4000 psi). They also studied the effect of aggregate shape and slab thickness on the BO test results. A total of 524 BO tests were performed. They concluded that BO readings for crushed aggregates were on average 10% higher than those for the rounded aggregates. Also, the BO test is less variable for crushed aggregate concrete. They also stated that the drilled core BO tests results were on average about 9% higher than the inserted sleeve BO test results. According to Naik et al. the drilled core test method is preferable, although both methods of obtaining the BO test specimen showed good correlation with the compressive strength of the in-place concrete, and also yielded equally consistent BO test results (see Tables 4.1, 4.2, and 4.3 and Figures 4.8 and 4.9). They discussed some of the difficulties encountered in inserting sleeves in harsh concrete or concrete with high amounts of bleeding. Additional statistical analysis was performed on the large amount of data that their investigations yielded.

TABLE 4.1 Results of Standard Cylinder Compressive Strength and BO Tests for Mixture 1 (30 MPa)

	Cylinder Compressive Strength (psi)		BO Readings (bar)							
			Inserted Sleeve Slab Thickness (in.)				Drilled Core Slab Thickness (in.)			
			5		7		5		7	
Test Age (days)	Actual	Average	Actual	Average	Actual	Average	Actual	Average	Actual	Average
	2120		41, 50		59, 59					
1	2210	2180	59, 57	55	57, 56	59	—	—	—	—
	2210		57, 64		62, 61					
	3360		76, 70		76, 72					
3	3380	3315	70, 76	73	73, 70	74	—	—	—	—
	3200		70, 77		77, 74					
	4085		78, 75		70, 86		104, 94		91, 87	
5	3925	3935	80, 83	79	77, 79	79	91, 98	97	89, 94	88
	3800		80		81		100		80	
	4155		67, 75		86, 82		95, 84		93, 84	
7	4070	4100	73, 80	73	79, 79	82	80, 88	87	80, 90	86
	4070		72		85		89		83	
	5040		104, 92		102, 90		123, 113		118, 120	
28	4950	4955	83, 96	94	91, 98	96	105, 105	112	118, 112	118
	4880		96		98		112		120	

TABLE 4.2 Results of Standard Cylinder Compressive Strength and BO Tests for Mixture 1 (45 MPa)

Test Age (Days)	Cylinder Compressive Strength (psi)		BO Readings (bar)							
			Inserted Sleeve Slab Thickness (in.)				Drilled Core Slab Thickness (in.)			
			5		7		5		7	
	Actual	Average	Actual	Average	Actual	Average	Actual	Average	Actual	Average
	2650		57, 58		61, 59					
1	2760	2705	68, 59	60	52, 68	61	—	—	—	—
	2705		60, 60		60, 65					
	4880		85, 82		71, 81					
3	4740	4820	79, 85	81	87, 70	76	—	—	—	—
	4845		72		71					
	5525		85, 87		89, 89		89, 87		89, 89	
5	5465	5560	89. 79	84	78, 69	83	85, 95	91	84, 83	87
	5685		78		89		100		92	
	5850		90, 88		92, 95		103, 96		94, 92	
7	5215	5735	83, 87	87	90, 97	91	106, 97	100	104, 107	95
	6135		85		80		97		81	
	6490		122, 103		95, 90		142, 125		105, 109	
28	6100	6320	113, 109	110	103, 95	97	119, 143	129	108, 95	103
	6365		103		101		115		100	

TABLE 4.3 Results of Standard Cylinder Compressive Strength and BO Tests for Mixture 1 (55 MPa)

Test Age (Days)	Cylinder Compressive Strength (psi)		BO Readings (bar)							
			Inserted Sleeve Slab Thickness (in.)				Drilled Core Slab Thickness (in.)			
			5		7		5		7	
	Actual	Average	Actual	Average	Actual	Average	Actual	Average	Actual	Average
	2775		92, 85		56, 59					
1	2760	2745	74, 80	85	74, 68	62	—	—	—	—
	2795		88, 91		67, 56					
	5020		108, 90		82, 97		98, 108		119, 108	
3	4635	4865	90, 78	93	106, 84	95	108, 94	97	92, 91	110
	4935		82, 92		97, 106		94, 79		90, 98	
	5555		107, 108		110, 95		110, 106		118, 111	
5	5215	5335	108, 114	106	95, 110	103	105, 116	106	115, 119	115
	5235		95		103		94		110	
	5820		117, 110		109, 112		117, 110		103, 106	
7	6225	5920	125, 109	112	110, 107	106	99, 108	108	113, 115	109
	5710		97		92		106		110	
	8310		119, 137		125, 120		113, 140		123, 124	
28	8455	8150	123, 110	124	109, 108	118	117, 131	130	137, 124	129
	7690		132		129		149		136	

4.5 Test Procedure

4.5.1 Inserting Sleeves in Fresh Concrete

Sleeves should be at center to center and edge distance of minimum 150 mm (6 in.). They are best pushed in-place by a rocking and twisting action, Figure 4.10. Concrete inside the sleeve and the top of plastic sleeve itself should then be tapped by fingers to insure good compaction for the BO specimen. Sleeves should then be moved gently up and down in-place and brought to the same level as the concrete surface

at its final position. For stiff mixes (i.e., low-slump concrete) a depression may occur within the confines of the sleeve during the insertion process. In such cases the sleeve should be filled with additional concrete, tapped with fingers, and slightly jiggled from side to side. On the other hand, for wet, high slump mixes, the sleeve may move upward due to bleeding. For such cases, sleeves should be gently pushed back in-place, as necessary, to the level of the finished concrete surface. Sometimes this process may have to be repeated until the uplift movement stops after the initial setting has occurred. A small weight (1 kg) may be placed on the sleeve in order to prevent its upward movement. Heavy grease, or other similar material, should be used to lubricate the plastic sleeves for its easier removal after the concrete hardens.

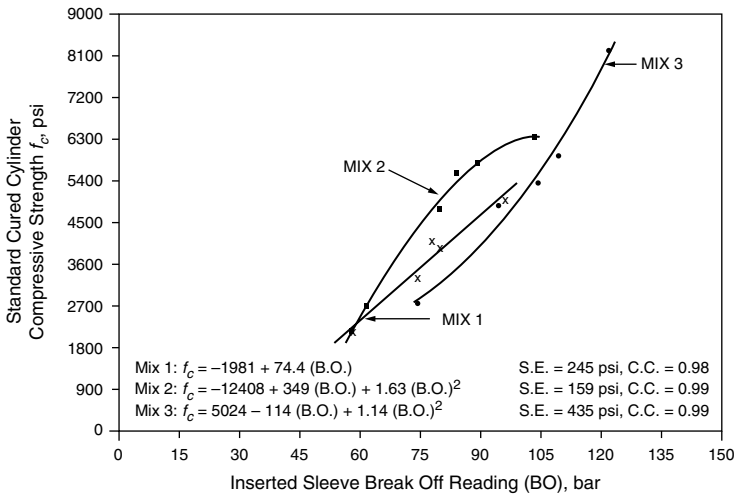

FIGURE 4.8 Plots of regression equations for inserted sleeve specimens for Mixtures 1, 2, and 3.

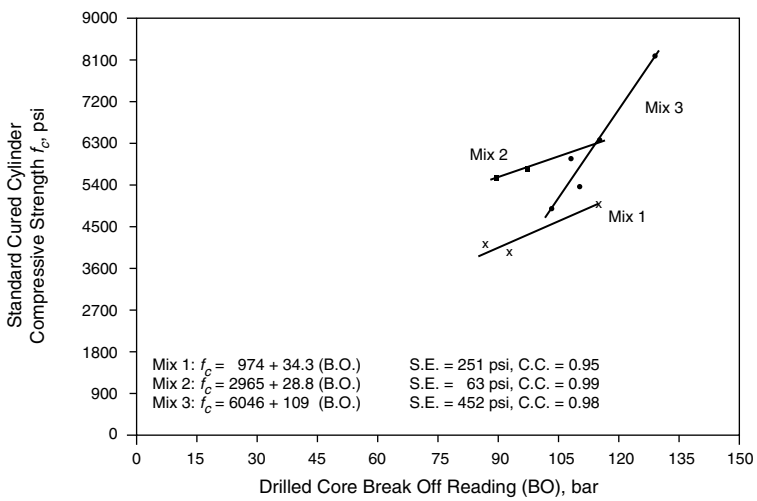

FIGURE 4.9 Plots of regression equations for drilled core specimens for Mixtures 1, 2, and 3

FIGURE 4.10 Inserting sleeve by rocking action.

4.5.2 Preparation for Core Drilling from Hardened Concrete

The finished concrete surface should be evaluated for sufficient smoothness in order to fix the vacuum plate of the core drilling machine. The core barrel should be perpendicular to the concrete surface at all times. The drilling process should be continued to the full depth required to produce a cantilever cylindrical core of 70 mm (2.76 in.) length, with a groove at the top of the core for setting the BO tester load cell. A slightly longer drilled core will not affect the BO reading, while a slightly shorter drilled core will affect the BO reading (see Figure 4.11).

4.5.3 Conducting the BO Test

At the time of the BO test, remove the inserted plastic sleeve by means of the key supplied with the tester (Figure 4.6). Leave the plastic ring in place. Remove loose debris from around the cylindrical slit and the top groove (see Figure 4.3). Select the desired range setting and place the load cell in the groove on the top of the concrete surface so that the load is applied according to Figure 4.3. The load should be applied to the test specimen at a rate of approximately one stroke of the hand pump per second. This rate is equivalent to about 0.5 MPa (70 psi) of hydraulic pressure per second. After breaking off the test specimen, record the BO manometer reading. This manometer reading can then be translated to the concrete strength using curves relating the BO reading to the desired concrete strength (i.e., flexural and/or compressive).

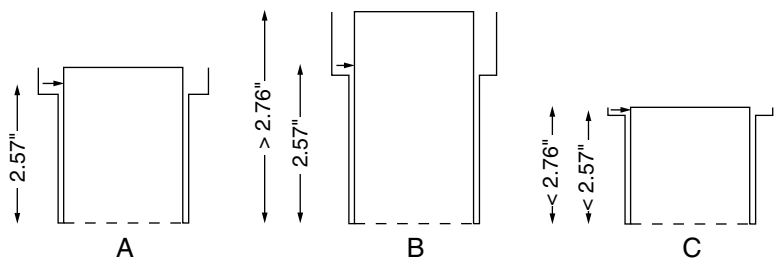

FIGURE 4.11 The BO drilled specimen dimensions: (A) The BO drilled specimen with the exact depth. (B) The BO drilled specimen with depth greater than 2.76 in. (C) The BO drilled specimen with depth less than 2.76 in.

4.5.4 The BO Tester Calibration Procedure

The BO tester should be calibrated, preferably each time before use, otherwise periodically. To calibrate the tester, follow these steps:

1. Set the calibrator gauge to zero.
2. Place the calibrator in the load cell (Figure 4.12).
3. Set the load cell on the high setting.
4. Apply the load to the calibrator by pumping the handle until the load cell manometer reading is 100.
5. Record the dial gauge reading and compare it with the expected value obtained from the manufacturers calibration chart (Figure 4.13). The dial gauge value should be within 4% of the manufacturer's chart value.
6. Repeat the above procedure for the low range setting.

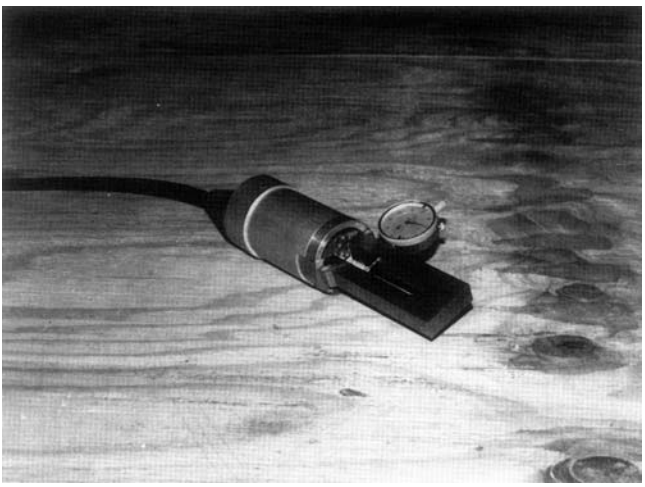

FIGURE 4.12 Calibrator placed in the load cell.

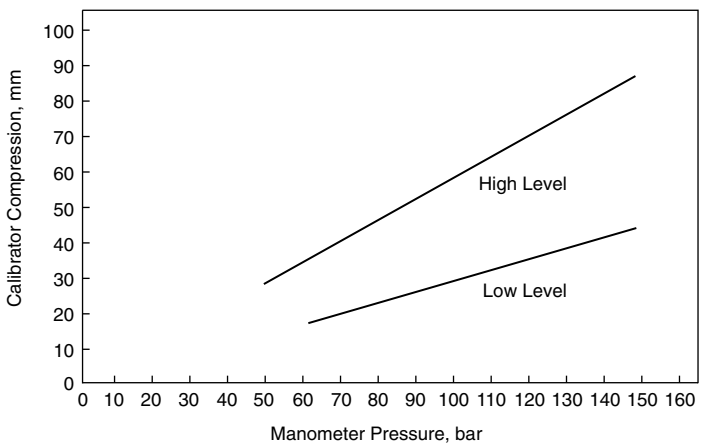

FIGURE 4.13 Calibrator chart as provided by the manufacturer.

Adjustment of the BO tester is necessary if error in the reading obtained is greater than ±4% of the expected value from the chart. For a well-calibrated tester, the needle on the manometer should move five bars per one hand stroke, while the first and/or second strokes might not move it that much. A good rate of applying the load would be one stroke per second.

4.5.5 Developing a Correlation Curve

The BO manufacturer provides correlation curves relating the BO reading and the compressive strength of the standard 150 ¥ 300-mm cylinders and 150-mm cubes. Figure 4.14 is the manufacturer's curves for the high-range setting of the load cell, while Figure 4.15 is for the low-range setting (see Section 4.4). This correlation is nonlinear and was empirically derived. The curve relating the BO reading and the compressive strength is concaved upward. This seems to indicate that the BO tester is less sensitive for higher concrete strengths. It should be noted that the manufacturer's curves consider many variables. However, knowing that concrete itself has inherent variability, a user should develop his or her own correlation curves for a particular concrete batch. Developing correlation curves for different types of concrete would efficiently increase the accuracy and dependability of the method in predicting the in-place strength.

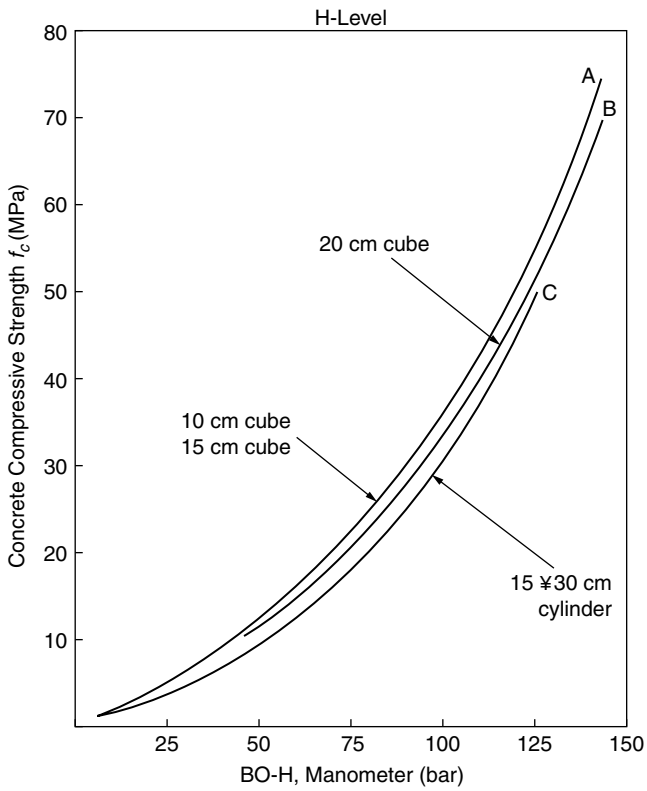

FIGURE 4.14 BO manometer reading vs. concrete compressive strength, as provided by the manufacturer, for the high-range setting.

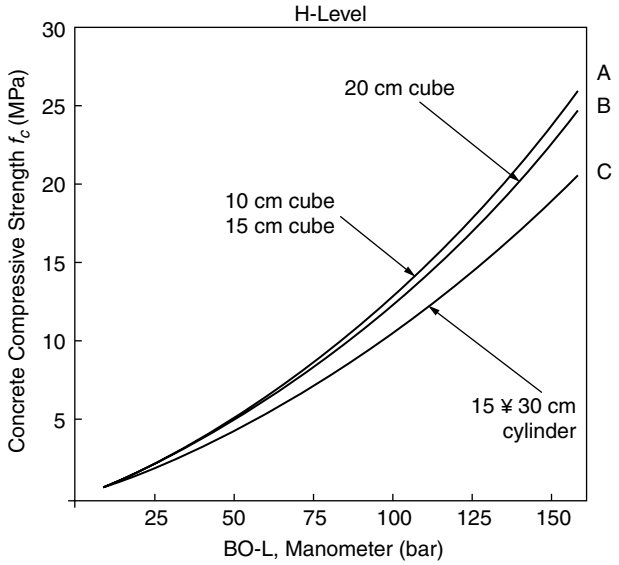

FIGURE 4.15 BO manometer reading vs. concrete compressive strength, as provided by the manufacturer, for the low-range setting.

The following precautions should be taken when developing data for correlations:

1. Keep the center-to-center and the edge distances of at least 150 mm (6 in.) in the process of inserting sleeves or drilling BO scores.
2. Obtain a minimum of five BO readings and three corresponding standard strength test specimens values, i.e., cylinders for compressive strength, and beams for flexural strength, for each test age.
3. An average of the five BO readings and the average of the three standard cylinder test results represent one point on the graph relating the BO reading to the desired standard strength of the concrete.
4. Cover the range of concrete strengths expected in the project, at early as well as at later ages, such as 1, 3, 5, 7, 14, and 28 days.

Regression equations between the mean values of the BO tests and standard strength tests should then be developed after sufficient data points are obtained for the correlation curve. The least square method can be applied to fit the best curve between the data points. The manufacturer's correlation curve could be used as a preliminary estimate only if no correlation chart has been obtained for the particular concrete under consideration. The strength value obtained from the manufacturer's correlation curves is considered only an approximation of the true in-place strength because it does not consider the combination of concrete making materials for the specific concrete under investigation.

4.6 Evaluation of Test Specimens

Before accepting a particular BO reading, the BO specimen tested should be examined to insure a "good" test. The BO test specimen must be perpendicular to the concrete surface. A minimum center to center and edge distance of 150 mm (6 in.) should be maintained. The failure plane should be approximately parallel to the concrete surface. It must be at a depth of 70 mm (2.76 in.) from the finished surface. The

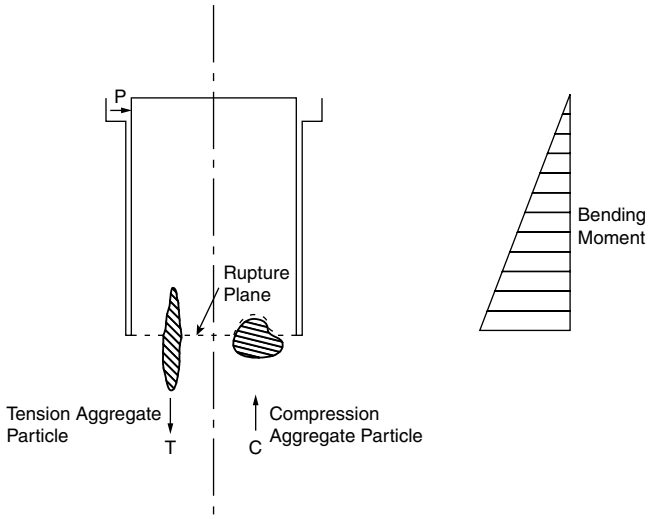

FIGURE 4.16 Rejected BO specimen due to presence of aggregate(s) in the failure plane.

presence of honeycombed concrete, excessive air voids, and/or reinforcement at the failure plane of test specimens could shift the rupture plane from its intended place. Such test specimen results should be rejected. The rejection criteria are somewhat dependent on the engineering judgment of the user. Figure 4.16 illustrates an example of irregular resistance mechanism to the applied BO force. In this special case, two fairly large aggregates exist in the rupture plane in such a way that the combination of the two particles could create a resistance couple. The rupture plane is forced to pass through the tensile particle, as illustrated in Figure 4.16, because the aggregate has a large aggregate-mortar bond area. Such cases, for example, could lead to a greater flexural resistance than that of other BO tests. Nishikawa and others[10,18] report rejection of very few tests. Dahl-Jorgensen[8] stated that less tests were rejected for the BO method than that for the pullout method. None of the published research reports on a statistical rejection technique that would provide a procedure for excluding bad test specimens, results, or personal judgment.

It is important to note that the inserted sleeve BO specimen tends to be trapezoidal in shape rather than cylindrical (the top diameter is 4 mm (0.16 in.) less than the bottom diameter), while it is exactly cylindrical in the case of the BO drilled core specimen. However, inserted sleeve BO specimen reading is not affected by the trapezoidal shape because the bottom diameter at the failure plane always remains 55 mm (2.17 in.).[13–15] In evaluating inserted sleeve specimens, it is also reported that the drilled core specimens give higher readings than the inserted sleeve specimens.[13–15] This is because in the case of the inserted sleeve specimens, the accumulation of bleed water under the bottom edge of the sleeve would tend to create a weaker zone of concrete exactly where the failure plane for the BO inserted sleeve test occurs.

4.7 Applications

The BO test can be used both for quality control and quality assurance. The most practical use of the BO test method is for determining the time for safe form removal, and the release time for transferring the force in prestressed or post-tension members. The BO method can also be used to evaluate existing structures. It has been reported that the BO test provides a more effective way for detecting curing conditions of concrete than the pullout and the standard cylinder tests.[7–9,12,16]

In 1982 the BO tester was used to control the time for safe form removal for a new Bank of Norway building and an apartment building in Oslo. In 1983 the BO tester was used in England. The BO tester has been used by the Norwegian Contractors Company, which was responsible for building off-shore platforms for the oil fields in the North Sea. The BO method can also be used to measure the bonding strength of overlays or the bonding between concrete and epoxy, but this usage has not been applied in the field.[12,16]

4.8 Advantages and Limitations

The main advantage of the BO test is that it measures in-place concrete (flexural) strength. The equipment is safe and simple; and the test is fast to perform, requiring only one exposed surface. The BO test does not need to be planned in advance of placing the concrete because drilled BO test specimens can be obtained. The test is reproducible to an acceptable degree of accuracy and correlates well with the compressive strength of concrete.

Two limitations for the BO test equipment are worth noting: (1) the maximum aggregate size; and (2) the minimum member thickness for which it can be used. The maximum aggregate size is 19 mm ($^3/_4$ in.) and the minimum member thickness is 100 mm (4 in.). However, the principle of the method can be applied to accommodate larger aggregate sizes or smaller members. The major disadvantage of the BO test is that the damage to the concrete member must be repaired if the member is going to be visible. However, this test is nondestructive since the tested member need not be discarded.

4.9 Standardization of the BO Method

In the 1980s, the BO method was standardized in England,[3] Norway,[19] and Sweden.[20] In 1990, ASTM adopted the method as Test Method C 1150.[21] The method, however, was not used frequently in the field. In 2002, ASTM discontinued the test method because "…the break-off test is not being used in North America, and there is little use in other parts of the world. Therefore, without feedback based on field experience, it is difficult to recommend meaningful revisions to this test method."[22] While the BO method is not used widely, there may be applications where it is a useful technique to assess in-place strength, and thus discussion of the method has been retained in this handbook.

References

1. Malhotra, V., Testing hardened concrete: nondestructive methods, *ACI Monog.*, No. 9, 1976.
2. Jones, R., A review of nondestructive testing of concrete, *Proc. Symp. Nondestructive Testing of Concrete and Timber*, Institute of Civil Engineers, London, June 1969, 1.
3. British Standard, B.S. 1881, Part 201, 1986, 17.
4. Methods of Mechanical Nondestructive Determination of Probable Compressive Strength of Concrete, Bulgarian National Standard 3816–65.
5. Vossitch, P., Outline of the various possibilities of nondestructive mechanical tests on concrete, *Proc. Int. Symp. Nondestructive Testing of Materials and Structures*, Vol. 2, Paris, 1959, 30.
6. Johansen, R., A New Method for Determination of In-Place Concrete Strength of Form Removal, 1st Eur. Colloq. on Construction Quality Control, Madrid, Spain, March 1976.
7. Byfors, J., Plain Concrete at Early Ages, Swedish Cement and Concrete Research Institute, Rep. No. Facks-10044, Stockholm, 1980.
8. Dahl-Jorgensen, E., In-situ Strength of Concrete, Laboratory and Field Tests, Cement and Concrete Research Institute, the Norwegian Institute of Technology, Rep. No. STF 65A, Trondheim, Norway, June 1982.
9. Johansen, R., In-situ Strength of Concrete, the Break-off Method, American Concrete Institute, Farmington Hills, MI, 1979, 45.

10. Nishikawa, A., A Nondestructive Testing Procedure for In-Place Evaluation of Flexural Strength of Concrete, Rep. No. JHRP 83-10, Joint Highway Research Project, School of Civil Engineering, Purdue University, West Lafayette, IN, 1983.
11. Smith, L., Evaluation of the Scancem Break-Off Tester, Ministry of Works and Development, Central Laboratories, Rep. No. 86/6, New Zealand, 1986.
12. Dahl-Jorgensen, E. and Johansen, R., General and Specialized Use of the Break-Off Concrete Strength Test Method, ACI, SP 82-15, 1984, 294.
13. Hassaballah, A., Evaluation of In-Place Crushed Aggregates Concrete by the Break-Off Method, M.S. thesis, Department of Civil Engineering and Mechanics, University of Wisconsin–Milwaukee, December 1987.
14. Salamech, Z., Evaluation of In-Place Rounded Aggregates Concrete by the Break-Off Method, M.S. thesis, Department of Civil Engineering and Mechanics, University of Wisconsin–Milwaukee, December 1987.
15. Naik, T.R., Salameh, Z., and Hassaballah, A., Evaluation of In-Place Strength of Concrete by the Break-Off Method, Department of Civil Engineering and Mechanics, University of Wisconsin–Milwaukee, March 1988.
16. Dahl-Jorgensen, E., Break-Off and Pull-Out Methods for Testing Epoxy-Concrete Bonding Strength, Project No. 160382, The Foundation of Scientific and Industrial Research of the Norwegian Institute of Technology, Trondheim, Norway, September 1982.
17. Carlsson, M., Eeg, I., and Jahren, P., Field Experience in the Use of Break-Off Tester, ACI, SP 82-14, 1984.
18. Barker, M. and Ramirez, J., Determination of Concrete Strengths Using Break-Off Tester, School of Civil Engineering, Purdue University, West Lafayette, IN, 1987.
19. Nordtest Method NTBUILD 212, Edition 2, Approved 1984-05.
20. Swedish Standard, SS 13723l9, Approved 1983-06.
21. ASTM C1150, Standard Test Method for the Break-Off Number of Concrete, *Annual Book of ASTM Standards*, Vol. 04.02, 1997.
22. ASTM C1150, Standard Test Method for the Break-Off Number of Concrete, *Annual Book of ASTM Standards*, Vol. 04.02, 640, 2002.

5

The Maturity Method*

5.1 Introduction

5.2 Historical Background
Maturity Functions • Strength–Maturity Relationships • Summary

5.3 Theoretical Basis
Strength Gain of Concrete • Maturity Functions • Experimental Results • Values of Activation Energy • Relative Strength Gain • Summary

5.4 Application of Maturity Method
Basic Principle • Maturity Instruments • Maturity Method Combined with Other Methods • Illustrative Examples • Maturity and Other Properties • Application to High-Strength Concrete • Application in Pavement and Bridge Construction • Summary

5.5 Standard Practice
Datum Temperature or Activation Energy • Strength–Maturity Relationship • Estimating In-Place Strength

5.6 Conclusion

Nicholas J. Carino
National Institute of Standards and Technology

This chapter reviews the history and technical basis of the maturity method, a technique for estimating the strength gain of concrete based on the measured temperature history during curing. The combined effects of time and temperature on strength gain are quantified by means of a maturity function. Various maturity functions are reviewed critically. It is shown that the traditional Nurse-Saul maturity function is inferior compared with the function based on the Arrhenius equation. The concept of equivalent age, which is the most convenient measure of maturity, is explained. The strength gain of a specific concrete mixture is estimated using the measured maturity and the strength vs. maturity relationship for that mixture. Various proposed strength-maturity relationships are reviewed. It is explained why the maturity method can only be used reliably to estimate relative strength. Examples are presented to illustrate how this technique can be used in combination with other in-place tests of concrete strength. The ASTM standard dealing with the method is also summarized.

5.1 Introduction

As is well known, the strength of a given concrete mixture, which has been properly placed, consolidated, and cured, is a function of its age and temperature history. At early ages, temperature has a dramatic effect on strength development. This temperature dependence presents problems in trying to estimate the in-place strength based on strength development data obtained under standard laboratory conditions.

*Contribution of the National Institute of Standards and Technology and not subject to copyright in the United States.

Around 1950, an approach was proposed to account for the combined effects of time and temperature on strength development of concrete. The motivation was the need for a method to estimate the effects of steam curing treatments on strength development. Subsequently, application of the method was extended to ordinary curing conditions. It was proposed that the measured temperature history during the curing period could be used to compute a single number that would be indicative of the concrete strength. Saul called this single factor "maturity," and he proposed the well-known "maturity rule" for estimating the strength of concrete.[1]

Following the publication of the maturity rule, there were reports of its validity.[2,3] There were, however, reports of cases where the method failed.[4-6] From the time of the initial proposal, extensive research has been performed and modifications have been proposed for improving the accuracy of strength estimated from temperature history. Today, the maturity method is viewed as a useful and simple means for accounting approximately for the complex effects of time and temperature on strength development. The method is used during the curing period and is not applicable to existing concrete structures. Various standards and recommended practices dealing with curing, cold weather protection, and formwork removal refer to the maturity method.[7–11]

The objective of this chapter is to provide the reader with the knowledge needed to correctly use the maturity method to estimate the strength of concrete in a structure while concrete is curing. The chapter begins with a brief review of the historical developments leading to current practice. This is followed by an analytical treatment of concrete strength gain to establish the basis for maturity method. After the theoretical development, practical aspects in applying the technique are discussed. Last, a standard practice[11] for implementing the maturity method is summarized.

5.2 Historical Background

A comprehensive review of the maturity method prior to 1971 was published by Malhotra.[12] Therefore, only a brief history is presented in this section. First, the various maturity functions that have been proposed to account for the effects of temperature and time on strength development are discussed. This is followed by a discussion of the relationships that have been proposed to represent strength development as a function of maturity.

5.2.1 Maturity Functions

Maturity functions are used to convert the actual temperature history of the concrete to a factor that is indicative of how much strength has developed. The roots of the earliest maturity function are found in a series of papers dealing with accelerated curing methods for concrete. In 1949, McIntosh[13] reported on experiments to develop procedures to estimate the strength development of concrete during electric curing. He suggested that the product of time and concrete temperature above a datum temperature could be used to summarize the effects of the curing history. A datum temperature of - 1.1∂C (30∂F) was suggested, and the product of time and temperature above the datum temperature was called the "basic age." However, it was found that when strength development at different temperatures was plotted as a function of basic age, there was not a unique relationship. McIntosh concluded that the strength development of concrete was governed by more complex factors than a simple product of temperature and time.

Soon after publication of McIntosh's work, Nurse[14] wrote on the principles of low-pressure steam curing. He also suggested that the product of time and temperature could be used to summarize the effects of different steam curing cycles. Nurse did not suggest using a datum temperature, and his calculations involved the curing chamber temperatures, not the actual concrete temperatures. Nevertheless, he showed that when the relative strength development was plotted as a function of the product of time and temperature, the data for different concretes and curing cycles fell reasonably close to a single nonlinear curve. This was the first evidence to show that the product of time and temperature could be used to approximate the combined effects of these two factors on strength development.

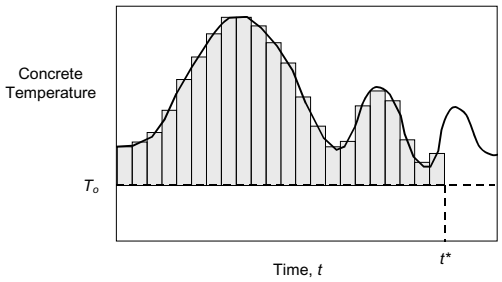

FIGURE 5.1 The Nurse–Saul maturity function.

In 1951, Saul[1] summarized the conclusions drawn from research on the principles of steam curing performed at the Cement and Concrete Association in England. The term *maturity* was for the first time linked to the product of time and temperature. Saul suggested that maturity should be calculated with respect to a "datum temperature," which is the lowest temperature at which strength gain is observed. Thus, maturity is computed from the temperature history using the following:

$$M = \sum_{0}^{t} (T - T_0)\Delta t \tag{5.1}$$

where

M = maturity* at age t
T = average temperature of the concrete during time interval Δt
T_0 = datum temperature

This equation has become known as the Nurse- Saul function. In using Equation 5.1, only time intervals in which the concrete temperature is greater than T_0 are considered as contributing to strength gain. If the concrete temperature is plotted vs. age, Equation 5.1 is simply equal to the area between the datum temperature and the temperature curve. This concept is demonstrated in Figure 5.1, which shows the temperature history at a particular point in a concrete member; the shaded area represents the maturity (temperature- time factor) at age t^*.

Saul recognized that once concrete has set it will continue to harden (gain strength) at temperatures below 0∂C (32∂F). Thus, he recommended a datum temperature of - 10.5∂C (13°F) for use in Equation 5.1. In 1956, Plowman[3] reported the results of a study designed to determine the temperature at which concrete, which has previously undergone setting, ceases to gain strength with time. Based on test data, Plowman suggested a value of - 12∂C (11∂F) for the datum temperature. Generally, a value of –10∂C (14∂F) has been used in subsequent applications of the Nurse–Saul function.

In his 1951 paper, Saul presented the principle that has become known as the "maturity rule":[1]

> Concrete of the same mix at the same maturity (reckoned in temperature–time) has approximately the same strength whatever combination of temperature and time go to make up that maturity.

In applying the rule to steam-cured concrete, Saul noted that this principle was valid provided the concrete temperature did not reach about 50∂C within the first 2 h or about 100∂C within the first 6 h after the start of mixing. If the early-age temperature rise was excessive, the Nurse–Saul maturity function underestimated strength during the first few hours of treatment and the strength at later ages was adversely affected. Thus, Saul recognized important limitations of the maturity rule and the Nurse–Saul maturity function. These limitations are discussed further in the next section.

*The "temperature- time factor" is the accepted term for this quantity.

The Nurse–Saul function can be used to convert a given temperature–time curing history to an equivalent age of curing at a reference temperature as follows:

$$t_e = \sum \frac{(T - T_0)}{(T_r - T_0)} \Delta t \tag{5.2}$$

where

t_e = equivalent age at the reference temperature
T_r = reference temperature

In this case equivalent age represents the duration of the curing period at the reference temperature that would result in the same maturity as the curing period at other temperatures. The equivalent age concept, originally introduced by Rastrup,[15] is a convenient method for using other functions besides Equation 5.1 to account for the combined effects of time and temperature on strength development.

Equation 5.2 can be written as follows:

$$t_e = \sum \alpha \, \Delta t \tag{5.3a}$$

where

$$\alpha = \frac{(T - T_0)}{(T_r - T_0)} \tag{5.3b}$$

The ratio α, which is called the "age conversion factor," has a simple interpretation: it converts a curing interval Δt to the equivalent curing interval at the standard reference temperature. For example, if T_0 = - 10∂C (14∂F), a curing period of 2 h at 43∂C (109∂F) is equivalent to 1.6 ¥ 2 = 3.2 h at 23∂C (73∂F). Note that according to Equation 5.3, the age conversion factor is a linear function of the curing temperature. This is an important characteristic of the Nurse–Saul function and it helps explain some of its observed deficiencies.

Saul's introduction of the maturity rule was an outgrowth of studies dealing with accelerated curing. In 1953, Bergstrom[2] demonstrated that the maturity method was equally applicable for curing at normal temperatures. He used the maturity method to analyze previously published data on the effects of temperature on strength development. To calculate maturity, Bergstrom assumed that the temperatures of the concrete specimens were the same as the ambient curing temperatures. He found that, for a given concrete, there was generally little deviation of the strength data from a common strength vs. maturity curve.

In 1954, Rastrup[15] proposed the following function for equivalent age, which was based on a "well-known axiom from physical chemistry which states: the reaction velocity is doubled if the temperature … is increased by 10∂C."

$$t_e = \sum 2^{(T - T_r)/10} \Delta t \tag{5.4}$$

For example, a curing period at 43∂C (109∂F) is equivalent to four times the same curing period at 23∂C (73∂F). Wastlund[16] reported, however, that subsequent studies at the Swedish Cement and Concrete Research Institute showed that over a wide temperature range the Rastrup function was not as accurate as the Nurse–Saul function in representing the effects of time and temperature.

In 1956, Plowman[3] presented a landmark paper on the maturity method. He made standard concrete cubes that were cured at temperatures varying between - 11.5 and 18∂C (11 to 64∂F). Cubes were tested at regular intervals, and he demonstrated that for each mixture there was a unique relationship between strength and maturity. An important detail in Plowman's procedure was that all specimens were initially

cured at a normal curing temperature (16 to 19∂C, or 61 to 66∂F) for 24 h before being exposed to the different curing temperatures. Thus, the early-age temperature histories of all specimens were identical and their long-term strengths were approximately equal. As will be made clearer, this is why Plowman was able to obtain unique strength–maturity relationships for each mixture.

In 1956, a series of papers dealing with the maturity method was presented at the first RILEM Symposium on Winter Concreting. McIntosh[4] reported on the results of a study in which specimens were exposed to different early-age temperatures. For equal maturities (based on the Nurse–Saul function), it was shown that specimens exposed to low early-age temperature were weaker at early maturities and stronger at later maturities than specimens exposed to a higher early-age temperature. It was concluded that a maturity function based on the product of time and temperature above a datum value cannot account for the "quality of cure" as affected by initial curing temperature. Two years later, Klieger[5] also noted that initial curing temperature influenced the shape of the strength–maturity relationship.

In 1962, Alexander and Taplin[6] reported the results of a study to determine whether strength gain of concrete and cement paste obeyed the maturity rule for curing at different temperatures (5, 21, and 42∂C, or 41, 70, and 108∂F). Maturity was calculated using the Nurse- Saul function. In agreement with previous observations of McIntosh and Klieger, they found that the curing temperature had systematic effects on the strength–maturity relationships of the pastes and concretes. The nature of the effects is summarized schematically in Figure 5.2. At the same value of low maturity, a high curing temperature results in greater strength than a low curing temperature. Conversely at later maturities, a high curing temperature results in lower strength. If Saul's maturity rule were correct, there should be a single strength–maturity curve.

In 1968, Verbeck and Helmuth[17] presented a qualitative explanation for the "crossover effect" illustrated in Figure 5.2. They suggested that a higher initial temperature results in more than a proportional increase in the initial rate of hydration. Therefore, during the early stage of curing, when there is rapid strength development, the strength of concrete cured at the high temperature is greater than that of concrete cured at a lower temperature despite having the same maturity according to the Nurse–Saul function. With rapid hydration, however, reaction products do not have time to become uniformly distributed within the pores of the hardening paste. In addition, "shells" made up of low permeability hydration products build up around the cement grains. The nonuniform distribution of hydration products leads to more large pores that reduce strength, and the shell impedes hydration of the unreacted portion of the grains at later ages. Thus, the lower long-term strength under high curing temperature may be a result of the inability of the cement grains to continue hydrating due to the "shell" of low permeability reaction products.

In the late 1960s, there surfaced a new interest in the maturity method. Swenson[18] used the method in a failure investigation to estimate the concrete strength at the time of the collapse. In the United States, Hudson and Steele[19,20] proposed the maturity method to estimate the 28-day strength of concrete based on tests at early ages. Their results were later incorporated into an ASTM Standard.[21]

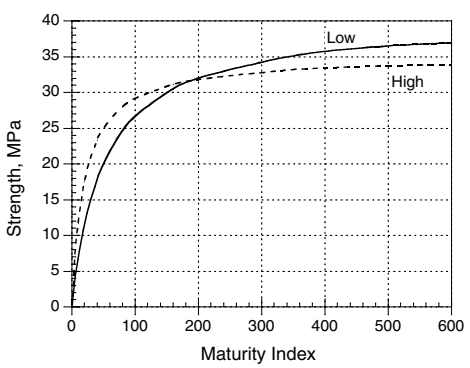

FIGURE 5.2 The effect of early-age curing temperature on the strength–maturity relationship.

Weaver and Sadgrove[22] used the equivalent age concept to develop a manual for formwork removal times under various temperature conditions. They suggested the following new expression to calculate the equivalent age at 20∂C (68∂F):

$$t_e = \frac{\sum (T + 16)^2}{1296} \Delta t \tag{5.5}$$

It was reported that Equation 5.5 gave better strength estimates at low maturity values than the Nurse–Saul function, Equation 5.2. In a later report,[23] Sadgrove noted that, at later maturities, the Nurse–Saul function was more accurate than Equation 5.5.

In the mid 1970s, several reports from Canada appeared dealing with application of the maturity method under field conditions. Bickley[24] reported using it during slipforming of the C.N. Tower in Canada; Mukherjee[25] reported its use for estimating the in-place strength of slabs; and Nisbett and Maitland[26] used the method for in-place strength estimation on a canal bypass project.

In 1960, Copeland et al.[27] suggested that the effects of temperature on the early rate of hydration of cement could be described by the Arrhenius equation. In 1977, Freiesleben Hansen and Pedersen[28] suggested the following expression for equivalent age based on the Arrhenius equation:

$$t_e = \sum_0 e^{\frac{-E}{R}\left[\frac{1}{273 + T} - \frac{1}{273 + T_r}\right]} \Delta t \tag{5.6}$$

where

t_e = equivalent age at the reference curing temperature
T = average temperature of concrete during time interval Δt, ∂C
T_r = reference temperature, ∂C
E = activation energy, J/mol
R = universal gas constant, 8.3144 J/(mol K)

In Equation 5.6, the exponential function is the age conversion factor and is expressed in terms of the absolute temperature. The exact shape of the curve describing the variation of the age conversion factor with temperature depends on the value of E, which according to Freiesleben Hansen and Pedersen had the following values:

for $T \geq 20$∂C

$$E = 33{,}500 \text{ J/mol} \tag{5.6a}$$

for $T < 20$∂C

$$E = 33{,}500 + 1470\ (20 - T) \text{ J/mol} \tag{5.6b}$$

At this point it is helpful to compare the various age conversion factors that have been proposed for computing equivalent age. Figure 5.3 shows the age conversion factors given by Equations 5.3 through 5.6 for a reference temperature of 20∂C (68∂F). There are several notable observations. For temperatures below 20∂C (68∂F), the three nonlinear equations give similar results and the age conversion factors are lower than those obtained from the linear Nurse–Saul function. For temperatures above 20∂C (68∂F), the linear function yields the lowest age conversion factors, and the nonlinear functions diverge. Equations 5.5 and 5.6 give similar results that are significantly lower than the Rastrup function, Equation 5.4. Which of these functions is the most accurate? In independent studies of various maturity functions, Byfors[29] and Naik[30] demonstrated that, over a wide temperature range, the function based on the Arrhenius equation, Equation 5.6, was best able to account for the effects of temperature on strength gain. The next section of this chapter discusses the basis for the maturity method and explains why Equation 5.6 has been found to be superior to other maturity functions.

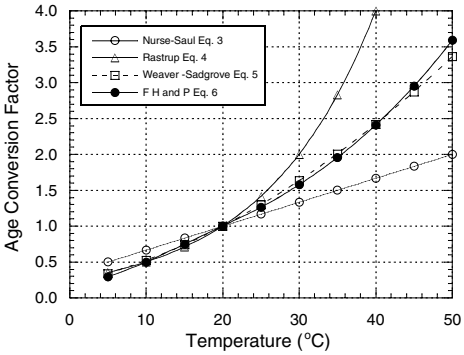

FIGURE 5.3 Various proposed functions to represent temperature dependence of the age conversion factor used to compute equivalent age.

As a result of its investigations of construction failures involving concrete, the U.S. National Bureau of Standards* (NBS) undertook research on the application of the maturity method as a tool for estimating in-place strength of concrete at early ages. Studies at the NBS demonstrated that the Nurse–Saul function was applicable under certain conditions, but they showed also that the function had deficiencies. Lew and Reichard[31] reported that the Nurse–Saul function could be used to estimate the development of other mechanical properties of concrete besides compressive strength. The development of indirect tensile strength, modulus of elasticity and pullout bond strength of steel bars under different curing temperatures could be related to maturity (temperature–time factor). The initial concrete temperature was constant for all specimens, and specimens were moved into the different temperature chambers soon after molding had been completed.

In a later study at NBS,[32] the applicability of the maturity method under simulated field conditions was investigated. Three different concrete mixtures were used to fabricate slabs containing push-out cylinder molds as described in ASTM C 873.[33] In addition, push-out cylinder molds were filled with concrete and stored in a moist curing room. The slabs were cured outdoors (during the spring). The objective was to determine whether the strength–maturity relationships for the field-cured push-out cylinders were the same as those for the companion laboratory-cured cylinders. The results of this study were perplexing: for one mixture there was good agreement between the strengths of field-cured and laboratory-cured specimens at equal temperature–time factors. For the other mixtures there were significant differences. Examination of the temperature histories of all specimens revealed that, for those two mixtures, the outdoor-cured specimens experienced different early-age temperatures than the laboratory-cured specimens. Specimens with higher early-age temperatures resulted in lower long-term strength. Therefore, a unique strength–maturity relationship did not exist for a single concrete mixture. Thus, the "crossover" effect reported in 1956 by McIntosh[4] resurfaced. Subsequent tests at the NBS confirmed the importance of early-age temperature on the resulting strength–maturity relationship, and it appeared that "early age" could be as early as the first 6 h.

NBS later embarked on a fundamental study of the maturity method to gain a basic understanding of the cause of the "crossover" effect and to develop alternative procedures to eliminate the problem.[34–37] The findings of this study are reviewed in Section 5.3, dealing with the basis of the maturity method, where the inherent deficiencies of the maturity rule and the Nurse–Saul function are explained.

5.2.2 Strength–Maturity Relationships

The previous subsection reviewed functions proposed to calculate a maturity index (temperature–time factor or equivalent age) based on the temperature history of the concrete. Proposed functions to relate

*Name has been changed to the National Institute of Standards and Technology.

concrete strength to the maturity index are considered next. In this discussion, the term *maturity* refers to either temperature–time factor computed using the Nurse- Saul function or equivalent age computed using any of the maturity functions.

In 1956, Nykanen[38] proposed an exponential strength–maturity relationship as follows:

$$S = S_{\infty}(1 - e^{kM}) \tag{5.7}$$

where

S = compressive strength
S_{∞} = limiting compressive strength
M = maturity index
k = a constant

The limiting compressive strength is a function of the water–cement ratio. The constant k is related to the initial rate of strength development. According to Nykanen, the value of k is expected to depend on the water–cement ratio and the type of cement.

Plowman[3] observed that when strength was plotted as a function of the logarithm of maturity (based on the Nurse–Saul function) the data fell very close to a straight line. Therefore, he suggested the following strength–maturity relationship:

$$S = a + b\log(M) \tag{5.8}$$

The constants a and b are related to the water–cement ratio of the concrete and the type of cement. The publication of this relationship led to controversial discussions.[39] The following major points were raised, indicating the limitations of Plowman's proposal:

- The relationship predicts ever-increasing strength with increasing maturity.
- The linear relationship is not valid at very early maturities.
- Only intermediate maturity values result in an approximately linear relationship between strength and the logarithm of maturity.

In 1956, Bernhardt[40] proposed a hyperbolic strength–maturity relationship. A similar function was independently proposed by Goral[41] to describe the development of strength with age at a constant temperature. Later, Committee 229 of the American Concrete Institute (ACI) adopted the same function to estimate concrete strength at different ages.[42] In 1971, Chin[43] proposed the same function and described a procedure to evaluate the function for given data. The hyperbolic strength–maturity function can be expressed in the following form:

$$S = \frac{M}{\frac{1}{A} + \frac{M}{S_{\infty}}} \tag{5.9}$$

where

M = maturity index
S_{∞} = limiting strength
A = initial slope of strength–maturity curve

The shape of this curve is controlled by the value of the initial slope. Figure 5.4A shows two curves that obey Equation 5.9, but have different initial slopes. As the initial slope increases, strength approaches the limiting strength S_{∞} more rapidly as maturity increases.

The hyperbolic equation can be transformed into the following linear equation:

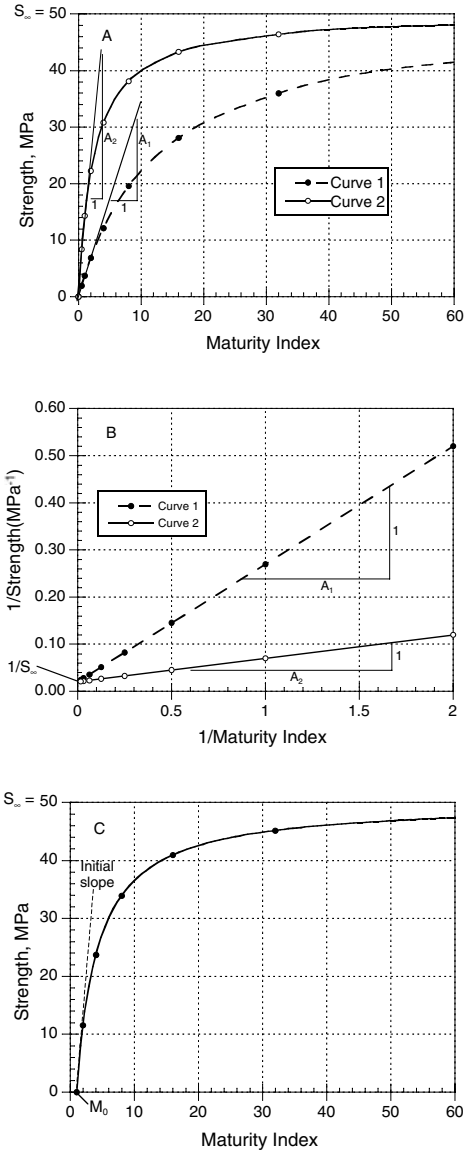

FIGURE 5.4 (A) Hyperbolic strength–maturity relationships having different initial slopes but the same limiting strength. (B) Plotting the reciprocal of strength vs. the reciprocal of maturity index transforms hyperbolic curves in Part A into straight lines. (C) Hyperbolic strength–maturity relationship using an offset maturity.

$$\frac{1}{S} = \frac{1}{S_{\cdot}} + \frac{1}{A}\frac{1}{M} \tag{5.10}$$

Thus, if test data obey the hyperbolic function, the data would lie on a straight line when the inverse of strength is plotted vs. the inverse of the maturity index. The intercept of the line equals the inverse of the limiting strength, and the slope of the line equals the inverse of the initial slope of the hyperbolic curve. Figure 5.4B shows the straight lines representing the two hyperbolas in Figure 5.4A. Because the hyperbolas have the same limiting strength, the straight lines have the same intercept. Note that a steeper straight line corresponds to a lower rate of initial strength gain.

Chin demonstrated that the hyperbolic function fitted his data well,[44] and a similar good fit was obtained in one of the NBS studies.[32] The author[45] of this chapter pointed out, however, that Equation 5.9 is not a good representation of the strength–maturity function at low values of maturity index. The reason is because Equation 5.9 assumes that strength development begins at $M = 0$. In reality, strength development does not begin until after setting has occurred. Therefore, following an idea first suggested by McIntosh,[4] the author introduced an "offset" maturity, M_0, to account for the fact that strength development does not begin until a finite value of the maturity index has been reached.[34] Thus, Equation 5.9 is modified into the following form:

$$S = \frac{M - M_0}{\frac{1}{A} + \frac{M - M_0}{S_u}} \tag{5.11}$$

Figure 5.4C is a plot of Equation 5.11. The hyperbola in Figure 5.4C is similar to curve 1 in Figure 5.4A, except that the curve has been shifted to the right by a value equal to M_0. The linear transformation of Equation 5.11 is similar to Equation 5.10 except that the term $(M - M_0)$ replaces M. If the offset maturity is not used, actual strength–maturity data at low maturities (generally corresponding to strengths below one half the limiting strength) will not follow a straight line when the inverse plot is used.[45]

Lew and Reichard[46] proposed another strength–maturity relationship. Based on their test data and previously published data, they recommended the following strength–maturity relationship:

$$S = \frac{K}{1 + D[\log(M - 16.70]^b} \tag{5.12}$$

This function was proposed as an improvement of Plowman's equation (Equation 5.8) in that strength approached a limiting value with increasing maturity. The coefficient b was found to vary between –1.5 and –4.3, depending on the water–cement ratio and type of cement. The coefficient D, which is related to the rate of strength gain, was also found to depend on water–cement ratio and type of cement. The coefficient K is the limiting strength, which was of course found to depend strongly on the water–cement ratio and to a lesser degree on the type of cement. The three coefficients for Equation 5.12 were based on using the Nurse–Saul maturity function with $T_0 = -12.2$∂C (10∂F). An offset maturity index, M_0, of 16.7∂C-days (30∂F-days) represented the maturity index below which compressive strength was effectively zero. Plots were provided[46] showing the variation of the coefficients for different water–cement ratios and cement types (ASTM Type I and III). It was suggested that a user could determine an approximate strength–maturity relationship for a particular concrete mixture by choosing the appropriate values of K, D, and b from the published figures.

Freiesleben Hansen and Pedersen[47] suggested that the strength–maturity relationship should be similar to the relationship between heat of hydration and maturity. They proposed the following strength–maturity relationship:

$$S = S_u \, e^{-\left(\frac{\tau}{t}\right)^{-a}} \tag{5.13}$$

where

S_u = limiting strength
M = maturity index
τ = characteristic time constant
a = shape parameter

This relationship attempts to model the early part of the strength gain curve of concrete in that rapid strength development begins after a certain maturity has been attained. Figure 5.5 shows three curves

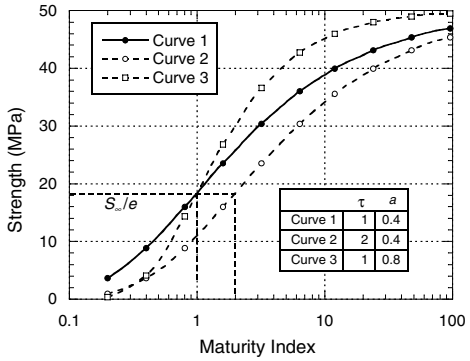

FIGURE 5.5 Effect of the time constant (a) and shape parameter ($\mathbf{t}$) on the strength–maturity relationship given by Equation 5.13.

that obey Equation 5.13, but have different values of the time constant and shape parameter. To accentuate the differences among the curves, strength is plotted as a function of the logarithm of maturity. Curve 2 has the same value of the shape parameter, a, as curve 1 but has a higher value of the time constant, $\mathbf{t}$. Curve 3 has the same value of $\mathbf{t}$ as curve 1 but has a higher value of a. The time constant has the following significance: when the maturity equals the value of $\mathbf{t}$, the strength = $S_\infty/e = 0.37\,S_\infty$. It is seen that changing the value of the time constant preserves the same general shape of the curve while shifting it to the left or right. Changing the value of the shape parameter alters the shape of the curve. As the value of a increases, the curve has a more pronounced S shape, as shown by curve 3.

Which of these various strength–maturity relationships best represents actual strength gain data? Table 5.1 lists compressive strength vs. age data for concrete cylinders cured in a water bath maintained at 23∂C (73∂F). The mixture had a water–cement ratio of 0.45 and was made with Type I cement. These data were used to obtain the best-fit curves for the strength–maturity relationships that have been discussed. The maturity index is taken to be the equivalent age at 23∂C (73∂F). Therefore, the ages in Table 5.1 are equivalent ages at 23∂C (73∂F). The strength data and the various best-fit curves are plotted in Figure 5.6. It is seen that for strength below about 50% of the limiting strength, all curves accurately describe strength development. At higher strength levels, however, the relationships proposed by Nykanen (Equation 5.7) and by Plowman (Equation 5.8) do not model strength gain as accurately as the others. For the data in Table 5.1, Equations 5.11, 5.12, and 5.13 provide accurate representations of the actual strength gain, and the only differences among them are the values of the limiting strength.

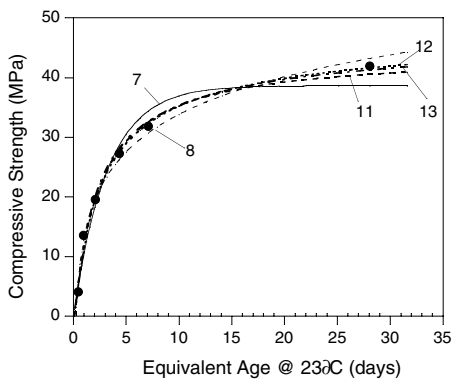

FIGURE 5.6 Comparison of various strength–maturity relationships with measured compressive strength of cylinders.

TABLE 5.1 Compressive Strength vs. Age at 22∂C (w/c = 0.45, Type I Cement)

Age (days)	Compressive Strength[a] (MPa)	(psi)
0.45	4.1	595
0.98	13.5	1960
2.06	19.5	2835
4.33	27.2	3950
7.11	31.8	4620
14.11	36.4	5290
28.06	41.9	6080

[a] 100 ¥ 200-mm (4 ¥ 8 in.) cylinders.
Source: Tank, R.C. and Carino, N.J., *ACI Mater. J.*, 88(1), 74, 1991.

5.2.3 Summary

This section has presented a brief review of the history of the maturity method. Various maturity functions have been proposed to account for the effects of time and temperature on the strength development of concrete. It is now generally recognized that the traditional Nurse–Saul function does not accurately represent time–temperature effects. Other maturity functions have been proposed that are more accurate than this traditional function. These functions are convenient to apply if the equivalent age approach is used to represent the maturity index.

This section has also reviewed some of the proposed functions to represent the relationship between maturity index and strength development. These relationships are useful in computer applications of the maturity method, where the functions are used to estimate the strength based on the measured maturity of the in-place concrete. Regardless of which relationship is chosen, the key point is that the coefficients that define the exact shape of the curves depend on the particular concrete mixture.

The next section presents a theoretical basis for the maturity method. At the same time, it explains why some maturity functions are superior to others.

5.3 Theoretical Basis

The Nurse–Saul function was proposed as an approximate method to account for the effects of time and temperature on concrete strength, but its theoretical basis was not explained. Its applicability was based on empirical evidence. In this section, the general form of the maturity function is derived, and it is shown that Equation 5.1 arises by assuming a specific type of behavior. It is also shown why other maturity functions are superior to the Nurse–Saul function.

5.3.1 Strength Gain of Concrete

The development of a mathematical expression to describe the compressive strength development of concrete is discussed first. The derivation follows ideas originally presented in 1956 by Bernhardt.[40] The rate of strength gain (dS/dt) at any age (t) is assumed to be a function of the current strength (S) and the temperature (T), that is,

$$\frac{dS}{dt} = f(S)\,k(T) \tag{5.14}$$

where

$f(S)$ = a function of strength
$k(T)$ = a function of temperature

Based on empirical evidence, Bernhardt proposed that

$$f(S) = S_\infty \left(1 - \frac{S}{S_\infty}\right) \tag{5.15}$$

where

S_∞ = limiting strength at infinite age

Note that when strength begins to develop $f(S) = S_\infty$. Therefore, the initial rate of strength development is

$$\left.\frac{dS}{dt}\right|_{S=0} = S_\infty\, k(T) \tag{5.16}$$

The temperature function $k(T)$ is called the *rate constant* because it affects the initial rate of strength development.

If S_∞ is assumed to be independent of curing temperature and Equation 5.14 is combined with Equation 5.15, the following integral equation is obtained:

$$\int_0^S \frac{dS}{\left(1 - \frac{S}{S_\infty}\right)^2} = S_\infty \int_{t_0}^{t} k(T)\, dt \tag{5.17}$$

Equation 5.17 departs from Bernhardt's original derivation by introducing the condition that strength gain does not begin until some time, t_0, after mixing. This approximation is introduced to account for the induction period between initial mixing and the start of strength gain described by Equation 5.16.

Note that the integral on the right side of Equation 5.17 involves the product of a temperature-dependent function and time. This integral is the general form of the maturity function, and it will be denoted as $M(t,T)$:

$$M(t,T) = \int_{t_0}^{t} k(T)\, dt \tag{5.18}$$

Integrating the left side of Equation 5.17 and rearranging terms, one obtains the following general strength–maturity relationship:

$$S = S_\infty \frac{M(t,T)}{1 + M(t,T)} \tag{5.19}$$

Comparing Equation 5.19 with Equation 5.9, one sees that they have similar forms. Hence there is a basis for the hyperbolic strength–maturity function proposed by Chin.[43]

Let us now take a closer look at the nature of the maturity function given by Equation 5.18 by considering strength development under constant and variable temperature curing.

5.3.2 Maturity Functions

5.3.2.1 Isothermal Conditions

When curing temperature is constant, the temperature function $k(T)$ has a constant value. Therefore, the maturity function becomes

$$M(t,T) = k_T(t - t_0) \tag{5.20}$$

where

k_T = value of the rate constant at the curing temperature

The strength–maturity relationship, Equation 5.19, becomes the following strength–age relationship:

$$S = S_u \frac{k_T(t - t_0)}{1 + k_T(t - t_0)} \tag{5.21}$$

A plot of Equation 5.21 would be identical to the hyperbolic curve shown in Figure 5.4C except that the units for the X-axis would be age rather than maturity index. An interesting feature of the hyperbolic curve is that the inverse of the rate constant $(1/k_T)$ equals the time beyond t_0 needed to reach 50% of the limiting strength.

An expression similar to Equation 5.21 was derived elegantly by Knudsen[48,49] using a completely different approach from that given here. He worked with the degree of hydration of cement rather than concrete strength. He considered the reaction kinetics of the individual cement grains and the particle size distribution of the grains. The key assumptions in Knudsen's derivation are as follows:

- All cement particles are chemically similar and need be classified only according to their size.
- The cement particles react independently.
- The particle size distribution is described by an exponential equation.
- The kinetic equation for hydration of each particle is also described by an exponential equation.

Knudsen called the results of his derivation the "dispersion model" because the particle size distribution of the cement grains was found to play a dominant role in the overall hydration behavior. According to Knudsen,[48–50] Equation 5.21 is valid when individual cement particles obey linear kinetics.*

Knudsen demonstrated[48,49] that the hyperbolic equation given by Equation 5.21 is valid for strength development and any other property of concrete that is directly related to the extent of cement hydration. In addition, he showed that the rate constant, k_T, depends on the particle size distribution of the cement and the rate constant for each particle (which is temperature dependent). The importance of the particle size distribution on the rate constant was also discussed by Bezjak and Jelenic.[51]

Knudsen's assumption that cement particles react independently is significant. As is well known, hydration products form in the water-filled spaces between cement particles. As the water–cement ratio is lowered, the distance between cement particles is reduced. Therefore, particle interference increases and one would expect the hydration rate to decrease. Thus, Knudsen[48] noted that the assumption of particle independence would be expected to be violated at very low water–cement ratios. Copeland and Kantro[52] showed, however, that for a low water–cement ratio, the effects of particle interference on hydration are not significant at early ages. Knudsen concluded that the assumption of independent particle reaction was not seriously violated at a water–cement ratio as low as 0.4.[48] Thus, it is expected that the rate constant should be independent of the water–cement ratio during the early stages of hydration.

*Parabolic kinetics applies when hydration is controlled by diffusion. For parabolic kinetics, Equation 5.21 is modified by substituting the term $\sqrt{t - t_0}$ in place of $(t - t_0)$.

In summary, the hyperbolic curve given by Equation 5.20 appears to be a soundly based approximation of the strength development of concrete under constant curing temperature. As was shown in Equation 5.18, the integral of the rate constant with respect to time is the general form of the maturity function. The following section examines how the temperature dependence of the rate constant affects the specific form of the maturity function when the curing temperature is not constant.

5.3.2.2 Variable Temperature Conditions

When the curing temperature is not constant, the temperature function $k(T)$ is not constant. Therefore, the temperature dependence of the rate constant must be considered in computing the maturity index. The simplest case is to assume a linear relationship, that is,

$$k(T) = K(T - T_0) \tag{5.22}$$

where

T_0 = the temperature corresponding to $k(T) = 0$
K = slope of the straight line

Substituting Equation 5.22 into Equation 5.17, one can express the maturity function as

$$M(t,T) = \int_{t_0}^{t} K(T - T_0)\,dt = K\int_{0}^{t}(T - T_0)\,dt - K\int_{0}^{t_0}(T - T_0)\,dt \tag{5.23}$$

The two terms on the right-hand side of Equation 5.23 are time–temperature factors based on the Nurse–Saul function, Equation 5.1. If these terms are called M and M_0, the maturity function is

$$M(t,T) = K(M - M_0) \tag{5.24}$$

Substituting Equation 5.24 into Equation 5.19, we obtain the following strength–maturity relationship:

$$S = S_u \frac{K(M - M_0)}{1 + K(M - M_0)} \tag{5.25}$$

It can be shown that Equation 5.25 is identical to Equation 5.11 by making the substitution $A = KS_u$.

The above derivation shows that if the rate constant, $k(T)$, is assumed to vary linearly with the curing temperature, the resulting maturity function is the traditional Nurse–Saul function. Thus, the fundamental assumption of the Nurse–Saul function is revealed, namely, the rate constant is a linear function of temperature.

At this point, it is helpful to examine the relationship between equivalent age and the general maturity function. Equivalent age represents the age at a reference curing temperature that results in the same maturity as under the actual curing temperature. Using Equation 5.18 and performing the integration from $t = 0$, we obtain the following:

$$t_e k_r = \int_{0}^{t} k(T)\,dt \tag{5.26a}$$

$$t_e = \int_{0}^{t} \frac{k(T)}{k_r}\,dt \tag{5.26b}$$

where

t_e = equivalent age at the reference temperature, T_r,
k_r = value of the rate constant at the reference temperature

Hence the ratio of value of the rate constant at any temperature to the value at the reference temperature equals a, the age conversion factor* previously mentioned. When the rate constant is a linear function of temperature, Equation 5.26b is similar to the previous Equation 5.2, which was based on the Nurse–Saul function.

There is, however, no technical basis for the linear temperature dependence of the rate constant. Since hydration is an exothermic chemical reaction, it is reasonable to assume that the rate constant should vary with temperature according to the Arrhenius equation, that is,

$$k(T) = b\, e^{\left(\frac{-E}{R(273+T)}\right)} \tag{5.27}$$

where

b = a constant
E = activation energy
R = universal gas constant

The age conversion factor obtained using Equation 5.27 is identical to the relationship proposed by Freiesleben Hansen and Pedersen,[28] which was previously given as Equation 5.6.

In summary, the mathematical form of the age conversion factor depends on the function used to represent the variation of the rate constant with temperature. Different rate constant vs. temperature functions account for the different curves in Figure 5.3. The next step is to examine how the actual variation of the rate constant with temperature compares with these proposed functions.

5.3.3 Experimental Results

Strength–age data for mortar cubes cured at constant temperatures of approximately 5, 12, 23, 32, and 43∂C (41, 54, 73, 90, and 109∂F) are used to compare the temperature dependence of the rate constant with the linear and Arrhenius functions. Two mortar mixtures, having water–cement ratios of 0.43 and 0.56, were used to prepare 51-mm (2-in.) cubes. The specimens were prepared in an environmental chamber at the above curing temperatures, and the molded cubes were stored in water baths maintained within ±1∂C (2∂F) of the nominal values. For each curing temperature, three cubes were tested in compression at each of seven test ages. Complete test results are given elsewhere.[34,37]

The strength–age data for each curing temperature was fitted by the hyperbolic relationship given by Equation 5.21, which can be transformed into the following linear equation:

$$\frac{1}{S} = \frac{1}{S_\infty} + \frac{1}{k_T S_\infty}\frac{1}{(t - t_0)} \tag{5.28}$$

There are several approaches to estimate the values of the three parameters (S_∞, k_T, and t_0). The simplest approach is to use a general least-squares curve fitting computer program (such as Reference 54). This procedure was used in Reference 34. Another approach involves trial and error. A value t_0 is assumed and the values of S_∞ and k_T are evaluated using linear regression analysis of the transformed data, that is, $1/S$ vs. $1/(t - t_0)$. The procedure is repeated for different values of t_0 until the best fit is obtained. A third alternative was suggested by Knudsen[48] and it is discussed here because of its usefulness if a general least-squares curve-fitting program is not available.

*This ratio has also been called the "affinity" ratio.[53]

First, the limiting strength, S_∞, is evaluated by considering strength–age data at later ages. For later age data, we can make the approximation $(t - t_0) = t$, and Equation 5.28 can be rewritten as follows:

$$\frac{1}{S} = \frac{1}{S_\infty} + \frac{1}{k_T S_\infty}\frac{1}{t} \tag{5.29}$$

Thus, a plot of $1/S$ vs. $1/t$ is a straight line. The intercept of the line is obtained from linear regression analysis, and the inverse of the intercept equals the limiting strength. It was found[37] that strength data for equivalent ages beyond about 7 days should be used for this step.

Using the estimated the value of S_∞, Equation 5.21 can be written in following form to estimate k_T and t_0:

$$\frac{S}{S_\infty - S} = -k_T t_0 + k_T t \tag{5.30}$$

Thus, a plot of $S/(S_\infty - S)$ vs. age is a straight line having a slope k_T, which can be evaluated by linear regression analysis. The value of t_0 is equal to the negative value of the intercept divided by the slope. It was found[37] that strength data for equivalent ages up to about 3 to 4 days should be used for this step to obtain the best estimates of k_T and t_0.

The complete results of the above two-step procedure are given in Reference 37, and the resulting values of k_T are listed in Table 5.2. Figure 5.7 shows the values of k_T in Table 5.2 plotted as a function of the curing temperature. It is seen that over the temperature range 5 to 43∂C (41 to 109∂F) the rate constant is a nonlinear function of temperature. These particular data show that water–cement ratio does not have a significant effect on the rate constant, which is consistent with Knudsen's findings.[48]

TABLE 5.2 Values of Rate Constant Based on Compression Tests of Mortar Cubes

w/c = 0.43		*w/c* = 0.56	
Curing Temperature (∂C)	k_T (day^{-1})	Curing Temperature (∂C)	k_T (day^{-1})
5.5	0.116	5.5	0.087
13.0	0.184	12.5	0.203
23.5	0.341	23.0	0.313
32.0	0.571	32.0	0.577
43.0	1.031	43.0	0.944

Source: Carino, N.J., *ASTM J. Cem. Concr. Aggregates*, 6(2), 61, 1984.

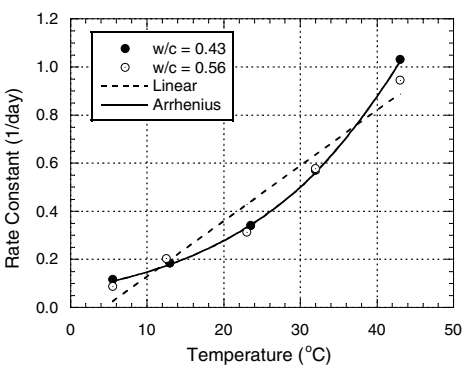

FIGURE 5.7 Variation of rate constant with temperature; results from tests compared with linear and Arrhenius equations.

First, consider whether the Arrhenius equation, Equation 5.27, describes the variation of the rate constant with curing temperature. By taking the natural logarithm of Equation 5.27, the following is obtained:

$$\ln k(T) = \ln b - \frac{E}{R}\frac{1}{(273+T)} \tag{5.31}$$

Thus, the Arrhenius equation is transformed into a linear relationship. The negative of the slope of the straight line is equal to the activation energy divided by the gas constant. Figure 5.8 shows the natural logarithms of the rate constant values in Table 5.2 plotted as a function of the reciprocal of the absolute temperature. Also shown is the best-fit straight line having the following equation:

$$\ln k(T) = 16.65 - 5255\frac{1}{(273+T)} \tag{5.32}$$

The straight line fits the data quite well, so it is concluded that the Arrhenius equation provides a good representation of $k(T)$ over the temperature range 5 to 43∂C (41 to 109∂F). Figure 5.7 shows the best-fit Arrhenius equation compared with the rate constant values.

Next, a straight line was fitted to the rate constant values. The best-fit straight line was found to have the following equation:

$$k(T) = 0.023(T - 4.4\,\partial C) \tag{5.33}$$

This straight line is plotted in Figure 5.7. There are two significant observations. First, the straight line does not accurately represent the observed variation of the rate constant with curing temperature. Therefore, the fundamental assumption in the Nurse–Saul function is not valid for these particular data. Second, the best-fit straight line crosses the temperature axis at 4.4∂C (40∂F). Therefore, if the Nurse–Saul function is used to approximate the effects of temperature over the range 5 to 43∂C (41 to 109∂F), the best results would be obtained by using a datum temperature of 4.4∂C (40∂F) instead of –10∂C (14∂F) as is commonly used.

The rate constant values in Table 5.2 can be converted to age conversion factors by dividing them by the estimated value of the rate constant at the reference temperature. In this discussion the reference temperature is taken to be 23∂C (73∂F). From Equation 5.32, the rate constant is approximately 0.33 day^{-1} at 23∂C (73∂F). The values of the age conversion factors are plotted vs. temperature in Figure 5.9.

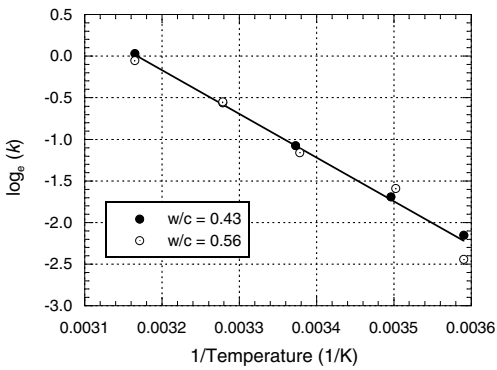

FIGURE 5.8 Natural logarithm of rate constant vs. the inverse of the absolute temperature (Arrhenius plot).

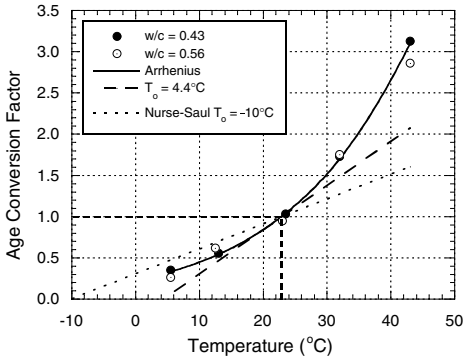

FIGURE 5.9 Variation of age conversion factor with temperature; comparison of data with various maturity functions.

The age conversion factor vs. temperature relationships based on various functions are also shown in Figure 5.9. The equation of the relationship based on the best-fit Arrhenius equation, Equation 5.32, is as follows:

$$a = e^{-5255\left(\frac{1}{273+T} - \frac{1}{296}\right)} \tag{5.34}$$

The dashed straight line is the relationship based on the best-fit straight line, Equation 5.33, and has the following equation:

$$a = \frac{(T - 4.4)}{18.6} \tag{5.35}$$

The dotted line is the linear age conversion factor vs. temperature relationship for a datum temperature of –10∂C (14∂F), as commonly used with the traditional Nurse–Saul maturity function, and has the following equation:

$$a = \frac{(T + 10)}{33} \tag{5.36}$$

Examination of Figure 5.9 shows that neither straight line is an accurate representation of the age conversion factor vs. temperature relationship over the indicated temperature range. The line representing the Nurse–Saul function with $T_0 = -10$∂C (14∂F) overestimates the age conversion factor at temperatures below the reference temperature of 23∂C (73∂F). Thus, using the traditional value of the datum temperature would overestimate the equivalent age. At temperatures above 23∂C, the opposite is true; that is, the equivalent age would be underestimated. On the other hand, using the straight line with $T_0 = 4.4$∂C (40∂F) always underestimates the equivalent age. The amount of underestimation increases as the temperature is farther away from the reference temperature.

The results in Figure 5.9 show that a maturity function that assumes a linear rate constant vs. temperature relationship will not accurately account for temperature effects when the curing temperature is significantly different from the reference temperature. If one wishes to use a linear maturity function because of its simplicity, accuracy can be improved greatly by using two values of the datum temperature. One value would be applicable when the curing temperature is below the reference temperature and the other value would be applicable above the reference temperature. Figure 5.10 illustrates this approach. It is seen that the variation of the rate constant for temperatures between 5 and 23∂C (41 and 73∂F) can be represented accurately by a straight line with a datum temperature of - 2∂C (28∂F). On the other hand,

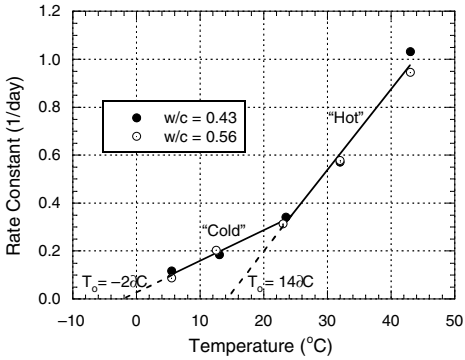

FIGURE 5.10 A bilinear approximation of age conversion factor vs. temperature relationship.

for temperatures between 23 and 43∂C (73 and 109∂F), a straight line with a datum temperature of 14∂C (57∂F) is a good approximation. The best values for the datum temperature depend on the actual shape of the rate constant vs. temperature function and the temperature range over which the linear approximation is made.[37]

5.3.4 Values of Activation Energy

A good maturity function must accurately represent the effect of temperature on the age conversion factor. In the previous section, it was shown that the Arrhenius function fitted experimental data well. Next, we examine the shape of the age conversion factor vs. temperature relationship in more detail.

The value of the activation energy, *E*, in the Arrhenius equation, Equation 5.27, determines the shape of the age conversion factor vs. temperature function. Figure 5.11 shows the variation of the age conversion factor with temperature for activation energy values of 40, 50, and 60 kJ/mol and using the values suggested by Freiesleben Hansen and Pedersen,[28] which were given in Equations 5.6a and 5.6b. The reference temperature is again taken as 23∂C (73∂F). The variation based on the Nurse–Saul function with T_0 = - 10∂C (14∂F) is also shown. It is seen that with increasing value of activation energy, the age conversion factor vs. temperature variation becomes more nonlinear. As a result, attempts to use a linear function as an approximation lead to greater errors for increasing values of activation energy. With this in mind, let us examine the values of activation energy that have been reported by others.

The value of the activation energy for a particular concrete can be determined in several ways. One approach is to make and cure concrete specimens at several different temperatures and analyze the strength–age data in the manner described above. There are, however, alternative possibilities. It has been

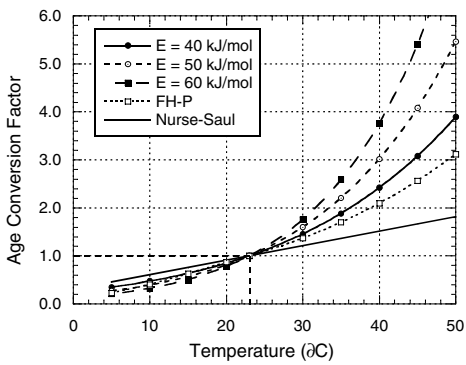

FIGURE 5.11 Effect of activation energy on the age conversion factor vs. temperature relationship using the Arrhenius function.

firmly established that the degree of hydration of cement correlates with the mechanical strength of concrete.[55,56] Thus, it is possible to determine the activation energy from hydration studies of cement pastes. This approach is supported by investigators[53,57,58] who have shown that activation energies based on heats of hydration are similar to those based on the mechanical strength of mortars. In addition, Bresson[59] and Gauthier and Regourd[57] report that similar activation energies are obtained from strength tests of mortar and concrete specimens. This was confirmed in a limited study by the author[37] and in a larger study by Tank and Carino.[60–62] Another approach is to measure the chemical shrinkage of cement pastes.[63,64] Thus, there is significant evidence showing that the activation energy for strength development can be determined without testing bulky concrete specimens.

There are limited published data on the activation energy for strength development of concrete. Table 5.3 lists some of the activation energies that have been reported for different types of cement and using different test methods. The results for ordinary portland cement (ASTM Type I) are in reasonable agreement except for the higher values reported by Geiker.[63,64] It should be mentioned that the values in Table 5.3 represent the activation energy to describe the temperature dependence of the initial rate of property development. Other procedures have been developed that determine activation energy at later stages of property development.[66,67]

Tank and Carino[60–62] conducted an extensive study of the isothermal strength development in concrete and mortar specimens made with different cementitious systems and having two water–cement ratios. The study had several objectives:

1. Verify the applicability of the hyperbolic strength–age model, Equation 5.21, for strength gain under constant temperature curing.
2. Confirm whether tests of mortar specimens result in the same activation energy values as tests of concrete.
3. Determine whether the water–cementitious materials ratio affects the values of activation energy.
4. Determine the effects of admixtures and cement replacements on activation energy.

Specimens were cured in constant temperature water baths at 10, 23, and 40∂C (50, 73, and 104∂F), and strength tests were performed at regular age intervals. The mortars had cement-to-sand proportions (volumetric) that were similar to the cement-to-coarse aggregate proportions of the corresponding concrete.

Tank and Carino found that test data for concrete and mortar specimens obeyed the hyperbolic strength–age model, and the model was used to evaluate the rate constants. Several rate constant vs. temperature functions were examined, including the Arrhenius equation. Table 5.4 summarizes the values of activation energies for the Arrhenius equation. In Figure 5.12A, the activation energy values obtained from mortar tests are compared with the values obtained from concrete tests. The straight line is the line

TABLE 5.3 Activation Energy Values

Cementitious Material	Type of Test	Activation Energy (kJ/mol)	Ref.
Type I (mortar)	Strength	42	34
Type I (mortar)	Strength	44	37
Type I (concrete)	Strength	41	37
OPC (paste)	Heat of hydration	42–47	57, 58
OPC + 70% BFS (paste)	Heat of hydration	56	57, 58
OPC (paste)	Chemical shrinkage	61	63
RHC (paste)	Chemical shrinkage	57	63
OPC (paste)	Chemical shrinkage	67	64
Type I/II (paste)	Heat of hydration	44	65
Type I/II + 50% BFS (paste)	Heat of hydration	49	65

Abbreviations: OPC = ordinary portland cement, BFS = ground blast furnace slag; RHC = rapid hardening cement.

TABLE 5.4 Activation Energy Values Based on Compressive Strength Tests of Concrete Cylinders and Mortar Cubes

	Activation Energy, kJ/mol			
	w/c = 0.45		*w/c* = 0.60	
Cementitious Material	Concrete	Mortar	Concrete	Mortar
Type I	63.6	61.1	48.0	43.6
Type II	51.1	55.4	42.7	41.1
Type III	43.6	40.1	44.0	42.6
Type I + 20% FA	30.0	33.1	31.2	36.6
Type + 50% slag	44.7	42.7	56.0	51.3
Type + Accelerator	44.6	54.1	50.2	52.1
Type I + Retarder	38.7	41.9	38.7	34.1

Source: Carino, N.J. and Tank, R.C., *ACI Mater. J.*, 89(2), 188, 1992.

of equality. It is seen that the results are uniformly distributed about the line. Thus, Tank and Carino verified that the activation energy for a concrete mixture could be obtained from the strength-gain data of mortar cubes.[62]

Figure 5.12B compares the activation energies for the two water–cementitious materials ratios (*w/cm*). Again, the straight line is the line of equality. In this case, the results are not so clear. For some mixtures, the water–cement ratio had no effect, which is in agreement with previous findings.[37,48] With Type I and

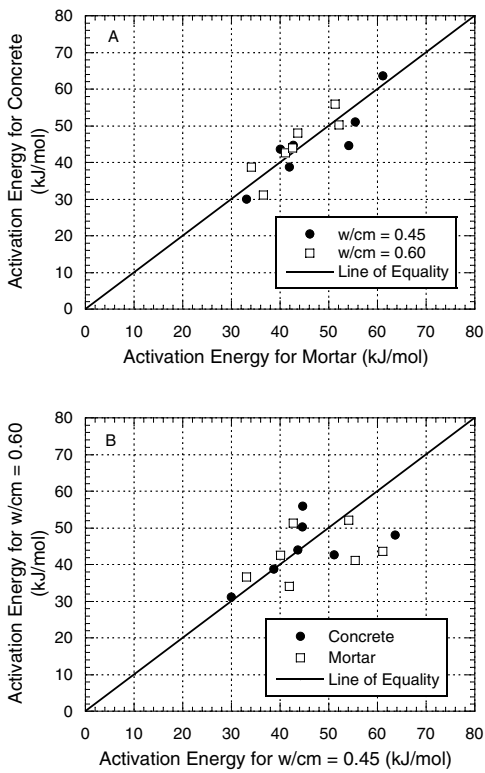

FIGURE 5.12 (A) Activation energy obtained from testing concrete cylinders compared with values obtained from testing mortar cubes. (B) Effect of water–cementitious materials ratio on activation energy.[62]

Type II cement, however, the low *w*/*cm* mixtures had significantly higher activation energies (see Table 5.4). On the other hand, the mixtures with Type I cement plus 50% slag (by mass) had higher values for the high *w*/*cm*. Clearly, more information is required to establish how the water–cement ratio relates to the activation energy.

Comparing the activation energies in Table 5.4 for the mixtures containing Type I cement one can see that use of admixtures or cement replacements alters the activation energy of the concrete. Thus, when admixtures and cementitious additions (fly ash, slag, or silica fume) are used, it is necessary to determine the activation energies for the particular combinations of ingredients in the concrete to be used in construction.

Carino and Tank[62] examined the following alternative relationship to the Arrhenius equation for describing the variation of the rate constant with temperature:

$$k(T) = Ae^{BT} \tag{5.37}$$

where

A = a constant, day^{-1}
B = temperature sensitivity factor, °C^{-1}

The constant A represents the value of the rate constant at $T = 0$∂C. The value of B indicates the sensitivity of the rate constant to changes in curing temperature. For a temperature increase equal to $1/B$, the rate constant increases by a value of approximately 2.72.

Carino and Tank found that Equation 5.37 fitted the results as well as the Arrhenius equation. They also found an empirical relationship between activation energy and temperature sensitivity factor:

$$B = 0.00135\,E \tag{5.38}$$

In Equation 5.38, E is expressed in units of kJ/mol. For example, if the activation energy is 45 kJ/mol, the corresponding value of B is 0.061°C^{-1}, and the rate constant increases by a factor of 2.72 for an increase of 16.4∂C in the curing temperature.

By using Equation 5.37, the expression for the age conversion factor becomes the following:

$$a = e^{B(T - T_r)} \tag{5.39}$$

Equation 5.39 is simpler to use than Equation 5.6 because one does not have to deal with the inverse of the absolute temperature.

This section has reviewed our understanding of values of activation energy that describe the age conversion factor vs. temperature relationship based on the Arrhenius equation. As a result of the scarcity of data, there does not yet exist a thorough understanding of the factors that affect the activation energy. As more data are accumulated, it may be possible to estimate the activation energy of a particular cement based on its chemical composition. When admixtures or supplementary cementitious materials are used, their effects on the activation energy must also be determined. This can probably only be done by testing the combinations of cement and admixtures that will be used in the field concrete.

When accuracy of strength estimations is not crucial, typical published values of activation energy can be used, such as those given in Tables 5.3 and 5.4. When maximum accuracy is desired, the value of activation energy for the particular combination of ingredients should be determined from testing. The applicable procedures are given in Section 5.5.

5.3.5 Relative Strength Gain

The maturity rule, as proposed by Saul,[1] states that samples of the same concrete will have equal strengths if they have equal maturities, irrespective of their temperature histories. In other words, there exists a

TABLE 5.5 Cylinder Strength vs. Age for Constant Temperature Curing

12∂C			21∂C			32∂C		
Age (days)	Strength (psi)	Strength (MPa)	Age (days)	Strength (psi)	Strength (MPa)	Age (days)	Strength (psi)	Strength (MPa)
0.92	705	4.9	0.51	510	3.5	0.37	980	6.8
1.8	1935	13.3	1.0	1680	11.6	0.8	1925	13.3
5.5	3710	25.6	3.0	3075	21.2	1.9	3040	20.9
12.1	4720	32.5	7.0	4210	29.0	5.0	4045	27.9
26.0	5390	37.1	13.2	4990	34.4	10.0	4530	31.2
46.0	6075	41.9	28.0	5490	37.8	20.8	4770	32.9
S_∞ =	6470	14.6		6060	41.8		5080	35.0
k_T =	0.265 day^{-1}		0.361 day^{-1}			0.815 day^{-1}		

Source: Carino, N.J., *ASTM J. Cem. Concr. Aggregates*, 6(2), 61, 1984.

unique strength–maturity relationship for a given concrete mixture. This section discusses why the traditional maturity rule is an approximation.

Thus far, it has been assumed that the limiting strength of a concrete mixture subjected to continuous curing is not affected by the early-age temperature history. However, it has been shown that higher early-age temperatures lower the limiting strength.[32,68–72] To illustrate the nature of this problem, Table 5.5 represents strength gain data for concrete cylinders cured at three different temperatures. The complete analysis of the data was reported in Reference 37. The data are plotted in Figure 5.13A along with the best-fit hyperbolic curves. It is clear that the curing temperatures affect not only the initial rate of strength development but also the limiting strength. Table 5.5 shows the limiting strengths and rate constants obtained by regression analysis of the data.

By fitting the Arrhenius equation (Equation 5.27) to the rate constant values in Table 5.5, one finds that the estimated value of the rate constant at a reference temperature of 23∂C (73∂F) equals 0.47 day^{-1}. The ages in Table 5.5 can be converted to equivalent ages at 23∂C (73∂F). Plotting strength vs. equivalent age to compare strength values at equal maturities, one obtains the results in Figure 5.13B. This plot clearly shows that the concrete does not have a unique strength–maturity relationship. Thus, the "maturity rule" will result in erroneous strength estimates, especially at later ages. At this point, the reader might conclude that the maturity method is not very useful. This is, however, not so.

The hyperbolic strength gain equation, Equation 5.21, can be converted to a relative strength gain equation:

$$\frac{S}{S_\infty} = \frac{k_T(t - t_0)}{1 + k_T(t - t_0)} \tag{5.40}$$

Introducing the age conversion factor

$$\alpha = \frac{k_T}{k_r} \tag{5.41}$$

the relative strength gain can be expressed in terms of equivalent age:

$$\frac{S}{S_\infty} = \frac{k_r\alpha(t - t_0)}{1 + k_r\alpha(t - t_0)} \tag{5.42}$$

Equation 5.42 states that there should be a unique relative strength vs. equivalent age curve having an initial slope equal to k_r. This equation has been referred to as the "rate constant model."[62] To test the validity of this assertion, the strength values in Table 5.5 were converted to relative strength by dividing

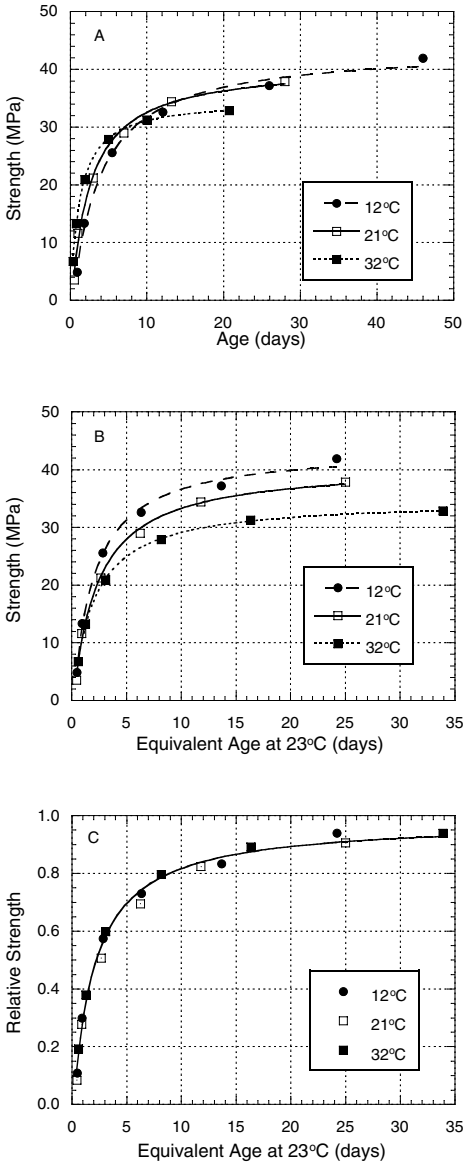

FIGURE 5.13 (A) Compressive strength vs. age for concrete cylinders cured at three temperatures (Type I cement, $w/c = 0.55$).[27] (B) Compressive strength vs. equivalent age at 23∂C for same data as Part A. (C) Relative compressive strength vs. equivalent age at 23∂C for same data as Part A.

them by their corresponding limiting strengths. Figure 5.13C is a plot of the relative strength vs. equivalent age. The data points are indeed grouped around a single curve, whose equation is:

$$\frac{S}{S_{\infty}} = \frac{0.47\,(t_e - 0.16)}{1 + 0.47\,(t_e - 0.16)} \tag{5.43}$$

The above discussion demonstrates that, while the early-age temperature affects the long-term strength, there is no significant effect of curing temperature on the relationship between equivalent age and relative strength. This leads to the following modified maturity rule:

Samples of a given concrete mixture that have the same equivalent age and that have had a sufficient supply of moisture for hydration will have developed equal fractions of their limiting strength irrespective of their actual temperature histories.

The significance of this modified maturity rule is that if one measures only the temperature of concrete while it is curing, only the relative strength gain can be estimated. Additional information is needed to estimate absolute strength values. This subject is discussed further in Section 5.4.

5.3.6 Summary

This section has discussed the theoretical basis of the maturity method, taking into account recent research on the subject. It was shown that under isothermal conditions, the strength gain of concrete could be described by a hyperbolic curve defined by three parameters:

1. The age when strength development is assumed to begin, t_0
2. A rate constant, k_T, which is related to the initial slope of the curve
3. The limiting strength, S.

These parameters can be estimated from regression analysis of strength–age data. It has been shown further that the parameters are temperature dependent.

To describe strength gain under variable temperature conditions, a maturity function is needed to account for the effect of time and temperature. It has been shown that the product of the rate constant and age is the general form of the maturity function. Thus, the key element in arriving at a valid maturity function is describing the relationship between the rate constant and the curing temperature.

The equivalent age approach is a convenient method for accommodating a variety of proposed maturity functions. Curing time intervals at a given temperature are converted to equivalent intervals at a reference temperature. The age conversion factor for each time interval is simply the value of the rate constant at the actual temperature divided by the value at the reference temperature.

If the rate constant is assumed to be a linear function of temperature, the resulting maturity function is identical to the Nurse–Saul function. The key parameter in this approach is the datum temperature, T_0, and it has been shown that the traditional value of - 10∂C is not necessarily the best value to use.

Tests have shown that over a wide temperature range, the rate constant is a nonlinear function of temperature. The Arrhenius equation has been found to describe accurately the relationship between the rate constant and curing temperature. In this case, the key parameter is the activation energy, which defines the temperature sensitivity of the rate constant. The value of activation energy depends on cement chemistry, cement fineness, and type and quantity of cement replacements and admixtures. It is not clear whether the water–cement ratio has a consistent effect on activation energy. For concretes made with ordinary portland cement and without admixtures, it appears that the activation energy is between 40 and 45 kJ/mol.

For greater accuracy in estimated strength, the activation energy for the particular concrete should be determined experimentally. However, the actual concrete mixture does not have to be tested. The required information can be obtained by monitoring the heat of hydration of cement paste, which includes the intended admixtures and cement replacements that may be used. Alternatively, the information can be obtained from the compressive strength development of mortar cubes. The mortar should have the same water–cement ratio as the concrete, and the ratio of cement to sand should be the same as the ratio of cement to coarse aggregate in the concrete.

Finally, it was shown that the limiting strength of a concrete mixture is affected by the early-age temperature history. Thus, there is not a unique strength- equivalent age relationship for a given concrete. There is, however, a unique relative strength vs. equivalent age relationship. This relationship can be developed from strength gain data obtained at a reference curing temperature. A modified maturity rule is proposed that suggests that relative strength can be estimated reliably from the measured temperature history. To estimate the absolute strength level, additional information about the concrete is required.

5.4 Application of Maturity Method

As with the other methods for estimating in-place strength of concrete that are discussed in this book, the maturity method has various applications in concrete construction.[73] It may be used to estimate in-place strength to assure that critical construction operations, such as form removal or application of post-tensioning, can be performed safely. It may be used to decide when sufficient curing has occurred and the concrete can be exposed to ambient conditions without endangering its long-term performance. In addition, it may serve as a tool in planning construction activities.

The method is also useful in laboratory work involving test specimens of different sizes. Because of the heat of hydration, specimens with lower surface-to-volume ratios experience higher early-age temperature rise than specimens with higher ratios. The maturity method can be used to ensure that differently sized specimens are tested at the same maturity. A good example is a testing program conducted to establish the correlation between an in-place test method and cylinder strength. Often the in-place tests are performed on large specimens that experience higher early-age temperatures than the companion cylinder specimens. Failure to perform companion tests at the same maturity will result in inaccurate correlations.

5.4.1 Basic Principle

Proper curing procedures[74] must be used to apply the maturity method for estimating strength development. It is essential that there is an adequate supply of moisture for hydration. If concrete dries out, strength gain ceases but the computed maturity index continues to increase with time. In such a case, strength estimates based on the maturity method are meaningless.

The basic principle in applying the maturity method is illustrated in Figure 5.14. Two phases are involved:

1. Laboratory testing
2. Field measurement of the in-place temperature history

The laboratory testing must be performed before attempting to estimate in-place strength. Two types of laboratory tests may be required. One is used to establish the temperature sensitivity of the rate constant for the particular materials in the concrete. This information, which can be obtained from mortar tests, is needed to develop the correct maturity function for the concrete. The second type of testing establishes

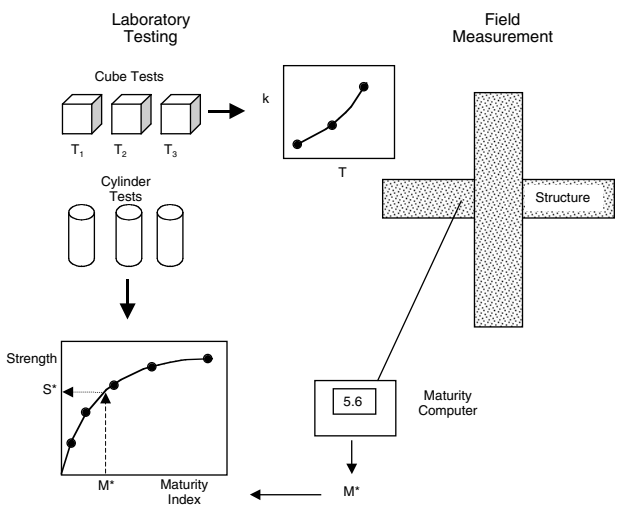

FIGURE 5.14 Schematic of procedures for using maturity method involving laboratory testing and field measurements.

the strength–maturity relationship for the concrete. The latter type of testing is always needed, whereas the need for the first type depends on the desired accuracy of the estimated strength. If maximum accuracy is desired, the activation energy value should be determined experimentally. If this is not the case, typical values of activation energy or datum temperature may be used.

In the field, the temperature history of the structure must be monitored to evaluate the in-place maturity. The in-place maturity is used with the strength–maturity relationship obtained from laboratory testing to estimate the in-place strength. Some of the available instruments for measuring in-place maturity are discussed in the next part of this section. The contractor, testing agency, and design engineer should hold a preconstruction meeting to select appropriate locations for temperature sensors. Consideration should be given to those portions of the structure that are critical because of unfavorable combinations of exposure and required strength. For example, in flat-plate, multistory construction, the slab–column joints are often the most highly stressed regions. During cold weather, corners of structures experience the most severe exposure.

5.4.2 Maturity Instruments

The temperature history of the structure is the basic information needed to evaluate the in-place maturity index (expressed as the temperature–time factor or equivalent age). Therefore, a device is needed to record temperature as a function of time. Analog strip chart recorders or digital data loggers connected to thermocouples embedded in the concrete have been used in the past. The measured thermal history was converted to a maturity index using maturity functions such as Equation 5.1 or Equation 5.6. The calculations have been automated using a personal computer with spreadsheet software.[75] This approach, however, requires manual entry of temperature values at regular time intervals, and is not practical.

A more convenient approach is to use commercial "maturity meters." These are instruments that monitor the temperature history and automatically perform the maturity index calculations. Concrete temperatures are monitored with reusable probes or with expendable thermocouple wires. The earliest models were single channel instruments based on the Nurse–Saul function with a datum temperature of - 10∂C (14∂F). In 1977, Freiesleben Hansen and Pedersen[28] introduced a single-channel maturity computer based on the Arrhenius equation. This instrument computed the equivalent age according to Equation 5.6 and used the relationship for activation energy given in Equations 5.6a and 5.6b.

Multichannel maturity computers have been developed that uses thermocouple wires as sensors, and some permit the use of either the Nurse–Saul function or the Arrhenius equation. In addition, the user can specify the value of the datum temperature or the activation energy. These multichannel meters, such as shown in Figure 5.15, permit each channel to be activated independently as the corresponding sensor is embedded in fresh concrete. Tikalsky et al.[76] compare the features of several commercial maturity meters.

FIGURE 5.15 Example of multichannel maturity meter using thermocouple wires to monitor in-place temperature. (Courtesy of American Engineering Testing, Inc.)

Hansen[77] developed a disposable "mini maturity meter" as an alternative to the more expensive maturity computers. The active component of this device is a glass capillary containing a fluid, as shown in Figure 5.16A. The instrument is based on the principle that the effect of temperature on the rate constant for evaporation of the fluid from the capillary tube is governed by the Arrhenius equation. Thus, the evaporation of the fluid and strength development of concrete are influenced by temperature in a similar manner. By choosing a fluid with activation energy similar to the concrete, the amount of evaporation at a given time is indicative of strength development in the concrete. The meter contains a fluid that is reported to have activation energy of 40 kJ/mol. The capillary tube of the mini-maturity meter is attached to a card that is marked in units of equivalent age at 20∂C (68∂F). The device was developed primarily for use during construction, and hence the scale is limited to an equivalent age of 5 days at 20∂C (68∂F). The card is attached to the removable cap of the plastic container. The meter is activated by removing the cap and breaking the capillary at the "0 days" mark (Figure 5.16B). The cap is replaced on the plastic container and the container is inserted into the fresh concrete. When it is desired to read the meter, the cap is removed and the position of the fluid is noted in units of equivalent days at 20∂C (68∂F).

Another novel idea for a "maturity meter" is based on measuring the chemical shrinkage of cement paste as it hydrates.[78] In this approach, cement paste at the same water–cement ratio as the concrete is placed in a vessel and covered with water. The vessel, known as a dilatometer, contains a small-diameter tube to monitor the decrease in water level as the paste hydrates and undergoes chemical shrinkage (Figure 5.17A). A layer of low-volatility fluid such as oil is used to prevent evaporation of water from the tube. The vessel would be placed in the fresh concrete so that the paste would experience the same temperature history as the concrete. The fall in water level with time would indicate the chemical shrinkage. Geiker[63] has shown that there is nearly a linear relationship between chemical shrinkage and strength, and that this relationship is independent of curing temperature. In addition, the ultimate value of chemical shrinkage was found to be affected by initial curing temperature in a similar manner as ultimate strength of mortar specimens. Thus, a meter based on chemical shrinkage would automatically account for the effects of early-age temperature on limiting strength. This is a significant advancement over maturity instruments based solely on temperature history because it would allow estimation of absolute strength rather than relative strength. To use such a device, a strength vs. chemical shrinkage correlation curve would be developed for the particular concrete mixture. Such a relationship is shown schematically in Figure 5.17B. The dilatometer would be filled with a sample of the field concrete, and measurement of in-place chemical shrinkage would be used to estimate the in-place strength. A practicable field instrument and test procedure based on chemical shrinkage has not been developed.

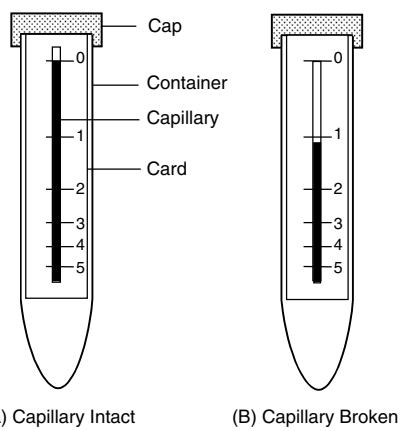

FIGURE 5.16 A disposable maturity meter that uses the evaporation of a liquid from a capillary tube as an indicator of maturity.

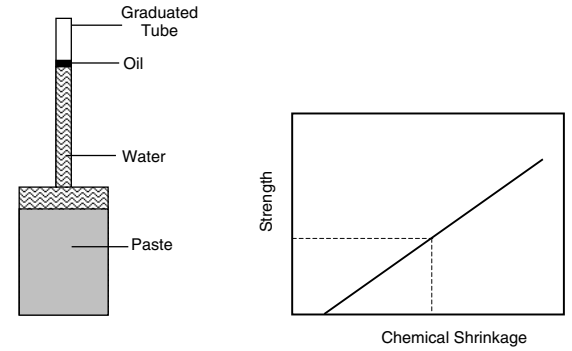

FIGURE 5.17 (A) Schematic of a maturity meter based on measuring chemical shrinkage; (B) schematic of strength–shrinkage relationship for estimating in-place strength.

In summary, a variety of commercial devices are available that can automatically compute the in-place maturity index. The user should keep in mind that maturity index calculations are based on specific values of datum temperature or activation energy. Hence, they will only correctly account for temperature effects if these values are applicable to the materials being used. For instruments based on the Nurse–Saul function it is possible to correct the displayed temperature–time factors for a different value of datum temperature using the following equation:

$$M_c = M_d - (T_0 - T_{0d})t \tag{5.44}$$

where

M_c = corrected temperature–time factor
M_d = displayed temperature–time factor
T_0 = the desired datum temperature
T_{0d} = the datum temperature used by the instrument
t = the elapsed time from when instrument was turned on

The readings of maturity computers based on the Arrhenius equation cannot be corrected for a different value of the activation energy. The user of such an instrument should refer to Figure 5.11 for an understanding of the effect of activation energy on the age conversion factor used to compute equivalent age.

5.4.3 Maturity Method Combined with Other Methods

There are several factors that can lead to errors in the estimated in-place strength based on the maturity method:

- Errors in batching that reduce the potential strength of the concrete
- High early-age temperatures that reduce the limiting strength of the concrete
- Improper curing procedures that cause concrete to dry below a critical level and cause hydration to cease
- Use of activation energy or datum temperature values that are not representative of the concrete mixture

Because of these limitations, it is not prudent to rely solely on measurements of in-place maturity to verify the attainment of a required level of strength before performing a critical construction operation. Therefore, as is discussed later, the ASTM standard practice[11] requires that maturity testing be supplemented with other tests. One approach is to use the maturity method along with other in-place tests of the concrete. For example, the maturity method has been used along with pullout tests.[79,80] As will be discussed, by combining the maturity method with other tests, the amount of required testing may be reduced without compromising safety.

One of the considerations in using in-place tests (such as pullout or probe penetration) is to know when these tests should be performed. If they are performed before the concrete reaches the required strength, they have to be repeated after additional curing. Premature testing may occur when a period of unusually cold weather occurs during the time between placement and testing. On the other hand, if the tests are performed after the concrete is well above the required strength level, unnecessary delays in construction activities may have occurred.

The proper time to perform the other in-place tests can be determined by measuring the in-place maturity. From the preestablished strength–maturity relationship, the user determines the maturity index value corresponding to the required strength. The in-place maturity index is monitored. When the necessary maturity index is attained, in-place tests are performed and the concrete strength is estimated from the correlation curve for that test. If the resulting estimated strength equals or exceeds the required strength, the construction activity can proceed. If the estimated strength is significantly less than the required value, the engineer may consider the following questions before deciding on the course of action:

- Were the sites of the in-place tests close enough to the locations of the temperature sensors, so that the maturity index values were indicative of the maturity of the concrete that was tested?
- Were proper curing procedures used to ensure an adequate supply of moisture?
- Is the value of the activation energy or datum temperature used to compute the maturity index reasonably accurate for the materials being used?

If the answer to any of these questions is "no," engineering judgment is required to decide whether the construction activity may proceed after additional curing, or whether additional curing and retesting are needed before beginning the activity.

If the answer to all of the above questions is "yes," it is reasonable to conclude that the low estimate of the in-place strength occurred because the concrete tested does not have the same potential strength as the concrete used to develop the strength–maturity relationship. In this case, the engineer must decide whether to require additional curing before beginning the scheduled activity, or whether there is sufficient concern to question the quality of the concrete.

5.4.4 Illustrative Examples

5.4.4.1 Strength–Maturity Relationship

The data reported in Table 5.1 are used to construct a strength–maturity relationship to illustrate how the maturity method could be applied on a project. These data are plotted in Figure 5.18A. Assume that the strength–maturity relationship obeys the hyperbolic equation presented in the previous section. The two-step procedure associated with Equations 5.29 and 5.30 is used to obtain the values of the parameters for the relative-strength vs. equivalent age relationship. Assume that the temperature of the test specimens was 23∂C (73∂F) throughout the testing period, so that the ages in Table 5.1 are equivalent ages at 23∂C.

First, the limiting strength is estimated by considering the data for tests beyond 4 days. Figure 5.18B shows the reciprocal of strength plotted against the reciprocal of age. From linear regression analysis, the intercept is 0.0222, which equals the reciprocal of the limiting strength. Therefore, the limiting strength is S_u = 1/0.0222 MPa = 45.0 MPa (6530 psi). Next, estimate the rate constant and the age when strength development begins by considering the first three test results in Table 5.1. In accordance with Equation 5.30, the quantity $S/(S_u - S)$ is plotted against age as shown in Figure 5.18C. From linear regression analysis, the slope of the line is found to be 0.40 day^{-1}, which is the value of the rate constant at 23∂C (73∂F). The intercept of the line with the age axis is 0.08 days. Thus, the hyperbolic strength–equivalent age relationship for this concrete mixture is

$$S(\text{MPa}) = 45.0\,\frac{0.40\,(t_e - 0.08)}{1 + 0.40\,(t_e - 0.08)} \tag{5.45}$$

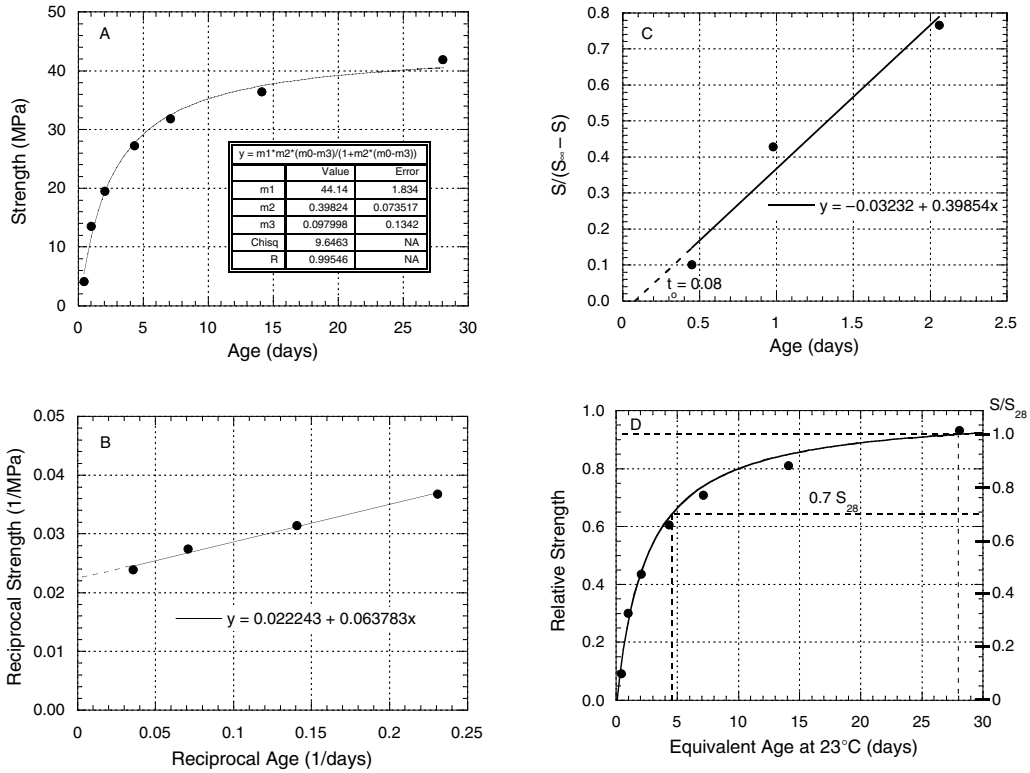

(A) and (B) (C) and (D)

FIGURE 5.18 (A) Strength vs. age[61] for curing at 22∂C; curve represents best fit of Equation 5.21. (B) Plot of reciprocal strength vs. reciprocal age to evaluate the limiting strength. (C) Plot to evaluate the rate constant and the age when strength development begins. (D) Relative strength vs. equivalent age at 23∂C (left scale is based on limiting strength and right scale is based on 28-day strength).

Alternatively, if proper software is available, the parameters S_∞, k, and t_0 can be determined directly by least-squares fitting. The resulting values for this approach are shown in the box in Figure 5.18A.

Equation 5.45 would correctly estimate in-place strength development if the early-age temperature in the field were close to 23∂C (73∂F). However, as was discussed in the previous section, the following relative strength vs. equivalent age curve would be applicable for other early-age temperatures:

$$RS_\infty = \frac{S}{S_\infty} = \frac{0.40\,(t_e - 0.08)}{1 + 0.40\,(t_e - 0.08)} \tag{5.46}$$

where

RS_∞ = fraction of limiting strength

Figure 5.18D shows Equation 5.46 along with the relative strength values obtained by dividing the strengths in Table 5.1 by the limiting strength of 45 MPa (6530 psi). The fit is good.

A more useful relationship would be to express relative strength in terms of the 28-day strength. If 28 days is substituted for the equivalent age in Equation 5.46, we obtain $S_{28}/S_\infty = 0.92$. Thus, the 28-day strength is 92% of the limiting strength, or conversely the limiting strength is 1/0.92 = 1.09 times the 28-day strength. Thus, Equation 5.46 can be rewritten as follows:

$$RS_{28} = \frac{S}{S_{28}} = \frac{(1.09)\,0.40\,(t_e - 0.08)}{1 + 0.40\,(t_e - 0.08)} \tag{5.47}$$

where

S_{28} = the 28-day strength
RS_{28} = fraction of the 28-day strength

To obtain the graph of the relationship between RS_{28} and equivalent age, the left-hand scale on Figure 5.18D is multiplied by 1.09. This new scale is shown on the right of Figure 5.18D.

5.4.4.1.1 Planning Construction

Next, the application of the maturity method for planning construction activities is discussed. First, Equation 5.47 is solved for equivalent age in terms of a desired strength ratio. Using general terms, one obtains the following:

$$t_e = \frac{RS_{28}}{k_r (f - RS_{28})} + t_0 \tag{5.48}$$

where

$f = \frac{S_\bullet}{S_{28}}$ (= 1.09 in this example)
k_r = the rate constant at the reference temperature (= 0.04 day^{-1} in this example)
t_0 = the equivalent age at start of strength development (= 0.08 days in this example)

Good engineering practice[81] recommends that, unless approved by the engineer/architect, supporting forms and shores should not be removed from horizontal members (beams and slabs) until at least 70% of the design strength has been attained. Assuming that the strength gain of concrete to be used for construction is described by Equation 5.46 and Figure 5.18D, the equivalent age at 23°C (73°F) needed to reach 70% of the 28-day design strength would be

$$t_e = \frac{0.7}{0.4(1.09 - 0.70)} + 0.08 \approx 4.6 \text{ days} \tag{5.49}$$

The equivalent age of 4.6 days would be the actual age only if the curing temperature were 23°C (73°F).

Now consider the time it would take to reach an equivalent age of 4.6 days for different constant curing temperature conditions. The maturity function based on the Arrhenius equation is used and it is assumed that the concrete has an activation energy of 40 kJ/mol. The age conversion factor would be

$$a = e^{\frac{-40000}{8.314}\left(\frac{1}{273 + T} - \frac{1}{296}\right)} \tag{5.50}$$

The following age conversion factor values are obtained for different concrete temperatures. The number of days needed to reach an equivalent age of 4.6 days at 23°C (73°F) is obtained by dividing the required equivalent age by the age conversion factors.

Temperature		Age Conversion Factor	Days to Reach t_e = 4.6 Days at 23°C (73°F)
°C	(°F)		
5	(41)	0.35	13.1
15	(59)	0.64	7.2
23	(73)	1.00	4.6
35	(95)	1.88	2.4
45	(113)	3.08	1.5

With this information, the contractor can analyze the economics of different construction schedules. For example, if the job were to be performed during cold weather, and if a 3-day cycle were desired for the re-use of forms, protection would have to be provided to ensure that the concrete temperature was maintained above about 30∂C (86∂F). The contractor could then decide whether it would be more economical to provide the needed protection or use a longer cycle time.

Maage and Helland[82] describe the use of the maturity method in a "curing technology system" that can be used to estimate in-place temperature histories for different construction scenarios. This type of simulation tool allows the contractor to avoid potential problems and establish optimal placement and curing procedures.

5.4.4.1.2 Evaluation of In-Place Tests

Finally, we discuss the use of the maturity method for rational interpretation of the results of other in-place tests used to verify the attainment of required strength during construction. The procedure is as follows:

- Based on the required strength, the 28-day design strength, and the relative strength–maturity relationship, compute the maturity index (time–temperature factor or equivalent age) at which the required strength is expected to be achieved.
- Perform the in-place tests and estimate the in-place concrete strength using the appropriate correlation for that test method.
- If the estimated strength based on the in-place tests equals or exceeds the required strength, perform the planned construction activity.
- If the estimated strength is less than the required strength, use the maturity method to analyze the in-place results and to help decide the appropriate action to take.

To illustrate the procedure, assume that concrete with a 28-day design strength of 40 MPa (5800 psi) is used in a post-tensioned structure, and the concrete must have a strength of 25 MPa (3600 psi) before post-tensioning can be applied. The equivalent age to achieve the required strength is computed using Equation 5.47. Thus, we have the following:

Concrete properties:

$k_r = 0.4$ day^{-1}	— Rate constant at reference temperature of 23∂C (73∂F)
$t_0 = 0.08$ days	— Equivalent age at start of strength gain
$S_\infty/S_{28} = 1.09$	— Ratio of limiting strength to 28-day strength
$S_{28} = 40$ MPa	— Given 28-day strength

Construction requirements:

$S_{req} = 25$ MPa	— Strength required for post-tensioning
$RS_{28} = 25/40 = 0.63$	— Required strength ratio

Equivalent age to attain required strength:

$t_e = 3.4$ days at 23∂C (73∂F) (from Equation 5.48)

Suppose that in-place tests are performed when the in-place equivalent age is 3 days, and based on these tests the estimated compressive strength of the concrete is 23 MPa (3300 psi). Because the estimated strength is less than the required strength and the tests were performed at less than the required equivalent age, the maturity method can be used to analyze the results.

First, Equation 5.47 is used to compute the relative strength that should have developed at an equivalent age of 3 days. Using the estimated in-place strength, the 28-day strength of the in-place concrete is estimated. Finally, the equivalent age needed to achieve the required strength is calculated. Thus, we have the following:

Evaluation of in-place testing results: Case 1

$t_e = 3$ days	— Equivalent age when in-place test performed
$RS_{28} = 0.59$	— Theoretical strength ratio at test age (Equation 5.47)
$S_e = 23$ MPa	— Estimated strength from in-place test result
$S_{28} = 23/0.59 = 39$ MPa	— Estimated 28-day strength of in-place concrete
$RS_{28} = 25/39 = 0.64$	— Needed strength ratio to achieve S_{req}
$t_e = 3.6$ days	— Equivalent age to achieve S_{req}

In this case, the in-place strength was lower than the required strength primarily because the tests were performed at an equivalent age of 3 days rather the computed required age of 3.4 days. The calculations indicate that the in-place concrete has the necessary strength potential and the required strength will be attained after additional curing. Thus, the post-tensioning can proceed according to plans after additional curing.

Now, consider the case where the estimated strength from the in-place tests is only 20 MPa (3200 psi). The evaluation of the results is as follows:

Evaluation of in-place testing results: Case 2

$t_e = 3$ days	— Equivalent age when in-place test performed
$RS_{28} = 0.59$	— Theoretical strength ratio at test age
$S_e = 20$ MPa	— Estimated strength from in-place test result
$S_{28} = 20/0.59 = 34$ MPa	— Estimated 28-day strength of in-place concrete
$RS_{28} = 25/34 = 0.74$	— Needed strength ratio to achieve S_{req}
$t_e = 5.3$ days	— Equivalent age to achieve S_{req}

In this case, it appears that the in-place concrete does not have the expected potential strength because the estimated 28-day strength of the in-place concrete is only 34 MPa (4900 psi) rather than the design value of 40 MPa (5800 psi). At this point, the engineer has to take a closer look at the three questions discussed at the end of the previous subsection. If the engineer is assured that sufficient moisture was provided and that the measured in-place maturity was representative of the maturity at the locations of the in-place tests, there is good reason to suspect a problem in the quality of the concrete. If the lower than expected design strength can be tolerated, it is only necessary to delay the post-tensioning until an equivalent age of 5.3 days has been attained. If the lower potential strength cannot be tolerated, additional investigation may be needed, and the questionable concrete may have to be removed.

The mathematical manipulations involved in the above analyses can be added to computer programs developed for the analysis of in-place test results. Spreadsheet software is a very convenient tool for analyzing in-place test data,[75,83] and the above procedures can be incorporated easily into such spreadsheets.

5.4.5 Maturity and Other Properties

The development of mechanical and transport properties of concrete is related to the degree of hydration of the cementitious materials. Thus, it would be expected that the early development of other properties besides compressive strength could be related to a maturity index. As was mentioned, Lew and Reichard[31] showed that the development of modulus of elasticity, splitting tensile strength, and pullout bond strength could be related to the temperature–time factor. More recently, Delatte et al.[84] related the development of splitting tensile strength and tensile bond strength of concrete overlays to the temperature–time factor. Yu and Ansari[85] studied the development of fracture energy under different curing temperatures. They demonstrated that the relationships discussed in Section 5.3 on the theoretical basis of the maturity method were applicable to analysis of the development of fracture energy. They found that the activation energy for development of fracture toughness was the same as for development of compressive strength. The values of fracture energy measured under different curing temperatures fell on the same curve when plotted as a function of equivalent age. Dilly and Zollinger[86] also related the development of fracture

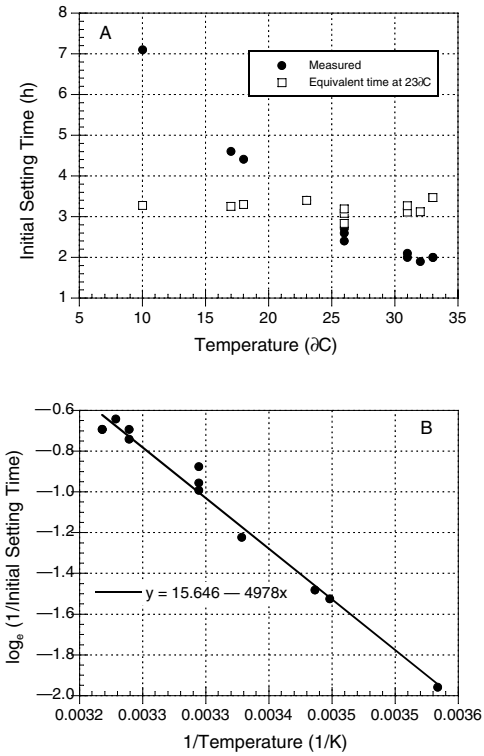

FIGURE 5.19 (A) Initial setting time vs. temperature. (B) Natural logarithm of the inverse of initial setting time vs. inverse of absolute temperature.[88]

strength to equivalent age. Pinto et al.[87] found that the development of compressional wave speed under different curing temperatures could be related to equivalent age.

Pinto and Hover[88] investigated whether the maturity method was applicable to the setting time of concrete measured in accordance with ASTM C 403/C 403M.[89] The solid circles in Figure 5.19A show the reported initial setting times as a function of the average temperature. They found that the setting time at different temperatures could be used to obtain an apparent activation energy to represent the temperature dependence of setting time. The inverses of the setting times were used as rate constants, and the natural logarithms of the rate constants were plotted as a function of the inverse of absolute temperature. As shown in Figure 5.19B, a straight line can be fitted to the transformed data. The slope of the line represents the negative of the apparent activation energy divided by the gas constant (Equation 5.31), and is referred to as Q in ASTM C 1074.[11] The value of Q in this case is 4978 1/K, which is close to the value of 5000 1/K recommended in ASTM C 1074 for concrete made with Type I cement. The measured setting times can be converted to the equivalent setting times at 23°C (73∂F) by using Equation 5.6. These values are shown as the open squares in Figure 5.19A. It is seen that the equivalent setting times are very close to the same value. Thus, by measuring setting times at two extreme temperatures, it is possible to estimate setting time for any temperature within the extremes.

5.4.6 Application to High-Strength Concrete

Beginning in the late 1980s, high-performance concrete became a popular research topic. In general, high-performance concretes have low water–cementitious materials ratios (*w*/*cm*) and may contain silica fume when high strength and low permeability are desired. High-range water-reducing admixtures are often used to provide workability. Carino et al.[90] investigated the applicability of the maturity method by testing low *w*/*cm* mortar mixtures cured at 7, 23, and 40∂C (45, 73, and 104∂F). Two water–cementitious materials ratios

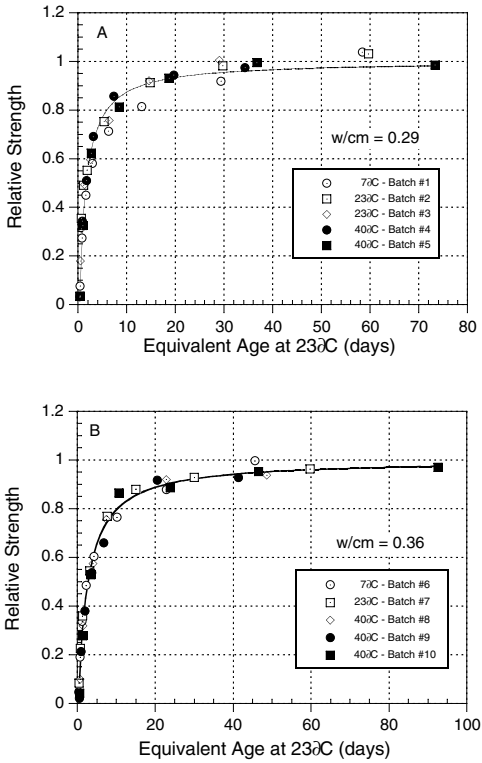

FIGURE 5.20 Relative strength vs. equivalent age at 23∂C for high-strength mortar mixtures: (A) *w/cm* = 0.29 and (B) *w/cm* = 0.36.[90]

were used: 0.29 and 0.36. Both mixtures included silica fume and a high-range water reducer. Strength–age data for each curing temperature were fitted with Equation 5.21 to determine the rate constant values. Equation 5.37 was used to represent the variation of the rate constant with temperature, and Equation 5.39 was used to compute the age conversion factor for calculating equivalent age at 23∂C (73∂F). Figure 5.20A and B shows the resulting relative strength vs. equivalent age curves for the two mortar mixtures. Thus, Carino et al.[90] concluded that the maturity method appeared to be applicable to the low *w/cm* mortar mixtures that were used. Of course, it remained to be shown whether the method was applicable to low *w/cm* concrete.

Pinto and Hover[91,92] studied the use of the maturity method with high-strength concrete. High-strength concrete was made with Type I portland cement and 10% (mass fraction of cement) silica fume. The water–cementitious materials ratio was 0.30. Five curing conditions were used:

1. Isothermal curing at 55°C (131°F)
2. Isothermal curing at 40°C (104°F)
3. Isothermal curing at 25°C (77°F)
4. Isothermal curing at 0°C (32°F)
5. Variable curing temperature to simulate cold weather conditions

Pinto and Hover examined three functions to represent strength development under the four constant-temperature curing conditions:

1. The exponential equation suggested by Freiesleben Hansen and Pedersen (Equation 5.13)
2. The "linear-hyperbolic" function (Equation 5.21)
3. The "parabolic-hyperbolic" function as proposed by Knudsen[48,49]

For each isothermal condition, the rate constant, k_T, was estimated from the best-fit equation of strength vs. time (for the exponential function the rate constant was taken as 1/t). The apparent activation energy was obtained by fitting Equation 5.31 to plots of logarithms of the rate constant vs. the inverse of the absolute temperate. The 95% confidence intervals for activation energy were as follows:[92]

- Exponential strength–age function: 25.8 ± 20.4 kJ/mol
- Linear-hyperbolic strength–age function: 33 ± 3.7 kJ/mol
- Parabolic-hyperbolic function: 48.4 ± 6.8 kJ/mol

The exponential model did not give reliable results as evidenced by the wide confidence interval.

The above values of apparent activation energy were used to compute equivalent ages using Equation 5.6, and the estimated values of limiting strength were used to calculate relative strength at each test age. It was concluded that the linear-hyperbolic model gave the least deviation of data points about a common curve.

For tests on specimens subjected to variable curing temperatures (designed to simulate actual field conditions), there was good overall agreement with the data from the isothermal curing conditions. This led Pinto and Hover[92] to conclude that the Arrhenius-based maturity function can be used with either isothermal or variable temperature curing conditions.

Myers[93] reported on a field trial of the maturity method in the construction of bridge decks made with normal strength concrete and high-strength concrete. Strength–maturity relationships for the different mixtures were developed in the laboratory in accordance with ASTM C 1074.[11] The 28-day strengths of the mixtures ranged from about 36 MPa (5250 psi) to 66 MPa (9630 psi). The reliability of the estimated strengths based on the maturity method was evaluated by testing field-cured cylinders at different ages. The temperature histories of the field-cured cylinders were assumed to equal those of the concrete decks measured with embedded thermocouples. When the strengths of the field-cured cylinders and the corresponding temperature–time factor were plotted, the points fell close to the preestablished strength–maturity relationships. The only exception occurred in one of the high-strength mixtures, where the strengths of the field-cured cylinders fell about 10% below the strength–maturity relationship. In this case, the early-age deck temperatures were greater than 50∂C (120∂F). This may have reduced the long-term strength of the field concrete. Nevertheless, Myers[93] concluded that the ranges between estimated and measured strength were acceptable. It was, however, recommended that restrictions on maximum field temperatures be enforced to minimize long-term strength reduction.

5.4.7 Application in Pavement and Bridge Construction

In the late 1980s and early 1990s, the Strategic Highway Research Program (SHRP) included several projects that addressed the maturity method. Roy et al.[94] reported on the use of the maturity method in curing technology. It was suggested that activation energy should be determined on the basis of the kinetics of cement hydration instead of the time-consuming method based on strength gain of mortar cubes as required by ASTM C 1074. Bickley[95] developed a field manual for implementing the maturity method and pullout test method. At the conclusion of the SHRP program, the Federal Highway Administration's Office of Technology Applications assembled a trailer that was driven around the United States to demonstrate new technologies to state highway engineers.[96] As a result of this effort, many state departments of transportation showed interest in incorporating this method into their standard practices.[97]

In 2000, engineers at the Pennsylvania Transportation Institute conducted a survey of state departments of transportation (DOT) to establish progress in the adoption of the maturity method.[76] Of 50 states, 44 responded to the survey, and 32 states indicated that they had conducted or were conducting research on implementing the method. The reported uses included determination of formwork removal times, determination of joint sawing times, and determination of opening times for pavements. Some states, such as Texas,[98] South Dakota,[99] Iowa,[100] and Indiana,[101] developed their own test methods, based essentially on ASTM C 1074.[11] Some of these methods were developed for estimating in-place flexural strength

and others were applicable to either flexural or compressive strengths. All protocols use the temperature–time factor, Equation 5.1, as the maturity function.

State DOT protocols include procedures for verifying during construction that previously established strength–maturity relationships are valid. For example, Texas[98] requires monitoring the temperature–time factor of selected specimens molded from samples of field concrete. At the preestablished level of temperature–time factor, the specimens are tested for strength. The measured strengths are compared with the estimated strength based on the strength–maturity relationship. If the difference between measured and estimated strengths is greater than 10%, a new strength–maturity relationship needs to be established for the project. The Texas protocol also requires enhanced batch plant inspection when the maturity method is used.

5.4.8 Summary

This section has discussed the essential elements for application of the maturity method. Three elements are required:

1. The maturity function for the concrete materials
2. A strength–maturity relationship for the concrete mixture to be used in construction
3. Measurement of the in-place thermal history

Selection of the proper maturity function is necessary to obtain the most accurate results, and it requires knowledge of the effects of curing temperature on the rate constant for strength development. A testing procedure using mortar cubes can be used to obtain this information.

The strength–maturity relationship is obtained from strength development data of concrete specimens. The temperature history of the specimens is recorded to evaluate the maturity index at the corresponding test ages. Regression analysis of the data can be used to construct a mathematical description for the strength–maturity index relationship.

Various instruments are available for monitoring the in-place temperature and computing maturity index values. In selecting a device, the user should be aware of the maturity function used by the equipment. State-of-the-art instruments permit the user to select the parameters for the maturity function.

Because of its inherent limitations, the maturity method should not be used alone to decide whether critical construction activities can be performed. Examples have been given to illustrate how the maturity method can be used with other in-place methods to verify the attainment of the required in-place strength.

It has been shown that maturity method can be used to estimate the development of other properties of concrete besides compressive strength. It has also been shown that the method is applicable to estimating strength development in high-strength concrete.

The next section summarizes the current ASTM Standard Practice governing the use of the maturity method.

5.5 Standard Practice

Procedures for using the maturity method have been standardized in ASTM C 1074.[11] The standard practice permits the user to express the maturity index either as a temperature–time factor using the Nurse–Saul function, Equation 5.1, or as an equivalent age using the Arrhenius equation, Equation 5.6. For the Nurse–Saul function, it is recommended that the datum temperature be taken as 0∂C (32∂F) if ASTM Type I cement is used without admixtures and the expected curing temperature is within 0 and 40∂C (32 and 104∂F). For the Arrhenius equation, an activation energy of 41.5 kJ/mol is recommended. For other conditions or when maximum accuracy is desired, the best value of the datum temperature or activation energy should be determined experimentally.

The ASTM standard provides procedures for developing the strength–maturity relationship and for estimating the in-place strength. In addition, a procedure is provided for obtaining the datum temperature or activation energy if that is desired.

5.5.1 Datum Temperature or Activation Energy

The procedure for determining the datum temperature or activation energy follows the approach discussed in Section 5.3 on the theoretical basis of the maturity method. Basically, mortar cubes made with the materials to be used in construction are cured at three temperatures. Two of the curing temperatures should be the minimum and maximum curing temperatures expected for the in-place concrete, and the third temperature should be midway between the extremes. The cubes are tested for compressive strength at regular time intervals.

The strength–age data for the mortar cubes are analyzed using Equation 5.21 to obtain the rate constant as a function of temperature. Several options are available depending on the data analysis capabilities of the user. One alternative is to measure the final setting times at the three curing temperatures using the penetration resistance method described in ASTM C 403/C 403M.[89] The final setting times are used to represent the ages when strength development is assumed to begin, that is, t_0. The reciprocals of the cube strengths are plotted as a function of reciprocals of the ages beyond the times of final setting. This approach is similar to using Equation 5.28 to represent the strength–age data. For each temperature, the least-squares best-fit straight line is determined, and the rate constant is obtained by dividing the intercept by the slope of the line. Another alternative is to use a two-step process in which the limiting strength is determined first by fitting Equation 5.29 and then the rate constant is determined by fitting Equation 5.30. The third alternative is to use a nonlinear curve-fitting computer program to fit Equation 5.21 to the strength–age data. The last approach is the most straightforward method and low-cost software is available for this purpose.

To obtain the datum temperature, the rate constants are plotted as a function of temperature and the best-fit straight line is determined. The intercept of the line with the temperature axis gives the datum temperature. To obtain the activation energy, the natural logarithms of the rate constants are plotted against the reciprocals of the absolute curing temperatures (Equation 5.31). The negative of the slope of the straight line equals the activation energy divided by the gas constant (referred to as Q in the standard).

5.5.2 Strength–Maturity Relationship

To develop the strength–maturity relationship, cylindrical concrete specimens are prepared using the mixture proportions and constituents of the concrete to be used in construction. These specimens are prepared according to the usual procedures for making and curing test specimens in the laboratory.

After the cylinders are molded, temperature sensors are embedded at the centers of at least two cylinders. The sensors are connected to instruments that automatically compute maturity index (Figure 5.21A).

The specimens are cured in a water bath or in a moist curing room. At ages of 1, 3, 7, 14, and 28 days, compression tests are performed on at least two specimens. At the time of testing, the average maturity index for the instrumented specimens is recorded. A time interval of 1/2 h or less should be used for recording temperature during the first 48 h, and longer time intervals are permitted for the remainder of the curing period.

A plot is made of the average compressive strength as a function of the average maturity index. A best-fit smooth curve is drawn through the data, or regression analysis may be used to determine the best-fit curve for one of the strength–maturity relationships discussed in the previous section. The resulting curve would be used to estimate the in-place strength of that concrete mixture.

The ASTM standard assumes that the initial temperature of the concrete in the field is approximately the same as the laboratory temperature when the cylinders were prepared. If the actual early-age temperatures are significantly greater than the laboratory temperatures, the limiting in-place strength is reduced. Thus, the in-place strength may be overestimated by the strength–maturity relationship.

5.5.3 Estimating In-Place Strength

The procedure for estimating in-place strength requires measuring the in-place maturity index. As soon as is practicable after concrete placement, temperature sensors are placed in the fresh concrete. As

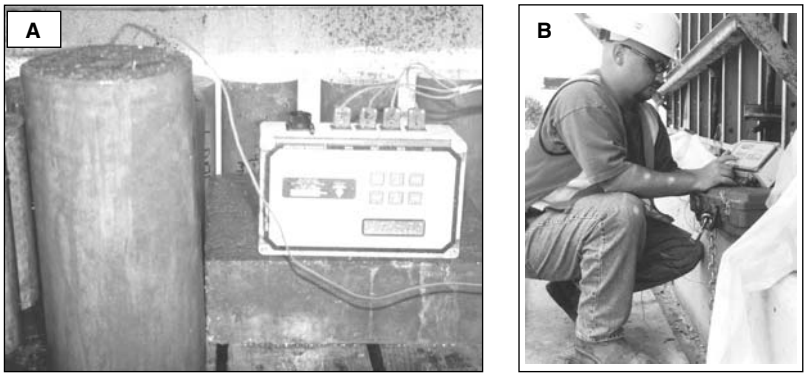

FIGURE 5.21 (A) Concrete cylinder instrumented with maturity meter and subjected to standard moist curing. (Courtesy of Texas Department of Transportation.) (B) Technician reading the accumulated maturity index to determine whether strength is sufficient for formwork removal. (Courtesy of Texas Department of Transportation.)

previously mentioned, the sensors should be installed at locations in the structure that are critical in terms of exposure conditions and structural requirements. The importance of this step cannot be over emphasized when the strength estimates are being used for timing the start of critical construction operations.

The sensors are connected to maturity instruments or temperature recording devices that are activated as soon as is practicable after concrete placement. When a strength estimate is desired, the maturity value from the maturity instrument is read (Figure 5.21B). Using the maturity index values and the previously established strength–maturity relationship, the user estimates the compressive strengths at the locations of the sensors.

Because the temperature history is the only measurement made in the field, there is no assurance that the in-place concrete has the correct mixture proportions. Therefore, the ASTM standard requires verification of the potential strength of the in-place concrete before performing critical operations, such as formwork removal or post-tensioning. Failure to do this can lead to drastic consequences in the event of such undetected batching errors as using excessive amounts of cement replacements or retarding admixtures. Alternative methods for verification of concrete strength include:

- Other in-place tests that measure an actual strength property of the in-place concrete
- Early-age compressive strength tests of standard-cured specimens molded from samples of the concrete in the structure and instrumented with maturity meters
- Compressive strength tests on specimens molded from samples of the concrete in the structure and subjected to accelerated curing

5.6 Conclusion

This chapter has provided the following:

- A review of the historical development of the maturity method
- A theoretical basis for the method
- A discussion on how the method may be applied during construction

The maturity method was initially proposed as a means to estimate strength development of concrete during accelerated curing, such as steam or electric curing. The idea was subsequently extended to ordinary curing conditions. The early work was empirical in nature. Recent work has attempted to establish a theoretical basis for the method and to explain the inherent approximations and limitations of the method.

A variety of maturity functions have been proposed to account for the effect of time and temperature on strength development. It has been shown that the product of the rate constant and age is the general form of an appropriate maturity function. The rate constant is related to the rate of strength development during the acceleratory period immediately following setting. Thus, the key element of a suitable maturity function is having the correct representation of the effect of temperature on the rate constant.

If the rate constant is assumed to be a linear function of temperature, the resulting maturity function is the traditional Nurse–Saul function. Test data show that, over a wide temperature range, the rate constant is not a linear function of temperature. Therefore, the Nurse–Saul function is inherently approximate and may overestimate or underestimate the effects of temperature on strength gain. It has been shown that if a straight-line approximation is used, the best-fit value of the datum temperature (temperature at which the rate constant equals 0) is not necessarily –10°C (14°F) as has been traditionally used in the Nurse–Saul function. Rather, the datum temperature depends on the temperature sensitivity of the rate constant and the temperature range over which the linear approximation is used.

A nonlinear function, such as the Arrhenius equation, can represent better the effect of temperature on strength development over wide temperature ranges. For the Arrhenius equation, the activation energy is the parameter that defines the temperature sensitivity of the rate constant. Recent work indicates that the activation energy depends on the cementitious components of the concrete and may also depend on water–cementitious materials ratio.

The equivalent age approach is the most flexible technique to represent the maturity index. In this case, the age conversion factor is used to convert a curing time interval at any temperature to an equivalent time interval at a reference temperature. The age conversion factor is simply the ratio of the value of the rate constant at any temperature to its value at the reference temperature.

An ASTM standard exists for application of the maturity method. The standard provides a procedure, based on testing mortar cubes, for obtaining the values of activation energy (or datum temperature) for the particular concrete mixture. This testing is required for maximum accuracy in estimating strength gain. The standard also provides a procedure for establishing the strength–maturity relationship of the concrete mixture. This relationship is obtained experimentally by testing cylindrical specimens at various values of maturity index. It must be emphasized that to estimate in-place strength accurately, one needs the correct maturity function. In addition, the early-age temperature of the in-place concrete must be similar to that of the specimens used to develop the strength–maturity relationship. The traditional maturity method cannot account for the effects of early-age temperature on limiting strength.

Because of the dependence of limiting strength on early-age curing temperature, a unique strength–maturity relationship does not exist for a given concrete mixture. It appears, however, that there is a unique relative strength vs. maturity index relationship. Thus, the only reliable information that can be obtained from measuring in-place maturity is relative strength gain. It is for this reason, and because the maturity method cannot detect batching errors, that the maturity method must be supplemented with other tests before performing critical construction operations.

The maturity method can be used along with other in-place tests. This approach provides the needed assurance of the in-place strength, and it permits rational interpretation of low estimated strengths based on in-place tests. A potential application is to use the maturity method along with other in-place methods to determine whether the in-place concrete meets contract strength requirements.

The maturity method is amenable to computer application because the maturity function and strength–maturity relationship can be represented by simple mathematical expressions. The Nordic countries have pioneered the use of the maturity method in computer programs designed to simulate the expected outcome of alternative construction schemes and concrete mixtures. For example, one can simulate the effects of cement content and amount of insulation on the in-place temperature history of a structural component exposed to different ambient conditions. The maturity method can then be used to estimate in-place strength based on the computed thermal history. Estimations based on this approach have been in good agreement with actual strength measurements.[82] The maturity method has also been used extensively in a series of Danish studies dealing with curing and control of early-age cracking.[102,103]

In the United States, the Federal Highway Administration has led in the incorporation of the maturity method in predictive models. Forster[104] describes models developed to predict the development of early-age cracking in concrete pavements. The models incorporate the maturity method to estimate the development of materials properties based on the computed temperature histories. A similar suite of models was also developed to predict interfacial bond failure in bonded concrete overlays. Such models permit the designer to identify the most favorable construction methods to reduce the likelihood of early-age cracking or bond failure.

In summary, the maturity method provides a simple procedure to account for the effects of temperature and time on strength development. In combination with other in-place strength tests discussed in this handbook, the maturity method is playing an expanded role in advanced concrete technology.

References

1. Saul, A.G.A., Principles underlying the steam curing of concrete at atmospheric pressure, *Mag. Concr. Res.,* 2(6), 127, 1951.
2. Bergstrom, S.G., Curing temperature, age and strength of concrete, *Mag. Concr. Res.,* 5(14), 61, 1953.
3. Plowman, J.M., Maturity and the strength of concrete, *Mag. Concr. Res.,* 8(22), 13, 1956.
4. McIntosh, J.D., The effects of low-temperature curing on the compressive strength of concrete, in *Proc. RILEM Symp. on Winter Concreting,* Session BII, Copenhagen, Danish Institute for Building Research, Copenhagen, 1956.
5. Klieger, P., Effects of mixing and curing temperatures on concrete strength, *J. Am. Concr. Inst.,* 54(12), 1063, 1958.
6. Alexander, K.M. and Taplin, J.H., Concrete strength, cement hydration and the maturity rule, *Aust. J. Appl. Sci.,* 13, 277, 1962.
7. Cold weather concreting, ACI 306R-88 (Reapproved 1997), Report by Committee 306, *Manual of Concrete Practice*, American Concrete Institute, Farmington Hills, MI.
8. Kukko, H. and Koskinen, I., Eds., RILEM Recommendations for Concreting in Cold Weather, Research Notes 827, Technical Research Centre, Espoo, Jan. 1988.
9. Freiesleben Hansen, P. and Pedersen, E.J., Vinterstobning af beton, Anvisning 125, Statens Byggeforskningsinstitut, Copenhagen, 1982 [in Danish].
10. In-place methods to estimate concrete strength, ACI 228.1R-95, Report by Committee 228, *Manual of Concrete Practice*, American Concrete Institute, Farmington Hills, MI, 1995.
11. Standard practice for estimating concrete strength by the maturity method, ASTM C 1074-98, *Annual Book of ASTM Standards,* Vol. 04.02, 2002.
12. Malhotra, V.M., Maturity concept and the estimation of concrete strength, Information Circular IC 277, Department of Energy Mines Resources (Canada), Nov. 1971.
13. McIntosh, J.D., Electrical curing of concrete, *Mag. Concr. Res.,* 1(1), 21, 1949.
14. Nurse, R.W., Steam curing of concrete, *Mag. Concr. Res.,* 1(2), 79, 1949.
15. Rastrup, E., Heat of hydration in concrete, *Mag. Concr. Res.,* 6(17), 79, 1954.
16. Wastlund, G., Hardening of concrete as influenced by temperature, General Report of Session BII, in *Proc. RILEM Symposium on Winter Concreting,* Copenhagen, Danish Institute for Building Research, Copenhagen, 1956.
17. Verbeck, G.J. and Helmuth, R.H., Structure and physical properties of cement paste, in *Proc. Fifth Int. Symp. on the Chemistry of Cement,* Part III, Tokyo, 1968, 1- 32.
18. Swenson, E.G., Estimation of strength gain of concrete, *Eng. J.*, Sept. 1967.
19. Hudson, S.B. and Steele, G.W., Prediction of potential strength of concrete from early tests, *Highway Res. Rec.,* 370, 25, 1971.
20. Hudson, S.B. and Steele, G.W., Developments in the prediction of potential strength of concrete from results of early tests, *Transp. Res. Rec.*, 558, 1, 1975.

21. Standard test method for developing early age compression test values and projecting later age strengths, ASTM C 918-02, *Annual Book of ASTM Standards*, Vol. 04.02, 2002.
22. Weaver, J. and Sadgrove, B.M., Striking times of formwork-tables of curing periods to achieve given strengths, Construction Industry Research and Information Association, Rep. 36, London, Oct. 1971.
23. Sadgrove, B.M., Prediction of strength development in concrete structures, *Transp. Res. Rec.,* 558, 19, 1975.
24. Bickley, J.A., Practical application of the maturity concept to determine in-situ strength of concrete, *Transp. Res. Rec.,* 558, 45, 1975.
25. Mukherjee, P.K., Practical application of maturity concept to determine in-situ strength of concrete, *Transp. Res. Rec.,* 558, 87, 1975.
26. Nisbet, E.G. and Maitland, S.T., Mass concrete sections and the maturity concept, *Can. J. Civ. Eng.*, 3, 47, 1976.
27. Copeland, L.E., Kantro, D.L., and Verbeck, G., Chemistry of hydration of portland cement, Part III: Energetics of the hydration of portland cement, in *Proc. Fourth Int. Symp. on Chemistry of Cement*, NBS Monograph 43, Washington, D.C., 1962, 453.
28. Freiesleben Hansen, P. and Pedersen, E.J., Maturity computer for controlled curing and hardening of concrete, *Nord. Betong*, 1, 19, 1977.
29. Byfors, J., Plain concrete at early ages, Swedish Cement and Concrete Research Institute Report 3:80, 1980.
30. Naik, T.R., Maturity functions for concrete cured during winter conditions, in *Temperature Effects on Concrete*, T.R. Naik, Ed., ASTM STP 858, 1985, 107.
31. Lew, H.S. and Reichard, T.W., Mechanical properties of concrete at early ages, *J. Am. Conc. Inst.,* 75(10), 533, 1978.
32. Carino, N.J., Lew, H.S., and Volz, C.K., Early age temperature effects on concrete strength prediction by the maturity method, *J. Am. Conc. Inst.,* 80(2), 93, 1982.
33. Standard test method compressive strength of concrete cylinders cast in place in cylindrical molds, ASTM C 873-99, *Annual Book of ASTM Standards*, Vol. 04.02, 2002.
34. Carino, N.J., Temperature effects on strength-maturity relation of mortar, NBSIR 81-2244, U.S. National Bureau of Standards, Mar. 1981.
35. Carino, N.J. and Lew, H.S., Temperature effects on strength-maturity relations of mortar, *J. Am. Conc. Inst.*, 80(3), 177, 1983.
36. Carino, N.J., Maturity functions for concrete, in *Proceedings, RILEM Int. Conf. on Concrete at Early Ages*, Paris, Ecole Nationale des Ponts et Chausées, Paris, Vol. I, 1982, 123.
37. Carino, N.J., The maturity method: theory and application, *ASTM J. Cem. Concr. Aggregates*, 6(2), 61, 1984.
38. Nykanen, A., Hardening of concrete at different temperatures, especially below the freezing point, in *Proc. RILEM Symp. on Winter Concreting*, Session BII, Copenhagen, Danish Institute for Building Research, Copenhagen, 1956.
39. Discussion of Reference 3, *Mag. Concr. Res.,* 8(24), 169, 1956.
40. Bernhardt, C.J., Hardening of concrete at different temperatures, in *Proc. RILEM Symp. on Winter Concreting*, Session BII, Copenhagen, Danish Institute for Building Research, Copenhagen, 1956.
41. Goral, M.L., Empirical time-strength relations of concrete, *J. Am. Conc. Inst.,* 53(2), 215, 1956.
42. Prediction of creep, shrinkage, and temperature effects in concrete structures, ACI 209R-92 (Reapproved 1997), Report of Committee 209, *Manual of Concrete Practice*, American Concrete Institute, Farmington Hills, MI.
43. Chin, F.K., Relation between strength and maturity of concrete, *J. Am. Conc. Inst.,* 68(3), 196, 1971.
44. Chin, F.K., Strength tests at early ages and at high setting temperatures, *Transp. Res. Rec.*, 558, 69, 1975.
45. Carino, N.J., Closure to discussion of Reference 32, *J. Am. Conc. Inst.,* 81(1), 98, 1984.

46. Lew, H.S. and Reichard, T.W., Prediction of strength of concrete from maturity, *Accelerated Strength Testing*, ACI SP-56, V.M. Malhotra, Ed., American Concrete Institute, Farmington Hills, MI, 1978, 229.
47. Freiesleben Hansen, P. and Pedersen, E.J., Curing of concrete structures, *CEB Inf. Bull.,* 166, May 1985.
48. Knudsen, T., On particle size distribution in cement hydration, in *Proceedings, 7th International Congress on the Chemistry of Cement,* Vol. II, Paris, Editions Septima, Paris, 1980, I-170- 175.
49. Knudsen, T., Modelling hydration of portland cement: the effects of particle size distribution, *Proc. Engineering Foundation Conf. on Characterization and Performance Prediction of Cement and Concrete,* July, Henniker, NH, 1982, 125.
50. Knudsen, T., The dispersion model for hydration of portland cement: I. General concepts, *Cem. Concr. Res.,* 14, 622, 1984.
51. Bezjak, A. and Jelenic, I., On the determination of rate constants for hydration processes in cement pastes, *Cem. Concr. Res.,* 10(4), 553, 1980.
52. Copeland, L.E. and Kantro, D.L., Chemistry of hydration of portland cement at ordinary temperature, in *The Chemistry of Cements*, Vol. I, H.F.W. Taylor, Ed., Academic Press, London, 1964, chap. 8.
53. Regourd, M., Structure and behavior of slag portland cement hydrates, in *Proc. 7th Int. Congr. on the Chemistry of Cement,* Paris, Vol. I, Editions Septima, Paris, 1980.
54. Filliben, J.J., DATAPLOT æ introduction and overview, U.S. National Bureau of Standards, Special Publication (SP) 667, June 1984 (program available from NTIS, Springfield, VA).
55. Alexander, K.M., Taplin, J.H., and Wardlaw, J., Correlation of strength and hydration with composition of portland cement, in *Proc. 5th Int. Symp. on the Chemistry of Cement*, Vol. III, Tokyo, 1968, Cement Association of Japan, Tokyo, 1969, 152.
56. Seki, S., Kasahara, K., Kuriyama, T., and Kawasumi, M., Effects of hydration of cement on compressive strength, modulus of elasticity and creep of concrete, in *Proc. 5th Int. Symp. on the Chemistry of Cement*, Vol. III, Tokyo, 1968), Cement Association of Japan, Tokyo, 1969, 175.
57. Gauthier, E. and Regourd, M., The hardening of cement in function of temperature, in *Proc. RILEM Int. Conf. on Concrete at Early Ages,* Vol. I, Paris, Ecole Nationale des Ponts et Chausées, Paris, 1982, 145.
58. Regourd, M., Mortureux, B., Gauthier, E., Hornain, H., and Volant, J., Characterization and thermal activation of slag cements, in *7th Int. Cong. on the Chemistry of Cement*, Vol. III, Paris, Editions Septima, Paris, 1980.
59. Bresson, J., Prediction of strength of concrete products, in *Proc. RILEM Int. Conf. on Concrete at Early Ages*, Vol. I, Paris, Ecole Nationale des Ponts et Chausées, Paris, 1982.
60. Tank, R.C., The Rate Constant Model for Strength Development of Concrete, Ph.D. dissertation, Polytechnic University, Brooklyn, NY, June 1988.
61. Tank, R.C. and Carino, N.J., Rate constant functions for strength development of concrete, *ACI Mater. J.*, 88(1), 74, 1991.
62. Carino, N.J. and Tank, R.C., Maturity functions for concrete made with various cements and admixtures, *ACI Mater. J.*, 89(2), 188, 1992.
63. Geiker, M., Studies of Portland Cement Hydration by Measurements of Chemical Shrinkage and Systematic Evaluation of Hydration Curves by Means of the Dispersion Model, Ph.D. dissertation, Technical University of Denmark, Lyngby, 1983.
64. Geiker, M. and Knudsen, T., Chemical shrinkage of portland cement pastes, *Cem. Concr. Res.,* 12(5), 603, 1982.
65. Roy, D.M. and Idorn, G.M., Hydration, structure, and properties of blast furnace slag cements, mortars and concrete, *J. Am. Conc. Inst.,* 79(6), 444, 1982.
66. Test method activation energy for the maturity method, TI-B 103(94), Danish Technological Institute, 1996.

67. Kjellsen, K.O. and Detwiler, R.J., Later-age strength prediction by a modified maturity model, *ACI Mater. J.*, 90(3), 220, 1993.
68. Barnes, B.D., Orndorff, R.L., and Roten, J.E., Low initial temperature improves the strength of concrete cylinders, *J. Am. Concr. Inst.,* 74(12), 612, 1977.
69. Dodson, C.J. and Rojagoplan, K.S., Field tests verify temperature effects on concrete strength, *Concr. Int.,* 1(12), 26, 1979.
70. Tashiro, C. and Tanaka, H., The effect of the lowering of initial curing temperature on the strength of steam cured mortar, *Cem. Concr. Res.,* 7(5), 545, 1977.
71. Al-Rawi, R.S., Effects of cement composition and w/c ratio on strength of accelerated cured concrete, *Cem. Concr. Res.,* 7(3), 313, 1977.
72. Butt, Y.M., Kolbasov, V.M., and Timashev, V.V., High temperature curing of concrete under atmospheric pressure, in *Proc. 5th Int. Symp. on the Chemistry of Cement*, Vol. III, Tokyo, 1968), Cement Association of Japan, Tokyo, 1969, 437.
73. Naik, T.R., Concrete strength prediction by the maturity method, *ASCE Eng. Mech. Div. J.,* 106(EM3), 465, 1980.
74. Guide to curing concrete, ACI 308R-01, Report by Committee 308, *Manual of Concrete Practice*, American Concrete Institute, Farmington Hills, MI.
75. Dilly, R.L., Beizai, V., and Vogt, W.L., Integration of time-temperature curing histories with PC spreadsheet software, *J. Am. Conc. Inst.,* 85(5), 375, 1988.
76. Tikalsky, P.J., Scheetz, B.F., and Tepke, D.G., Using the concrete maturity meter for QA/QC, Pennsylvania Transportation Institute, Report PA-2000-0126+97-04(22), Jan. 2001.
77. Hansen, A.J., COMA-Meter æ the mini maturity meter, *Nord. Betong*, Sept. 1981.
78. Knudsen, T. and Geiker, M., Chemical shrinkage as an indicator of the stage of hardening, in *Proc. RILEM Int. Conf. on Concrete at Early Ages*, Vol. I, Paris, Ecole Nationale des Ponts et Chausées, Paris, 1982, 163.
79. Peterson, C.G. and Hansen, A.J., Timing of loading determined by pull-out and maturity tests, in *RILEM Int. Conf. on Concrete at Early Ages*, Vol. I, Paris, Ecole Nationale des Ponts et Chausées, Paris, 1982, 173.
80. Parsons, T.J. and Naik, T.R., Early age concrete strength determination by pullout testing and maturity, in *In Situ/Nondestructive Testing of Concrete*, V.M. Malhotra, Ed., ACI SP-82, American Concrete Institute, Farmington Hills, MI., 1984, 177.
81. Guide to formwork for concrete, Report of ACI Committee 347, *Manual of Concrete Practice*, American Concrete Institute, Farmington Hills, MI, 2001.
82. Maage, M. and Helland, S., Cold weather concrete curing planned and controlled by microcomputer, *Concr. Int.,* 10(10), 34, 1988.
83. Carino, N.J. and Stone, W.C., Analysis of in-place test data with spreadsheet software, in *Computer Use for Statistical Analysis of Concrete Tests Data*, ACI SP-101, P. Balaguru and V. Ramakrishnan, Eds., American Concrete Institute, Farmington Hills, MI, 1987, 1.
84. Delatte, N.J., Williamson, M.S., and Fowler, D.W., Bond strength development with maturity of high-early-strength bonded concrete overlays, *ACI Mater. J.*, 97(2), 201, 2000.
85. Yu, B.J. and Ansari, F., Method and theory for nondestructive determination of fracture energy in concrete structures, *ACI Struct. J*, 93(5), 602, 1996.
86. Dilly, R.L. and Zollinger, D.G., Mode I fracture strength based on pullout force and equivalent age, *ACI Mater. J.*, 95(3), 304, 1998.
87. Pinto, R.C.A., Hobbs, S.V., and Hover, K.C., The maturity approach in concrete technology — going beyond compressive strength, in *Proc. Fifth CANMET/ACI Int. Conf. on Recent Advances in Concrete Technology,* ACI SP 200, V.M. Malhotra, Ed., American Concrete Institute, Farmington Hills, MI, 2001, 749.
88. Pinto, R.C.A. and Hover, K.C., Application of maturity approach to setting times, *ACI Mater. J.*, 96 (6), 686, 1999.

89. Standard test method for time of setting of concrete mixtures by penetration resistance, ASTM C 403/C 403M-99, *Annual Book of ASTM Standards*, Vol. 04.02, 2002.
90. Carino, N.J., Knab, L.I., and Clifton, J.R., Applicability of the maturity method to high-performance concrete, NISTIR-4819, U.S. National Institute of Standards and Technology, May, 1992 (available from NTIS, Springfield, VA, 22161, PB93-157451/AS).
91. Pinto, R.C.A. and Hover, K., Application of maturity functions to high-strength concretes, in *High-Strength Concrete: An International Perspective*, ACI SP 167, J.A. Bickley, Ed., American Concrete Institute, Farmington Hills, MI, 1996, 229.
92. Pinto, R.C.A. and Hover, K.C., Further studies on the utilization of maturity functions to a high-strength concrete mixture, in *4th Int. Symp. on High-Strength/High-Performance Concrete,* Paris, 1996, 711.
93. Myers, J.J., The use of the maturity method as a quality control tool for high-performance concrete bridge decks, in *Proc. PCI/FHWA/FIB Int. Symp. on High Performance Concrete,* L.S. Johal, Ed., Precast/Prestressed Institute, Chicago, 2000, 316.
94. Roy, D.M., Scheetz, B.E., Sabol, S., Brown, P.W., Shi, D., Licastro, P.H., Idorn, G.M., Andersen, P.J., and Johanson, V., Maturity model and curing technology, SHRP-C-625, Strategic Highway Research Program, National Research Council, Washington, D.C., 1993.
95. Bickley, J.A., Field manual for maturity and pullout testing on highway structures, Strategic Highway Research Program Report (SHRPC-376), National Research Council, Washington, D.C., 1993
96. Crawford, G.L., Wathne, L., and Mullarky, J.I., On the road testing roads, *Public Roads*, July/Aug. 2002, available at http://www/tfhrc.gov/pubrds/02jul/04.htm.
97. Maturity meters: A concrete success, *FOCUS*, Oct. 2002, U.S. Department of Transportation, Federal Highway Administration, available at http://www.tfhrc.gov/focus/oct02/01.htm.
98. Texas Department of Transportation, Estimating concrete strength by the maturity method, Tex-426-A, Manual of Testing Procedures, 2002.
99. South Dakota Department of Transportation, Procedure for estimating concrete strength by maturity method, SD 407, Materials Manual, Section 400 Concrete, 1997.
100. Iowa Department of Transportation, Method of testing the strength of portland cement concrete using the maturity method, IM 383, Office of Materials, 2002.
101. Indiana Department of Transportation, Strength of portland cement concrete pavement (PCCP) using the maturity method, ITM 402-99T, Materials & Tests Division, 1999.
102. Schaumann, J., Haugaard, M., and Jensen, P.F., Curing guideline, HETEK Report 121, Road Directorate, Denmark Ministry of Transport, 1997.
103. Pedersen, E.S. et al., Control of early age cracking in concrete — guidelines, HETEK Report 120, Road Directorate, Denmark Ministry of Transport, 1997.
104. Forster, S.W., HIPERPAV — guidance to avoid early-age cracking in concrete pavements, in *Proc. 2000 CANMET/ACI Int. Conf. on Durability of Concrete,* ACI SP-192, V.M. Malhotra, Ed., American Concrete Institute, Farmington Hills, MI, 2000, 1109.

6

Pull-Off Test and Permeation Tests

Graeme D. Henderson
Dr. Doran and Partners

P.A. Muhammed Basheer
The Queen's University of Belfast

Adrian E. Long
The Queen's University of Belfast

6.1 Introduction
6.2 *In Situ* Strength Assessment
Classification of Various Test Methods • Pull-Off Test
6.3 Measuring Concrete Permeation Properties
Transport Processes
6.4 Description of Test Methods
Absorption Tests • Permeability Tests
6.5 Concluding Remarks

In situ testing of concrete to assess its strength and durability is now common. Whereas there is a general acceptance of *in situ* tests for assessing the strength of concrete, the same is not true for permeability testing due to the effect of *in situ* moisture condition on the measured permeation properties. This chapter describes one of the methods that has been used successfully to assess near-surface strength of concrete — the pull-off test. This is followed by a review of some of the *in situ* tests that can be used to measure the water absorption, water permeability, and gas permeability of concrete.

6.1 Introduction

One of the spinoffs from the technological era in which we are living is that all industrial processes are being refined and streamlined in an attempt to improve their efficiency. The construction industry is no exception; the main aim of most design engineers and project planners/managers is to design the most economically viable structure and then construct it as quickly as possible. Although in many cases this approach has resulted in successful projects with the client receiving a cost-effective final product, there have been other cases where the final product has not satisfied exactly the design specifications and ultimately the client has incurred extra expense rectifying these problems.

In an attempt to eradicate these problems, many novel *in situ* testing techniques have been invented to allow an assessment of the concrete during the construction period and on completion of the structure before it goes into service. This chapter describes the pull-off strength testing technique and some of the techniques available for measuring the permeation properties of concrete. This is not intended to be a complete listing and discussion of all available permeation tests, but rather a brief summary of some of the more popular methods.

6.2 *In Situ* Strength Assessment

In most countries in the world, the strength properties of the concrete in a structure are assessed indirectly by measuring the strength of cubes or cylinders that are made in a standard manner from the concrete

supplied to the site. While this is well accepted by industry, it has its limitations in that problems are not detected until it is too late as testing is generally carried out at 7 and 28 days. In addition, and fortunately infrequently, it can be the subject of abuse æ either by making cubes prior to the addition of further water to the mixture or, in extreme cases, by the contractor supplying cubes from a specially prepared mixture that will meet the specifications. Furthermore, cubes or cylinders manufactured and cured in a standard manner do not represent the quality of concrete in the structure.

Both these shortcomings could be eliminated by measuring the properties of the concrete *in situ*. This also permits the effectiveness of the consolidation and curing processes to be incorporated in providing a reliable indication of the condition of the finished product. Another advantage to be gained from *in situ* strength testing is that the speed of the overall construction program could be increased if an accurate assessment of the *in situ* strength were made because this would allow a much faster "turnaround" for formwork and back-propping.

6.2.1 Classification of Various Test Methods

A wide range of tests is available for estimating the *in situ* strength of concrete and many of them are discussed in various chapters of this handbook. These various tests can be classified into the following groups:

1. *Destructive tests:* These conventional methods enable the strength of the concrete to be measured by way of cores or cubes cut from the concrete, however, this is not possible in all cases and especially in slender members. Alternatively, complete structural members can be load-tested to prescribed design loads, in which case the extent of damage to the structure may be considerable.
2. *Nondestructive tests:* By definition, strength properties are not measured directly so some other properties are measured and the strength estimated by correlation. Naturally, these methods have the great advantage that the concrete is not damaged.
3. *Partially destructive tests:* In these tests, the concrete is tested to failure but the damage resulting is localized and the member under test is not weakened to any significant extent. One such partially destructive strength test is the pull-off test, which is discussed in Section 6.2.2.

6.2.2 Pull-Off Test

The pull-off test is based on the concept that the tensile force required to pull a metal disk, together with a layer of concrete, from the surface to which it is attached, is related to the compressive strength of the concrete. There are two basic approaches that can be used. One is where the metal disk is attached directly to the concrete surface and the stressed volume of concrete lies close to the face of the disk, and the other is where surface carbonation or skin effects are present and these can be avoided by the use of partial coring to an appropriate depth. Both these approaches are illustrated in Figure 6.1. At least two commercial pull-off testing systems are available: one developed at The Queen's University of Belfast and another developed at the Danish Technical University using the pull-out test loading equipment. The Danish system is known commercially as the "007- Bond Test." Both approaches are similar in principle. The discussion presented here focuses mainly on the technique developed at The Queen's University although most of it is applicable to the Danish and other systems.

The first version of the pull-off test produced at The Queen's University was developed in the early 1970s as a means of assessing the compressive strength of concrete beams made with high-alumina cement. The first step is to remove any laitance from the concrete surface to expose the top of the coarse aggregate particles. This is usually done using some sort of abrasion, typically a wire brush. The exposed concrete surface and metal disk are then de-greased to ensure good bonding of the adhesive. The adhesive is generally a two-part epoxy system. A thin uniform layer of adhesive is spread over the disk area and the disk is pressed firmly onto the concrete surface (Figure 6.1). Excess adhesive that is squeezed out during this process should be removed before it sets. The curing time

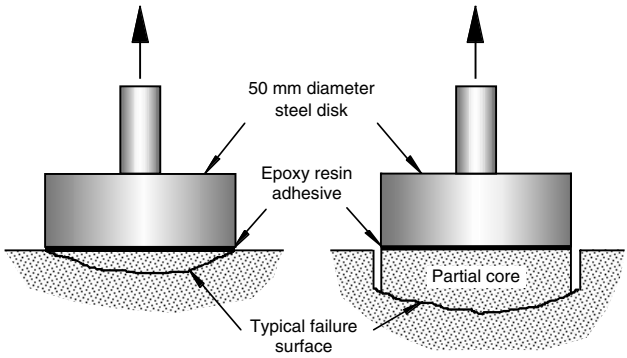

FIGURE 6.1 Schematic of the pull-off test showing the two procedures that can be used.

needed for the adhesive depends on the type of epoxy used and the surrounding environmental conditions, although in most situations a curing time of no more than 24 h is required. After the adhesive has cured sufficiently, the metal disk is "pulled" from the concrete surface. The apparatus used for applying and recording this tensile force is known as a "Limpet" and this applies a maximum tensile force of 10 kN at a rate of approximately 6 kN/min through a threaded rod screwed into the metal disk. From the recorded tensile force a nominal pull-off tensile strength is calculated on the basis of the disk diameter (usually 50 mm). To convert this pull-off tensile strength into a cube (or cylinder) compressive strength, a previously established empirical correlation chart is used; one such typical chart is shown in Figure 6.2.

The main advantage of the pull-off test is that it is simple and quick to perform. The entire process of preparing the surface and bonding the metal disk should take no more than 15 min. Another advantage is that the damage caused to the concrete surface after a test is not severe. The main limitation of the method is the curing time required for the adhesive. In most situations, it is normal practice to apply the disks one day and complete the test the next day. There is, however, a potential problem by doing this in that, if the surface preparation has not been completed in the correct way or if the environmental conditions are unfavorable, then this may cause the adhesive to fail. Thus, the test result is meaningless; however, this will not be discovered until after the test has been completed. To compensate for this type of problem, it is recommended that at least six disks be used to estimate the compressive strength and, if necessary, one of the individual test results can be eliminated if an adhesive failure has occurred.

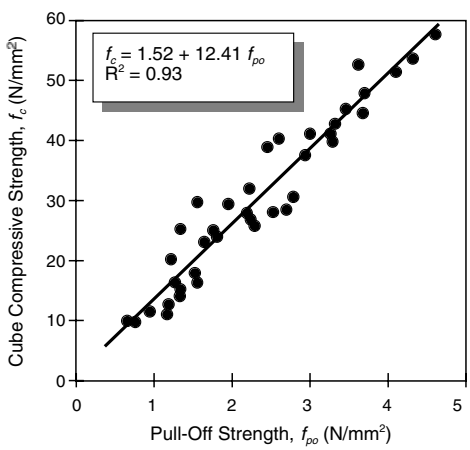

FIGURE 6.2 Example of compressive strength correlation for the pull-off test. (From Murray, A.McC., Ph.D. thesis, The Queen's University of Belfast, 1984.)

However, with the advances that have taken place in the development of adhesives for the construction industry, this particular limitation is becoming less of a problem.

Another aspect of the pull-off test worth considering is the correlation used to determine the compressive strength. The single factor that has the greatest effect on this relationship is the type of coarse aggregate used in the concrete, the greatest difference being between natural gravels and crushed rocks.[1] Therefore, care should always be taken to ensure that the correlation being used is applicable in that situation. Another criticism of the pull-off test is that only a surface layer of concrete no more than 5 mm thick is actually tested. However, if the partial coring technique shown in Figure 6.1 is used, then the concrete will be tested at the depth to which the coring is completed. This approach of partial coring is also used quite extensively for testing the bond strength of concrete repair mortars.

6.3 Measuring Concrete Permeation Properties

The main cause of nearly all concrete deterioration is the penetration into concrete of aggressive substances, for example, carbon dioxide, chloride ions, or sulfates. In most of these cases, water is also required to sustain degradation. Therefore, durability can be improved significantly by producing concrete that is highly resistant to the ingress of external harmful substances. This approach is summarized well by a quote from Mehta:[2] "Impermeability of concrete should be the first line of defense against any of the physiochemical deterioration processes."

If this concept is to be used to ensure durable concrete, then to assess the potential durability of *in situ* concrete it is necessary to measure the near-surface transport properties of the concrete because it is the surface zone concrete (or "covercrete") that is largely responsible for controlling durability. In this section, details are provided of some of the test techniques available for measuring the near-surface transport properties. This is not intended to be a complete, detailed discussion of all available test techniques but rather a brief description of some of the most commonly used methods and their advantages and disadvantages. One general point that must be borne in mind when discussing these tests is that few of them measure absolute values of fundamental transport properties; what they do provide is an index or relative value and this is useful for comparing one concrete with another.

6.3.1 Transport Processes

The following is a brief description of the main transport processes that describe the movement of aggressive substances through concrete.

Adsorption: This is the process by which molecules adhere to the internal surface of concrete. It can be either by physical forces of adhesion (van der Waals forces) or as a result of chemical bonds.[3-5]

Absorption: This is the process by which concrete takes in liquid by capillary suction to fill the pore space available. The rate at which liquid enters the pores is termed absorptivity or sorptivity.[4-6]

Diffusion: This is the process by which a liquid, gas, or ions migrate through concrete under the action of a molar concentration gradient. It is generally defined by a diffusion coefficient or a diffusivity value.[4,6,7]

Permeability: This is the property of concrete that describes resistance to a fluid penetration under the action of a pressure gradient.[4,8] Quite often, permeability is confused with porosity, and vice-versa. Porosity, however, is merely a measure of the proportion of the total volume occupied by pores, usually expressed as a percentage.[7] It is conceivable, although somewhat improbable, that a concrete could be porous and impermeable if it contained a series of disconnected air pockets separated by impermeable material.[4]

6.4 Description of Test Methods

6.4.1 Absorption Tests

Absorption tests involve the intake of a fluid due to capillary suction in the pores.[9] Under perfect conditions, the magnitude of capillary rise follows a linear relationship with the square root of time

elapsed, and the constant of proportionality is called the sorptivity. Ideally, this is the property that should be measured in an absorption test.[9] There are, however, practical limitations that hinder this, for example, difficulty in achieving a unidirectional penetration of water and problems of determining the water penetration depth without actually splitting open the concrete specimen. Because of these difficulties, the absorption characteristics of concrete are usually measured indirectly by one of the following types of test.

6.4.1.1 Standpipe Tests

One of the simplest techniques available for measuring the water absorption characteristics of concrete is the standpipe test. This consists essentially of a vertical tube of suitable diameter glued onto the horizontal concrete surface to be tested. Water is filled into the tube up to a certain level and then allowed to be absorbed by the concrete. The amount of water absorbed per unit of time is reported as an index of water absorptivity.

There are different versions of this type of test reported in the technical literature; however, in this discussion only a brief description of three different methods is given. The first version is commonly referred to as the "chimney method."[10] Its main features are that it has a constant head of 100 mm, a standpipe diameter of 67 mm, and the water absorptivity index is calculated from the amount of water absorbed over a 6-day period (measurements are taken every 24 h for the entire duration of the 6 days). The second method is known as "Karsten's pipe test."[11] This has a falling head of 100 mm, a 60-mm-diameter standpipe, and the volume of water absorbed between minute 5 and minute 15 from the start of the test is used as a measure of the absorptivity. The third approach is called the "Australian test."[12] This has a 200-mm falling head, a 100-mm-diameter standpipe, and the water absorptivity index is determined from a graphical relationship developed between the head and time. This graphical relationship can be developed either by observing the head for 2 h or by measuring the time until the head has fallen by 100 mm. Although all of these tests are simple to carry out on site, they each have a low level of sensitivity and thus are not that successful at detecting different levels of concrete performance. Therefore, they are not used extensively.

6.4.1.2 Initial Surface Absorption Test (ISAT)

The initial surface absorption is defined as the rate of flow of water into the concrete surface per unit area at a stated interval from the start of the test at a constant applied head and temperature.[13] The first version of a test to measure this property was proposed by Glanville in 1931.[14] This was further developed into a commercial test by Levitt[15] and was incorporated into the British Standards in 1970.[16] A brief description of the British Standards version of this test is presented here.

The main components and general arrangement of the ISAT are shown in Figure 6.3. A circular cap with a surface area of at least 5000 mm^2 is clamped tightly onto the concrete surface and filled with water from a reservoir. To ensure that all the air is removed from the cap during this operation, the flexible tube (connected to the capillary) should not be connected to the outlet. Another requirement to ensure that no air is trapped is that the cap should be made from a transparent material to allow the detection of air bubbles. After the cap has been filled, the flexible tube is connected to the outlet. The other end of the tube is connected to a horizontal, calibrated glass capillary tube. To commence a test the reservoir is filled with water to a level that is 200 mm above the concrete surface (the same height as the horizontal capillary tube). Once this has been achieved and there are no leaks or air bubbles in the system, the inlet tap from the reservoir is closed. The movement of the water in the capillary tube is then monitored. This monitoring should take place over a 2-min period at intervals of 10 min, 30 min, 1 h, and 2 h after the start of the test. From the movement of the water in the calibrated capillary tube, the initial surface absorption value can be calculated in units of $mL/m^2/s$. The reason for measuring absorption at specified intervals after the start of the test is that water absorption of a dry surface is initially high but decreases as the water-filled length of the capillaries increases. A recommendation in the British Standard[17] suggests that it is not necessary for the test be conducted at 2 h after the start of the test because there will probably be only a small amount of movement in the capillary tube.

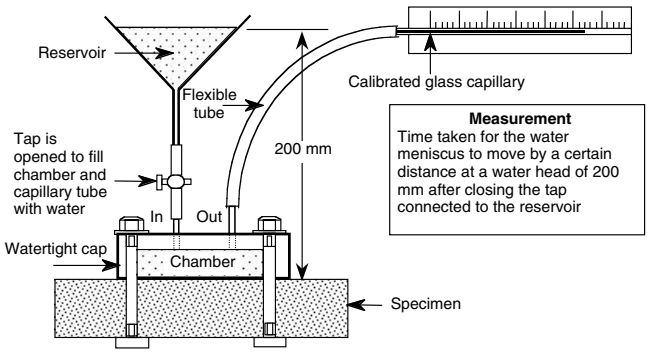

FIGURE 6.3 Schematic of initial surface absorption test (ISAT).

The main advantage of the ISAT is that it is a quick and simple nondestructive *in situ* test method that can be used to measure water penetration into a concrete surface. It can also be used on exposed aggregate and profiled surfaces provided a watertight seal is achieved. The difficulty of ensuring a watertight seal is probably one of the greatest limitations of this test because of the problems achieving this in practice. Another limitation is that the measured property is greatly affected by the moisture condition of the concrete. This, however, applies to nearly all near-surface absorption and air permeability tests and is best summarized by a quote from Neville:[7] "A low value of initial surface absorption may be due either to the inherent low absorption characteristics of the concrete tested or else to the fact that the pores in poor-quality concrete are already full of water." Another disadvantage is that the 200-mm head of water is considered quite low, and although the results may be related to surface weather exposure they are of little relevance to behavior under high water pressures. In view of these advantages and disadvantages, the main application of the ISAT is as a quality control test for precast concrete units that can be tested whenever they are "dry." The technique can also be used as a comparative test on *in situ* concrete for assessment of potential durability.

6.4.1.3 Autoclam Sorptivity Test

The idea for the "Clam" test was first reported by Montgomery and Adams[18] in the early 1980s. Initially, it was only a water permeability test. It was then modified and the "Universal Clam" was produced. This could measure both water and air permeability. Although the test was quite advanced at the time, it still was essentially a manual test with piston movement (which controlled the pressure) performed by a micrometer screw.

In the early 1990s, Basheer[19] completed further development work that not only standardized the tests but also made the whole process fully automatic. This version of the Clam, the "Autoclam," is controlled by a microprocessor and has a complete data acquisition and transfer facility to enable computer analysis of the results. Three types of test are now possible: water absorption, air permeability, and water permeability. The Autoclam is commercially available. In this section, the water absorption test is described, and in a later section the air and water permeability tests are presented.

The first step for all three Autoclam tests is to clamp or glue a steel base ring onto the concrete surface (Figure 6.4A). If clamping is being used, a rubber ring is placed between the base ring and the concrete to ensure an air- and water-tight seal. The base ring usually has an internal diameter of 50 mm. The actual Autoclam test apparatus is then clamped onto the base ring. This overall arrangement is shown in Figure 6.4B. For a water absorption test, both the priming and bleed valves are opened and the piston is raised to the top of the cylinder using the controller. Using a syringe, the user introduces water into the test area through the priming valve with air escaping through the bleed valve. After a steady flow of water out of the bleed valve has been achieved, the bleed valve is closed and, using the syringe, the water pressure is increased to slightly below 0.02 bar. The priming valve is then closed and the test started by means of the control panel. At this point, a stepper motor increases the water pressure to exactly 0.02

bar and the test commences. An applied pressure of 0.02 bar is used because this corresponds to a water head of approximately 200 mm, which is the same as in the ISAT. As the test commences, water is absorbed immediately into the concrete and thus the pressure tends to decrease; however, the piston moves downward to maintain the pressure. This piston travel is monitored every minute for 15 min and, knowing the cross-sectional area of the piston, the volume of water absorbed can be determined. If the cumulative volume of water absorbed is plotted against the square root of time, a linear relationship is achieved and the gradient of this relationship is reported as the sorptivity index, in units of $m^3/\div min$. Start-up errors can be avoided if only the portion of the straight-line relationship between minute 5 and minute 15 is used.

The main advantages of this test are that it is relatively simple and easy to perform, the recorded results have a high level of accuracy, and the apparatus is completely portable allowing easy use on-site and in the laboratory. The disadvantages are generally the same as the ISAT; the main problem is the practical difficulties in clamping the base ring onto the concrete surface.

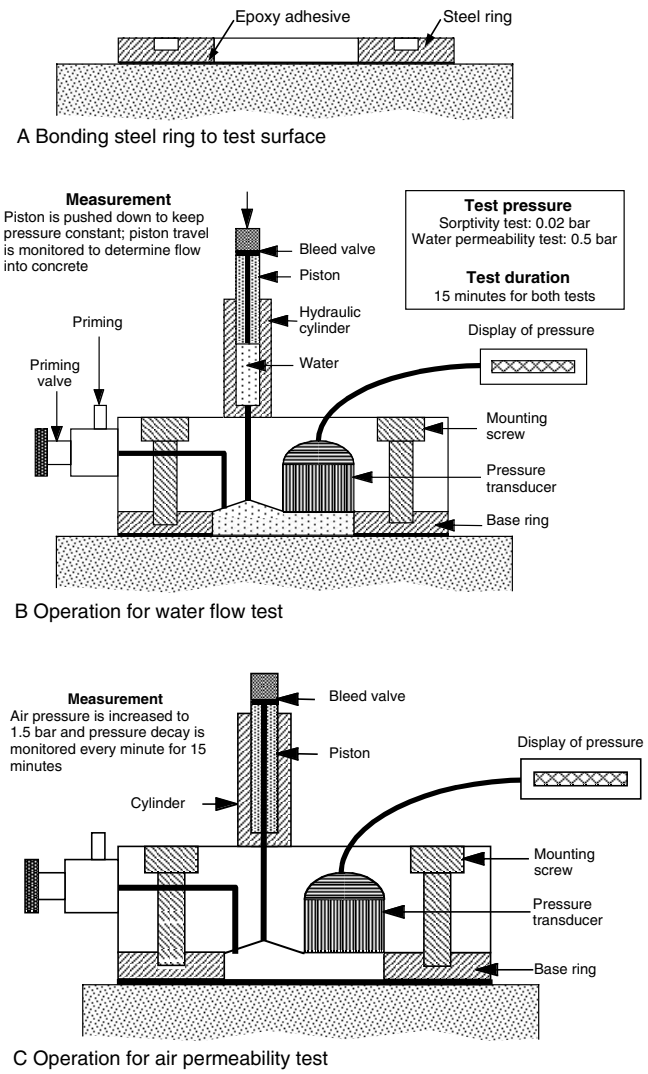

FIGURE 6.4 Schematic of Autoclam tests. (From Basheer, P.A.M., Ph.D. thesis, The Queen's University of Belfast, 1991.)

6.4.1.4 Figg Water-Absorption Test

The development of this test, known as a "drill-hole" absorptivity test, was first reported by Figg in 1973.[20] The commercial trade name for the apparatus is the "Poroscope." A schematic showing the apparatus and test setup is presented in Figure 6.5. The first step in performing a test is to drill a hole, 10 mm in diameter and 40 mm deep, normal to the concrete surface with a masonry bit. After thorough cleaning of the hole, a silicone plug is placed into the hole to leave a 20-mm-long cavity, 20 mm below the concrete surface. A hypodermic needle with a very fine canula passing through it is inserted through the silicone plug until the canula touches the bottom of the cavity. A two-way connector and various flexible tubes are used to connect the hypodermic needle to a syringe and a horizontal calibrated capillary tube set 100 mm above the bottom of the cavity. The syringe is used to inject water through the canula into the cavity. As water enters through the canula, air in the cavity escapes through the flexible tubes. When the system is full of water and a check has been made to ensure no air is trapped, the syringe is isolated. At this point the concrete being tested is subjected to a water head of approximately 100 mm. As time elapses, water is absorbed into the concrete and thus the meniscus in the capillary tube moves. The time required for this meniscus to move 50 mm is taken as a measure of the water absorption of the concrete. This obtained value is called the absorption index and is measured in seconds. Obviously, a higher absorption index value corresponds to a better-quality concrete.

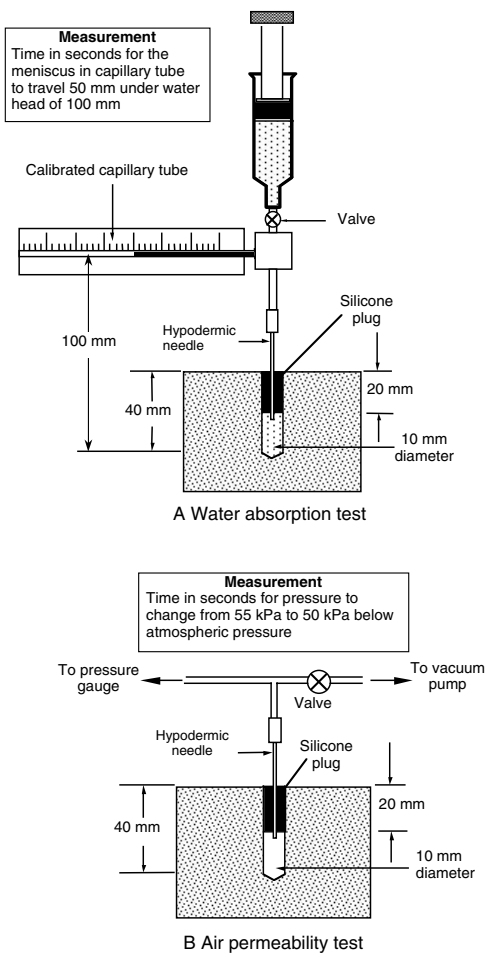

FIGURE 6.5 Schematic of Figg tests.

The main advantages of the Figg water absorption test are that it is a simple and easy test to complete and the cost of the equipment is relatively low. One of the main limitations is that during drilling of the hole microcracks may be formed in the surrounding concrete, which may defeat the purpose of the test by altering the absorption mechanism. Another possible limitation is that, because this test involves concrete that is approximately 20 mm below the surface, this test cannot be used to assess the performance of surface treatments, for example, surface penetrants or controlled permeability formwork. Bungey,[13] however, has also described this limitation as an advantage because the recorded results are not influenced by localized surface effects such as carbonation of the outer few millimeters of concrete.

6.4.2 Permeability Tests

Permeability tests measure the flow of a liquid or gas into the concrete under the action of a pressure gradient. They can be either steady state or nonsteady state depending on the condition of flow established within the pore system of the concrete.

6.4.2.1 Autoclam Water and Air Permeability Tests

In the absorption tests described in the previous section, to ensure that water penetration is governed by sorptivity of the concrete, a low water pressure is used (a water head of no more than 200 mm in each case). To measure the permeability of concrete, the same type of tests (in principle) is used, but to establish a suitable pressure gradient, much higher test pressures are used. This is the case with the Autoclam water permeability test, which uses the same apparatus and setup as the Autoclam sorptivity test (Figure 6.4). The only difference between the two is the water pressure used during the actual test. For the water permeability test, the water pressure is maintained at 1.5 bar compared with 0.02 bar for the water absorption test. The test principle and procedure is exactly the same in both cases with the water permeability index calculated in the same way as the sorptivity index.

The third test that can be completed by the Autoclam apparatus is the air permeability test. The overall apparatus and arrangement for this test are shown in Figure 6.4C. The main difference between the air permeability test and water absorption or permeability test is that during an air test the piston is positioned at the bottom of the cylinder. Using a syringe attached to the priming valve, the user increases the air pressure inside the test chamber to slightly above 0.5 bar. The priming valve is then closed and the test is started by means of the control panel. The test apparatus monitors the pressure decay automatically every minute for 15 min or until the pressure has dropped to zero. The plot of the natural logarithm of pressure against time is linear, and the gradient of the linear regression line between minute 5 and minute 15 (for tests lasting for 15 min) is reported as the air permeability index with units of $\log_e$ (bar)/min. If the pressure drops to zero before the end of the 15-min test duration, the data from the start of the test are used to determine the permeability index.

Air and water permeability indices, as opposed to coefficients of permeability, are the reported properties from these tests because steady state is not achieved during any of the tests. Similar to the Autoclam sorptivity test, the Autoclam air and water permeability tests also have the advantage that they are quick and simple to perform both on-site and in the laboratory.

6.4.2.2 Figg Air Permeability Test

The overall arrangement for the Figg air permeability test is shown in Figure 6.5B. The hole preparation and layout for the air test is the same as the water test (Figure 6.5A). The only difference between the two tests is in the apparatus used to complete the test. For the air test, a three-way connector connects the hypodermic needle to a digital manometer and a hand-operated vacuum pump. To complete a test, the pump is used to reduce the pressure in the cavity to 55 kPa below atmospheric pressure. A valve is then closed to isolate the vacuum pump. Subsequently, air flows into the cavity and the pressure increases. The time taken for the pressure to increase by 5 kPa, that is, to a cavity pressure of –50 kPa is recorded using a stopwatch and this is reported as the air permeability index. Similar to the Figg water test, a higher air permeability index value corresponds to a less permeable concrete. The advantages and

disadvantages of the Figg water absorption test discussed in the previous section also apply to the Figg air permeability test.

6.4.2.3 Schönlin Air Permeability Test

As discussed in the previous sections, the main limitation of the Figg testing apparatus is that a hole needs to be drilled into the concrete surface to complete the test. This causes damage to the concrete surface and the drilling operation may also cause microcracking that may affect the permeation properties being measured. In an attempt to eradicate these problems, the Schönlin test was developed. This test is almost identical in concept to the Figg air permeability test. The main difference between the two methods is that the Schönlin test is completed on the surface of the concrete.

A schematic showing the setup for the Schönlin test is presented in Figure 6.6. As can be seen in this figure, a 50-mm-diameter chamber of known volume is placed on the concrete surface. A vacuum pump is used to evacuate the chamber to a pressure less than 99 kPa below atmospheric pressure.[21] The valve to the pump is then closed, and the time when the vacuum reaches a pressure of - 95 kPa is taken as the start of the test. The time required for the vacuum to reach a pressure of - 70 kPa is measured and, knowing the volume of the chamber, the air permeability index in units of m^2/s can be calculated. If the concrete being tested has a very low permeability, then instead of waiting until a vacuum pressure of - 70 kPa is achieved, the vacuum pressure change during a 2-min interval is used to calculate the air permeability index.

The main advantage of the Schönlin test is that, because a vacuum is created in the chamber, no permanent attachment or clamping arrangement is required to hold the test apparatus in position. This test, just as all the other tests described previously, is also considerably influenced by the moisture condition of the concrete. In an attempt to eliminate this problem, Schönlin and Hilsdorf[21] suggested that the concrete surface should be dried with hot air for 5 min before the start of a test. This appears to be quite a good idea; however, to achieve the maximum benefit some form of moisture measurement technique needs to be employed to establish the exact moisture condition of the concrete.

6.4.2.4 Surface Airflow Test

The surface airflow test (SAF) is based on a method used by the petroleum industry to determine the permeability of rock cores.[22] A schematic of the apparatus is shown in Figure 6.7. To complete a test, a vacuum plate is placed on the concrete surface. Valves A, B, and C (shown in Figure 6.7) are closed. The vacuum pump is started and allowed to stabilize at a vacuum pressure of approximately - 83 kPa. Because of the capacity of the pump, this should take no more than 15 s. Valve A is then opened allowing the vacuum to be created inside the vacuum plate (again, a pressure of - 83 kPa should be achieved relatively quickly). After the vacuum has been created, valve A is closed and valve B is opened. To maintain the vacuum pressure, the air that has permeated into the vacuum chamber through the concrete is drawn out through the flow meter. After a period of approximately 15 seconds, to allow the system to stabilize,

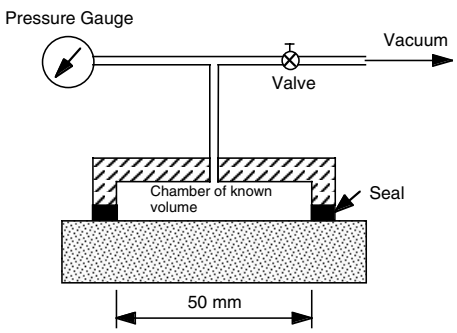

FIGURE 6.6 Schematic of Schönlin surface air permeability test.

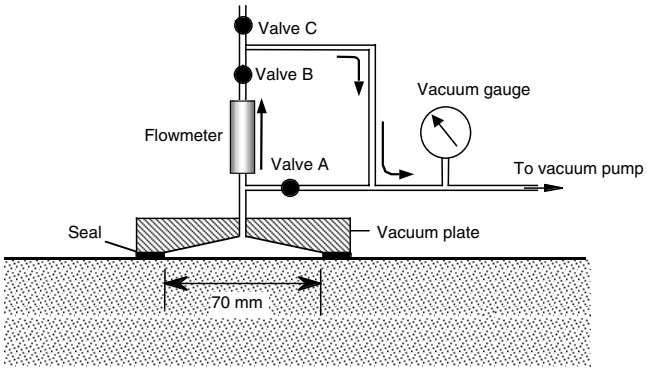

FIGURE 6.7 Schematic of surface airflow test.

the flow rate of the air is measured using a flowmeter as shown Figure 6.7. This flow rate is used as a measure of the surface air permeability. Similar to the Schönlin test, if it is suspected that the surface layer has high moisture content, the surface should be dried with hot air.

6.5 Concluding Remarks

This chapter has presented a brief description of the pull-off strength testing technique and a short discussion of the principles, advantages, and disadvantages of some of the techniques available for measuring the permeation properties of concrete. The intention of this chapter has not been to provide a complete exhaustive list and details of all possible test techniques but rather a brief description of some of the most popular test techniques. If more detailed information about any of the test techniques is required, then the appropriate references quoted should be consulted.

References

1. Murray, A. McC., The Development and Application of the Pull-Out Test for Concrete Strength, Ph.D. thesis, The Queen's University of Belfast, 1984.
2. Mehta, P.K., Concrete technology at the crossroads — problems and opportunities, in *Concrete Technology æ Past, Present and Future, Proc. V. Mohan Malhotra Symposium*, P.K. Mehta, Ed., ACI SP-144, 1994, 1.
3. Feldman, R.F. and Sereda, P.J., A model for hydrated portland cement paste as deduced from sorption-length changes and mechanical properties, *RILEM Bull.*, 1(6), 509, 1968.
4. The Concrete Society, Permeability testing of site concrete — a review of methods and experiences, Technical Report 3, London, Aug. 1988.
5. McCurrich, L.H., In-situ permeability of concrete æ a review of testing and experience, Concrete Society Technical Report, 1985.
6. Rose, D.A., Water movement in unsaturated porous materials, *RILEM Bull.,* 29, 119, Dec. 1965.
7. Neville, A.M., *Properties of Concrete*, 4th ed., Longman, London, 1995.
8. Perraton, D. and Aitcin, P.C., Permeability as seen by the researcher, in *High Performance Concrete: From Material to Structure*, Y. Mailer, Ed., E. & F.N. Spon, London, 1992.
9. Basheer, P.A.M., A brief review of methods for measuring the permeation properties of concrete in-situ, in *Proc. Inst. Civ. Eng. Struct. Bldgs.*, Tech. note 603, 99, 1993, 74.
10. Soroka, L., Permeability of lightweight aggregate concrete, in *Proc. 2nd Int. CIB/RILEM Symp. on Moisture Problems in Buildings*, Rotterdam, Sept. 1974.
11. Meyer, A., The importance of the surface layer for the durability of concrete structures, *Katharine and Bryant Mather Int. Conf. on Concrete Durability*, J.M. Scanlon, Ed., ACI SP-100, American Concrete Institute, Farmington Hills, MI, 1987, 48.

12. Farahbakhsh, B., Permeability Studies of Concrete, M.Sc. thesis, Department of Civil and Structural Engineering, University of Manchester Institute of Science and Technology, Manchester, U.K., 1989.
13. Bungey, J.H., *Testing of Concrete in Structures*, 2nd ed., Surrey University Press, Surrey, U.K., 1989.
14. Glanville, W.H., The permeability of portland cement concrete, Building Research Establishment, Tech. Paper, 3, 1931.
15. Levitt, M., Non-destructive testing of concrete by the initial surface absorption method, in *Proc. Symp. Non-destructive Testing of Concrete and Timber*, ICE, London, 1969, 23.
16. British Standards Institution, Methods of testing hardened concrete for other than strength, BSI London, BS 1881: Part 5, 1970.
17. British Standards Institution, Methods of testing hardened concrete for other than strength, BSI London, BS 1881: Part 208, 1996.
18. Montgomery, F.R. and Adams, A., Early experience with a new concrete permeability apparatus, in *Proc. Structural Faults æ 85*, ICE, London, 1985, 359.
19. Basheer, P.A.M., "Clam" Permeability Tests for Assessing the Durability of Concrete, Ph.D. thesis, The Queen's University of Belfast, 1991, 438 pp.
20. Figg, J.W., Methods of measuring air and water permeability of concrete, *Mag. Concr. Res.,* 25(85), 213, 1973.
21. Schönlin, K. and Hilsdorf, H., Evaluation of effectiveness of curing concrete structures, in *Katharine and Bryant Mather Int. Conf. on Concrete Durability*, J.M. Scanlon, Ed., ACI SP-100, American Concrete Institute, Farmington Hills, MI, 1987, 207.
22. Whiting, D. and Cady, P.D., Method of field measurement of concrete permeability, in *Condition Evaluation of Concrete Bridges Relative to Reinforcement Corrosion*, Vol. 7, SHRP-S/FR-92-109, National Research Council, Washington, D.C., 1992.

7

Resonant Frequency Methods*

7.1 Introduction
7.2 Resonant Frequency Method
Test Equipment · Vibration Generating Section · Vibration Sensing Section · Operation of the Sonometer · Calculation of Dynamic Moduli of Elasticity and Rigidity and Poisson's Ratio
7.3 Other Methods of Resonant Frequency Testing
7.4 Factors Affecting Resonant Frequency and Dynamic Modulus of Elasticity
Influence of Mix Proportions and Properties of Aggregates · Specimen-Size Effect · Influence of Curing Conditions
7.5 Resonant Frequency and Durability of Concrete
Deterioration of Concrete in Freezing and Thawing Cycling · Corrosion of Concrete in Aggressive Media
7.6 Reproducibility of Test Results
7.7 Correlation between Dynamic Modulus of Elasticity and Strength Properties of Concrete
7.8 Comparison of Moduli of Elasticity Determined from Longitudinal and Transverse Frequencies
7.9 Comparison of Dynamic and Static Moduli of Elasticity
7.10 Specialized Applications of Resonance Tests
7.11 Damping Properties of Concrete
Logarithmic Decrement · Damping Constant
7.12 Standardization of Resonant Frequency Methods
7.13 Limitations and Usefulness of Resonant Frequency Methods

V. Mohan Malhotra
Department of Natural Resources Canada, Ottawa

Vasanthy Sivasundaram
Department of Natural Resources Canada, Ottawa

This chapter presents a review of resonant frequency method of testing concrete nondestructively. The background and the theoretical basis of this method are briefly discussed, and the test method standardized originally by ASTM is detailed. The method of resonant frequency testing using impact is also described. The factors affecting resonant frequency and dynamic modulus of elasticity, study of durability of concrete by means of resonant frequency testing, and the correlations between dynamic modulus of elasticity and static modulus of elasticity and strength properties of concrete are presented. A brief discussion of the damping properties of concrete is also given. Specialized applications of this test method and its usefulness and limitations are discussed. An extensive reference list is included.

7.1 Introduction

An important dynamic property of any elastic system is the natural frequency of vibration. For a vibrating beam of given dimensions, the natural frequency of vibration is mainly related to the dynamic modulus of elasticity and density. Hence, the dynamic modulus of elasticity of a material can be determined from the measurement of the natural frequency of vibration of prismatic bars and the mathematical relationships existing between the two. These relationships were derived for solid media considered to be homogeneous, isotropic, and perfectly elastic, but they may be applied to heterogeneous systems, such as concrete, when the dimensions of the specimens are large in relation to the size of the constituents of the material.

For flexural vibrations of a long-thin rod, the following equation or its equivalent may be found in any complete textbook on sound:[1]

$$N = \frac{m^2 k}{2\pi L^2}\sqrt{\frac{E}{d}} \tag{7.1}$$

and solving for E

$$E = \frac{4\pi^2 L^4 N^2 d}{m^4 k^2} \tag{7.2}$$

where

E = dynamic modulus of elasticity
d = density of the material
L = length of the specimen
N = fundamental flexural frequency
k = radius of gyration of the section about an axis perpendicular to the plane of bending
k = $t/12$ for rectangular cross section where t = thickness
m = a constant (4.73 for the fundamental mode of vibration)

The dynamic modulus of elasticity can also be computed from the fundamental longitudinal frequency of vibration of a specimen, according to the following equation:[2]

$$E = 4L^2 dN^2 \tag{7.3}$$

Equations 7.1 and 7.3 were obtained by solving the respective differential equations for the motion of a bar vibrating: (1) in flexure in the free-free mode, and (2) in the longitudinal mode.

Thus, the resonant frequency of vibration of a concrete specimen or structure directly relates to its dynamic modulus of elasticity and, hence, its mechanical integrity. The method of determining the dynamic elastic moduli of solid bodies from their resonant frequencies has been in use for the past 55 years. However, until up to the last few years, resonant frequency methods had been used almost exclusively in laboratory studies. In these studies, natural frequencies of vibration are determined on concrete prisms and cylinders in order to calculate the dynamic moduli of elasticity and rigidity, the Poisson's ratio, and for monitoring the degradation of concrete during durability tests.

7.2 Resonant Frequency Method

This method was first developed by Powers[3] in the United States in 1938. He determined the resonant frequency by matching the musical tone created by concrete specimens, usually 51 × 51 × 241-mm prisms, when tapped by a hammer, with the tone created by one of a set of orchestra bells calibrated according

to frequency. The error likely to occur in matching the frequency of the concrete specimens to the calibrated bells was of the order of 3%. The shortcomings of this approach, such as the subjective nature of the test, are obvious. But this method laid the groundwork for the subsequent development of more sophisticated methods.

In 1939 Hornibrook[4] refined the method by using electronic equipment to measure resonant frequency. Other early investigations on the development of this method included those by Thomson[5] in 1940, by Obert and Duvall[2] in 1941, and by Stanton[6] in 1944. In all the tests that followed the work of Hornibrook, the specimens were excited by a vibrating force. Resonance was indicated by the attainment of vibrations having maximum amplitude as the driving frequency was changed. The resonant frequency was read accurately from the graduated scale of the variable driving audio oscillator. The equipment is usually known as a sonometer, and the equipment has been used to measure various dynamic moduli of concrete.[7–15]

7.2.1 Test Equipment

The testing apparatus required by ASTM C 215-85, entitled "Standard Test Method for Fundamental Transverse, Longitudinal, and Torsional Frequencies of Concrete Specimens,"[7] is shown schematically in Figure 7.1. Equipment meeting the ASTM requirements has been designed by various commercial organizations. One of the commercially available sonometers is shown in Figure 7.2. The resonant frequency test equipment presently used in monitoring the long-term deterioration of massive concrete blocks (dimension 305 × 305 × 915-mm) exposed to sea water in Treat Island, Maine, is shown in Figure 7.3.

The testing apparatus consists primarily of two sections, one generates mechanical vibrations and the other senses these vibrations.[8]

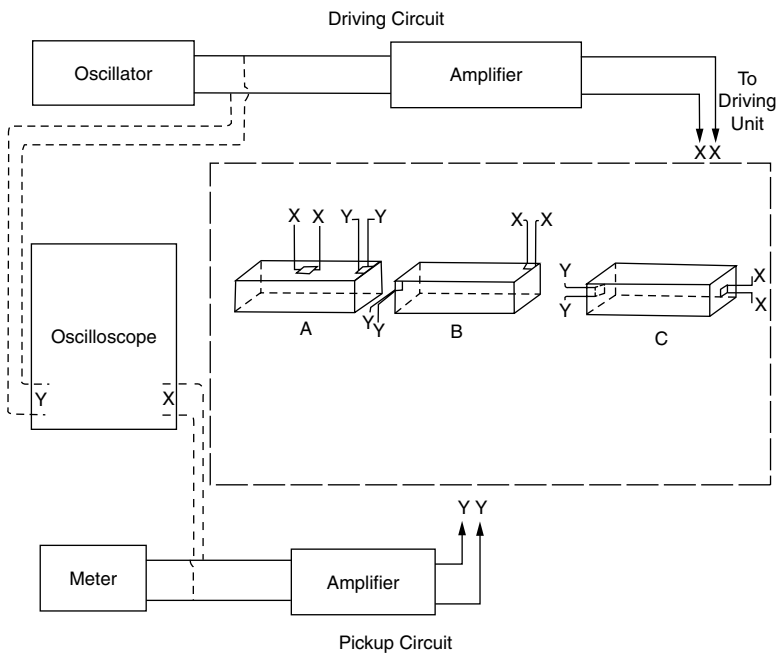

FIGURE 7.1 Schematic diagram of a typical apparatus for the forced resonance method showing driver and pick-up positions for the three types of vibration. (A) Transverse resonance. (B) Torsional resonance. (C) Longitudinal resonance. (Adapted from ASTM C 215-85, *Annual Book of ASTM Standards*, Vol. 04.02, 1986, p. 123.)

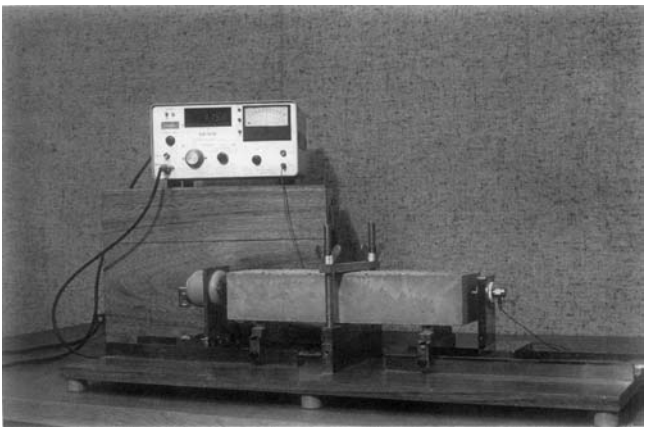

FIGURE 7.2 Longitudinal resonance testing of a 76 × 102 × 406-mm concrete prism by a sonometer.

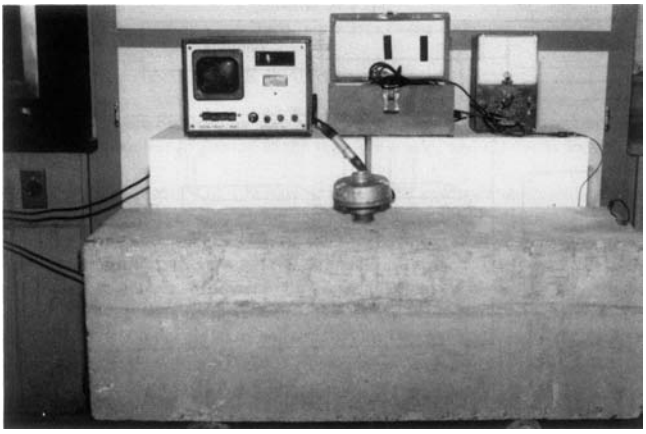

FIGURE 7.3 The resonant frequency test equipment used in monitoring the deterioration of 305 × 305 × 915-mm concrete blocks exposed to sea water in Treat Island, Maine.

7.2.2 Vibration Generating Section

The principal part of this section is an electronic audio-frequency oscillator, which generates electrical audio-frequency voltages. The oscillator output is amplified to a level suitable for producing mechanical vibrations. The relatively undistorted power output of the amplifier is fed to the driver unit for conversion into mechanical vibrations.

7.2.3 Vibration Sensing Section

The mechanical vibrations are sensed by a piezoelectric transducer. The transducer is contained in a separate unit and converts mechanical vibrations to electrical AC voltage of the same frequencies. These voltages are amplified for the operation of a panel-mounted meter which indicates the amplitude of the transducer output. As the frequency of the driver oscillator is varied, maximum deflection of the meter needle indicates when resonance is attained. Visible indications that the specimens are vibrating at their fundamental modes can be obtained easily through the use of an auxiliary cathode-ray oscilloscope, and its use is generally recommended.

7.2.4 Operation of the Sonometer

Some skill and experience are needed to determine the fundamental resonant frequency using a meter-type indicator because several resonant frequencies may be obtained corresponding to different modes of vibration. Specimens having either very small or very large ratios of length to maximum transverse direction are frequently difficult to excite in the fundamental mode of transverse vibration. It has been suggested that the best results are obtained when this ratio is between three and five.

The supports for the specimen under test should be of a material having a fundamental frequency outside the frequency range being investigated and should permit the specimen to vibrate without significant restriction. Ideally, the specimens should be held at the nodal points, but a sheet of soft sponge rubber is quite satisfactory and is preferred if the specimens are being used for freezing and thawing studies.

The fundamental transverse vibration of a specimen has two nodal points, at distances from each end of 0.224 times the length. The vibration amplitude is maximum at the ends, about three fifths of the maximum at the center, and zero at the nodal points. Therefore, movement of the pickup along the length of the specimen and observation of the meter reading will show whether the specimen is vibrating at its fundamental frequency.

For fundamental longitudinal and torsional vibrations, there is a point of zero vibration (node) at the midpoint of the specimen and the maximum amplitude is at the ends.

Sometimes in resonance testing of concrete specimens, two resonant frequencies may appear which are close together. Kesler and Higuchi[12] believed this to be caused by a nonsymmetrical shape of the specimen that causes interference due to vibration of the specimen in some direction other than that intended. Proper choice of specimen size and shape should practically eliminate this problem; for example, in a specimen of rectangular cross section the above problem can be eliminated by vibrating the specimen in the direction parallel to the short side.

In performing resonant frequency tests, it is helpful to have an estimate of the expected fundamental frequency. Table 7.1 shows the approximate ranges of fundamental longitudinal and flexural resonant frequencies of standard concrete specimens given by Jones.[13]

7.2.5 Calculation of Dynamic Moduli of Elasticity and Rigidity and Poisson's Ratio

The dynamic moduli of elasticity and rigidity and the Poisson's ratio of the concrete can be calculated by equations given in ASTM C 215-02. These are modifications of theoretical equations applicable to specimens that are very long in relation to their cross section, and were developed and verified by Pickett[9] and Spinner and Tefft.[10] The corrections to the theoretical equations in all cases involve Poisson's ratio and are considerably greater for transverse resonant frequency than for longitudinal resonant frequency. For example, a standard 102 × 102 × 510-mm prism requires a correction factor of about 27% at the fundamental transverse resonance, as compared with less than 0.5% at the fundamental longitudinal resonance.[13,15] The longitudinal and flexural modes of vibration give nearly the same value for the dynamic

TABLE 7.1 Approximate Ranges of Resonant Frequencies of Concrete Prism and Cylinder Specimens

	Approximate Range of Resonant Frequency, Hz	
Size of Specimens (mm)	Transverse	Longitudinal
152 × 152 × 710-mm prism	550–1150	1800–3200
102 × 102 × 510-mm prism	900–1600	2500–4500
152 × 305-mm cylinder	2500–4500	4000–7500

From Jones, R., *Non-Destructive Testing of Concrete*, Cambridge University Press, London, 1962. With permission.

modulus of elasticity. The dynamic modulus of elasticity may range from 14.0 GPa, for low quality concretes at early ages, to 48.0 GPa for good quality concrete at later ages.[11] The dynamic modulus of rigidity is about 40% of the modulus of elasticity.[14]

7.3 Other Methods of Resonant Frequent Testing

A method for determining fundamental frequencies was proposed by Gaidis and Rosenburg[16] as an alternative to the ASTM C 215 method. In this method, the concrete specimen is struck with a small hammer. The impact causes the specimen to vibrate at its natural frequencies. The amplitude and frequency of the resonant vibrations are obtained using a spectrum analyzer that determines the component frequencies via the fast Fourier transform. The amplitude of the specimen response vs. frequency is displayed on the screen of a cathode ray tube, and the frequencies of major peaks can be read directly.

In operation, the pick-up accelerometer is fastened to the end of the specimen with microcrystalline wax, and the specimen is struck lightly with a hammer. The output of the accelerometer is recorded by the waveform analyzer and recorded signal is processed to obtain the frequency response. On the resulting amplitude vs. frequency curve, a dot marker may be moved to coincide with the peak, and the frequency value of the peak is displayed on the screen (Figure 7.4). Some typical results obtained with this method and those obtained with ASTM C 215 are shown in Table 7.2. The advantages of this method over the forced-resonance procedure in ASTM C 215 are the greater speed of testing, and capability of testing specimens having a wide range of dimensions. However, the initial high cost of equipment appears to be a disadvantage. In 1991, this impact resonance procedure was adopted by ASTM as an alternative to the existing procedure.

7.4 Factors Affecting Resonant Frequency and Dynamic Modulus of Elasticity

A number of factors affect the resonant frequency measurements, the dynamic modulus of elasticity, or both. Some of these are discussed below.

7.4.1 Influence of Mix Proportions and Properties of Aggregates

The dynamic modulus of elasticity of concrete is affected by the elastic moduli of its constituent materials and their relative proportions. According to Jones,[13] for a given composition of cement paste, that is, the

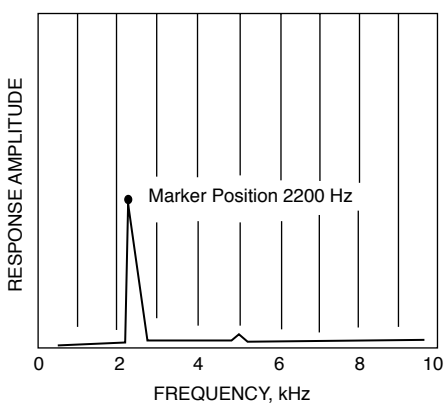

FIGURE 7.4 The amplitude of specimen response vs. frequency, displayed on a cathode-ray tube. (Adapted from Reference 16.)

TABLE 7.2 Fundamental Transverse Frequencies of Concrete Determined Using ASTM C 215 and the Impact-Resonance Method

Prism Size, mm	ASTM C 215 Method Frequency (Hz)	Spectrum Analyzer Frequency (Hz)
76.2 × 102 × 406	1762	1760
76.2 × 102 × 406	1725	1720
76.2 × 102 × 406	728	620
76.2 × 102 × 406	1936	1860
76.2 × 102 × 406	1912	1920
76.2 × 102 × 406	1243	980
25.4 × 25.4 × 279	1148	1160
25.4 × 25.4 × 279	1077	1060
25.4 × 25.4 × 279	977	980
25.4 × 25.4 × 279(γ)	501	400

γ damaged by freezing and thawing cycling.
From Gaidis, J.M. and Rosenburg, M., *Cem. Concr. and Aggr.*, 8, 117, 1986.

same water-cement ratio, the elastic modulus of hardened concrete increases with an increase in the percentage of total aggregate. It has also been reported that an increase in the amount of mixing water or in the volume of entrapped air reduces the dynamic modulus of elasticity.[13]

In a recent CANMET study* of concretes incorporating high volumes of low-calcium fly ashes, the values of static and dynamic elastic moduli were found to be relatively high in relation to the strength. The higher values are believed to be caused by the unhydrated fly ash particles acting as fine filler in the concrete.

7.4.2 Specimen-Size Effect

Obert and Duvall[2] demonstrated that for a given concrete, the value of the dynamic modulus of elasticity varies depending on the size of specimen used in the measurements. The larger specimens, because of their dimensions and weight, have lower resonant frequencies. Kesler and Higuchi[12] found that longer beams resonating at lower frequencies gave higher elastic moduli than did proportionately smaller beams. On the other hand, Jones[13] found little change in the dynamic modulus for different specimens having a frequency range of 70 to 10,000 Hz. Thornton and Alexander[17] pointed out that, if other parameters remain unchanged, the resonant frequency of the fundamental flexural mode will increase with the increase in thickness or with the decrease in length of the specimen.

7.4.3 Influence of Curing Conditions

Obert and Duvall[2] have shown that although the dynamic modulus of elasticity depends on the moisture content, the change in the elastic modulus with drying is rather small after about 3 or 4 days of air drying. Further, it has been shown that a large decrease in the dynamic modulus of elasticity occurs over the first 48 h of oven drying but the subsequent change is small. Oven drying, even at as low a temperature as 34°C, causes an irreversible reduction of the elastic modulus. A possible explanation is that shrinkage results in micro-cracking of paste with subsequent reduction in its stiffness and thus affecting the value of the dynamic modulus of elasticity.

Kesler and Higuchi[18] in their studies have concluded:

1. For the same curing conditions, the dynamic modulus of elasticity increases as the strength increases.

*Unpublished CANMET data.

2. If the concrete is kept moist, the modulus of elasticity increases with age, and if the concrete is allowed to dry, the modulus of elasticity decreases with age.

However, studies on large blocks incorporating large amounts of supplementary cementing materials have indicated that longer periods of air-drying do not cause any detrimental effects on the static and dynamic moduli of elasticity. These findings have been confirmed by pulse-velocity measurements as well. The strength gain in these concretes over longer periods of time due to the pozzolanic reaction of the supplementary materials appears to cause the increase in elastic moduli.

Jones[13] reported significant differences in the values of elastic moduli determined from flexural and longitudinal resonance tests on beam specimens moist-cured for 25 days and subsequently air-cured for 150 days. The above difference is believed to have been caused by the loss of moisture resulting in gradients for moisture content, elastic modulus, and density in each dimension of the beam. These gradients would affect the flexural and longitudinal modes of vibration in different ways.

The effects of curing conditions on the resonant frequency and dynamic modulus of elasticity are rather critical. Unless special curing conditions are required, water-curing is to be preferred and the specimen should be in a water-saturated or saturated-surface-dry condition at the time of test. This will help in achieving more reproducible results.

7.5 Resonant Frequency and Durability of Concrete

The determination of flexural resonance has been employed to advantage in studying the effects of successive accelerated freezing and thawing cycles and aggressive environments on concrete specimens. The advantages of resonance methods in this regard are:

1. The repeated tests can be carried out on the same specimens over a very long period, and the number of test specimens to be cast is therefore greatly reduced.
2. The results obtained with flexural resonance methods on the same specimen are more reproducible than those obtained with destructive tests on a group of supposedly duplicate specimens.

7.5.1 Deterioration of Concrete in Freezing and Thawing Cycling

Extensive studies of changes in dynamic modulus of elasticity with the deterioration of concrete subject to repeated cycles of freezing and thawing have been reported by Hornibrook,[4] Thomson,[5] Long and Kurtz,[19] Axon et al.,[20] and Malhotra and Zoldners.[21–23] Results of one such study are shown in Figure 7.5.

The ASTM Method C 666-84, entitled "Standard Test Method for Resistance of Concrete to Rapid Freezing and Thawing," specifies resonant frequency methods for studying the deterioration of concrete specimens subjected to repeated cycles of freezing and thawing. The standard requires the calculation of the relative dynamic modulus of elasticity and durability factor.

Wright and Gregory[24] suggested the use of the resonant frequency values rather than the values of dynamic elastic modulus as a criterion for evaluating the results of freezing and thawing tests. This is because the calculations for the dynamic elastic modulus are based on the assumption that concrete is isotropic and homogeneous material, which it is not. The calculations in ASTM C 666 use the square of the resonant frequency values to evaluate the test results. Changes in the shape factor, due to dimensional changes during the test, are ignored.

7.5.2 Corrosion of Concrete in Aggressive Media

A number of studies have been reported in which resonance methods have been used to determine the damage sustained by concrete in aggressive media such as acidic or alkaline environments.

In one study, the corrosive effect of ammonium nitrate-based fertilizers on blended natural pozzolan-portland cement concretes was investigated by testing for dynamic modulus of elasticity and density for 8 weeks.[25] It was observed that the corrosive effect increased with nitrification of the alkaline

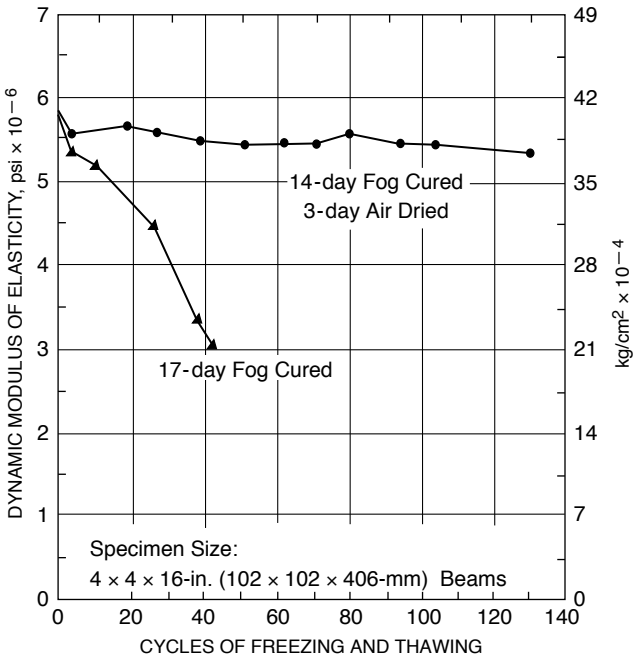

FIGURE 7.5 Effect of cycles of freezing and thawing on dynamic modulus of elasticity. (Adapted from Reference 19.)

medium, and the concretes made with pozzolan-substituted cements were more damaged than the portland cement concretes. Studies dealing with the determination of the dynamic elastic modulus of concrete specimens made from five different types of cements and subjected to the action of ammonium nitrate solution have been reported by Chefdeville.[26] In his investigation, the percentage reduction in the dynamic elastic modulus of elasticity of the concrete specimens was calculated by subjecting the specimens to resonant frequency testing at predetermined intervals. It was found that the reduction in the dynamic elastic modulus is somewhat similar to that obtained in the freezing and thawing studies. The corrosive effects of dilute sulfuric acid and acetic acids on concrete prisms have also been reported by Stuterheim et al.[12-b]

7.6 Reproducibility of Test Results

Limited data are available on the reproducibility of the dynamic modulus of elasticity based on resonance tests. Jones[13] has published data indicating that for standard-size prisms and cylinders the reproducibility of dynamic modulus of elasticity is superior to that obtained in static tests (Table 7.3). According to Jones, the greater variability of the static elastic modulus results is due to greater errors introduced in the testing procedure rather than to greater variability between specimens. On the other hand, each of the measurements needed to determine the dynamic elastic modulus by resonance methods, that is, the resonant frequency, length, and density, can be measured accurately.

ASTM C 215 gives the following precision statement for fundamental transverse frequency only, determined on concrete prisms as originally cast.

Single-Operator Precision — Criteria for judging the acceptability of measurements of fundamental transverse frequency obtained by a single operator in a single laboratory on concrete specimens made from the same materials and subjected to the same conditions are given in below. These limits apply over the range of fundamental transverse frequency from 1400 to 3300 Hz.

TABLE 7.3 Comparison of Reproducibility of the Standard Methods of Measuring Static and Dynamic Young's Modulus of Elasticity

Size of Specimen (mm)	Young's Modulus of Elasticity	No. of Specimens	Standard Error of 3 Results (MPa)
152 × 305-mm cylinder	Static	3	604
76 × 76 × 305-mm prisms	Static	3	1000
152 × 152 × 710-mm prisms	Dynamic	3	270
102 × 102 × 510-mm prisms	Dynamic	3	350
76 × 76 × 305-mm prisms	Dynamic	3	370

From Jones, R., *Non-Destructive Testing of Concrete*, Cambridge University Press, London, 1962. With permission.

Test Results for Single Operator in a Single Laboratory

	Coefficient of Variation, %[a]	Acceptable Range of Two Results, % of Average[a]
Within-batch single specimen	1.0	2.8
Within-batch, average of 3 specimens[b]	0.6	1.7
Between-batch, average of 3 specimens per batch	1.0	2.8

[a] These numbers represent, respectively, the 1S% and D2S% limits as described in Practice C 670.
[b] Calculated as described in Practice C 670.

Note 1 — The coefficients of variation for fundamental transverse frequency have been found to be relatively constant over the range of frequencies given for a range of specimen sizes and age or condition of the concrete, within limits.

The different specimen sizes represented by the data include the following (the first dimension is the direction of vibration):

76 by 102 by 406 mm (3 by 4 by 16 in.)

102 by 76 by 406 mm (4 by 3 by 16 in.)

89 by 114 by 406 mm ($3^1/_2$ by $4^1/_2$ by 16 in.)

76 by 76 by 286 mm (3 by 3 by $11^1/_4$ in.)

102 by 89 by 406 mm (4 by $3^1/_2$ by 16 in.)

76 by 76 by 413 mm (3 by 3 by $16^1/_4$ in.)

The multilaboratory coefficient of variation for averages of three specimens from a single batch of concrete has been found to be 3.9% for fundamental transverse frequencies over the range from 1400 to 3300 Hz (Note 2). Therefore, two averages of three specimens from the same batch tested in different laboratories should not differ by more than 11.0% of their common average (see Note 6).

Note 2 — These numbers represent, respectively, the 1S and D2S limits as described in Practice C 670, where 1S is the estimate of the standard deviation characteristic of the total statistical population and D2S is the difference between two individual test results that would be equaled or exceeded in the long run in only 1 case in 20 in the normal and correct operation of the method.

7.7 Correlation between Dynamic Modulus of Elasticity and Strength Properties of Concrete

Several investigators[27–34] have attempted to establish empirical relationships between the dynamic modulus of elasticity and strength of concrete. Some of these correlations appear to hold for the particular type of concrete investigated, but it is doubtful that any generalized relationships can be given. Therefore, if the flexural and compressive strengths of concrete are to be estimated from the dynamic modulus of elasticity, it is essential first to establish an experimental relationship between these strengths and the dynamic modulus of elasticity.

Jones[13] stated that no general relationship exists between the dynamic elastic modulus of concrete and its flexural or compressive strength. Nevertheless, he concluded that limited correlations are obtained when the changes in the dynamic elastic modulus and strength are produced by changes in the age of the concrete, the degree of compaction, the water-cement ratio, or by deterioration.

Notwithstanding the above limitations, relationships, between the strength parameters and the dynamic modulus of elasticity have been reported by various researchers.[31,34] Two such relationships are illustrated in Figures 7.6 and 7.7.

7.8 Comparison of Moduli of Elasticity Determined from Longitudinal and Transverse Frequencies

In routine calculation of dynamic elastic modulus, only the transverse frequencies are determined because it is generally easier to determine the transverse resonant frequency. However, Batchelder and Lewis[35] have shown that excellent correlation exists between the elastic moduli calculated from the transverse and longitudinal frequencies (Figure 7.8).

In his studies, Jones[13,15] found that for wet concretes there was no appreciable difference in the dynamic modulus of elasticity determined from the transverse and longitudinal modes of vibration. However, when the beams were allowed to dry, the dynamic elastic modulus calculated from the transverse vibrations was lower than that calculated from longitudinal vibrations. This was attributed to the moisture gradients within the concrete beams.

7.9 Comparison of Dynamic and Static Moduli of Elasticity

A considerable amount of work has been carried out by various researchers to establish the relationship between the dynamic elastic modulus and static elastic modulus obtained from conventional stress-strain

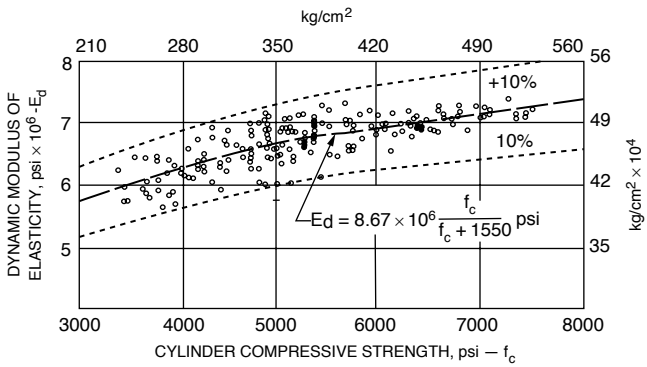

FIGURE 7.6 Relationship between dynamic modulus of elasticity and compressive strength of concrete. (Adapted from Reference 31.)

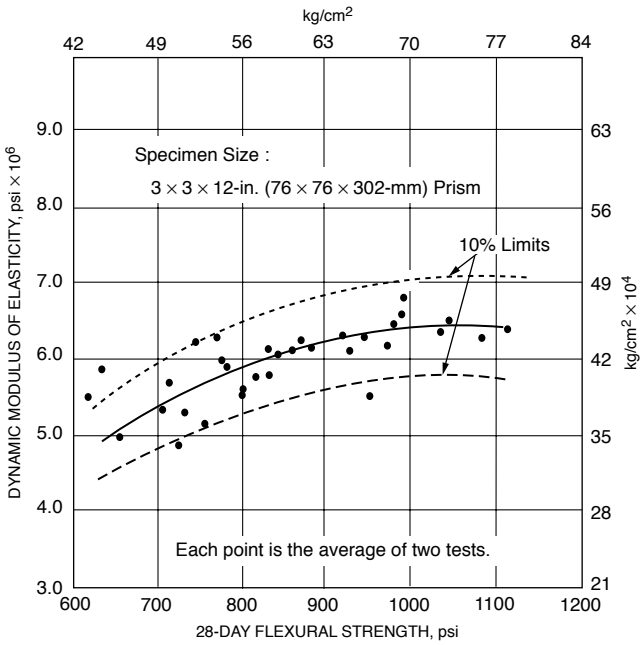

FIGURE 7.7 Relationship between dynamic modulus of elasticity and 28-day flexural strength of concrete. (Adapted from Reference 34.)

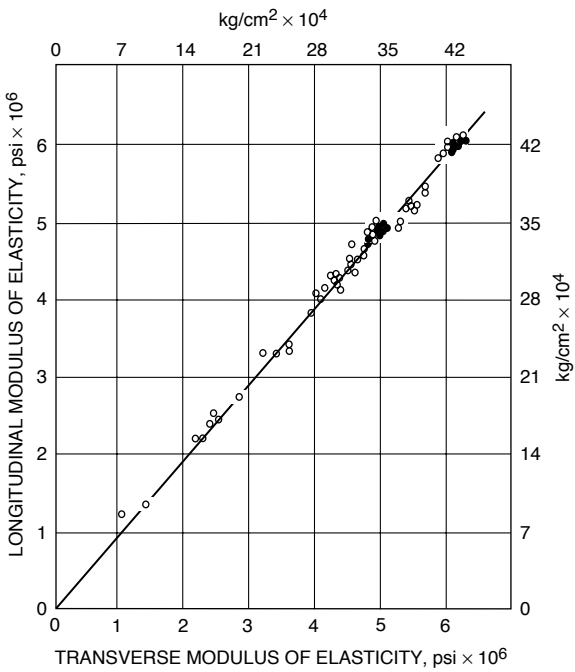

FIGURE 7.8 Comparison of dynamic moduli of elasticity determined from longitudinal and transverse frequencies. (Adapted from Reference 35.)

tests conducted at low rates of loading as in ASTM C 469. It should be noted that resonance tests subject the concrete to very low strains compared to static load tests. The following observations may be made from the investigations by Powers,[3] Stanton,[6] Sharma and Gupta,[31] Whitehurst,[36] Klieger,[37] and Philleo:[38]

1. The dynamic modulus of elasticity is generally somewhat higher than the static elastic modulus; the difference depends upon the degree of precautions taken during the conduct of the experiments and the applications of the correction factors allowed for in the equations for the computations of the dynamic elastic modulus.
2. As the age of the specimen increases, the ratio of static elastic modulus to dynamic modulus also increases and more nearly approaches 1.0.*
3. For higher static moduli of elasticity, the values for both dynamic and static moduli of elasticity show close agreement.

Figure 7.9 shows the relationship between static and dynamic elastic moduli for high-strength concrete as developed by Sharma and Gupta.[31]

Hansen[39] reported an investigation in which concretes with paste contents of 32 and 50%, each having water-cement ratios of 0.40 and 0.60, were investigated together with a concrete with 20% replacement of cement by silica fume. This study showed that the static elastic modulus determined according to ASTM C 469 could be predicted from the dynamic elastic modulus computed using the resonance technique. It was also shown that the entire static elastic modulus vs. strength relationship for each concrete could be predicted from early age measurements of dynamic elastic modulus and compressive strength. Figure 7.10 shows the excellent agreement of the results of this study to those obtained by Kesler and Higuchi.[18]

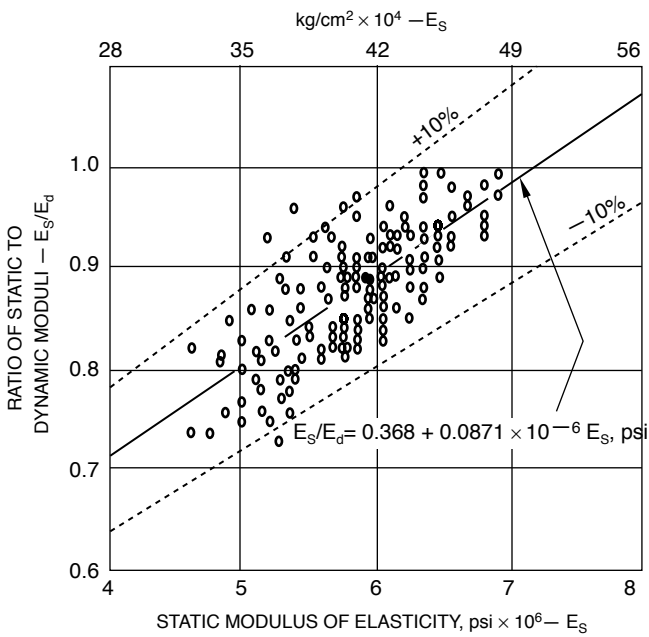

FIGURE 7.9 Relationship between static modulus of elasticity and ratio of static to dynamic moduli. (Adapted from Reference 31.)

*On the basis of tests of 2-year-old specimens reported by Witte and Price,[6] the static elastic modulus in compression was equivalent to 89% of the dynamic modulus, while the static elastic modulus in flexure was equal to 88% of the dynamic modulus. When the tests were repeated after the specimens were 3 years old, these values were found to be 96 and 87%, respectively.

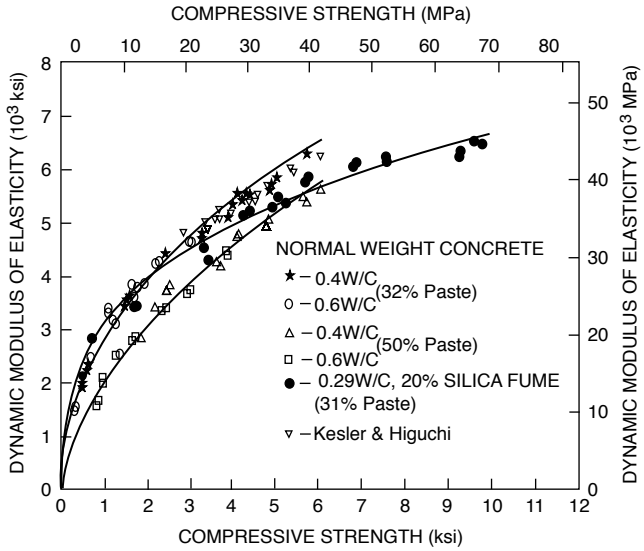

FIGURE 7.10 Dynamic modulus of elasticity for concretes containing river gravel. (Adapted from Reference 39.)

Figure 7.11 shows the elastic modulus-compressive strength curves obtained from early-age results (less than 3 days) as well as those obtained over the entire age span investigated. The predicted modulus of elasticity values are within 5% and 1% for the two systems with and without silica fume, respectively, when compared with those calculated from regression curves, based on data up to 28 days.

7.10 Specialized Applications of Resonance Tests

Gatfield[40] has reported a relatively simple and inexpensive technique for fatigue tests of plain concrete using the resonant frequency method. In his method, significant vibratory strains up to 120×10^{-6} are induced on concrete specimens in flexure. The local failures caused by the loading are determined by measuring the changes in flexural resonant frequency. Also, studies on creep and relaxation of concrete using the resonant frequency techniques have been reported by Chang and Kesler.[41,42]

The variations in the dynamic elastic modulus measured before and after the test specimens were subjected to loading-unloading cycles have been published by Daxelhofer.[12-k] It was concluded that the stressing of concrete even for a short time affected the dynamic elastic modulus, which showed a decrease of 3 to 3.5% at 28 days.

Thornton and Alexander[17] observed in a study that the dynamic elastic modulus of large concrete structures, and hence, their mechanical integrity, can be assessed by measuring the fundamental resonant frequency of vibration. In this investigation, mathematical and physical modeling tests of large concrete piers were performed in order to establish the range of frequencies expected when actual tests were performed. Following the laboratory modeling, resonant frequency measurements were performed on the actual piers by setting the structures in motion by impact loading, and the frequency content of the vibrations was determined by waveform analyzers. The results indicated that the piers were structurally sound, and it was shown that by exciting a structure with an impact force and analyzing the output, reliable data of overall structural integrity could be obtained.

7.11 Damping Properties of Concrete

Damping is the property of a material causing free vibrations in a specimen to decrease in amplitude as a function of time. In concrete technology it is short-term decay that is of interest rather than long-term effects. Several investigators, particularly Thomson,[5] Obert and Duvall,[2] Kesler and Higuchi,[18] and

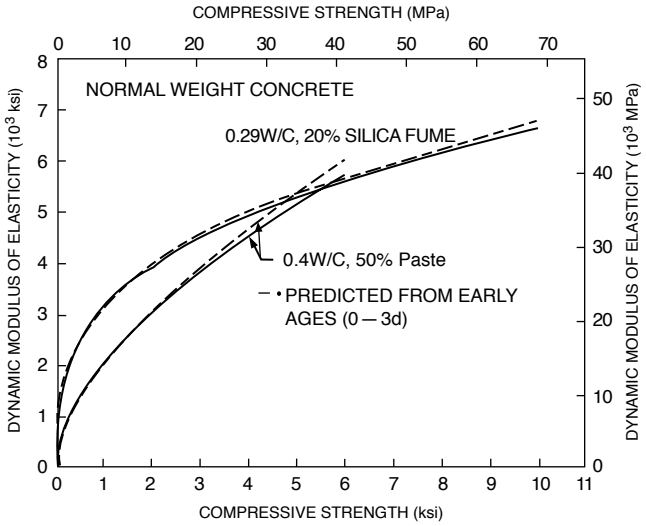

FIGURE 7.11 A comparison between dynamic elastic modulus vs. compressive strength curves predicted from early ages, and curing times up to about 28 days. (Adapted from Reference 39.)

Shrivastava and Sen,[30] Swamy and Rigby[14] have shown that certain properties of concrete can be related to its damping ability.

There are several methods of determining the damping characteristics of a material, but two common methods used for concrete are

1. The determination of logarithmic decrement, δ, which is the natural logarithm of the ratio of any two successive amplitudes in the free vibration of the specimen
2. Calculation of the damping constant Q from the resonance curve of the test specimen

7.11.1 Logarithmic Decrement

The logarithmic decrement is the natural logarithm of the ratio between the amplitudes of successive oscillations in the damped sine wave produced by the decay of free vibrations of a specimen, and it is given by the following equation:

$$\delta = ln\frac{h_1}{h_2} \tag{7.4}$$

where

δ = logarithmic decrement
h_1 and h_2 = amplitudes of two successive vibrations after the driving force has been removed from the specimen

The amplitudes h_1 and h_2 can be obtained by using an oscilloscope to record the decay of vibrations at resonance after the driving oscillator is turned off. The image on a cathode-ray oscilloscope can be photographed, and the amplitudes h_1 and h_2 can easily be measured off the developed film. If a digital oscilloscope is used, the amplitudes can be measured directly from the display using the cursor controls.

7.11.2 Damping Constant

The damping constant Q is given by the equation

$$Q = \frac{f_0}{f_2 - f_1} \tag{7.5}$$

where

Q = damping constant
f_0 = resonant frequency of vibrations
f_1, f_2 = frequencies on either side of resonance at which the amplitude is 0.707 times the amplitude at resonance

The values of f_1 and f_2 can be determined if an output meter is employed for resonance indication. After locating the fundamental resonance, the oscillator is detuned on each side of the resonance frequency until the output meter reads 0.707 times the reading at resonance. The frequencies at which this occurs are the frequencies f_1 and f_2.[13] In general, hardened concrete has Q values between 50 and 200; the higher the value of Q the smaller the decrease in successive amplitudes of vibration.

Figure 7.12 is a resonance curve to illustrate how the damping constant is determined. In this case the value of f_0 is 1990 Hz and the values of f_2 and f_1, at which the amplitude was 0.707 times the amplitude at resonance are 1996 and 1984 Hz, respectively. This gives a Q value of 1990/12 = 166.

The relationship between the damping constant and the logarithmic decrement is as follows:

$$Q = \frac{\pi}{\delta} \tag{7.6}$$

Substituting the value of δ from Equation 7.4:

$$Q = \frac{\pi}{ln\frac{h_1}{h_2}} \tag{7.7}$$

Table 7.4 gives values of the damping constant for rock specimens obtained using the resonance curve method and the decay procedure. According to Obert and Duvall,[2] of the above two methods, the resonance curve approach is the more accurate and the less difficult to measure.

The damping in concrete is a complex phenomenon. According to Swamy and Rigby,[14] most of the damping in concrete occurs in the matrix, with some in the interfacial boundaries, and less in the aggregate. The presence of air voids in dry specimens contributes little to the damping, whereas moisture in the matrix is a major contributor to the damping ability of concrete.

In measuring the parameters associated with the damping properties of concrete, considerable care should be taken to use supports that exert low restraint on the concrete specimens. Otherwise, substantial energy losses would be introduced, resulting in erroneous test data.

The study of the vibrational characteristics of structures, such as frequency, damping, and mode shape is called modal analysis.[17] The relationship between the modal properties and the factors influencing them is complex. Generally factors such as geometry, elastic modulus, and boundary conditions significantly affect the modal properties.

Thornton and Alexander[43] observed that the resonant frequencies and the damping functions can be calculated by the input of parameters of geometry, restraint, and dynamic elastic modulus of the total structure into a finite element program, calibrated from measurements made at the completion of construction, when the structure is known to be sound. These values then can be compared with actual data measured from the structure at a later time to detect any anomalies.

In one field investigation, impact-resonance measurements were made on the walls of both the prototype and the model of a concrete building.[43] Measurements of mode shapes, resonant frequencies, and damping factors were made on the prototype before soil was moved against the outside walls and

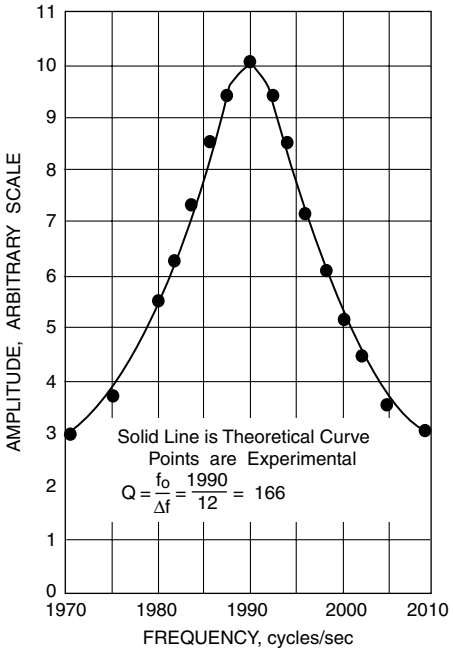

FIGURE 7.12 Representative resonance curve. (Adapted from Reference 2.)

TABLE 7.4 Damping Constant as Determined from the Width of Resonance Cure and from the Logarithmic Decay of Free Vibration

Material	Damping Constant Q	
	Resonance	Decay
Granite No. 50	456	444
Granite No. 51	435	417
Granite No. 47	297	286
Granite No. 48	280	256
Granite No. 49	250	270
Sandstone No. 39	83	86
Sandstone No. 41	59	54
Sandstone No. 42	61	61

From Obert, L. and Duvall, W.I., in *Proc. ASTM*, 41, 1053, 1941. With permission.

afterward. When the wall was covered by soil, the resonant frequency of the fundamental mode was found to increase by 30% together with an increase in damping. Later, the prototype wall was subjected to blast loading and sustained minor structural damage. Again, the impact-resonance measurements were repeated after removing the soil away from the wall. Compared with the initial measurements (without soil), the resonant frequency was found to be decreased slightly, and the damping was found to be decreased significantly.

Thornton and Alexander[43] have reported another investigation in which tests made on a dam showed that the damping was about 3 or 4% of critical damping. When damping is less than critical, the motion is oscillatory, and it is non-oscillatory otherwise. When cylinders made from the dam concrete were tested, supported at the nodes with narrow supports, the damping of the specimens was found to be only 0.37% of critical damping. Although size may have been a factor, the boundary conditions were considered more critical in influencing the damping. The damping was found to be (1) 0.55%, (2) 0.86%, and (3) 1.5% of critical damping, when the cylinders were tested (1) lying on the soil, (2) embedded 50

mm deep in the soil, and (3) embedded 75 mm deep in the soil, respectively. In all the above, damping was determined from measurements of the fundamental resonant frequency of the flexural mode, and the frequency was not found to change significantly. The above indicates the ability of the boundary conditions to influence damping.

7.12 Standardization of Resonant Frequency Methods

The ASTM Test Method C 215 "Standard Test Method for Fundamental Transverse, Longitudinal, and Torsional Frequencies of Concrete Specimens" was published first in 1947 and since then has been revised periodically.[7] The last revision to this Standard was in 2002. In 1991, the impact-resonance procedure was added as an alternative to the forced resonance procedure.

The significance and use statement of the test method as given in ASTM C 215-02 is as follows:[7]

5.1 This test method is intended primarily for detecting significant changes in the dynamic modulus of elasticity of laboratory or field test specimens that are undergoing exposure to weathering or other types of potentially deteriorating influences.

5.2 The value of the dynamic modulus of elasticity obtained by this test method will, in general, be greater than the static modulus of elasticity obtained by using Test Method C 469. The difference depends, in part, on the strength level of the concrete.

5.3 The conditions of manufacture, the moisture content, and other characteristics of the test specimens (see section on Test Specimens) materially influence the results obtained.

5.4 Different computed values for the dynamic modulus of elasticity may result from widely different resonant frequencies of specimens of different sizes and shapes of the same concrete. Therefore, it is not advisable to compare results from specimens of different sizes or shapes.

7.13 Limitations and Usefulness of Resonant Frequency Methods

Although the basic equipment and testing procedures associated with the resonant frequency techniques have been standardized in various countries, and commercial testing equipment is easily available, the usefulness of the tests is seriously limited for the following reasons:

1. Generally, these tests are carried out on small-sized specimens in a laboratory rather than on structural members in the field because resonant frequencing is affected considerably by boundary conditions and the properties of concrete. The size of specimens in these tests is usually 152 × 305-mm cylinders or 76 × 76 × 305-mm prisms.
2. The equations for the calculation of dynamic elastic modulus involve "shape factor" corrections. This necessarily limits the shape of the specimens to cylinders or prisms. Any deviation from the standard shapes can render the application of shape factor corrections rather complex.

Notwithstanding the above limitations, the resonance tests provide an excellent means for studying the deterioration of concrete specimens subjected to repeated cycles of freezing and thawing and to deterioration due to aggressive media. The use of resonance tests in the determination of damage by fire and the deterioration due to alkali-aggregate reaction have also been reported by Chefdeville[26] and Swamy and Al-Asali.[44]

The resonant frequency test results are often used to calculate the dynamic modulus of elasticity of concrete but the values obtained are somewhat higher than those obtained with standard static tests carried out at lower rates of loading. The use of dynamic modulus of elasticity in design calculations is not recommended.

Various investigators have published correlations between the strength of concrete and its dynamic modulus of elasticity. The indiscriminate use of such correlations to predict compressive and/or flexural strength of concrete is discouraged unless similar relationships have been established in the laboratory for the particular concrete under investigation.

References

1. Rayleigh, J.W., *Theory of Sound*, 2nd ed., Dover Press, New York, 1945.
2. Obert, L. and Duvall, W.I., Discussion of dynamic methods of testing concrete with suggestions for standardization, *Proc. ASTM*, 41, 1053, 1941.
3. Powers, T.C., Measuring Young's modulus of elasticity by means of sonic vibrations, *Proc. ASTM*, 38, Part II, 460, 1938
4. Hornibrook, F.B., Application of sonic method to freezing and thawing studies of concrete, ASTM Bull. No. 101, December 1939, 5.
5. Thomson, W.T., Measuring changes in physical properties of concrete by the dynamic method, *Proc. ASTM*, 40, 1113, 1940. Also, discussion by T.F. Willis and M.E. de Reus, pp. 1123–1129.
6. Stanton, T.E., Tests comparing the modulus of elasticity of portland cement concrete as determined by the dynamic (sonic) and compression (scant at 1000 psi) methods, ASTM Bull. No. 131, Dec. 1944, 17. Also, discussion by L.P. Witte and W.H. Price, pp. 20–22.
7. Standard Test Method for Fundamental Transverse, Longitudinal, and Torsional Resonant Frequencies of Concrete Specimens (ASTM C 215-02), *Annual Book of ASTM Standards*, Vol. 04.02, ASTM, West Conshohocken, PA, 2003
8. Malhotra, V.M., Testing of hardened concrete: nondestructive methods, Monogr. No. 9, American Concrete Institute, Detroit, 1976, 52.
9. Pickett, G., Equations for computing elastic constants from flexural and torsional resonant frequencies of vibration of prisms and cylinders, *Proc. ASTM*, 45, 846, 1945.
10. Spinner, S. and Tefft, W.E., A method for determining mechanical resonance frequencies and for calculating elastic moduli from these frequencies, *Proc. ASTM*, 61, 1221, 1961.
11. Orchard, D.F., *Concrete Technology*, Vol. 2, Practice, John Wiley & Sons, New York, 1962, 181.
12. Kesler, C.E. and Higuchi, Y., Problems in the sonic testing of plain concrete, Proc. Int. Symp. on Nondestructive Testing of Materials and Structures, Vol. 1, RILEM, Paris, 1954, 45. Other contributions dealing with sonic tests and published in this symposium are listed below:

Vol. 1

(a) Cabarat, R., Measurement of elastic constants by an acoustical procedure, 9.
(b) Stutterheim, N., Lochner, J.P.A., and Burger, J.F., A method for determining the dynamic Young's modulus of concrete specimens developed for corrosion studies, 18.
(c) Takabayashi, T., Comparison of dynamic Young's modulus and static modulus for concrete, 34.
(d) Arredi, F., Nondestructive tests on concrete specimens performed in the hydraulic structures laboratory of the engineering faculty of Rome, 55.
(e) Takano, S., Determination of concrete strength by a nondestructive method, 61.
(f) Higuchi, Y., Studies presented by the author, 69.
(g) Fujita, K.I., Nondestructive method for concrete, 71.
(h) Ban, S., Activity of the committee on nondestructive concrete inspection of the ASTM, 74.
(i) Kilian, G., Evolution of the mechanical and elastic properties of concretes as a function of age, the proportion of binder and the nature of the aggregates, 75.
(j) Report by Lazard, 80.
(k) Daxelhofer, J.P., Concrete anisotropy brought out by the measurement of the dynamic modulus, 89.
(l) Daxelhofer, J.P., Remarks on the use of sonic methods for investigating the liability to frost damage of concretes at the materials testing laboratory of the Lausanne Polytechnical School, 98.
(m) Daxelhofer, J.P., Note on the static and dynamic moduli of a concrete, 106.
(n) Daxelhofer, J.P., Note on the variation of the dynamic modulus in function of the water content of a lightweight concrete, 108.
(o) Elvery, R.H., Symposium on the non-destructive testing of concrete, 111.
(p) Beauzee, C., Errors of measurement in the determination of the modulus of elasticity by the sonic method, 120.

(q) Jones, R., The testing of concrete by an ultrasonic pulse technique, 137.
(r) Chefdeville, J., The qualitative control, 166.
(s) Andersen, J., Apparatus for determination of sound velocity in concrete and execution of the measurements, 179.
(t) Nerenst, P., Speed of propagation in concrete determined by a condensing chronograph, 184.
(u) Nerenst, P., Wave velocity as influenced by curing conditions and age, 200.
(v) Andersen, J., The use of sound-velocity measurements for practical tests of concrete, 205.

Vol. 2

(w) Kameda, Y., Awaya, K., and Yokoyama, I., The nondestructive testing of concrete, 209.
(x) Voellmy, A., Vibration testing of concrete in structures in Switzerland, 216.
(y) Magnel, G. and Huyghe, G., Determination of the strength of a concrete by a nondestructive process, 219.
(z1) Okushima, M. and Kosaka, Y., Four reports, 248.
(z2) Borges, F., Some uses of ultrasounds at the Laboratorio Nacional de Engenharia Civil, 252.
(z3) Mamillan, M., The use of sonic methods for the study of freestones, 259.
(z4) Dawance, G., Application of the vibration test to the study of rocks and rock masses, 275.
(z5) Nondestructive testing of bituminous concrete. Relationship between the speed of sound propagation and the temperature of the concrete, 277.
(z6) Moles, A., A geoseismic apparatus for investigating the compactness of soils, 282.

13. Jones, R., *Non-Destructive Testing of Concrete*, Cambridge University Press, London, 1962.
14. Swamy, N. and Rigby, G., Dynamic properties of hardened paste, mortar, and concrete, Materials and Structures/Research and Testing (Paris), 4(19), 13, 1971.
15. Jones, R., The effect of frequency on the dynamic modulus and damping coefficient of concrete, *Mag. Concr. Res. (London)*, 9(26), 69, 1957.
16. Gaidis, J.M. and Rosenberg, M., New test for determining fundamental frequencies of concrete, *Cement Concr. Aggregates*, CCAGDP, 8(2), 117, 1986.
17. Thornton, H. and Alexander, A., Development of impact and resonant vibration signature for inspection of concrete structures, ACI Spec. Publ. SP 100, American Concrete Institute, 1987, 667.
18. Kesler, C.E. and Higuchi, Y., Determination of compressive strength of concrete by using its sonic properties, *Proc. ASTM*, 53, 1044, 1953.
19. Long, B.G. and Kurtz, H.J., Effect of curing methods on the durability of concrete as measured by changes in the dynamic modulus of elasticity, *Proc. ASTM*, 43, 1051, 1943.
20. Axon, E.O., Willis, T.F., and Reagel, F.V., Effect of air-entrapping portland cement on the resistance to freezing and thawing of concrete containing inferior coarse aggregate, *Proc. ASTM*, 43, 981, 1943.
21. Malhotra, V.M. and Zoldners, N.G., Durability Studies of Concrete for Manicouagan-2 Project, Mines Branch Investigation Rep. IR 64-69, Department of Energy, Mines and Resources, Ottawa, July 1964.
22. Malhotra, V.M. and Zoldners, N.G., Durability of Non-Air-Entrained Concrete Made with Type I and Modified Type II Cements, Mines Branch Investigation Rep. IR 65-86, Department of Energy, Mines and Resources, Ottawa, September 1965.
23. Malhotra, V.M. and Zoldners, N.G., Durability of Non-Air-Entrained and Air-Entrained Concretes Made with Type I and Modified Type II Cements, Mines Branch Investigation Rep. IR 67-29, Department of Energy, Mines and Resources, Ottawa, February 1967.
24. Wright, P.J.F. and Gregory, J.M., An investigation into methods of carrying out accelerated freezing and thawing tests on concrete, *Mag. Concr. Res. (London)*, 6(19), 39, 1955.
25. Akman, M.S. and Yildrim, M., Loss of durability of concrete made from portland cement blended with natural pozzolans due to ammonium nitrate, *Durability of Building Mater. (Amsterdam)*, 4(4), 357, 1987.

26. Chefdeville, J., Application of the Method toward Estimating the Quality of Concrete, RILEM Bull. (Paris), No. 15, August 1953, Special Issue-Vibrating Testing of Concrete, 2nd part, 61.
27. Long, B.G., Kurtz, H.J., and Sandenaw, T.A., An instrument and a technique for field determination of the modulus of elasticity and flexural strength of concrete (pavements), *ACI J. Proc.*, 41(3), 217, 1945.
28. Sweet, H.S., Research on concrete durability as affected by coarse aggregate, *Proc. ASTM*, 48, 988, 1948.
29. L'Hermite, R., The strength of concrete and its measurement, *Ann. L'Institut Technique Bâtiment Travaux Publics (Paris)*, 12, 3, 1950.
30. Shrivastava, J.P. and Sen, B., Factors affecting resonant frequency and compressive strength of concrete, *Indian Concr. J. (Bombay)*, 37(1), 27, 1963, and 37(3), 105, 1963.
31. Sharma, M.R. and Gupta, B.L., Sonic modulus as related to strength and static modulus of high strength concrete, *Indian Concr. J. (Bombay)*, 34(4), 139, 1960.
32. Kaplan, M.F., Effects of incomplete consolidation on compressive and flexural strengths, ultrasonic pulse velocity, and dynamic modulus of elasticity of concrete, *ACI J. Proc.*, 56(9), 853, 1960.
33. Kaplan, M.F., Ultrasonic pulse velocity, dynamic modulus of elasticity, Poisson's ratio and the strength of concrete made with thirteen different coarse aggregates, RILEM Bull. (Paris), New Series No. 1, March 1959, 58.
34. Malhotra, V.M. and Berwanger, C., Correlations of Age and Strength with Values Obtained by Dynamic Tests on Concrete, Mines Branch Investigation Rep. IR 70-40, Department of Energy, Mines and Resources, Ottawa, June 1970.
35. Batchelder, G.M. and Lewis, D.W., Comparison of dynamic methods of testing concretes subjected to freezing and thawing, *Proc. ASTM*, 53, 1053, 1953.
36. Whitehurst, E.A., Evaluation of concrete properties from sonic tests. ACI Monogr. No. 2, American Concrete Institute/Iowa State University Press, Detroit, 1966.
37. Klieger, P., Long-term study of cement performance in concrete. Chapter 10 — Progress Report on Strength and Elastic Properties of Concrete, *ACI J. Proc.*, 54(6), 481, 1957.
38. Philleo, R.E., Comparison of results of three methods for determining Young's modulus of elasticity of concrete, *ACI J. Proc.*, 51(5), 461, 1955.
39. Hansen, W., Static and dynamic modulus of concrete as affected by mix composition and compressive strength, ACI Spec. Publ. SP 95, American Concrete Institute 1986, 115.
40. Gatfield, E.N., A Method of Studying the Effect of Vibratory Stress, Including Fatigue, on Concrete in Flexure, paper presented to the RILEM Technical Committee on Nondestructive Testing of Concrete, Varna, Bulgaria, September 3–6, 1968.
41. Chang, T.S. and Kesler, C.E., Correlation of sonic properties of concrete with creep and relaxation, *Proc. ASTM*, 56, 1257, 1956.
42. Chang, T.S. and Kesler, C.E., Prediction of creep behavior in concrete from sonic properties, Proc. Highw. Res., Board, 35, 436, 1956.
43. Thornton, H. and Alexander, A., Development of Nondestructive Testing Systems for In Situ Evaluation of Concrete Structures, Tech. Rep. REMB-CS-10, Waterways Experiment Station, Corps of Engineers, Vicksburg, MI, December 1987.
44. Swamy, R.N. and Al-Asali, M.M., Engineering properties of concrete affected by alkali-silica reaction, *ACI Mater. J.*, 85(5), 367, 1988.

8

The Ultrasonic Pulse Velocity Method

8.1 Historical Background
8.2 Theory of Wave Propagation
8.3 Pulse Velocity Test Instrument
8.4 The Pulse Velocity Method
8.5 Factors Affecting Pulse Velocity
Effects of Concrete Properties • Other Effects • Temperature of Concrete
8.6 Standardization of the Pulse Velocity Method
8.7 Applications
Estimation of Strength of Concrete • Establishing Homogeneity of Concrete • Studies on the Hydration of Cement • Studies on Durability of Concrete • Measurement of Surface Crack Depth • Determination of Dynamic Modulus of Elasticity
8.8 Advantages and Limitations
Appendix 8.1

Tarun R. Naik
University of Wisconsin–Milwaukee

V. Mohan Malhotra
Department of Natural Resources Canada, Ottawa

John S. Popovics
University of Illinois at Urbana–Champaign

The ultrasonic pulse velocity method has been used successfully to evaluate the quality of concrete for more than 60 years. This method can be used for detecting internal cracking and other defects as well as changes in concrete such as deterioration due to aggressive chemical environment and freezing and thawing. By using the pulse velocity method it is also possible to estimate the strength of concrete test specimens and in-place concrete.

The pulse velocity method is a truly nondestructive method, as the technique uses mechanical waves resulting in no damage to the concrete element being tested. A test specimen can be tested again and again at the same location, which is useful for monitoring concrete undergoing internal structural changes over a long period of time.

8.1 Historical Background

Concrete technologists have been interested in determining the properties of concrete by nondestructive tests for decades. Many test methods have been proposed for laboratory test specimens using vibrational methods beginning in the 1930s. Powers,[1] Obert,[2] Hornibrook,[3] and Thomson[4] were the first to conduct extensive research using vibrational techniques such as the resonant frequency method (see Chapter 7).

World War II accelerated research regarding nondestructive testing using stress wave propagation methods (see also Chapter 14 by Carino on stress wave propagation methods). The development of the pulse velocity method began in Canada and England at about the same time. In Canada, Leslie and Cheesman[5] developed an instrument called the soniscope. While in England, Jones[6] developed an

instrument called the ultrasonic tester. In principle, both the soniscope and the ultrasonic tester were quite similar, with only minor differences in detail. Since the 1960s, pulse velocity methods have moved out of laboratories and to construction sites.[7] Malhotra[8] has compiled an extensive list of papers published on this subject. Many nations have adopted standardized procedures to measure pulse velocity in concrete.

8.2 Theory of Wave Propagation

Three types of propagating mechanical waves (also called stress waves) are created when the surface of a large solid elastic medium is disturbed by a dynamic or vibratory load: (1) compressional waves (also called longitudinal or P-waves), (2) shear waves (also called transverse or S-waves), (3) and surface waves (also called Rayleigh waves). The compressional waves propagate through the solid medium in a fashion analogous to sound waves propagating through air. Each wave type propagates with its characteristic velocity. For a given solid, compressional waves have the highest velocity and surface waves the lowest. In concrete, the velocities of the shear and surface waves are typically 60 and 55%, respectively, of the compressional wave velocity.[9] The particular velocity of a wave depends on the elastic properties and density of the medium. For elastic, homogeneous solid media the compressional wave velocity is given by the following:[9]

$$V = \sqrt{\frac{KE}{\rho}} \tag{8.1}$$

where

V = compressional wave velocity,
$K = (1 - \mu)/((1 + \mu)(1 - 2\mu))$
E = dynamic modulus of elasticity
ρ = density
μ = dynamic Poisson's ratio

The value of K varies within a fairly narrow range. For example, as μ increases from 0.15 to 0.25 (67% increase), the associated K value increases from 1.06 to 1.20 (12% increase). Thus, variations in E and ρ have a more significant effect on V than variations in μ For concrete, V typically ranges from 3000 to 5000 m/s.

The frequency f and wavelength λ of propagating wave motion are related by the velocity of propagation: $V = f\lambda$. The frequency is reported in units of hertz (or cycles per second) and the wavelength in units of distance (e.g., mm). In a given medium, an increase in wave frequency therefore dictates a decrease in the wavelength, and vice versa. When a propagating wave pulse impinges on an interface with a medium having distinct material properties, a portion of the wave energy is scattered away from the original wave path (see also Chapter 14). For example, voids, cracks, and aggregate particles in concrete act to scatter some of the initial energy of the compressional wave pulse away from the original wave path. The magnitude of the scattering is especially intense if the wavelength of the propagating wave is the same size or smaller than the size of the scatterer, resulting in rapid wave attenuation.[10] For concrete, the upper limit of usable frequency is about 500 kHz as the associated wavelength is approximately 10 mm, which is in the size range of the coarse aggregate particles. As a result, the path length that can be effectively traversed at this upper limit of frequency before the wave pulse becomes completely scattered is only several centimeters. Greater path lengths can be traversed using lower frequencies (thus larger wavelengths): a frequency of 20 kHz can usually traverse up to 10 m of concrete.[10]

In the ultrasonic pulse velocity test method, an ultrasonic wave pulse through concrete is created at a point on the surface of the test object, and the time of its travel from that point to another is measured. Knowing the distance between the two points, the velocity of the wave pulse can be determined. Portable pulse velocity equipment is available today for concrete testing to determine the arrival time of the first wavefront. For most test configurations, this is the direct compressional wave, as it is the fastest wave.

8.3 Pulse Velocity Test Instrument

The test instrument consists of a means of producing and introducing a wave pulse into the concrete (pulse generator and transmitter) and a means of sensing the arrival of the pulse (receiver) and accurately measuring the time taken by the pulse to travel through the concrete. The equipment may also be connected to an oscilloscope, or other display device, to observe the nature of the received pulse. A schematic diagram is shown in Figure 8.1. A complete description is provided in ASTM Test Method C 597.[11]

Portable ultrasonic testing units are available worldwide. The equipment is portable, simple to operate, and may include a rechargeable battery and charging unit. Typically, pulse times of up to 6500 μs can be measured with 0.1-μs resolution. The measured travel time is prominently displayed. The instrument comes with a set of two transducers, one each for transmitting and receiving the ultrasonic pulse. Transducers with frequencies of 25 to 100 kHz are usually used for testing concrete. Transducer sets having different resonant frequencies are available for special applications: high-frequency transducers (above 100 kHz) are used for small-size specimens, relatively short path lengths, or high-strength concrete, whereas low-frequency transducers (below 25 kHz) are used for larger specimens and relatively longer path lengths, or concrete with larger size aggregates. These transducers primarily generate compressional waves at predominantly one frequency, with most of the wave energy directed along the axis normal to the transducer face. A commonly used instrument is shown in Figure 8.2.

8.4 The Pulse Velocity Method

The basic idea on which the pulse velocity method is established is that the velocity of a pulse of compressional waves through a medium depends on the elastic properties and density of the medium, as shown in Equation 8.1.

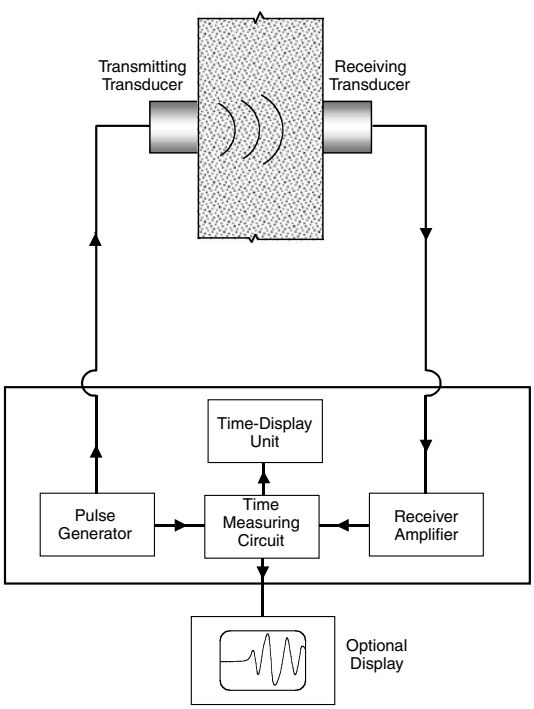

FIGURE 8.1 Schematic diagram of pulse velocity test circuit. (Adapted from Reference 11.)

FIGURE 8.2 Pulse velocity instrument. (Courtesy of James Instruments, Inc.)

The transmitting transducer of the pulse velocity instrument transmits a wave into the concrete and the receiving transducer, at a distance L, receives the pulse through the concrete at another point. The pulse velocity instrument display indicates the transit time, Δt, it takes for the compressional wave pulse to travel through the concrete. The compressional wave pulse velocity V, therefore, is

$$V = \frac{L}{\Delta t} \tag{8.2}$$

The compressional pulse transmitted through the concrete undergoes scattering at various aggregate–mortar boundaries. By the time the pulse reaches the receiving transducer it becomes transformed into a complex waveform, which contains multiply reflected compressional waves and shear waves. Of course, compression waves traveling the fastest arrive first at the receiver.

To transmit or receive the pulse, the transducers must be in full contact with the test object; otherwise an air pocket between the test object and transducer may introduce an error in the indicated transit time. This error is introduced because only a negligible amount of wave energy can be transmitted through air. Many couplants available in the market can be used to eliminate air pockets and to assure good contact; petroleum jelly has proved to be one of the superior couplants. Other couplants are grease, liquid soap, and kaolin-glycerol paste. The couplant layer should be as thin as possible. While applying constant pressure on the transducers, repeated readings at a particular location should be taken until a minimum value of transit time is obtained. If the concrete surface is very rough, thick grease should be used as a couplant. In some cases, the rough surface may have to be ground smooth, or a smooth surface may have to be established with the use of plaster of Paris or suitable quick-setting cement paste or quick-setting epoxy mortar. The leveling paste should be allowed to set before proceeding with the pulse velocity test. An exponential receiver probe with a tip diameter of only 6 mm may also be used to receive the pulse in very rough surfaces, e.g., locations where the surface mortar is scaled off due to fire or weathering action. It must be emphasized, however, that this probe is good only for receiving the signal. A smooth surface is still required for the transmitting transducer.

The pulse velocity for ordinary concrete is typically 3700 to 4200 m/s. Therefore, for a 300-mm path length, the travel time is approximately 70 to 85 μs. It is obvious that the instrument must be very accurate to measure such a short transit time. The path length should also be carefully measured. Because the pulse velocity method is a wave propagation technique, any sources creating even the slightest wave motion in the element under test (e.g., jackhammers) should be eliminated during the time of the test. Many other factors also affect the pulse velocity. They are discussed in detail in the next section.

There are three possible configurations in which the transducers may be arranged, as shown in Figure 8.3A to C. These are (1) direct transmission; (2) semidirect transmission; and (3) indirect or surface transmission. The direct transmission method, Figure 8.3A, is the most desirable and the most satisfactory

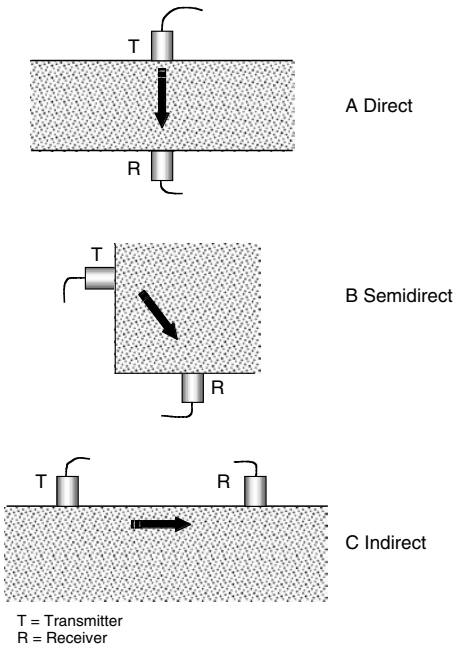

FIGURE 8.3 Pulse velocity measurement configurations. (A) Direct method. (B) Semidirect method. (C) Indirect surface method.

arrangement because maximum energy of the pulse is transmitted and received with this arrangement. The semidirect transmission method, Figure 8.3B, can also be used quite satisfactorily. However, care should be exercised that the transducers are not too far apart; otherwise the transmitted pulse might attenuate and a pulse signal might not be detected. This method is useful in avoiding concentrations of reinforcements. The indirect or surface transmission method, Figure 8.3C, is least satisfactory because the amplitude of the received signal is significantly lower than that received by the direct transmission method. This method is also more prone to errors and a special procedure may be necessary for determining the pulse velocity.[12] First, the location of the transmitting transducer is fixed and the receiver location is changed in fixed increments along a line, and a series of transit time readings are taken. The direct distance between the two transducers is plotted on the *X*-axis and the corresponding pulse transit time is plotted on the *Y*-axis (Figure 8.4). The inverse of the slope of this plot is the pulse velocity along the line.

When this surface method is used, the pulse propagates in the concrete layer near the surface. The near-surface concrete is sometimes of a composition slightly different from the concrete in the lower layer. For example, the concrete near the surface of a slab has higher amounts of fine materials than the concrete in the lower portion of the slab. Thus, velocities measured by the surface transmission method are typically lower than those measured with direct transmission. This behavior, however, can be turned into a means to detect and estimate the thickness of a layer of different quality material. A layer of lower quality concrete may occur due to improper construction practices (e.g., poor vibration and finishing, poor curing, cold joints due to delay, incorrect placement), damage due to weathering action (e.g., freezing and thawing, sulfate attack, and corrosion of reinforcement and other embedded items), and damage by fire. The layer thickness can be estimated by using the surface transmission procedure. When the two transducers are closer together, the fastest travel path is through the upper layer of concrete, and as the transducers are moved further apart, the fastest travel path is the combined path through both layers. The pulse velocity through the upper layer (V_1) and the lower layer (V_2) will be indicated on the plot by the different slopes of the two straight lines fitted to the data (Figure 8.4). The distance X in Figure 8.4 at which the change in these slopes occurs is measured and the thickness of the upper layer, t, is estimated from the following equation:[9]

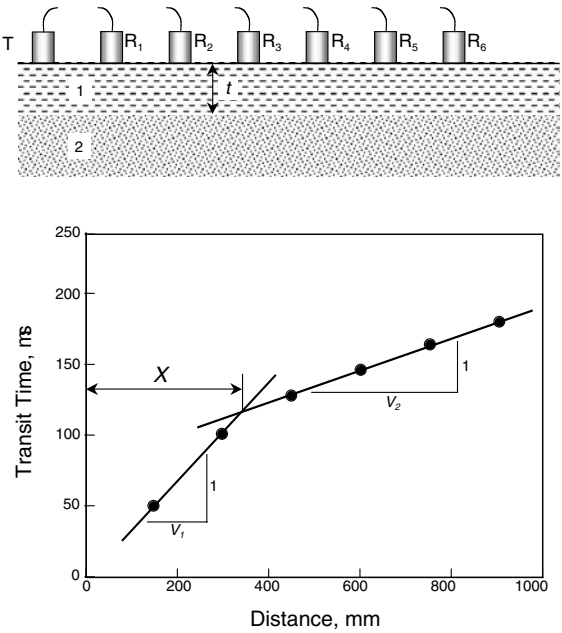

FIGURE 8.4 Use of surface method to determine depth of deterioration, *t*.

$$t = \frac{X}{2}\sqrt{\frac{V_2 - V_1}{V_2 + V_1}} \tag{8.3}$$

This method is only suitable when the upper layer (the poor-quality layer) is distinct, is of reasonably uniform thickness, and $V_2 > V_1$. Benedetti proposed a more realistic model for the interpretation of surface velocity measurements, which assumes a linear distribution of elastic modulus within a fire-damaged layer.[13]

8.5 Factors Affecting Pulse Velocity

Although it is relatively easy to conduct a pulse velocity test, it is important that the test be conducted such that the pulse velocity readings are reproducible and that they are affected only by the properties of the concrete under test rather than by other factors. The factors affecting the pulse velocity can be divided into two categories: (1) factors resulting directly from concrete properties; and (2) other factors. These influencing factors are discussed below.

8.5.1 Effects of Concrete Properties

8.5.1.1 Aggregate Size, Grading, Type, and Content

Many investigators have found that the pulse velocity is affected significantly by the type and amount of aggregate.[14–19] In general, the pulse velocity of cement paste is lower than that of aggregate. Jones[18] reported that for the same concrete mixture and at the same compressive strength level, concrete with rounded gravel had the lowest pulse velocity, crushed limestone resulted in the highest pulse velocity, and crushed granite gave a velocity that was between these two. On the other hand, type of aggregate had no significant effect on the relationship between the pulse velocity and the modulus of rupture. Additional test results by Jones,[10] Bullock and Whitehurst,[14] and Kaplan[20] indicate that at the same strength level the concrete having the higher aggregate content gave a higher pulse velocity. The effects of varying

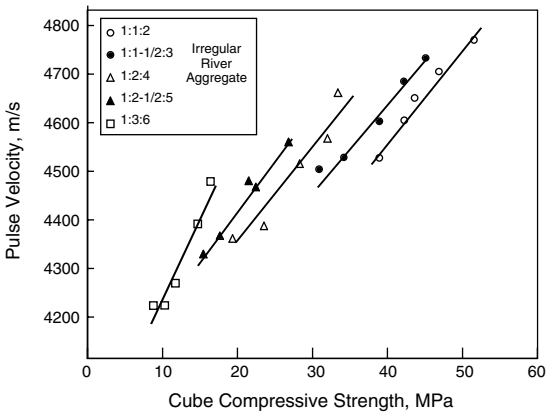

FIGURE 8.5 Effect of cement:fine aggregate:coarse aggregate proportions on the relationship between pulse velocity and compressive strength. (Adapted from Reference 10.)

the proportion of coarse aggregate in a concrete mixture on the pulse velocity vs. compressive strength relationship are shown in Figure 8.5.[10] The figure shows that for a given value of pulse velocity, the higher the aggregate–cement ratio, the lower the compressive strength.

8.5.1.2 Cement Type

Jones[18] reported that the type of cement did not have a significant effect on the pulse velocity. The rate of hydration, however, is different for different cements and it will influence the pulse velocity. As the degree of hydration increases, the modulus of elasticity will increase and the pulse velocity will also increase. The use of rapid-hardening cements results in higher strength for a given pulse velocity level.[21]

8.5.1.3 Water–Cement Ratio

Kaplan[20] studied the effect of water- cement (*w/c*) ratio on the pulse velocity. He has shown that as the *w/c* increases, the compressive and flexural strengths and the corresponding pulse velocity decrease assuming no other changes in the composition of the concrete.

8.5.1.4 Admixtures

Air entrainment does not appear to influence the relationship between the pulse velocity and the compressive strength of concrete.[18] Other admixtures will influence the pulse velocity in approximately the same manner as they would influence the rate of hydration. For example, the addition of calcium chloride will reduce the setting time of concrete and will increase the rate by which the pulse velocity increases.

8.5.1.5 Age of Concrete

The effect of age of concrete on the pulse velocity is similar to the effect on the strength development of concrete. Jones[18] reported the relationship between the pulse velocity and age. He showed that velocity increases very rapidly initially but soon flattens. This trend is similar to the strength vs. age curve for a particular type of concrete, but pulse velocity reaches a limiting value sooner than strength. He further concluded that once the pulse velocity curve flattens, experimental errors make it impossible to estimate the strength with accuracy.[10]

8.5.2 Other Effects

8.5.2.1 Transducer Contact

The influence of improper transducer contact was discussed in Section 8.4. If sufficient care is not exercised in obtaining a good contact (e.g., inconsistent pressure applied to transducers), an incorrect pulse velocity reading may result.

8.5.2.2 Temperature of Concrete

Temperature variations between 5 and 30∂C have been found to have an insignificant effect on the pulse velocity.[21] For temperatures beyond this range, the corrections in Table 8.1 are recommended.[22]

8.5.2.3 Moisture and Curing Condition of Concrete

The pulse velocity for saturated concrete is higher than for air-dry concrete. Moisture generally has less influence on the velocity in high-strength concrete than on low-strength concrete because of the difference in the porosity.[21] A 4 to 5% increase in pulse velocity can be expected when dry concrete with high w/c ratio is saturated.[10] Kaplan[23] found that the pulse velocity for laboratory-cured specimens were higher than for site-cured specimens. He also found that pulse velocity in columns cast from the same concrete were lower than in the site-cured and laboratory-cured specimens.

8.5.2.4 Path Length

Theoretically the path length traveled by the wave and the frequency of the wave (which is the same as the frequency of the transducer) should not affect the propagation time; therefore, they should not affect the pulse velocity. However, in practice, smaller path lengths tend to give more variable and slightly higher pulse velocity because of the inhomogeneous nature of concrete.[10] RILEM[24] has recommended the following minimum path lengths:

1. 100 mm for concrete having maximum aggregate size of 30 mm
2. 150 mm for concrete having maximum aggregate size of 45 mm

8.5.2.5 Size and Shape of a Specimen

In most cases, the pulse velocity is not dependent on the size and the shape of a specimen. However, Equation 8.1 is valid only for a medium having an infinite extent. This requirement is easily satisfied for a finite-dimension test specimen by requiring that the smallest lateral dimension of the specimen be greater than the wavelength of the pulse. For concrete having a pulse velocity of about 3700 m/s and for a transducer frequency of 54 kHz, the wavelength is about 68 mm. Therefore, a specimen made from this concrete, when tested with a transducer having a frequency of 54 kHz, should have a minimum lateral dimension of 70 mm. If the least lateral dimension of this specimen is less than 70 mm, then Equation 8.1 may not be an accurate relationship, especially for longer path lengths. For such situations, it would be advisable to use a higher-frequency transducer, thus reducing the wavelength and the corresponding least lateral dimension requirement. The maximum size aggregate should also be smaller than the wavelength; otherwise, the wave energy will attenuate to the point that no clear signal may be detected at the receiving transducer. RILEM[24] recommendations for least lateral dimension and corresponding maximum size aggregate are given in Table 8.2.

8.5.2.6 Level of Stress

Pulse velocity is generally not affected by the level of stress in the element under test. However, when the concrete is subjected to a very high level of static or repeated stress, say, 65% of the ultimate strength or greater, microcracks develop within the concrete, which will reduce the pulse velocity considerably.[25,26]

TABLE 8.1 Corrections for Pulse Velocity Due to Temperature Changes

	Correction (%)	
Concrete Temperature (∂C)	Air-Dried Concrete	Water-Saturated Concrete
60	+5	+4
40	+2	+1.7
20	0	0
0	–0.5	–1
Under –4	–1.5	–7.5

Source: From BS 1881 Part 203, 1986.

TABLE 8.2 Frequency of Transducer vs. Least Lateral Dimension

Minimum Frequency of Transducer (kHz)	Smallest Lateral Dimension (or Max. Size Aggregate) (mm)	Range of Path Length (mm)
60	70	100–700
40	150	200–1500
20	300	>1500

Source: From RILEM Recommendation NDT1, Paris, Dec. 1972.

8.5.2.7 Presence of Reinforcing Steel

One of the most significant factors that influences the pulse velocity of concrete is the presence of steel reinforcement. The pulse velocity in steel is 1.4 to 1.7 times the pulse velocity in plain concrete. Therefore, pulse velocity readings in the vicinity of reinforcing steel are usually higher than that in plain concrete. Whenever possible, test readings should be taken such that the reinforcement is avoided in the wave path. If reinforcements cross the wave path, correction factors should be used. The correction factors that are used are those recommended by RILEM[23] and British Standards.[22] Appendix 8.1 provides specific information about the correction factors. Chung[27,28] has demonstrated the importance of including bar diameters as a basic parameter in the correction factors. However, the RILEM recommendations involve only two basic parameters: the pulse velocity in the surrounding concrete and the path lengths within the steel and concrete. Bungey[29] also provides correction factors that include bar diameters. It should be emphasized, however, that in heavily reinforced sections it might not be possible to obtain accurate measurements of the concrete pulse velocity.

8.6 Standardization of the Pulse Velocity Method

Many nations have developed standardized procedures to measure pulse velocity. Several standards are compared by Komlos et al.[30] In the United States, ASTM Committee C09 initiated the development of a standard for pulse velocity in the late 1960s. A tentative standard was issued in 1968. A standard test method was issued in 1971 and no significant changes have been made in the standard since then.[11] The Significance and Use statement of the test method, as given in the ASTM C 597-02, is as follows:[11]

> The pulse velocity, V, of longitudinal stress waves in a concrete mass is related to its elastic properties and density according to the following relationship (see also Equation 8.1):
>
> $$V = \sqrt{\frac{E(1-\mu)}{\rho(1+\mu)(1-2\mu)}} \tag{8.4}$$
>
> where
>
> E = dynamic modulus of elasticity
> μ = dynamic Poisson's ratio
> ρ = density
>
> This test method is applicable to assess the uniformity and relative quality of concrete, to indicate the presence of voids and cracks, and to evaluate the effectiveness of crack repairs. It is also applicable to indicate changes in the properties of concrete, and in the survey of structures, to estimate the severity of deterioration or cracking.* When used to monitor changes in condition over time, test locations are to be marked on the structure to ensure that tests are repeated at the same positions.

*Naik, T.R. Evaluation of an 80-Year-Old Concrete Dam, paper presented at the ACI meeting in Seattle, WA, October 1987 (available from the UWM Center for By-Products Utilization, University of Wisconsin–Milwaukee).

The degree of saturation of the concrete affects the pulse velocity, and this factor must be considered when evaluating test results. In addition, the pulse velocity in saturated concrete is less sensitive to changes in its relative quality.

NOTE 1 — The pulse velocity of saturated concrete may be up to 5% higher than in dry concrete.

The pulse velocity is independent of the dimensions of the test object provided reflected waves from boundaries do not complicate the determination of the arrival time of the directly transmitted pulse. The least dimension of the test object must exceed the wavelength of the ultrasonic vibrations.

[NOTE 2 is omitted because it is not relevant to the significance and use of the pulse velocity method.]

The accuracy of the measurement depends upon the ability of the operator to determine precisely the distance between the transducers and of the equipment to measure precisely the pulse transit time. The received signal strength and measured transit time are affected by the coupling of the transducers to the concrete surfaces. Sufficient coupling agent and pressure must be applied to the transducers to ensure stable transit times. The strength of the received signal is also affected by the travel path length and by the presence and degree of cracking or deterioration in the concrete tested.

NOTE 3 — Proper coupling can be verified by viewing the shape and magnitude of the received waveform. The waveform should have a decaying sinusoidal shape. The shape can be viewed by means of outputs to an oscilloscope or digitized display inherent in the device.

The results obtained by the use of this test method are not to be considered as a means of measuring strength nor as an adequate test for establishing compliance of the modulus of elasticity of field concrete with that assumed in the design. The longitudinal resonance method in Test Method C 215 is recommended for determining the dynamic modulus of elasticity of test specimens obtained from field concrete because Poisson's ratio does not have to be known.

NOTE 4 — When circumstances permit, a velocity-strength (or velocity-modulus) relationship may be established by the determination of pulse velocity and compressive strength (or modulus of elasticity) on a number of samples of a concrete. This relationship may serve as a basis for the estimation of strength (or modulus of elasticity) by further pulse-velocity tests on that concrete. Refer to ACI 228.1R for guidance on the procedures for developing and using such a relationship.

The procedure is applicable in both field and laboratory testing regardless of size or shape of the specimen within the limitations of available pulse-generating sources.

Since the pulse velocity in steel could be up to double that in concrete, the pulse velocity measured in the vicinity of the reinforcing steel will be higher than in plain concrete of the same composition. Where possible, avoid measurements close to steel parallel to the direction of pulse propagation.

8.7 Applications

The pulse velocity method has been applied successfully in the laboratory as well as in the field.[31–48] Furthermore, it can be used for quality control, as well as for the analysis of deterioration. Figure 8.6 illustrates the application of the pulse velocity method on a concrete structure.

8.7.1 Estimation of Strength of Concrete

The pulse velocity method may provide a means of estimating the strength of both *in situ* and precast concrete although there is no physical relation between the strength and velocity. The strength can be estimated from the pulse velocity by a pre-established graphical correlation between the two parameters, an example of which is shown in Figure 8.7. The relationship between strength and pulse velocity is not unique, and is affected by many factors, e.g., aggregate size, type, and content; cement type and content;

FIGURE 8.6 Application of pulse velocity technique on a concrete structure. (Courtesy of James Instruments, Inc.)

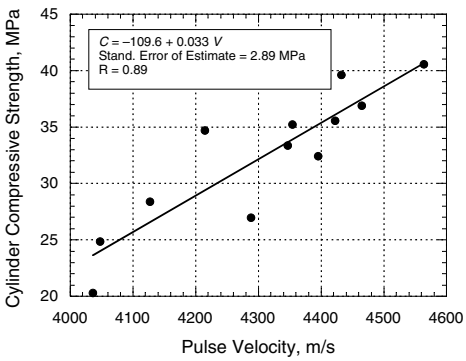

FIGURE 8.7 Example strength vs. velocity relationship for estimation of strength of concrete.

water–cement ratio; and moisture content. The effect of such factors has been studied by many researchers.[15,17,20,23] They have clearly pointed out that no attempts should be made to estimate compressive strength of concrete from pulse velocity values unless similar correlations have been previously established for the type of concrete under investigation. RILEM,[24] the British Standard,[22] and American Concrete Institute (ACI)[49] provide recommended practices to develop the relationship between pulse velocity and compressive strength, which can be later used for estimating the *in situ* strength based on the pulse velocity. Phoon et al.[50] recently proposed a probabilistic model to predict compressive strength from ultrasonic pulse velocity. By using the model together with field data, a consistent statistical quality assurance criterion may be established.

8.7.2 Establishing Homogeneity of Concrete

The pulse velocity method is suitable for the study of homogeneity of concrete, and, therefore, for relative assessment of quality of concrete. Heterogeneity is defined as interior cracking, deterioration, honeycombing, and variations in mixture proportions. Heterogeneities in a concrete member will cause variations in the pulse velocity. For example, the diffraction of a wave pulse around an internal air void will cause an increase in the time of propagation for an assumed path through the void center. Thus, the apparent velocity will decrease. However, only large voids, generally larger than the transducer contact face, will cause measurable reduction in velocity.[10] Also, *in situ* concrete strength varies in a structure because of the variations in source and proportions of materials, uniformity of mixing, and due to inadequate or variable consolidation. The

pulse velocity method is highly effective in establishing comparative data and for qualitative evaluation of concrete. For obtaining these qualitative data, a system of measuring points, i.e., a grid pattern, may be established. Depending on the quantity of the concrete to be evaluated, the size of the structure, the variability expected, and the accuracy required, a grid of 300 mm spacing, or greater, should be established. Generally about 1 m spacing may be adequate depending on the thickness of the element being tested. Other applications of this qualitative comparison of *in situ* or test specimen concrete are (1) to check the variation of density of concrete to evaluate the effectiveness of consolidation; (2) for locating areas of honeycombed concrete; and (3) localizing internal cracks and voids.

Researchers[18,34–37,51,52] have reported results of carefully conducted surveys for determining the homogeneity of concrete in various types of structures. Of many such surveys carried out on existing structures, one that deserves mention is that reported in 1953 by Parker[34] of the Hydro-Electric Power Commission of Ontario, Canada. The survey was made on a dam built in 1914. A total of 50,000 readings were taken, most of them with 300-mm spacings. The pulse velocities measured on the structure ranged from below 1525 to over 5185 m/s, and these values were used, with success, to determine areas of advanced deterioration. Rhazi et al.[51] report the use of multiple velocity data to map subsurface anomalies within a concrete gravity retaining wall built in the 1940s. Olson and Sack[52] report the use of multiple velocity data to successfully assess the condition of larger concrete structures. Some thousands of pulse velocity measurements have been made on 29 concrete dams during the period of 1948 to 1965. McHenry and Oleson[37] cite ten of these case histories in which velocity measurements have been a valuable supplement to other observations for settling questions regarding repair or maintenance of dams.

8.7.3 Studies on the Hydration of Cement

The pulse velocity method has the advantage that it is truly nondestructive. Therefore, changes in the internal structure of concrete can be monitored on the same test specimen. Many researchers have published information on successful application of the pulse velocity method for monitoring the setting and hardening process of cement paste, mortar, and concrete.[7,18,38–42,53,54] The method is particularly useful for detecting changes during the first 36 h after adding water to the concrete mixture. A very significant practical use of the method is the evaluation of the rate of setting for different types of cements or admixtures to be used for a given project.

Whitehurst[41] reported results of tests on 102 ¥ 102 ¥ 406-mm concrete prisms, using various types of cement. The concretes used had zero slump and, immediately after casting, the end plates of the forms were removed. Pulse velocity tests using the soniscope were made periodically, from shortly after the specimens were cast until 8 h or more had elapsed. Initial velocities of the order of 1220 m/s were observed, and during the first few hours the velocities increased at a rapid rate. After periods varying from $4^1/_2$ to $8^1/_2$ h, the rate of increase suddenly changed and continued at a much slower pace. The point at which this occurred was taken as the time of setting of concrete. The results of Whitehurst,[41] together with those reported by Cheesman,[42] are shown in Figure 8.8.

8.7.4 Studies on Durability of Concrete

Aggressive environments will damage the structure of concrete and decrease the pulse velocity. Deterioration caused by freezing and thawing, sulfate exposure, alkali-silicate reactivity, and corrosion of embedded items can be detected by the pulse velocity method and have been studied by various investigators.[5,18,38,43,55,56] Progressive deterioration of either a test specimen or *in situ* concrete can be monitored by conducting repetitive tests on the same concrete element. Deterioration of concrete due to fire exposure has also been investigated by the pulse velocity method.[13,28,44]

8.7.5 Measurement of Surface Crack Depth

This aspect of the pulse velocity technique has been studied by various researchers.[5,45–48] As indicated earlier, the ultrasonic pulse transmits a very small amount of energy through air. Therefore, if a pulse

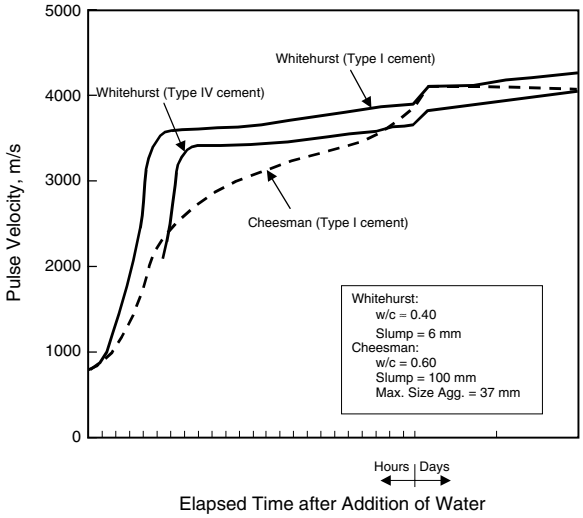

FIGURE 8.8 Relationship between pulse velocity and setting of concrete. (Adapted from References 41 and 42.)

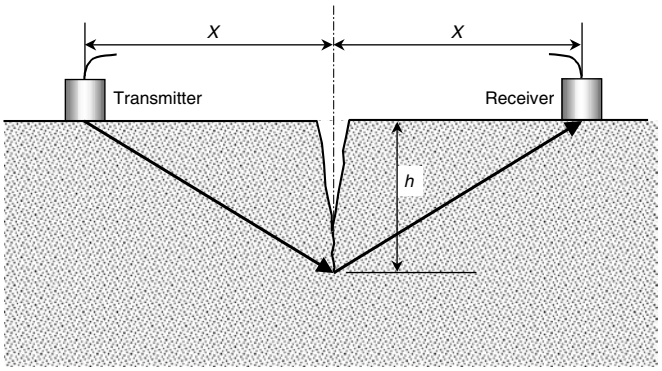

FIGURE 8.9 Scheme for measurement of surface crack depth, *h*.

traveling through the concrete comes upon an air-filled crack or a void whose projected area perpendicular to the path length is larger than the area of the transmitting transducer, the pulse will diffract around the defect. Thus, the pulse travel time will be greater than that through similar concrete without any defect. The pulse velocity method, therefore, is effective in characterizing surface cracks. It should be pointed out that the application of this technique in locating flaws has serious limitations. For example, if cracks and flaws are small or if they are filled with water or other debris thus allowing the wave to propagate through the flaw, or if the crack tip is not well defined, the pulse velocity will not significantly decrease, implying that no flaw exists.

The depth of an air-filled surface crack can be estimated by the pulse velocity method as shown in Figure 8.9. The depth, *h*, is given by Equation 8.5:

$$h = \frac{X}{T_2}\sqrt{T_1^2 - T_2^2} \tag{8.5}$$

where

X = distance to the transducer from the crack (note that both transducers must be placed equidistant from the crack)

T_1 = transit time around the crack
T_2 = transit time along the surface of the same type of concrete without any crack (note that the surface path length for T_1 and T_2 must be equal)

It should be pointed out that for Equation 8.5 to be valid, the crack must be perpendicular to the concrete surface. A check should be made to determine if the crack is perpendicular to the surface or not. This can be done as follows.[24] Place both transducers equidistant from the crack and obtain the transit time. Move each transducer, in turn, away from the crack. If the transit time decreases, then the crack slopes toward the direction in which the transducer was moved.

8.7.6 Determination of Dynamic Modulus of Elasticity

The velocity of a compressional wave traveling through an elastic material is uniquely defined by the elastic constants and density of the material by wave propagation theory (see Equation 8.1). Therefore, it is possible to compute the modulus of elasticity of a material if the ultrasonic pulse velocity is measured where the values of Poisson's ratio and density are known or assumed. This approach has an advantage over other standardized techniques, which make use of vibration frequencies, in that the testing is not restricted to specially shaped laboratory specimens. Several researchers report the estimation of dynamic (low-strain) modulus of elasticity from pulse velocity measurements in concrete.[5,7,31,32] Nevertheless, the estimation of the dynamic modulus of elasticity in concrete from ultrasonic pulse velocity measurements is not normally recommended for two reasons: (1) the error resulting from inaccurate estimation of Poisson's ratio is not insignificant and (2) Equation 8.1 is appropriate for homogeneous materials only, leaving the validity for inhomogeneous composite materials, such as concrete, in doubt.[31,57] Usually, the dynamic modulus of elasticity estimated from pulse velocity measurements is higher than that obtained from vibration measurements, even when the value of Poisson's ratio is known.[31]

8.8 Advantages and Limitations

The pulse velocity method is an excellent means for investigating the uniformity of concrete. The test procedure is simple and the available equipment in the market is easy to use in the laboratory as well as in the field.

The testing procedures have been standardized by ASTM and other organizations, and test equipment is available from several commercial sources. With the availability of small portable digital instruments, which are relatively inexpensive and easy to operate, ultrasonic testing adds a new dimension to quality control of concrete in the field.

Ultrasonic pulse velocity tests can be carried out on both laboratory-sized test specimens and concrete structures. This fact, combined with the knowledge that ultrasonic techniques provide an effective means of delineating both surface and internal cracks in concrete structures, enhances the usefulness of these tests.

Inasmuch as a large number of variables affect the relations between the strength parameters of concrete and its pulse velocity, the use of the latter to estimate the compressive and/or flexural strengths of concrete is not recommended unless previous correlation testing has been performed.

Appendix 8.1: Effect of Reinforcing Bars

The pulse velocity measured in reinforced concrete in the vicinity of reinforcing bars is often higher than in plain concrete of the same composition. This is because the compressional pulse velocity in steel is 1.4 to 1.7 times that in plain concrete and, under certain conditions, the first pulse to arrive at the receiving transducer travels partly in concrete and partly in steel. The apparent increase in pulse velocity depends on the proximity of the measurements to the reinforcing bar, the dimensions and number of the reinforcing bars, their orientation with respect to the propagation path, and the pulse velocity in the surrounding concrete.[22,24,29]

Axis of Reinforcing Bar Perpendicular to Direction of Propagation

The influence of the presence of the reinforcing bars can be calculated assuming that the pulse traverses the full diameter of each bar during its path. If there are n different bars of diameter Q_i (i = 1 to n) directly in the path of the pulse, with their axes perpendicular to the path of propagation (see Figure 8.10A), then[22]

$$\frac{V_c}{V} = 1 - \frac{L_s}{L}\left(1 - \frac{V_c}{V_s}\right) \tag{8.6}$$

where

V = the pulse velocity in the reinforced concrete, i.e., the measured pulse velocity
V_c = the pulse velocity in the plain concrete
V_s = the pulse velocity in the steel
L = the total path length

$L_s = \sum_1^n Q_i$, the path length through steel

Values of V_c/V are given in Table 8.3 for different amounts of steel in three types of concrete, which could be rated as very poor, fair, and very good materials, respectively.

In practice V_c/V is likely to be slightly higher than values given in Table 8.3 because of misalignment of the reinforcing bars and because only a small fraction of the pulse energy will actually traverse the full diameter of each bar.

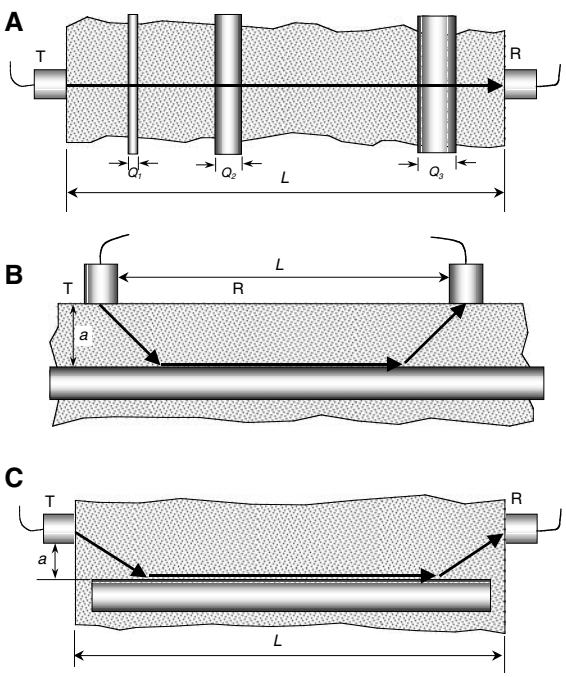

FIGURE 8.10 Measurements on reinforced concrete. (A) Reinforcing bar perpendicular to direction of propagation. (B) Reinforcing bar parallel to test surface. (C) Reinforcing bar parallel to direction of propagation.

TABLE 8.3 Influence of Steel Reinforcement — Line of Measurement Perpendicular to Axis of Bar

$$\frac{V_c}{V} = \frac{\text{pulse velocity in plain concrete}}{\text{measured pulse velocity in reinforced concrete}}$$

L_s/L	Very poor quality, V_c = 3000 m/s	Fair quality, V_c = 4000 m/s	Very good quality, V_c = 5000 m/s
1/12	0.96	0.97	0.99
1/8	0.94	0.96	0.98
1/6	0.92	0.94	0.97
1/4	0.88	0.92	0.96
1/3	0.83	0.89	0.94
1/2	0.75	0.83	0.92

Axis of Bar Parallel to Direction of Propagation

If the edge of the bar is located at a distance a from the line joining the nearest points of the two transducers and the path length between transducers is L, then the transit time T in either of the configurations of Figure 8.10B or C is[22]

$$T = \frac{L}{V_s} + 2a\sqrt{\frac{V_s^2 - V_c^2}{V_s V_c}} \tag{8.7}$$

for

$$\frac{a}{L} \pounds \frac{1}{2}\sqrt{\frac{V_s - V_c}{V_s + V_c}} \tag{8.8a}$$

There is no influence of the steel when[22]

$$\frac{a}{L} > \frac{1}{2}\sqrt{\frac{V_s - V_c}{V_s + V_c}} \tag{8.8b}$$

The difficulty of applying Equations 8.7 and 8.8 lies in deciding on the velocity (V_s) of propagation of the pulse along the steel bar. Propagation of the pulse is influenced by geometrical dispersion in the steel bar. The value for V_s is likely to be between about 5900 m/s (i.e., the compressional wave velocity in steel) and 5200 m/s (i.e., the bar velocity* in steel).

Corrections to the measured pulse velocity in the direction parallel to the reinforcement are given in Table 8.4. This table also indicates that, for bars that span most of the section, the lateral displacement of the line of measurement from the axis of the bar will usually be of the order of 0.2 to 0.25 L before the influence of the steel becomes negligible.

Two-Way Reinforcement

Steel reinforcement in two or more directions complicates the interpretation of pulse velocity measurements. Corrections based on Table 8.3 and Table 8.4 may be calculated for simple well-defined systems of reinforcement but it may become impossible to make any reliable corrections for more complicated, heavily reinforced concrete.

*A guided wave is likely to set up and to propagate along the length of a long cylindrical bar. This "bar wave" has a lower velocity than the compressional wave.

TABLE 8.4 Influence of Steel Reinforcement — Line of Measurements Parallel to Axis of Bar

$$\frac{V_c}{V} = \frac{\text{pulse velocity in plain concrete}}{\text{measured pulse velocity in reinforced concrete}}$$

a/L	$\frac{V_c}{V_s} = 0.90$	$\frac{V_c}{V_s} = 0.80$	$\frac{V_c}{V_s} = 0.71$	$\frac{V_c}{V_s} = 0.60$
0	0.90	0.80	0.71	0.60
1/20	0.94	0.86	0.78	0.68
1/15	0.96	0.88	0.80	0.71
1/10	0.99	0.92	0.85	0.76
1/7	1.00	0.97	0.91	0.83
1/5	1.00	1.00	0.99	0.92
1/4	1.00	1.00	1.00	1.00

References

1. Powers, T.C., Measuring Young's modulus of elasticity by means of sonic vibrations, *Proc. ASTM*, 38(Part II), 460, 1938.
2. Obert, L., Sonic method of determining the modulus of elasticity of building materials under pressure, *Proc. ASTM,* 39, 987, 1939.
3. Hornibrook, F.B., Application of sonic method to freezing and thawing studies of concrete, *ASTM Bull.,* 101, 5, 1939.
4. Thomson, W.T., Measuring changes in physical properties of concrete by the dynamic method, *Proc. ASTM,* 40, 1113, 1940.
5. Leslie, J.R. and Cheesman, W.J., An ultrasonic method of studying deterioration and cracking in concrete structures, *ACI J. Proc.,* 46(1), 17, 1949.
6. Jones, R., *The Application of Ultrasonic to the Testing of Concrete,* Research, London, 1948, 383.
7. Whitehurst, E.A., *Evaluation of Concrete Properties from Sonic Tests,* ACI Monograph 2, American Concrete Institute, Detroit, MI, 1966, 94 pp.
8. Malhotra, V.M., *Testing Hardened Concrete: Nondestructive Methods,* ACI Monograph 9, American Concrete Institute, Detroit, MI, 1976.
9. ACI Committee 228, *Nondestructive Test Methods for Evaluation of Concrete in Structures,* ACI 228.2R-98, American Concrete Institute, Farmington Hills, MI, 1998.
10. Jones, R., *Non-Destructive Testing of Concrete*, Cambridge University Press, London, 1962.
11. ASTM Test Designation C 597-02, Standard Test Method for Pulse Velocity through Concrete, *Annual Book of ASTM Standards*, Vol. 04.02, West Conshohocken, PA, 2003.
12. Qixian, L. and Bungey, J.H., Using compression wave ultrasonic transducers to measure the velocity of surface waves and hence determine dynamic modulus of elasticity for concrete, *Constr. Build. Mater.*, 10(4), 237, 1996.
13. Benedetti, A., On the ultrasonic pulse propagation into fire damaged concrete, *ACI Struct. J.*, 95(3), 259, 1998.
14. Bullock, R.E. and Whitehurst, E.A., Effect of certain variables on pulse velocities through concrete, *Highway Res. Board Bull.,* 206, 37, 1959.
15. Sturrup, V.R. Vecchio, R.J., and Caratin, H., *Pulse Velocity as a Measure of Concrete Compressive Strength,* ACI SP 82-11, American Concrete Institute, Farmington Hills, MI, 1984, 201.
16. Swamy, N.R. and Al-Hamed, A.H., The use of pulse velocity measurements to estimate strength of air-dried cubes and hence *in situ* strength of concrete, Malhotra, V.M., Ed., ACI SP 82, American Concrete Institute, Farmington Hills, MI, 1984, 247.
17. Anderson, D.A. and Seals, R.K., Pulse velocity as a predictor of 28 and 90 day strength, *ACI J.,* 78, 116, 1981.

18. Jones, R., Testing of concrete by an ultrasonic pulse technique, RILEM Int. Symp. on Nondestructive Testing of Materials and Structures, Paris, Vol. 1, Paper No. A-17 January 1954, 137. *RILEM Bull.*, 19(Part 2), Nov. 1954.
19. Popovics, S., Rose, J.L., and Popovics, J.S. The behavior of ultrasonic pulses in concrete, *Cem. Concr. Res.*, 20, 259, 1990.
20. Kaplan, M.F., The effects of age and water to cement ratio upon the relation between ultrasonic pulse velocity and compressive strength of concrete, *Mag. Concr. Res.*, 11(32), 85, 1959.
21. Jones, R. and Facaoaru, I., Recommendations for testing concrete by the ultrasonic pulse method, *Mater. Struct. Res. Testing* (Paris), 2(19), 275, 1969.
22. BS 1881, Part 203, Recommendations for Measurement of Velocity of Ultrasonic Pulses in Concrete, British Standards Institution, London, 1986.
23. Kaplan, M.F., Compressive strength and ultrasonic pulse velocity relationships for concrete in columns, *ACI J.,* 29(54-37), 675, 1958.
24. RILEM Recommendation NDT 1, Testing of concrete by the ultrasonic pulse method, Paris, Dec. 1972.
25. Popovics, S. and Popovics, J.S., Effect of stresses on the ultrasonic pulse velocity in concrete, *RILEM Mater. Struct.*, 24, 15, 1991.
26. Wu, T.T and Lin, T.F., The stress effect on the ultrasonic velocity variations of concrete under repeated loading, *ACI Mater. J.*, 95(5), 519, 1998.
27. Chung, H.W., Effect of embedded steel bar upon ultrasonic testing of concrete, *Mag. Concr. Res.* (London), 30(102), 19, 1978.
28. Chung, H.W. and Law, K.S., Diagnosing *in situ* concrete by ultrasonic pulse technique, *Concr. Int.,* 42, Oct. 1983.
29. Bungey, J.H., *The Influence of Reinforcement on Ultrasonic Pulse Velocity Testing*, Malhotra, V.M., Ed., ACI SP 82, American Concrete Institute, Farmington Hills, MI, 1984, 229.
30. Komlos, K., Popovics, S., Nurnbergerova, T., Babal, B., and Popovics, J.S., Ultrasonic pulse velocity test of concrete properties as specified in various standards, *Cem. Concr. Composites*, 18, 357, 1996.
31. Philleo, R.E., Comparison of results of three methods for determining Young's modulus of elasticity of concrete. *ACI J.,* 26(5), 461, 1955. Discussions, 472-1, Dec. 1955.
32. Goodell, C.E., Improved sonic apparatus for determining the dynamic modulus of concrete specimens, *ACI J.,* 27(47-4), 53, 1950.
33. Galan, A., Estimate of concrete strength by ultrasonic pulse velocity and damping constant, *ACI J.,* 64(64-59), 678, 1967.
34. Parker, W.E., Pulse velocity testing of concrete, *Proc. ASTM,* 53, 1033, 1953.
35. Whitehurst, E.A., Soniscope tests concrete structures, *ACI J. Proc.,* 47(6), 433, 1957.
36. Breuning, S.M. and Bone, A.J., Soniscope applied to maintenance of concrete structures, *Proc. Highway Res. Board,* 33, 210, 1954.
37. McHenry, D. and Oleson, C.C. Pulse velocity measurements on concrete dams, in *Trans. 9th Int. Congr. on Large Dams,* Istanbul, 1967, Q34, R5, V. 3, 73.
38. Chefdeville, J., Application of the method toward estimating the quality of concrete, *RILEM Bull.* 15, Paris, Special Issue-Vibration Testing of Concrete, Part 2, Aug., 59. 1953.
39. Van der Winder, N.G.B. and Brant, A.W., *Ultrasonic Testing for Fresh Mixes,* Concrete, Cement and Concrete Association, Wexham Springs, U.K., 1977, 25.
40. Woods, K.B. and McLaughlin, J.F., Application of pulse velocity tests to several laboratory studies of materials, *Highway Res. Board Bull.,* 206, 1959.
41. Whitehurst, E.A., Use of soniscope for measuring setting time of concrete, *Proc. ASTM,* 51, 1166, 1951.
42. Cheesman, W.J., Dynamic testing of concrete with the soniscope apparatus, *Proc. Highway Res. Board,* 29, 176, 1949.
43. Neville, A.M., A study of deterioration of structural concrete made with high alumina concrete, *Proc. Inst. Civ. Eng.* (London), 25, 287, 1963.

44. Zoldners, N.G., Malhotra, V.M., and Wilson, H.S., High-temperature behavior of aluminous cement concretes containing different aggregates, *Proc. ASTM,* 63, 966, 1963.
45. Sturrup, V.R., Evaluation of pulse velocity tests made by Ontario hydro, Bull. 206, Highway Research Board, 1959, 1.
46. Jones, R., A method of studying the formation of cracks in a material subjected to stress, *Br. J. Appl. Phys.* (London), 3, 229, 1952.
47. Knab, L.J., Blessing, G.V., and Clifton, J.R., Laboratory evaluation of ultrasonics for crack detection in concrete, *ACI J.,* 80, 17, 1983.
48. Rebic, M.P., The distribution of critical and rupture loads and determination of the factor of crackability, *ACI J.,* 80, 17, 1983.
49. ACI Committee 228, *In-Place Methods to Estimate Concrete Strength*, ACI 228.1R-95, American Concrete Institute, Farmington Hills, MI, 1995.
50. Phoon, K.K., Wae, T.H. and Loi, C.S., Development of statistical quality assurance criterion for concrete using ultrasonic pulse velocity method, *ACI Mater. J.*, 96(5), 568, 1999.
51. Rhazi, J. Kharrat, Y., Ballivy, G., and Rivest, M., Application of acoustical imaging to the evaluation of concrete in operating structures, S. Pessiki and L. Olson, Eds., ACI SP 168, American Concrete Institute, Farmington Hills, MI, 1997, 221.
52. Olson, L.D. and Sack, D.A., Nondestructive evaluation of concrete dams and other structures, *Proc. SPIE* (The International Society for Optical Engineering), 2457, 113, 1995.
53. Keating, J., Hannant, D.J., and Hibbert, A.P., Correlation between cube strength, ultrasonic pulse velocity and volume change for oil well cement slurries, *Cem. Concr. Res.*, 19, 714, 1989.
54. Sayers, C.M. and Dahlin, A., Propagation of ultrasound through hydrating cement pastes at early times, *J. Adv. Cem. Based Mater.*, 1, 12, 1993.
55. Bungey, J.H., Ultrasonic testing to identify alkali-silica reaction in concrete, *Br. J. NDT*, 33(5), 227, 1991.
56. Selleck, S.F., Landis, E.N., Peterson, M.L., Shah, S.P., and Achenbach, J.D., Ultrasonic investigation of concrete with distributed damage, *ACI Mater. J.*, 95(1), 27, 1998.
57. Neville, A.M., *Properties of Concrete*, 4th ed., John Wiley & Sons, New York, 1996, 63.

9

Combined Methods

9.1 Introduction
9.2 Historical Development
9.3 Combined Ultrasonic Pulse Velocity and Hardness Measurement Techniques
Theoretical Considerations · Description of Test Methods · Development of Test Methods for Practical Applications · Limitations and Advantages of Combined Pulse Velocity and Rebound Number Technique · Application of Combined Test Methods
9.4 Conclusions

Aleksander Samarin
Consultant

This chapter describes the theoretical and empirical based concepts as well as the history of development of combined nondestructive test methods for hardened concrete.

Of a number of purely nondestructive tests, the rebound (Schmidt) hammer and the ultrasonic pulse velocity combinations are the most commonly used. In the majority of cases, the need for *in situ* concrete strength evaluation arises as a result of suspect quality of concrete. By developing a prior correlation for a range of concrete grades and types, having only the source of coarse aggregate and a broad age group in common, it is possible to obtain good indication of the *in situ* strength of concrete, expressed as the value of a test result of a standard laboratory compressive specimen.

The quality of concrete, using combined nondestructive methods, is evaluated through the measurements and correlation of the surface hardness, density, elastic constants and the predicted compressive strength.

Use of combined methods is generally justifiable only if a reliable correlation for a particular type of concrete is developed prior to the evaluation of the subject quality concrete. The benefit of the small additional reliability of a combined test vs. a single nondestructive test should be assessed against the additional time, cost, and complexity of combined techniques.

9.1 Introduction

Although the need for nondestructive *in situ* testing of concrete has long been realized, it is seldom used in its own right for quality control and compliance purposes. In fact, the practice is to bring in a destructive (e.g., cores), a semi-destructive (e.g., pullout or break-off tests), or a nondestructive *in situ* test at the postmortem stage, either following noncompliance of a standard specimen test result or on observing signs of deterioration and distress in a structure.

Occasionally, nondestructive *in situ* tests are used to evaluate the "quality" of existing structural members for the purpose of subsequent modifications to that structure. The "quality" of concrete in practice is still commonly described in terms of its uniaxial compressive strength, evaluated statistically from the results of standard laboratory specimens, cast, compacted, cured, and tested under strictly prescribed conditions. There is, of course, a very good reason for maintaining this system. In those

countries where ready-mixed concrete can be purchased from a premixed concrete manufacturer, this method remains the only fair and reasonable way of evaluating the potential quality, i.e., strength of concrete as supplied to a building site.

However, with the present emphasis on the design of reinforced concrete structures according to the limit state concepts, there seems to be much greater need for better definition of the relationship between concrete quality and variability in actual structures and in standard, laboratory-cured test specimens of the same concrete. A combination of these *in situ* tests, if properly used, can improve some of these correlations. The extent to which the correlation can be improved should be balanced, however, by the additional time, cost, and resources required to use combined methods.

9.2 Historical Development

In the preceding chapters several nondestructive and semi-destructive (or partially destructive) test methods have been described. These methods were developed to evaluate the strength, or strength related properties of concrete. In order to predict the strength of *in situ* concrete more accurately, a number of investigators have tried to apply more than one nondestructive method at the same time.

Some of the pioneering work in this field, carried out in the 1950s and 1960s, was reported by Kesler and Higuchi,[1] Skramtaev and Leshchinsky,[2] Wiebenga,[3] Facaoaru,[4] and McLeod.[5] Combined methods, as used in this chapter, refers to techniques in which one test improves the reliability and precision of the other in evaluating a property of concrete, e.g., strength or elastic modulus. When an additional test is used to provide new, but supporting information (e.g., location of reinforcing steel, using a covermeter), the tests are not considered promising by their investigators.

Dynamic modulus of elasticity and damping constant, as determined from resonance tests by Kesler and Higuchi,[1] were reported to correlate well with the compressive strength of concrete, regardless of its mix proportions, age, or moisture content. The accuracy of prediction was considered to be within 5%. Laboratory techniques were used, as the method was unsuitable for *in situ* measurements.

Wiebenga[3] used ultrasonic pulse velocity in place of dynamic modulus of elasticity and the damping constant as well as pulse attenuation in his laboratory tests. In each case, the use of either damping constant or pulse attenuation improved the accuracy of the predicted compressive strength. Galan[6] also used the combination of ultrasonic pulse velocity and the damping constant to estimate the *in situ* strength of concrete. The damping constant was determined by calibrating experimental curves of an oscillogram with the corresponding damped reverberated impulses. According to Galan, good correlation between the strength of concrete and the two acoustic characteristics, i.e., pulse velocity and damping constant, can be established. The pulse velocity expresses the elastic properties and the damping constant represents the inelastic behavior of concrete.

In the majority of cases, the differences between the estimated strength values and the values obtained by destructive testing was of the order of 5%, i.e., similar to the accuracy of the laboratory tests by Kesler and Higuchi. Most of the recent research work using the above technique has been conducted in the eastern European countries.

The portable ultrasonic pulse velocity units currently used in Western countries have digital displays and are not equipped with oscilloscopes. Thus the application of pulse attenuation techniques combined with the ultrasonic pulse velocity would require additional equipment. It would also require highly skilled technical personnel, which can render this test method cost ineffective.

By far, the most popular combination, however, is the method based on the measurement of ultrasonic pulse velocity in conjunction with hardness measurements. This was confirmed by a number of surveys, such as Jones and Facaoaru[7] and Malhotra and Carette.[8] Historically, most of the credit for the development of this combined method should be attributed to Skramtaev and Leshchinsky,[2] Wiebenga,[3] MacLeod[5] and particularly to Facaoaru,[4,7,9] and for the promotion and popularization of the method to Malhotra.[8,10–12] Several isolated reports on the use of other types of combinations were published from time to time. For example, MacDonald and Ramakrishman[13] considered pulse velocity and maturity, and Parsons and Naik[14] used the pullout test and maturity. However, the only recorded practical application

at present seems to be the combination of ultrasonic pulse velocity and hardness measurements, and all other combinations, however theoretically promising, should thus be considered only as research and development.

9.3 Combined Ultrasonic Pulse Velocity and Hardness Measurement Techniques

9.3.1 Theoretical Considerations

Fundamental aspects of the hardness methods are given in Chapter 1 and those of ultrasonic pulse velocity in Chapter 5. However, a brief summary is given to highlight the major aspects of these tests.

Hardness scales are arbitrarily defined measures of the resistance of a material to indentation under static or dynamic load or resistance to scratch, abrasion, wear, cutting or drilling. Concrete test hammers evaluate surface hardness as a function of resiliency, i.e., the ability of a hammer to rebound or spring back. One of the original papers on the subject was published by Schmidt.[15] ASTM Method C 805 describes the test method for determining the rebound number of hardened concrete, and methods of hammer use and calibration are also given in the B.S. 1881:Part 202.

The propagation of a longitudinal or compressional disturbance and also a transverse or shear disturbance in a semi-infinite solid was explained by Poisson in 1828. Chree[16] and Lord Rayleigh[17] subsequently showed that by transmitting ultrasonic waves through blocks of different materials it was possible to measure the values of the elastic constants for these solids. The method was particularly useful for a material such as glass, for which the behavior under static loading causes considerable difficulty of interpretation.

The interpretation of the pulse velocity measurements in concrete is complicated by the heterogeneous and to some degree anisotropic nature of this material. The wave velocity is not determined directly, but is calculated from the time taken by a pulse to travel a measured distance. A piezoelectric transducer emitting vibrations at its fundamental frequency is placed in contact with the concrete surface so that the vibrations travel through the concrete and are received by another transducer, which is in contact with the opposite face of the test object.

In theory, a for a semi-infinite elastic solid there is a unique relationship between the longitudinal wave velocity and the density, modulus of elasticity, and Poisson's ratio. The ultrasonic pulses produce relatively low stresses and strains and the behavior of concrete subjected to this test method can be considered elastic for all practical considerations (see Figure 9.1). Thus at least some of the theoretical correlations should retain a degree of validity in practical applications.

ASTM Method C 597 and B.S. 1881:Part 203 describe the standard test methods for determination of pulse velocity through concrete.

9.3.2 Description of Test Methods

The nondestructive testing of *in situ* concrete may be carried out for a number of reasons. The final objective of the evaluation, as well as the type and the extent of the available information, which is essential for interpreting the results will generally influence the selection of a particular method. Arbitrarily, the combined methods based on ultrasonic pulse velocity and rebound hammer techniques can be divided into two main groups.

In the first group, the prime objective is to determine the rate of strength gain in concrete and/or the variation in the strength within a group of concrete batches, mixed to the same proportions. All the ingredients of each mix (e.g., cement, aggregate, and admixture type) as well as their proportions are generally known in this case.

A classical example of this application is the SONREB method, developed largely due to the efforts of RILEM Technical Committees 7 NDT and 43 CND, and under the chairmanship of Facaoaru[18] has been adopted in Romania. A general relationship between compressive strength of concrete, rebound hammer

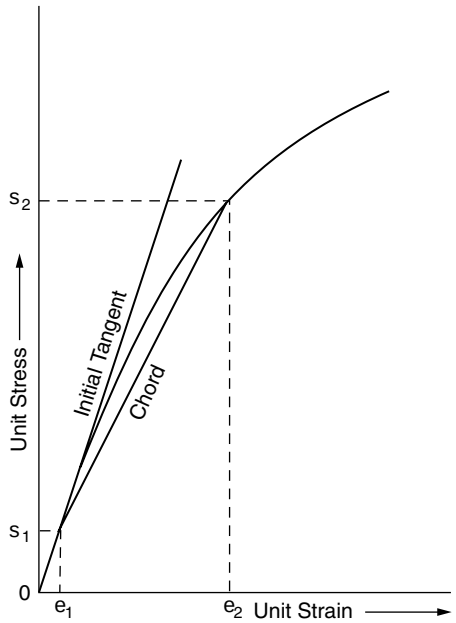

FIGURE 9.1 Typical relationship between the initial tangent and a chord modulus of elasticity for concrete. 0 to ϵ_1 is the range of potential disturbance in a static test, but also an elastic range in the dynamic test.

number, and ultrasonic pulse velocity, in accordance with the tentative recommendations for "*In Situ* Concrete Strength Estimation by Combined Non-Destructive Methods," RILEM Committee TC 43 CND, 1983, forms the basis of SONREB technique. Figure 9.2 shows this relationship in the form of a nomogram. By knowing the rebound number and pulse velocity, the compressive strength is estimated.

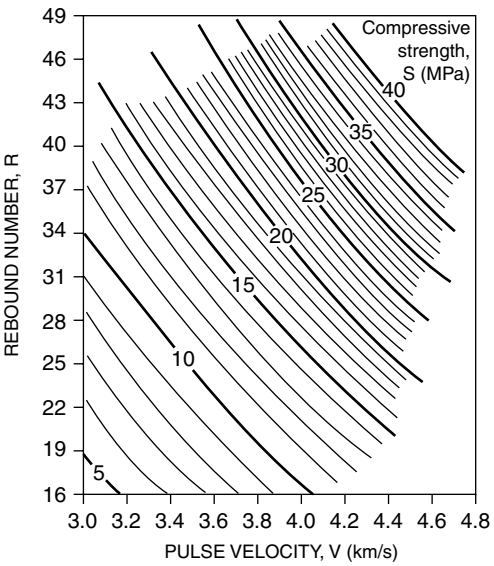

FIGURE 9.2 ISO-strength curves for reference concrete in SONREB method.

A series of correction coefficients, developed for a specific concrete grade and type are then applied in order to improve the accuracy of prediction obtained from the nomogram. The following coefficients are used, according to Facaoaru:[18]

Cc = coefficient of influence of cement type
Cd = coefficient of influence of cement content
Ca = coefficient of influence of petrological aggregate type
Cg = coefficient of influence of aggregate fine fraction (less than 0.1 mm)
Co = coefficient of influence of maximum size of aggregate

The accuracy of the estimated strength (the range comprising 90% of all the results) is considered to be

1. 10 to 14% when the correlation relationship is developed with known strength values of cast specimens or cores and when the composition is known
2. 15 to 20% when only the composition is known

In the second group, the prime objective is to determine the potential compressive strength of *in situ* concrete when its quality is considered to be suspect. Even if the intended mix ingredients and proportions are known (and quite often this is not the case), low compressive strength results, poor field performance, or even concrete appearance may lead to the belief that, due to either a mechanical malfunction or a human error, these ingredients and proportions differ from the designed values. Thus for the second group, we can say that the combined test method is used when concrete mix ingredients and proportions are *not* known.

The general approach for the second case is to develop a correlation relationship between pulse velocity and rebound hammer readings and compressive strength of standard laboratory specimens cast from the locally manufactured concretes. These forms of general correlation at least reduce the uncertainties due to variable ingredients and variations in mix proportions, as the sources of local raw materials are usually limited.

The accuracy (again shown as the range comprising 90% of all the results) when only specimens or cores are available is indicated by Facaoaru[18] to be between 12 and 16%. There are, however, ways in which this accuracy can be improved.

9.3.3 Development of Test Methods for Practical Applications

As already mentioned, in the majority of cases the need for *in situ* concrete strength evaluation arises as a result of the suspect, and hence unknown, quality of the concrete in a structure.

In an ordinary concrete between 60 and 70% of the absolute volume is taken up by aggregate and the rest by cement paste, consisting of hydrated and unhydrated cement grains, chemically bound and free water, and entrained (small voids) or entrapped (larger voids) air. Subject to availability in a particular country or region, part of the cementitious material may be ground granulated blast furnace slag, fly ash, silica fume, or some other pozzolanic or reactive siliceous material. The paste may also contain chemical admixtures. The strength characteristics of a given cement paste, subjected to the influence of a particular environment, will be a function of *time*, and the strength characteristics of a given *aggregate*, for all practical purposes, can be considered time independent and a function of its petrological type only.

Thus, even in concrete of suspect quality and unknown composition, there are two variables which can be identified with a reasonable degree of accuracy, namely, *petrological type of the aggregate* and *approximate age of the concrete*. Aggregate can be identified by removing some of the matrix in an out-of-sight part of a structural member. Coarse aggregate is particularly easy to identify in this way and, in the majority of commercial grade concretes, coarse aggregate content is significantly higher than the fine.

Establishment of a series of specific correlations between the combination of rebound hammer number (R) and ultrasonic pulse velocity (V) and the compressive strength (S) of concretes, each containing a *particular aggregate type* and being of a *particular age group*, was completed in the early 1970s by Samarin and Smorchevsky.[19,20] Because the transit time of an ultrasonic pulse through concrete consists of the

sum of transit times through aggregate and paste, the identification of *aggregate type* and *time* dependent properties of cement paste eliminates two major uncontrollable variables of the general correlation. The accuracy of the estimated compressive strength can thus be measurably improved. Yet another factor which can improve the accuracy of prediction, particularly over a wide range of concrete strength levels, is the provision for nonlinearity of some functions.

Work by Samarin[20] has shown that for Australian concretes the relationship between rebound hammer number (R) and the compressive strength (S) is nearly linear, and curve fitting analyses indicated that a fourth order function gives the best correlations between ultrasonic pulse velocity (V) and the compressive strength (S) for the same concretes. Thus the general equation for the rebound hammer correlation relationship is

$$S = a_0 + a_1 R \tag{9.1}$$

where a_0, a_1 are constants.
The general equation for the pulse velocity correlation relationship is of the form:

$$S = b_0 + b_1 V^4 \tag{9.2}$$

where b_0, b_1 are also constants.

It is worth mentioning that the almost universally accepted empirical relationship between the elastic modulus of concrete (E) and the compressive strength of concrete (S) is of the following general form:

$$E = A\ S^{0.5} \tag{9.3}$$

where A is a constant, depending on concrete density, statistical evaluation of strength and the selected system of measures. At the same time, the theory of propagation of stress waves through an elastic medium states that for a compression wave the following functional relationship is valid:

$$E = B\ V^2 \tag{9.4}$$

where B is a constant, depending on density and Poisson's ratio. Equating the right hand sides of Equations 9.3 and 9.4, we see that strength (S) is related to the fourth power of the pulse velocity (V), confirming the general validity of Equation 9.2.

Detailed consideration of the above derivation was given by Samarin and Meynink.[21] It was considered convenient in this work to divide concrete into three age groups, namely:

1. 7 days and younger
2. Over 7 days but less than 3 months
3. 3 months and older

It is known, for example as reported by Elvery and Ibrahim,[22] that the sensitivity of ultrasonic pulse velocity to concrete strength is very high in the first few days, but after about 5 to 7 days (depending on curing conditions) the results become considerably less reliable. Most of the concrete that is identified as being suspect is subsequently tested *in situ* at the age of between 1 and 3 months. The majority of the laboratory test data, for which the correlations have been developed, also fall into this period.

To develop a correlation relationship for each *age group* and *aggregate type*, concretes having a wide range of strength grades and mix composition are cast into standard laboratory (cylindrical) specimens. Compaction, curing, capping, etc. are carried out strictly according to the requirements of the relevant standards. Just prior to a compression strength test, each specimen is placed in a horizontal rig and the transit time of an ultrasonic pulse through the length of a capped cylinder is recorded. The pulse velocity is calculated as the ratio of the length over the transit time. The specimen is then placed in a compression machine and a load of approximately 1.4 MPa (200 psi) is applied, while 15 rebound hammer readings are taken around the circumference of the cylinder. A similar technique can be used with a cube or a

prismatic specimen. The specimen is then tested in unconfined compression, using a test method that complies with the relevant standard requirements.

When the multiple correlation relationship for each *aggregate type* and each *age group* is developed, the results, as compared with correlations between compressive strength and ultrasonic pulse velocity alone, or between compressive strength and rebound hammer reading alone, indicate:

1. An increase in the multiple correlation coefficient above the correlation coefficient for rebound number alone for pulse velocity alone
   (Note that correlation coefficients for rebound number and strength are generally higher [better] than those for pulse velocity and strength.)
2. A decrease in the standard error of estimate for a multiple correlation relationship compared with relationships between rebound number and strength alone and between pulse velocity and strength alone

The degree of improvement due to the combined technique depends on a number of factors. Of these, the most significant (in the order of importance) appear to be

1. Grouping concretes for a particular multiple-regression analysis according to the petrological type of the coarse aggregate.
2. Use of least-squares curve fitting to establish the correct form of the relation between concrete strength and each independent variable separately. (For Australian concretes, the correlation between compressive strength and rebound hammer is very near linear, and pulse velocity has to be raised to the fourth power in order to produce near optimum curve-fitting in its functional relationship to strength.)
3. In establishing the multiple correlation relationship, a reasonably wide range of strength grades of concrete (say, from 20 to 50 MPa) all manufactured using identical coarse aggregate, should be used.

A typical multiple correlation relationship for Australian concrete in a form of a nomogram is shown in Figure 9.3. Early age effect puts greater emphasis on pulse velocity.

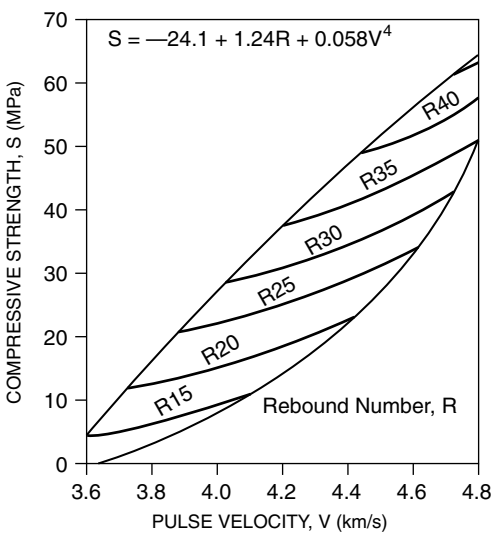

FIGURE 9.3 Nomogram for concrete of a particular aggregate type and age.

Development of a general multiple correlation equation for a particular country or even for a given district, for example as reported by Shah,[23] does not take into consideration the coarse aggregate effect and the benefit of a combined effect is reduced.

The curve fitting model used for each independent variable can have a significant effect on the relation to strength. Malhotra and Carette[8] in their analysis using multiple correlation methods compare their own test data with the correlations obtained by Samarin and Meynink[21] and Bellander.[24] In each case, when nonlinearity of pulse velocity vs. strength was not taken into account, the effect of the combined method was either of little significance, or there was no improvement at all due to multiple correlation.

A variety of nonlinear and linear multiple correlation equations were considered by different research workers and the results are compiled in Table 9.1. In every case, when nonlinearity between the pulse velocity (V) and strength (S) was taken into account the significance of the combined effect was enhanced.

9.3.4 Limitations and Advantages of Combined Pulse Velocity and Rebound Number Technique

First of all, most of the limitations that apply to the rebound number method by itself (Chapter 1) and also to the ultrasonic pulse velocity method by itself (Chapter 5) are likely to affect the reliability, sensitivity, and reproducibility of the results obtained by the combined technique. However, there are exceptions in those cases when a variation in properties of concrete produces opposite effects on the result of each component test. Most notable of these is the effect of variability of moisture content in concrete. An increase in the moisture content increases the ultrasonic pulse velocity but decreases the value of the rebound hammer number. This aspect of the combined method was reported by Bellander,[24] and it is also shown in Table 9.2 from unpublished research by Meynink and Samarin. In the work by Meynink and Samarin, the objective was to assess the influence of curing and the moisture condition of a specimen on the predicted vs. measured strength. The following method was employed:

Seven sets of cylinders (2 per set) cast from the same mix were subjected to the following curing regimes prior to testing in compression.

1. 28 days in water in 23°C
2. 28 days in water at 23°C, 2 h in oven at 65°C
3. 26 days in water at 23°C, 2 days in 50% relative humidity (RH), 23°C environment
4. 7 days in water at 23°C, 21 days in 50% RH, 23°C environment
5. As for Number 4 but prior to testing, rewetted by immersion in water for 2 h
6. 7 days in water at 23°C, 7 days in 50% RH, 23°C environment, 7 days in oven at 65°C, 7 days in oven at 110°C
7. As for Number 6 but prior to testing, rewetted by immersion in water for 2 h

The mix was typical of a concrete in Australia containing a natural normal weight aggregate and blended cement. With the exception of high temperature treatments 6 and 7, the strength calculated from a regression equation was within 1 MPa (about 145 psi) of measured strength for all curing and moisture conditions.

These results give further confidence in the combined technique developed by Samarin et al.[19–21] on the basis of prior correlations, when only the aggregate type and the age of concrete is known or can be identified. Results of heat treated specimens indicate that concrete exposed to fire may not be suitable for evaluation by the combined pulse velocity and hardness measurement technique. This view is confirmed by a detailed study of the effects of high temperatures on the reliability of strength estimates from combined nondestructive tests by Logothetis and Economou.[29]

Chung and Law[30] concluded that both the pulse velocity and the compressive strength of concrete are reduced by fire attack, but that the rate of reduction is not the same. It seems that, in order to evaluate the extent of fire damage, a prior multiple regression correlation relationship using the combined technique should be developed for concrete of a given composition subjected to a range of high temperatures.

TABLE 9.1 Various Multiple Regression Correlations Suggested by Different Researchers for Estimating Compressive Strength of Concrete

Researchers	Form of Multi-Regression Equation	Significance of the Combined Effect
McLeod[5]	$S = K_0 + k_1 R + k_2 V$	Significant in some cases, but not in others
Di Maio, et al.[25]		
Tanigawa, et al.[26]		
Knaze and Beno[27]	$S = a_0 + a_1 R + a_2 R^2$	Use of nomogram "Curves of Equal
	$S = b_0 + b_1 V + b_2 V^2$	Strength"; effect considered significant
Bellander[24]	$S = k_0 + k_1 R^3 + k_2 V$	Significant to a certain degree
Weibinga[3]	$\log_e S = k_0 + k_1 R + k_2 V$	Significant (within test conditions)
Shah[23]		
Tanigawa, et al.[26]		
Schickert[28]	$S = k_0 R^n V^m$	Some evidence of significant effect
Samarin et al.[19–21]	$S = k_0 + k_1 R + k_2 V^4$	Significant
Tanigawa et al.[26]	$S = V(a_0 + a_1 R + a_2 R^2 + a_3 R^3)$	Significant (but possibly too complex)

TABLE 9.2 Effect of Curing Conditions and Moisture Content of Concrete on the Reliability of Predictions Using Combined Techniques

	Description of Curing of Cylinders	Pulse Velocity (km/s)	Rebound Number	Compressive Strength (MPa) Predicted	Compressive Strength (MPa) Actual
1.	28 days moist	4.59	27.3	35.5	35.0
2.	28 days moist, dry surface by 65°C (2 h)	4.57	27.9	36.0	35.0
3.	26 days moist, dry surface by 50% RH (2 days)	4.56	29.1	37.0	38.0
4.	7 days moist, dry at 50% RH (21 days)	4.43	29.3	34.5	35.5
5.	7 days moist as for (4) but rewetted	4.41	27.2	31.5	31.5
6.	7 days moist/very dry in oven	4.10	28.9	28.0	39.0
7.	7 days moist as for (6) but rewetted	3.94	27.3	23.5	31.0

The change in ultrasonic pulse velocity due to the presence of reinforcing bars in the direction of propogation of the pulse was investigated by a number of researchers, among whom the work by Chung[31] deserves particular mention. If the position of steel is known or can be located by a covermeter, corrections as given by Chung,[31] or as shown in B.S. 1881:Part 203:1986, can be applied. However, complicated steel patterns in the direction of the ultrasonic pulse must be avoided.

The effect of incomplete consolidation of concrete on the accuracy of strength prediction using the combined method developed by Samarin et al.[19–21] was investigated by Samarin and Thomas.[32] Reduction in the concrete strength due to the lack of consolidation was correctly estimated by the combined nondestructive test. In superplasticized concrete, the estimated strength tended to be conservative, i.e., the actual results were slightly higher than predicted. The effect of concrete surface treatments, such as curing compounds and particularly surface treatments designed to improve abrasion resistance, was investigated by Sadegzadeh and Kettle.[33] The ultrasonic pulse velocity readings were not found to be significantly sensitive to surface treatments. The rebound hammer readings were affected by finishing techniques and curing regimes, but not by the *liquid* surface treatments. Hence, care must be taken in applying combined nondestructive test methods to concretes with abrasion-resistant surface treatments. Similar considerations may apply to very old, surface-carbonated concretes.

9.3.5 Application of Combined Test Methods

In evaluating the *in situ* properties of concrete, one must take into account the potential differences between strengths in the lower and upper parts of structural members, and the extent to which this

difference is affected by the size and the shape of a structural element. Wiebenga,[34] in his general report on the subject, states that the differences in strength between the upper and lower parts of walls and columns can often be 20 to 30% and in some cases the strength is up to 50% lower in the bottom parts of these members.

Destructive tests can be influenced by a number of factors, and these should be taken into consideration when comparison is made or correlations are established with the nondestructive tests. For example, Meynink and Samarin[35] found that the cores drilled in a horizontal direction generally give lower results than vertical cores taken at the same location.

Subject to the above considerations, combined methods for which prior correlations were developed for the local concrete materials have been successfully used for nondestructive *in situ* strength evaluation of concrete. Most of the reported cases of practical applications of the combined technique were in Europe and in Australia. The SONREB method, in which all concrete mix ingredients and proportions are usually known in advance, found practical use in Europe, as previously mentioned and reported by Facaoaru.[18] The application of this technique by Pohl[36] in the solution of a structural repair problem of a concrete silo resulted in considerable cost saving on the project. The main advantage of a nondestructive test is the possibility of obtaining a very large number of spot readings at a relatively low cost and without affecting the integrity of a structure.

Use of the combined nondestructive technique developed by Samarin et al.[19–21] became a routine method for evaluating the *in situ* quality of suspect concrete in many parts of Australia, and examples of its applications in a variety of projects involving office buildings, hospitals, and precast yards were given by Meynink and Samarin[35] and by Samarin and Dhir.[37] Some examples highlighting the practical use of this technique in Scotland were also reported.[37]

9.4 Conclusions

Combined nondestructive methods refer to techniques in which one test is used to improve the reliability of the *in situ* concrete strength estimated by means of another test alone.

The validity of a combined technique can be evaluated from the degree of improvement this additional test provides to the accuracy and reproducibility of predictions, vs. the additional cost and complexity of the combined method and the extent to which it is practicable to perform the additional tests *in situ*.

Of the various combinations proposed by different researchers and from the reported data it seems that only the combined techniques based on the ultrasonic pulse velocity and surface hardness measurement have been adopted in some parts of the world for practical evaluation of the *in situ* compressive strength of concrete. Presently, other combined techniques should be considered as being in the research and development phase.

The limitations of a combined method are usually those pertinent to the limitations of each component test, except when a variation in the properties of concrete affects the component test, except when a variation in the properties of concrete affects the component test results in opposite directions. In this case, the errors can be self-correcting. Development of a prior correlation relationship is essential if the estimates from the combined tests are to be meaningful. The more information that can be obtained about the concrete ingredients, proportions, age, curing conditions, etc. the more reliable the estimate is likely to be.

When testing suspect quality concrete of unknown composition, it is highly desirable to develop a prior correlation relationship in which factors such as aggregate type and approximate age of concrete are introduced as constants. For most *in situ* concretes an approximate age and petrological type of aggregate can be determined, thus reducing the number of uncontrollable variables in the equation by two.

The most important influences on the accuracy and reliability of strength estimates seem to be the coarse aggregate type in the concrete and the form of the multiple-regression equation. Nonlinear correlation relationships appear to provide more accurate estimates.

When a reliable prior correlation relationship exists for a particular concrete type, the use of combined nondestructive techniques provides a realistic alternative to destructive testing. It is often possible to perform a large and thus a representative number of tests at a reduced cost compared with coring, and without an adverse effect on the integrity of a structural element.

References

1. Kesler, C.E. and Higuchi, Y., Determination of compressive strength of concrete by using its sonic properties, *Proc. ASTM*, 53, 1044, 1953.
2. Skramtaev, B.G. and Leshchinsky, M.Yu., Complex methods for non-destructive tests of concrete in constructions and structural works, RILEM Bull., Paris, New Series No. 30, March 1966, 99.
3. Wiebenga, J.G., A comparison between various combined non-destructive testing methods to derive the compressive strength of concrete, Rep. kB1-68-61/1418, Inst. TNO Veor Bouwmaterialen en Bouwconstructies, Delft, the Netherlands, 1968.
4. Facaoaru, I., Non-destructive testing of concrete in Romania, Proc. Symp. on Non-destructive Testing of Concrete and Timber, London, June 1969, Institute of Civil Engineers, London, 1970, 39.
5. MacLeod, G., An assessment of two non-destructive techniques as a means of examining the quality and variability of concrete in structures, Rep. Cl/sfB/Eg/(A7q)UDC 666.972.017.620 179.1 42.454, Cement and Concrete Association, London, July 1971.
6. Galan, A., Estimate of concrete strength by ultrasonic pulse velocity and damping constant, *ACI J.*, 64(10), 678, 1967.
7. Jones, R. and Facaoaru, I., Analysis of answers to a questionnaire on the ultrasonic pulse technique, RILEM, *Materials and Construction*, 1(5), 457, 1968.
8. Malhotra, V.M. and Carette, G.C., In situ testing for concrete strength, CANMET publication: Progress in Concrete Technology, Malhotra, V.M., Ed., Canada, 1980, 749.
9. Facaoaru, I., The correlation between direct and indirect testing methods for in-situ concrete strength determination, Proc. RILEM Conf., Quality Control of Concrete Situations, Stockholm, June 1979, Vol. 1, 147.
10. Malhotra, V.M., *Testing Hardened Concrete: Non-Destructive Methods*, ACI Monogr. No. 9, American Concrete Institute, Iowa State University Press, Detroit, 1979.
11. Malhotra, V.M., In-situ strength evaluation of concrete, in *Concrete International, Design and Construction*, Vol. 1, No. 9, September 1979, 40.
12. Malhotra, V.M., Ed., *In Situ/Nondestructive Testing of Concrete*, ACI Spec. Publ., SP-82, American Concrete Institute, Detroit, 1984.
13. MacDonald, C.N. and Ramakrishman, V., Quality control of concrete using pulse velocity and maturity concepts, Proc. RILEM Conf., Quality Control of Concrete Structures, Stockholm, June 1979, Vol. 2, 113.
14. Parsons, T.J. and Naik, T.R., Early ages concrete strength determination by pullout testing and maturity, ACI, SP-82 (Ref. 12), Detroit, 1984, 177.
15. Schmidt, E., Concrete testing hammer, *Schweiz. Bauz. (Zurich)*, 68(28), 378, 1958 (in German).
16. Chree, C., On longitudinal vibrations, *Q. Math. J.*, 23, 317, 1889.
17. Lord Rayleigh (Strutt, J.W.), *The Theory of Sound*, Vol. 1, 2nd ed., Macmillan, London, 1894, chaps. 5, 7, and 8.
18. Facaoaru, I., Romanian achievements in nondestructive strength testing of concrete, ACI, SP-82 (Ref. 12), Detroit, 1984, 35.
19. Samarin, A. and Smorchevsky, G., The non-destructive testing of concrete, Central Research Laboratory, Internal Tech. Rep. No. 54, 1973.
20. Samarin, A., Use of combined ultrasonic and rebound hammer method for determining strength of concrete structural members, Central Research Laboratory, Internal Tech. Rep., Ready Mixed Concrete Ltd. Tech. Bull., 1967.

21. Samarin, A. and Meynink, P., Use of combined ultrasonic and rebound hammer method for determining strength of concrete structural members, *Concr. Int. Design Construction*, 3(3), 25, 1981.
22. Elvery, R.H. and Ibrahim, L.A.M., Ultrasonic assessment of concrete strength at early ages, *Mag. Concr. Res.*, 28(97), 181, 1976.
23. Shah, C.B., Estimation of strength of in situ concrete, *Indian Concr. J.*, 56(11), 292, 1982.
24. Bellander, U., Hallfasthet I fardig Komstruktion – Del 3 – oforstorande metoder, Laboratorie-Och Faltforsok. (Concrete strength in finished structure – Part 3 – non-destructive testing methods.) Investigations in laboratory and in situ, CBI Forskning Research, 3, 1977.
25. Di Maio, A.A., Traversa, L.P., and Giovambattista, A., Nondestructive combined methods applied to structural concrete members, *ASTM J. Cement Concrete Aggregates*, 7(2), Winter, 1985, 89.
26. Tanigawa, Y., Baba, K., and Mori, H., Estimation of concrete strength by combined nondestructive testing method, ACI, SP-82, (Ref. 12), 57.
27. Knaze, P. and Beno, P., The use of combined nondestructive testing methods to determine the compressive strength of concrete, RILEM, *Materials and Structures*, 18(105), 207, 1985.
28. Schickert, G., Critical reflections on nondestructive testing of concrete, RILEM, *Materials and Structures*, 17(99), 217, 1984.
29. Logothetis, L.L. and Economou, Chr., The influence of high temperatures on calibration of non-destructive testing for concrete, RILEM, Materials and Structures, 14(79), 1981.
30. Chung, H.W. and Law, K.S., Diagnosing in situ concrete by ultrasonic pulse technique, *Concr. Int. Design Construction*, 7(2),42, 1985.
31. Chung, H.W., Effects of embedded steel bars upon ultrasonic testing of concrete, *Mag. Concr. Res.*, 30(102), 19, 1978.
32. Samarin, A. and Thomas, W.A., Strength evaluation of incompletely consolidated conventional and superplasticised concrete-combined non-destructive tests, *Proc. 10th Austr. Road Research Board Conference*, Sydney, Vol. 10, Part 3, 25–29 August 1980, 107.
33. Sadegzadeh, M. and Kettle, R., Indirect and non-destructive method for assessing abrasion resistance of concrete, *Mag. Concr. Res.*, 38(137), 183, 1986.
34. Wiebenga, J.G., Strength of concrete, General Rep. on Session 2.1, RILEM Symp., Quality Control of Concrete Structures, Stockholm, June 17–21, 1979, Proc., 115.
35. Meynink, P. and Samarin, A., Assessment of compressive strength of concrete by cylinders, cores and non-destructive tests, RILEM Symp., Quality Control of Concrete Structures, Stockholm, June 17–21, 1979, Vol. 1, 127.
36. Pohl, E., Combined non-destructive testing methods to assess the strength of in situ concrete for silo, RILEM Symp., Quality Control of Concrete Structures, Stockholm, June 17–21, 1979, Vol. 1, 151.
37. Samarin, A. and Dhir, R.K., Determination of in situ concrete strength: rapidly and confidently by nondestructive testing, ACI SP-82 (Ref. 12), Detroit, 1984, 77.

10

Magnetic/Electrical Methods

10.1 Introduction
10.2 Magnetic Methods
Introduction · Theory · Test Methods
10.3 Electrical Methods
Introduction · Theory · Electrical Properties of Concrete · Test Methods

Kenneth R. Lauer
University of Notre Dame

The initial portion of the chapter briefly describes the theory of magnetic induction, magnetic flux leakage, and nuclear magnetic resonance to facilitate an understanding of equipment used to locate reinforcement and determine the moisture content of concrete.

The remaining portion of the chapter discusses the electrical nature of concrete and the mechanism of reinforcement corrosion as a preliminary to understanding the use of electrical capacitance and resistance to measure moisture content, pavement thickness, and corrosion of reinforcement.

Where possible, the accuracy of current magnetic and electrical apparatus is indicated.

10.1 Introduction

Magnetic and electrical methods are used in a number of ways to evaluate concrete structures. These methods are used to (1) locate reinforcement and measure member thickness by inductance; (2) measure the moisture content of concrete by means of its electrical properties and the nuclear magnetic resonance of hydrogen atoms; (3) measure the corrosion potential of reinforcement; (4) determine pavement thickness by electrical resistivity; and (5) locate defects and corrosion in reinforcement by measuring magnetic flux leakage.

Magnetic and electrical methods have received considerable attention in recent years. Their underlying principles range in complexity as do their practical applications in the field.

10.2 Magnetic Methods

10.2.1 Introduction

Materials containing iron, nickel, and cobalt are strongly attracted to themselves and to each other when magnetized; they are called ferromagnetic materials. Other materials, such as oxygen, which are weakly attracted by magnetic fields, are called paramagnetic materials.

In 1905, the magazine *Revue de Met* mentioned for the first time the possibility of detecting defects such as cracks, laminations, etc. in ferromagnetic materials by means of magnetic fields. In 1919,

E.W. Hoke applied for the first patent in the United States on a magnetic inspection method, which was granted in 1922.

Magnetic nondestructive testing techniques used in conjunction with concrete involve the magnetic properties of the reinforcement and the response of the hydrogen nuclei to such fields. Because of the need to control the magnetic field, electromagnets are used in most instances.

10.2.2 Theory

At the present time, three different aspects of magnetic field phenomena are used in the nondestructive testing of reinforced concrete: (1) alternating current excitation of conducting materials and their magnetic inductance; (2) direct current excitation resulting in magnetic flux leakage fields around defects in ferromagnetic materials; and (3) nuclear magnetic resonance.

10.2.2.1 Magnetic Induction

This technique is only applicable to ferromagnetic materials. Test equipment circuitry resembles a simple transformer in which the test object acts as a core (Figure 10.1). There is a primary coil, which is connected to a power supply delivering a low frequency (10 to 50 Hz) alternating current, and a secondary coil, which feeds into an amplifier circuit. In the absence of a test object, the primary coil induces a small voltage in the secondary coil, but when a ferromagnetic object is introduced near the coils, a much higher secondary voltage is induced. The amplitude of the induced signal in the secondary coil is a function of the magnetization characteristics, location, and geometry of the object.

The inductance of a coil can be reduced by bringing a conducting surface near the coil. It can be shown that the effect of a conducting plate on the coil is the same as the effect of a second coil, identical to the first, carrying a current equal and opposite to the coil current and located on the coil axis at a distance $2d$ from the original coil, where d is the coil-to-plate distance. The second coil is said to be the image of the first. The voltage induced in the first coil is seen to have two components. The first of these is due to the self-inductance of the coil in space, and the second is due to the mutual inductance between the coil and the plate. Thus the induced voltage is seen to be the sum of two components, one a constant and the other a function of coil-to plate spacing. As a result the inductance of the coil can be used to measure coil-to place distance, d, if the relationship between mutual inductance and d is known.

The probe unit consists of a highly permeable U shaped magnetic core on which two coils are mounted. An alternating current is passed through one of these coils and the current induced in the other coil is measured. The induced current depends upon the mutual inductance of the coil and upon the presence of the steel reinforcing bars. For a given probe the induced current is controlled by the distance between the reinforcement and the probe. This relationship between induced current and distance from the probe to the reinforcement is not linear because the magnetic flux intensity decreases with the square of the distance. As a result, calibrated scales on commercial equipment are nonlinear. The magnetic permeability of concrete, even though low, will have some effect on the reading.

10.2.2.2 Flux Leaking Theory

Fundamentals of this theory have been explained in detail in a number of texts.[2–4] When ferromagnetic materials are magnetized, magnetic lines of force (or flux) flow through the material and complete a magnetic path between the poles. These magnetic lines of flux increase from zero at the center of the specimen and increase in density and strength toward the outer surface. When the magnetic lines of flux are contained within the ferromagnetic object, it is difficult, if not impossible, to detect them in air space surrounding the member. However, if the surface is disrupted by a crack or defect, its magnetic permeability is drastically changed and leakage flux will emanate from the discontinuity. Measurement of the intensity of this leakage flux provides a basis for nondestructive identification of such discontinuities. Figure 10.2 illustrates how a notch or defect distorts the magnetic lines of flux causing leakage flux to exist in the surface of the ferromagnetic material.

Automatic flux leakage inspection systems use magnetic field sensors to detect and measure flux leakage signals. Flux leakage sensors usually have small diameters in order to have adequate sensitivity for

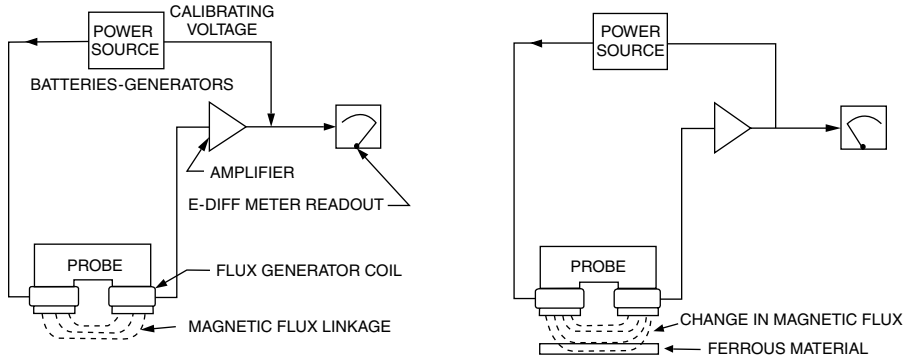

FIGURE 10.1 Principle of operation of induction meter used to locate reinforcement. (From Malhotra, V.M., Testing Hardened Concrete: Nondestructive Methods, ACI Monogr. No. 9, The Iowa State University Press, Ames, and American Concrete Institute, Detroit, 1976. With permission.)

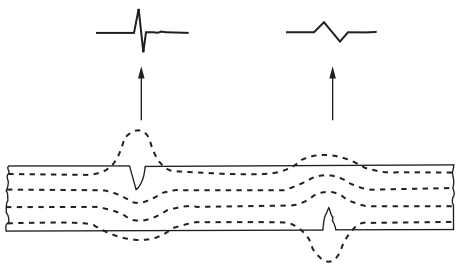

FIGURE 10.2 Effect of defects on flux pattern and measurement.

detecting short length defects. Probes are typically spring loaded to provide constant lift-off (distance between probe and surface). Signals from probes are transmitted to the electronics unit where they can be filtered and analyzed by a continuous spectrum analyzer.

A majority of the sensors are inductive coil sensors or solid-state Hall effect sensors (electromotive forces developed as a result of the interaction of a steady current flowing in a steady magnetic field). Magnetic diodes and transistors, whose output current or gain change with magnetic field intensity, can also be used. To a lesser extent, magnetic tape systems have also been used.

The more highly magnetized the ferromagnetic object, the higher its leakage flux intensity from a given defect. The amount of leakage flux produced also depends on defect geometry. Broad, shallow defects will not produce a large outward component of leakage flux; neither will a defect whose long axis is parallel to the lines of flux. The latter are more easily detected with circular magnetic fields. Internal defects in thick parts may not be detected because the magnetic lines of flux nearly bypass the defect with little leakage. Defects oriented so that they are perpendicular to the surface and at right angles to the lines of flux will be more easily detected than defects laying at an angle with respect to the surface or flux lines. Defects lying at a shallow angle to the surface and oriented in the direction of the flux lines produce the weakest lines of leakage flux.

10.2.2.3 Nuclear Magnetic Resonance (NMR)

This technique is based on the interaction between nuclear magnetic dipole moments and a magnetic field. This interaction can be used as a basis for determining the amount of moisture present in a material by detection of a signal from the hydrogen nuclei in water molecules. The term resonance is used because the frequency of gyroscopic precession of the magnetic moments is detected in an applied magnetic field.

Several methods of generating and detecting *NMR* signals are available. The method preferred for most practical applications is the transient or pulsed method because measurements can be made rapidly and the data obtained provide a maximum amount of information about the investigated species. Detailed information on this method is available in several texts.[5–7]

10.2.3 Test Methods

10.2.3.1 Depth of Concrete Cover

The induction principle resulted in the development of equipment for determining the location, sizes, and depth of reinforcement.[8,9] In 1951 an apparatus called the "covermeter" was developed in England by the Cement and Concrete Association in conjunction with the Cast Stone and Cast Concrete Products Industry.[8] Their reports indicate the effectiveness of this type of equipment for both plastic and hardened concrete. Refined versions are now available, using more sophisticated electronic circuits, which can detect reinforcement at depths of 12 in. A typical meter is shown in Figure 10.3.

Meters must be recalibrated for different probes. The probes are highly directional. A distinct maximum in induced current is observed when the long axis of the probe and reinforcement are aligned and when the probe is directly above the reinforcement. By using spacers of known thickness, the size of reinforcing bars between 3/8 and 2 in. (9.52 mm and 57.33 mm) can be estimated.

British Standard 4408 pt 1 suggests a basic calibration procedure involving a cube of concrete of given proportions with reinforcing bars at specified distances from the surface.[10]

These meters can be used to estimate the thickness of concrete members accessible from both sides. If a steel plate is aligned on one side with the probe on the other side, the measured induced current will indicate the thickness of the slab. The equipment must be especially calibrated for this use.

Commercial reinforcement bar locaters are portable, inexpensive instruments that can be easily used. Accuracy of ±2% or 0.1 in. up to depths of 6 in. for any bar size has been claimed. A bar size accuracy of ±10% to a depth of 8 in. is also indicated. The latest equipment utilizes headphones that can detect by tone, a 3/4-in. bar at 12-in. depth. Tone trigger levels can be preset for depths less than 6 in. If cover determinations are carried out on a grid system over the concrete surface, equi-depth contours can be constructed which clearly illustrate the variability in depth of cover and any regions where it is less than satisfactory. An example of this type of map is illustrated in Figure 10.4.

The use of a hand-held instrument in mapping the cover of reinforcement in a bridge deck is very time consuming. The U.S. Federal Highway Administration developed a "Rolling Pachometer," which

FIGURE 10.3 A meter used to locate reinforcement. Instrument includes a standard probe, a special probe for magnetic concrete, headphones and a spacer block for rebar measurement. (Courtesy of NDT James Instrument Inc.)

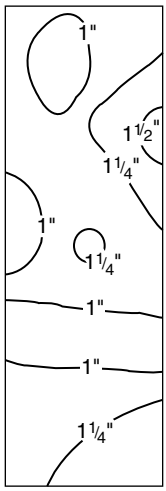

FIGURE 10.4 Depth of concrete cover on a reinforced concrete bridge deck.

proved to be accurate, reliable, and capable of gathering data at a rate 20 times that of conventional hand-held methods.[11] The second generation system contains a modified hand-held meter, a battery operated, two channel, pressurized ink recorder; a speedometer; and associated electronics. The electronics include an amplifier, filters, voltage regulators, adjustable high and low reinforcing bar limit controls, a magnetic sensor, and counters for processing and displaying distance marks on the chart graph. A constant scan speed of 1 mph is required. The speedometer works in conjunction with the magnetic sensor which is located on one of the wheels. Pulses from the sensors, which are processed and used to indicate speed, are also fed into counters which trigger a distance mark on the left side of the chart paper (Figure 10.5). These distance marks occur every 18 in. of travel and, when used with the manual event

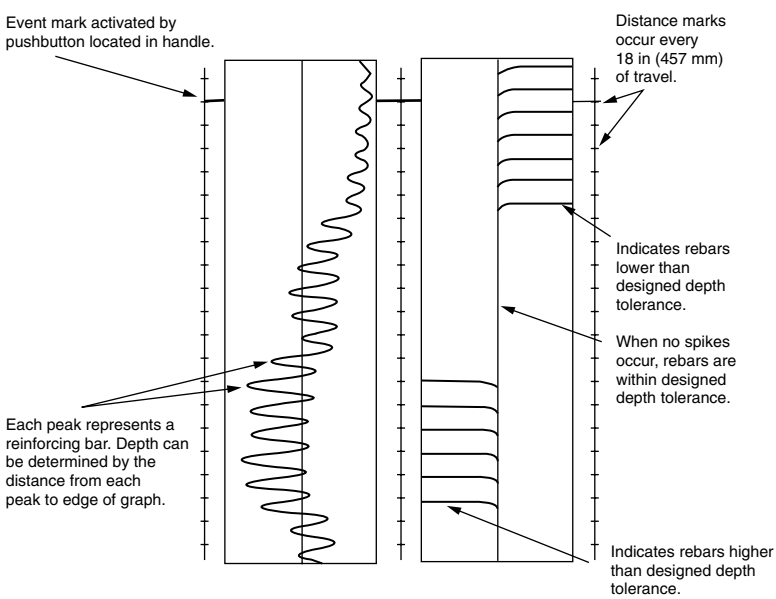

FIGURE 10.5 Typical chart recorder presentation of "Rolling Pachometer." (Adapted from Reference 11.)

marker switch, can be correlated to a particular area of interest on the bridge. The manual event mark is displayed on the left side of the chart paper.

Data, representing variations of the signal as the probe passes over the reinforcing bars, are displayed on the left channel of the chart paper. The sinusoidal nature of the recorded data represents the peaks associated with a reinforcing bar and, by measuring the distance of each peak to the edge of the chart paper graph, depth of cover can be determined from a calibration curve. High and low limit controls permit identification of reinforcing bars either higher or lower than the allowed tolerances for the specified depth. This is indicated on the right-hand channel. A spike to the left of center indicates a rebar that is lower than the preset limit. A spike to the right of center indicates a rebar that is higher than the preset limit.

Calibration curves for the apparatus are developed by constructing a test track with simulated bridge deck construction.

Repeatability, stability, and operation of the rolling instrument under various temperature extremes proved excellent. In comparison with other calibrated, hand-held meters, the results were also very good. A constant bias was, however, noted in both systems during the test of a particular bridge. The peaks indicated that the rebars were closer to the surface than when measured by coring operations. The error ranged from 1/8 to 1/4 in. depending upon the depth of the reinforcing bars. This bias effect was caused by the presence of magnetic aggregate particles. As a result, each bridge deck requires calibration with coring to correct for this kind of bias. The system is considered to be accurate within ±0.25 in.

The accuracy of test systems using the induction principle are reduced by factors that affect the magnetic field within the range of the instrument. They include presence of more than one reinforcing bar — laps and second layers; metal tie wires and bar supports; and variations in the iron content of the aggregate and cement. As depth/spacing ratios increase, it becomes more difficult to discern individual bars. The operating temperature range of battery-operated models is generally relatively small, and such instruments will not function satisfactorily at temperatures below freezing.

10.2.3.2 Magnetic Field Method of Detecting Flaws in Reinforcement

Currently used inspection procedures rely heavily on rust staining, cracking, and spalling of concrete as an indication of problems with reinforcing steel. There is a great need for a practical nondestructive *in situ* method for detecting deterioration in the reinforcing steel of prestressed concrete highway bridge members. Of primary interest is the need to detect a 10% loss or greater of area due to corrosion and fracture of reinforcing bars and strands. Figure 10.6 illustrates regions of particular interest. A magnetic field method based on leakage flux was considered to have the most promise for this application and was investigated by the U.S. Federal Highway Administration.[12]

This magnetic field method consists of applying a steady-state magnetic field to the beam under inspection and the use of a scanning magnetic field sensor to detect perturbances in the applied field caused by anomalies such as deterioration or cracks. The magnetizing field is produced by a dc excited electromagnet and a Hall-effect device is used as the magnetic field sensor. The experiments included varying degrees of deterioration, influence of adjacent unflawed steel elements, type of tendon duct, type of reinforcing steel, transverse rebar configuration, etc. Figure 10.7 illustrates typical magnetic responses for different steel configurations and degrees of deterioration. The results of the laboratory evaluation indicated good overall sensitivity to loss-of-section and excellent sensitivity to fracture with minimal degradation to signal response in the presence of a steel duct.

Field test results showed signatures with features similar to those observed in the laboratory as well as several prominent anomalous indications. From analyses of test data and field investigations it was determined that steel elements (chairs) were present in the structure which were completely unanticipated and were not indicated on the drawings. A method involving the "subtracting out" of configurational steel signatures so that signatures from deterioration and fracture could be recognized, proved successful. Additional work at the Ferguson Laboratory of The University of Texas at Austin confirmed the ability of the method to detect fractures in reinforcing strands as they developed from fatigue due to cyclic loadings.[13]

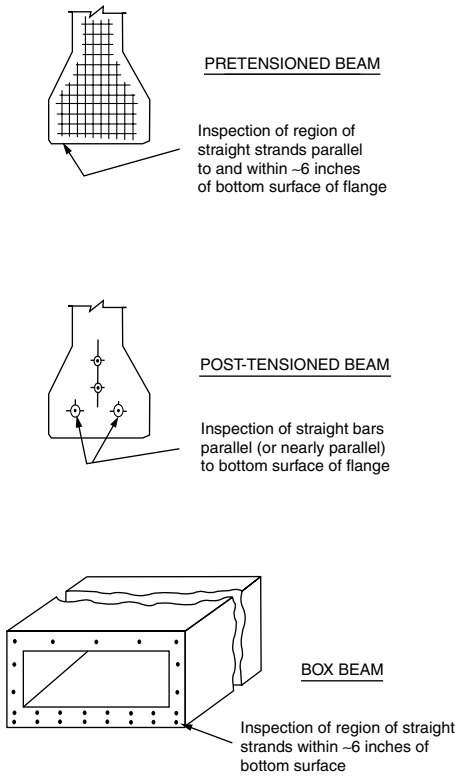

FIGURE 10.6 Critical reinforcement in structural bridge members. (Adapted from Reference 12.)

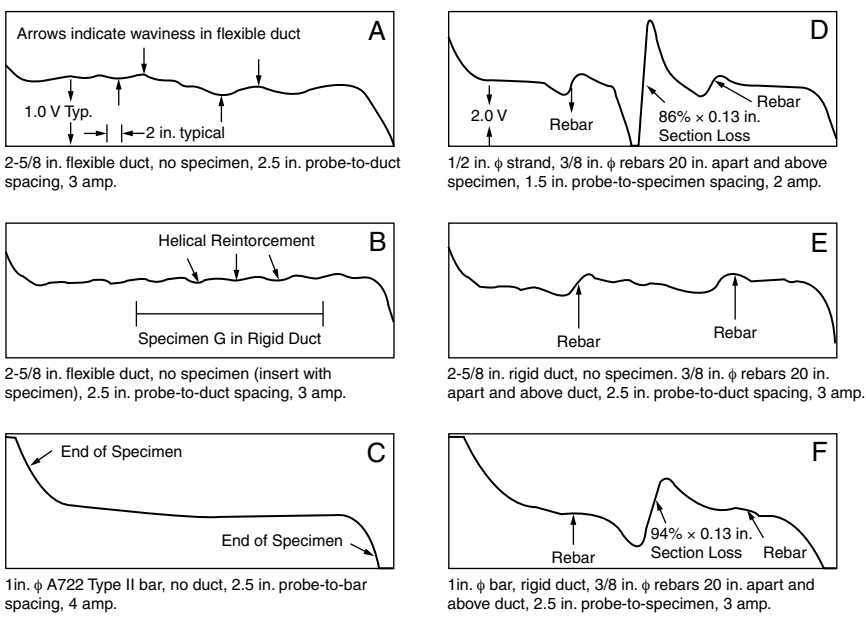

FIGURE 10.7 Selected magnetic signatures from laboratory investigations of flux leakage instrument. (Adapted from Reference 12.)

10.2.3.3 Nuclear Magnetic Resonance Method of Determining Moisture Content

Corrosion of reinforcing steel in structural concrete is known to be caused by the combined action of chloride ions, moisture, and oxygen. Matzkanin et al. report on the development, fabrication, and evaluation of a nondestructive instrument for measuring the moisture content in reinforced concrete bridge decks.[14] This instrument is based on nuclear magnetic resonance (NMR) which is an electromagnetic method capable of determining the amount of moisture present in a material by detection of a signal from the hydrogen nuclei in water molecules. The transient (or pulsed) method is the most suitable one for practical applications.

The following discussion comes from the report by Matzkanin et al.[14] For transient NMR measurement, the material is exposed to a static magnetic field of intensity, H_o, and to a pulsed radiofrequency (RF) magnetic field, H_1 corresponding to the NMR frequency of the nuclei of interest. For hydrogen nuclei the NMR frequency is 2.1 MHz in a magnetic field of 494 O_ϵ(3.9×10^4 A/m). The H_1 field is generated by a transmitter which produces adequate power to cause the required RF current to flow in a tuned detection coil. Following each transmitter pulse (sequence) the NMR response of the excited nuclei induce a transient RF voltage in the detection coil. The prototype NMR Moisture Measurement System utilizes a two pulse sequence which provides the capability of distinguishing between NMR signals from free moisture and signals from bound hydrogen. For the application of NMR to moisture measurement in concrete bridge decks, a sensor assembly is required in which the test specimen is external to both the RF coil and magnet structure. A schematic illustration of the approach utilized in the prototype measurement system developed in this program is shown in Figure 10.8. A U-shaped magnet provides a magnetic bias field, H_o, extending outward from the open ends of the "U." The field direction is represented by the dashed line in Figure 10.8. The RF coil is a flat spiral located in the plane of the two magnet faces; two direction lines of the RF field, H_1, are shown in the figure. At a selected distance interval below the plane of the RF coil and magnet poles, the resonance relationship between the magnetic field intensity and RF frequency for hydrogen NMR can occur. The size, shape, and location of the sensitive region are determined by the magnitude and gradients of the magnetic bias field and the RF field.

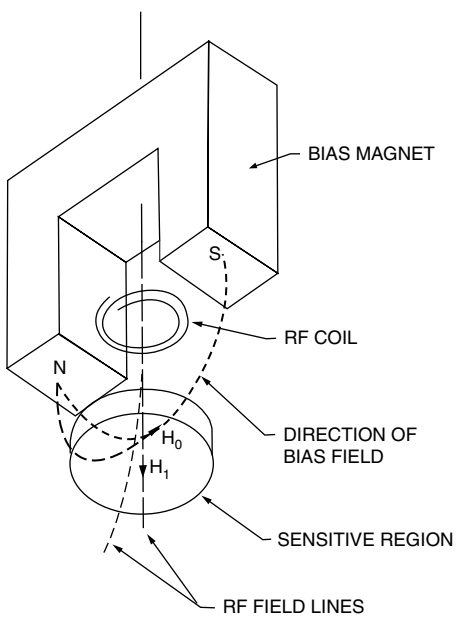

FIGURE 10.8 Schematic illustration of NMR detection for a specimen external to the RF coil and magnet structure. (Adapted from Reference 14.)

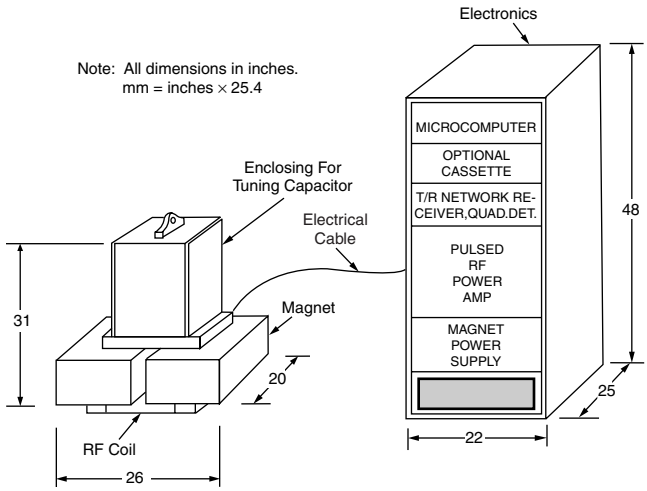

FIGURE 10.9 Diagram of sensor assembly and electronics assembly for NMR bridge deck moisture measurement system. (Adapted from Reference 14.)

Specifications for the system indicate a moisture content range of from 1 to 6% by weight of the material with an accuracy of ±0.2% moisture for depths up to 2.75 in. and ±0.4% moisture for depths from 2.75 to 3.75 in. The measurement time per location was estimated at 2 min. A prototype instrument was developed for the Federal Highway Administration.[14] The two assemblies comprising the prototype NMR Moisture Measurement System have exterior dimensions as shown in Figure 10.9. The electronics assembly contains the RF pulse generators operating at 2.1 MHz, amplifiers, signal processing components, and magnet power supply. The sensor assembly contains the electromagnet capable of producing the required hydrogen NMR field of 494 O_ϵ(3.9×10^4 A/m) at distances up to 6 in. (152 mm) away, the NMR detection coil and the tuning capacitor.

10.3 Electrical Methods

10.3.1 Introduction

The changes in electrical properties of concrete have been investigated as a basis for understanding durability and the development of various nondestructive tests. The properties include electrical resistance, dielectric constant, and polarization resistance.

10.3.2 Theory

10.3.2.1 Electrical Nature of Concrete

The evaporable water content of concrete varies with water-to-cement ratio, degree of hydration, and degree of saturation. This water contains ions, primarily Na^+, K^+, Ca^{++}, SO^{--}, and OH^-, whose concentrations vary with time. As a result the conduction of electricity by moist concrete could be expected to be essentially electrolytic as suggested by Nickkanin.[15] Tests by Hammond and Robson support this view.[16] Much of the following presentation of the theory is based on a paper by Monfore.[17]

The resistance of an electrolyte, or any other material, is directly proportional to the length and inversely proportional to the cross-sectional area. Thus

$$R = \rho \frac{L}{A} \tag{10.1}$$

where

R = resistance in ohms
ρ = resistivity in ohm-cm
L = length in cm, and
A = cross-sectional area in cm^2

Resistivity, ρ, is essentially constant for a given material under constant conditions and is numerically equal to the resistance of a 1-cm cube of the material.

Ohm's law states that the direct current through a metallic conductor is directly proportional to the potential applied and inversely proportional to the resistance of the conductor, i.e.,

$$I = \frac{E}{R} \tag{10.2}$$

where

I = current in amperes
E = potential in volts

If the conductor is an electrolyte, the passage of direct current (movement of ions) will cause polarization and the establishment of a potential at the electrodes that opposes the applied potential. In such a case the current is

$$I = \frac{E_a - E_p}{R} \tag{10.3}$$

where

E_a = the applied potential in volts
E_p = the polarization potential in volts, or back emf, as it is frequently called

Polarization potential (back emf) results from reactions that take place at the electrodes, reactions that depend upon the ions present and the materials of the electrodes. Thin films of oxygen, hydrogen, or other gases may be formed on the electrodes and may influence the potential created.

The use of alternating current does not avoid these polarization effects. Investigators such as Hammond and Robson suggest that the behavior of concrete can be modeled by a capacitor and resistor in parallel.[16] The current through such a combination is

$$I = \frac{E}{Z} \tag{10.4}$$

where

I = current in amperes
E = potential in volts
Z = impedance in ohms

For the particular case of a resistor and capacitor in parallel

$$Z = \frac{R}{\left(1 + \omega^2 C^2 R^2\right)^{1/2}} \tag{10.5}$$

where

ω = $2\pi f$, f being in hertz, Hz (cycles per second)
C = capacitance in farads

Another way of evaluating the model for alternating current is

$$I = j\omega FE\epsilon \tag{10.6}$$

where

F = a factor taking into account the geometry of the electrodes
E = the potential difference between the electrodes, volts
ω = $2\pi f$

and

ϵ = the complex dielectric constant defined as

$$\epsilon = \epsilon' - j\epsilon'' \tag{10.7}$$

where

ϵ' = the dielectric constant of the material and

$$\epsilon'' = \frac{1}{R\omega} \tag{10.8}$$

The complex dielectric constant, ϵ, of a material is a measure of the extent and speed with which its molecular dipoles are aligned by an electric field. The real component, ϵ', is a measure of the extent of alignment, and the complete component ϵ'', is a measure of the speed of alignment, or frictional loss of electrical energy.

The ϵ-value of free water is about 40 times that of most solids, including cement and stone. It is about 8 times that of chemically bound water. the ϵ-value of moist concrete is a complex function of the dielectric properties of its components and the fact that its water exists in three states — unbound or free, chemically bound, and physically adsorbed.

Despite the complex relationship between a material's moisture content and its dielectric constant, this property has been used in the evaluation of moisture content.

10.3.2.2 Mechanism of Reinforcement Corrosion

The corrosion of steel in concrete is an electrochemical process that requires a flow of electrical current for the chemical corrosion reactions to proceed. It is similar to a corrosion cell of two dissimilar metals in which a current flow is established between two metals because of the difference in their electrical potential. A separate cathodic metal is not required for corrosion of steel. This is because different areas of the bar may develop "active sites" with higher electrochemical potentials, and thus set up anode-cathode pairs as illustrated in Figure 10.10, and corrosion occurs in localized anodic areas. The development of active sites can be caused by a variety of conditions, such as different impurity levels in the iron, different amounts of residual strain, or different concentrations of oxygen or electrolyte in contact with the steel.

For corrosion of steel embedded in concrete to occur, a number of conditions must be met:

1. The provision of anode-cathode sites
2. Maintenance of an electrical circuit
3. Presence of moisture and oxygen

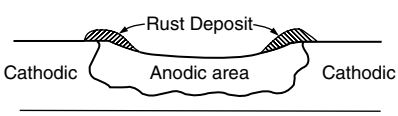

FIGURE 10.10 Rusting of an isolated steel bar.

Even with activity sites present reinforcement will not corrode if the normal highly alkaline conditions present in concrete prevail (a pH of about 12 to 12.5). At this level of alkalinity a passive oxide film forms on the surface of the reinforcement which prevents corrosion. This passive iron oxide layer is, however, destroyed when the pH is reduced o about 11.0 or below, and the normal porous oxide layer forms during corrosion. This critical reduction in pH occurs when calcium hydroxide, which maintains the high pH in cement paste, is converted to calcium carbonate by atmospheric carbonation. Chloride ions have the special ability to destroy the passive oxide film even at high alkalinities. The amount of chloride required to initiate corrosion depends on the pH of the solution in contact with the steel. Comparatively small quantities are needed to offset the alkalinity of portland cement. Concretes with a low permeability will limit the rate of corrosion by limiting the rate of diffusion of oxygen. Figure 10.11 is a summary of the relationships involving these variables.[18] If the values of pH, chloride content, and oxygen concentration result in a point below the curved surface, there is no corrosion.

The electrical potential differences, or voltage, between the anode and cathode may be measured by a voltmeter. The difference in measured voltage is not, however, very meaningful. It has been known for some time that the electrode potential of the steel in concrete is an indicator of corrosion feasibility. This electrode potential shows if a particular electrochemical reaction at the electrode is possible or impossible. For any chemical or electrochemical reaction, the thermodynamics and kinetics of the reaction determine the extent to which the reaction occurs. The thermodynamic factors determine if a reaction is possible and the kinetic factors determine the rate at which the reaction can proceed under a given set of conditions. In our case, the electrode potential is the thermodynamic factor, while concrete resistivity and availability of oxygen are the kinetic factors.

10.3.3 Electrical Properties of Concrete

Little information exists in the literature relative to electrical properties of concrete. The most comprehensive studies are those of Hammond and Robson[16] and Monfore.[17]

Moist concrete behaves essentially as an electrolyte with a resistivity in the order of 10^4 ohm-cm, a value in the range of semiconductors. Oven-dried concrete has a resistivity in the order of 10^{11} ohm-cm, a reasonably good insulator. The resistivity to direct current may be different since there is a greater polarizing effect.

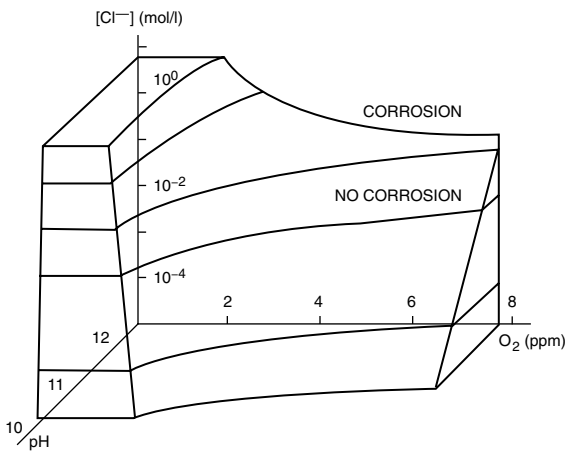

FIGURE 10.11 Regions of corrosion and no corrosion as a function of pH, chloride concentration, and oxygen concentration. (Adapted from Reference 18.)

TABLE 10.1 Polarization Potential and Resistance Under Varying D.C. Potential

Applied D.C. Potential (volts)	Polarization Potential, E_p (volts)	Resistance, R (ohms)
4 and 6	1.77	327
6 and 8	1.78	325
8 and 10	1.75	328

Note: Table 10.2 gives additional information on concrete of different ages.

From Monfore, G.E., *J. PCA Res. Dev. Lab.,* 10(2), 1968. With permission.

TABLE 10.2 Polarization Potential and Resistance of Concrete

Concrete	Age (days)	Applied D.C. Potential (volts)	Polarization Potential, E_p (volts)	Resistance, R (ohms)
A	7	4 and 6	1.84	412
A	28	4 and 6	1.84	514
A	90	4 and 6	1.85	642
B	7	4 and 6	1.80	308
B	28	4 and 6	1.76	435
B	90	4 and 6	1.77	598

From Monfore, G.E., *J. PCA Res. Dev. Lab.*, 10(2), 1968. With permission.

Table 10.1 indicates essentially constant values of polarization potentials and resistance under varying applied D.C. voltages (see Equation 10.3). Table 10.2 gives additional information on concrete of different ages.

These data indicate an increase in resistance with age, probably as a result of a decrease in free water due to hydration. The polarization potential remained constant under different applied potentials.

Table 10.3 shows the effect of frequency to be minor in terms of resistance but substantial in terms of capacitance. The values of calculated impedance was essentially equal to the measured resistance.

The effect of potential on resistance or impedance was slight as shown in Table 10.4.

Since the resistivity of electrolytes decreases with increasing temperature, the resistivity of moist paste, mortar and concrete would also be expected to decrease with increasing temperature. Measurements of the resistivity of paste over a temperature range of 40 to 100°F indicated an average decrease in resistivity of 1% per degree increase in temperature.[17]

TABLE 10.3 Effect of Frequency at Constant Potential

Frequency (Hertz)	Resistance, R (ohms)	Capacitance, C (microfarads)	Impedance, Z (ohms)
100	571	0.07217	570.8
1000	561	0.00301	560.4
10000	551	0.00040	551.0

Note: The effect of potential on resistance or impedance was slight as shown in Table 10.4.

From Monfore, G.E., *J. PCA Res. Dev. Lab.*, 10(2), 1968. With permission.

TABLE 10.4 Effect of Potential at a Frequency of 1000 Hertz

Applied Potential (volts)	Resistance, *R* (ohms)	Capacitance, *C* (microfarads)	Impedance, *Z* (ohms)
2	964.4	0.00140	964.4
4	962.8	0.00207	962.7
6	962.0	0.00267	961.8
8	961.4	0.00295	961.3

From Monfore, G.E., *J. PCA Res. Dev. Lab.*, 10(2), 1968. With permission.

10.3.4 Test Methods

10.3.4.1 Capacitance Instruments for Measuring Moisture Content

Experimental investigations at frequencies up to 100 MHz have shown that both the real and imaginary components (see Equation 10.7) of the dielectric constant of building materials increase significantly with increasing moisture conent.[16,18,19] The relationships are different for different materials. Bell et al. indicated that the moisture content of laboratory concrete specimens could be determined to ±0.25% for values less than 6% using a 10 MHz frequency.[18] Jones confirmed that high frequencies (10 to 100 MHz) minimize the influence of dissolved salts and finally electrical contacts.[19]

Capacitance instruments are available to measure the moisture content of building materials. Various electrode configurations are available. The electrodes are attached to a constant frequency alternating current source and establish an electric field in the material to be tested. Current flow or power loss indicating moisture content is then measured. Most instruments are portable and easily operated. Figure 10.12 shows a moisture meter which works on this principle. A recent investigation by Knab et al. suggests that further study is required to establish the reliability of this method.[20] it is suggested that instruments be calibrated for a particular material. This would involve relating the measured power loss with the moisture content determined by a direct method such as heating in an oven.

FIGURE 10.12 Meter designed to measure moisture content of solids based on capacitance. (Courtesy of NDT James Instruments Inc.)

10.3.4.2 Electrical Resistance Probe for Measuring Moisture Content

The resistance probe method involves measuring the electrical resistance of a material, which decreases as the moisture content increases. Most instruments consist of two closely spaced probes and a meter-battery assembly enclosed in a housing. The probes are usually insulated except at the tips so that the region being measured lies between the tips of the probes. By having the probe penetrate soft materials the moisture content at various depths can be measured. This type of instrument should be calibrated for the particular material being tested.

These simple, inexpensive instruments do not determine moisture contents precisely. However, a resistance-type meter has been used to trace moisture movement through concrete.[21]

Resistivity measurements can be used to estimate the probability of significant corrosion when half-cell potential tests show that corrosion is possible.[22] In general it has been shown that if:

1. The resistivity is greater than 12,000 ohm-cm, corrosion is unlikely to occur
2. The resistivity is in the range 5000 to 12,000 ohm-cm, corrosion will probably occur
3. The resistivity is less than 5000 ohm-cm, corrosion is almost certain to occur

10.3.4.3 Resistivity and Pavement Thickness

The resistance to the passage of electric current is different for different materials. Since concrete and subgrade have different characteristics the change in slope of a resistivity vs. depth curve will indicate pavement thickness.[22] A method for measuring resistivity, as illustrated in Figure 10.13, was suggested by Robertshaw and Brown[23] Four electrodes are spaced equally. A current I is passed through the outer electrodes, C_1 and C_2 while the potential drop E between the inner electrodes, P_1 and P_2, is measured. The resistivity is calculated as:

$$\rho = \frac{2\pi AE}{I} \tag{10.9}$$

where A is the electrode spacing in cm.

When testing a concrete pavement the electrode system may be spaced at a 1- or 2-in. spacing for the initial readings and the system expanded in 1-in. increments for successive readings extending to a spacing equal to the pavement depth plus 3 to 6 in.

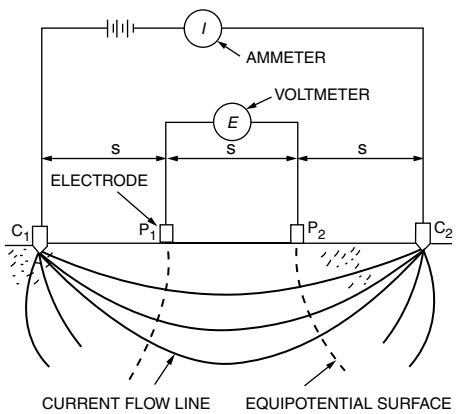

FIGURE 10.13 Vertical section along line of electrodes showing lines of current flow and equipotential surface in homogeneous materials. (From Robertshaw, J. and Brown, P.D., *Proc. Inst. Civil Engineers (London)*, 4(5), Part I, 645, 1955. With permission.)

When plotting resistivity against electrode spacing or depth, a change in resistivity is normally encountered in the base layer that will produce a recognizable trend in the curve towards a higher or lower resistivity, signifying the presence of the underlying material.

The Moore Cumulative Curve Method of depth determination indicates a graphical treatment of data from this test procedure.[24] The assumption is made that equipotential hemispheres with a radius A are established around each current electrode (C_1 and C_2) (see Figure 10.13). Every point on the surface of the hemisphere has the same potential. By placing the potential electrodes P_1 and P_2 at points on the surface where these hemispheres intersect the ground surface, it is possible to measure a potential drop that applied equally well at a depth A below the surface. As the electrode system is expanded to involve greater depth, the bottom of the hemispherical zones may involve a layer of differing electrical resistivity, which produces a trend towards lower or higher resistivity and gives an indication of depth to the layer producing the resistivity change. The resistivity values are plotted against electrode spacing or depth as shown by the dashed-line curve of Figure 10.14. The solid line curve is a cumulative plotting of the data. The first point is the same value as the first point of the dashed-line curve plotted to a condensed scale. The second point is the sum of the resistivities for the first and second point, etc. Using a constant increment of depth throughout, the solid-line curve constitutes a graphical integration of the dashed-line curve. Straight lines drawn through the plotted points in the vicinity of a rend in the dashed-line curve intersect to give the depth to the subsurface layer producing the trend. Other intersections obtained in the cumulative curve were discounted as not being significant in the analysis, in the absence of additional recognizable trends in the dashed-line curve (see expanded scale dashed-line curve in Figure 10.14).

The Pennsylvania Department of Transportation built a modified version of this equipment.[25] The number of probes was increased from 4 to 48, spaced 1 in. apart. By use of a resistivity bridge read out device and push-button switches, spacing can be selected automatically, instead of physically moving the probes. As a result the instrument is capable of reading to a depth of 15 in. in approximately 5 min., one quarter the time required by the original instrument. An analysis of field data indicates at least 15 determinations are required per test area to provide a mean value no more than 1/4 in. greater than the average measured thickness.[25] Concern about the determination of the inflection point were allayed by a comparison among different operators. A comparison of three operators showed no significant difference at the 95% confidence level.

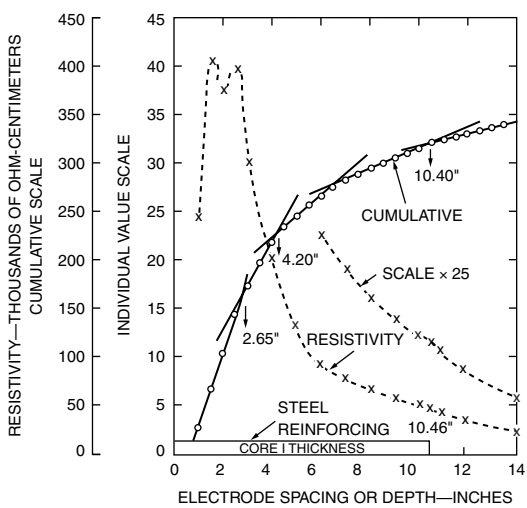

FIGURE 10.14 Earth resistivity test of reinforced concrete pavement on cement treated base. (Adapted from Reference 24.)

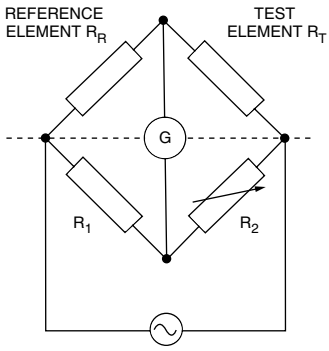

FIGURE 10.15 Basic circuit for electrical resistance probe technique.

10.3.4.4 Electrical Resistance Probe for Reinforcement Corrosion

This technique is based on electrical resistance measurements on a thin section of *in situ* reinforcement.[22] Its resistance is inversely proportional to its thickness; as the thin slice is gradually consumed by corrosion it becomes thinner with a corresponding increase in resistance. As indicated in Figure 10.15, to facilitate measurements the probe is incorporated into a Wheatstone bridge network. One are of the probe is protected from corrosion while the other arm is the inplace portion of the reinforcement. The measured resistance ratio can be used to monitor the corrosion rate.

$$R = \rho\frac{\ell}{A} = \rho\frac{\ell}{W}\left(\frac{1}{t}\right) = \frac{K}{t} \tag{10.10}$$

where

R = the resistance of the inplace specimen
ρ = the resistivity of the inplace specimen
ℓ = the length of the inplace specimen
W = the width of the inplace specimen
A = the cross-sectional area of the inplace specimen
t = the thickness of the inplace specimen and

K is a constant, therefore

$$\frac{R_T}{R_R} = \frac{K_T/t_T}{K_R/t_R} = \frac{K^*}{t_T} \tag{10.11}$$

where

R_T = the resistance of the exposed arm
R_R = the resistance of the protected arm
t_T = the thickness of the specimen in the exposed arm
t_R = the thickness of the specimen in the protected arm

K^*, K_T, and K_R = constants
initially $t_T = t_R$, and

$$\frac{t_T - t_T^1}{a} = \text{ rate of corrosion in } \mu\text{m year}^{-1} \tag{10.12}$$

during an exposure period of "a" years.

where

t_T = the initial thickness of the exposed arm at $a = 0$, and
t_T = the thickness of exposed arm after exposure of "a" years.

Changes in temperature are automatically taken into account because both arms of the probe are located at the same place and are consequently exposed to the same temperature profile. In practice, the thickness of the specimens in the arms of the probe are in the range of 50 to 500 mm. The thinner the probe the shorter the life but the greater its sensitivity. The probes and AC bridge network can be made up in an electronics laboratory and are also available commercially.

The only significant disadvantages are the need for positioning the exposed arm of the probes during construction and the concerns of associated sampling techniques required for locating the probes in large structures subject to localized corrosion.

10.3.4.5 Half-Cell Potential Measurements

The measurement of electrode potential of steel reinforcement is made using the experimental arrangement shown in Figure 10.16. An electrical connection is made to the reinforcement at a convenient position enabling electrode potentials to be measured at any desired location by moving the half cell over the concrete surface in an orderly manner. The surface of the concrete being investigated is usually divided up into a grid system. The results can then be plotted in the form of an equipotential contour diagram (Figure 10.17).[26–29] The reinforcement in a structure is usually electrically continuous so that only one electrical connection is needed, but if there is a doubt over electrical continuity additional connections can be made or continuity tested. The potential difference between the reinforcement and the half cell is measured using a high impedance voltmeter. The two most commonly used half cells are the saturated calomel electrode and the saturated copper/copper sulfate electrode (CSE). The latter is more durable and has had considerable use.[26–29] It is described in detail in ASTM Test Method C876.[29]

The value of the potential measured is used to estimate the likelihood of corrosion but cannot indicate the corrosion rate.[23] The interpretations of these potentials varies with investigator and agency.[26–30] Generally accepted values representing corroding and noncorroding conditions are given in ASTM C876.[29]

1. If potentials over an area are more positive than –0.20 V CSE, there is greater than 90% probability that no reinforcing steel corrosion is occurring.
2. If potentials over an area in the range of –0.20 to –0.35 V CSE, corrosion activity of the reinforcing steel in that area is uncertain.

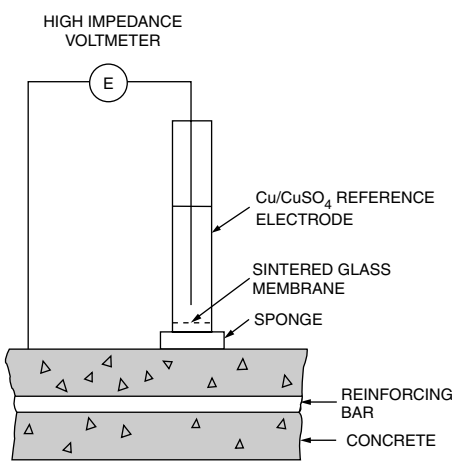

FIGURE 10.16 System for measuring electrode potential of reinforcement.

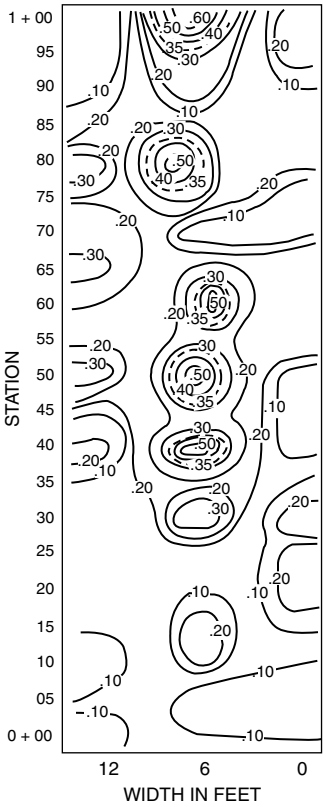

FIGURE 10.17 Equi-potential contour map. (From Van Deveer, J.R., *J. Am. Concr. Inst.,* Proc. V. 72, No. 12, 699, 1975. With permission.)

3. If potentials over an area are more negative than –0.35 V CSE, there is a greater than 90% probability that reinforcing steel corrosion is occurring in that area.

Positive readings, if obtained, generally indicate a poor connection with the steel, insufficient moisture in the concrete, or the presence of stray currents and should not be considered valid.

According to ASTM C876, the difference between two half-cell readings taken at the same location with the same cell should not exceed 10 mV when the cell is disconnected and reconnected. The difference between two half-cell readings taken at the same location with two different cells should not exceed 20 mV. The chief limitation is that it does not give information about the rate of corrosion.

10.3.4.6 Polarization Resistance and Reinforcement Corrosion

The National Bureau of Standards has developed a prototype portable system for measuring the corrosion rate of steel in concrete bridge decks.[18,31,32] A small, portable computer system is used to control the measurement of polarization resistance of steel in concrete. The polarization resistance is used to compute the corrosion current, which indicates the rate at which the steel is corroding. The polarization technique employs a three electrode system having the steel specimen as one electrode, a voltage reference as a second electrode, and a counter electrode as a third electrode from which polarizing current is applied to the specimen. The circuit used for these measurements is that of Holler,[33] which incorporates a Wheatstone bridge for iR compensation as illustrated in Figure 10.18.[32] The iR error is an error that arises when potential measurements are made in the presence of an electric current in a resistive medium.

The NBS equipment was successfully used on three bridge decks. Ongoing studies are assessing the reliability and accuracy of the data obtained in the field.

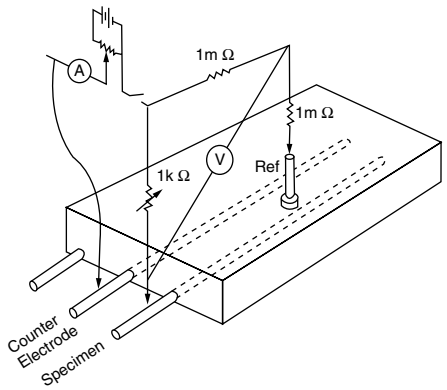

FIGURE 10.18 Holler's circuit for measuring iR compensation polarization resistance and compensation for IR error. (Adapted from Reference 31.)

References

1. Malhotra, V.M., Testing Hardened Concrete: Nondestructive Methods, ACI Monogr. No. 9, The Iowa State University Press, Ames, and American Concrete Institute, Detroit, MI, 1976.
2. Mix, P.E., *Introduction to Nondestructive Testing*, John Wiley & Sons, New York, 1987.
3. Lord, W., A survey of electromagnetic methods of nondestructive testing, in *Mechanics of Nondestructive Testing*, Stinchcomb, W.W., Ed., Plenum Press, New York, 1980, chap. 3.
4. Lord, W., Ed., *Electromagnetic Methods of Nondestructive Testing*, Vol. 3, Gordon and Breach, New York, 1985.
5. Abragam, A., *The Principles of Nuclear Magnetism*, Clarendon Press, Oxford, 1961.
6. Sliehter, C.P., *Principles of Magnetic Resonance*, Harper & Row, New York, 1963.
7. Andrew, E.R., *Nuclear Magnetic Resonance*, Cambridge University Press, Cambridge, England, 1955.
8. Determining the position of reinforcement in concrete, *Engineering (London)*, 175(4555), 640, 1953.
9. Rebut, P., Non-destructive apparatus for testing reinforced concrete: checking reinforcement with the "Pachometer" (in French), *Rev. Malenaux (Paris)*, 556, 31, 1962.
10. British Standard 4408 p.1, Non-destructive methods of test for concrete — electromagnetic cover measuring devices, British Standards Institution, London.
11. Moore, K.R., Rapid measurement of concrete cover on bridge decks, *Public Roads*, 39(2), 1975.
12. Kusenberger, F.N. and Barton, J.R., Detection of flaws in reinforcing steel in prestressed concrete bridge members, Rep. No. FHWA/AD-81/087, Federal Highway Administration, Washington, D.C., 1981.
13. Barton, J.R., personal communication, 1987.
14. Matzkanin, G.A., De Los Santos, A., and Whiting, D.A., Determination of moisture levels in structural concrete using pulsed NMR (Final Report), Southwest Research Institute, San Antonio, Texas, Federal Highway Administration, Washington, D.C., Report No. FHWA/RD-82-008, April 1982.
15. Nikkanin, P., On the electrical properties of concrete and their applications, Valtion Teknillinen Tutkinuslaitos, Tiedotus, Sarja III, Rakennus 60 (1962), in French with English summary.
16. Hammond, E. and Robson, T.D., Comparison of electrical properties of various cements and concretes, *The Engineer*, 199, 78 and 115, 1955.
17. Monfore, G.E., The electrical resistivity of concrete, *J. PCA Res. Dev. Lab.*, 10(2), 1968.
18. Bell, J.R., Leonards, G.A., and Dolch, W.L., Determination of moisture content of hardened concrete and its dielectric properties, *Proc. ASTM*, 63, 996, 1963.

19. Jones, R., A review of the non-destructive testing of concrete, Proc. Symp. on Non-Destructive Testing of Concrete and Timber, Institution of Civil Engineers, London, June 1969, 1.
20. Knab, R., Mathey, R.G., and Jenkins, D., Laboratory evaluation of nondestructive methods to measure moisture in built-up roofing systems, National Bureau of Standards Building Science Series 1311, 1981.
21. Bracs, G., Balint, E., and Orchard, D.F., Use of electrical resistance probes in tracing moisture permeation through concrete, *J. Am. Concr. Inst. Proc.*, 67(8), 642, 1970.
22. Vassie, P.R., Evaluation of techniques for investigating the corrosion of steel in concrete, Department of the Environment, Department of Transport, TRRL Report SR397, Crowthorne, 1978.
23. Robertshaw, J. and Brown, P.D., Geophysical methods of exploration and their application to civil engineering problems, Proc. Institution of Civil Engineers (London), 4(5), Part I, 645, 1955.
24. Moore, R.W., Earth resistivity tests applied as a rapid nondestructive procedure for determining thickness of concrete pavements, Highway Research Record, No. 218, 1968, 49, Transportation Research Board, Washington, D.C.
25. Weber, W.G., Jr., Grey, R.L., and Cady, P.D., Rapid measurement of concrete pavement thickness and reinforcement location — field evaluation of nondestructive systems, National Cooperative Highway Research Program Report 168, 1976, Transportation Research Board, Washington, D.C.
26. Van Deveer, J.R., Techniques for evaluating reinforced concrete bridge decks, *J. Am. Concr. Inst.*, December 1975, No. 12, Proc. 72, 697.
27. Browne, R.D., The corrosion of concrete marine structures: the present situation, Concrete Structures — Proc. Int. Conf. Trondheim, Taper, 1978, 177.
28. Okada, K., Kobayashi, K., and Miyagawa, T., Corrosion monitoring method of reinforcing steel in offshore concrete structures, Malhotra, V.M., Ed., SP-82 of American Concrete Institute — *In Situ/ Nondestructive Testing of Concrete*, 1984.
29. Standard Test Method for Half Cell Potentials of Reinforcing Steel in Concrete, ASTM C 876-91(1999), *Annual Book of ASTM Standards*, V. 04.02, ASTM, West Conshohocken, PA, 2002.
30. Stratfull, R.F., Half cell potentials and the corrosion of steel in concrete, Highway Research Report, No. 433, 12, Transportation Research Board, Washington, D.C.
31. Esalante, E., Cohen, M., and Kohn, A.H., Measuring the corrosion rate of reinforcing steel in concrete, NBSIR B4-2853, National Bureau of Standards, Washington, D.C.
32. Esalante, E., Whitenton, E., and Qiu, F., Measuring the rate of corrosion of reinforcing steel in concrete — final report, NBSIR 86-3456, National Bureau of Standards, Washington, D.C.
33. Holler, H.D., Studies of galvanic couples, *J. Electrochem. Soc.*, 97, 271, 1950.

11

Methods to Evaluate Corrosion of Reinforcement*

11.1 Introduction
11.2 Principles of Corrosion
Electrolytic Cell • Electrical Potential • Polarization
11.3 Corrosion of Steel in Concrete
11.4 Half-Cell Potential Method
Data Analysis • Limitations
11.5 Concrete Resistivity
11.6 Polarization Resistance
Principle • Instrumentation • Limitations
11.7 Summary

Nicholas J. Carino
National Institute of Standards and Technology

A critical step in selecting the most appropriate repair strategy for a distressed concrete structure is to determine the corrosion status of reinforcing bars. Because of the complexity of the corrosion process, it is prudent to involve personnel who are experienced in the corrosion of steel in concrete. The corrosion engineer may employ a variety of tools to help make an assessment of the corrosion conditions. This chapter provides an overview of the corrosion of steel in concrete and presents some nondestructive electrochemical tools that are commonly used in corrosion investigations. The objective is to provide the basic information to allow effective communication with the corrosion engineer. Electrochemical principles involved in the corrosion of steel in concrete are reviewed. Subsequently, the half-cell potential method, the concrete resistivity test, and the linear polarization method are discussed. The principles of operation and the inherent limitations of these methods are emphasized.

11.1 Introduction

The corrosion of ordinary steel is inevitable. This is because, under atmospheric conditions, the iron in the steel is unstable and there is a natural tendency for it to revert to a more stable state, which is iron oxide.[1] To understand why there is this tendency, consider how steel is produced. First, the iron ore, which contains iron oxide, is mined. The ore is processed by using a large amount of energy to separate the iron from the ore. This is done in the blast furnace, and the resulting material is an impure form of iron called pig iron. The pig iron, which contains large amounts of carbon, is refined by removing the majority of the impurities and adding small amounts of other alloying elements to improve the mechanical properties of the resulting steel. The energy used in the production process results in a material that

*Contribution of the National Institute of Standards and Technology, not subject to copyright in the United States.

is in a higher energy state at room temperature than the iron ore from which it came. The laws of thermodynamics dictate that materials have a tendency to revert to the lowest energy state that is in equilibrium with the environment. For iron at ordinary atmospheric conditions, the lowest energy state is as an oxide, that is, a type of rust. Thus, the presence of atmospheric oxygen provides the necessary ingredient to form the iron oxide. At ordinary temperatures, the transformation is very slow, but if water is also present, the transformation proceeds rapidly, and the iron turns to rust.

The above-simplified explanation is intended to point out that it is not surprising that steel corrosion is a widespread problem. In the case of reinforcing steel in concrete structures, the objective is to prevent the onset of corrosion for the design life of the structure, which differs depending on the type of structure. For ordinary buildings, 50 years may be a reasonable expectation. For other monumental structures, such as long-span bridges, hundreds of years may be desirable. Thus, the goal of the construction team is to design a structure, and to build it correctly, so that it will have a good chance of reaching the design life.

Fortunately, steel in concrete develops a protective oxide film that provides a barrier to the transformation of the iron to rust. The passive oxide is similar to the "mill scale" that forms on hot rolled steel when it cools to room temperature. It is well known that the mill scale provides a protective barrier to steel. The oxide, however, is brittle and is easily removed, as evidenced by the rapid corrosion of the bent portions of reinforcing bars. In reinforced concrete, a passive oxide coating forms because of the alkaline conditions (high pH, normally about 12.5) in the pores of the cement paste.[2,3] There are two major causes for the breakdown of the passive oxide coating: carbonation and the presence of chloride ions.

Carbonation refers to reactions between carbon dioxide and alkalis in the pore solution of the cement paste.[2,3] Typical reactions are as follows:

$$Ca(OH)_2 + CO_2 \rightarrow CaCO_3 + H_2O \tag{11.1}$$

$$2NaOH + CO_2 \rightarrow Na_2CO_3 + H_2O \tag{11.2}$$

As a result of these reactions, the pH of the pore solution decreases (even below a value of pH 9), and conditions are no longer favorable for maintaining the passive coating on the reinforcing steel. The steel becomes susceptible to corrosion. The penetration of the "carbonation front" depends on the quality of the cover concrete (water–cement ratio and degree of hydration) and the degree of saturation of the pores in the cement paste. The rate of penetration is low for dry concrete and for saturated concrete, and it is a maximum when the concrete is in equilibrium with ambient relative humidities between about 40% and 80%.[3]

The presence of chloride ions also breaks down the passive coating. The exact mechanism for this breakdown is not known with certainty,[4] but it is known that it happens when the chloride ion content reaches a "threshold value." As pointed out by Rosenberg et al.,[3] there are many factors that affect the threshold chloride ion concentration, such as the following:

- Mixture proportions
- Type of cement
- Water–cement ratio
- Sulfate content
- Curing conditions, age, and environmental history of the concrete
- Whether the concrete is carbonated
- Temperature and degree of saturation of the concrete
- Physical conditions of the steel surface

For this reason, there is no single minimum value of chloride ion concentration that will break down the passive film. In the United States, the general guideline is 0.2% of acid-soluble chloride by mass of cement,[5] but others suggest a higher level of 0.4%.[6] The term *acid-soluble* refers to the chloride ion content

measured when the sample is prepared by acid dissolution. There is controversy over whether the threshold value should be based on "acid-soluble" or "water-soluble" chlorides.

Electrochemical methods are used to evaluate corrosion activity of steel reinforcement. As is the case with other nondestructive test (NDT) methods, an understanding of their underlying principles and inherent limitations is needed to obtain meaningful results. In addition, an understanding of the factors involved in the corrosion of steel in concrete is essential for reliable interpretation of data from this type of testing. This chapter provides basic information about three commonly used methods:

1. Half-cell potential
2. Concrete resistivity
3. Polarization resistance

The science of corrosion is complex, and, unfortunately, it is not covered in the typical civil engineering curriculum. As a result, practicing engineers involved in repair of concrete may lack the basic knowledge for understanding the underlying principles of NDT methods used to assess corrosion activity in concrete. Therefore, before describing the test procedures, we provide a brief discussion of the principles of corrosion. The presentation is greatly simplified to permit explanation of the basic concepts. Readers should consult other references for additional information on the electrochemistry of corrosion and the factors affecting corrosion of steel in concrete.[3,5,7–10]

11.2 Principles of Corrosion

11.2.1 Electrolytic Cell

Corrosion is an electrochemical process, which means that it involves chemical reactions (gain and loss of electrons) and electrical current (motion of charges through a conductor). The classic approach for understanding the mechanism of corrosion is to consider the operation of an electrolytic, or galvanic, cell.[11] An electrolytic cell is a system involving two electrodes and two types of chemical reactions, one of which supplies electrons and the other that consumes electrons. To maintain electrical neutrality and sustain the chemical reactions, electrical charge transfer occurs through external and internal pathways connecting the two electrodes where these reactions take place. Electrons flow through the external connection and ions flow between the two solutions surrounding the electrodes.

Figure 11.1 illustrates the basic components of an electrolytic cell. One metal electrode is immersed in an ionic solution containing the positive ions of the metal. The other electrode is made of a different metal immersed in an ionic solution containing the positive ions of that metal. For simplicity, this example uses two metals for the electrodes, so that the electrode reactions involve metal atoms and ions. The electrode reactions, however, do not have to involve the actual electrode materials. The electrodes are connected externally by an electrical conductor. There is also an internal connection (salt bridge) that permits movement of ions between the two solutions. One electrode is the *anode* where a *half-cell oxidation reaction* occurs, by which the electrode material dissolves and enters solution as positive ions leaving behind electrons. This anodic reaction can be written as follows:

$$A \rightarrow A^{n+} + ne \tag{11.3}$$

where A represents an atom, A^{n+} is a positively charged ion, and e represents an electron. Thus, each atom of material A loses n electrons as it enters solution as a positively charged ion. This is the corrosion reaction for the cell.

The other electrode is the *cathode* and a *half-cell reduction reaction* occurs on its surface. The cathodic reaction involves the combination of electrons with positive ions in the solution to produce atoms that deposit on the electrode. The cathodic reaction can be represented as follows:

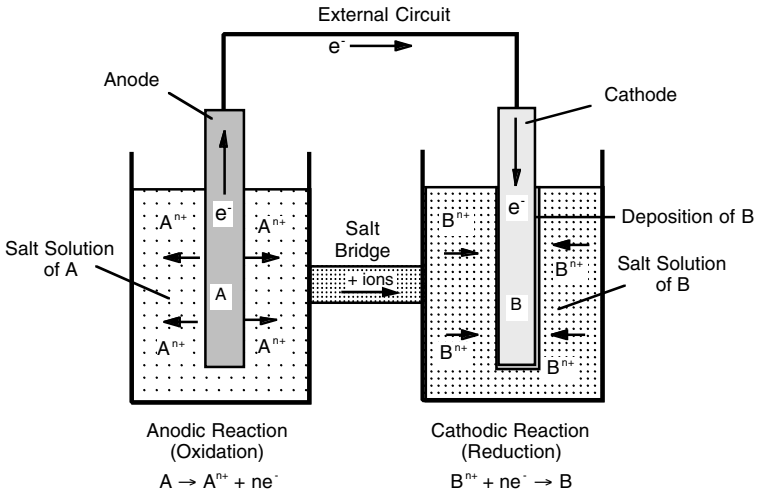

FIGURE 11.1 Example of an electrolytic cell; oxidation occurs at the anode and reduction occurs at the cathode. (Adapted from Reference 11.)

$$B^{n+} + ne \rightarrow B \tag{11.4}$$

As a result of these two reactions, there is an increase in positive ions in the solution containing the anode and a depletion of positive ions in the solution containing the cathode. To sustain the half-cell reactions, there must be a connection between the two solutions so that electrical neutrality is maintained. In this case there would be a flow of positive ions from the anodic half-cell to the cathodic half-cell.

If a conductor does not connect the electrodes, there is no net corrosion of the cathode and no net deposition at the cathode. The word *net* is used, because at both electrodes some atoms enter solution and some are deposited, but the rates are equal so that there is no net change at the electrodes. The rate at which the atoms are dissolved and deposited on the electrode at its equilibrium condition defines the *equilibrium exchange current*, which is a misnomer since the net current is actually zero.[8]

In summary, an electrolytic cell can be two electrodes made of dissimilar metals immersed in ionic solutions (electrolytes). The electrodes are connected externally by an electrical conductor and there is a means for ionic transfer between the electrolytes. The anode is consumed (corrodes) and reaction products are deposited on the cathode.

11.2.2 Electrical Potential

The ease with which the half-cell reactions occur is governed by their *half-cell potentials,* which are measured in volts. These potentials affect how vigorously the anode corrodes when the external circuit is completed. Half-cell potentials are usually expressed for the oxidation reaction; that is, they represent the ease with which atoms will give up electrons and enter solution as positive ions. A half-cell potential cannot be measured for a single electrode; therefore, it is referenced to the potential of a standard reduction reaction in which hydrogen ions gain electrons to form hydrogen gas.[12] The half-cell potential depends on the ionic concentration of the solution in which the electrode is immersed and on the temperature of the solution. S*tandard half-cell potentials* are measured for unit concentrations of the solutions at a standard temperature. The more negative the value of the standard half-cell potential, the greater is the tendency of the metal to lose its electrons, that is, to corrode.

Suppose that the external circuit in Figure 11.1 is replaced with a high-impedance voltmeter, which means that there is no current in the external circuit. This is referred to as the *open-circuit* condition. The voltmeter reads a voltage that equals the difference between the half-cell potentials of the anodic and cathodic reactions.[11] For example, suppose one electrode is iron in a standard solution of iron ions

and the other electrode is zinc in a standard solution of zinc ions. The standard half-cell potential for the oxidation of iron is –0.44 V, and the standard half-cell potential for the oxidation of zinc is –0.76 V.[8] The greater negative potential for the zinc electrode means that it tends to give up its electrons more readily than iron. If the positive terminal of the voltmeter is connected to the zinc electrode, the voltmeter would read –0.32 V, which is the difference between –0.76 V and –0.44 V. If the positive terminal of voltmeter had been connected to the cathode, the reading would be +0.32 V. The zinc electrode is the anode and the iron is the cathode. If a conductor replaces the voltmeter, current (electrons) would flow from the zinc to the iron. The zinc electrode would dissolve and iron would deposit on the iron electrode.

11.2.3 Polarization

Next, the magnitude of the current when the external circuit of an electrolytic cell is completed is discussed. This will establish the corrosion rate of the anode. Figure 11.2A shows an electrolytic cell with the electrodes connected to a high-impedance voltmeter. As explained above, the voltmeter would read a voltage equal to the difference of the half-cell potentials for the electrode reactions. This is the *equilibrium* or *open-circuit potential*.[8] When the electrodes are connected with a low-resistance material, they will be at the same potential. The potential of the electrodes can be measured by introducing a reference electrode and measuring the potential with a voltmeter as shown in Figure 11.2B. The measured potential will be a value between the half-cell potentials of the electrodes. Thus, the anode will be at a more positive potential than its half-cell potential, and the cathode will be at a more negative potential than its half-cell potential. Thus, the current between the electrodes leads to a change from the equilibrium half-cell potential of each electrode. This potential change is called *polarization*.[8,13] The difference between the equilibrium half-cell potential and the electrode potential with current is the *overpotential*.

Every half-cell possesses a characteristic *polarization curve* that represents the relationship between overpotential and the net current into or out of the electrode. Figure 11.3 shows idealized (and simplified) polarization curves for the anode and cathode of an electrolytic cell.[3,8–10] The horizontal axis is a log scale, so that the relationship is nonlinear in terms of actual current. In addition, the current is usually expressed as a *current density*, which is the net electrode current per unit surface area of the electrode. The points A and C correspond to the half-cell equilibrium conditions with no net current at the electrodes, and the difference between the potential values is the equilibrium potential of the cell. The curves show that the net current out of the anode increases as its potential is made more positive, and the net current into the cathode increases as its potential become more negative. These polarization curves permit the determination of the corrosion current density and the corrosion potential of the short-circuited electrolytic cell. When the cell is in a stable condition, the net current out of the anode has to

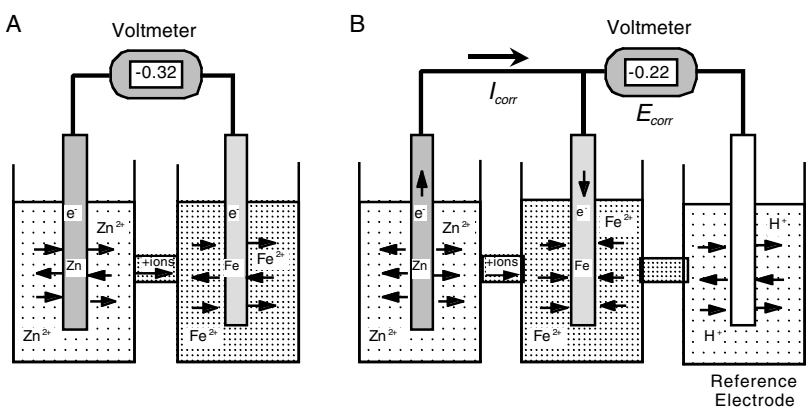

FIGURE 11.2 Electrolytic cell: (A) with no external current, the voltmeter reads the equilibrium voltage; (B) short-circuited cell with electrodes at same potential.

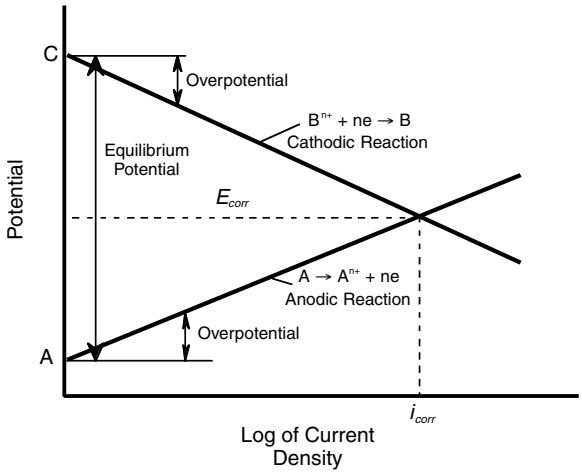

FIGURE 11.3 Polarization curves for short-circuited electrolytic cell showing stable cell potential and corrosion current. (Adapted from Reference 3.)

equal the net current into the cathode. Thus, the intersection of the polarization curves defines the corrosion potential, E_{corr}, and corrosion current density, i_{corr}, of the electrolytic cell. Note that Figure 11.3 shows both curves with equal current density at the half-cell equilibrium conditions (points A and C). In reality, the current densities at points A and C represent the equilibrium exchange currents for the half-cells and would not necessarily be equal.[8]

The corrosion current density can be converted to loss of electrode in terms of mass or thickness per unit of time. This is accomplished by using Faraday's law.[7,14,15]

In summary, when a conductor connects the anode and cathode of an electrolytic cell, corrosion occurs at the anode. The polarization curves of the anodic and cathodic half-cell reactions are the key for understanding the corrosion rate of the cell. There are several ASTM standards that should be consulted for additional information on terminology and procedures for developing these polarization curves.[13,14,16,17]

11.3 Corrosion of Steel in Concrete

With the above simplified explanation of an electrolytic cell, our attention can be turned to a reinforcing bar embedded in moist concrete, as shown in Figure 11.4. The water in the pores of the paste contains various dissolved ions and serves as the electrolyte. If the passive coating on the steel is lost, due to carbonation or to the presence of chloride ions above the critical concentration, conditions are set up for corrosion. Heterogeneities in the surface of the steel, such as differences in grain structure and composition, and local differences in the electrolyte, due to the heterogeneous nature of concrete, cause a region of the bar to act as an anode and another region to act as a cathode. Because the anode and cathode are on the same bar, there is an electrical connection between the two. Thus, we have a short-circuited electrolytic cell, analogous to Figure 11.2B.

At the anode, iron atoms lose electrons and move into the surrounding concrete as ferrous ions. This process is represented by the following oxidation (or anodic) reaction:

$$Fe \rightarrow Fe^{2+} + 2e^{-} \tag{11.5}$$

The electrons flow through the bar to cathodic sites, where they combine with water and oxygen that are present in the concrete. The reduction reaction at the cathode is represented as follows:

$$H_2O + 1/2\ O_2 + 2e^{-} \rightarrow 2OH^{-} \tag{11.6}$$

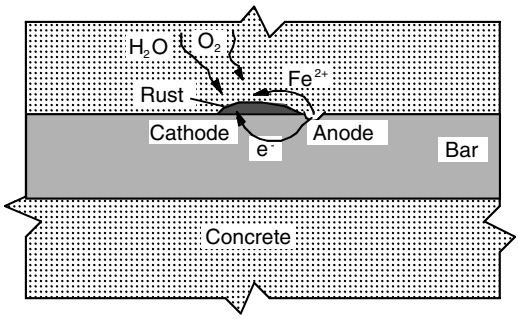

FIGURE 11.4 Localized corrosion of steel bar embedded in concrete; iron is dissolved at anode and rust forms at cathode.

To maintain electrical neutrality, the ferrous ions migrate through the pores of the paste to the cathode where they combine with the OH^- ions to form hydrated iron oxide, or rust. Thus, when the bar is corroding, there is a flow of electrons through the bar and a flow of ions through the concrete. The corrosion current would be governed by the polarization curves for the two half-cell reactions given above.

From the above discussion, it can be concluded that corrosion of embedded steel in concrete requires the following conditions:

- Loss of passivation
- Presence of moisture
- Presence of oxygen

If any of these are absent, there is no corrosion. If there are limited amounts of water or oxygen, corrosion proceeds at a slow rate. These factors are discussed further because they are important in understanding the corrosion process.

The short-circuited electrolytic cell in Figure 11.2 has a bridge that allows unrestricted flow of ions between the cell solutions to maintain electrical neutrality. For the bar embedded in concrete, the concrete provides the bridge between the anode and cathode to allow the movement of ions. The pore structure of the paste and the degree of saturation of the capillary pores control the ease with which the ions move through the concrete. In short, the mobility of the ions is controlled by the electrical conductance of the paste. Figure 11.5A shows an electrolytic cell in which the bridge between the solutions is replaced by a resistor. The resistor restricts the flow of charge between the cells, and this in turn reduces the corrosion current compared with the electrolytic cell in Figure 11.2B. The polarization curves in Figure 11.5B help explain why the corrosion current is reduced. The driving voltage due to the difference between the half-cell equilibrium potentials of the cathode and anode $(E_c - E_a)$ is dissipated in polarizing the electrodes and overcoming the electrolytic resistance of the concrete:[10]

$$E_c - E_a = \eta_a + |\eta_c| + I_{\text{corr}}R \tag{11.7}$$

where η_a and η_c are the overpotentials of the electrodes, R is the electrolytic resistance, and I_{corr} is the corrosion current. The corrosion current is lower than the case where the resistance is zero (Figure 11.2 and Figure 11.3). Figure 11.5C shows an equivalent circuit of the corroding bar.[10] The polarized electrodes are shown as resistors and this is usually referred to as "reaction resistance."[18] If the electrolytic resistance decreases from R_1 to R_2, less of the cell potential is required to overcome the electrolytic resistance, the overpotentials increase, and the corrosion current increases.

If the amount of oxygen in the concrete is less than needed for the cathodic reaction, a condition known as *concentration polarization* occurs, and the corrosion current is reduced.[8–10] This is illustrated in Figure 11.6. Because of the limited amount of oxygen for the cathodic reaction, the cathodic polarization curve is no longer a linear function of the logarithm of the current density. Instead, there is a

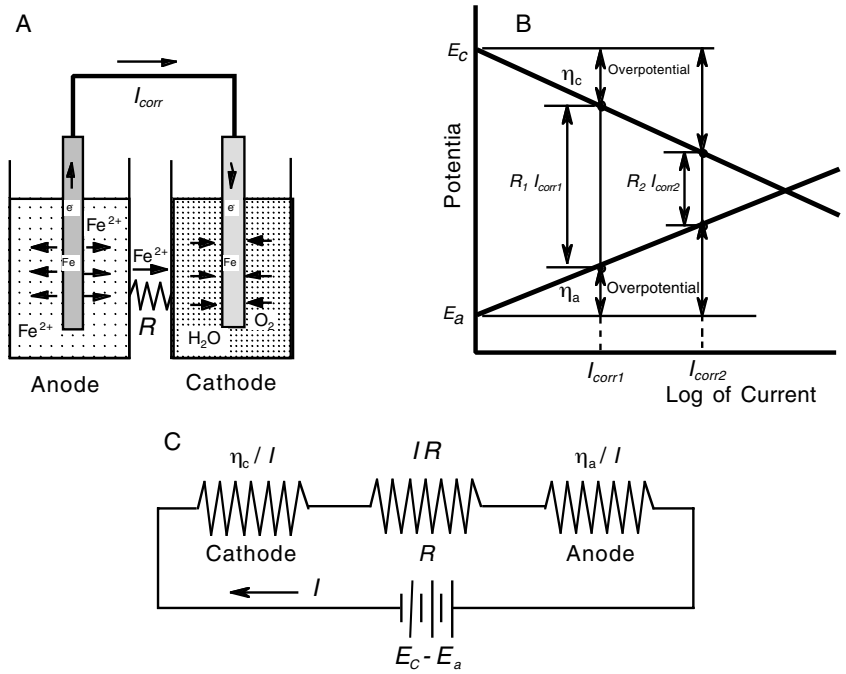

FIGURE 11.5 (A) Electrolytic cell analogy of corroding steel bar in concrete; (B) polarization curves showing effect of concrete resistance (ohmic polarization); (C) equivalent electric circuit of corroding bar. (Adapted from Reference 10.)

limiting value of the cathodic current density and the polarization curve is asymptotic as shown in Figure 11.6. The limiting current density depends on the concentration of oxygen in the paste, the diffusion coefficient of oxygen through the paste, and other factors.[9] As shown in Figure 11.6, because of concentration polarization at the cathode, the corrosion current is reduced. This is why the corrosion rate of steel in submerged concrete is very low. The low concentration of oxygen limits the cathodic current density, and thereby limits the corrosion current between anodic and cathodic sites. Note that the corrosion potential shifts to a more negative value, but the corrosion current is reduced compared with the conditions represented by Figure 11.2. This is important in the interpretation of half-cell potential, as discussed in the next section.

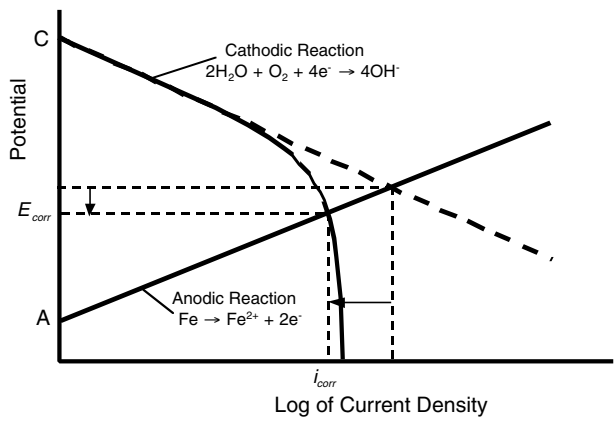

FIGURE 11.6 Polarization curves to illustrate concentration polarization; the corrosion current is limited by the rate of the cathodic reaction.

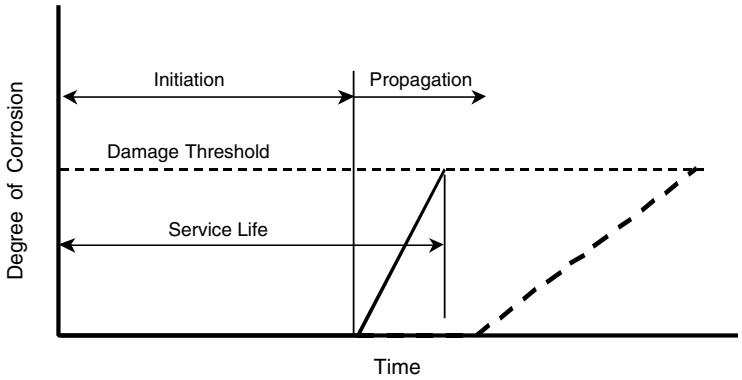

FIGURE 11.7 Model proposed by Tutti[2] to represent corrosion process of steel in concrete.

In summary, when steel in concrete loses its passive layer, corrosion occurs due to naturally occurring anodic and cathodic sites. However, the rate of corrosion depends on the electrical resistance of the concrete surrounding the anodic and cathodic sites and on the availability of oxygen. If the paste has low porosity, the resistance will be high, the oxygen diffusion coefficient will be low, and the corrosion rate will be low.

Tutti[2] provided a conceptual model to represent the service life of a reinforced concrete structure that is susceptible to steel corrosion. Figure 11.7 shows the degree of corrosion as a function of time. During the *initiation* period, there is no corrosion, but chloride ions or the carbonation front penetrates from the surface to the reinforcement. When the steel loses its passive layer, the *propagation* phase begins and the degree of corrosion increases rapidly with time. The rate of corrosion during the propagation phase is affected by the factors listed above. The service life is denoted by the time when the degree of corrosion has reached a level where the strength or serviceability of the structure is reduced below a critical level. The dashed line in Figure 11.7 represents a structure with a longer service life because of a longer initiation period and reduced rate of corrosion during the propagation phase. With this simple model, it is easy to explain why increased concrete cover and low water–cement-ratio concrete are two effective means for increasing service life.

11.4 Half-Cell Potential Method

Now that some of the basic principles underlying corrosion of steel in concrete have been reviewed, our attention can be turned to the methods that can be used to assess the corrosion conditions in a reinforced concrete structure. When there is active corrosion, current flow (in the form of ion migration) through the concrete between anodic and cathodic sites is accompanied by an electric potential field surrounding the corroding bar (Figure 11.8). The equipotential lines intersect the surface of the concrete and the potential at any point can be measured using the *half-cell potential method.* By mapping equipotential contours on the surface, those portions of the structure where there is a high likelihood of corrosion activity are identified by their high negative potentials.[18–20]

The standard test method is given in ASTM C 876[21] and is illustrated in Figure 11.8. The apparatus includes a copper–copper sulfate half-cell, connecting wires, and a high-impedance voltmeter. This half-cell is composed of a copper bar immersed in a saturated copper sulfate solution. It is one of many half-cells that can be used as a reference to measure the electrical potential of embedded bars. The measured voltage depends on the type of half-cell, and conversion factors are available to convert readings obtained with other references cells to the copper–copper sulfate half-cell. The positive terminal of the voltmeter is attached to the reinforcement and the negative terminal is attached to the copper–copper sulfate half-cell. A high impedance voltmeter (normally greater than 10 MΩ) is used so that there is very little current through the circuit. As shown in Figure 11.8, the copper–copper sulfate half-cell makes electrical contact

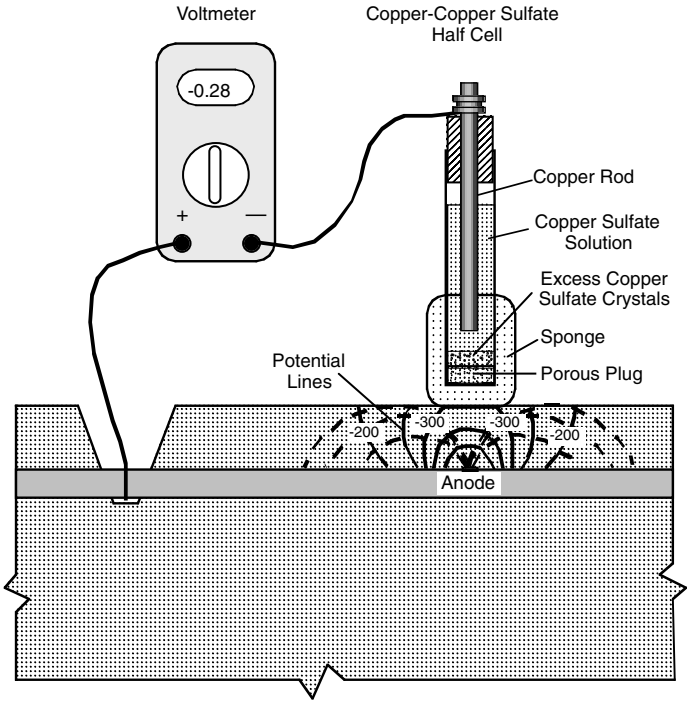

FIGURE 11.8 Apparatus for half-cell potential method described in ASTM C 876[21] to measure surface potential associated with corrosion current.

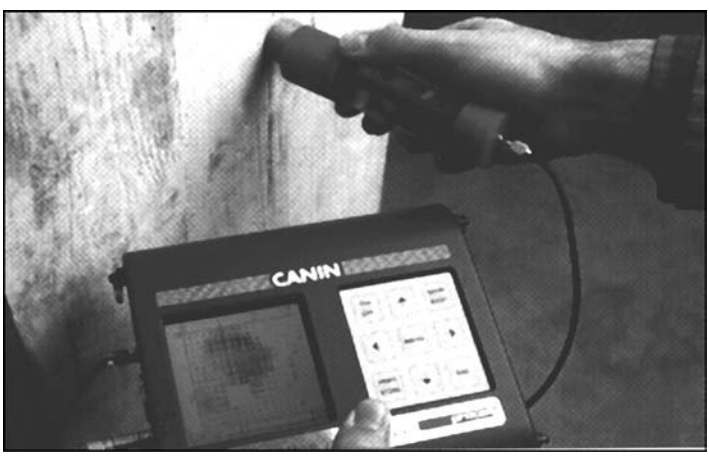

FIGURE 11.9 Example of half-cell potential apparatus. (Courtesy of Proceq SA.)

with the concrete by means of a porous plug and a sponge that is moistened with a wetting solution (such as liquid detergent). Figure 11.9 shows an example of a computer-based device for making half-cell potential measurements. This particular instrument stores data acquired at different test points and displays equipotential contours.

If the bar were corroding, the excess electrons in the bar would tend to flow from the bar to the half-cell. Because of the way the terminals of the voltmeter are connected in the electrical circuit shown in Figure 11.8, the voltmeter indicates a negative voltage (see ASTM G 3[16] for standard conventions related to electrochemical measurements). The measured half-cell potential is the *open-circuit potential*, because

it is measured under the condition of no current in the measuring circuit (ASTM G 15[13]). A more negative voltage reading at the surface is interpreted to mean that the embedded bar has more excess electrons, and there is, therefore, a higher likelihood that the bar is corroding.

The half-cell potential readings are indicative of the probability of corrosion activity of the reinforcing steel located beneath the copper–copper sulfate reference cell.[22] However, this is true only if that reinforcing steel is electrically connected to the bar attached to the voltmeter. To assure that this condition exists, electrical resistance measurements between widely separated reinforcing bars should be carried out (ASTM C 876[21]). This means that access to the reinforcement has to be provided. The method cannot be applied to concrete with epoxy-coated reinforcement or concrete with coated surfaces.

Testing is usually performed at points arranged in a grid. The required spacing between test points depends on the particular structure. Excessive spacing can miss points of activity or provide insufficient data for proper evaluation, while closer spacing increase the cost of the survey. In surveying bridge decks, ASTM C 876[21] recommends a spacing of 1.2 m. If the differences in voltages between adjacent points exceed 150 mV, a closer spacing is suggested. However, others have suggested that spacing should be about one-half of this value to obtain a reliable assessment of the extent of the corrosion.[23] Test equipment are available that include multiple cells and wheeled apparatus to speed data collection at close spacing.

A key aspect of the test is to assure that the concrete is sufficiently moist to complete the circuit necessary for a valid measurement. If the measured value of the half-cell potential varies with time, pre-wetting of the concrete is required and ASTM C 876[21] provides two approaches for doing this. When pre-wetting is necessary, there should be no free surface water between test points at the time of potential measurement. The concrete is sufficiently moist if the measured potential at a test point does not change by more than ±20 mV within a 5-min period (ASTM C 876[21]). If stability cannot be achieved by pre-wetting, it may be because of stray electrical currents or excessive electrical resistance in the circuit. In either case, the half-cell potential method should not be used. When testing is performed outside of the range of 17 to 28°C, a correction factor (see ASTM C 876[21]) is applied to the measured voltages.

11.4.1 Data Analysis

According to ASTM C 876,[21] half-cell potential readings should be used in conjunction with other data, such as chloride content, depth of carbonation, findings of delamination surveys, and the exposure conditions, to formulate conclusions about corrosion activity. Data from a half-cell potential survey can be presented in two ways: (1) as an equipotential contour map or (2) as a cumulative frequency diagram. Irrespective of the presentation method, reports of potential surveys must indicate clearly the reference electrode that was used.

The equipotential contour map is used most often to summarize survey results. It is created by locating the test points on a scaled plan view of the test area. The half-cell voltage readings at each test point are marked on the plan, and contours of equal voltage values are sketched. Figure 11.10 is an example of an equipotential contour map adapted from ASTM C 876. The contour interval should not exceed 100 mV. Computer-based test equipment is available to generate these contour maps.

The cumulative frequency diagram is obtained by plotting the potential data on normal probability paper, according to the procedure in ASTM C 876, and drawing the best-fit straight line through the data. The cumulative frequency diagram is used to determine the percentage of half-cell potential readings that are more negative than a certain value, and can be used to identify those potential values associated with different levels of corrosion activity.[18]

According to ASTM C 876,[21] two techniques can be used to evaluate the results: (1) the *numeric* technique or (2) the *potential difference* technique. In the numeric technique, the value of the potential is used as an indicator of the likelihood of corrosion activity. The appendix of ASTM C 876[21] gives the following guidelines (for the copper–copper sulfate reference electrode):

- If the potential is more positive than –200 mV (relative to the copper–copper sulfate half-cell), there is a high likelihood that no corrosion is occurring at the time of the measurement.
- If the potential is more negative than –350 mV, there is a high likelihood that there is active corrosion.

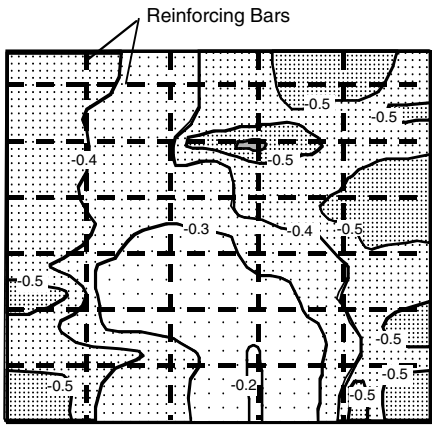

FIGURE 11.10 Example of equipotential contours from half-cell potential survey. (Based on Reference 21.)

- Corrosion activity is uncertain when the voltage is in the range of –200 to –350 mV.

However, it is stated that, unless there is positive evidence to suggest their applicability, these numeric criteria should not be used in the following conditions:

- Carbonation extends to the level of the reinforcement
- Evaluation of indoor concrete that has not been subjected to frequent wetting
- Comparison of corrosion activity in outdoor concrete with highly variable moisture or oxygen content
- To formulate conclusions about changes in corrosion activity due to repairs which changed the moisture or oxygen content at the level of the steel

The above precautions are recommended because of the importance of concrete resistivity and oxygen availability on actual corrosion rates. Figure 11.11 illustrates the generally poor correlation between half-cell potential and corrosion current density as measured by the polarization resistance method to be described.[24] As will be discussed, a corrosion current density less than 0.1 μA/cm^2 has been suggested as indicative of negligible corrosion and a value greater than 1 μA/cm^2 as indicative of high corrosion. Figure 11.11 shows that strict application of the limits suggested in ASTM C 876[21] can lead to incorrect inferences about the true corrosion activity.

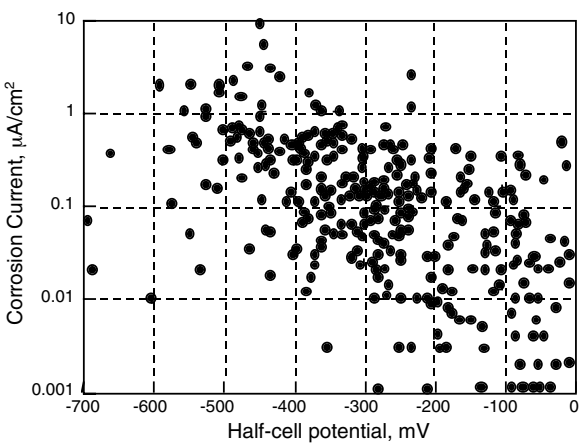

FIGURE 11.11 Comparison of corrosion current density (i_{corr}) with half-cell potential. (Adapted from Reference 24.)

In the potential difference technique, the areas of active corrosion are identified on the basis of the potential gradients. In the equipotential contour plot, the close spacing of the voltage contours indicates regions of high gradients. Some practitioners use the change in potential over a given surface area as an indicator of active corrosion, such as a change greater than 100 mV over 5 m^2. It is generally accepted that the potential difference technique is more reliable for identifying regions of active corrosion than is the use of numerical limits.[18,19,25–27]

11.4.2 Limitations

As has been stated, valid potential readings can be obtained only if the concrete is sufficiently moist, and the user must understand how to recognize when there is insufficient moisture for a meaningful measurement. In addition, there are several factors that can affect the magnitude of the potentials so that they are not indicative of the true corrosion conditions.[18–20] For example, a surface layer with high resistance results in less negative surface potentials; this can mask underlying corrosion activity. On the other hand, cathodic polarization due to the lack of oxygen results in more negative potentials (see Figure 11.6), while the actual corrosion rate is reduced. Increasing cover tends to result in similar surface potential readings irrespective of the underlying differences in corrosion activity.

Because of the many factors that have to be considered in this type of corrosion testing, a corrosion specialist is recommended to properly interpret half-cell potential surveys under one of the following conditions (ASTM C 876[21]):

- The concrete is saturated with water.
- The concrete is carbonated to the depth of the reinforcement.
- The steel is coated (galvanized).

Potential surveys should be supplemented with tests for carbonation and soluble chloride ion content. Finally, it needs to be made clear that the results of a potential survey are indicative of corrosion activity at the particular time of testing, and the activity can be expected to change with changes in environmental conditions.

11.5 Concrete Resistivity

The half-cell potential method provides an indication of the likelihood of corrosion activity at the time of measurement. It does not, however, furnish direct information on the *rate of corrosion* of the reinforcement. As has been discussed, after a bar loses its passivity, the corrosion rate depends on the availability of oxygen for the cathodic reaction. It also depends on the electrical resistance of the concrete, which controls the ease with which ions migrate through the concrete between anodic and cathodic sites. Electrical resistance, in turn, depends on the microstructure of the paste and the moisture content of the concrete. Thus, a useful test in conjunction with a half-cell potential survey is the measurement of the *resistivity* of the concrete. The resistivity is numerically equal to the electrical resistance of a unit cube of a material and has units of resistance (in ohms) times length.[28] The resistance R of a conductor of area A and length L is related to the resistivity ρ as follows:

$$R = \rho \frac{L}{A} \tag{11.8}$$

There is no ASTM test method for measuring the in-place resistivity of concrete. One technique that has been used successfully is shown in Figure 11.12.[28–30] This is based on the classical four-electrode system described by Wenner,[31] which has been incorporated into a standard test method for measuring soil resistivity (ASTM G57[32]). The four equally spaced electrodes are electrically connected to the concrete surface by using, for example, a conducting cream.[29] The outer electrodes are connected to a source of alternating current, and the two inner electrodes are connected to a voltmeter. The "apparent" resistivity is given by the following expression:[29,31]

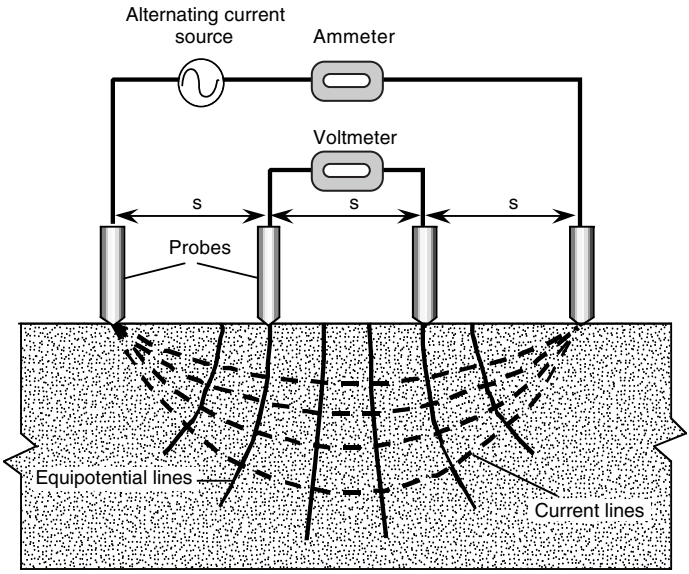

FIGURE 11.12 Four-probe resistivity test. (Adapted from Reference 30.)

$$\rho = \frac{2\pi s V}{I} \tag{11.9}$$

The word *apparent* is used because Wenner derived Equation 11.9 under the assumption that the material is semi-infinite and homogeneous. Thus, the relationship gives the correct measure of resistivity when these assumptions are satisfied. Any deviations from Wenner's assumptions lead to differences between the calculated "apparent" resistivity and the true resistivity of the material.[29]

Millard et al.[29] have carried out experimental and analytical studies to establish the magnitudes of the errors between the apparent and true resistivities when Equation 11.9 is applied to a finite-sized concrete member. One variable to consider is the minimum electrode spacing. Because concrete is made of paste and aggregates, which have different resistivities, the spacing should be large enough so that a representative average resistivity of concrete is measured. The minimum spacing depends on the maximum size of coarse aggregate: the larger the aggregate, the greater is the required minimum spacing. The spacing also determines the depth of the material that affects the measurements. The greater the spacing, the greater is the depth of concrete that contributes to the measurements. If the member is too shallow relative to the electrode spacing, there are boundary effects and the Wenner relationship is not a good approximation. Figure 11.13 shows an example of a four-probe device for measuring concrete resistivity.

Based on their studies, Millard et al.[29] recommend an electrode spacing of 50 mm as sufficient for typical concrete mixtures, and the width and depth of the member should be at least four times the electrode spacing. In addition, the edge distance should not be less than twice the electrode spacing. When these minimum dimensions are not satisfied, the apparent resistivity calculated by Equation 11.9 will exceed the true resistivity. Other factors that affect the calculated resistivity are the presence of a thin surface layer of low-resistivity concrete and the presence of reinforcing bars. Both of these conditions will result in an apparent resistivity that is lower than the true value. The effect of reinforcing bars is related strongly to the depth of cover and less so to the bar diameter. If possible, resistivity measurements should be conducted midway between two bars. When depth of cover is low and bar spacing is small, it may be possible to apply a correction factor if the diameter and location of the reinforcement are known.[29]

FIGURE 11.13 Example of commercial apparatus to measure concrete resistivity. (Courtesy of Proceq SA.)

Another technique for measuring resistivity is incorporated into one of the linear polarization devices to be described in the next section.[33] A special probe is used to measure ambient temperature, ambient relative humidity, and concrete resistivity in conjunction with the measurement of polarization resistance. In this case, the resistance measurement is affected by the concrete between the reinforcing bar and the point on the surface where the probe is located. The author is not aware of publications on comparisons of the resistivities measured by the four-electrode device and this single-probe device. The developers of the single-probe device offer the recommendations shown in Table 11.1 for relating concrete resistivity to the risk of corrosion.[24] On the other hand, Bungey[30] quotes the guidelines shown in Table 11.2. The dissimilarity of the entries in these tables emphasizes the need for a better understanding of the relationship between concrete resistivity and corrosion risk when reinforcement has lost its passivity.

TABLE 11.1 Relationship between Concrete Resistivity and Corrosion Risk

Resistivity, kΩ · cm	Corrosion Risk
>100 to 200	Negligible corrosion; concrete is too dry
50 to 100	Low corrosion rate
10 to 50	Moderate to high corrosion rate when steel is active
<10	Resistivity does not control corrosion rate

Source: Feliú, S. et al., in *Techniques to Assess the Corrosion Activity of Steel Reinforced Concrete Structures*, ASTM STP 1276, N.S. Berke et al., ASTM, West Conshohocken, PA, 1996, 107.

TABLE 11.2 Relationship between Concrete Resistivity and Likelihood of Significant Corrosion

Resistivity, kΩ · cm	Likelihood of Significant Corrosion (Nonsaturated Concrete)
>20	Low
10 to 20	Low/moderate
5 to 10	High
<5	Very high

Source: Bungey, J.H., *Testing of Concrete in Structures*, 2nd ed., Chapman & Hall, New York, 1989.

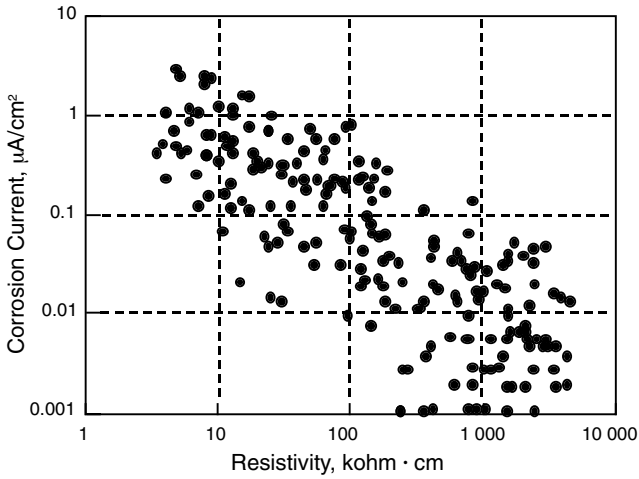

FIGURE 11.14 Comparison of corrosion current density (i_{corr}) and resistivity from field measurements. (Adapted from Reference 24.)

Figure 11.14 shows the relationship between concrete corrosion rate (measured as explained in the next section) and concrete resistivity.[24] In comparison with Figure 11.11, it is evident that, when steel loses its passivity, concrete resistivity correlates with corrosion rate better than does half-cell potential.

In summary, measurement of concrete resistivity provides additional information to assist in assessing the likelihood of different levels of corrosion activity. It is a useful supplement to a half-cell potential survey. A high resistivity indicates that, even though the steel is actively corroding as determined from the potential survey, the corrosion rate may be low. As mentioned, the resistivity of concrete is related to the ease with which ions can migrate through the concrete under the action of the potential field surrounding anodes and cathodes. The resistivity increases as the capillary pore space in the paste is reduced. This explains why high-quality concrete is of such critical importance for long service life under corrosion-inducing conditions.

11.6 Polarization Resistance

To overcome a major drawback of the half-cell potential method, namely, that it does not indicate directly the corrosion rate, several approaches have been investigated for measuring the in-place corrosion rate.[34] Among these methods, the *linear polarization resistance* method appears to be gaining the most acceptance[35] and draft standard test methods have been proposed.[36] This section provides an overview of the method, but it is emphasized that a qualified corrosion engineer should be retained to assure meaningful results.

11.6.1 Principle

The polarization resistance technique is a well-established method for determining corrosion rate by using electrolytic test cells (ASTM G 59[17]). The technique basically involves measuring the change in the open-circuit potential of the short-circuited electrolytic cell when an external current is applied to the cell. For a small perturbation about the open circuit potential, there is a linear relationship between the change in voltage, ΔE, and the change in applied current *per unit area* of electrodes, Δi. This ratio is called the *polarization resistance*, R_p:

$$R_p = \frac{\Delta E}{\Delta i} \tag{11.10}$$

Because the current is expressed per unit area of electrode that is polarized, the units of R_p are ohms times area. It has been pointed out that R_p is not a true resistance in the usual sense of the word,[37] but the term is widely used (ASTM G 15[13]).

Stern and Geary[38] established the underlying relationships between the corrosion rate of the anode and the polarization resistance. No attempt is made to explain these relationships other than to state that they are derived from the slopes of the anodic and cathodic polarization curves (refer to Figure 11.3). The corrosion rate (expressed as corrosion current density, i.e., current per unit area) is inversely related to the polarization resistance (ASTM G 59[17]):

$$i_{corr} = \frac{B}{R_p} \tag{11.11}$$

where

i_{corr} = corrosion current density, ampere/cm^2
B = a constant, V
R_p = polarization resistance, ohms · cm^2

The constant B is a characteristic of the polarization curves and a value of 26 mV is commonly used for steel that is actively corroding in concrete.[39]

11.6.2 Instrumentation

The basic apparatus for measuring the polarization resistance of reinforcing bars in concrete is the three-electrode system shown in Figure 11.15.[40,41] This basic configuration is often referred to as a "3LP" device, because it involves three electrodes. One electrode is composed of a reference half-cell, and the reinforcement is a second electrode called the *working electrode*. The third electrode is called the *counter electrode*, and it supplies the polarization current to the bar. Supplementary instrumentation measures the voltages and currents during different stages of the test. Such a device can be operated in the *potentiostatic* mode, in which the current is varied to maintain constant potential of the working electrode; or it can be operated in the *galvanostatic* mode, in which the potential is varied to maintain constant current from the counter electrode to the working electrode.

A summary of the main steps for using the 3LP device to measure polarization resistance in the potentiostatic mode is as follows:[36]

- Make an electrical connection to the reinforcement (the working electrode).
- Locate the bar whose corrosion rate is to be measured, wet the concrete surface, and locate the device over the center of the bar.
- Measure the open-circuit potential, E_o, of the reinforcement relative to the reference electrode, i.e., measure the half-cell potential (Figure 11.15A).
- Measure the current from the counter electrode to the working electrode that is necessary to produce a –4 mV change in the potential of the working electrode (Figure 11.15B).
- Repeat the previous step for different values of potential, namely, –8, and –12 mV beyond the corrosion potential.
- Calculate the area of bar that is affected by the measurement.
- Plot the potential vs. the current per unit area of the bar, and determine the slope of the best-fit straight line. This is the polarization resistance.

An uncertainty in obtaining the polarization resistance by the above procedure is the area of the steel bar that is affected by the current from the counter electrode. In the application of the 3LP device, it is

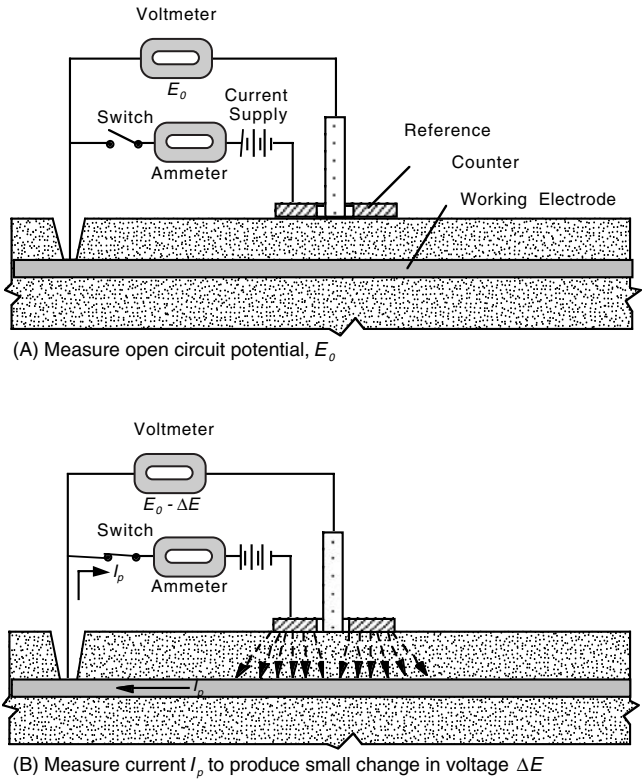

FIGURE 11.15 Three-electrode, linear polarization method to measure corrosion current.

assumed that current flows in straight lines perpendicular to the bar (working electrode) and the counter electrode. Thus, the affected bar area is taken as the bar circumference multiplied by the length of the bar below the counter electrode. Numerical simulations of current flow, however, show that the above assumption is incorrect and that the current lines are not confined to the region directly below the counter electrode.[35,39] In an effort to better control the current path from the counter electrode to the bar, a device has been developed that includes a fourth electrode, called a *guard* or *auxiliary electrode*, that surrounds the counter electrode.[39,42,43] Figure 11.16 is a schematic of this type of corrosion meter. The guard electrode is maintained at the same potential as the counter electrode. As a result, the current flowing from the counter electrode to the working electrode is confined to the region below the counter electrode and the nonuniform lateral spreading of the current is reduced. Figure 11.17 shows the use of a commercial linear polarization device on a structural element.

A comparative study, involving laboratory and field tests, was conducted of three commercially available corrosion rate devices.[35] Field test sites were chosen in three different environments that would represent the range of conditions that might be encountered in practice. Measurements were made on bridge structures at identical locations using the three devices. One of the devices was of the 3LP type and the other two used guard electrodes. It was found that the 3LP device gave higher values of corrosion current at the same test sites. From laboratory measurements on slabs it was concluded that the device developed in Spain,[42] which had a guard electrode, gave corrosion rates closest to the true corrosion currents measured independently by standard polarization resistance techniques. Each device, however, was capable of distinguishing between passive and active sites, and there were well-defined relationships between the corrosion currents measured by the different devices. It was concluded that each device could be used to estimate the corrosion rate in a structure.

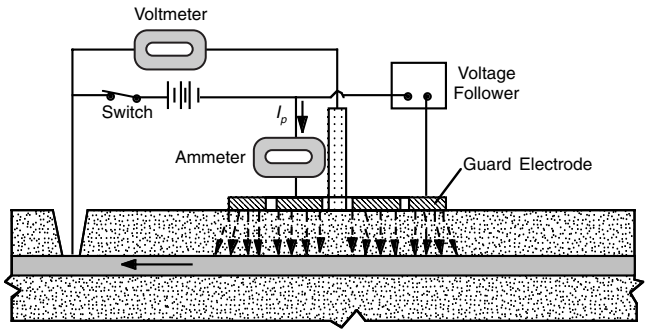

FIGURE 11.16 Linear polarization technique using guard electrode to confine the current from counter electrode to reinforcement. (Adapted from Reference 24.)

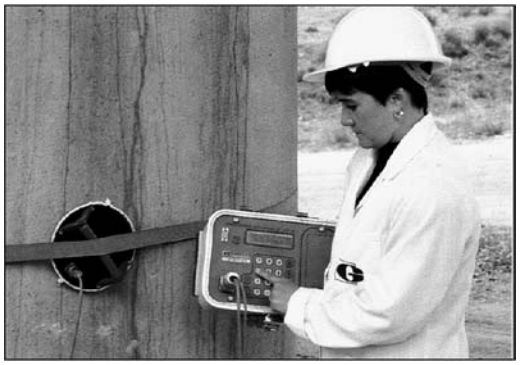

FIGURE 11.17 Example of linear polarization apparatus. (Courtesy of James Instruments, Inc.)

11.6.3 Limitations

The corrosion rate measured using polarization resistance represents the rate at the time of the test. The corrosion rate at a particular point in a structure is expected to depend on several factors, such as the moisture content of the concrete, the availability of oxygen, and the temperature. Thus, the corrosion rate at any point in an exposed structure would be expected to have seasonal variations. Such variations were observed during multiple measurements that extended over a period of more than 1 year.[44] To project the amount of corrosion that would occur after an extended period, it is necessary to repeat the corrosion rate measurements at different times of the year. As suggested by Clemeña et al.,[44] several alternatives could be used to predict the future condition of the reinforcement:

- Use the maximum measured corrosion rates to obtain a conservative estimate of remaining life.
- Use the yearly average corrosion rate at a typical or the worst location in the structure.
- Use the minimum and maximum corrosion rates to estimate the range of remaining life.

The corrosion rate is calculated from the polarization resistance by the use of the constant B, which is typically assumed equal to 26 mV. This constant, however, is related to the anodic and cathodic activity.[33] Feliú et al.[24] have pointed out that a value of 26 mV is reasonable for actively corroding bars, but a value twice as large is applicable under less active conditions. Thus, there is an inherent uncertainty in the calculated corrosion rate that can be as high as a factor of two.

At this time, there are no standard procedures for interpreting corrosion rate measurements obtained with different devices. As has been mentioned, different devices result in different corrosion rate values at the same test site. Thus, current guidelines are for specific test devices. For example, based on years

TABLE 11.3 Relationship between Corrosion Current Density Measured with Guard-Ring Device and Corrosion Risk

Corrosion Current Density, $\mu A/cm^2$	Corrosion Risk
<0.1	Negligible
0.1 to 0.5	Low
0.5 to 1	Moderate
>1	High

Source: Based on References 15 and 24.

of experience from laboratory and field testing, the guidelines shown in Table 11.3 have been developed for interpreting corrosion rate measurements using the guard ring device.[15,24]

As has been mentioned, corrosion current densities can be converted to metal loss by using Faraday's law (ASTM G 102[14]). For example, 1 $\mu A/cm^2$ corresponds to about 0.012 mm/year of section loss.[33] This assumes that corrosion is occurring uniformly on the bar, which is the typical condition with carbonation-induced corrosion. Chloride-induced corrosion, however, is associated with localized corrosion, or pitting. It has been reported that the depth of local pitting may be four to eight times the average depth of corrosion.[24] This factor should be considered if the effect of section loss on structural capacity is a concern.

There are other limitations that should be considered when planning corrosion rate testing. Some of these have been outlined in a proposed test method[36] and are as follows:

- The concrete surface has to be smooth (not cracked, scarred, or uneven).
- The concrete surface has to be free of water-impermeable coatings or overlays.
- The cover depth has to be less than 100 mm.
- The reinforcing steel cannot be epoxy coated or galvanized.
- The steel to be monitored has to be in direct contact with the concrete.
- The reinforcement is not cathodically protected.
- The reinforced concrete is not near areas of stray electric currents or strong magnetic fields.
- The ambient temperature is between 5°C and 40°C.
- The concrete surface at the test location must be free of visible moisture.
- Test locations must not be closer than 300 mm to discontinuities, such as edges and joints.

In summary, testing instruments based on linear polarization resistance have been developed for estimating the instantaneous corrosion rates. These are based on measuring the change in open-circuit potential when a small current is applied to the reinforcing bar. The calculations make certain assumptions about how much of the underlying bar is polarized during the test. As a result, different devices will give different corrosion rates if testing were done at the same point. Any particular device is able to differentiate between regions of high and low corrosion rates. It is important to understand that a corrosion rate measurement represents the conditions at the time of the test. Changes in the factors that affect corrosion rate, such as temperature, concrete resistivity, and oxygen availability, will change the corrosion rate. Thus, it is difficult to extrapolate service life based on one measurement. Measurements need to be repeated under different seasonal conditions to have an understanding of the average corrosion rate over an extended time period.

11.7 Summary

This chapter has reviewed the principles of three nondestructive techniques that can be used to investigate the status of corrosion in reinforced concrete members. These methods may be used to assess conditions for the planning of concrete repairs, or they may be used for assessing the performance of a specific repair system.

The basics of the corrosion process have been reviewed by presenting the behavior of electrolytic cells. The key to understanding corrosion phenomena is the polarization curve, which summarizes the net electrode current as a function of the electrode potential. Simplified polarization curves have been used to explain concepts such as the corrosion potential, cathodic polarization, and resistance effects. These basic concepts were used to explain the corrosion behavior when a bar embedded in concrete loses its protective passive film.

The three techniques covered in the chapter are half-cell potential, concrete resistivity, and polarization resistance. Each provides distinct information related to the corrosion status. The half-cell potential provides an assessment of the likelihood that there is active corrosion in the structure. It does not, by itself, provide information on the corrosion rate. One of the controlling factors for corrosion rate is the concrete resistivity, and measurement of concrete resistivity is a useful complement to the half-cell potential survey. The polarization resistance technique allows measurement of half-cell potential along with the actual corrosion current. The latter can be used to estimate the rate of section loss of the bar. It is emphasized that any of these measurements represent the conditions at the time of testing. Care must be exercised in extrapolating "one-time" measurements to estimate long-term corrosion.

Any assessment of the status of corrosion should include two additional determinations: depth of carbonation and chloride ion profiles. The former is a relatively simple measurement. The measurement of chloride profiles is a more involved process, and there is still debate over whether water-soluble or total chlorides is the key parameter.

Finally, corrosion of steel in concrete is a complex and not completely understood process. Experienced individuals should perform assessment of corrosion.

Acknowledgments

The majority of the text within the sections on half-cell potential and polarization resistance was originally drafted by the author for inclusion in a report being prepared by Committee 228 on nondestructive testing of the American Concrete Institute.[45] The author acknowledges the contributions of committee members in the preparation of the final version of these sections.

References

1. Smith, C.O., *The Science of Engineering Materials*, 2nd ed., Prentice-Hall, Englewood Cliffs, NJ, 1977, chap. 13.
2. Tutti, K., Service life of structures with regard to corrosion of embedded steel, in *Performance of Concrete in Marine Environment*, ACI SP-65, American Concrete Institute, Farmington Hills, MI, 1980, 223.
3. Rosenberg, A., Hansson, C., and Andrade, C., Mechanisms of corrosion of steel in concrete, in *Materials Science of Concrete I,* J.P. Skalny, Ed., American Ceramic Society, Westerville, OH, 1989, 285.
4. Hime, W.G., The corrosion of steel–random thoughts and wishful thinking, *Concr. Int.*, 15(10), 54, 1993.
5. ACI 222R-01, Protection of metals in concrete against corrosion, Report of ACI Committee 222, in *Manual of Concrete Practice*, American Concrete Institute, Farmington Hills, MI, 2002.
6. Browne, R.D., Mechanisms of corrosion of steel in concrete in relation to design, inspection, and repair of offshore and coastal structures, in *Performance of Concrete in Marine Environment*, ACI SP-65, American Concrete Institute, Farmington Hills, MI, 1980, 169.
7. Evans, U.R., *The Corrosion and Oxidation of Metals: Scientific Principles and Practical Applications*, Edward Arnold Press, London, 1980.
8. Fontana, M.G., *Corrosion Engineering*, 3rd ed., McGraw-Hill, New York, 1986.
9. Uhlig, H.H., *Corrosion and Corrosion Control: An Introduction to Corrosion Science and Engineering*, 2nd ed., John Wiley & Sons, New York, 1971.

10. West, J.M., *Basic Corrosion and Oxidation*, 2nd ed., Halstead Press, New York, 1986.
11. Brown, T.L. and LeMay, H.E., Jr., *Chemistry, the Central Science*, 4th ed., Prentice-Hall, Englewood Cliffs, NJ, 1988, chap. 20.
12. Guy, A.G., *Essentials of Materials Science*, McGraw-Hill, New York, 1976.
13. Terminology relating to corrosion and corrosion testing, ASTM G 15, *2002 Annual Book of ASTM Standards,* Vol. 03.02, ASTM, West Conshohocken, PA, 2002.
14. Practice for calculation of corrosion rates and related information from electrochemical measurements, ASTM G 102, *2002 Annual Book of ASTM Standards,* Vol. 03.02, ASTM, West Conshohocken, PA, 2002.
15. Andrade, C. and Alonso, C., Corrosion rate monitoring in the laboratory and on-site, *Constr. Build. Mater.*, 10(5), 315, 1996.
16. Practice for conventions applicable to electrochemical measurements in corrosion testing, ASTM G 3, *2002 Annual Book of ASTM Standards,* Vol. 03.02, ASTM, West Conshohocken, PA, 2002.
17. Practice for conducting potentiodynamic polarization resistance measurements, ASTM G 59, *2002 Annual Book of ASTM Standards,* Vol. 03.02, ASTM, West Conshohocken, PA, 2002.
18. Elsener, B., Müller, S., Suter, M, and Böhni, H., Corrosion monitoring of steel in concrete-theory and practice, in *Corrosion of Reinforcement in Concrete*, C.L. Page, K.W.J. Treadway, and P.B. Bamforth, Eds., Elsevier Applied Science, New York, 1990, 348.
19. Elsener, B. and Böhni, H., Potential mapping and corrosion of steel in concrete, in *Corrosion Rates of Steel in Concrete,* ASTM STP 1065, N.S. Berke, V. Chaker, and D. Whiting, Eds., ASTM, West Coshohocken, PA, 1990, 142.
20. Browne, R.D., Geoghegan, M.P., and Baker, A.F., Analysis of structural condition from durability tests, in *Corrosion of Reinforcement in Concrete Construction,* A.P. Crane, Ed., Society of Chemical Industry, London, 1983, 193.
21. Test method for half-cell potential of uncoated reinforcing steel in concrete, ASTM C 876, *2002 Annual Book of ASTM Standards,* Vol. 04.02, ASTM, West Conshohocken, PA, 2002.
22. Van Daveer, J.R., Techniques for evaluating reinforced concrete bridge decks, *J. Am. Concr. Inst.*, 72(12), 697, 1975.
23. Clemeña, G.G., Jackson, D.R., and Crawford, G.C., Benefits of using half-cell potential measurements in condition surveys of concrete bridge decks, *Transp. Res. Rec.,* 1347, 46, 1992.
24. Feliú, S., González, J.A., and Andrade, C., Electrochemical methods for on-site determinations of corrosion rates of rebars, in *Techniques to Assess the Corrosion Activity of Steel Reinforced Concrete Structures*, ASTM STP 1276, N.S. Berke, E. Escalante, C. Nmai, and D. Whiting, Eds., ASTM, West Conshohocken, PA, 1996, 107.
25. Dawson, J.L., John, D.G., Jafar, M.I., Hladky, K., and Sherwood, L., Electrochemical methods for the inspection and monitoring of corrosion of reinforcing steel in concrete, in *Corrosion of Reinforcement in Concrete*, C.L. Page, K.W.J. Treadway, and P.B. Bamforth, Eds., Elsevier Applied Science, New York, 1990, 358.
26. Naish, C.C., Harker, A., and Carney, R.F.A., Concrete inspection: interpretation of potential and resistivity measurements, in *Corrosion of Reinforcement in Concrete*, C.L. Page, K.W.J. Treadway, and P.B. Bamforth, Eds., Elsevier Applied Science, New York, 1990, 314.
27. Takewaka, K., Matsumoto, S., and Khin, M., Nondestructive and quantitative evaluation for corrosion of reinforcing steel in concrete using electro-chemical inspection system, in *Evaluation and Rehabilitation of Concrete Structures and Innovations in Design,* V.M. Malhotra, Ed., ACI SP 128, American Concrete Institute, Farmington Hills, MI, 1992, 339.
28. Millard, S.G., Harrison, J.A., and Edwards, A.J., Measurement of the electrical resistivity of reinforced concrete structures for the assessment of corrosion risk, *Br. J. NDT*, 31(11), 617, 1989.
29. Millard, S.G., Ghassemi, M.H., and Bungey, J.H., Assessing the electrical resistivity of concrete structures for corrosion durability studies, in *Corrosion of Reinforcement in Concrete*, C.L. Page, K.W.J. Treadway, and P.B. Bamforth, Eds., Elsevier Applied Science, New York, 1990, 303.
30. Bungey, J.H., *Testing of Concrete in Structures*, 2nd ed., Chapman & Hall, New York, 1989.

31. Wenner, F., A method of measuring earth resistivity, *Bull. Bur. of Stand.*, 12(4), 469, 1915.
32. Test method for field measurement of soil resistivity using the Wenner four-electrode method, ASTM G 57, *2002 Annual Book of ASTM Standards,* Vol. 03.02, ASTM, West Conshohocken, PA, 2002.
33. Broomfield, J., Field measurement of the corrosion rate of steel in concrete using a microprocessor controlled unit with a monitored guard ring for signal confinement, in *Techniques to Assess the Corrosion Activity of Steel Reinforced Concrete Structures*, ASTM STP 1276, N.S. Berke, E. Escalante, C. Nmai, and D. Whiting, Eds., West Conshohocken, PA, 1996, 91.
34. Rodríguez, P., Ramírez, E. and González, J.A., Methods for studying corrosion in reinforced concrete, *Mag. Concr. Res.,* 46(167), 81, 1994.
35. Flis, J., Sehgal, A., Li, D., Kho, Y.T., Osseao-Asare, K, and Cady, P.D., Condition evaluation of concrete bridges relative to reinforcement corrosion, Vol. 2: Method for measuring the corrosion rate of reinforcing steel, SHRP-S/FR-92-104, Strategic Highway Research Program, National Research Council, Washington, D.C., 1992.
36. Cady, P.D. and Gannon, E.J., Condition evaluation of concrete bridges relative to reinforcement corrosion, Vol. 8: Procedure manual, SHRP-S/FR-92-110, Strategic Highway Research Program, National Research Council, Washington, D.C., 1992.
37. Stern, M. and Roth, R.M., Anodic behavior of iron in acid solutions, *J. Electrochem. Soc.,* 104(6), 390, 1957.
38. Stern, M. and Geary, A.L., Electrochemical polarization: I. A theoretical analysis of the shape of polarization curves, *J. Electrochem. Soc.,* 104(1), 56, 1957.
39. Feliú, S., González, J.A., Andrade, C., and Feliú, V., Polarization resistance measurements in large concrete specimens: mathematical solution for unidirectional current distribution, *Mater. Struct. Res. Testing* (RILEM), 22(129), 199, 1989.
40. Escalante, E., Elimination of IR error in measurements of corrosion in concrete, in *The Measurement and Correction of Electrolyte Resistance in Electrochemical Tests*, ASTM STP 1056, L.L. Scribner and S.R. Taylor, Eds., ASTM, West Conshohocken, PA, 1989, 180.
41. Clear, K.C., Measuring rate of corrosion of steel in field concrete structures, *Transp. Res. Rec.,* 1211, 28, 1989.
42. Feliú, S, González, J.A., Feliú, S., Jr., and Andrade, M.C., Confinement of the electrical signal for *in situ* measurement of polarization resistance in reinforced concrete, *ACI Mater. J.,* 87(5), 457, 1990.
43. Feliú, S., González, J.A., Escudero, M.L., Feliú, S., Jr., and Andrade, M.C., Possibilities of the guard ring for electrical signal confinement in the polarization measurements of reinforcements, *J. Sci. Eng. Corrosion*, 46(12), 1015, 1990.
44. Clemeña, G.G., Jackson, D.R., and Crawford, G.C., Inclusion of rebar corrosion rate measurements in condition surveys of concrete bridge decks, *Transp. Res. Rec.,* 1347, 37, 1992.
45. ACI 228.2R-98, Nondestructive test methods for evaluation of concrete in structures, Report of ACI Committee 228, *ACI Manual of Concrete Practice*, American Concrete Institute, Farmington Hills, MI, 1999.

Notation

The following symbols are used in this chapter:

A = area of electrical conductor (cm^2)
B = a constant (V)
E_a = equilibrium half-cell potential of anode (V)
E_c = equilibrium half-cell potential of cathode (V)
E_o = open-circuit potential of reinforcement (V)
E_{corr} = corrosion potential (V)

I = current (A)
I_{corr} = corrosion current (A)
i_{corr} = corrosion current density (A/cm^2)
R = resistance (Ω)
R_p = polarization resistance ($\Omega \cdot$ cm^2)
s = electrode spacing (mm)
L = length of electrical conductor (cm)
ΔE = change in voltage (V)
Δi = change in current per unit area of polarized electrode (A/cm^2)
η_a = overpotential of anode (V)
η_c = overpotential of cathode (V)
ρ = resistivity ($\Omega \cdot$ cm)

12

Radioactive/Nuclear Methods

12.1 Introduction
12.2 General Principles
Source, Interaction, and Detection · Radiation Safety
12.3 Radiometry
Historical Background · Test Equipment and Procedures · Case Histories · Advantages and Limitations
12.4 Radiography
Historical Background · Test Equipment and Procedures · Case Histories · Advantages and Limitations
12.5 Neutron-Gamma Techniques
Historical Background · Test Equipment, Procedures, and Case History · Advantages and Limitations

Terry M. Mitchell
Federal Highway Administration

Radioactive and nuclear methods can be useful analytic or diagnostic tools, but, with an exception or two, are not widely used in concrete testing currently. The methods are based on directing radiation from sources such as radioisotopes and X-ray generators against or through fresh or hardened concrete samples. The radiation collected after interaction with the concrete provides information about physical characteristics such as composition, density, and structural integrity.

Gamma radiometry is the most widely used method, primarily for density determinations on roller-compacted and bridge deck concretes. Radiography is used occasionally in concrete laboratories for studying microstructure and in the field for confirming the integrity in structural concrete. Infrequently used, neutron-gamma techniques provide composition information on fresh or hardened concrete. The radioactive and nuclear methods are fast and accurate, but their use has been limited by the often complex technology involved, high initial costs, and training and licensing requirements.

Where possible, the accuracy of current magnetic and electrical apparatus is indicated.

12.1 Introduction

Radioactive and nuclear methods for testing concrete have been the subject of numerous research studies but, with an exception or two, are not widely used. The methods are generally fast and accurate and often provide information not available to any other means. On the other hand, their limited use is likely due to often complex technology, high initial costs, and training and licensing requirements. Another factor which limits the effectiveness of these, as well as many other nondestructive methods, is the heterogeneous nature of concrete itself, whether within a small sample, across a construction site, or from one project to another. Nevertheless, many of the radioactive and nuclear methods can be very useful analytic or diagnostic tools, and the disadvantages cited should not be overstressed.

The methods available use radiation produced by radioisotope sources, X-ray generators, and nuclear reactors to bombard fresh or hardened concrete samples. The radiation that is transmitted through, attenuated by, or emitted by the concrete is then collected and analyzed. The collected radiation can provide information about physical characteristics such as composition, density, and structural integrity.

12.2 General Principles

Although "radioactive" and "nuclear" have specific and distinct meanings, they are often used interchangeably in nondestructive testing contexts to refer to test methods that use the interaction of wave or particle radiation with matter to supply analytic or diagnostic information about the material. (In this chapter, the methods will be referred to, generically, as "nuclear methods.")

The nuclear methods used to test concrete can be separated into three categories: (1) radiometry; (2) radiography; and (3) neutron-gamma techniques. Radiometry describes techniques in which a radiation source and a detector are placed on the same or opposite sides of a concrete sample; a portion of the radiation from the source passes through the concrete and reaches the detector where it produces a series of electrical pulses. When these pulses are counted, the resulting count or count rate is a measure of the dimensions or physical characteristics, e.g., density or composition, of the concrete sample. Radiography describes techniques in which a radiation source and photographic film (the radiation detector) are placed on opposites sides of a concrete sample. After exposing the film, the result is a photographic image of the sample's interior, which is primarily used to locate defects in the concrete. Neutron-gamma techniques, rarely used in the concrete industry, are those in which a concrete sample is irradiated with neutrons, one type of radiation, and gamma rays, a second type, are emitted and detected. The result is a series of counts that are a measure of the composition of the concrete.

12.2.1 Source, Interaction, and Detection

Each nuclear testing method is a system composed of a radiation source, a mode of interaction with the concrete, and a radiation detector. A general description of each of these three components is needed before focussing on individual nuclear techniques.

Sources generate two types of radiation, electromagnetic waves and particles. The electromagnetic waves employed in nondestructive testing of concrete are gamma rays and X-rays. Wave radiation is characterized by the energy it carries, usually expressed in units of electron volts, eV (or kilo electron volts, keV, or mega electron volts, MeV). Gamma rays are emitted from reactions inside an atomic nucleus and typically carry energies from a few keV to several MeV. X-rays are emitted from interactions outside the nucleus among orbital and free electrons. They typically have energies from a few eV up to 100 keV, although much higher energies can be produced in X-ray tubes. Neutrons are the only particles of interest in concrete testing. They are uncharged particles that are also characterized by the energy they carry. Neutrons with energies greater than 10 keV are described as "fast," between 0.5 eV and 10 keV as "epithermal," and less than 0.5 eV as "slow."

The interaction of gamma and X-rays with concrete can be characterized as penetration with attenuation. That is, if a beam of gamma rays strikes a sample of concrete, some of the radiation will pass through the sample; a portion will be removed from the beam by absorption; and another portion will be removed by being scattered out of the beam (when gamma rays scatter, they lose energy and change direction). If the rays are travelling in a narrow beam, the intensity I of the beam falls off exponentially according to the relationship:

$$I = I_0 e^{-\mu x} \tag{12.1}$$

where

I_o = the intensity of the incident beam
x = the distance from the surface where the beam strikes
μ = the linear absorption coefficient

For the gamma and X-ray energies common in nuclear instruments used to test concrete, the absorption coefficient includes contributions from a scattering reaction, called Compton scattering, and an absorption reaction, called photoelectric absorption. In Compton scattering, a gamma or X-ray loses energy and is deflected into a new direction by a collision with a free electron. In photoelectric absorption, a gamma or X-ray is completely absorbed by an atom, which then emits a previously bound electron. The relative contributions of Compton scattering and photoelectric absorption are a function of the energy of the incident gamma or X-rays. In concrete, Compton scattering is the dominant process for gamma or X-ray energies in the range from 60 keV to 15 MeV, while photoelectric absorption dominates below 60 keV.

The amount of Compton scattering that occurs at a given gamma or X-ray energy is a function of the density of the sample being irradiated. The amount of photoelectric absorption that occurs is chiefly a function of the chemical composition of the sample, and increases as the fourth power of the atomic number of the elements present. (The latter effect is one of the reasons lead, with an atomic number of 82, is such a good absorber of X-rays.)

The interaction of neutrons with concrete can also be characterized as penetration with attenuation, although the reactions are different than those for gamma and X-rays. Except for nuclear reactors, most sources used to test concrete generate fast neutrons. Neutrons are scattered by collisions with atoms of the various elements in a concrete sample, losing energy and changing direction in each collision. Hydrogen atoms are the most effective scatterers, by far, and collisions with hydrogen atoms rapidly change neutrons from fast to slow. A measurement of the number of slow neutrons present therefore serves as an indicator of how much hydrogen is present in a sample, and since the only hydrogen present in concrete typically is in water molecules, slow neutron detection can be used as a measure of water content.

Neutrons are also absorbed in concrete, and, in general, slow neutrons are more likely to be absorbed than fast neutrons. Unlike the photoelectric absorption process for gamma and X-rays, which increases as atomic number increases, the absorption process for slow neutrons shows no such regular relationship. Although atoms of all elements absorb neutrons to some extent, certain elements, e.g., boron and cadmium, are much stronger absorbers than others. Absorption plays a minor role in neutron-based test methods, except in the neutron-gamma methods.

When neutrons are absorbed, many of the capturing atoms become radioactive. The newly formed atoms are usually unstable isotopes which subsequently decay, emitting gamma rays (or other types of radiation) with energies characteristic of the isotope. Some of these gamma rays are emitted almost instantly, others are emitted over a period of time ranging from seconds to years, depending on the isotope. If the gamma rays of specific energies are counted during specified time periods, the quantities of various elements present in a concrete sample can be established. Counting the gamma rays emitted almost instantly is the basis for neutron capture gamma ray analysis, while counting those emitted after some delay is the basis for neutron activation analysis.

Radiation detectors are the third component of a nuclear testing method. Having interacted with the concrete sample, the radiation carries information about sample properties or structure. The task of the detector and the associated electronics is to collect, process, and analyze that information to put it in a form useful to the engineer.

Radiography methods generally employ photographic film as detectors (although photosensitive paper, fluorescent screens, and electronic detectors are also used), while radiometry and neutron-gamma methods employ gas-filled tubes or scintillation crystals (crystals which transform incident radiation into flashes of light). In X- and gamma radiography, the rays strike the film emulsion and expose it much the same as light exposes conventional photographic film. Neutron radiography is slightly more complex

since neutrons will not expose the film emulsion directly; the neutrons are forced to strike a screen of a material that absorbs them and then emits secondary radiation that exposes the film.

The detectors for radiometry and neutron-gamma methods absorb a portion of the radiation and turn it into electrical pulses or currents, which can be counted or analyzed. In Geiger-Müller tubes, for example, gamma or X-rays ionize some of the gas in the tube; when the amount of ionization is then multiplied by a high voltage applied across the tube, it produces an electrical pulse that indicates radiation has interacted in the tube. Geiger-Müller tubes are used widely in nuclear density gauges. Neutrons do not ionize the gas in a gas-filled tube directly, but they are absorbed by boron trifluoride or ^{3}He in a tube; the latter cases emit secondary radiation that ionizes the gas in the tube and produces electrical pulses. Gas-filled neutron detectors are widely used in moisture gauges in agriculture and civil engineering applications.

Scintillation crystals are used primarily in the neutron-gamma methods, where knowing the energy of the detected gamma rays is useful. When gamma rays are absorbed in a scintillation crystal (sodium iodide is a typical crystal material), they produce tiny flashes of light. A photomultiplier tube turns the light into electrical pulses, the amplitudes of which are directly proportional to the energies of the gamma rays absorbed. Pulse height analyzers allow counts to be made over a single gamma ray energy range or over many such ranges to provide a distribution of counts as a function of energy. Scintillation crystal detection in neutron-gamma methods has uses such as establishing the amount of chloride ion present in concrete bridge decks or the amount of cement in freshly mixed or cured concrete samples.

After the brief discussion of radiation safety that follows, the remainder of this chapter will be devoted to examining radiometry, radiography, and neutron-gamma methods in more detail. The discussion of each of the three methods includes historical background, descriptions of the test equipment and procedures, case histories, and advantages and disadvantages. Appropriate references are also provided.

12.2.2 Radiation Safety

With few exceptions, anyone who owns radioactive sources or who performs any of the nuclear testing procedures discussed in this chapter must hold a license from the appropriate governmental authority. Licensing requirements are imposed to ensure that neither employees nor the general public are unnecessarily exposed to radiation and that an appropriate radiation safety program is in place. License applications typically require a listing of the individuals responsible for the radiation safety program (and the training they have received), descriptions of the training required for individuals using any of the sources, a description of the facilities and of the radiation monitoring equipment available, and an outline of the radiation safety program. Licensing requirements should not discourage potential users of nuclear testing methods, but should be regarded as promoting and insuring safe usage. More information about radiation safety for the nuclear testing methods is available in References 1 to 3.

12.3 Radiometry

12.3.1 Historical Background

Gamma radiometry is widely used in highway construction for density determinations on soil, soil-aggregates, and asphalt concrete, in the paper and pulp industry for thickness monitoring, and in other industries, but is just beginning to gain acceptance for testing portland cement concretes (PCC). Neutron radiometry, likewise, is widely used in highway construction (on soils and asphalt concrete), in well-logging, and in roofing rehabilitation, but is rarely used in testing PCC.

The development of gamma radiometry techniques did not really begin until radioisotope sources became widely available with the advent of nuclear reactors (after World War II). Malhotra[4] reported Smith and Whiffin as the first users of gamma radiometry on concrete in 1952; they made direct transmission measurements using a ^{60}Co source* inserted in a hole in a concrete block and a Geiger-Müller tube detector

*Isotope radiation sources such as ^{60}Co are identified by the chemical symbol for the element (Co for cobalt) preceded by the isotope's atomic weight (60) in a superscript.

external to the block. The apparatus allowed measurements of variations in density with depth in order to evaluate the effectiveness of an experimental surface-vibrating machine.

In his 1976 survey, Malhotra[4] reported gamma radiometry had been used for measuring the *in situ* density of structural concrete members, the thickness of concrete slabs, and the density variations in drilled cores from concrete road slabs. With the possible exception of its application in Eastern Europe for monitoring density in precast concrete units, radiometry was still an experimental nondestructive testing tool for concrete at that time. Density monitoring applications increased in the highway industry after a 1972 report by Clear and Hay[5] showed the importance of consolidation in increasing the resistance of concrete to penetration by chloride ions. A number of U.S. state and Canadian province highway agencies began to use commercially available nuclear gauges to evaluate the density achieved in bridge deck overlays, particularly overlays employing low slump, low water-cement ratio mixes. In 1979, The American Association of State Highway and Transportation Officials (AASHTO) adopted a standard method, T 271, for the "Density of Plastic and Hardened Portland Cement Concrete in Place by Nuclear Methods,"[6] and, in 1984, the American Society for Testing and Materials (ASTM) followed with a slightly different version, Test Method C 1040.[7]

Most recently, Whiting et al.[8] showed the strong influence of consolidation on several critical properties of concrete including strength, bond to reinforcing steel, and resistance to chloride ion penetration. They also evaluated several existing nuclear (gamma radiometric) gauges and strongly recommended their use for monitoring consolidation during construction.[9] They pointed out the value of density monitoring in evaluating the quality of concrete construction itself, rather than just the quality of the materials being delivered to the job site. Currently no procedures are in standard use to measure the in-place quality of concrete immediately after placement; that quality is not assessed until measurements such as strength, penetration resistance, and/or smoothness can be made after the concrete has hardened.

Gamma radiometry is also being used extensively for monitoring the density of roller-compacted concretes.[10,11] Densification is critical to strength development in these mixtures of cement (and pozzolans), aggregates, and a minimal amount of water. After placement, the concrete is compacted by rollers, much the same as asphalt concrete pavements. Commercially available nuclear gauges have become standard tools for insuring these concretes are adequately compacted.

Gamma radiometry has found limited application in composition determinations on PCC. When radioisotope sources emit low energy (below 60 keV) gamma rays, photoelectric absorption is the predominant attenuation mechanism, rather than Compton scattering. Since the absorption per atom increases as the fourth power of the atomic number Z, it is most sensitive to the highest Z element present in a sample. Noting that calcium in portland cement is the highest Z element present in significant quantities in PCC (in mixtures containing non-calcareous aggregates), Berry[12] used ^{241}Am (60 keV gammas) in a prototype backscatter device for measuring the cement content of fresh concrete. Mitchell[13] refined the technique, and the resulting instrument was reported to measure cement contents to within ±8% (at a 95% confidence level) for siliceous aggregate mixtures and to within ±11% for calcareous aggregate mixtures. Because of the sensitivity of photoelectric absorption to Z, the cement content procedure required calibration on a series of mixtures of different cement contents for a given aggregate source. This sensitivity to aggregate composition remains a barrier to further application of the technique.

A shortlived but interesting application of gamma radiometry was in pavement thickness determinations.[14] Gamma ray absorption is a function of the thickness of a specimen (see Equation 12.1). Therefore, a source could be placed beneath a PCC pavement, and, if a detector were positioned directly over the source, the count recorded by the detector would be a function of the pavement thickness. Researchers placed thumbtack-shaped ^{46}Sc sources on a pavement subbase before a PCC pavement was placed. The sources were difficult to locate after the concrete was placed, however, and the technique was abandoned albeit with a recommendation that it merited further research.

Neutron radiometry has seen few applications for testing PCC although neutron moisture gauges are widely used in other industries. In 1976, Malhotra's[4] out-of-the-practice included only a single reference to the use of neutron gauges on concrete, by Bhargava in 1969. Bhargava[15] used a neutron moisture gauge to measure the water content at three locations (top, middle, and bottom) of 6 in. × 12 in. × 5 ft-

(150 mm × 1.5-m) mortar and concrete columns. In another application Lepper and Rodgers[16] used commercially available neutron moisture gauges with the probe placed at the center of 1/2 and 1 ft^3 (14 and 28 dm^3) volumes (unit weight measures) of fresh PCC. The latter researchers found that the gauges could establish water contents to within ±3 to 6% of the actual value at a 95% confidence level; the accuracy depended on the gauge model and the sample volume.

12.3.2 Test Equipment and Procedures

All gamma radiometry systems are composed of (1) a radioisotope source of gamma rays; (2) the object (concrete) being examined; and (3) a radiation detector and counter. Measurements are made in either of two modes: direct transmission (Figure 12.1) or backscatter (Figure 12.2).

In direct transmission, the specimen, or at least a portion of it, is positioned between the source and the detector. The source and detector may both be external to the concrete sample (Figure 12.1A), e.g., in making density scans on cores or thickness determinations on pavements; the source may be

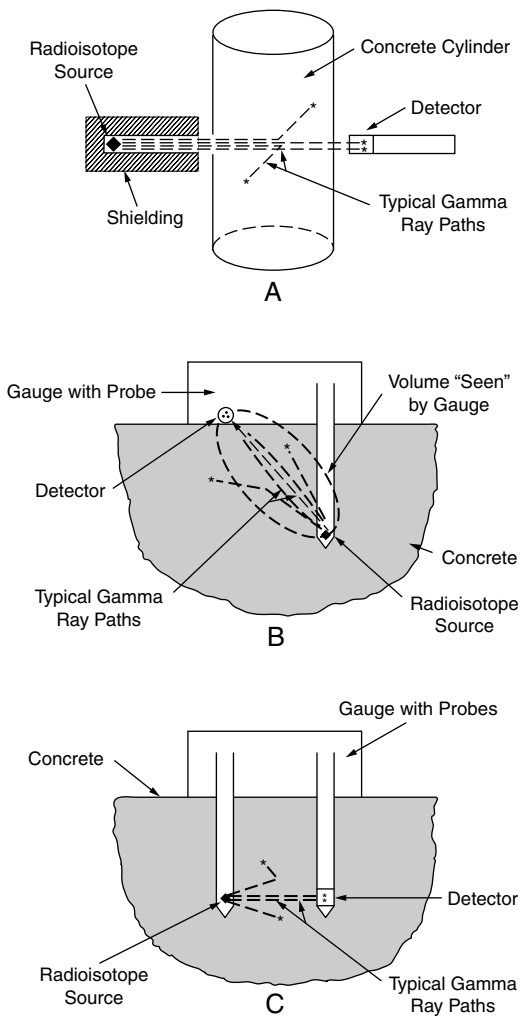

FIGURE 12.1 Gamma radiometry schematics — direct transmission mode: (A) source and detector both external to concrete; (B) source internal, detector external; and (C) source and detector both internal.

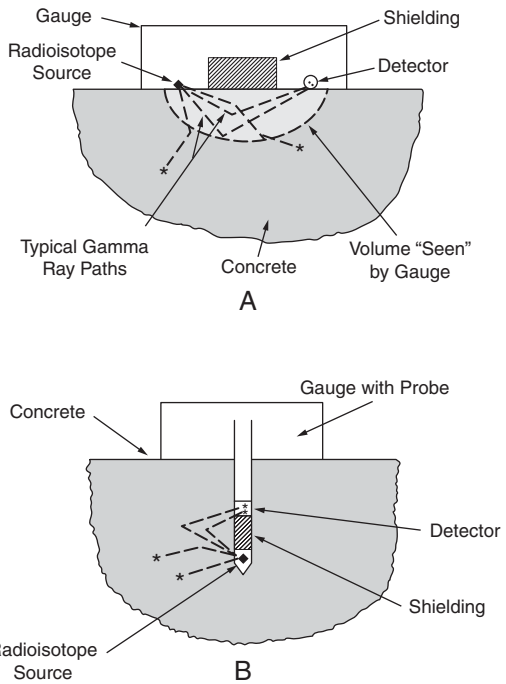

FIGURE 12.2 Gamma radiometry schematics — backscatter mode: (A) source and detector both external to concrete; and (B) both in probe internal to concrete.

inside the concrete and the detector outside (Figure 12.1B), e.g., is determining the density of a newly placed pavement or bridge deck; or the source and detector may both be inside the concrete (Figure 12.1C), e.g., in determining the density of a particular stratum in a newly placed pavement or in a hardened cast concrete pile.

In direct transmission, the gamma rays of interest are those that travel in a straight (or nearly straight) line from the source to the detector. Gamma rays that are scattered through sharp angles, or are scattered more than once, generally do not reach the detector. The fraction of the originally emitted radiation that reaches the detector is primarily a function of the density of the concrete, and of the shortest distance between the source and the detector through the concrete, as shown in Equation 12.1. Typical gamma ray paths are shown in Figure 12.1. The actual volume of the concrete through which gamma rays reach the detector, i.e., the volume that contributes to the measurement being made, is usually ellipsoidal in shape (see, e.g., Figure 12.1B), with one end of the volume at the source, the other at the detector. Sources typically used in direct transmission devices allow measurements to be made through 2 to 12 in. (500 to 300 mm) of concrete.

In backscatter measurement, the source and the detector are next to each other, although separated by radiation shielding. No portion of the concrete sample lies on a direct path between the source and detector. The source and detector may both be external to the concrete (Figure 12.2A), e.g., in determining the density of a newly placed pavement or bridge deck from the top surface of the concrete; or they may both be in a probe that is inserted in the concrete (Figure 12.2B), e.g., in a borehold in a cast pile.

In backscatter, only gamma rays that have been scattered one or more times within the concrete can reach the detector. The shielding prevents radiation from traveling directly from the source to the detector. Examples of gamma ray paths are shown in Figure 12.2A. Each time a gamma ray is scattered it changes direction and loses some of its energy. As its energy decreases, the gamma ray becomes increasingly susceptible to photoelectric absorption. Consequently, backscatter measurements are more sensitive to

the chemical composition of the concrete sample than are direct transmission measurements in which unscattered gamma rays form the bulk of the detected radiation.

Backscatter measurements made from the surface are usually easier to perform than direct transmission measurements which require access to the interior or opposite side of the concrete. However, backscatter has another shortcoming besides sensitivity to chemical composition: the concrete closest to the source and detector contributes more to the radiation count than does material further away. For typical commercially available backscatter density gauges, the top 1 in. (25 mm) of a concrete sample yields 50 to 70% of the density reading, the top 2 in. (50 mm) yield 80 to 95%, and there is almost no contribution from below 3 in. (75 mm). The actual volume of the concrete through which gamma rays reach the detector is roughly half of an ellipsoid (see Figure 12.2A), with one end of the ellipsoid at the source, the other at the detector.

The source, detector, and shielding arrangement can be modified to somewhat increase the depth to which a backscatter gauge will be sensitive. One of the most depth-sensitive gauges is a prototype device built for mounting on the back of a slipform paver for continuous density monitoring;[17] slightly over 70% of the device's reading comes from the top 2 in. (50 mm) of concrete and about 5% comes from below $3^1/_2$ in. (90 mm). Using a gauge model with minimal depth sensitivity may be desirable for applications such as measuring density of a thin (1- to 2-in. [25 to 50 mm] thick) overlay on a bridge deck. (Backscatter measurement has a third disadvantage, sensitivity to surface roughness, but this is rarely a concern for measurements on concrete.)

Gamma radiometry systems for monitoring density generally use ^{137}Cs (662 keV) sources, but ^{226}Ra (a wide range of gamma ray energies, which can be treated as equivalent, on the average, to a 750 keV emission) and ^{60}Co (1.173 and 1.332 MeV) are employed in some. These sources are among the few that have the right combination of long half-life* and sufficiently high initial gamma ray energy for density measurements. The half-life of ^{137}Cs, for example, is 30 years.

Most commercially available density gauges employ gas-filled Geiger-Müller (G-M) tubes as gamma ray detectors because of their ruggedness and reliability. Some prototype devices have employed sodium iodide scintillation crystals as detectors. The crystals are more efficient capturers of gamma rays than G-M tubes. They also can energy discriminate among the gamma rays they capture, a feature that can be used to minimize chemical composition effects in backscatter mode operation. However, the crystals are temperature and shock sensitive and, unless, carefully packaged, they are less suitable for field applications than the G-M detectors.

Portable gauges for gamma radiometry density determinations are widely available. A typical gauge is able to make both direct transmission and backscatter measurements, as shown in Figures 12.1B and 12.2A, respectively. The gamma ray source, usually 8 to 10 mCi** of ^{137}Cs, is located in the tip of a retractable (into the gauge case) stainless steel rod. The movable source rod allows direct transmission measurements to be made at depths up to 8 or 12 in. (200 or 300 mm), or backscatter measurements when the rod is retracted into the gauge case. The typical gauge would have one or two G-M tubes inside the gauge cause about 10 in. (250 mm) from the source rod. With the source rod inserted 6 in. (150 mm) deep into the concrete, the direct transmission source-to-detector distance would be about 11 in. (280 mm).

Detailed procedures for both direct transmission and backscatter measurements are given in ASTM Standard Test Method C 1040.[7] Density measurements require establishment of calibration curves (count rate vs. sample density) prior to conducting a test on a concrete sample. Calibration curves are created using fixed density blocks, typically of granite, limestone, aluminum, and/or magnesium. Method C 1040 encourages users to adjust the calibration curves for local materials by preparing fresh concrete samples

*The rate at which radioisotope sources emit radiation decreases with time; the half-life is the period of time in which the rate decreases by a factor of two.

**The curie (Ci) has traditionally been the unit for measuring activity of a radioisotope source; it is defined as exactly 3.7×10^{10} disintegrations/second. The curie is being replaced by an SI unit, the becquerel (Bq), which is equivalent to 2.703×10^{-11} Ci.

in fixed volume containers (the containers must be at least 18 × 18 × 6 in. [450 × 450 × 150 mm] for backscatter measurements). The nuclear gauge readings on the concrete in such a container are compared with the density established gravimetrically, i.e., from the weight and volume of the sample, and the calibration curve is shifted accordingly.

In-place tests on concrete are straightforward. For a direct transmission measurement, the most common configuration is that shown in Figure 12.1B; the gauge is seated with the source rod inserted into a hole, which has been formed by a steel auger or pin. For a backscatter measurement, the most common configuration is shown in Figure 12.2A, with the gauge seated on the fresh or hardened concrete at the test location. Care must be taken to insure reinforcing steel is not present in the volume "seen" by the gauge; reinforcing steel can produce a misleadingly high reading on the gauge display. Counts are accumulated, typically over a 1- or 4-min period, and the density is determined from the calibration curve (or read directly off a gauge in which the calibration curve has been internally programmed).

Tests with other gamma radiometry configurations (Figures 12.1A, 12.1C, and 12.2B) employ the same types of sources and detectors. Various shielding designs are used around both sources and detectors in order to collimate the gamma rays into a beam and focus it into a specific area of a sample. The two probe direct transmission technique (Figure 12.1C) needs additional development but has considerable potential for monitoring consolidation at particular depths, for example, below the reinforcing steel in reinforced concrete pavements. Iddings and Melancon used a commercially available gauge with a 5 mCi ^{137}Cs source and a 1-in. diameter × 1-in. (25 mm × 25 mm) sodium iodide scintillation crystal, respectively, in two probes that were separated by 12 in. (300 mm) of concrete.[18] They reported the effective vertical layer thickness for density measurements with this system to be about 1 in. (25 mm).

Neutron radiometric procedures usually employ a source/detector configuration similar to that used in gamma backscatter probes, as in Figure 12.2B. The probe might contain a 100 mCi fast neutron source (^{241}Am/Be) and a gas-filled BF_3 or ^{3}He detector. Because the detector is almost totally insensitive to fast neutrons, no shielding is employed between it and the source. The response of a neutron radiometry gauge arises from a much larger volume of concrete than does that of a gamma backscatter gauge. For example, a neutron radiometry probe completely surrounded by concrete with a water content of 250 lb/yd^3 (150 kg/m^3) will effectively be seeing the concrete up to 14 in. (350 mm) away; a gamma backscatter probe in the same concrete will be seeing the concrete no more than 4 in. (100 mm) away.

12.3.3 Case Histories

As noted previously, Malhotra[4] reported examples of radiometric techniques for measuring *in situ* density of structural concrete members, thickness of concrete slabs, and density variations in drilled cores. The principal applications of gamma radiometry recently have been in monitoring the density of conventional PCC bridge decks and pavements and of roller-compacted concrete (RCC) pavements and other structures during construction. Examples are presented here of what can be achieved with these techniques:

12.3.3.1 Static Gamma Radiometry on Conventional PCC and RCC Pavements

Tayabji and Whiting[9] reported on two field tests using commercially available nuclear density gauges on PCC pavement. A typical data collection effort is shown in Figure 12.3A, where measurements are being taken during slipform paving operations from a platform that was part of a dowel inserter.[19] Readings were taken in the direct transmission mode, with a 10 mCi ^{137}Cs source inserted 8 in. (200 mm) into the pavement. The technician made a 15-s count at every third stop of the inserter unit, i.e., at about 42-ft (13-m) intervals. Measurements were made at eight locations in each of eight lots. The average consolidation in the eight lots ranged from 98.9 to 100.2% of the rodded unit weight, with standard deviations within the lots ranging from 0.5 to 1.3%.

Figure 12.3B shows a similar density gauge being used on a newly placed RCC pavement. Density monitoring is critical on RCC projects since high density is needed to develop adequate flexural strength. On a pavement project such as the one shown in the figure, the concrete behind the paver typically has a density of 95% of the laboratory maximum, but will reach 98% after additional roller compaction.

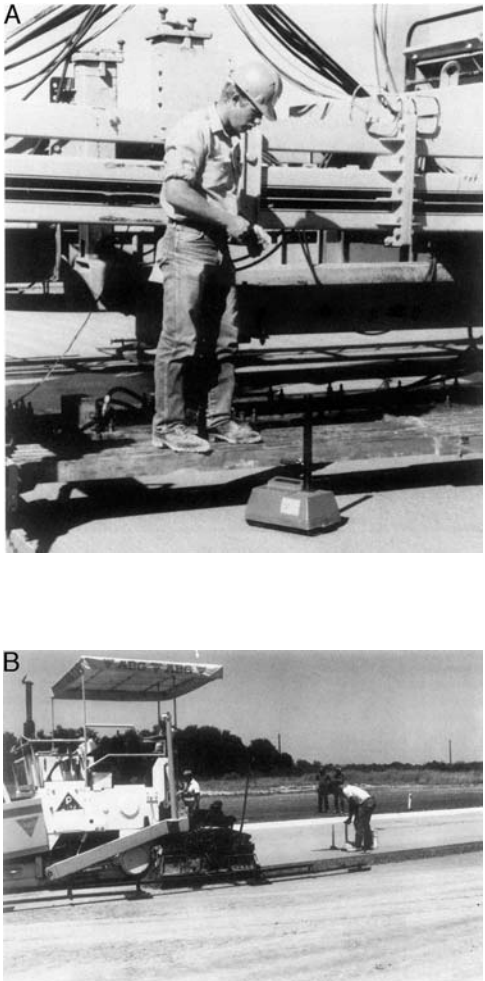

FIGURE 12.3 Static nuclear density gauges in use during construction of (A) conventional PCC pavement[19] and (B) roller-compacted concrete.[11] (A, Photo courtesy of FHWA; B, Photo courtesy of Kirby T. Meyer, P.E. Austin, TX. Reprinted with permission from Malisch, W.R., *Conc. Constr.*, 33, 13, 1988.)

Ozyildirim[20] cautions that static gauges are not suitable for exact determination of degree of consolidation in the field, because variations in component proportions or air content within acceptable ranges can cause variations in the maximum density attainable.

12.3.3.2 Dynamic Gamma Radiometry on Pavements

Figure 12.4 is a photograph of the Consolidation Monitoring Device (CMD) in use over a newly placed, conventional PCC pavement. The CMD is a noncontact backscatter density gauge, shown here with the source/detector unit mounted on a track on the back of a slipform paver. The unit rides back and forth transversely while the paver moves forward, thus monitoring the density of a significant portion of the pavement. The CMD uses a 500 mCi ^{137}Cs source and a 1-3/4 in. diameter × 4 in. long (45 × 102 mm) sodium iodide scintillation crystal. Results indicate that the device is capable of duplicating core density measurements within a ±/2-1/4 lb/ft^3 (±/36 kg/m^3) range at a 95% confidence level.[17] The CMD appears to be effective for tasks such as establishing proper vibrator operation, alerting vibrator malfunctions, and detecting significant changes in mixture composition, i.e., too little or too much air entrainment.

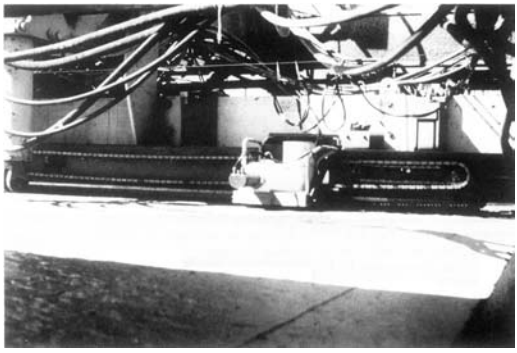

FIGURE 12.4 Dynamic nuclear density gauge (Consolidation Monitoring Device) in use during construction of conventional PCC pavement.[17] (Photo courtesy of FHWA.)

12.3.4 Advantages and Limitations

Gamma radiometry offers engineers a means for rapidly assessing the density, and therefore the potential quality, of concrete immediately after placement. Table 12.1 summarizes the advantages and limitations of backscatter and direct transmission gamma radiometry techniques and of neutron radiometry as well.

Direct transmission gamma radiometry has been used for density measurements on hardened concrete, but its speed, accuracy, and need for internal access make it most suitable for quality control measurements before newly placed concrete undergoes setting. Backscatter gamma radiometry is limited by its inability to respond to portions of the concrete much below the surface, but it can be used over both fresh and hardened concrete and can be used, in noncontact devices, to continuously monitor density over large areas. Gamma radiometry techniques have gained some acceptance in density monitoring of bridge deck concrete and fairly widespread acceptance for density monitoring of roller-compacted concrete pavement and structures.

TABLE 12.1 Radiometry

Technique	Advantages	Limitations
Gamma radiometry for density	Technology well-developed Rapid Simple, rugged and portable equipment Moderate initial cost Minimal operator skills	Requires license to operate Requires radiation safety program
Backscatter mode	Suitable for fresh or hardened concrete Can scan large volumes of concrete continuously	Limited depth sensitivity Sensitive to concrete's chemical composition and surface roughness
Direct transmission mode	Very accurate Suitable primarily for fresh concrete Low chemical sensitivity	Requires access to inside or opposite side of concrete
Neutron radiometry for water content	Rapid Accurate Large sample size minimizes effects of concrete's heterogeneity	Technology needs further development Requires calibration on local concrete materials Requires license to operate Requires radiation safety program

Although widely used in other industries, neutron radiometry techniques have been only minimally developed for water content measurements in concrete.

12.4 Radiography

12.4.1 Historical Background

X-radiography techniques were developed around the turn of the century and came to be used extensively in the 1920s. As with gamma radiometry, the development of gamma radiography techniques followed the ready availability of radioisotope sources after World War II.

X- and gamma radiography procedures are used primarily for examining welded products and castings for defects, e.g., for slag inclusions or porosity in welds and for gas cavities, blowholes, or cracks in castings. In the mid-1970s, Barton stated that X- and gamma radiography had become a $500 million a year business in the United States alone.[21]

Usage of X- and gamma radiography on concrete has developed very slowly. Malhotra[4] reported Mullins and Pearson making the first published field application in 1949; they used X-rays to show variations in density and to locate reinforcing bars. The same author reported finding only one other field application of X-rays up to the time of his writing (1976): a study on bond stress in prestressed concrete beams. The only field X-ray work on concrete recently has been done with the Scorpion II system developed in France.[22,23] The prototype Scorpion II includes a linear accelerator X-ray source mounted on a movable crane; the resulting system is designed for evaluation of prestressed concrete bridges. The equipment has been used for examining the quality of grouting and of concrete and for establishing the location and condition of prestressing cables.

Gamma radiography has enjoyed somewhat greater success in field applications, particularly in the U.K. Malhotra[4] summarized applications including determining the position and condition of reinforcing steel, establishing the location and extent of voids in concrete and in the grouting of post-tensioned concrete, and the detection of variable consolidation in concrete. The first generation Scorpion device used gamma ray sources for many of the same applications as those discussed previously for its successor (the higher energy X-rays generated by Scorpion II's linear accelerator double the thickness of the concrete that can be examined).[23] The British Standards Institution has adopted a standard for gamma radiography, BS 1881: Part 205, which indicates the usefulness of radiography for locating and identifying steel and voids in structural concrete.[24] The British standard includes a number of recommendations for investigators considering radiographic examination of concrete.

Both X- and gamma radiography have also been used in the laboratory to study the internal structure of concrete. Malhotra[4] summarized applications prior to 1976, which included studies of microcracking before and during loading and of crack propagation. The only laboratory application subsequent to 1976 appears to be by Slate, whose work included further studies of microcracking.[25]

Neutron radiography is also a relatively young field, only widely used since the mid-1960s. Typically more expensive than X- and gamma radiography, it finds is principal uses in applications where its interactions with particular elements in a sample are stronger than those of X- or gamma rays, or in hostile environments where intense gamma radiation is already present. Hawkesworth[26] cites the following five areas where neutron radiography is advantageous:

1. Highly radioactive objects, such as nuclear reactor fuel rods
2. Hydrogenous materials, such as seals, gaskets, and explosives
3. Materials containing high neutron absorbers such as boron and cadmium
4. Samples in which hydrogenous material or high neutron absorbers are embedded in heavy metals, such as copper, brass, lead, or steel, which are low neutron absorbers
5. Materials where the correct balance among different isotopes is important, e.g., new reactor fuel

Another author[27] says "…three applications, inspection of explosive devices, inspection of aircraft gas-cooled turbine blades for residual core material, and inspection of nuclear fuel pins, make up well over 90% of today's (1976) neutron radiography market."

The only applications of neutron radiography for testing concrete have been the recent work by Najjar et al.[28] in the United States, by Reijonen and Pihlajavaara[29] in Finland, and by Mo Da-Wei et al.[30] in China. The first group used the technique to study microcracking, the second used it to determine the thickness of the carbonated layer, and the third used it to study the water permeability of concrete samples.

12.4.2 Test Equipment and Procedures

As shown in Figure 12.5, all radiography systems are composed of (1) a beam from a radiation source; (2) the object being examined; and (3) an image collector. In X-radiography, the radiation source is an X-ray tube. When high voltage is applied to the tube, X-rays are emitted with energies proportional to the voltage. According to Malhotra,[4] X-ray sources used on concrete in laboratory studies typically produce maximum energies ranging from 30 to 125 keV. The French Scorpion II, designed for field applications, generates X-rays up to 4.5 MeV. In gamma radiography, a radioisotope source emits gamma rays continuously. The commonly used sources include ^{60}Co (which emits 1.17 and 1.33 MeV gammas), ^{137}Cs (0.67 MeV gammas), and ^{192}Ir (gammas at a number of energies between 0.21 and 0.61 MeV). Source selection depends on the planned application: the energy, half-life, exposure time required, and cost may all be considerations.

After the radiation beam traverses the sample, it is collected and turned into an image on photographic film. Steel attenuates gamma and X-rays much more than concrete does (reducing the intensity of a ^{60}Co beam by 1/2 requires 0.87 in. [22 mm] of steel or 2.7 in. [69 mm] of concrete), while air attenuates much less effectively than concrete. These differences in attenuation therefore can yield a photographic image of the internal structure of the concrete. Exposure times can range from a few seconds to an hour or longer, depending on the thickness of the concrete sample. Film selection depends on the range of thicknesses and densities being analyzed. Intensifying screens, usually of lead foil, can be used adjacent to the film to reduce exposure times and to minimize blurring due to secondary radiation. Once generated, the X- or gamma rays are collimated and the resulting beam is directed against the concrete sample. The radiation is attenuated, primarily by scattering out of the beam; the amount of attenuation depends on the thickness and density of the concrete and the initial energy of the radiation. The thickness of a typical concrete, which will reduce the intensity of a radiation beam by 1/2, is 1.9 in. (48 mm) for ^{192}Ir, 2.1 in. (53 mm) for ^{137}Cs, 2.7 in. (69 mm) for ^{60}Co, and 5.3 in. (135 mm) for a 4.5 MeV X-rays from an accelerator. The effect is multiplicative, so that, for a ^{137}Cs source, 4.2 in. (107 mm) of concrete reduces the beam intensity to 1/4 of its original value, 6.3 in. (160 mm) to 1/8 of its original value, etc. Beyond a certain thickness the beam intensity is reduced to a point that clear images cannot be obtained and collection times are impractically long. Figure 12.6 shows typical concrete thicknesses that can be

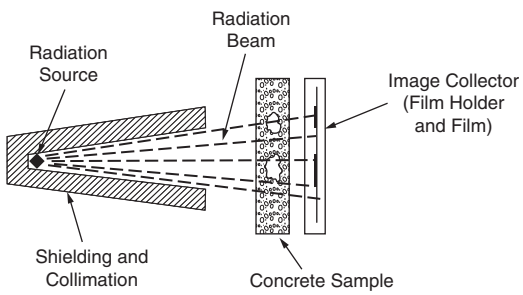

FIGURE 12.5 Radiography schematic.

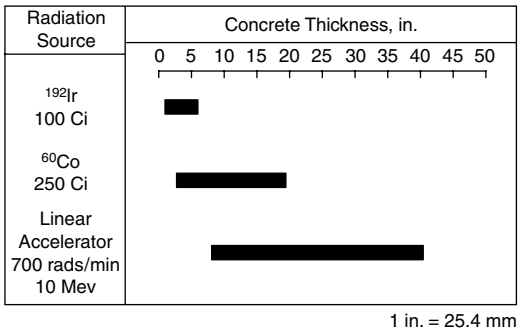

FIGURE 12.6 Concrete thickness ranges for three typical gamma radiography sources. (Adapted from Reference 23. Original figure courtesy of Laboratoire Régional des Ponts-et-Chausées de BLOIS.)

examined in the field for three of the radiation sources. In laboratory studies, e.g., of microcracking, concrete test specimens are less than 1 in. (25 mm) thick and X-rays in the 100 keV range are appropriate.

Radioscopy, in which a special fluorescent screen collects the image and converts it, in real time, into a television image, has been used to a limited extent on concrete, e.g., in a modification of the Scorpion system.[23] The maximum concrete thickness that can practically be viewed by a radioscopy system is only about 3/4 of that possible with a radiography system.

X-ray tomography also has potential applications as a radiographic technique on concrete.[31,32] Tomographic equipment, now widely used in medicine, collects radiographic information along a single plane through the object, repeats the process from various perspectives around it, and then uses a computer to construct an image of the internal structure. Tomography systems are very expensive and, up to now, have only been used in a limited way in research studies on concrete.

In neutron radiography, three types of sources are used, depending on the application. For laboratory studies, neutron beams from nuclear research reactors are the most effective sources. Accelerators are used in field applications, as are radioisotopes such as ^{124}Sb/Be and ^{252}Cf. Nuclear reactor beams produce the clearest images in the shortest exposure times. Accelerators produce more intense beams and hence have shorter exposure times than do radioisotopes; the latter are the most portable and require the least operator skill.

The laboratory studies on concrete have involved irradiating samples ranging from slices 0.15 in. (3.8 mm) thick to cylinders 2 in. (50 mm) in diameter.[28–30] The neutron beam is attenuated by (1) hydrogen-produced scattering, in the case of moisture studies; or (2) absorption by a high neutron absorber such as gadolinium, in the case of cracking studies. In the latter case, the concrete sample is impregnated, prior to irradiation, with a compound containing the absorbing element; the compound acts as a contrasting agent.

Photographic film is again used for image collection but cannot be directly exposed by neutrons. The film must instead be wrapped in a converted, gadolinium foil for example, which turns the neutrons into light or charged particles, which will then expose the film. Exposure times again depend on the thickness of the sample, and typically are an hour or longer. Najjar[33] provides useful information on both experimental equipment and sample preparation.

12.4.3 Case Histories

The principal applications of radiography to concrete to date are primarily in two categories: (1) X-, gamma, and neutron radiography in laboratory studies of internal microstructure, particularly of microcracking, and (2) X- and gamma radiography in field studies of macrostructure, e.g., the location of reinforcing steel and of voids or areas of inadequate consolidation. Two examples are presented here of what can be achieved with these techniques.

12.4.3.1 X- and Neutron Radiography for Microcracking

Malhotra[4] summarized much of the pre-1976 work in X- and gamma radiography of the microstructure of concrete. Two later articles by Najjar et al.[28,34] illustrate the effectiveness of the two techniques in microcracking studies. Figures 12.7A and B show X- and neutron radiographs, respectively, of a 0.15-in. (3.8 mm) thick slice of a 4-in. (102-mm) diameter concrete sample that had been loaded to just beyond the peak compressive stress. Figures 12.8A, B, and C show, respectively, a conventional photograph, a conventional X-radiograph, and a contrasting-agent X-radiograph of a 0.30-in. (7-mm) thick slice of a 4-in. (102-mm) diameter sample, also loaded to just beyond the peak stress. For both figures, specimens of the desired thickness were sawed from concrete cylinders that had been loaded to the desired level. The specimens were then cleaned, ground, and polished.

The X-radiography in Figure 12.7A was accomplished with a 150-kV industrial X-ray machine operated at 40 kV, 5-mA current, and 2 min of exposure time on a fine-grained Kodak Type T X-ray film. The X-radiography shown in Figures 12.8B and C was accomplished with a 150-kV veterinary medicine diagnostic X-ray machine operated at 44-kV, 150-mA current, and 0.33 s of exposure time on Kodak Type X-OMATG film. The neutron radiography was accomplished with a beam of slow neutrons generated from the TRIGA Mark II nuclear reactor at Cornell University. The neutron flux was approximately 10^6 neutrons/cm^2/s at the specimen. The slow neutrons passed through the specimen and the film, and then a portion were absorbed by a 25-mm thick gadolinium foil; the secondary radiation from this absorption exposed the film.

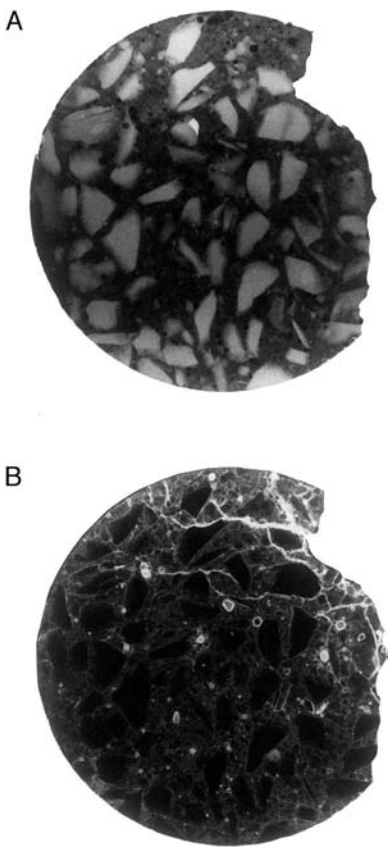

FIGURE 12.7 (A) X-radiograph of 4-in. diameter, 0.15-in. thick (102 × 3.8 mm) slice of concrete after loading to peak stress; (B) neutron radiograph of some specimen.[28] (Copyright ASTM. Reprinted with permission.)

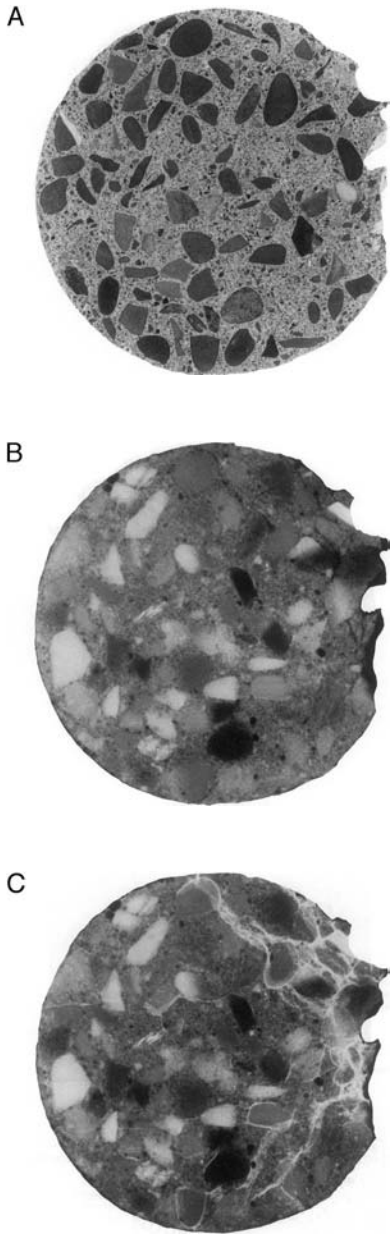

FIGURE 12.8 (A) Conventional photograph of 4-in. diameter, 0.30-in. thick (102 × 7-mm) slice of concrete after loading to peak stress; (B) conventional radiograph of same specimen; and (C) X-radiograph of same specimen after treatment with contrasting agent.[34] (Copyright ASTM. Reprinted with permission.)

Figures 12.7B and C show the quality of images of microcracking that can be obtained from radiography when contrasting agents are employed. In Figure 12.7B a gadolinium nitrate solution was applied to the polished specimen surface and allowed to penetrate into the cracks and voids; in Figure 12.8C the surface was treated similarly with a lead nitrate solution. The two agents are efficient absorbers, respectively, of neutrons and X-rays, thus highlighting the microcracks in the radiographs. It should be noted that the radiographs are not images of the surface but are images of the full thickness of the specimen, so care must be taken in interpreting and establishing the effective width and depth of the cracks.

12.4.3.2 X- and Gamma Radiography for Macrostructure

Figure 12.9 is a photograph of the French-built Scorpion II system in use on a prestressed concrete bridge structure. The handling arm, shown extended to beneath the bridge, includes a miniaturized linear accelerator that can generate X-rays with energies up to 4.5 Mev. The detector, either a film cassette for radiography or an image converter and camera for radioscopy, is positioned in the interior of the concrete girder.

Figure 12.10A is a photograph of Scorpion II's radioscopic image of a prestressing cable anchorage in concrete; Figure 12.10B is a schematic of the cable anchorage and interpretation of the radiograph. The radioscopic image was observed through 14 in. (360 mm) of concrete in real time; a sensitive electronic camera (25 images/s and 10^{-4} lux) captured the image of the fluorescent screen and displayed it on a television monitor. The radioscopic image is not sharp but does clearly show the large voids ("heterogeneity") behind the anchorage and the smaller voids ("bad contact") on the front side.

FIGURE 12.9 Scorpion II X-radiography system on prestressed concrete bridge structure. (Photo courtesy of Laboratoire Régional des Ponts-et-Chausées de BLOIS.)

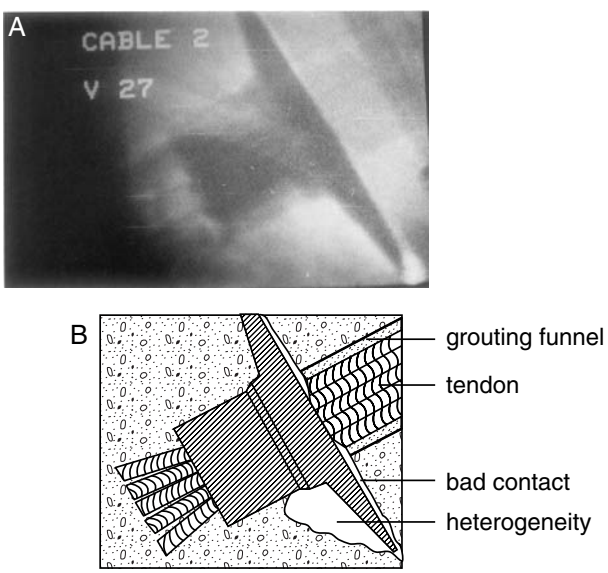

FIGURE 12.10 Scorpion X-radioscopic image of prestressing cable anchorage in concrete: (A) photograph of radioscopic image; (B) schematic of cable anchorage and interpretation of photograph. (Photo courtesy of Laboratoire Régional des Ponts-et-Chausées de BLOIS.)

It should be noted that a radiograph of a thick concrete member is based on the entire thickness; therefore, thin cracks of planar defects perpendicular to the radiation beam will have little effect on the beam and may not be detectable in the radiograph.

12.4.4 Advantages and Limitations

X- and gamma radiography offer researchers a means for visually examining the internal microstructure of concrete specimens and offer engineers a means for inspecting the quality of construction and materials in concrete structures. Table 12.2 summarizes the advantages and limitations of the two techniques and of neutron radiography as well. X-ray techniques are fast; they are capable of viewing interiors of concrete sections up to 3 ft (1 m) thick; they can generate radiation at the optimum energy level for a given specimen thickness; and they require minimal shielding since radiation emission can be terminated by turning off the electrical power supply. On the other hand, X-ray equipment is expensive and must be operated carefully because of high voltages and high radiation levels. Until recent miniaturization of X-ray generators such as in the Scorpion II system, gamma radiography equipment has generally been more portable. Gamma ray equipment is less expensive and is easier to operate because electrical power is not necessary. The continuous radioactivity from the gamma ray sources requires more shielding and additional safety interlocks to prevent accidental exposures.

Neutron radiography is currently a tool for researchers to use in examining the internal microstructure of concrete specimens. It is most useful where specimens contain elements that interact more readily with neurons than with X- or gamma radiation.

TABLE 12.2 Radiography

Technique	Advantages	Limitations
All radiography techniques		Expensive Require skilled operators Require license to operate Require radiation safety program Thin cracks or planar defects perpendicular to radiation beam may be difficult to detect
X-ray	Useful for examining internal macrostructure, e.g., steel location and voids, or microstructure, e.g., steel location and voids, or microstructure Fast View through concrete up to 18 in. (0.5 m) thick View through concrete up to 3 ft (1 m) thick Minimal shielding Energy adjustable for different applications	Primarily a research tool Very expensive initially Potential high voltage hazard
Gamma ray	Useful for examining internal macrostructure, e.g., steel location and voids, or microstructure More portable than X-ray Less expensive than X-ray No electrical power required	View through concrete up to 18 in. (0.5 m) thick Long exposure times
Neutron	Useful for examining microstructure	Primarily a research tool Very expensive initially Little advantage over other radiography methods for most applications on concrete

12.5 Neutron-Gamma Techniques

12.5.1 Historical Background

Neutron-gamma techniques, which include neutron activation analysis (NAA) and neutron capture-prompt gamma ray analysis (NCGA), are important tools in criminal forensics, authentication of art objects, and establishment of trace elements in pollutants; as yet they have only served as a research aid, for composition measurements, on concrete. Malhotra[4] summarized the pre-1976 work on concrete, stating that the neutron-gamma techniques were "largely undeveloped for application to concrete and little published data were available on their laboratory and field use for this application."

In the decade following Malhotra's statement, applications to concrete have continued at a very limited pace. Iddings and Arman[35] reported construction of field NAA equipment for measuring the cement content of fresh concrete, of hardened concrete in place, and of concrete cores. Taylor[36] developed a multielement analyzer which used both NAA and NCGA to establish cement, water, and fine and coarse aggregate contents of fresh concrete. And Rhodes et al.[37] constructed a mobile device for nondestructively measuring the chloride content of concrete bridge decks.

12.5.2 Test Equipment, Procedures, and Case History

Neutron-gamma systems are composed of three components: (1) a source of neutrons; (2) the sample being examined; and (3) a gamma ray collection and counting system. When samples can be brought into the laboratory, research nuclear reactors are the optimum neutron source. However, all of the devices named in the previous section were designed for testing concrete in the field and employed radioisotope sources, either ^{239}Pu/Be (^{239}Pu emits alpha particles that are captured by the Be to produce neutrons) or ^{252}Cf (^{252}Cf emits neutrons directly as a result of spontaneous fission). ^{252}Cf source sizes typically are 200 to 500 mg, which generate 5 to 12 × 10^8 neutrons/s.

Neutron-gamma systems work best with high neutron levels from the sources. Because this means sources are highly radioactive and because neutrons are very penetrating radiation, the mobile neutron-gamma systems require considerable shielding. For example, the shield for Iddings' field system was a 36 in. (90 mm) diameter sphere of borated water extended polyester, along with a small lead shield; the total assembly weighed some 800 lb (350 kg).[35]

Sample sizes can be relatively large, e.g., up to 10 in. diameter by 8 in. high (250 mm × 200 mm) in the Iddings' experiments; this can be helpful in minimizing the effects of concrete's characteristic heterogeneity. Because of the high radiation levels at the sources, test procedures require remote controls to transfer the sample into the vicinity of the source or to bring the source out of its shield into the vicinity of the sample.

The neutrons interact with the various elements present in the sample in three principal ways: (a) absorption by atoms and prompt (almost immediate) emission of characteristic gamma rays; (b) inelastic scattering by atoms, also with prompt emission of gamma rays; and (c) absorption by atoms, which decay and emit characteristic gamma rays over a longer period of time (seconds, minutes, or longer, after the irradiation occurs). The first two interactions are the basis for NCGA, the third for NAA.

Each element present in a sample has a different probability of capturing (ort scattering) neutrons. When neutrons are absorbed, the resulting atom is in an excited state, and the atom can emit radiation of various types to return to a more stable state. When gamma rays are emitted, either as prompt or activation gammas, they have an energy or energies characteristic of the element. The number of gamma rays of a specific energy emitted in a specified period of time can then be related to the amount of the element present in the sample. Scintillation crystals are generally used in the detecting and counting system because of their absorption efficiency and their capability for resolving gamma ray energies.

The distinction between the two neutron-gamma techniques is based on the time at which the radiation detection and count is made: the NCGA measurements require the irradiation and the counting to be done simultaneously; in NAA the source and sample are separated after irradiation and the sample and

detector are brought together, after some delay period (to allow potentially interfering gamma ray emissions to die down), for the counting.

The Iddings NAA system for measuring the cement content of fresh concrete is an example of a typical prototype neutron-gamma system.[35] The device employed 140 μg of ^{252}Cf and a 5-in. diameter × 5-in. long (127 mm × 127 mm) sodium iodide scintillation crystal and determined the cement content of a 5-in. diameter × 5-in. high container of concrete. The sample was brought adjacent to the source, irradiated for 4-min, and then removed. After a 1-min radioactive decay period, the 3.09 and 4.05 Mev gamma rays (8.5-min half-life) characteristic of ^{49}Ca were counted for 4 min. In concretes containing siliceous coarse and fine aggregates, the cement is the only component containing a significant quantity of calcium. The system required initial calibration with samples having known cement contents and using the same cement and aggregates as would be used in subsequent "unknown" samples. Results indicated the Iddings NAA system could establish cement contents in typical concretes with siliceous aggregates within 10% of the actual value (at a 95% confidence level).

Other irradiation, decay, and counting period combinations and detection over other gamma ray energy levels allow other elements to be measured quantitatively. The Rhodes instrument, for example, is based on the detection and counting of the capture and activation gamma rays emitted by ^{35}Cl and ^{37}Cl, respectively, for detecting the chloride ion level in bridge deck concrete.[37] Techniques based on adding small quantities of an easily irradiated and detected element, such as indium, to concrete are considered periodically as a quality control tool: concrete samples from construction projects could be irradiated to verify their cement content.[38]

12.5.3 Advantages and Limitations

Neutron-gamma techniques have some potential for field composition measurements on both fresh and hardened concrete because of their speed, accuracy, and large sample sizes. However, no systems have been commercially developed for concrete because (1) heavy shielding is required; (2) electronics are complex and expensive for a system with a limited commercial market; and (3) interferences from elements other than the one(s) of interest force frequent recalibrations and limit accuracy with some component compositions, e.g., calcareous aggregates.

References

1. *Metals Handbook*, 8th ed., Vol. 11, *Nondestructive Inspection and Quality Control*, Boyer, H.E., Ed., American Society for Metals, Metals Park, Ohio, 1976, 114.
2. Code of Federal Regulations, Title 10, Energy, Parts 0 to 50, U.S. Government Printing Office, Washington, D.C., 1988.
3. Kerr, G.W., Regulatory control for neutron radiography, in *Practical Applications of Neutron Radiography and Gaging*, ASTM STP 586, Berger, H., Ed., American Society for Testing and Materials, Philadelphia, 1976, 93.
4. Malhotra, V.M., Testing hardened concrete: nondestructive methods, ACI Monogr. No. 9, American Concrete Institute, Detroit, 1976, 109.
5. Clear, K.C. and Hay, R.E., Time-to-Corrosion of Reinforcing Steel in Concrete Slabs, Vol. 1, Effect of Mix Design and Construction Parameters, Rep. FHWA-RD-73-32, U.S. Federal Highway Administration, Washington, D.C., 1973.
6. Standard Method of Test for Density of Plastic and Hardened Portland Cement Concrete in Place by Nuclear Methods, AASHTO Designation T 271-83(2000), *Methods of Sampling and Testing*, 21st ed., American Association of State Highway and Transportation Officials, Washington, D.C., 2001.
7. Standard Test Methods for Density of Hardened and Unhardened Concrete in Place by Nuclear Methods, ASTM Designation C 1040-93(2000) *Annual Book of ASTM Standards,* Vol. 04.02, Concrete and Aggregates, ASTM, West Conshohocken, PA, 2002.

8. Whiting, D., Seegebrecht, G.W., and Tayabji, S., Effect of degree of consolidation on some important properties of concrete, in *Consolidation of Concrete*, ACI SP-96, Gebler, S.H., Ed., American Concrete Institute, Detroit, MI, 1987, 125.
9. Tayabji, S.D. and Whiting, D., Field evaluation of concrete pavement consolidation, *Transp. Res. Rec.*, 1110, 90, 1988.
10. Schrader, E.K., Compaction of roller compacted concrete, in *Consolidation of Concrete*, ACI SP-96, Gebler, S.H., Ed., American Concrete Institute, Detroit, MI, 1987, 77.
11. Malisch, W.R., Roller compacted concrete pavements, *Concr. Construction*, 33, 13, 1988.
12. Berry, P.F., Radioisotope X- and Gamma-Ray Methods for Field Analysis of Wet Concrete Quality: Phase II — Instrument Design and Operation, Rep. ORO-3842-2, U.S. Atomic Energy Commission, Washington, D.C., 1970.
13. Mitchell, T.M., Measurement of cement content by using nuclear backscatter-and-absorption gauge, *Transp. Res. Rec.*, 692, 34, 1978.
14. Weber, W.G., Jr., Grey, R.L., and Cady, P.D., Rapid measurement of concrete pavement thickness and reinforcement location, Rep. NCHRP 168, Transportation Research Board, Washington, D.C., 1976.
15. Bhargava, J., Nuclear and radiographic methods for the study of concrete, Civil Engineering and Building Construction Series 60, ACTA Polytechnica Scandinavia Publishing Office, Stockholm, 1969.
16. Lepper, H.A., Jr. and Rodgers, R.B., Nuclear methods for determining the water content and unit weight of fresh concrete, *J. Mater.*, JMLSA, 6(4), 826, 1971.
17. Mitchell, T.M., Lee, P.L., and Eggert, G.J., The CMD: a device for continuous monitoring of the consolidation of plastic concrete, *Public Roads*, 42, 148, 1979.
18. Iddings, F.A. and Melancon, J.L., Feasibility of Development of a Nuclear Density Gage for Determining the Density of Plastic Concrete at a Particular Stratum, Rep. FHWA/LA-81/149, Louisiana Department of Transportation and Development, Baton Rouge, LA, 1981.
19. Whiting, D.A. and Tayabji, S.D., Relationship of Consolidation to Performance of Concrete Pavements, Rep. FHWA/RD-87/095, U.S. Federal Highway Administration, Washington, D.C., 1988.
20. Ozyildrim, H.C., Evaluation of a Nuclear Gage for Controlling the Consolidation of Fresh Concrete, Rep. FHWA/VA-81/41, Virginia Department of Highways and Transportation, Richmond, VA, 1981.
21. Barton, J.P., Neutron radiography — an overview, in *Practical Applications of Neutron Radiography and Gaging*, ASTM STP 586, Berger, H., Ed., American Society for Testing and Materials, Philadelphia, 1976, 5.
22. Champion, M. and Dufay, J.-C., Naissance du SCORPION: système de radioscopie télévisée par rayonnement pour l'inspection des ouvrages en béton, *Rev. Gen. Routes Eerodromes*, 589, 7, 1982.
23. Dufay, J.-C. and Piccardi, J., Scorpion: premier système de radioscopie télévisée haute énergie pour le contrôle non destrucif des ouvrages d'art en béton précontraint, *Bull Liaison Lab. P. & Ch.*, 139, 77, 1985.
24. Recommendations for radiography of concrete, BS 1981: Part 205, British Standards Institute, London, 1986.
25. Slate, F.O., Microscopic observation of cracks in concrete, with emphasis on methods developed and used at Cornell University/X-ray technique for studying cracks in concrete with emphasis on methods developed and used at Cornell University, in *Fracture Mechanics of Concrete*, Witmann, F.H., Ed., Elsevier, 1984, chap. 3, sections 1 and 2.
26. Hawkesworth, M.R., Neutron radiography in industry, in *Recent Developments in Nondestructive Testing*, The Welding Institute, Cambridge, U.K., 1978, 13.
27. Underhill, P.E. and Newacheck, R.L., Miscellaneous applications of neutron radiography, in *Practical Applications of Neutron Radiography and Gaging,* ASTM STP 586, Berger, H., Ed., American Society for Testing and Materials, Philadelphia, 1976, 252.

28. Najjar, W.S., Aderhold, H.C., and Hover, K.C., The application of neutron radiography to the study of microcracking in concrete, *Cement Concr. Aggregates*, 8(2), 103, 1986.
29. Reijonen, H. and Pihlajavaara, S.E., On the determination by neutron radiography of he thickness of the carbonated layer of concrete based upon changes in water content, *Cement Concr. Res.*, 2, 607, 1972.
30. Da-Wei, M., Chao-Zong, Z., Zhi-Ping, G., Yi-Si, L., Fu-Lin, A., Qi-Tian, M., Zhi-Min, W., and Huiz-Han, L., The application of neutron radiography to the measurement of the water permeability of concrete, in *Proc. 2nd World Conf. on Neutron Radiography*, Barton, J.P., Farny, G., Person, J.-L., and Rottger, H., Eds., D. Reidel, Boston, 1986, 255.
31. Gilboy, W.B. and Foster, J., Industrial applications of computerized tomography with X- and gamma-radiation, in *Research Techniques in Nondestructive Testing*, Vol. 6, Sharpe, R.S., Ed., Academic Press, London, 1985, 255.
32. Morgan, I.L., Ellinger, H., Klinksiek, R., and Thompson, J.N., Examination of concrete by computerized tomography, *J. Am. Concr. Inst.*, Proc. 77(1), 23, 1980.
33. Najjar, W.S., The Development and Application of Neutron Radiography to Study Concrete, with Emphasis on Microcracking, Ph.D. thesis, Cornell University, Ithaca, NY, 1987.
34. Najjar, W.S. and Hover, K.C., Modification of the X-radiography technique to include a contrast agent for identifying and studying microcracking in concrete, *Cement Conc. Aggregates*, 10(1), 15, 1988.
35. Iddings, F.A. and Arman, A., Determination of Cement Content in Soil-cement Mixtures and Concrete, Rep. FHWA-LA-LSU-NS-2, Louisiana Department of Highways, Baton Rouge, 1976.
36. Howdyshell, P.A., A Comparative Evaluation of the Neutron/Gamma and Kelly-Vail Techniques for Determining Water and Cement Content of Fresh Concrete, Rep. CERL SP-M-216, Construction Engineering Research Laboratory, Champaign, IL, 1977.
37. Rhodes, J.R., Stout, J.A., Sieberg, R.D., and Schindler, J.S., In Situ Determination of the Chloride Content of Portland Cement Concrete Bridge Decks, Rep. FHWA/RD-80/30, U.S. Federal Highway Administration, Washington, D.C., 1980.
38. Frevert, E., Zerstörungsfreie Feststellung des Zementgehaltes von Beton, in *Radiation and Isotope Techniques in Civil Engineering,* Proc. Conf. of EURISOTOP Office, Brussels, 1970, 717.

13

Short-Pulse Radar Methods

13.1 Introduction
13.2 Principle of Short-Pulse Radar
Behavior of Microwave at the Interface of Two Different Materials · Propagation of Microwave Energy through a Material
13.3 Instrumentation
13.4 Applications
Detection of Delamination in Concrete · Determination of the Degree of Hydration of Cement · Determination of Water Content in Fresh Concrete · Measurement of Thickness
13.5 Standardization of Short-Pulse Radar Methods
13.6 Conclusions

Gerardo G. Clemeña
Virginia Transportation Research Council

Short-pulse radar is a powerful scientific tool with a wide range of applications in the testing of concrete. It is gaining acceptance as a useful and rapid technique for nondestructive detection of delaminations and other types of defects in bare or overlaid reinforced concrete decks. It also shows potential for other applications — such as monitoring of cement hydration or strength development in concrete, study of the effect of various admixtures on curing of concrete, determination of water content in fresh concrete, and measurement of the thickness of concrete members.

To facilitate the understanding of these applications, the physical principles behind short-pulse radar are presented. The advantages and limitations of radar in these applications are also discussed.

13.1 Introduction

Experiments in the early 1900s proved the feasibility of transmitting electromagnetic (EM) waves through space as a beam and receiving the reflected signal from an airborne object in the path of the beam. Because of the military significance of this technology, it experienced a rapid advancement during World War II. Subsequent refinement in microwave* sources and detection circuits made it possible to accurately locate planes. These applications were made possible by the realization that different objects have their own characteristic scattering and reflection properties toward EM waves and that EM waves travel through free space with a constant speed, equivalent to that of light. Such detection systems were eventually called radar, which is an acronym for **ra**dio **d**etection **a**nd **r**anging.

Since much of this technology was also applicable to transmission of EM signals through solids, experiments were conducted in the early 1950s using radar as a tool for probing solids, such as rock and

*An EM wave which has a wavelength between about 0.3 and 30 cm, corresponding to frequencies on the order of 1 to 100 GHz.

soil. It was quickly recognized that the speed of microwave and its amplitude as a function of distance traveled in a solid could vary significantly from one material to another, and that these properties can be used to identify and profile subsurface geological features. This led to the development in the late 1960s of several types of radar systems, which were called ground-probing radars (GPR) because of their original intended applications.

Since then, GPR has been put to a variety of uses, including determining the thickness and structure of glaciers, locating ice in permafrost,[1] finding sewer lines and buried cables,[2] measuring the thickness of sea ice,[3] profiling the bottom of lakes and rivers,[4] examining the subsurface of the moon,[5] detecting buried containerized hazardous wase,[6] and measuring scouring around bridge foundations.[7]

The earliest study on the use of GPR in areas related to civil engineering, but not to concrete itself, was that reported in 1974 by Bertram et al., which dealt with the inspection of airfield for voids underneath pavements.[8] This study was followed by other studies, which included locating undermining underneath concrete sidewalks[9] and pavements.[10,11] As the following discussion will show, GPR can be used to test concrete for other purposes. Because of the nature of the microwave pulses that are employed by the radar systems used and because the applications are no longer limited to the probing of subsurface geological features, GPR is more appropriately called short-pulse radar.

13.2 Principle of Short-Pulse Radar

Short-pulse radar is the electromagnetic analog of sonic and ultrasonic pulse-echo methods. It is governed by the processes involved in the propagation of electromagnetic energy through materials of different dielectric constants.

13.2.1 Behavior of Microwave at the Interface of Two Different Materials

Consider the behavior of a beam of EM energy (such as microwave) as it strikes an interface, or boundary, between two materials of different dielectric constants (see Figure 13.1). A portion of the energy is reflected, and the remainder penetrates through the interface into the second material. The intensity of the reflected energy, *AR*, is related to the intensity of the incident energy, *AI*, by the following relationship

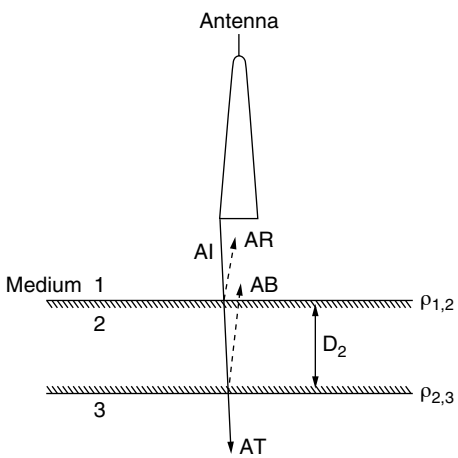

FIGURE 13.1 Propagation of EM energy through dielectric boundaries.

$$\rho_{1,2} = \frac{AR}{AI} = \frac{\eta_2 - \eta_1}{\eta_2 + \eta_1} \tag{13.1}$$

where

$\rho_{1,2}$ = the reflection coefficient at the interface, and
η_1, η_2 = the wave impedances of materials 1 and 2, respectively, in ohms.

For any nonmetallic material, such as concrete or soil, the wave impedance is given by

$$\eta = \sqrt{\frac{\mu_0}{\epsilon}} \tag{13.2}$$

where

μ_0 = the magnetic permeability of air, which is $4\pi \times 10^{-7}$ henry/meter, and
ϵ = the dielectric constant of the material in farad/meter.

(Metals are perfect reflectors of EM waves, because the wave impedances for metals are zero.) Since the wave impedance of air, η_0 is

$$\eta_0 = \sqrt{\frac{\mu_0}{\epsilon_0}} \tag{13.3}$$

and if we define the relative dielectric constant, ϵ_r, of a material as

$$\epsilon_r = \frac{\epsilon}{\epsilon_0} \tag{13.4}$$

where ϵ_0 = the dielectric constant of air, which is 8.85×10^{-12} farad/meter. Then, we may rewrite Equation 13.2 as

$$\eta = \frac{\eta_0}{\sqrt{\epsilon_r}} \tag{13.5}$$

and Equation 13.1 as

$$\rho_{1,2} = \frac{\sqrt{\epsilon_{r1}} - \sqrt{\epsilon_{r2}}}{\sqrt{\epsilon_{r1}} + \sqrt{\epsilon_{r2}}} \tag{13.6}$$

where ϵ_{ri} and ϵ_{r2} are the relative dielectric constants of materials 1 and 2, respectively.

Equation 13.6 indicates that when a beam of microwave strikes the interface between two materials, the amount of reflection ($\rho_{1,2}$) is dictated by the values of the relative dielectric constants of the two materials. If material 2 has larger relative dielectric constant than material 1, then $\rho_{1,2}$ would have a negative value, i.e., with the absolute value indicating the relative strength of the reflected energy and the negative sign indicating that the polarity of the reflected energy is opposite of that arbitrarily set for the incident energy.

13.2.2 Propagation of Microwave Energy through a Material

After penetrating the interface and into material 2, the wave propagates through material 2 with a speed, V_2, given by

$$V_2 = \frac{C}{\sqrt{\epsilon_{r2}}} \tag{13.7}$$

where C is the propagation speed of EM waves through air, which is equivalent to the speed of light, or 1 ft/ns (0.3 m/ns). As the wave propagates through material 2, its energy is attenuated as follows:

$$A = 12.863 \times 10^{-8} f \sqrt{\epsilon_{r2}} \left\{ \sqrt{1 + \tan^2 \delta} - 1 \right\}^{1/2} \tag{13.8}$$

where

A = attenuation, in decibel/meter*
f = wave frequency, in Hz

and the loss tangent (or dissipation factor) is related to σ, the electrical conductivity (in mho/meter) of the material by:

$$tan\delta = 1.80 \times 10^{10} \frac{\sigma}{f \epsilon_{r2}} \tag{13.9}$$

When the remaining microwave energy reaches another interface, a portion will be reflected back through material 2 as given by Equation 13.6. The resulting two-way transit time (t_2) of the microwave energy through material 2 can be expressed as

$$t_2 = \frac{2D_2}{V_2} = \frac{2D_2\sqrt{\epsilon_{r2}}}{C} \tag{13.10}$$

where D_2 is the thickness of material 2.

We shall discuss later how some of these basic principles serve as the basis for the various applications in which short-pulse radar is already being used routinely or has shown promise.

13.3 Instrumentation

Short-pulse radar systems are used in applications related to inspection of concrete. These radar systems operate by transmitting a single pulse that is followed by a "dead time" in which reflected signals are returned to the receiver. A basic radar system consists of a control unit, a monostatic antenna (i.e., an antenna that is used for both transmitting and receiving), an oscillographic recorder, and a power converter for DC operation (see Figure 12.2). In the inspections of sizeable concrete structures, such as bridge decks and pavements, a multi-channel instrumentation tape recorder is mandatory due to the relatively fast rate at which the inspection has to be carried out. In addition, tape-recorded radar signals are amenable to treatment by signal processing techniques that facilitate data analysis and interpretation.

In the inspection of concrete, it is desirable to use a radar antenna with relatively high resolution or short pulse width, such as 1 ns or preferably less. The two commercially available antennas that are often

*Decibel is a unit for describing the ratio of two intensities or powers; if I_1 and I_2 are two amounts of intensity, the first is said to be n decibels greater, where $n = 10 \log (I_1/I_2)$.

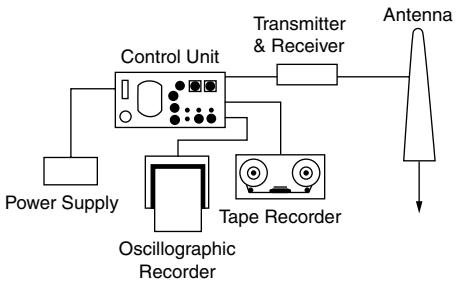

FIGURE 13.2 Components of a typical short-pulse radar system.

cited in the literature have pulse widths of approximately 1 ns. With such antennas the thinnest layers of a concrete that can be distinguished or accurately measured, if it is assumed that the concrete has a dielectric constant of 6, would be 1.2 to 2.4 in. (3.1 to 6.1 cm), depending on the radar system.

Figure 13.3 shows one of these antennas, which is referred to as a "bowtie" antenna because of the physical shape of its transmitting and receiving element within the housing. This particular antenna has a center frequency of 900 MHz and a characteristic pulse width of 1.1 ns. At 12 in. (0.3 m) away from an object, it provides a coverage of approximately 12 in. × 15 in. (0.30 m × 0.38 m). The other commercially available antenna is called a "horn" antenna, because of its outer appearance. It is usually used in a noncontact manner, as it is scanned over the surface of the concrete.

It is quite difficult to estimate a radar system's depth of penetration before the inspection is actually performed, especially the penetration into reinforced concrete, since penetration is affected by the moisture content of the concrete and the amount and type of reinforcement. However, for dry and unreinforced concrete the penetration can be as much as 24 in. (0.61 m).

In operation, a circuit within the radar control unit that is shown in Figure 13.3B generates a trigger pulse signal at a rate of 50 kHz, i.e., a pulse at every 20 s. Each trigger pulse, in turn, causes a solid-state impulse generator in the transmitting antenna to produce a pulse with a very fast rise time, which is then electrically discharged from the antenna in the transducer as a short burst of electromagnetic energy. The resulting pulse is then radiated into the material being examined.

As the radiated pulses travel through the material, different reflections will occur at interfaces that represent changing dielectric properties. Each reflected electromagnetic pulse arrives back at the receiving antenna at a different time that is governed by the depth of the corresponding reflecting interface and the dielectric constant of the intervening material (see Equation 13.10). A receiver circuit reconstructs the reflected pulses at an expanded time scale by a time-domain sampling technique. The resulting replicas of the received radar signals are amplified and further conditioned in the control unit before they are fed to an output.

The analog output can be displayed on an oscilloscope, an oscillographic recorder, or a facsimile gray-scale graphic recorder. It can also be recorded on magnetic tape for future processing or analysis. On an oscilloscope or an oscillographic recorder, the received radar signals may appear similar to the wave form illustrated in Figure 13.4A, depending on the radar system used. For the particular contact radar system from which this waveform was obtained, the received signal consists of three basic components. At the top is the transmitted pulse, or the feed-through of the transmitted pulse into the receiver section, that serves as a time reference. Immediately following the transmitted pulse is a strong surface reflection, the shape of which is indicative of the shape of the radar pulse transmitted by the antenna. Then at a later time equal to the pulse travel time from the surface to an interface and back to the antenna, the interface reflection appears. The vertical scale is the time scale, which can be calibrated by a pulse generator that produces pulses at equally spaced time durations. If the wave speed in the material is known the time scale can be converted to a corresponding depth scale.

A facsimile graphic recorder will print the portions of the waveforms that exceed a selected threshold amplitude. As the antenna is scanned across the surface, the positive and negative peaks in the waveforms

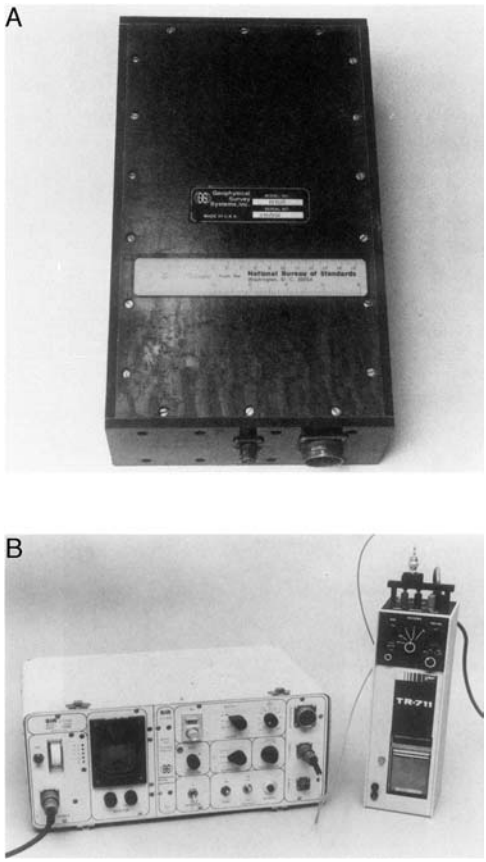

FIGURE 13.3 (A) A "bowtie" radar antenna, and (B) A control unit and an oscillographic recorder.

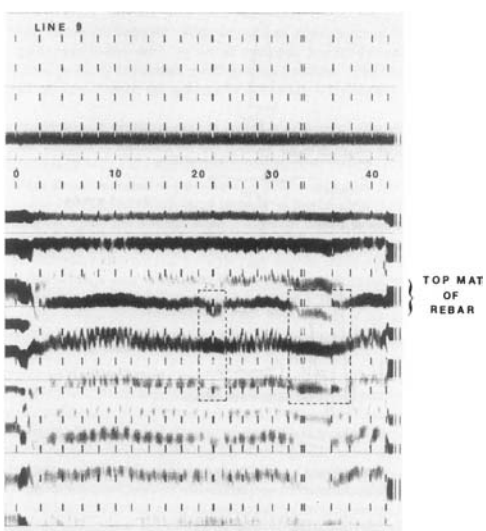

FIGURE 13.4 (A) A single waveform as seen by the receiver, and (B) a display of cascade of waveforms by facsimile graphic recorder as antenna is scanned horizontally above a subsurface interface. (With permission from Geophysical Survey Systems, Inc.)

are displayed as bands of varying gray tones, whereas the zero crossings between peaks are displayed as narrow while lines, as shown in Figure 13.4B. Notice that the main feature throughout the profile at varying times (or depths) is a group of three closely related bands across the chart, each of which represents reflection of portions of the transmitted pulse from an interface. The darkness of each band is directly proportional to the extent by which the amplitude of the corresponding peak exceeds the print threshold in the recorder. (The triple band is the characteristic of the particular radar system with which the radar signals were obtained. This characteristic is, of course, undesirable since it limits the ability of this system to discriminate neighboring interfaces that are spaced closer than the typical width of a group of bands.)

13.4 Applications

13.4.1 Detection of Delamination in Concrete

A major problem with the reinforced concrete bridge decks located in coastal areas or areas where de-icing salts are used on roadways during winter is the premature deterioration of the concrete. The intrusion of chloride from these salts into the concrete causes the embedded reinforcement to corrode, which eventually cause the concrete to crack or delaminate. Marine structures are also subjected to this type of deterioration.

The simplest method for detecting delamination in concrete involves sounding the concrete with a hammer or heavy chains, which produces a characteristic hollow sound when delamination is present. Although the method is effective, it is adversely affected by the presence of traffic noises. Since sounding is a contact method, its use requires closure of traffic lanes, which is often costly and undesirable. Because of the need for an alternative to the sounding method, the use of noncontact and nondestructive methods such as infrared thermography[12,13] and radar[14–18] have been studied.

13.4.1.1 Principle

When a beam of microwave energy is directed at a reinforced concrete slab (see Figure 13.5), a portion of the energy is reflected from the surface of the concrete, and the remaining energy penetrates this interface. The surface reflection has a negative polarity since the dielectric constant of concrete, which has been reported to range from 6 when dry to about 12 when saturated,[10] is considerably higher than that of air, which is 1. (It must be noted that the actual *in situ* relative dielectric constant of concrete, and most materials, will vary because it is affected to varying degrees by not only its water content but also by its conductivity, mineral composition, etc.)

As the remaining microwave energy propagates into the concrete, a portion of the beam will be completely reflected and scattered as it strikes the top mat of reinforcement. This reflection will also have a negative polarity, since the dielectric constant of metal is infinite compared with that of the surrounding concrete. The remaining energy will continue deeper into the concrete slab until a portion of it strikes the second mat of reinforcement and the same reflection and scattering processes occurs. Eventually, some portion of the original beam of microwave energy will reach the bottom of the concrete slab, and some of it will be reflected at the concrete/air interface to give a positive reflection signal. The remainder will penetrate through this interface and be lost from the receiving antenna.

When the concrete slab is delaminated, usually at the level of the top mat of reinforcement, there is an additional reflection from the deteriorated section. This additional reflection, usually of negative polarity, serves as an indicator of the presence of a delamination in the concrete slab.

13.4.1.2 Test Procedures

To inspect concrete members, including bridge decks, an antenna is placed with its transmitting face parallel to and at a distance from the surface of the concrete. For the inspection of bridge decks, the distance found to be most suitable is 8 to 12 in. (0.2 to 0.3 m). However, if the concrete member is relatively thick and the expected deterioration is deep of if the antenna does not have sufficient power

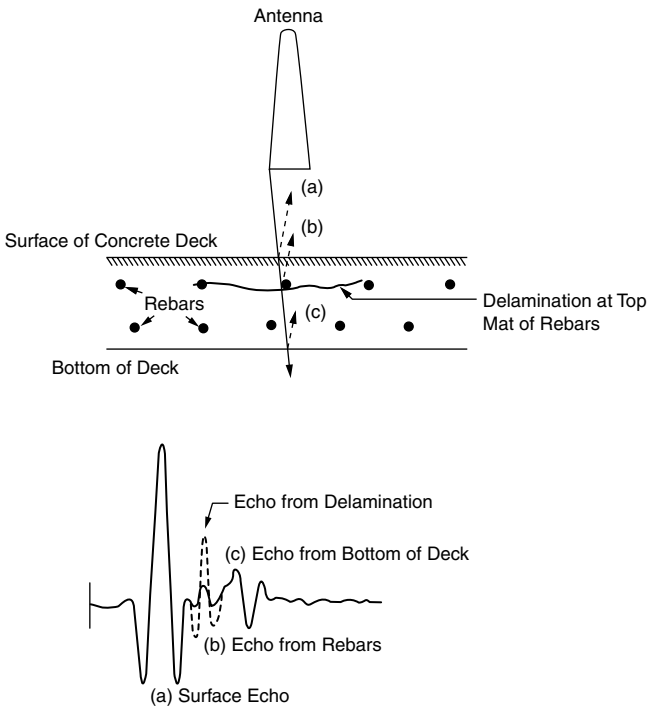

FIGURE 13.5 Radar echoes from the cross section of a reinforced concrete deck. The presence of a delamination causes additional reflection of the incident energy.

or penetration, the antenna may be placed directly above the concrete. With the various adjustments in the control unit — such as range, gain, sensitivity, etc. — set at optimum levels, the resulting radar signal is recorded with a properly calibrated oscillographic recorder. This is often called the static mode of measurement, since the antenna is stationary with respect to the concrete being inspected.

In the inspection of bridge decks, in which a relatively large concrete area has to be inspected, the antenna is mounted on the front or the rear of an inspection vehicle, which is also instrumented with a horizontal distance-measuring device. If a single antenna radar system is used, the vehicle has to make several passes over each traffic lane from one end of a deck to the other at a selected speed (usually in the range of 5 to 10 mi/h, or 8 to 16 km/h). During each pass the antenna scans a different area in the lane. The stream of radar signals are recorded continuously with an instrumentation tape recorder. With a two-antenna or a multiple-antenna radar system, a single pass may be made over each lane. (It must be emphasized that when a lane is scanned with a two-antenna radar system in a single pass only, a significant portion of the lane will be missed.) This procedure creates continuous recordings of the stream of reflections from the entire depth of the deck along the paths of the antenna. These recordings are played back at a later time for signal interpretation.

13.4.1.3 Interpretation of Radar Signals

Perhaps the most difficult aspect of the inspection is the interpretation of the radar signals for locating delaminations or any other defects in the concrete. One procedure that has been used to analyze the tape-recorded streams of signals consisted of displaying the waveforms on an oscilloscope, photographing the display with a synchronized shutterless motion picture camera, and then projecting the image in the film on a viewing screen.[15] The image, which resembles "cascading waveforms," is basically an array of closely spaced waveforms with topographic features that differentiate delaminated concrete from sound concrete.

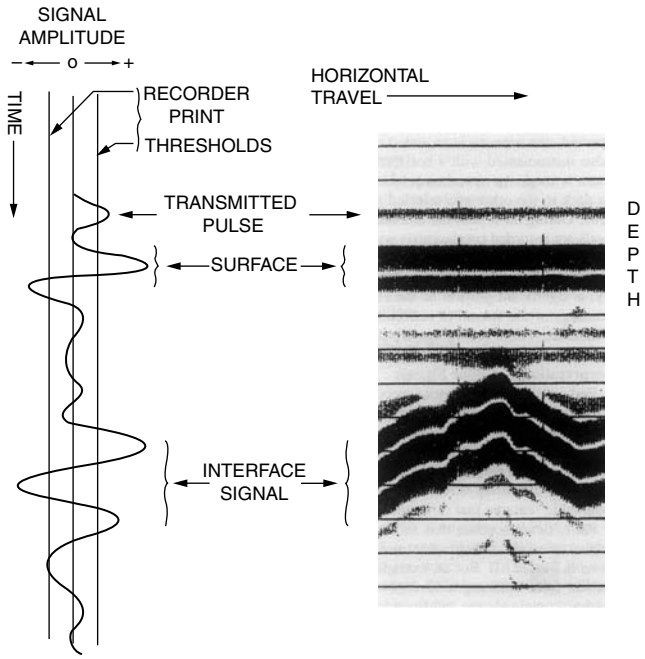

FIGURE 13.6 Radar scan of a 42-ft (14-m) section of a concrete bridge deck as displayed on a facsimile graphic recorder.

An easier procedure that achieved the same effect is to playback the stream of radar signals on a facsimile graphic recorder,[17] which provides a graphic chart similar to that shown in Figure 13.4B. For an example, Figure 13.6 shows a graphic profile of the radar signals obtained from scanning a 42-ft (14-m) section of a concrete bridge deck. This section of concrete contained two confirmed delaminations at the top mat of rebars, which were approximately 4 and 6 ft (1.2 to 1.8 m) long. The delaminations appeared, in this and other profiles, as recognizable depressions.

The signature for concrete delaminations often assumed the shape of a depression on the graphic profile (see Figure 13.7), because as the antenna moves over a delamination the major reflection at any instant would be that part of the microwave beam that is perpendicular to the nearest plane of delamination.[19] Although it has not been extensively confirmed by honeycombing, may be distinguished by other signatures or as irregularities in the graphic profiles.

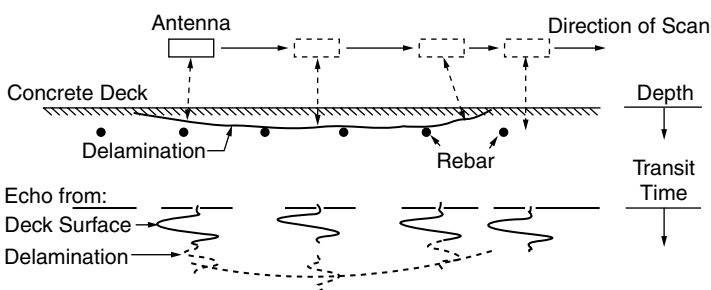

FIGURE 13.7 Development of an idealized radar signature (a depression) for a delamination in a concrete deck. (Echoes from the top mat of rebars are not shown.)

Although the use of the facsimile recorder is a simple and reasonably effective procedure, it is not completely objective. Furthermore, it can become cumbersome and time-consuming when large areas of bridge decks are involved. Consequently, computerized procedures based on simple physical models of concrete bridge decks have been developed. These models are based on predictions of how the radar waveform may be affected by such varying physical conditions as the thickness of the concrete over the top mat of rebars, salt and moisture content, spacing at the rebars, etc.[20–24]

13.4.1.4 Advantages and Limitations

13.4.1.4.1 Advantages

Radar has some advantages that are very desirable in the inspection of bridge decks and other concrete structures. Unlike infrared thermography, which has been found to be relatively effective provided proper ambient conditions exist during inspection,[12,13] radar is free of such restriction.

Since radar yields information on the structural profile across the depth of the object being tested, it is at present the only commercially available nondestructive method for the inspection of concrete bridge decks that have asphalt overlays, which constitute a significant portion of bridges. Under favorable conditions, radar can also detect localized loss of bond between the overlay and the concrete, in addition to detecting delaminations in the concrete.

Since it is unnecessary for the antenna to be in contact with a bridge deck, the disruption to traffic during radar inspection is minimal.

13.4.1.4.2 Limitations

Some efforts have been made to estimate the accuracy of radar in locating delaminations in bridge decks. Cantor et al. reported that 90% of the area that was predicted by radar to be distressed in a deck was confirmed as such as coring, and 91% of the area that was predicted to be sound concrete was confirmed.[16] In another study,[17] which involved comparison of the results of radar surveys on several bridge decks performed prior to the removal of the overlays, it was found that on the average radar detected only 80% of the existing concrete delamination, while falsely identifying 8% of the area tested as delaminated. The results from both studies indicated that radar occasionally gave an indication of delamination in what was actually sound concrete. Radar also failed to locate some of the delaminated areas, especially those that were only 1 ft (0.3 m) wide or less; partly because the strong reflections from the rebars tend to mask reflections from delaminations, which would be relatively weak when the concrete is dry.

This inaccuracy is partly due to the inherent limitation of current radar antennas to resolve consecutive reflections arriving at time intervals which are shorter than the characteristic pulse width of the antenna. Therefore, depending on the dielectric constant of the concrete, the reflection from a small delamination at the level of rebars that are relatively close to the surface may not be resolved from the reflection at the surface.

The presence of interfering signals, such as reverberations, in the radar signals from the "bowtie" antenna is a contributing factor too. Another cause of inaccuracy is the lack of a complete understanding of the relationship between different radar signatures and the various types of defects that are encountered in these concrete structures and how these signatures are affected by the condition in the structure, especially moisture content.

13.4.2 Determination of the Degree of Hydration of Cement

The durability of a concrete is greatly influenced by the degree of hydration attained by he cement. Therefore, a nondestructive method that can be used satisfactorily for determining the degree of hydration, especially for in-place concrete at an early age, can be a very useful tool. The use of microwave radar measurements for this application has not yet received wide interest, which is evidenced by the scarcity of literature on the topic.

In 1972 Rzepecka et al. reported that it was feasible to test concrete for strength during the curing process by observing changes in the dielectric property.[25] In 1982 Gorur et al. reported the use of laboratory microwave equipment and a relatively small wave-guide to monitor the curing of cement

paste.[26] In 1983 the use of a portable short-pulse radar system to monitor the hydration of concrete blocks by using reflection measurements was reported.[27]

13.4.2.1 Principle

When portland cement is mixed with water, the various components in the cement undergo chemical reactions with the water (hydration) to form the tobermorite gel and other products that provide the desirable cementing action in a concrete. As these hydration processes progress, some of the mix water is consumed by the reactions. Since "free" water has a relatively high dielectric constant of 80 in contrast to approximately 5 for chemically bound water,[28] the dielectric properties of concrete at early ages are very much influenced by the degree of hydration. Therefore, the degree of hydration can be monitored by continuous measurement of the dielectric properties of the concrete as it cures.

13.4.2.2 Test Procedures

The dielectric property of concrete that is relatively convenient to deal with and simple to measure is its reflectivity or reflection coefficient. When a microwave beam is directed at the surface of a concrete specimen, the reflectivity of the concrete is the ratio of the energy reflected from its surface to the incident energy, in accordance with Equation 13.1.

A simple and effective setup for measuring these parameters is illustrated in Figure 13.8. After a fresh batch of concrete is mixed, it is placed into a plywood box that is at least 20 in (50-cm) wide by 20 in (50 cm) long by 3 in. (7.5-cm) deep. After the concrete has been consolidated and trowelled until its surface is reasonably flat, the antenna is centered 12 in. (30 cm) above the surface of the concrete. (An open-ended 12-in. (30-cm) high box made of 1-in. (2.5-cm) thick styrofoam is a convenient means of supporting the antenna above the concrete.) The amplitude of the reflection from the surface of the fresh concrete (*AS*) can then be measured with a calibrated oscilloscope or recorded on an oscillographic recorder. Figure 13.9A shows a typical waveform recorded from a fresh concrete specimen.

To measure the amplitude of the initial microwave pulse striking the surface of the concrete (*AI*), a piece of aluminum plate that measures at least 20 in. × 20 in. (50 cm × 50 cm) is placed on the surface of the concrete. (This causes the microwave pulse that would otherwise strike the surface of the concrete to be completely reflected back to the antenna.) The amplitude *AI* is similarly measured with an oscilloscope or oscillographic recorder. An example of this waveform is shown in Figure 13.9B. The reflection coefficient, or reflectively, of the fresh concrete can be calculated from the expression

$$\rho = \frac{AS}{AI} \times \frac{AOI}{AOS} \tag{13.11}$$

where *AOS* and *AOI* are the radar signals traveling through air from the transmitting to the receiving antenna during the measurements of *AS* and *AI*, respectively. These parameters serve as convenient means to correct for electronic drifts in the radar system.

If desired, it is also possible to follow the hydration of the cement during curing by measuring the amplitude of the reflection from the bottom of the concrete. However, owing to the high reflectivity at

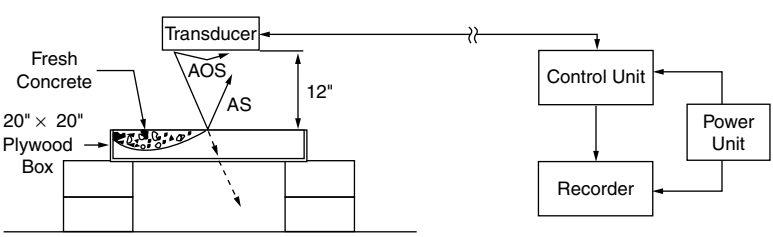

FIGURE 13.8 Measurement of the reflection of microwave pulses from the surface of fresh concrete. (The thickness of the specimen was 3.0 in. [7.5 cm].)

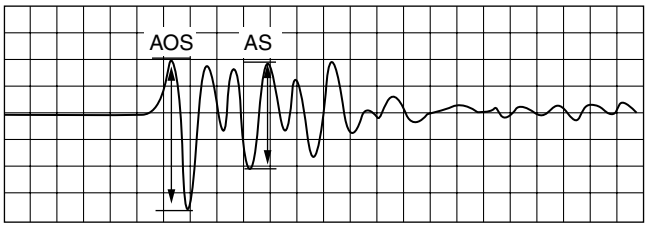

A

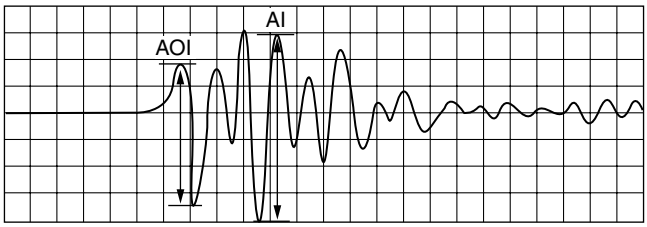

B

FIGURE 13.9 Waveforms of reflections from: (A) a concrete specimen (*AS*), and (B) an aluminum plate resting on top of the concrete (*AI*).

the surface of concrete and their high attenuation during the first few days after their casting, this reflection would generally be too weak to observe during that period. This can be remedied by placing aluminum foil in the bottom of the wooden box before placing the concrete.

These measurements are repeated as often as necessary and for as long as the change in the dielectric properties if the concrete is significant and of interest. From the measured reflectivity of the concrete surface at any age, the relative dielectric constant of the concrete (ϵ_{r2}) can be calculated using Equation 13.6, which becomes

$$\rho = \frac{1 - \sqrt{\epsilon_{r2}}}{1 + \sqrt{\epsilon_{r2}}} \tag{13.12}$$

since ϵ_{r1} equals 1.

If there is appreciable bleeding in the concrete, the measured reflectivity may represent the free water content in the surface layer of the fresh concrete more than the free water in the bulk of the concrete. In such cases, the dielectric constant of the entire thickness of the concrete specimen can be indirectly measured, as indicated in Equation 13.10, by using the two-way transit time of the reflection from the bottom of the specimen. Unfortunately, if the water-cement ratio of the concrete is high, or the concrete is too thick, or there is too much reinforcement, this reflection may be too weak to detect, especially during the first few days after the placing of the concrete. In such cases, aluminum foil or a metal plate can be placed at the bottom of the concrete to enhance the reflection, or the antenna can be placed directly on top of the concrete,[27] or an antenna with more penetration but less resolution can be used.

13.4.2.3 Example Test Data

Radar measurements can be utilized to compare concrete made with different types of cement. For example, Figure 13.10 shows the changes in the observed reflectivities and relative dielectric constants of two different concrete mixtures, starting 2 h after their mixing and continuing through the first 28 days.[29] These concrete mixtures were made with the same aggregates and water-cement ratio (0.48) but

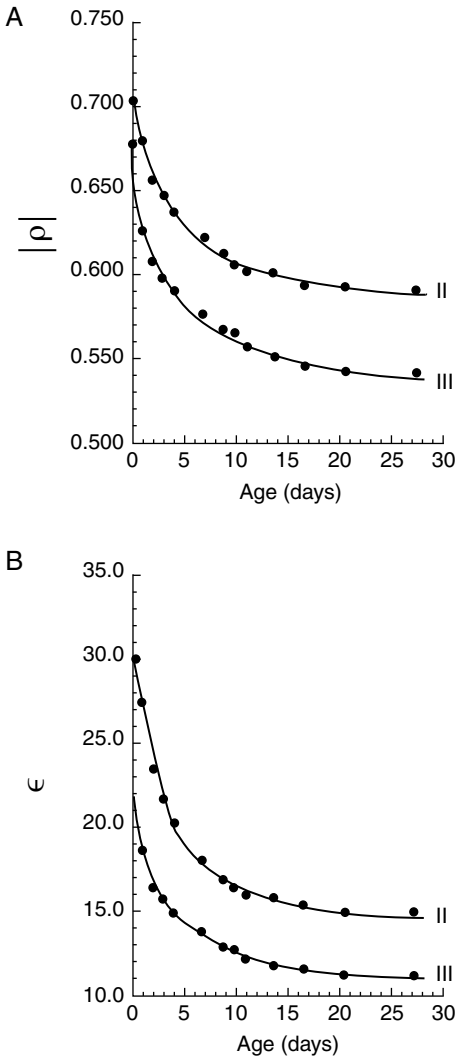

FIGURE 13.10 Influence of age on the reflectivity and the dielectric constant of concrete mixtures containing Type II and Type III cements.

with different types of cement (Type II and Type III). The concrete containing Type III cement exhibited a faster decrease in reflectivity and relative dielectric constant compared with the concrete containing Type II cement. This difference is a manifestation of the higher content of relatively fast reacting tricalcium silicate and tricalcium aluminate in Type III cement.

Since the dielectric properties and strength of a concrete are both affected by the same hydration processes, these properties can be related, if desired. Figure 13.11 shows a correlation of the compressive strength of each of the above two concrete mixtures, as measured by testing cylinders, which were prepared from these mixtures, at 1, 2, 4, 7, 10, 14, and 28 days after casting, with their corresponding reflectivities at the same ages. It can be seen that there was a very strong linear correlation between these two properties, with a correlation coefficient of 0.97 for all the data combined.

13.4.2.4 Advantages and Limitations

The standard deviation associated with the measurement of reflectivity, based on triplicate waveforms that were typically recorded during each measurement, was estimated to be approximately ±0.009. The

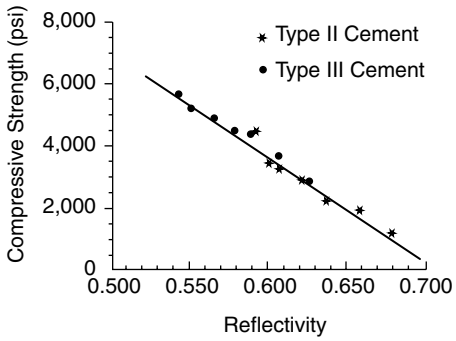

FIGURE 13.11 Correlation between the reflectivity and compressive strength of two concrete mixtures with the same w/c of 0.48 but different types of cement. (*Note:* 145 psi = 1 MPa).

repeatability of results is sensitive to fluctuation in the measurement setup, especially the position of the antenna with respect to the concrete surface.

There is indication that the effect of admixtures and pozzolans on the hydration rate of a concrete may also be manifested in the reflectivity of the concrete surface; therefore, it may be possible to use radar to supplement other techniques in the study of these materials.

13.4.3 Determination of Water Content in Fresh Concrete

Control of proper water and cement content during concrete batching operations is very important, since these factors have great influence on the durability of the concrete. Radar has recently been studied as a rapid and yet reasonably accurate method for determining the water content of fresh concrete mixtures.[30]

13.4.3.1 Principle

One of the bases for this potential application of radar is the very same principle involved in the monitoring of cement hydration in concrete. Figure 13.12 shows the observed amplitudes of the reflection from the bottom of three concrete specimens made with the same materials but of different water-cement ratios.[27,29] These data indicate that the dielectric property of a concrete is dependent on the amount of unreacted water in the concrete, which in turn is dependent on not only its age but also the amount of mixing water used.

The other basis for this potential application is the dependency of the attenuation of microwave pulses, during its travels through fresh concrete, on the relative dielectric constant of the concrete, as expressed in Equation 13.8. Since the dielectric constant and, therefore, the tendency of a concrete to attenuate microwave pulses is directly proportional to its water content, the ability of the concrete to transmit the microwave pulses must be inversely proportional to its water content.

Therefore, the water content of fresh concrete mixtures may be indirectly determined through measurement of either their microwave reflectivity or their transmission properties.

13.4.3.2 Test Procedures

To measure water content through measurement of reflectivity, the experimental setup discussed earlier and illustrated in Figure 13.8 can be used. For measurement of transmittance, however, a setup such as that illustrated in Figure 13.13, which utilized two identical antennas, has been used.[30] In this setup, one antenna functioned only as a transmitter while the other functioned only as a receiver; this arrangement was made possible through the use of a manufacturer-supplied electronic circuit, "breakout box," that interferes with the normal dual functions of each antenna.

Figure 13.14 shows a typical recorded waveform of the microwave energy (*AT*) that had reached the receiver after propagating through a layer of fresh concrete. The transmission property of the fresh

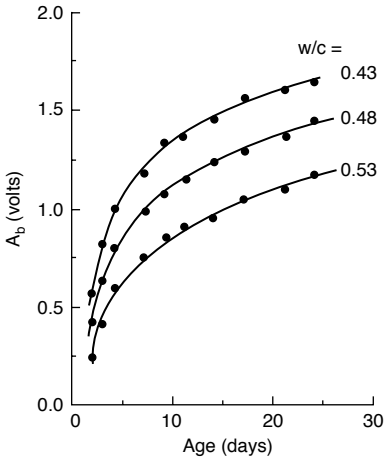

FIGURE 13.12 Influence of age and *w/c* on the intensity of reflection from the bottom of an 8-in. (20.3-cm) thick concrete specimen.

concrete was then expressed in terms of a quantity (T), which is defined as the ratio of AT to the amplitude of the initial microwave pulses striking the surface of the concrete (AI), i.e.,

$$T = \frac{AT}{AI} \tag{13.13}$$

Immediately after AT was measured, the receiving antenna was disconnected to allow the transmitting antenna to resume its normal dual function and the measurement of AI according to the procedure that has been described earlier.

Since the potential benefit of this application is to allow for timely adjustment of the water content of any batch of fresh concrete mixture, if necessary, the measurement of either reflectivity or transmission should be performed as soon as the materials are uniformly mixed.

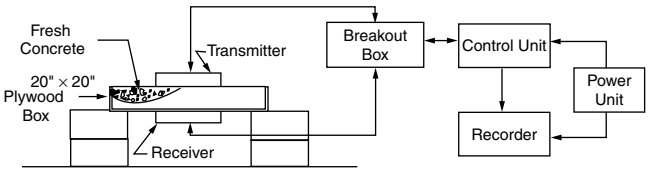

FIGURE 13.13 Measurement of transmission through a layer of freshly mixed concrete.

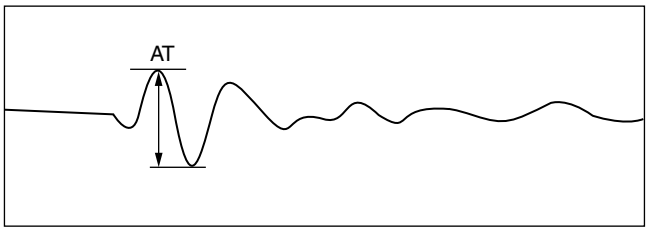

FIGURE 13.14 Waveform of transmission through a layer of fresh concrete.

13.4.3.3 Example Test Data

Figure 13.15 shows a plot of measured reflectivities of a series of four air-entrained concrete mixtures vs. their known water-cement ratios.[30] These mixtures contained the same amounts of fine and coarse aggregates, cement, and air-entraining agent; the only variable is the amount of mix water, or water-cement ratio, which ranged from 0.45 to 0.60. (Since the amount of cement used in these mixtures was constant, the water contents of these mixtures were expressed in terms of water-cement ratios.) It is evident that there is a reasonably good linear correlation between these parameters.

If instead of reflectivity, the measured transmission through these same concrete mixtures was correlated with their water-cement ratio (see Figure 13.16), a strong inverse linear relationship between these parameters was obtained.[30]

13.4.3.4 Advantages and Limitations

The use of radar to determine the water content of fresh concrete is a relatively new application and therefore has not been studied extensively yet. In perhaps the only study conducted to date, it was reported that, for the procedure used, the error associated with the measurement of water-cement ratio by the reflectivity method was estimated to be less than ±0.038 (at a 95% confidence level); and the standard deviation was ±0.011.[30] Although this degree of accuracy does not compare favorably to those reported for the modified Kelly-Vail method and the microwave-oven drying method,[31] which have received extensive study in the last several years, the method has merit and should be studied further to improve its reliability.

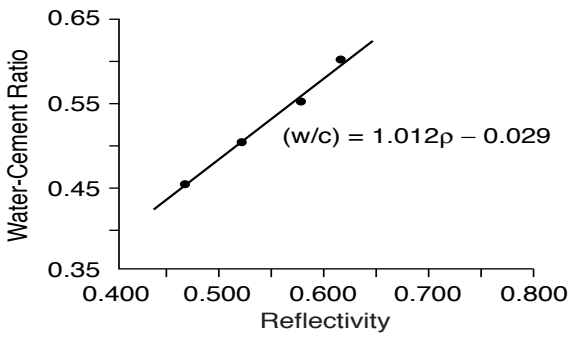

FIGURE 13.15 Relationship between reflectivity and *w/c* for concrete mixtures (containing Type II cement, granite aggregates, air-entraining agent, and water reducer) at about 3 min after mixing.

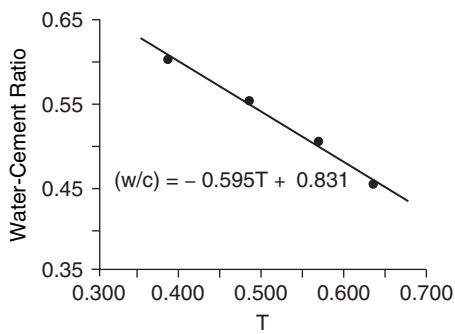

FIGURE 13.16 Relationship between transmission value and *w/c* for concrete mixtures (containing Type II cement, granite aggregates, air-entraining agent, and water reducer) at about 3 min after mixing.

The error that was associated with the use of the transmission method to measure water-cement ratio was estimated to be ±0.024, at a 95% confidence level; with a standard deviation of ±0.005.[30] This accuracy is better than that corresponding to the reflectivity method and at least equal to that of the modified Kelly-Vail method.

A disadvantage with either of these radar methods is that a calibration line is probably necessary for every combination of materials used, because it appears that the type of cement, aggregate, and additive used can influence the parameters in the relationship between water content and reflectivity or transmission value.

The potential advantages of these radar methods are their speed and simplicity. The necessary handling of the fresh concrete sample prior to the use of either procedures is minimal, since it involves only transferring sufficient amount of the fresh concrete into a suitable sample container and consolidation of the concrete. After a calibration line appropriate to the selected concrete materials has been established, the actual measurement of either reflectivity or transmission usually requires less than 30 s, which is faster than even the fastest of the two nonradar methods, which requires at least 15 min.

Another potential advantage is that these methods are amenable to automation. In a large capacity ready-mix plant, the procedure could conceivably be setup in such a manner that either the reflectivity or the transmission of fresh concrete could be measured automatically and continuously with the aid of microprocessors along a production line.

13.4.4 Measurement of Thickness

In the construction of concrete pavements, strict compliance with the specified minimum slab thickness is important in ensuring long service life for the new pavements. To ensure compliance, cores are extracted at specified intervals in each newly constructed lane for direct measurement. In addition to being time consuming and costly, this destructive inspection method creates undesirable discontinuities in the pavements. Radar has been tested as a possible alternative for this application.[32]

13.4.4.1 Principle

According to Equation 13.10, assuming that the dielectric constant of a concrete slab is uniform and known, the two-way transit time of microwave pulses through the concrete is directly proportional to the thickness of slab.

13.4.4.2 Test Procedure

There are two ways by which this relationship may be applied in the nondestructive measurement of concrete slab thickness. First, the relative dielectric constant of the concrete at each test location can be calculated from the measured surface reflectivity. Then, the thickness of the slab at that location can be calculated from this relative dielectric constant and the measured two-way transit time.

The second approach involves the establishment of a suitable calibration line to relate slab thickness and the two-way transit time. From a review of the reflection waveforms recorded for all randomly selected test locations, several locations that appear to provide a suitable range of measured two-way transit times are selected for direct measurements of slab thickness by coring or any other preferred method. Then the measured slab thicknesses and transit times at these selected locations are correlated through a linear regression analysis to establish the calibration line from which the thickness of the slab at all other test locations may be estimated.

The first approach is susceptible to error, because the relative dielectric constant as determined from the surface reflectivity may not be representative of the entire thickness of the concrete. The second approach is susceptible to error too, because it assumes that the relative dielectric constant of the concrete is uniform at all test locations.

13.4.4.3 Example Test Data

Figure 13.17 shows the reflection waveform recorded for one of 51 locations in a continuously reinforced concrete pavement where the use of radar to determine slab thickness was studied.[32] This waveform consists of the reflections from the surface of the pavement, from the rebars, and from the bottom of the slab, and sandwiched between the latter two reflections is the reverberation from the rebars.

In the investigation, a calibration line was established from the cores and radar data at seven locations selected from the 51 locations. Using the resulting calibration line, the thickness of the concrete slab at each of the remaining locations was estimated from its respective measured transit times. Figure 13.18 shows that these estimates compare favorably with the lengths of the cores, with absolute errors ranging from 0.0 to 0.9 in. (0.0 to 2.25 cm). This presence of a range of errors likely reflects the fallacy of the assumption, that the concrete at all locations have the same relative dielectric constant, which is inherent in this procedure. Further, some of these errors exceeded the ±0.25 in. (0.63 cm) that is considered acceptable for compliance testing.

13.4.4.4 Advantages and Limitations

The success of thickness measurement using radar depends on a reasonably detectable reflection from the backside (or the bottom) of the concrete member (or slab), because this allows for the precise identification of the reflection and, therefore, the accurate measurement of the transit time. Conditions that would prevent the reflection from being precisely detected include the presence of reinforcement, relatively high attenuation of the microwave pulses by the concrete, insufficient difference between the relative dielectric constants of the concrete and the subbase, and slabs that are too thick.

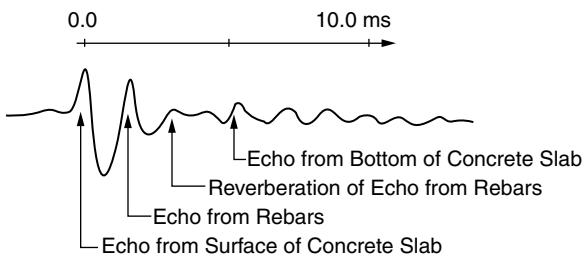

FIGURE 13.17 Radar echoes recorded at a test location on a continuously reinforced concrete pavement.

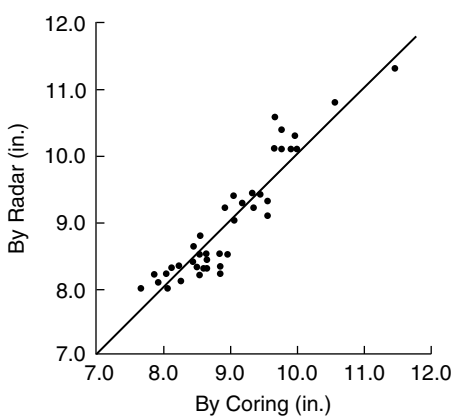

FIGURE 13.18 Comparison between concrete slab thickness as determined by coring and by radar using a calibration line. (*Note:* 1 in. = 25.4 mm.)

For some pavements, it is likely that there may be only small differences between the relative dielectric constants of the concrete and the subbase materials, so that this reflection would be very weak and difficult to identify, particularly when the concrete has cured long enough that its dielectric constant has approached that of the subbase. Consequently, prior to an actual inspection, it is difficult to predict how precise the radar will be in measuring the thickness of a particular pavement.

It is possible that the reflection may be more pronounced, if the measurement is made during the period between 3 to 10 days after the concrete is placed — when its relative dielectric constant is still relatively high (see Figure 13.10) and its ability to attenuate microwave pulses is probably low enough.

13.5 Standardization of Short-Pulse Radar Methods

ASTM Committee D04 on Road and Paving Materials has adopted two standard test methods on the use of short-pulse (or ground-penetrating) radar for pavement and bridge deck evaluation. One method, ASTM D 4748, was originally adopted in 1987 and is used to determine the thickness of "bound" pavement layers.[33] Bound pavement layers are the upper layers of a pavement system and consist of materials such as portland cement concrete or bituminous concrete. The procedure is based on the principles discussed in Section 13.4.4. The significance and use statement of the 1998 version of the test method is as follows:

3.1 This test method permits accurate and nondestructive thickness determination of bound pavement layers. As such, this test method is widely applicable as a pavement system assessment technique.

3.2 Although this test method, under the right conditions, can be highly accurate as a layer-thickness indicator, consistently reliable interpretation of the received radar signal to determine layer thicknesses can be performed only by an experienced data analyst. Such experience can be gained through use of the system and through training courses supplied by various equipment manufacturers or consulting companies. Alternatively, the operator may wish to use computer software to automatically track the layer boundaries and layer thickness, where applicable.

The other method, ASTM D 6087, was originally adopted in 1997 and is used to detect delaminations in concrete bridge decks covered with asphaltic concrete wearing surfaces.[34] The principles involved in the use of short-pulse radar to detect delaminations were covered in Section 13.4.1. The test method recommends the attenuation technique for analyzing recorded signals. In this approach, the amplitude of the echo signal from the bottom of the slab is used as an indicator of the presence of a delamination. When the bottom echo amplitude is less than a specified fraction of the maximum amplitude from all scans, a delamination is likely to be present. The significance and use section of the 2003 version of the test method is as follows:

3.1 This test method provides information on the condition of concrete bridge decks overlaid with asphaltic concrete without necessitating removal of the overlay, or other destructive procedures.

3.2 A systematic approach to bridge deck rehabilitation requires considerable data on the condition of the decks. In the past, data has been collected using the traditional methods of visual inspection supplemented by physical testing and coring. Such methods have proven to be tedious, expensive and of limited accuracy. Consequently, radar provides a mechanism to rapidly survey bridges in a noncontact, nondestructive manner.

3.3 Information on the condition of asphalt-covered, concrete bridge decks is needed to estimate bridge deck condition for maintenance and rehabilitation, to provide cost-effective information necessary for rehabilitation contracts.

13.6 Conclusions

Short-pulse radar is proving to be a powerful scientific tool with a wide range of applications, including the nondestructive detection of delaminations in bare or overlaid reinforced concrete bridge decks. Its

accuracy and ability to detect other types of defects existing in concrete bridge decks and other structures need improvement, and it is believed that this can be achieved through improvements in the resolution of the antenna and by increasing the understanding of the various radar signatures encountered in these structures.

In addition to the detection of delaminations in concrete, radar shows potential for other applications such as the monitoring of cement hydration or strength development in concrete, the study of the effect of various admixtures and additives on concrete, the rapid determination of water content in fresh concrete, the measurement of the thickness of concrete members, and the locating of rebars. These potential applications have not yet received wide attention, as is evident in the scarcity of literature.

References

1. Bertram, C.L., Campbell, K.J., and Sandler, S.S., Locating large masses of ground ice with an impulse radar system, in *Proc. 8th Int. Symp. on Remote Sensing*, Willow Run Laboratory, University of Michigan, Ann Arbor, October 1972.
2. Morey, R.M. and Harrington, W.S., Jr., Feasibility Study of Electromagnetic Subsurface Profiling, Rep. EPA-R2-72-082. U.S. Environmental Protection Agency, Washington, D.C., October 1972.
3. Campbell, K.J. and Orange, A.S., A continuous profile of sea ice and freshwater ice thickness by impulse radar, *Polar Rec.*, 17, 31, 1974.
4. Morey, R.M., Applications of downward looking impulse radar, in *Proc. 13th Annu. Canadian Hydrographic Conf.*, Canada Centre for Inland Waters, Burlington, Ontario, Canada, March 1974.
5. Porcello, L.J., The Apollo lunar sounder radar system, in *Proc. Inst. Electrical and Electronic Engineers*, 62, 769, 1974.
6. Lord, A.E. and Koerner, R.M., Nondestructive Testing Techniques to Detect Contained Subsurface Hazardous Waste, Rep. No. EPA/600/2-87/078, Drexel University, Philadelphia, September 1987.
7. Haeni, P. and Trent, R.E., Measuring scour with ground-penetrating radar, sonar, and seismic geographical methods, presented at the 67th Annu. Meet. of the Transportation Research Board, Washington, D.C., January 11 to 14, 1988.
8. Bertram, C.L., Morey, R.M., and Sander, S.S., Feasibility Study for Rapid Evaluation of Airfield Pavements, Rep. No. AFWL-TR-71-178, U.S. Air Force Weapons Laboratory, June 1974.
9. Clemeña, G.G. and McGhee, K.H., Applicability of radar subsurface profiling in estimating sidewalk undermining, *Transp. Res. Rec.*, 752, 21, 1980.
10. Kovacs, A. and Morey, R.M., Detection of Cavities Under Concrete Pavement, CRREL Rep. 82-18, U.S. Army Cold Regions Research and Engineering Laboratory, Hanover, NH, July 1983.
11. Clemeña, G.G., Sprinkle, M.M., and Long, R.R., Jr., Use of ground-penetrating radar for detecting voids under a jointed concrete pavement, *Transp. Res. Rec.*, 1109, 1, 1987.
12. Clemeña, G.G. and Mickeel, W.T., Jr., Detection of delamination in bridge decks with infrared thermography, *Transp. Res. Rec.*, 664, 180, 1978.
13. Holt, F.B. and Manning, D.G., Detecting delamination in concrete bridge decks, *Concr. Int.*, 2, 34, 1980.
14. Alongi, A.V., Radar Examination of Condition of Two Interstate Highway Bridges, Penetradar Corp., Niagara Falls, N.Y.
15. Cantor, T. and Kneeter, C., Radar and acoustic emission applied to the study of bridge decks, suspension cables and masonry tunnel, *Transp. Res. Rec.*, 676, 27, 1978.
16. Cantor, T. and Kneeter, C., Radar as applied to evaluation of bridge decks, *Transp. Res. Rec.*, 852, 37, 1982.
17. Clemeña, G.G., Nondestructive inspection of overlaid bridge decks with ground-penetrating radar, *Transp. Res. Rec.*, 899, 21, 1983.
18. Manning, D. and Holt, F., Detecting deterioration in asphalt-covered bridge decks, *Transp. Res. Rec.*, 899, 10, 1983.

19. Clemeña, G.G., Survey of Bridge Decks with Ground-Penetrating Radar — A Manual, Rep. VTRC 86-R3, Virginia Transportation Research Council, Charlottesville, VA, July 1985.
20. Alongi, A., Cantor, T., Kneeter, C., and Alongi, A., Jr., Concrete evaluation by radar — theoretical analysis, *Transp. Res. Rec.*, 853, 31, 1982.
21. Ulriksen, C.P.F., Application of Impulse Radar to Civil Engineering, Doctoral Thesis, Lund University, Lund, Sweden, 1982.
22. Chung, T., Carter, C.R., Manning, D.G., and holt, F.B., Signature Analysis of Radar Waveforms Taken on Asphalt Covered Bridge Decks, Rep. ME-84-01, Ontario Ministry of Transportation and Communications, Ontario, Canada, June 1984.
23. Maser, K.R., Detection of progressive deterioration in bridge decks using ground-penetrating radar, in *Proc. Experimental Assessment of Performance of Bridges*, ASCE Convention, Boston, MA, October 1986.
24. Alongi, A., Jr., personal communication, 1987.
25. Rzepecka, M.A., Hamid, A.K., and Soliman, A.H., Monitoring of concrete curing process by microwave terminal measurements, IEEE Trans. on Industrial Electronics and Control Instrumentation, 19, 120, 1972.
26. Gorur, K., Smit, M.K., and Witman, F.H., Microwave study of hydrating cement paste at early age, *Cement Concr. Res.*, 12, 447, 1982.
27. Clemeña, G.G., Microwave Reflection Measurements of the Dielectric Properties of Concrete, Rep. VTRC-84-R10, Virginia Transportation Research Council, Charlottesville, VA, 1983.
28. Hasted, J.B., The dielectric properties of water, *Prog. Dielectrics*, 3, 101, 1961.
29. Clemeña, G.G., unpublished data, 1987.
30. Clemeña, G.G., Determining Water Content of Fresh Concrete by Microwave Reflection or Transmission Measurement, Rep. VTRC-88-R3, Virginia Transportation Research Council, Charlottesville, VA, 1987.
31. Head, W.J., Phillippi, P.A., Howdyshell, P.A., and Lawrence, D., Evaluation of selected procedures for the rapid analysis of fresh concrete, *Cement Concr. Aggregates*, 5, 88, 1983.
32. Clemeña, G.G. and Steele, R.E., Inspection of the Thickness of In-Place Concrete with Microwave Reflection Measurements, Rep. VTRC-88-R16, Virginia Transportation Research Council, Charlottesville, VA, 1988.
33. ASTM D 4748-98, Standard Test Method for Determining the Thickness of Bound Pavement Layers Using Short-Pulse Radar, *Annual Book of ASTM Standards*, Vol. 04.03, ASTM, West Conshohocken, PA, 2003.
34. ASTM D 6087-03, Standard Test Method for Evaluating Asphalt-Covered Concrete Bridge Decks Using Ground Penetrating Radar, *Annual Book of ASTM Standards*, Vol. 04.03, ASTM, West Conshohocken, PA, 2003.

14

Stress Wave Propagation Methods*

14.1 Introduction
14.2 Wave Types
Wave Types • Wave Speed • Reflection and Refraction
14.3 Test Methods
Pulse-Echo • Impact-Echo • Impulse-Response Method • Spectral Analysis of Surface Waves Method
14.4 Summary

Nicholas J. Carino
National Institute of Standards and Technology

This chapter presents a review of nondestructive testing methods based on the use of stress waves. The pulse-echo, impact-echo, impulse-response, and spectral analysis of surface waves techniques for evaluation of concrete are discussed. The principles, test procedures, signal processing, and representative applications of each method are presented. It is shown that the common feature of the methods is that inferences about internal conditions of concrete structures are made based on the effect that the structure has on the propagation of stress waves. The methods differ in the source of the stress waves, the testing configuration, instrumentation, the characteristics of the measured response, and the signal processing techniques that are used. These differences make each method particularly suitable for specific applications. This chapter supplements Chapter 8 on the ultrasonic pulse velocity method.

14.1 Introduction

Except for visual inspection, the use of acoustic methods is the oldest form of nondestructive testing. Striking an object with a hammer and listening to the "ringing" sound is a common way of detecting the presence of internal voids, cracks, or delaminations. The method is subjective, as it depends on the experience of the operator, and it is limited to detecting near-surface defects. Despite these inherent limitations, sounding is a useful method for detecting near-surface delaminations, and a standard practice is available.[1] The sounding technique is not discussed any further in this chapter.

In 1929, Solokov in the then U.S.S.R. first suggested the use of ultrasonic waves to find defects in metal objects.[2] It was, however, not until World War II spurred the development of sophisticated electronic instrumentation in the 1940s that significant progress was made. Ultrasonic** pulse-echo flaw detectors were first introduced in 1942 by Firestone of the University of Michigan and, independently, by Sproule

*Contribution of the National Institute of Standards and Technology; not subject to copyright in the United States. This chapter is a revision of the chapter co-authored with Mary J. Sansalone in the previous edition of this handbook.

**_Ultrasonic_ refers to sound waves with frequencies above the audible range, which is generally taken to be about 20 kHz. Most ultrasonic pulse-echo devices operate at 1 MHz or greater.

in England. Since that time, ultrasonic pulse-echo testing of metals, plastics, and other homogeneous materials has developed into an efficient, reliable, and versatile nondestructive test method.[3]

The development of echo-techniques and equipment for ultrasonic evaluation of less ideal materials, such as concrete, has been hindered by the difficulties inherent in obtaining and interpreting a signal record from a heterogeneous material. Because high-frequency (1 MHz or greater) stress pulses cannot penetrate far into concrete, none of the commercially available transducers is satisfactory for pulse-echo testing of concrete. An alternative approach is to generate low-frequency stress waves using mechanical impact. Several techniques have been developed for testing concrete, and are being used in field inspections. Standard test methods have been adopted for some of these methods, as discussed below.

This chapter begins with a review the basic principles of stress wave propagation in solids. Next, the methods that are used for evaluation of concrete structures are discussed. Test procedures, signal processing, and representative applications of each method are presented.

14.2 Basic Principles

This section provides background information on elastic wave propagation in solids, which is applicable to the techniques to be discussed. It supplements the discussion in Chapter 8 on the ultrasonic pulse velocity method.

14.2.1 Wave Types

When a stress is applied suddenly to the surface of a solid, the disturbance that is generated travels through the solid as stress waves, which are analogous to sound waves traveling through air. There are three primary modes of stress wave propagation through isotropic, elastic media: dilatational, distortional, and Rayleigh waves. Dilatational and distortional waves, which are commonly referred to as compression and shear waves, or P- and S-waves, are characterized by the direction of particle motion with respect to the propagation direction of the disturbance, or the wave front. In a P-wave, particle motion is parallel to the propagation direction; in the S-wave, particle motion is perpendicular to the propagation direction. A P-wave is associated with normal stress, while an S-wave is associated with shearing stress. P-waves can propagate in all types of media; S-waves can propagate only in media with shear stiffness, that is, in solids. A Rayleigh wave, also called a surface wave or R-wave, propagates along the surface of a solid, and particle motion is retrograde elliptical.

The wave front defines the leading edge of a stress wave as it propagates through a medium. There are three idealized types of wave fronts: planar, spherical, and cylindrical. The shapes of the P-, S-, and R-wave fronts depend on the characteristics of the source used to generate the waves. For example, when the stress waves are generated by impact at a point on the surface of a solid, the resulting P- and S-waves travel into the solid along hemispherical wave fronts, and the R-wave travels away from the impact point along a cylindrical wave front.

14.2.2 Wave Speed

In most applications of stress wave propagation, the input is a pulse of finite duration and the resulting disturbance propagates through the solid as transient waves. The propagation of transient stress waves through a heterogeneous bounded solid, such as a structural concrete member, is a complex phenomenon. A basic understanding of the relationship between the physical properties of a material and the wave speed can be acquired from the theory of wave propagation in infinite, isotropic, elastic media.[4]

In infinite elastic solids, the P-wave speed, C_p, is a function of Young's modulus of elasticity, E, the density, ρ, and Poisson's ratio, ν:

$$C_p = \sqrt{\frac{E(1-\nu)}{\rho(1+\nu)(1-2\nu)}} \tag{14.1}$$

In bounded solids, such as thin plates or long rods, P-wave speed can vary depending on the lateral dimensions of the solid relative to the component wavelength(s) of the propagating wave. For rodlike structures, such as piles, P-wave speed is independent of Poisson's ratio if the rod diameter is much less than the wavelength(s) of the propagating wave.[5] In this case, the P-wave speed is called the *bar-wave speed*, C_b, and is given by the following equation:

$$C_b = \sqrt{\frac{E}{\rho}} \tag{14.2}$$

For a Poisson's ratio of 0.2, a typical value for concrete, the P-wave speed in an infinite solid is 5% higher than the bar-wave speed in a long thin rod.

The S-wave speed, C_s, in an infinite solid is given by the following equation:

$$C_s = \sqrt{\frac{G}{\rho}} \tag{14.3}$$

where

G = shear modulus of elasticity = $E/2(1+\nu)$

A useful parameter is the ratio, α, of the S- to P-wave speeds:

$$\alpha = \frac{C_s}{C_p} = \sqrt{\frac{(1-2\nu)}{2(1-\nu)}} \tag{14.4}$$

For a Poisson's ratio of 0.2, α is 0.61.

R-waves propagate at a speed, C_R, that is given by the following approximate formula:[6]

$$C_R = \frac{0.87+1.12\nu}{1+\nu} C_s \tag{14.5}$$

For Poisson's ratio of 0.2, the R-wave speed is 92% of the S-wave speed, or 56% of the P-wave speed.

14.2.3 Reflection and Refraction

When a P- or S-wave front is incident on a boundary between dissimilar media, "specular" reflection occurs. (The term *specular reflection* is used since the reflection of stress waves is similar to the reflection of light by a mirror.) As shown in Figure 14.1A, stress waves can be thought of as propagating along ray paths. The geometry of ray reflection is analogous to that of light rays, that is, the angle of reflection of any ray is equal to the angle of incidence, θ, for that ray.

At a boundary between two different media only a portion of a stress wave is reflected. The remainder penetrates into the underlying medium (wave refraction). The angle of refraction, β, is a function of the angle of incidence, θ, and the ratio of wave speeds, C_2/C_1, in the different media, and is given by Snell's law:

$$\sin\beta = \frac{C_2}{C_1}\sin\theta \tag{14.6}$$

Unlike light waves, however, stress waves can change their mode of propagation when striking a boundary at an oblique angle. Depending on the angle of incidence, a P-wave can be partially reflected as both P- and S-waves and can be refracted as both P- and S-waves. Since an S-wave propagates at a lower speed than a P-wave, it will reflect and refract at angles (determined using Snell's law), θ_s and β_s, that are less than the angles of reflection and refraction for a P-wave, as shown in Figure 14.1B.

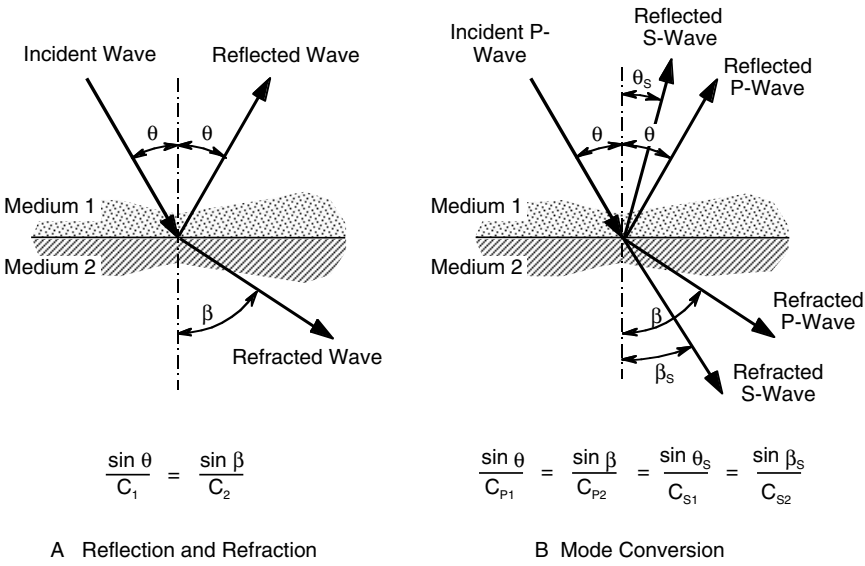

FIGURE 14.1 The behavior of a P-wave incident on an interface between two dissimilar media: (A) reflection and refraction; (B) mode conversion.

The relative amplitudes of reflected waves depend on the mismatch in specific acoustic impedances at the interface, the angle of incidence, the distance of an interface from the pulse source, and the attenuation along the wave path. The influence of each of these factors is considered in the following discussion.

The portion of an incident ray of a P-wave that is reflected at an interface between two media depends on the specific acoustic impedances of each medium. The specific acoustic impedance, Z, of a medium is

$$Z = \rho C_p \tag{14.7}$$

Specific acoustic impedance values for P-waves in selected materials are given in Table 14.1.[7] Equation 14.7 is also valid for S-waves if the S-wave speed is used to calculate specific acoustic impedance.

TABLE 14.1 Specific Acoustic Impedances

Material	Density (kg/m³)	P-Wave Speed (m/s)	Specific Acoustic Impedance (kg/m² · s)
Air	1.205	343	0.413
Concrete[a]	2300	3000–4500	$6.9–10.4 \times 10^6$
Granite	2750	5500–6100	$15.1–16.8 \times 10^6$
Limestone	2690	2800–7000	$7.5–18.8 \times 10^6$
Marble	2650	3700–6900	$9.8–18.3 \times 10^6$
Quartzite	2620	5600–6100	$14.7–16.0 \times 10^6$
Soil	1400–2150	200–2000	$0.28–4.3 \times 10^6$
Steel	7850	5940	46.6×10^6
Water	1000	1480	1.48×10^6

[a] The density of concrete depends on the mixture proportions, the relative densities of the mixture ingredients, and moisture content. The given density is a typical value for ordinary normal density concrete.

The amplitude in a reflected ray is maximum when the angle of incidence of the ray is normal to the interface. For normal incidence, the amplitude of the reflected ray relative to the amplitude of the incident ray can be determined using the following equation:

$$R_n = \frac{Z_2 - Z_1}{Z_2 + Z_1} \tag{14.8}$$

where

R_n = the reflection coefficient for normal incidence
Z_1 = the specific acoustic impedance of medium 1
Z_2 = the specific acoustic impedance of medium 2

If Z_1 is greater than Z_2, R_n is negative, indicating that the reflected wave will have the opposite sign, that is, a phase change occurs. This means that the stress changes sign. For example, if the stress in an incident P-wave is compressive, the stress in the reflected P-wave is tensile. If Z_2 is greater than Z_1, no phase change occurs.

For incident angles other than normal to an interface, the reflection coefficients depend on the angle of incidence, and they can be determined using the formulas in Krautkramer and Krautkramer,[8] which are applicable for plane waves (wave front is a plane) incident on plane boundaries. The formulas in Reference 8 were used to calculate the P-wave reflection coefficients for a concrete/air interface, which are shown in the upper left of Figure 14.2. It is assumed that the incident wave has amplitude equal to unity. A similar figure can be constructed for an incident S-wave.[9] Figure 14.2 is composed of three graphs. The graph in the upper left gives the reflection coefficients, R_P, for the reflected P-wave. The graph in the lower right gives the reflection coefficients, R_s, for the mode-converted S-wave. The graph in the upper right gives the angular relationship between the incident wave and the mode-converted wave, which is determined by Snell's law. The drawing in the lower left shows an illustrative example. Note that for rays of a P-wave with low angles of incidence, R_p is approximately equal to one and R_s is small. This is important in the application of the impact-echo method to be discussed.

In the previous discussion it was assumed that reflection and refraction of wave fronts occurred at planar interfaces between two dissimilar media. This type of analysis is also applicable to flaws or discontinuities within a medium. The ability (sensitivity) of stress wave propagation methods to detect flaws or discontinuities depends on the component frequencies (or wavelengths) in the propagating wave and on the size of the flaw or discontinuity. A general rule is that to be detectable, the size of flaw must be approximately equal to or larger than the wavelengths in the propagating wave. Wave speed, C, frequency, f, and wavelength, λ, are related by the following equation:

$$C = f\,\lambda \tag{14.9}$$

For example, to detect a flaw with a diameter of about 0.1 m, it is necessary to introduce into the concrete (P-wave speed of about 4000 m/s) a stress pulse that contains frequencies greater than approximately 40 kHz (wavelengths less than approximately 0.1 m).

As a wave propagates through a solid its amplitude decreases with path length due to attenuation (scattering and absorption) and divergence (beam spreading). Divergence causes the amplitude of spherical waves to decrease in proportion to the inverse of the distance from the source. In evaluation of concrete, low-frequency (long-wavelength) waves must be used to reduce the attenuation of wave energy due to scattering (reflection and refraction from mortar–aggregate interfaces). If the wavelength of the propagating wave is less than the size of the aggregate, the mismatch in acoustic impedances between mortar and aggregate particles scatters incident waves at each mortar–aggregate interface. For example, if the maximum size aggregate is 25 mm in a concrete with a P-wave speed of 4000 m/s, frequencies lower than 4000/0.025 = 160 kHz should be used to reduce scattering. The concrete will appear homogeneous to these lower frequency waves. Use of low-frequency waves, however, reduces the sensitivity of

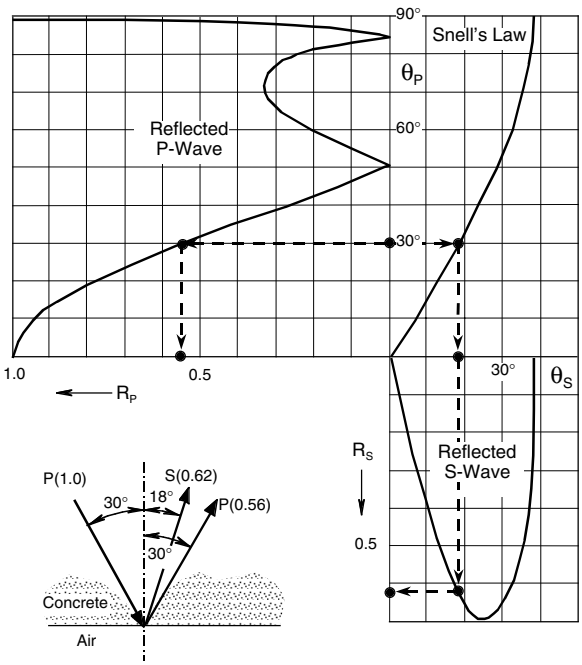

FIGURE 14.2 Reflection coefficients at a concrete/air interface for an incident P-wave as a function of the incidence angle (Poisson's ratio = 0.2).[7]

the propagating waves to small flaws. Thus, there is an inherent limitation in the flaw size that can be detected within concrete using stress wave propagation methods.

14.3 Test Methods

Several test methods based on stress wave propagation are used for nondestructive testing of concrete structures. The echo methods (impact-echo and pulse-echo) are used for thickness measurements, flaw detection, and integrity testing of piles. The impulse-response method is also used to test piles and slablike structures. The spectral analysis of surface waves (SASW) method is used to determine the thickness of pavements and elastic moduli of layered pavement systems. The following sections describe the principles of these methods, the required test equipment, and the signal processing techniques. Typical applications for each method are presented.

14.3.1 Pulse-Echo

14.3.1.1 Principle

In the traditional pulse-echo method,[3] a transmitter introduces a stress pulse into an object at an accessible surface. The pulse propagates into the test object and is reflected by flaws or interfaces. The surface response caused by the arrival of reflected waves, or echoes, is monitored by either the transmitter acting as a receiver (true pulse-echo) or by a second transducer located near the pulse source (pitch–catch). Figure 14.3 illustrates the principle of these echo methods. The receiver output is displayed on a display device, and the display is called a time-domain waveform. By using the time base of the display, the round-trip travel time of the pulse is determined. If the wave speed in the material is known, this travel time can be used to determine the depth of the reflecting interface using the following equation:

$$T = \frac{1}{2}\Delta t\ C_p \tag{14.10}$$

where

Δt = the round-trip travel time
T = the depth
C_p = the P-wave speed

The factor of one half is used because the actual depth is one half the travel path of the wave. This equation is approximate for a pitch–catch system and is applicable only if the separation between the sending and receiving transducers is small.

14.3.1.2 Signal Processing

Time-domain analysis has been used exclusively in all applications where pulse-echo or pitch–catch methods have been used to test concrete structures. Figure 14.4 shows a waveform obtained from a 0.235-m-thick concrete slab using an experimental pitch–catch test system.[10] The start of the transmitted pulse and the arrival of the P-wave echo reflected from the bottom of the slab are indicated on the waveform by the letters A and C, respectively. Using the time base of the display, the elapsed time, Δt, between points A and C was determined to be 106 μs. Therefore, solving for C_p in Equation 14.10, the P-wave speed is 4430 m/s.

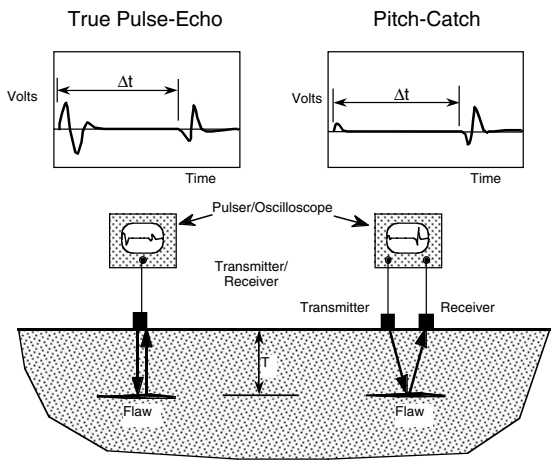

FIGURE 14.3 Schematic of pulse-echo and pitch–catch techniques.

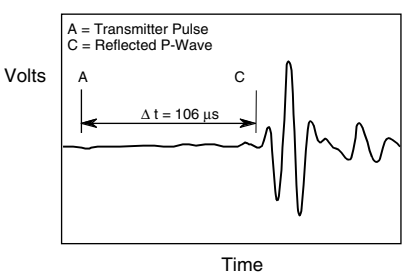

FIGURE 14.4 Waveform obtained from pitch–catch test on concrete slab. (Adapted from Reference 10.)

14.3.1.3 Instrumentation

The key components of a pulse-echo or pitch–catch test system are the transmitting and receiving transducer(s) and the system that is used to record and display waveforms.

The majority of modern transducers use piezoelectric materials to generate and receive stress waves. Generally, these materials are manufactured ceramics such as lead zirconate titanate (PZT) and lead metaniobate. A piezoelectric material subjected to an electrical field will change dimension suddenly, and then it will oscillate and gradually "ring down" to its initial state. Conversely, a piezoelectric material subjected to deformation generates an electrical charge that is proportional to the applied strain. Thus, a single transducer can be used for both generation and reception of stress waves. A fluid couplant, such as oil, grease, or other viscous fluid, is needed between the transducer and the test object to transmit and receive the low-amplitude stress waves used in pulse-echo testing.

When a transmitting transducer is excited by a high-voltage pulse, its vibration time-history is approximately that of a damped sinusoidal curve. The vibration has a characteristic (or resonant) frequency. When a single transducer is used as the transmitter and receiver, the transmitted pulse must be sufficiently short so as not to overlap with the arrival of the echoes. The transducer must be damped or the "ringing" (vibrations) of the piezoelectric element will render it unresponsive to echoes. The more heavily a transducer is damped, however, the less sensitive it is to the displacements caused by the arrival of echoes. Thus, an acceptable balance must be achieved in the design and construction of a piezoelectric pulse-echo transducer. The development of a suitable pulse-echo transducer for testing concrete is a difficult undertaking. Although some success has been reported,[11] most researchers have resorted to pitch–catch systems. In this case a heavily damped transducer is used to send the pulse, and a lightly damped transducer is used to receive the echoes.

The following discussion summarizes some of the considerations in the design of ultrasonic transducers used as pulse sources. Most of the energy transmitted into the test object is contained within a cone-shaped region that has its apex at the transducer. The ratio of transducer diameter, d, to the wavelength of the transmitted waves, λ, determines the radiation pattern of the stress pulse. Figure 14.5 shows the directional characteristics in concrete for $d/\lambda = 4$, $d/\lambda = 1$, and $d << \lambda$ (a point source). These figures represent the variation of the wave amplitude with the direction of radiation. The radial distances from the origin to the curves represent the relative amplitude, and it is seen that the highest amplitude occurs in the direction of the transducer axis. As d/λ decreases, the apex angle of the cone increases; that is, the directionality of the pulse decreases. With decreasing directionality, the pulse probes a greater volume of material, and it becomes more difficult to identify the boundaries of internal defects as the transducer is scanned across the test object. It is generally much simpler to interpret test results using a transducer that emits a focused beam ($d/\lambda = 4$). If a 100-kHz focused transducer ($d/\lambda = 4$) were to be used to evaluate concrete with a P-wave speed of 4000 m/s, the transducer must have a diameter of 0.16 m, which is quite large. This shows the inherent difficulty in trying to develop a successful pulse-echo system for concrete.

In summary, low-frequency transducers are needed for testing concrete. It is difficult, however, to construct low-frequency transducers that generate short-duration, focused stress pulses. As illustrated in the previous example, the size of the required transducer becomes large, which makes the transducer cumbersome and creates difficulties in coupling the transducer to the surface of concrete. Because of these difficulties, there are no commercially available transducers for pulse-echo testing of concrete in the field.

An alternative approach is to replace the transmitting transducer with a mechanical impactor. Although this has the disadvantage of producing a nonfocused spherical wave front, it has the advantage of simplicity and providing high-energy input. This procedure has been incorporated into ASTM D 5882,[12] a test method for integrity testing of piles. In these applications, the test object is essentially a slender rod and the wave energy is naturally focused by the side boundary of the pile.

14.3.1.4 Applications

Since the early 1960s, experimental pulse-echo and pitch–catch systems have been developed for concrete. Successful applications have been limited to measuring the thickness of thin slabs, pavements, and walls,

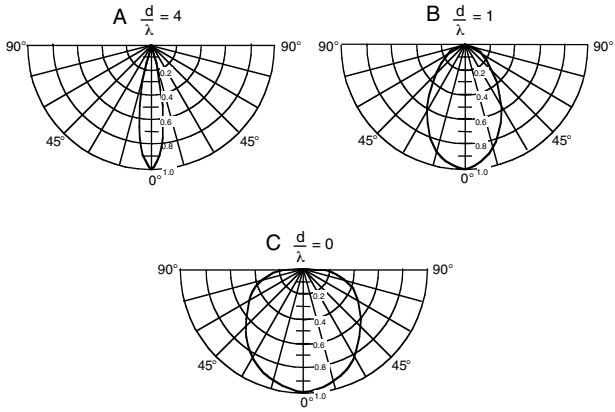

FIGURE 14.5 Polar diagrams of radiation patterns for transducers with various ratios of diameter to wavelength (Poisson's ratio = 0.2).

measuring the length of piles, and, in one instance, locating surface-opening cracks in submerged structures. Each of these applications is reviewed in the following paragraphs. For specific details on the construction and characteristics of the various transducers, the reader is referred to the cited references.

In 1964, Bradfield and Gatfield[13] of England reported the development of an echo technique for measuring the thickness of concrete pavements. Using two 100-kHz resonant transducers (0.16 m tall, 0.10 m wide, and 0.25 m long) in a pitch–catch arrangement, they were able to measure the 0.3-m thickness of a concrete specimen with an accuracy of 2%. This system could not be field-tested because of the impracticality of the test configuration. Besides being bulky, the transducers were coupled to the concrete by a large plastic block that required a smooth flat concrete surface for good coupling. Difficulties were also reported in obtaining reflections from roughly textured bottom surfaces.

In 1968, Howkins, et al.[14] at IIT Research Institute independently investigated available echo techniques in an attempt to identify a feasible method for pavement thickness measurements. Using a pitch–catch technique similar to that developed by Bradfield and Gatfield, the IIT researchers were able to measure the thickness of 0.18- and 0.25-m-thick portland cement concrete slabs and 0.13-m-thick asphalt concrete slabs with an accuracy of 2%. It was concluded, however, that the transducer arrangement was not practical for field use.

A pitch–catch system was developed at The Ohio State University in the late 1960s to measure pavement thickness.[15] A large transmitter was needed to produce a focused pulse with a low resonant frequency. The transmitter was a hollow cylinder, with a 0.46-m outer diameter, a 0.15-m inner diameter, and a 200-kHz resonant frequency. The receiving transducer was placed at the center of the transmitter. Thicknesses were measured with accuracies of ±3% at more than 90% of the pavement test locations. The accuracy and good performance of the Ohio State thickness gauge was confirmed in independent field tests conducted in 1976 by Weber et al.[16] They concluded that the Ohio State instrument needed to be redesigned to better withstand the rigors of field use before it could be considered as practical nondestructive testing equipment.

Claytor and Ellingson[17] at Argonne National Laboratory attempted to use a pulse-echo system to measure the thickness of 0.305-m thick refractory concrete specimens. It was found that for frequencies below 100 kHz, the use of a single transducer was impractical because the ringing after transducer excitation obscured the echo signal. Tests were also carried out using two transducers in a pitch–catch arrangement; however, the transmitting transducer generated strong R-waves that interfered with the reception of the echo signal by the receiving transducer. To reduce R-wave interference, large-diameter (0.18-m) transducers were constructed. As the response of a transducer is an averaged phenomenon over the contact area, the sensitivity of a larger diameter transducer to localized surface disturbances (R-waves) was reduced and the thickness of the concrete specimens could be determined.

In 1977, Forrest[18] at the Naval Civil Engineering Laboratory reported the use of a pulse-echo system for measuring the length of concrete piles. A large transducer with a resonant frequency of 12 kHz was used to measure the length of piles up to 24 m. A pulse-echo system works for long piles because there is sufficient time for transducer ringing to dampen before a reflection from the bottom of the pile arrives.

In 1984, Smith[19] demonstrated that R-waves could be used to detect surface opening cracks in submerged concrete structures, such as concrete tanks and offshore structures. Two 500-kHz, 0.025-m-diameter, P-wave transducers were used as transmitter and receiver. When a transmitted P-wave strikes the surface of a submerged solid at a critical angle (defined by Snell's law, Equation 14.6), mode conversion occurs producing an R-wave that propagates along the solid–liquid interface. As the R-wave propagates, mode conversion also occurs, producing a P-wave that radiates into the liquid at the same critical angle. The receiving transducer picks up this P-wave. The distance between the two transducers can be adjusted to optimize the amplitude of the received signal. If the path of the propagating R-wave is crossed by a crack, reflection occurs and the receiving transducer will not pick up a signal. If a crack is favorably oriented (a crack at 90° to the propagating wave is the best orientation), the P-wave produced by mode conversion of the reflected R-wave will be picked up by the transmitting transducer. From an analysis of the received signals obtained from a complete scan, that is, from moving the transducers parallel to and over the surface of the test object in a prearranged pattern, surface opening cracks were located.

In 1983, Thornton and Alexander[10,20] at the U.S. Army Engineer Waterways Experiment Station (WES) developed a pitch–catch system, concentrating their efforts mainly on transducer development. Their system used a transmitting transducer made of four plates of lead metaniobate forming a 120-mm square. The mosaic transducer had high damping and a resonant frequency of about 190 kHz. The receiver was made of PZT. The transducers were coupled to the concrete with castor oil, and a relatively flat surface was needed to achieve proper coupling of the transducer faces. Slab thickness measurements up to 0.25 m were reported.[10,20] Figure 14.4, presented earlier, is an example of a measurement made using the WES pitch–catch system.

14.3.2 Impact-Echo

The idea of using impact to generate a stress pulse is an old idea that has the great advantage of eliminating the need for a bulky transmitting transducer. The stress pulse generated by impact at a point, however, does not have the directionality of a pulse from a large-diameter transducer. The energy propagates into a test object in all directions, and reflections may arrive from many directions. For this reason, impact methods are used primarily for testing piles. The pile boundary acts as a waveguide and confines most of the energy within the pile. In the 1980s, Sansalone and Carino[7] developed an impact method for testing of thin concrete structures, and they coined the term "impact-echo" to describe their technique.

14.3.2.1 Principle

The principle of the impact-echo technique is illustrated in Figure 14.6. A stress pulse is introduced into a test object by mechanical impact on the surface. The stress pulse propagates into the object along spherical wave fronts as P- and S-waves. In addition, a surface wave (R-wave) travels along the surface away from the impact point. The P- and S- stress waves are reflected by internal interfaces or external boundaries. The arrival of these reflected waves, or echoes, at the surface where the impact was generated produces displacements that are measured by a receiving transducer and recorded by a data acquisition system. Because of the radiation patterns associated with P- and S-waves,[7,9] if the receiver is placed close to the impact point, the waveform is dominated by the displacements caused by P-wave arrivals. As discussed below the success of the method depends, in part, on using an impact of the correct duration.

14.3.2.2 Signal Analysis

A pulse generated by impact is composed of low-frequency waves that have the ability to penetrate concrete. For a point source, however, the pulse propagates in all directions (Figure 14.5C) rather than as a focused beam such as in ultrasonic pulse-echo systems. If a ray strikes a favorably oriented reflector

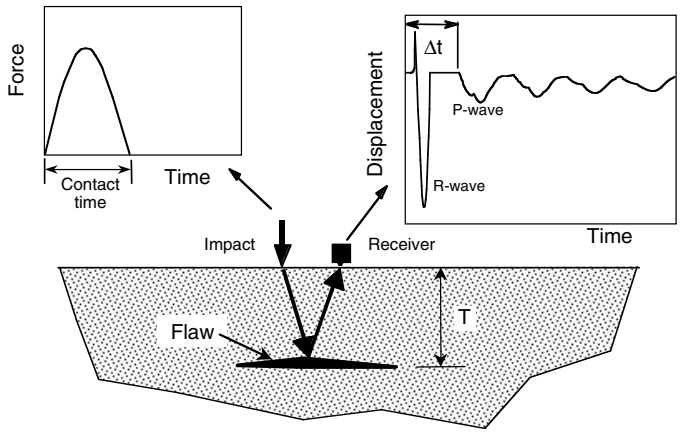

FIGURE 14.6 Principle of the impact-echo method.

within a test object, the ray is reflected back to the receiver and a surface displacement is recorded. The waveform can be simple or complex depending on the test object. Interpretation of waveforms in the time domain using Equation 14.10 as described above has been successful for long slender structures, such as piles and drilled shafts. These types of structures are waveguides; that is, the geometry of the structure acts to focus the energy in the propagating wave within a narrowly defined boundary. In addition, there is sufficient time between the generation of the stress pulse and the reception of the wave reflected from the bottom surface or from an inclusion or other flaw so that the arrival time of the reflected wave is generally easy to determine even if long duration impacts produced by hammers are used. An example of a waveform obtained from an impact test of a pile is shown in Figure 14.7.[21] In this example, an accelerometer is used as the receiving transducer. Time zero in the waveform is the start of the impact. The R-wave produced by the impact caused the first set of peaks, and the echo from the bottom of the 15.3-m pile gives rise to the second set of lower-amplitude peaks. The time from the start of the impact to the arrival of the echo is about 7.5 ms. When applied to testing piles, this impact method is generally referred to as "low strain integrity testing" and is described in ASTM D 5882.[12]

For relatively thin structures such as slabs and walls, time-domain analysis is feasible if short-duration impacts are used, but it is time-consuming and can be difficult depending on the geometry of the structure.[7,9,22] An alternative approach, which is much quicker and simpler, is frequency analysis of the displacement waveforms.[23–25] The principle of frequency analysis is as follows. In Figure 14.6, the stress pulse generated by the impact propagates back and forth between the flaw and the top surface of the plate. Each time the pulse arrives at the top surface it produces a characteristic downward displacement.

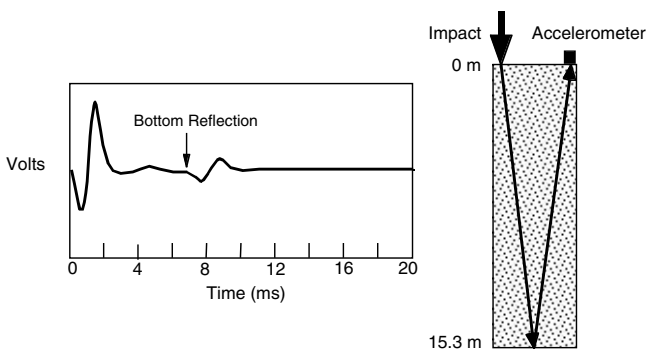

FIGURE 14.7 Waveform from impact test of a pile. (Adapted from Reference 21.)

Thus, the waveform is periodic, and the period is equal to the travel path, $2T$, divided by the P-wave speed. Because frequency is the inverse of the period, the frequency, f, of the characteristic displacement pattern is

$$f = \frac{C_{pp}}{2T} \tag{14.11}$$

where C_{pp} is the *plate P-wave speed* determined from an impact-echo test on a part of the structure of known thickness. Thus, if the dominant frequency in a waveform can be determined, the thickness of the plate (or distance to a reflecting interface) can be calculated:

$$T = \frac{C_{pp}}{2f} \tag{14.12}$$

In the early research[7] leading to the development of the impact-echo method, it was assumed that the wave speed across the thickness of the plate is the same as the P-wave speed in a large solid, as given by Equation 14.1. Subsequent, and more rigorous, research[26] led to the conclusion that the wave speed across the thickness of the plate was approximately 96% of the P-wave speed, that is, $C_{pp} = 0.96C_p$. According to Sansalone and Streett,[25] "this difference occurs because multiple reflections of P-waves excite a particular mode of vibration in the plate — the thickness mode — and the displacements caused by this mode produce the principal periodic patterns in the waveform."

In practice, the frequency content of the digitally recorded waveforms is obtained using the fast Fourier transform (FFT) technique.[27] This technique is based on the principle of the Fourier transform, which states that any waveform can be represented as a sum of sine curves, each with a particular amplitude, frequency, and phase shift. The FFT is used to calculate the amplitude spectrum of the waveform, which gives the relative amplitude of the component frequencies in the waveform.

Figure 14.8A shows an amplitude spectrum obtained from an impact-echo test performed over a solid portion of a 0.5-m-thick concrete slab.[28] In the amplitude spectrum, there is a frequency peak at 3.42 kHz, which corresponds to multiple reflections of the P-wave between the bottom and top surfaces of the slab. Using Equation 14.11 and solving for C_{pp}, the plate P-wave speed is calculated to be 3420 m/s. Figure 14.8B shows the amplitude spectrum obtained from a test over a portion of the slab containing a disk-shaped void.[28] The peak at 7.32 kHz results from multiple reflections of the P-wave between the top of the plate and the void. Using Equation 14.12, the calculated depth of the void is $3420/(2 \times 7320) = 0.23$ m, which compares favorably with the planned depth of 0.25 m.

The resolution in the amplitude spectrum obtained using the FFT, that is, the frequency difference between adjacent discrete points, is equal to the sampling frequency used to capture the waveform divided by the number of points in the waveform record. For example, if the sampling frequency is 500 kHz and there are 1024 points in the waveform, the frequency resolution is (500/1024) kHz = 0.488 kHz. This imposes a limit on the resolution of the depth calculated according to Equation 14.12. Because depth and frequency are inversely related, it can be shown that for a fixed resolution in the frequency domain, the resolution of the calculated depth improves as the frequency increases, that is, as depth decreases.

In using the impact-echo method to determine the locations of flaws within an object, tests are performed at regularly spaced points along "scan" lines marked on the surface. Examination of the amplitude spectra from these scans reveals the depth and approximate size of defects that may be present. A classical technique for visualization of the location of defects along a given scan is to create a "waterfall plot" of the individual spectra. In a waterfall plot, the spectra are plotted consecutively in the order corresponding to the test location along the scan line. Figure 14.9 is an example of a waterfall plot that was obtained for a scan across a section of a 0.5-m thick, reinforced concrete slab containing two disk-shaped voids.[28] The waveforms at each test point are shown on the left and the corresponding spectra are on the right. Spectrum 1 with a single large-amplitude peak at 3.91 kHz is typical of spectra obtained over the solid portion of the slab. Using Equation 14.11, the plate P-wave speed in the slab is 3910 m/s.

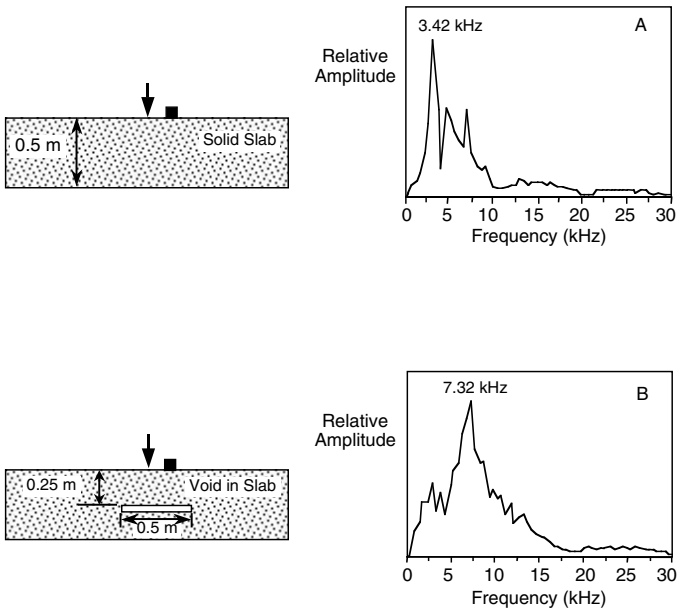

FIGURE 14.8 Examples of amplitude spectra: (A) test over a solid portion of concrete slab; (B) test over a disk-shaped void embedded in same slab.[28]

Spectra 2, 3, and 6 reveal the presence of voids. Equation 14.12 can be used to calculate the depth of each void. The peak at 7.81 kHz in spectrum 3 corresponds to reflections from a void at 3910/2(7810) = 0.25 m, and the peak at 15.9 kHz in spectrum 6 corresponds to reflections from a void at 3910/2(15900) = 0.12 m. These calculated depths agree with the planned depths of the artificial voids. Note that in spectra 3 and 6 there is a high-amplitude peak at 3.42 kHz. This peak is associated with refraction of the P-wave around the flaw and reflection from the bottom of the slab. This shift of the thickness frequency to a lower value has been found to occur in a variety of cases when flaws are present, and can be used as further evidence that the slab is not solid at that test point.[25]

The information contained in a waterfall plot can be further processed to produce a cross-sectional view of the test object along the scan line. The technique that has been developed is called "spectral peak plotting."[29] The series of operations that are performed for each spectrum in the scan is illustrated in Figure 14.10 and outlined as follows:

1. Locate the peak in the spectrum that has the highest amplitude.
2. Normalize the amplitude values by dividing by the highest amplitude.
3. Select a threshold value for the relative amplitude.
4. Locate all peaks in the spectrum whose relative amplitudes exceed the threshold value.
5. For each peak selected in step 4, compute the depth corresponding to the frequency values using the plate P-wave speed and Equation 14.12.
6. Using the depth calculated in step 5, plot the depths at the test point along the scan line.

The above procedure can be incorporated into a computer program that uses the individual spectra as input and generates a plot of the cross section along the scan line.[29] Spectral peak plotting permits a rapid assessment of impact-echo results by allowing the user to "see" reflectors inside the test object.

The spectra in Figure 14.9 were processed using a spectral peak–plotting computer program, and the resulting computer-generated cross section is shown in Figure 14.11. For this case, the maximum depth for the plot was chosen as 0.5 m; therefore, each tick mark along the depth axis represents 0.05 m. The tick marks along the top surface represent the individual test locations. The depth calculated at each test point is plotted as a "dash" between the midpoints of adjacent test points. The presence of the two voids

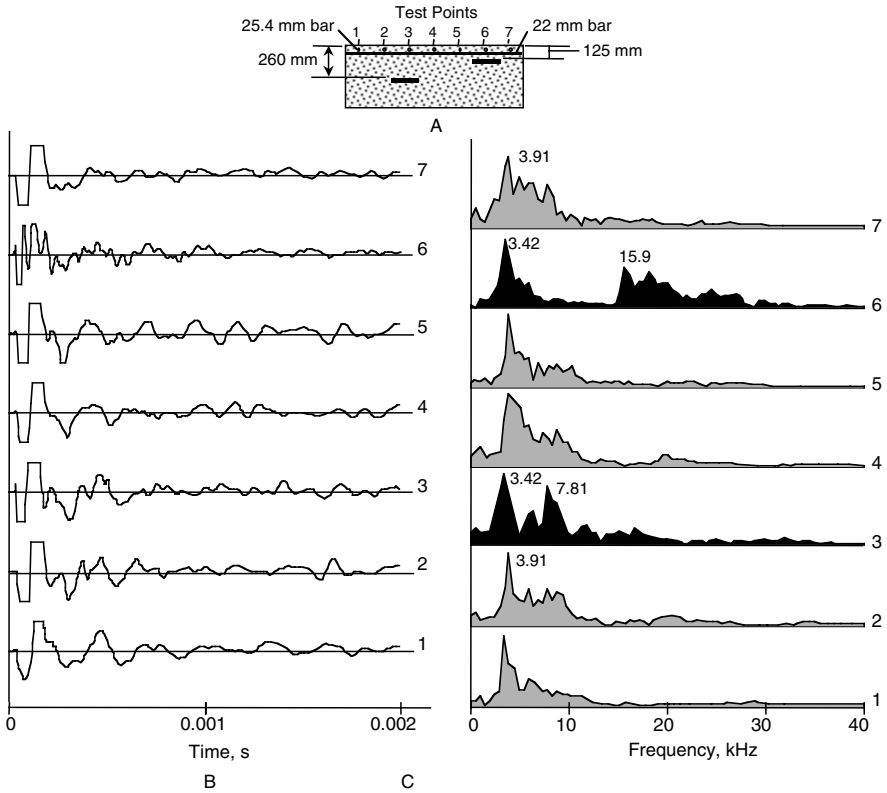

FIGURE 14.9 Impact-echo results across section of 0.5-m-thick slab containing 0.2-m-diameter disk-shaped voids: (A) slab cross section; (B) waveforms; and, (C) amplitude spectra.[28]

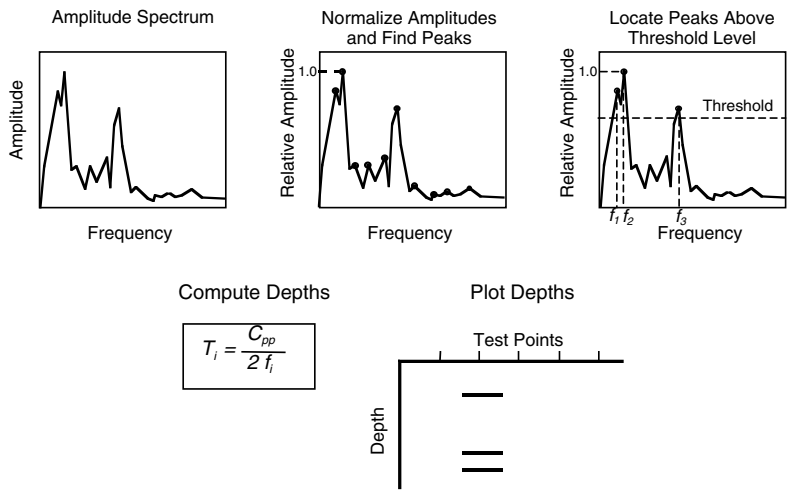

FIGURE 14.10 Spectral peak plotting procedure for constructing cross-section of test object from amplitude spectra.

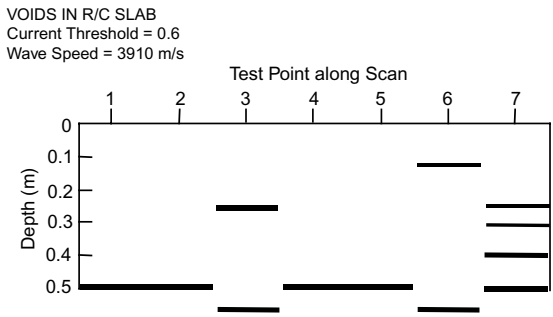

FIGURE 14.11 Spectral peak plot of the amplitude spectra shown in Figure 14.9C.

in the slab can be seen clearly. Note the apparent increase in slab thickness where flaws are present. Spectral peak plotting may not be practical in cases where the peaks associated with internal flaw are of low amplitude. Refer to Sansalone and Streett[25] for descriptions of other signal processing techniques that can be used to help simplify amplitude spectra.

14.3.2.3 Instrumentation

An impact-echo test system is composed of three components: an impact source; a receiving transducer; and a data acquisition system with appropriate software for signal analysis and data management.

The selection of the impact source is a critical aspect of a successful impact-echo test system. The force-time history of an impact may be approximated as a half-cycle sine curve, and the duration of the impact is the "contact time," as shown in Figure 14.6. The contact time determines the frequency content of the stress pulse generated by the impact.[23] The shorter the contact time, the higher the range of frequencies contained in the pulse. Thus, the contact time determines the size of the defect that can be detected by impact-echo testing. As the contact time decreases and the pulse contains higher-frequency (shorter-wavelength) components, smaller defects can be detected. In addition, short-duration impacts are needed to accurately locate shallow defects. The stress pulse must have frequency components greater than the frequency corresponding to the flaw depth (Equation 14.11). As an approximation, the highest-frequency component of significant amplitude in a pulse equals the inverse of the contact time. For example, for a contact time of 100 μs, the maximum frequency having significant amplitude is about 10 kHz. For a P-wave speed of 4000 m/s, a pulse with a contact time shorter than 100 μs would be needed to determine the depth of defects shallower than about 0.2 m. Thus, for impact-echo testing of slablike structures, short duration impacts are preferable. Experience, however, has shown that as the contact time decreases, the amplitude spectra become more complex. In practical applications, it advisable to use a range of contact times beginning with longer durations and then using shorter durations.[25]

Many impact sources have been tried. In evaluation of piles, hammers are used.[30–34] Hammers produce energetic impacts with long contact times (greater than 1 ms) that are acceptable for testing long, slender structures but are not suitable for detecting flaws within thin structures such as slabs or walls. Impact sources with shorter-duration impacts (20 to 60 μs), such as small steel spheres and spring-loaded spherically tipped impactors, have been used for detecting flaws within slab and wall structures ranging from 0.15 to 1 m thick.[7,9,22,24,25,35,36] Steel spheres are convenient impact sources because they produce well-defined pulses (approximately a half-cycle sine curves), and the contact time is proportional to the diameter of the sphere.[7,25,37]

In integrity testing of piles, geophones (velocity transducers) or accelerometers have been used as the receiving transducer.[30–34] For impact-echo testing of slab and wall structures, Sansalone and Carino[7] were the first to use a conically tipped, piezoelectric displacement transducer as the receiver. This transducer responds to surface displacement over a broad frequency range. It was developed at the National Bureau of Standards (now the National Institute of Standards and Technology) as a secondary reference standard for calibrating acoustic emission transducers.[38] A thin lead strip was used to provide acoustic coupling between the conical transducer and the test surface. No viscous liquid couplants were required.

FIGURE 14.12 Example of impact-echo test instrument. (Courtesy of Impact-Echo Instruments, LLC.)

The data acquisition system should have a sampling frequency of at least 500 kHz, and it may be a digital waveform analyzer, a portable computer with data acquisition hardware and software, or a dedicated impact-echo instrument. The optimal sampling frequency depends on the thickness of the test object, but a high sampling rate has been found effective for testing relatively thin members. Pratt and Sansalone[39] were the first to develop a portable impact-echo test system. That system included a conically tipped displacement transducer and integral steel spheres attached to spring rods as impact sources. A portable computer was used for data acquisition and signal analysis. Today, several impact-echo test systems are commercially available. Figure 14.12 shows a commercial system that uses a rugged laptop computer for data acquisition and analysis. The conically tipped transducer is within the metal housing and steel balls on spring steel rods are used as the impact source.

14.3.2.4 Applications

Since the early 1970s, impact methods have been widely used for evaluation of concrete piles.[30–34] Steinbeck and Vey[31] were among the first to apply the technique to piles. A pulse was introduced at the top surface by impact and the returning echo was monitored by an accelerometer mounted on the same surface. The time-domain signal record was used to detect partial or complete discontinuities, such as voids, abrupt changes in cross section, very weak concrete, and soil intrusions, as well as the approximate location where such irregularities existed. In the absence of major imperfections the location of the bottom of a sound pile could be determined. The success of the method (also known as *seismic* or *sonic echo*) depends on the pile length and the characteristics of the surrounding soil; echoes from the bottom of a long pile in a stiff, dense soil with an acoustic impedance similar to that of concrete may be too weak to be detected.[30]

Carino and Sansalone initiated experimental and theoretical studies at the National Bureau of Standards in 1983 to develop an impact method for testing structures other than piles. The result of that work was the impact-echo method that has been described here. Details of these early studies may be found in the cited references.[7,9,22,23,28,35,36,40–46] In the laboratory, they used the method to detect various types of interfaces and simulated defects in concrete slab and wall structures, including cracks and voids in plain and reinforced concrete, the depth of surface-opening cracks, voids in prestressing tendon ducts, honeycombed concrete, the thickness of slabs and overlays, and delaminations in slabs with and without asphalt concrete overlays. Most of theses early experimental studies were controlled-flaw studies where specimens containing flaws at known locations were constructed and tested. Two of their early studies were carried out on specimens constructed by other researchers for "blind" studies to evaluate nondestructive test methods based on stress wave propagation. These studies involved detecting delaminations

in a reinforced concrete slab[35] and locating voids in tendon ducts in a 1-m-thick reinforced wall that was built to simulate a wall for an arctic offshore structure.[46] In both of these studies, the locations of the flaws were not known prior to testing; the impact-echo method successfully detected the flaws in both studies.

In conjunction with their early experimental studies, Sansalone and Carino performed a series of numerical studies using the finite-element method. Because there are no theoretical solutions for calculating the transient impact response of a bounded solid containing flaws, the finite-element method was used for this purpose. The results of these studies form the theoretical basis for the initial development of the impact-echo method. Variations in the parameters important in impact-echo testing were easily studied using finite-element models. Conclusions were drawn about the effect of contact time of the impact, flaw size and depth, and specimen geometry on waveforms and spectra.[7,40–43] Other finite-element studies were performed subsequently by Sansalone and co-workers to develop an understanding of transient wave propagation in other applications besides testing slablike structures.[24,25]

The impact-echo method for structures other than piles has been used in the field.[25,28,34,47–49] As an early example, the method was used successfully to detect pockets of unconsolidated concrete below cooling pipes in a 0.15-m-thick ice-skating rink slab.[28] Briefly, portions of the slab were known to contain pockets of unconsolidated concrete about 50 to 100 mm in length below the small-diameter, closely spaced, cooling pipes. Regions of the skating rink slab were selected for testing. The thickness of the slab was measured at existing core-holes in the slab. A plate P-wave speed of 4000 m/s was obtained from impact-echo tests performed adjacent to these holes. To be able to detect the small voids, an impact with a contact time of about 20 μs was used.

Figure 14.13A shows the cross section obtained using spectral peak plotting of the amplitude spectra along one scan line. The results indicate that this scan was carried out over generally sound concrete because, except for test point 10, the cross section shows only the bottom of the slab. In contrast, Figure 14.13B shows the cross section obtained along a scan line in an area of the slab believed to contain voids. The presence of voids is indicated by lines within the slab and by the multiple lines associated with the bottom of the slab. Note that this portion of the slab is considerably thinner than that shown in Figure 14.13A. Thus, it was shown that, by using an appropriate short-duration impact, the impact-echo method could identify the presence of small voids in a thin slab.

Since the initial studies in the 1980s, a number of additional studies were carried out at Cornell University, which expanded the range of successful applications.[24,25] These include fundamental studies on the detection of voids in tendon ducts,[50,51] and the impact response produced by thin layers of dissimilar materials embedded in concrete.[52] Analytical and experimental studies provided a clear understanding of the influence of delaminated regions and steel reinforcing bars on impact-echo waveforms.[53,54] Similarly, analytical and experimental studies were used to examine the minimum crack width required for crack detection by impact-echo testing.[55,56] The method was also found to be applicable to testing hollow cylindrical structures, such as mine shafts and tunnel liners.[57–59]

Lin and Sansalone[60–62] extended the application of the method to transverse testing of prismatic members, such as columns and beams. It has been found that reflections from the perimeter of these members cause complex modes of vibration. Figure 14.14 shows an example of the shapes associated with the modes of vibration of round and square beams or columns.[60] These modes result in amplitude spectra with many peaks (compare with Figure 14.8), and the depth of the member is not related to the dominant frequency in the spectrum according to Equation 14.12. Nevertheless, it has been shown that defects can still be detected within beams and columns, and successful field applications have been reported.[25,47] To avoid the complexities associated with these cross-sectional modes, the smallest lateral dimension of the structure should be at least five times the thickness.[25]

The impact-echo method has also been applied to evaluate the quality of the bond between an overlay and base concrete.[63,64] Although it is not possible to estimate the bond strength, the impact-echo method may be used to determine whether there is extensive porosity at the interface. The method has also been used for nondestructive evaluation of masonry structures.[65] Potential users of the impact-echo method

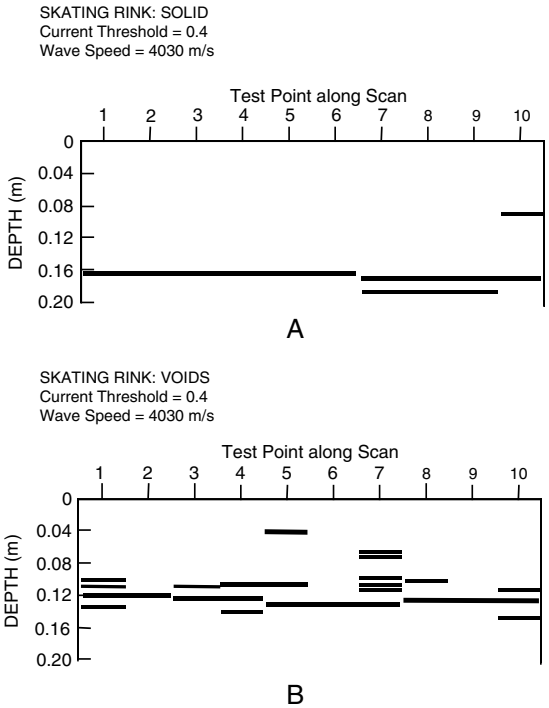

FIGURE 14.13 Spectral peak plots of impact-echo results for ice-skating rink slab: (A) cross section in portion of slab containing sound concrete; (B) cross section in portion of slab containing voids.[29]

should refer to the textbook by Sansalone and Streett[25] for comprehensive coverage of the theory of the method and recommendations for field applications.

The development of a standard test method for flaw detection using impact-echo is difficult because of the many variables and conditions that may be encountered in field-testing. The types of defects can vary from the rather simple case of delaminations or voids to the complex case of distributed microcracking. The type of structure can vary from the simple case of a slab to the complex case of a rectangular beam or column. The measurement of the thickness of a platelike structure, however, is a relatively straightforward application that is amenable to standardization. In 1998, ASTM adopted a test method on the use of the impact-echo method to measure the thickness of platelike concrete members.[66] In this case, a plate is defined as a structure or portion of a structure in which the lateral dimensions are at least six times the thickness.

ASTM Test Method C 1383 includes two procedures. Procedure A, which is shown in Figure 14.15A, is used to measure the P-wave speed in the concrete. This measurement is based on the travel time of the P-wave between two transducers a known distance apart. The background research for this technique is provided in References 26, 67, and 68. Procedure B, shown in Figure 14.15B, is to determine the thickness frequency using the impact-echo method from which the plate thickness is calculated using the measured P-wave speed and Equation 14.12. As was previously discussed, the P-wave speed obtained by Procedure A is multiplied by 0.96 when Equation 14.12 is used to calculate thickness. The data analysis procedure in ASTM C 1383 considers the systematic errors associated with the digital nature of the data in Procedures A and B. The thickness is reported with an uncertainty that is related to the sampling interval in Procedure A and the duration of the recorded signal in Procedure B.[26,68] Limited comparisons of measured pavement thickness with the length of drilled cores demonstrated that the impact-echo results were within 3% of the core lengths.[25,68]

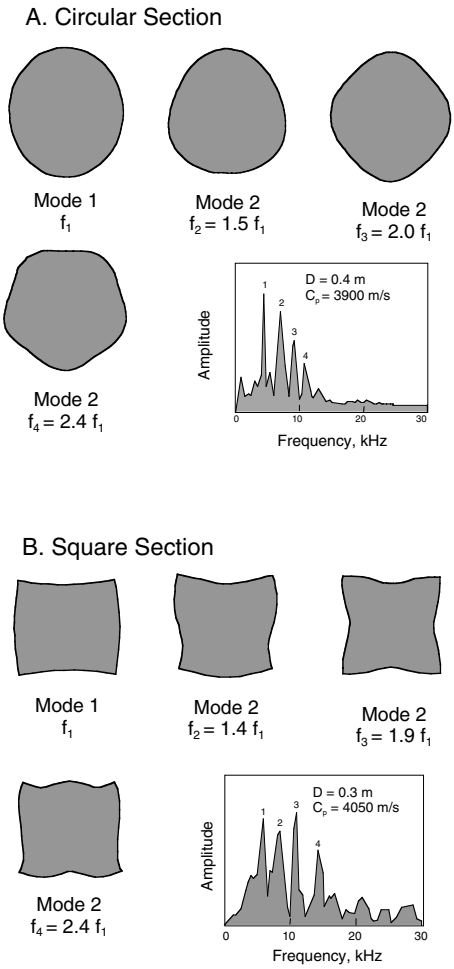

FIGURE 14.14 Mode shapes and amplitude spectra for impact-echo tests of solid round and square columns. (Based on Reference 60.)

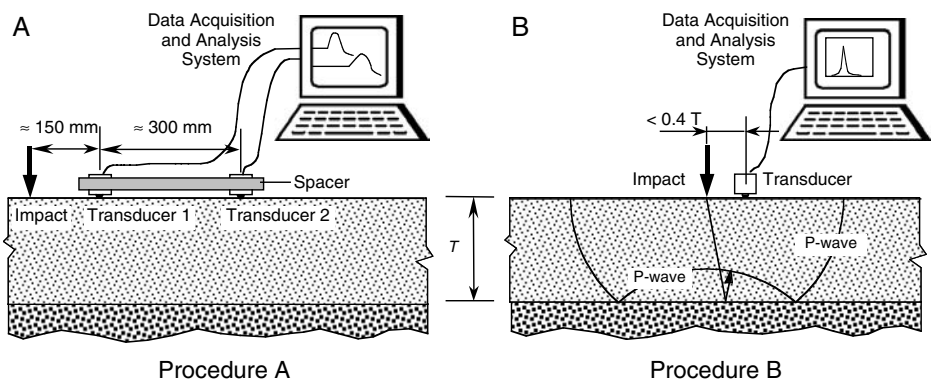

FIGURE 14.15 ASTM C 1383 procedures for measuring thickness of slablike concrete structures: (A) procedure to determine P-wave speed, and (B) procedure to determine thickness frequency.

14.3.3 Impulse-Response Method

14.3.3.1 Principle

Another variant of the impact method is known as impulse-response, transient dynamic response, or impedance testing.[30,34,69–71] The principle of this method is similar to the impact-echo method. A stress pulse is generated by mechanical impact on the surface of an object. The force-time function of the impact is monitored by using an instrumented hammer or by using a hammer to strike a load cell. A transducer located near the impact monitors the movement of the surface as it vibrates in response to the impact. The waveforms of the force and motion transducers are recorded and processed on a dynamic signal analyzer or computer with appropriate software. The analysis reveals information about the condition of the structure.

14.3.3.2 Signal Processing

To calculate the dynamic response of a structure to a given input, the force-time function of the input is convolved* with the impulse response function of the structure. The impulse response is the response of the structure to an input having a force-time function that is a single spike at time zero (impulse). The impulse-response function is a characteristic of a structure, and it changes depending on material properties, geometry, support conditions, and the existence of flaws or cracks. Alternatively, the impact response can be calculated in the frequency domain by multiplying the Fourier transform of the force input with the Fourier transform of the impulse-response function.[73]

In the impulse-response method, the time history of the impact force, and the time history of the response of the structure are recorded, and the impulse response is calculated. This can be accomplished by deconvolution or, in the frequency domain, by dividing the Fourier transform of the response waveform by the Fourier transform of the impact force-time function. In the frequency domain, the resultant response spectrum indicates structural response as a function of the frequency components of the input. Digital signal processing techniques are used to obtain the impulse-response function, often referred to as the transfer function. A procedure for computing the transfer function is outlined in Higgs[70] and involves the following steps:

1. Calculate the Fourier transforms of the measured force-time function, $f(t)$, and the measured response, $v(t)$. These will be denoted as $F(\omega)$ and $V(\omega)$.
2. Using the complex conjugate** of the Fourier transform of the force-time function, $F^*(\omega)$, compute the cross-power spectrum, $V(\omega) \cdot F^*(\omega)$.
3. Compute the power spectrum of the force-time function, $F(\omega) \cdot F^*(\omega)$.
4. Divide the cross-power spectrum by the power spectrum to obtain the transfer function:

$$H(\omega) = \frac{V(\omega) \cdot F(\omega)}{F(\omega) \cdot F(\omega)} \tag{14.13}$$

To improve the results, the test can be repeated, and average power spectra can be used to compute the transfer function. These calculations can be carried out automatically with a dynamic signal analyzer or a computer with appropriate software.

Depending on the measured physical quantity of the structural response, the response spectrum obtained by the division in Equation 14.13 has different meanings. Typically, velocity is measured and the resulting impulse-response spectrum has units of velocity/force, which is referred to as "mobility," and the spectrum is often called a "mobility plot." At frequency values corresponding to resonant frequencies of the structure, mobility values are maximum. Figure 14.16 shows an idealized mobility plot

*The convolution of two functions $f(x)$ and $g(x)$ is $h(x) = \int(u)g(x - u)du$. See Reference 72 for an explanation of the convolution integral.

**The complex conjugate of a vector $\mathbf{F} = x + iy$ is $\mathbf{F}^* = x - iy$, where $i = \sqrt{-1}$

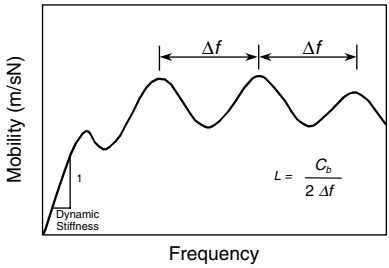

FIGURE 14.16 Idealized mobility plot for a pile. (Adapted from Reference 69.)

for a pile.[69] The series of peaks corresponds to the fundamental and higher modes of vibration; the difference between any two adjacent peaks, Δf, is equal to the fundamental longitudinal frequency.[30,69,70]

The length, L, of the pile can be calculated using the following equation:

$$L = \frac{C_b}{2\,\Delta f} \tag{14.14}$$

where C_b is the bar-wave speed (see Equation 14.2). Note the similarity between this equation and Equation 14.12.

In addition to length, other information can be obtained from impulse-response tests on pile structures.[69,74] At low frequencies, the pile and soil vibrate together, and the mobility plot provides information on the dynamic stiffness of the soil-pile structure.[30,69] In this low frequency range, the mobility plot is approximately a straight line and the slope of the straight line represents the dynamic flexibility of the pile head. The dynamic stiffness is the inverse of the dynamic flexibility. Thus, mobility plots with steeper initial slopes correspond to a lower dynamic stiffness of the pile head. The pile head stiffness is a function of the dynamic stiffness of the pile and the dynamic stiffness of the surrounding soil.

14.3.3.3 Instrumentation

The components of a typical impulse-response test system are the impact source that can be an instrumented hammer or a hammer striking a load cell that is located on the surface of the test object, a geophone (low-frequency velocity transducer), and a two-channel dynamic signal analyzer or portable computer with data acquisition and signal analysis capabilities.

14.3.3.4 Applications

The impulse-response method evolved from a forced vibration method first used in France by Paquet and Briard in 1968.[75] In forced vibration testing, an electrodynamic vibrator was attached to the top of the pile, and the pile response was measured. To obtain the response spectrum, the response was measured for different applied frequencies. Thus, considerably more effort was required compared with the impulse-response technique. Many examples of integrity testing of piles using forced vibration and impulse-response have been reported.[21,30,69–71,74]

To illustrate how the method works, impulse-response spectra obtained from two test piles with the same dimensions are shown in Figure 14.17.[21] Figure 14.17A is the response spectrum obtained from a sound pile. The P-wave speed in this pile was 4140 m/s. The initial straight-line part of the curve was used to determine the dynamic stiffness, which was reported to be 2150 kN/mm. The fundamental longitudinal frequency of 138 kHz was calculated by determining the average frequency difference between four successive peaks. Using Equation 14.13, the length of the pile was calculated to be 15.0 m. The known length of the pile was 15.2 m.[21]

For comparison, Figure 14.17B shows the response spectrum obtained from the second test pile that contained a defect across the full width of the pile at a depth of 9.8 m. The P-wave speed in this pile was 4200 m/s. The measured dynamic stiffness of 1715 kN/mm was lower than that for the sound pile. The

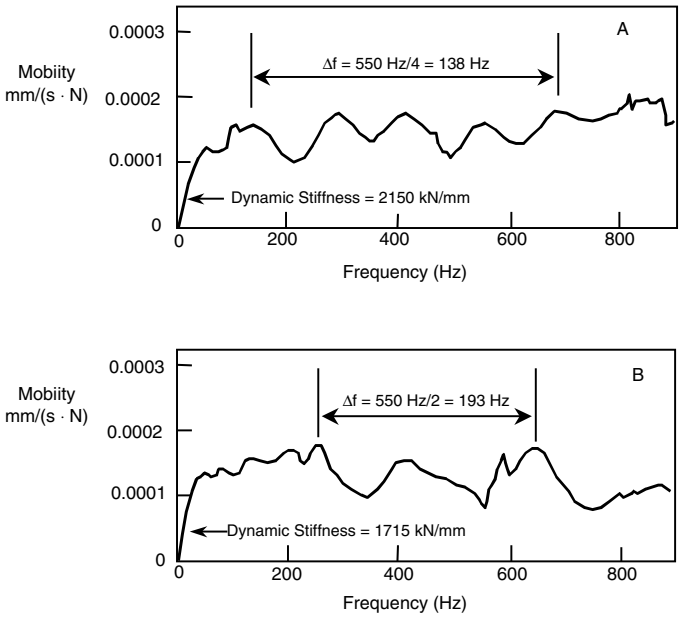

FIGURE 14.17 Mobility plots: (A) sound pile; (B) pile containing a defect across its full width. (Adapted from Reference 21.)

peaks in the response curve are much less regular than for the sound pile. The fundamental frequency was estimated to be 193 Hz. This was obtained by averaging the difference between three successive frequency peaks as shown on Figure 14.17B. By using Equation 14.13, the depth to the reflecting interface was calculated to be about 11 m. Thus, the presence of the defect was indicated by a reduction in the dynamic stiffness and an increase in the fundamental resonant frequency.

The results obtained from actual piles can be complicated by a number of factors that make interpretation of response spectra more difficult than the above examples. Davis and Dunn[69] list the following complicating factors:

- Variations in the diameter of a pile
- Variations in the quality of concrete within a pile
- Variations in the stiffness and damping characteristics of the soil through which the pile passes
- Possible exposure of the top part of the pile above the ground surface

In addition, the length-to-diameter ratio (L/D) for a pile relative to the damping characteristics of the soil must be considered. Higgs[70] states that for L/D greater than 20, test results are not likely to be definitive unless the pile passes through a soft soil deposit onto a rigid stratum.

A simple guide taken from Higgs[70] is shown in Table 14.2. This table offers insight into how results obtained from impulse-response tests on a series of piles might be interpreted. It also demonstrates how the variables calculated from the response spectrum (pile length, dynamic stiffness, and the geometric mean of the mobility, N) are interrelated.

Testing of piles by the impulse-response method is covered in ASTM Test Method D 5882.[12] In that standard, the method is called the "transient response method." Other successful applications besides testing of piles have been reported.[76–78] In these other applications, the method is often used on a comparative basis to identify portions of a structure with anomalous response spectra. This allows determination where other nondestructive tests should be performed or where invasive sampling should be carried out.

TABLE 14.2 Interpretation of Impulse-Response Tests on Piles

Stiffness	Length	N Value[a]	Interpretation
As expected	As built	As expected	Regular pile
Low	As built	High	Possible reduction in pile section or lower grade concrete in pile
Very low	Short	Low	Fault at depth indicated
High	Near or as built	Low	General oversized pile section
Very high	Short	Low	Bulb at depth indicated
High	Multiple	Variable/low	Irregular pile section in pile shaft (enlargements)
Low	Multiple	Variable/high	Irregular pile section in pile shaft (constrictions), or changeable quality of concrete
High	As built	As expected	
Low	As built	As expected	Regular pile with strong anchorage; low settlement expected Regular pile with weak anchorage; high settlement expected

[a] The N-value is the geometric mean of the mobility values in the resonance portion of the response spectrum.
Source: Higgs, J., *Concrete*, Oct., 31, 1979. With permission.

14.3.4 Spectral Analysis of Surface Waves Method

14.3.4.1 Principle

In the late 1950s and early 1960s, Jones[79,80] reported on the use of surface waves to determine the thickness and elastic stiffness of pavement slabs and of the underlying layers. The method involved determining the relationship between the wavelength and velocity of surface vibrations as the vibration frequency was varied. Apart from the studies reported by Jones there seems to have been little use of this technique for testing concrete pavements. In the early 1980s, however, researchers at The University of Texas at Austin began studies of a surface wave technique that involved an impactor instead of a steady-state vibrator. Digital signal processing was used to develop the relationship between wavelength and velocity. The technique was called "spectral analysis of surface waves" (SASW).[81,82]

In the SASW method, a transient stress pulse is generated by impact on the surface of the test site. Two receivers, located as shown in Figure 14.18, monitor the movement of the surface as the waves produced by the impact propagate past the receivers. Because the amplitude of particle motion in the R-wave is large at the surface compared with the amplitude of motion in the P- and S-waves, surface movement caused by the R-wave dominates the measured response. The waveform measured by the two receivers contains information that is used to construct the stiffness profile of the underlying materials.

The R-wave produced by impact contains a range of frequencies or components of different wavelengths. This range depends on the contact time of the impact; the shorter the contact time, the broader the range of frequencies or wavelengths. The amplitude of particle motion in each component of the R-wave decays exponentially with depth. At a depth below the surface of about 1.5 wavelengths, the

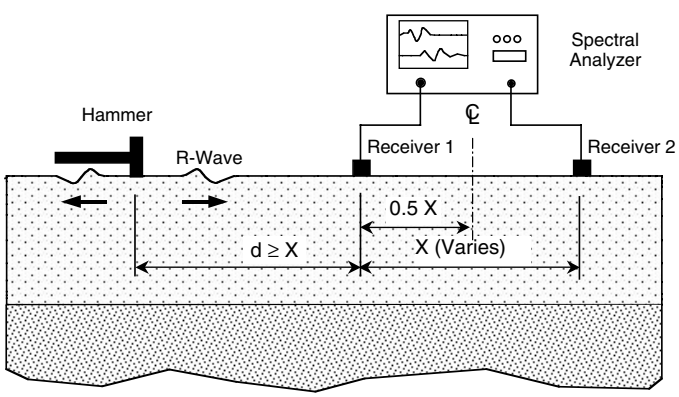

FIGURE 14.18 Schematic of the SASW test method.

amplitude in each component wavelength is one tenth the amplitude at the surface. Thus, longer-wavelength components penetrate more deeply, and this is the key to gaining information about the properties of the underlying layers.

In the SASW method, the impact is chosen so that there are high-frequency (short-wavelength) components in the R-wave that will propagate entirely within the top layer of the layered system. These components propagate with a speed determined by the S-wave speed (depends on shear modulus of elasticity and density) and Poisson's ratio of the top layer (see Equations 14.3 and 14.5). Lower-frequency components penetrate into the underlying layer or layers; and their speed of propagation will be affected by the properties of these layers. Thus, a layered system is a dispersive medium for R-waves, which means that different frequency components in the R-wave will propagate with different speeds, which are called "phase velocities."[83]

Phase velocities are calculated by determining the time it takes for each component frequency to travel between the two receivers. These travel times are determined from the phase difference of the frequency components when they arrive at the receivers. The meaning of "phase difference" is illustrated in Figure 14.19, which shows two points, A and B, on a sine curve with a characteristic period equal to τ. The frequency, f, of the sine curve is the inverse of the period. The phase difference between points A and B is defined as:

$$\phi = \frac{\Delta t}{\tau} 360° = \Delta t \ f \ 360° \tag{14.15}$$

where Δt is the time difference between points A and B. In the SASW method, the waveforms from the two receivers are processed, as explained in the next section, to obtain the phase differences of the component frequencies. Thus, for each frequency, the travel time between the receivers, Δt_f, can be calculated:

$$\Delta t_f = \frac{\phi}{360° f} \tag{14.16}$$

From the travel time, the speed of a component frequency, $C_{R(f)}$, can be determined since the distance, X, between the two receivers is known:

$$C_{R(f)} = \frac{X}{\Delta t_f} = X \frac{360°}{\phi} f \tag{14.17}$$

The wavelength, λ_f, corresponding to a component frequency is calculated using the following equation:

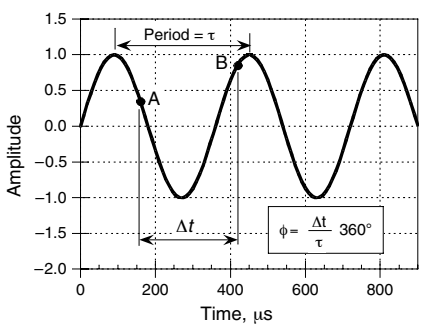

FIGURE 14.19 Definition of phase difference between two points on a periodic waveform.

$$\lambda_f = \frac{C_{R(f)}}{f} = X\frac{360^\circ}{\phi} \tag{14.18}$$

By repeating these calculations for each component frequency, a plot of phase velocity vs. wavelength is obtained. Such a plot is called a "dispersion curve" and is used to obtain the stiffness profile.

An iterative process called "inversion" is used to obtain the approximate stiffness profile at the test site from the experimental dispersion curve.[83–87] First, a numerical model of the test site is created and divided into layers of varying thickness. The number and thicknesses of the layers depend on expected stiffness gradients in the underlying materials. For widely varying properties, thinner layers are needed to accurately define the stiffness profile.[84] Each layer is assigned a density, Poisson's ratio, and shear modulus of elasticity. With this information, the solution for surface wave propagation in a layered system is determined and a theoretical dispersion curve is calculated for the assumed layered system.[84,85] The theoretical dispersion curve is compared with the experimental dispersion curve. If the curves match, the analysis is completed and the assumed stiffness profile is correct. If there are significant discrepancies, the properties of the assumed layered system are changed or refined and a new theoretical curve is calculated. This iterative process continues until there is good agreement between the theoretical and experimental dispersion curves. The user should be experienced in selecting plausible starting values of the elastic constants and have the ability to recognize whether the final values are reasonable. Convergence cannot be assumed to indicate that the correct values have been determined, because it is possible for different combinations of layer thicknesses and elastic moduli to result in similar dispersion curves. Because inversion is time-consuming, automated methods have been developed.[86,87]

14.3.4.2 Signal Processing

The phase information needed to construct the experimental dispersion curve can be obtained from the experimental waveforms by digital signal processing. A brief explanation of the analysis procedure is given here and the reader is referred to the cited references for further details.

Figure 14.20 is an example of waveforms recorded by the two receivers during an SASW test. (The receiver closest to the impact point is connected to channel 1 of the signal analyzer.) The first step is to calculate the cross power spectrum, G_{12}, of the two waveforms as follows:

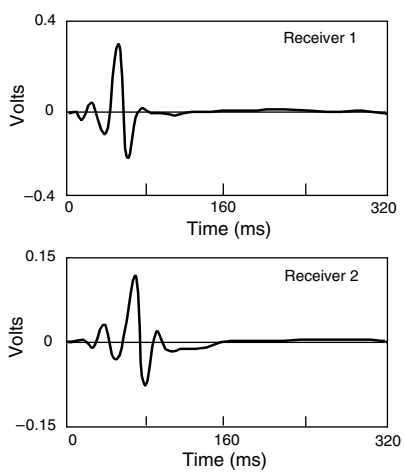

FIGURE 14.20 Waveforms obtained from an SASW test on a pavement. (Adapted from Reference 85.)

$$G_{21} = (S_2)(S_1^*) \tag{14.19}$$

where

S_2 = the Fourier transform of the waveform recorded on channel 2
S_1^* = the complex conjugate of the Fourier transform of the waveform recorded on channel 1

To improve the quality of the data, a test is typically repeated about three to five times, and the average cross power spectrum is used in subsequent steps.[88]

The cross power spectrum can be represented by its amplitude and phase spectra. An example of a phase spectrum is shown in Figure 14.21. The phase spectrum gives the phase difference between the two receivers for each component frequency.* Applying Equation 14.17, the phase difference for each frequency component is used to compute the phase velocity of that component. Finally, by using Equation 14.18, the wavelength of each component is calculated, and the experimental phase velocity vs. wavelength curve is established, that is, the experimental dispersion curve.

The coherence function is also generally calculated as a means of assessing the quality of observed signals.[85] The coherence function spectrum is obtained from power spectra and is defined as

$$\gamma^2 = \frac{G_{21} G_{21}^*}{G_{11} G_{22}^*} \tag{14.20}$$

where

G_{21}^* = the complex conjugate of the average cross power spectrum
G_{11} = the averaged auto power spectrum $(S_1)(S_1^*)$ of the channel 1 waveform
G_{22} = the average auto power spectrum $(S_2)(S_2^*)$ of the channel 2 waveform

A coherence value close to one at a given frequency indicates good correlation between that frequency component in the input signal and in the measured waveform. A low coherence can indicate the presence of noise or other problems in the measured signals.[85] In constructing the experimental dispersion curves, frequencies (wavelengths) with low coherence values are not considered.

14.3.4.3 Instrumentation

There are three components to a SASW test system: the impact source (which is usually a hammer); two receivers, which are geophones (velocity transducers) or accelerometers; and a two-channel spectral analyzer or computer system for recording and processing the waveforms.

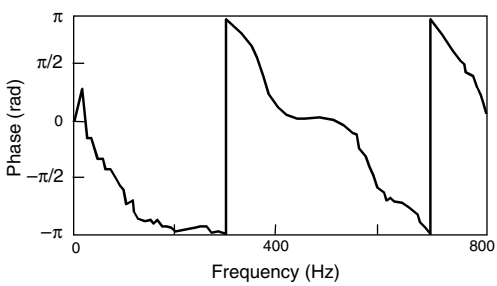

FIGURE 14.21 Phase spectrum of averaged cross power spectrum determined from five waveforms such as those shown in Figure 14.18. (Adapted from Reference 85.)

* Phase spectrum is usually plotted so that the phase angle axis ranges from $-\pi$ to π radians. Hence the spectrum "folds over" when the phase angle reaches $-\pi$ radians, giving the phase spectrum a "sawtooth" pattern.

The general test configuration is shown above in Figure 14.18. It has been found that because of experimental limitations, reliable phase velocities are calculated only for components with wavelengths greater than one half the receiver spacing and less than three times the spacing.[89] Thus, to construct a reliable dispersion curve over a wide range of wavelengths, tests are repeated with different receiver spacings. The test arrangement used commonly is illustrated in Figure 14.22, which is known as the common receivers midpoint (CRMP) geometry.[84,89] In this arrangement, the receivers are always located equidistant from a chosen centerline. The receivers are first located close together, and for subsequent tests the receiver spacing is increased by a factor of two. The source is moved so that the distance between source and nearest receiver is equal to or greater than the distance between the two receivers. As a check on the measured phase information, for each receiver spacing, a second series of tests is carried out by reversing the position of the source. Typically, five receiver spacings are used at each test site. For tests of concrete pavements, the closest spacing is usually about 0.15 m.[85] Sheu et al.[90] provide additional guidance on positioning the source and receivers relative to boundaries to minimize the effects of the reflected surface wave.

The required characteristics of the impact source depend on the stiffnesses of the layers, the distances between the two receivers, and the depth to be investigated.[89] When investigating concrete pavements, the receivers are located relatively close together. In this case, a small hammer is required so that a short-duration pulse is produced with sufficient energy at frequencies up to about 10 to 20 kHz. As an approximation, the highest-frequency component with significant energy can be taken as the inverse of the pulse duration (contact time). As the depth to be investigated increases, the distance between receivers also increases, and an impact that generates a pulse with greater energy at lower frequencies is required. Thus, heavier hammers, such as a sledgehammer, are used.

The two receiving transducers measure vertical surface velocity or acceleration. The selection of transducer type depends in part on the test site.[89] For tests at soil sites where deep layers are to be investigated and larger receiver spacings are used, geophones are generally used because of their superior low-frequency sensitivity. For tests of concrete pavements where shallower depths are investigated and closer spacings are used, the receivers must provide accurate measurements at higher frequencies. Thus, for pavements a combination of geophones and accelerometers is often used.[89]

14.3.4.4 Applications

The SASW method has been used to determine the S-wave speed profiles of soil sites and stiffness profiles of flexible and rigid pavement systems.[81,82,88,89,91,92] The method has also been used for the monitoring the curing of concrete slabs by measuring the increase in wave speed with time,[93] and for evaluation of surface damage and repairs.[94]

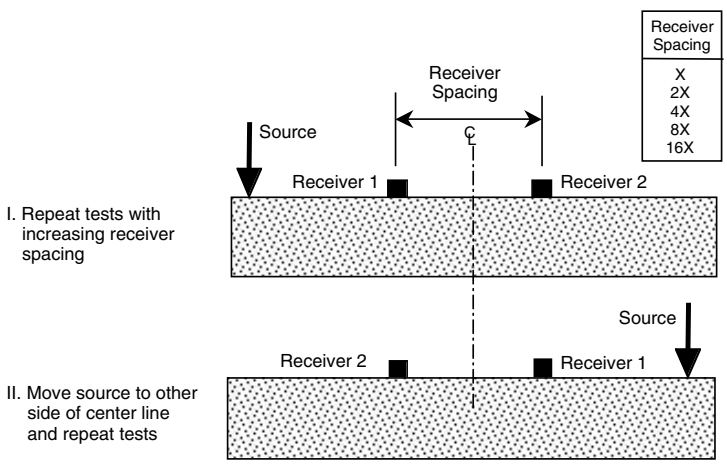

FIGURE 14.22 Common receivers midpoint geometry used in repeated SASW tests to improve reliability.

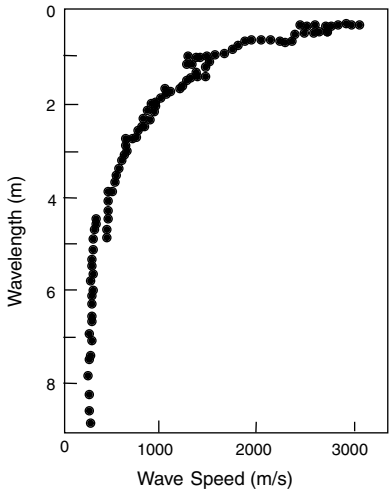

FIGURE 14.23 Experimental dispersion curve from SASW tests on concrete pavement. (Adapted from Reference 89.)

An example of the use of the SASW method for testing reinforced concrete pavement systems is presented here. Concrete pavement systems present the most difficult challenge for the SASW method because the large contrast in stiffness between the concrete pavement and the underlying subgrade makes the inversion procedure numerically difficult.[89] Nazarian and Stokoe,[89] however, developed a technique that has been shown to be successful in a number of studies on concrete pavements. At many of these sites they were able to verify their results by comparison with pavement and soil profiles obtained from boreholes. Following are some typical results.

At one test site,[89] accelerometers were used so that frequencies up to 12.5 kHz could be measured. Figure 14.23 shows the experimental dispersion curve obtained from this series of tests. The S-wave speed profile obtained after inversion is shown in Figure 14.24A. This profile shows that the S-wave speed in the concrete is 2950 m/s. This speed was found to be representative of the good-quality concrete used in construction of the pavement. For comparison, Figure 14.24B shows the profile obtained from borings. Borings showed that the pavement system consisted of approximately 255 mm of reinforced concrete, 100 mm of asphalt–concrete base, 150 mm of lime-treated subbase, and subgrade. The shape of the S-wave speed profile obtained from the SASW testing is in excellent agreement with the actual depths of the subsurface layers. If desired, the S-wave speed profile can be converted to a profile of Young's modulus of elasticity. This requires knowledge of the density and Poisson's ratio for each of the layers. It must be realized, however, that the computed stiffnesses are representative of behavior only at the low strain levels associated with the SASW test.

14.4 Summary

This chapter has reviewed test methods that are based on stress wave propagation. The principles, instrumentation, signal processing techniques, and representative applications of each test method have been discussed. The common feature of the various methods is that inferences about internal conditions of concrete structures are made based on the effect that the structure has on the propagation of stress waves. In all cases, stress waves are introduced into the test object and the surface response is monitored. Access to only one surface is required. Depending on the details of the testing configuration and the measured response, different information is gained about the structure.

Conceptually, the pulse-echo method is the simplest technique. The method involves measuring the travel time from the generation of the stress pulse to the arrival of the reflected echo. Knowing the wave

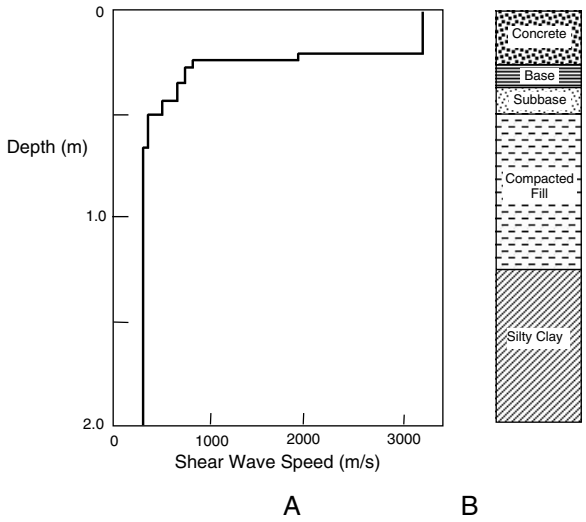

FIGURE 14.24 (A) S-wave speed profile obtained from inversion of dispersion curve shown in Figure 14.23; (B) soil profile obtained from borehole. (Adapted from Reference 89.)

speed, one can calculate the depth of the reflector. A reflector is any interface where there is a change in the specific acoustic impedance, such as that occurring at an internal defect or the boundaries of the structure. Development of practical pulse-echo test systems for concrete has been hindered by the difficulties inherent in developing an adequate low-frequency transducer that can emit a short-duration pulse. Some success has been achieved in the laboratory. Maximum penetration is limited, however, and a practical field system is yet to be developed.

The impact-echo method uses mechanical impact to generate a high-energy stress pulse. Surface displacements are measured near the impact point. The stress pulse undergoes multiple reflections between the test surface and the reflecting interface, and results in a periodic surface motion. This permits frequency analysis of the recorded surface displacement waveforms. The dominant frequency in the amplitude spectrum is used to determine the depth of the reflecting interface from the known wave speed. The amplitude spectra along a scan line can be used to construct a cross section of the structure, which displays the location of the reflecting interfaces. The theoretical basis of the impact-echo method has been established using numerical simulations of transient wave propagation in various types of bounded solids. The ability of the method to detect a variety of defects has been demonstrated. Several commercial impact-echo test systems are available, and a standard test method has been developed for measuring the thickness of slablike structures.

The impulse-response method is similar to the impact-echo method, except that the force-time history of the impact is recorded and more complex signal processing is used. The frequency content of the received waveform is correlated with the frequency content of the force-time function, from which inferences can be made about structural conditions. The method is widely used for testing piles, and a standard test method has been developed. Information about pile length, presence of defects, and overall pile head stiffness is obtained from the test results. The method is also used for comparative testing of slablike structures. Commercial test systems are available.

The SASW method uses signal processing techniques similar to those used in the impulse-response method, but information about the structure is extracted from the surface wave created by impact. It is the most complex of the impact methods covered in this review. The SASW method is based on the principle that the various wavelength components in the impact-generated surface wave penetrate to different depths in the test structure. By monitoring the surface motion at two points a known distance apart, information is extracted about the speed of the various wavelength components that can then be

used to infer the elastic properties of the underlying materials. It has been used successfully to construct the stiffness profiles of pavement systems. It is a computationally intensive test method.

The three impact techniques appear similar in terms of the physical test procedure. By using different sensors and signal processing methods, the user can obtain different information about the test object. Each method is best for particular kinds of applications. Persons interested in using nondestructive testing methods based on stress wave propagation will probably find it advantageous to develop the ability to use all the methods so that the most appropriate one can be used for a particular situation. Users are cautioned, however, that these methods require a relatively high level of expertise and training compared with some of the other methods covered in this handbook.

Impact techniques are a departure from the high-frequency, pulse-echo technology, which works so well for metals, to test methods where low-frequency stress waves are generated by mechanical impact. This appears to be the key for overcoming many of the difficulties involved with testing heterogeneous materials with stress waves. With new developments in automation and signal processing, these methods will find increasing use as routine tools for evaluating internal conditions of concrete structures.

References

1. ASTM D 4580, Practice for Measuring Delaminations in Concrete Bridge Decks by Sounding, *Annual Book of ASTM Standards,* Vol. 04.03, ASTM, West Conshohocken, PA, 2002.
2. Slizard, J., Ed., *Ultrasonic Testing*, John Wiley & Sons, New York, 1982.
3. ASTM E 114, Practice for Ultrasonic Pulse-Echo Straight Beam Examination by the Contact Method, *2002 Annual Book of ASTM Standards,* Vol. 03.03, ASTM, West Conshohocken, PA, 2002.
4. Timoshenko, S.P. and Goodier, J.N., *Theory of Elasticity*, 3rd ed., McGraw-Hill, New York, 1970.
5. Banks, B., Oldfield, G., and Rawding, H., *Ultrasonic Flaw Detection in Metals*, Prentice-Hall, Englewood Cliffs, NJ, 1962.
6. Viktorov, I., *Rayleigh and Lamb Waves*, translated by W.P. Mason, Plenum Press, New York, 1967.
7. Sansalone, M. and Carino, N.J., Impact-echo: a method for flaw detection in concrete using transient stress waves, NBSIR 86-3452, National Bureau of Standards (NTIS PB 87-104444/AS), Sept. 1986.
8. Krautkramer, J. and Krautkramer, H., *Ultrasonic Testing Fundamentals*, Springer-Verlag, New York, 1969.
9. Carino, N.J., Laboratory study of flaw detection in concrete by the pulse-echo method, in *In Situ/ Nondestructive Testing of Concrete*, Malhotra, V.M., Ed., ACI SP-82, American Concrete Institute, Farmington Hills, MI, 1984, 557.
10. Thornton, H.T. and Alexander, A.M., Development of nondestructive testing systems for in-situ evaluation of concrete structures, Tech. Rep. REMR-CS-10, Waterways Exp. Sta., U.S. Army Corps of Engineers, December 1987.
11. Hillger, W., Imaging defects in concrete by ultrasonic pulse-echo techniques, in *Proc. Third International Conf. on Struct. Faults and Repair,* July, University of Edinburgh, Engineering Technics Press, 2003, 59.
12. ASTM D 5882, Test Method for Low Strain Integrity Testing of Piles, *Annual Book of ASTM Standards,* Vol. 04.08, ASTM, West Conshohocken, PA, 2002.
13. Bradfield, G. and Gatfield, E., Determining the thickness of concrete pavements by mechanical waves: directed beam method, *Mag. Concr. Res.*, 16(46), 49, 1964.
14. Howkins, S. et al., Measurement of pavement thickness by rapid and nondestructive methods, NCHRP Report 52, 1968.
15. Mailer, H., Pavement thickness measurement using ultrasonic techniques, *Highway Res. Rec.*, 378, 20–28, 1972.
16. Weber, W., Jr., Grey, R., and Cady, P., Rapid measurement of concrete pavement thickness and reinforcement location C field evaluation of nondestructive systems, NCHRP Report 168, 1976.

17. Claytor, T. and Ellingson, W., Development of ultrasonic methods for the nondestructive inspection of concrete, in *Proc. Ultrasonics Symp.,* Halifax, Nova Scotia, July 1983.
18. Forrest, J., In-situ measuring techniques for pile length, TN-1475, Civil Eng. Lab., Naval Constr. Battalion Center, Port Hueneme, CA, March 1977.
19. Smith, R., The use of surface scanning waves to detect surface opening cracks in concrete, in *In Situ/Nondestructive Testing of Concrete*, Malhotra, V. M., Ed., ACI SP-82, American Concrete Institute, Farmington Hills, MI, 1984, 557.
20. Alexander, A.M. and Thornton, H.T., Jr., Ultrasonic pitch–catch and pulse-echo measurements in concrete, in *Nondestructive Testing of Concrete*, Lew, H.S., Ed., ACI SP-112, American Concrete Institute, Farmington Hills, MI, 1989, 21.
21. Olson, L. and Church, E., Survey of nondestructive wave propagation testing methods for the construction industry, in *Proc. 37th Annual Highway Geology Symp.,* Helena, MT, Aug. 1986.
22. Carino, N.J., Sansalone, M., and Hsu, N.N., A point source–point receiver technique for flaw detection in concrete, *J. Am. Conc. Inst*., 83 (2), 199, 1986.
23. Carino, N.J., Sansalone, M., and Hsu, N.N., Flaw detection in concrete by frequency spectrum analysis of impact-echo waveforms, in *International Advances in Nondestructive Testing*, 12th ed., McGonnagle, W.J., Ed., Gordon & Breach Science, New York, 1986, 117.
24. Sansalone, M, Impact-echo: the complete story, *ACI Struct. J*., 94(6), 777, 1997.
25. Sansalone, M. and Streett, W.B., *Impact-Echo: Nondestructive Testing of Concrete and Masonry*, Bullbrier Press, Jersey Shore, PA, 1997.
26. Sansalone, M., Lin, J.M., and Streett, W.B., A procedure for determining P-wave speed in concrete for use in impact-echo testing using a P-wave speed measurement technique, *ACI Mater. J*., 94(6), 531, 1997.
27. Stearns, S., *Digital Signal Analysis*, Hayden, Rochelle Park, NJ, 1975.
28. Sansalone, M. and Carino, N.J., Laboratory and field study of the impact-echo method for flaw detection in concrete, in *Nondestructive Testing of Concrete*, Lew, H.S., Ed., ACI SP-112, American Concrete Institute, Farmington Hills, MI, 1989, 1.
29. Carino, N.J. and Sansalone, M., Impact-echo: a new method for inspecting construction materials, in *Proc. Conf. Nondestructive Testing and Evaluation for Manufacturing and Construction,* dos Reis, H.L.M., Ed., Hemisphere, Washington, D.C., 1990, 209.
30. Stain, R., Integrity testing, *Civ. Eng.* (London), April, 53, 1982.
31. Steinbach, J. and Vey, E., Caisson evaluation by stress wave propagation method, *J. Geotech. Eng. Div*. ASCE, 101(GT4), 361, 1975.
32. Vankuten, H. and Middendorp, P., Testing of foundation piles, *Heron*, 26(4), 3, 1982.
33. Brendenberg, H., Ed., *Proc. of the Int. Seminar on the Application of Stress-Wave Theory on Piles,* Stockholm, 1980.
34. Olson, L.D. and Wright, C.C., Seismic, sonic, and vibration methods for quality assurance and forensic investigation of geotechnical, pavement, and structural systems, in *Proc. Conf. Nondestructive Testing and Evaluation for Manufacturing and Construction,* dos Reis, H.L.M., Ed. Hemisphere, Washington, D.C., 1990, 263.
35. Sansalone, M. and Carino, N.J., Detecting delaminations in concrete slabs with and without overlays using the impact-echo method, *J. Am. Conc. Inst*., 86(2), 175, 1989.
36. Sansalone, M. and Carino, N.J., Impact-echo method: detecting honeycombing, the depth of surface-opening cracks, and ungrouted ducts, *Concr. Int.*, 10(4), 38, 1988.
37. Goldsmith, W., *Impact: The Theory and Physical Behavior of Colliding Solids*, Edward Arnold Press, London, 1965, 24–50.
38. Proctor, T.M., Jr., Some details on the NBS conical transducer, *J. Acoust. Emission*, 1(3), 173, 1982.
39. Pratt, D. and Sansalone, M., Impact-echo signal interpretation using artificial intelligence, *ACI Mater. J.*, 8(2), 178, 1992.

40. Sansalone, M. and Carino, N.J., Transient impact response of thick circular plates, *J. Res. Natl. Bur. Stand.*, 92(6), 355, 1987.
41. Sansalone, M. and Carino, N.J., Transient impact response of plates containing flaws, *J. Res. Natl. Bur. Stand.*, 92(6), 369, 1987.
42. Sansalone, M., Carino, N.J., and Hsu, N.N., A finite element study of transient wave propagation in plates, *J. Res. Natl. Bur. Stand.*, 92(4), 278, 1987.
43. Sansalone, M., Carino, N.J., and Hsu, N.N., A finite element study of the interaction of transient stress waves with planar flaws, *J. Res. Natl. Bur. Stand.*, 92(4), 279, 1987.
44. Sansalone, M., Carino, N.J., and Hsu, N.N., Finite element studies of transient wave propagation, in *Review of Progress in Quantitative Nondestructive Evaluation*, Vol. 6A, Thompson, D.O. and Chimenti, D.E., Eds., Plenum Press, New York, 1987, 125.
45. Sansalone, M., Carino, N.J., and Hsu, N.N., Flaw detection in concrete and heterogeneous materials using transient stress waves, *J. Acoust. Emission*, 5(3), S2, 1986.
46. Carino, N.J. and Sansalone, M., Detecting voids in metal tendon ducts using the impact-echo method, *ACI Mater. J.*, 89(3), 296, 1992.
47. Poston, R. and Sansalone, M., Detecting cracks in beams and columns of a post-tensioned parking garage using the impact-echo method, in *Innovations in Nondestructive Testing*, SP-168, Pessiki, S. and Olson, L., Eds., American Concrete Institute, Farmington Hills, MI, 1997, 199.
48. Poston, R.W., Whitlock, A.R., and Kesner, K.E., Condition assessment using nondestructive evaluation, *Concr. Int.*, 17(7), 36, 1995.
49. Hendrikson, C., Impact-echo testing, *Concr. Int.*, 17(5), 55, 1995.
50. Jaeger, B., Sansalone, M., and Poston, R., Detecting voids in grouted tendon ducts of post-tensioned concrete structures using the impact-echo method, *ACI Struct. J.*, 93 (4), 462, 1996.
51. Jaeger, B.J., Sansalone, M.J., and Poston, R.W., Using impact-echo to assess tendon ducts, *Concr. Int.*, 19(2), 42, 1997.
52. Lin, Y., Sansalone, M., and Carino, N.J., Finite element studies of the impact-echo response of plates containing thin layers and voids, *J. Nondest. Eval.*, 9(1), 27, 1990.
53. Cheng, C. and Sansalone, M., The impact-echo response of concrete plates containing delaminations: numerical, experimental, and field studies, *Mater. Struct.* (RILEM), 26(159), 274, 1993.
54. Cheng, C. and Sansalone, M., Effects on impact-echo signals caused by steel reinforcing bars and voids around bars, *ACI Mater. J.*, 90(5), 421, 1993.
55. Cheng, C. and Sansalone, M., Determining the minimum crack width that can be detected using the impact-echo method, Part 1: Experimental study, *Mater. Struct.* (RILEM), 28(176), 74, 1995.
56. Cheng, C. and Sansalone, M., Determining the minimum crack width that can be detected using the impact-echo method, Part 2: Numerical fracture analyses, *Mater. Struct.* (RILEM), 28(177), 125, 1995.
57. Lin, J.M. and Sansalone, M., The transverse elastic impact response of thick hollow cylinders, *J. Nondest. Eval.*, 12(2), 139, 1993.
58. Lin, J.M. and Sansalone, M., Impact-echo response of hollow cylindrical concrete structures surrounded by soil and rock, Part I: Numerical studies, *Geotech. Test. J.* (ASTM), 17(2), 207, 1994.
59. Lin, J.M. and Sansalone, M., Impact-echo response of hollow cylindrical concrete structures surrounded by soil and rock, Part II: Experimental studies, *Geotech. Testing J.* (ASTM), 17(2), 220, 1994.
60. Lin, Y. and Sansalone, M., Transient response of thick circular and square bars subjected to transverse elastic impact, *J. Acoust. Soc. Am.,* 91(2), 885, 1992.
61. Lin, Y. and Sansalone, M., Transient response of thick rectangular bars subjected to transverse elastic impact, *J. Acoust. Soc. Am*, 91(5), 2674, 1992.
62. Lin, Y. and Sansalone, M., Detecting flaws in concrete beams and columns using the impact-echo method, *ACI Mater. J.*, 89(4), 394, 1992.
63. Lin, J.M. and Sansalone, M., Impact-echo studies of interfacial bond quality in concrete, Part I: Effects of unbonded fraction of area, *ACI Mater. J.,* 93(3), 223, 1996.

64. Lin, J.M., Sansalone, M., and Poston, R., Impact-echo studies of interfacial bond quality in concrete, Part II: Effects of bond tensile strength, *ACI Mater. J.*, 93(4), 318, 1996.
65. Williams, T.J., Sansalone, M., Streett, W.B., Poston, R., and Whitlock, R., Nondestructive evaluation of masonry structures using the impact-echo method, *TMS J.*, 15(1), 47, 1997.
66. ASTM C 1383, Standard Test Method for Measuring the P-Wave Speed and Thickness of Concrete Plates Using the Impact-Echo Method, *Annual Book of ASTM Standards*, Vol. 04.02, ASTM, West Conshohocken, PA, 2002.
67. Lin, J.M. and Sansalone, M., A procedure for determining P-wave speed in concrete for use in impact-echo testing using a Rayleigh wave speed measurement technique, in *Innovations in Nondestructive Testing*, SP-168, Pessiki, S. and Olson, L., Eds., American Concrete Institute, Farmington Hills, MI, 1997, 137.
68. Sansalone, M., Lin, J.M., and Streett, W.B., A procedure for determining concrete pavement thickness using P-wave speed measurements and the impact-echo method, in *Innovations in Nondestructive Testing*, SP-168, Pessiki, S. and Olson, L., Eds., American Concrete Institute, Farmington Hills, MI, 1997, 167.
69. Davis, A. and Dunn, C., From theory to field experience with the nondestructive vibration testing of piles, *Proc. Inst. Civ. Eng.*, 57(2), 571, 1974.
70. Higgs, J., Integrity testing of piles by the shock method, *Concrete*, Oct., 31, 1979.
71. Davis, A.G. and Hertlein, B.H., Developments of nondestructive small-strain methods for testing deep foundations: a review, *Transp. Res. Rec.,* 1331, 15, 1991.
72. Bracewell, R., *The Fourier Transform and Its Applications*, 2nd ed., McGraw-Hill, New York, 1978.
73. Papoulis, A., *Signal Processing*, McGraw-Hill, New York, 1977.
74. Finno, R.J. and Gassman, S.L., Impulse response evaluation of drilled shafts, *J. Geotech. Geoenviron. Eng.*, 124(10), 965, 1998.
75. Paquet, J. and Briard, M., Controle non destrucht des pieux en beton, *Ann. Inst. Tech. Batim. Trav. Publics*, 337, 49, 1976.
76. Davis, A.G. and Hertlein, B.H., Assessment of bridge deck repairs by a nondestructive technique, in *Proc. NATO Advanced Research Workshop on Bridge Evaluation, Repair, and Rehabilitation,* April 30–May 2, Baltimore, MD, Nowak, A.J., Ed., Kluwer Academic, Boston, 1990, 229.
77. Davis, A.G., Evans, J.G., and Hertlein, B.H., Nondestructive evaluation of concrete radioactive waste tanks, *J. Perf. Const. Fac.,* ASCE, 11(4), 161, 1997.
78. Nazarian, S., Reddy, S., and Baker, M., Determination of voids under rigid pavements using impulse response method, in *Nondestructive Testing of Pavements and Backcalculation of Moduli,* 2nd ed., von Quintas, H.L., Bush, A.J. and Baladi, G.Y., Eds., ASTM STP 1198, ASTM, Philadelphia, 1994.
79. Jones, R., Surface wave technique for measuring the elastic properties and thickness of roads: theoretical development, *Br. J. Appl. Phys.*, 13, 21, 1962.
80. Jones, R., A vibration method for measuring the thickness of concrete road slabs *in situ*, *Mag. Concr. Res.*, 7(20), 97, 1955.
81. Heisey, J.S., Stokoe, K.H., II, and Meyer, A.H., Moduli of pavement systems from spectral analysis of surface waves, *Transp. Res. Rec.*, 853, 22, 1982.
82. Nazarian, S., Stokoe, K.H., II, and Hudson, W.R., Use of spectral-analysis-of-surface-waves method for determination of moduli and thicknesses of pavement systems, *Transp. Res. Rec.*, 930, 38, 1983.
83. Krstulovic-Opara, N., Woods, R.D., and Al-Shayea, N., Nondestructive testing of concrete structures using the Rayleigh wave dispersion method, *ACI Mater. J.*, 93(1), 75, 1996.
84. Rix, G.J. and Leipiski, E.A., Accuracy and resolution of surface wave inversion, in *Recent Advances in Instrumentation, Data Acquisition and Testing in Soil Dynamics*, Bhatia, S.K. and Blaney, G.W., Eds., Geotech. S.P. 29, ASCE, Reston, VA, 1991, 17.
85. Nazarian, S. and Stokoe, K.H., II, In-situ determination of elastic moduli of pavement systems by spectral-analysis-of-surface-waves method (theoretical aspects), Res. Rep. 437-2, Center for Transportation Research, The University of Texas, Austin, 1986.

86. Nazarian, S. and Desai, M.R., Automated surface wave method: field testing, *J. Geotech. Eng.* (ASCE), 119(7), 1094, 1993.
87. Yuan, D. and Nazarian, S., Automated surface wave method: inversion technique, *J. Geotech. Eng.* (ASCE), 119(7), 1112, 1993.
88. Nazarian, S. and Stokoe, K.H., II, Nondestructive testing of pavements using surface waves, *Transp. Res. Rec.*, 930, 1984.
89. Nazarian, S. and Stokoe, K.H., II, In-situ determination of elastic moduli of pavement systems by spectral-analysis-of-surface-waves method (practical aspects), Res. Rep. 368-1F, Center for Transportation Research, The University of Texas at Austin, 1986.
90. Sheu, J.C., Stokoe, K.H., II, and Roesset, J.M., Effect of reflected waves in SASW testing of pavements, *Transp. Res. Rec.,* 1196, 1989.
91. Nazarian, S. and Stokoe, K.H., II, Use of surface waves in pavement evaluation, *Transp. Res. Rec.,* 1070, 1986.
92. Rix, G.J. and Stokoe, K.H., II, Stiffness profiling of pavement subgrades, *Transp. Res. Rec.,* 1235, 1, 1989.
93. Rix, G.J., Bay, J.A., and Stokoe, K.H., II, Assessing *in situ* stiffness of curing portland cement concrete with seismic tests, *Transp. Res. Rec.,* 1284, 8, 1990.
94. Kalinski, M.E., Nondestructive characterization of damaged and repaired areas of a concrete beam using the SASW method, in *Innovations in Nondestructive Testing*, SP-168, Pessiki, S. and Olson, L., Eds., American Concrete Institute, Farmington Hills, MI, 1997, 111.

15

Infrared Thermographic Techniques

15.1 Introduction
15.2 Historical Background
15.3 Theoretical Considerations
15.4 Testing Equipment
15.5 Testing Procedures
15.6 Case Histories
15.7 Advantages and Limitations
15.8 Summary

Gary J. Weil
Entech Engineering, Inc.

Infrared thermography, a nondestructive, remote sensing technique, has proved to be an effective, convenient, and economical method of testing concrete. It can detect internal voids, delaminations, and cracks in concrete structures such as bridge decks, highway pavements, garage floors, parking lot pavements, and building walls. As a testing technique, some of its most important qualities are that (1) it is accurate; (2) it is repeatable; (3) it need not inconvenience the public; and (4) it is economical. This chapter provides a summary of the historical development of this technique, discusses the underlying theory, describes the test equipment, and gives example case histories.

15.1 Introduction

Concrete is one of the world's most useful building materials. It is used in almost every phase of society's infrastructure: from the buildings that house people to the roads and bridges that allow us to travel from place to place; from the dams that help control nature's forces to the launchpads that help us explore the heavens. This building material has strength and rigidity along with versatility, but it does have its limits. Most concrete structures have a design life of 20 to 25 years, and when they begin to deteriorate they do so slowly at first and then gradually progress to failure. This failure can be expensive in terms of both dollars and lives, but this scenario can be avoided. Planned restoration can extend the life of concrete structures almost indefinitely, and testing of concrete structures to establish the existing conditions is the basis of economically viable restoration. For any testing technique to be widespread, it must have the following qualities:

1. It must be accurate.
2. It must be repeatable.
3. It must be nondestructive.
4. It must be able to inspect large areas as well as localized areas.
5. It must be efficient in terms of both labor and equipment.
6. It must be economical.

7. It must not be obtrusive to the surrounding environment.
8. It must not inconvenience the structure's users.

One technique for testing in-place concrete has emerged during the past 30 years that fulfills all of these requirements. That technique is called infrared thermographic testing. During its gestation period, it has been used to test concrete on bridge decks, highways, dams, garages, airport taxiways, and buildings. It has shown itself to be both accurate and efficient in locating subsurface voids, delaminations, as well as poor binding, moisture entrapment, and other anomalies in concrete structures.

15.2 Historical Background

Infrared thermographic investigation techniques are based on the fundamental principle that materials with subsurface anomalies, such as voids caused by corrosion on reinforcing steel, or voids caused by poor concrete consolidation called honeycombing, or pooling fluids such as water infiltration, in a material affect heat flow through that material. These changes in heat flow cause localized differences in surface temperature. Thus, by measuring surface temperatures under conditions of heat flow into or out of the material, one can determine the presence and location of any subsurface anomalies.

The first documented experimental paper on using infrared thermography to detect concrete subsurface delaminations was published by the Ontario Ministry of Transportation and Communication in 1973. It illustrated effective methods, although they depended on relatively crude, inefficient techniques.[1] Using these basic techniques, additional research was performed.[2] These later studies were performed on concrete bridge decks, again located in Canada. They were based on the use of a simple infrared imager to measure surface temperatures, without the use of computer enhancements. They were carried out using a variety of techniques, such as both daytime and nighttime data collection. They proved that infrared thermographic techniques could be used to detect concrete subsurface delaminations on bridge decks.

During the next 10 years, the Ontario Ministry of Transportation and Communications was a strong advocate of research on these infrared thermographic techniques. At the same time, research was progressing in the United States,[3,4] and continued into the late 1980s.[5–10] An early study was performed for the Wisconsin Department of Transportation along a four-lane, 16-mi (27-km) portion of Interstate 90/94. In this study, videotape was used to record both visible and infrared images of the highway. These tests used manual methods to transfer the delamination data to scaled plan drawings.

In 1983, major concrete bridge deck delamination analysis was performed on the Dan Ryan Expressway located in Chicago. This investigation was significant because it showed that infrared thermography could be used efficiently on congested highways. The fieldwork was performed from a mobile van with traffic control provided by two signboard vehicles behind the data collection van. Permanent lane closure was not required, thereby reducing costs and inconvenience, particularly for the motorists using the expressway. Field data on the 11-mi (17.6-km), eight-lane expressway in Chicago was collected in 14 h during five separate days, significantly less time than would have been needed for other inspection techniques such as chain dragging, deflectometer, sounding, or coring.

In 1985, concrete pavement delamination inspections were performed on the Poplar Street Bridge entrance and exit ramps and bridge decks spanning the Mississippi River at St. Louis, Missouri for the Illinois Department of Transportation. The bridges are a major part of the highway system on Interstate 55-70 and include approximately 40 lane-mi (65 km) of bridge deck roadways. These were crucial structures because more than 90% of the traffic between Missouri and Illinois, near St. Louis, crossed these bridges. Traffic stoppages had to be kept to a minimum. Five techniques were evaluated: (1) visual inspections, (2) infrared thermography, (3) ground penetrating radar, (4) corings, and (5) chloride measurements. The various tests were performed by separate firms, and the results were analyzed by an independent engineering firm. All data were recorded on a scaled computer-aided design (CAD) system to allow overlaying of the data and comparisons of the results of the various techniques at individual

locations as well as overall statistics. infrared thermography proved to be the most accurate nondestructive method as well as the most efficient and economical to perform.

One of the largest individual infrared thermographic inspections occurred in 1987 at the Lambert St. Louis International Airport. This involved testing concrete taxiways. The concrete slabs ranged from 14 to 18 in. (360 to 460 mm) in thickness. The rules set up by the airport engineering department dictated that the testing had to be performed during low air traffic periods (11:00 P.M. to 5:00 A.M.) and no loading gates could be blocked. The field inspection was completed in five working nights. Approximately 2,000,000 ft^2 (186,000 m^2) of concrete was inspected with production rates approaching 1,000,000 ft^2 (93,000 m^2) per night. In addition to determining individual slab conditions, the use of an infrared thermography–based system with computer enhancements allowed the determination of damage caused by traffic patterns and underground erosion caused by soil migration and subsurface moisture problems.

15.3 Theoretical Considerations

An infrared thermographic scanning system measures surface temperatures only, but the surface temperatures of a concrete mass depend on three factors: (1) the subsurface configuration, (2) the surface conditions, and (3) the environment.

The subsurface configuration effects are based on the principle that heat cannot be stopped from flowing from warmer to cooler areas; it can only be moved at different rates by the insulating effects of the materials through which it is flowing. Various types of construction materials have different insulating abilities or thermal conductivities. In addition, differing types of concrete defects have different thermal conductivity values. For example, a dead air void caused by "honeycombing" or corrosion-related "delaminations" has a lower thermal conductivity than its surrounding solid concrete.

There are three ways of transferring thermal energy from a warmer to a cooler region: (1) conduction, (2) convection, and (3) radiation. Sound concrete should have the least resistance to conduction of heat, and the internal convection and radiation effects should be negligible. However, the various types of anomalies associated with poor concrete, namely, voids and low density, decrease the thermal conductivity of the concrete by reducing the energy conduction properties, without substantially increasing the convection effects because dead air spaces do not allow the formation of convection currents.

For heat energy to flow, there must be a heat source. Because concrete testing can involve large areas, the heat source should be both low cost and capable of giving the concrete surface an even distribution of heat. The sun fulfills both these requirements. Allowing the sun to warm the surface of the concrete areas under test will normally supply the required energy. During nighttime hours, the process may be reversed with the warm concrete acting as the heat source and the clear night sky acting as the heat sink.

For concrete areas not accessible to sunlight, an alternative is to use the heat storage ability of Earth to draw heat from the concrete under test. The important point is that to use infrared thermography, heat must be flowing through the concrete. It does not matter in which direction it flows.

The second important factor to consider when using infrared thermography to measure temperature differentials due to anomalies is the surface condition of the test area. As noted above, there are three ways to transfer energy. Radiation is the process that has the most profound effect on the ability of the surface to transfer energy. The ability of a material to radiate energy is measured by the emissivity of the material. This is defined as the ability of the material to radiate energy compared with a perfect blackbody* radiator. This is strictly a surface property. The emissivity value is higher for dark, rough surfaces and lower for smooth, shiny surfaces. For example, rough concrete may have an emissivity of 0.95 whereas shiny copper metal may have an emissivity of only 0.05. In practical terms, this means that when using thermographic methods to collect temperature values on large areas of concrete, the engineer must be

*A blackbody is a hypothetical radiation source that radiates the maximum energy theoretically possible at a given temperature. The emissivity of a blackbody equals 1.0.

aware of differing surface textures caused by such things as broom-textured spots, rubber tire tracks, oil spots, or loose sand and dirt on the surface.

The final factor that affects the temperature measurement of a concrete surface is the environmental system that surrounds that surface. Various parameters affect the surface temperature measurements:

1. *Solar Radiation:* Testing should be performed during times of the day or night when the solar radiation or lack of solar radiation would produce the most rapid heating or cooling of the concrete surface.
2. *Cloud Cover:* Clouds will reflect infrared radiation, thereby slowing the heat transfer process to the sky. Therefore, nighttime testing should be performed during times of little or no cloud cover to allow the most efficient transfer of energy from the concrete.
3. *Ambient Temperature:* This should have a negligible effect on the accuracy of the testing because the important consideration is the rapid heating or cooling of the concrete surface. This parameter will affect the length of time (i.e., the window) during which high-contrast temperature measurements can be made. It is also important to consider if water is present. Testing while ground temperatures are lower than 32°F (0°C) should be avoided, as ice can form, thereby filling subsurface voids.
4. *Wind Speed:* High gusts of wind have a definite cooling effect and reduce surface temperatures. Measurements should be taken at wind speeds lower than 15 mph (25 km/h).
5. *Surface Moisture:* Moisture tends to disperse the surface heat and mask the temperature differences and thus the subsurface anomalies. Tests should not be performed while the concrete surface is covered with standing water or snow.

Once the proper conditions are established for thermal data collection, a relatively large area should be selected for calibration purposes. This should encompass concrete areas both good and bad (i.e., areas with voids, delaminations, cracks, or powdery concrete). Each type of anomaly will display a unique temperature pattern depending on the conditions present. If, for example, the data collection process is performed at night, most anomalies will be between 0.01°C and 5°C cooler than the surrounding solid concrete depending on configuration (Figure 15.1). A daylight survey will show reversed results; i.e., concrete surfaces above damaged areas will be warmer than the surrounding sound concrete.

15.4 Testing Equipment

In principle, to test concrete for subsurface anomalies, all that is really needed is a sensitive contact thermometer. However, even for a small test area, thousands of readings would have to be made simultaneously to outline the anomaly precisely. Because this is not practical, high-resolution infrared thermographic radiometers are used (Figure 15.2) to inspect large areas of concrete efficiently and quickly. This type of equipment allows large areas to be scanned, and the resulting data can be displayed as pictures with areas of differing temperatures designated by differing gray tones in a black-and-white image or by various colors on a color image. A wide variety of auxiliary equipment can be used to facilitate data recording and interpretation.

A complete thermographic data collection and analysis system can be divided into four main subsystems. The first is the infrared sensor head that normally can be used with interchangeable lenses. It is similar in appearance to a portable video camera. The scanner's optical system, however, is transparent only to short-wave infrared radiation with wavelengths in the range of 3 to 5.6 μm, or to medium-wave infrared radiation with wavelengths in the range of 8 to 12 μm. Normally the infrared radiometer's highly sensitive detector is cooled by liquid nitrogen to a temperature of –196°C, and it can detect temperature variations as small as 0.1°C. Alternative methods of cooling the infrared detectors are available that use either compressed gases or electric cooling. These last two cooling methods may not give the same resolution, because they cannot bring the detector temperatures as low as liquid nitrogen. In addition, compressed gas cylinders may present safety problems during storage or handling. New types of cooling include mechanical Stirling coolers that are capable of bringing temperatures as low as liquid nitrogen.

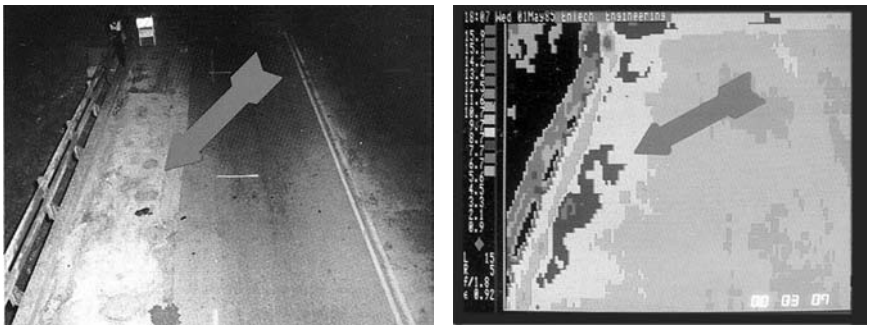

FIGURE 15.1 Color figure follows p. 15-10.) Visual and thermal images of powdery concrete on the Martin Luther King Bridge in St. Louis, Missouri. Red areas on thermal image represent powdery concrete.

FIGURE 15.2 Infrared thermographic radiometer.

Several manufacturers have developed detectors capable of detecting infrared wavelengths at normal room temperatures. These uncooled sensors, coupled with new array-type sensors hold promise for the future of lower-cost radiometers.

The second major component of the infrared scanning system is a real-time microprocessor coupled to a black-and-white or color display monitor. With this component, cooler items being scanned are normally represented by darker gray tones, and warmer areas are represented by lighter gray tones. To make the images easier to interpret for those unfamiliar with interpreting gray-tone images, a color monitor may also be installed. The microprocessor will quantize the continuous gray-tone energy images into two, three, or more "buckets" of energy levels and assign them contrasting visual colors representing relative temperatures. Thus, the color monitor displays the different temperature levels as contrasting colors and patterns, which are easier to decipher.

The third major component of the infrared data collection system is the data acquisition and analysis equipment. It is composed of an analog-to-digital converter for use with analog sensors, a computer with a high-resolution color monitor, and data storage and analysis software. The computer allows the transfer of instrumentation videotape or live images of infrared scenes to single-frame computer images. The images can then be stored individually and later retrieved for enhancement and individual analysis. The use of the computer allows the engineer in charge of testing to set specific analysis standards based on invasive sample tests, such as corings, and apply them uniformly to the entire pavement. Standard, off-the-shelf image analysis programs may be used or custom-written software may be developed.

FIGURE 15.3 Infrared thermographic radiometer sensor and optics mounted on a custom-designed mobile van designed to hold the electronic processing and computer enhancement systems.

The fourth major component consists of various types of image recording and retrieving devices. These are used to record both visual and thermal images. They may be composed of instrumentation videotape recorders, still-frame film cameras with both instant and 35 mm or larger formats, or computer digital images.

All the above equipment may be carried into the field or parts of it may be left in the laboratory for additional use. If all of the equipment is transported to the field to allow simultaneous data acquisition and analysis, it is prudent to use an automotive van to set up and transport the equipment. This van should include power supplies for the equipment, either batteries and inverter or a small gasoline-driven generator. The van should also include a method to elevate the scanner head and accompanying video camera to allow scanning of the widest area possible depending on the system optics used (Figure 15.3).

Several manufacturers produce infrared thermographic equipment. Each manufacturer's equipment has its own strengths and weaknesses. These variations are in a constant state of change as manufacturers alter and improve their equipment. Therefore, equipment comparisons should be made before purchase.

15.5 Testing Procedures

To perform an infrared thermographic inspection, a movement of heat must be established in the structure. The first example deals with the simplest and most widespread situation. Assume that we desire to test an open concrete bridge deck surface. The day preceding the inspection should be dry with plenty of sunshine. The inspection may begin either 2 to 3 h after sunrise or 2 to 3 h after sunset; both are times of rapid heat transfer. The deck should be cleaned of all debris. Traffic control should be established to prevent accidents and to prevent traffic vehicles from stopping or standing on the pavement to be tested. The infrared radiometer should be mounted in a mobile van along with other peripheral equipment such as recorders for data storage and a computer for assistance in data analysis. The scanner head and either a regular film-type camera or a standard video camera should be aligned to view the same sections being tested.

The next step is to locate a section of concrete deck and, by chain dragging (sounding), coring, or ground-penetrating radar, establish that it is sound concrete. Image the reference area and set the equipment controls so that an adequate temperature image is viewed and recorded. Next, locate a section of concrete deck known to be defective by containing a void, delamination, or powdery material, again by using either chain dragging, coring, or ground-penetrating radar. Image this reference area and again make sure that the equipment settings allow the viewing of both the sound and defective reference areas in the same image with the widest contrast possible. These settings will normally produce a sensitivity scale such that the full-scale represents no more than 5°C.

If a black-and-white monitor is used, better contrast images will normally be produced when the following convention is used: black is defective concrete and white is sound material. If a color monitor

or computer-enhanced screen is used, three colors are normally used to designate definite sound areas, definite defective areas, and indeterminate areas. As has been mentioned, when tests are performed during daylight hours, the defective concrete areas will appear warmer, whereas during tests performed after dark, defective areas will appear cooler.

Once the controls are set and traffic control is in place, the van may move forward as rapidly as images can be collected, normally 1 to 30 mph (2 to 50 km/h). If it is desired to mark the pavement, white or metallic paint may be used to outline the defective deck areas when the pavement is covered by black asphalt and orange-colored paint when plain concrete is being investigated. At other times, videotape may be used to document the defective areas, or a scale drawing may be produced complete with bridge deck reference points. Production rates as high as 1,200,000 ft^2/day (112,000 m^2/day) have been attained. During long testing sessions, reinspection of the reference areas should be performed approximately every 2 h, with more calibration retests scheduled during the early and later periods of the session when the testing "window" may be opening or closing.

For inside areas where the sun cannot be used for its heating effect, it may be possible to use the same techniques, except for using the ground as a heat sink. The equipment should be set up in a similar fashion to that designed above, except that the infrared radiometer's sensitivity will have to be increased. Once the data are collected and analyzed, the results should be plotted on scale drawings of the area inspected. Defective areas should be clearly marked so that trends can be observed. Computer enhancements can have varying effects on the accuracy and efficiency of the inspection systems. Image contrast enhancements can improve the accuracy of the analysis by bringing out fine details, and automatic plotting and area analysis software can improve the efficiency in preparing the finished report.

A word of caution: When inspecting areas that contain shadow-causing areas, such as bridges with superstructures or parapet walls, or pavements near buildings, it is preferable to perform the investigation after sundown (Figure 15.4). Because the shadows will constantly move, their resulting temperature variations will average out to a uniform level.

Many of the above basic techniques are included in ASTM D4788, "Test Method for Detecting Delaminations in Bridge Decks Using Infrared Thermography." Since 1988, this consensus standard has been the basis for over 900 bridge and other pavement investigations performed by the author throughout the world.

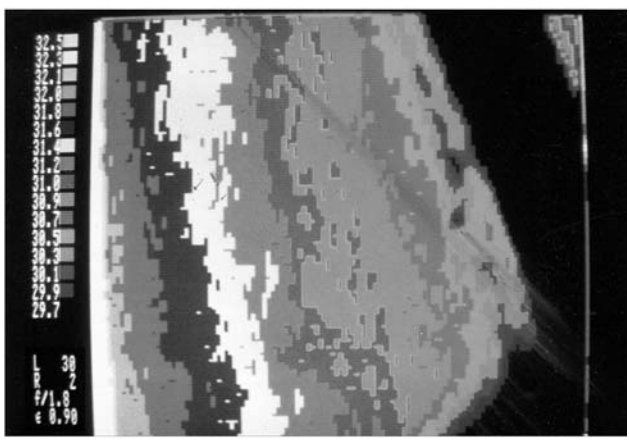

FIGURE 15.4 Color figure follows p. 15-10.) Computer-enhanced thermographic image of concrete pavement next to a three-story building. Bands of temperature are caused by shadows restricting solar energy being absorbed by pavement as shadows move.

15.6 Case Histories

To illustrate some diverse applications for infrared thermographic concrete testing, five case histories are reviewed:

1. Bridge deck concrete
2. Airport taxiway concrete
3. Garage deck concrete
4. Swimming pool concrete
5. Tunnel wall concrete

Each of these investigations highlights a different important application of this nondestructive, remote-sensing evaluation technique.

The first case history reviews the inspection of an asphalt overlaid concrete deck on the nation's busiest truck bridge, the three-lane, 3500-ft-long (1070-m) Peace Bridge over the Niagara River between Fort Erie, Ontario, Canada and Buffalo, New York (Figure 15.5). The investigation took place during the night in early August. Core drilling was performed from midnight to approximately 4:30 A.M. The coring process was designed to assist in the infrared thermography and ground-penetrating radar data depth calibration and required that two representative deck pavement cores be collected. The cores were collected in the center lane (Figure 15.6). At approximately midnight, the investigators began driving a customized data collection vehicle from the east abutment toward the west abutment. Each driven lane pass took approximately 15 min during which time traffic was routed around the data collection vehicle and an associated traffic control vehicle supplied by the Peace Bridge Authority. No lane traffic was permanently halted.

A second case study involves the inspection of over 3125 slabs of reinforced concrete on the taxiway of one of the busiest airports in America, Lambert St. Louis International Airport. This inspection was performed during August and the field inspection took a total of 7 nights, during 2 of which no data collection could be done because of rain.

Because air traffic flow could not be interrupted on the taxiways, the inspection was performed from 11:00 P.M. to 5:00 A.M. when traffic was light. To move the infrared equipment about rapidly and to move in and out of air traffic flow quickly, a van was used to carry all the infrared testing equipment along with associated surveying tools, such as power supplies, drawing equipment, and various recording devices. The van was custom-designed to allow the scanner head and visual cameras to be raised to a 14 ft (4.8 m) height during scanning runs to allow the surveying of a slab 25 ft (8.0 m) wide by 25 ft (8.0 m) long in a single view. Production rates, which included the scanning operation, storage of images on computer disks and videotape, occasional 35-mm photographs, and all analysis allowed the inspection of up to 500,000 ft^2 (46,500 m^2) per night.

Prior to beginning the inspection, reference and calibration areas were determined for sound concrete and for concrete with subsurface voids and delaminations. These areas were rescanned at regular intervals during the inspection to ensure that equipment settings allowed for accurate data collection. This

FIGURE 15.5 Front and side views of the nation's busiest truck bridge over the Niagara River between Fort Erie, Ontario, Canada and Buffalo, New York, U.S.A.

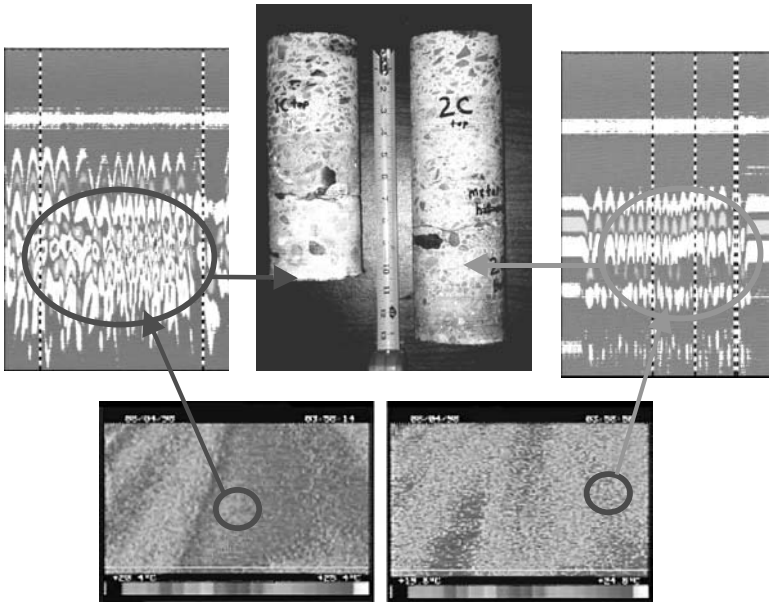

FIGURE 15.6 **(Color figure follows p. 15-10.)** Infrared thermograms (bottom) detecting solid concrete (light blue) and half-depth delaminated concrete (dark blue and purple) and confirming ground-penetrating radar profiles (top left and top right) and corings (center).

information was fed continuously into a computer and a color monitor was used to assist in location of anomalies. To speed data interpretation, the thermal data presented on the monitor were divided into three categories represented by three colors: green for solid concrete; yellow for concrete areas with minor temperature deviations most likely caused by minor surface deterioration; and red for concrete areas with serious subsurface cracks/voids. The computer was also used to determine the area on each slab that appeared in the above colors. These data were used to designate each individual slab for no corrective action, spot repairs, or major replacement.

The third case history involves the inspection of parking garage concrete and adjacent roadway concrete at the same facility, Lambert St. Louis International Airport. The same techniques as described above were used, but particular attention was paid to the expansion joint areas between concrete slabs. Figure 15.7 shows one of the computer-enhanced thermograms and a visual picture of an expansion joint in good condition. Figure 15.8 shows a nearby joint in a deteriorated subsurface condition. The surface visual photograph shows no visual surface deterioration. The deteriorated areas were confirmed and rehabilitated the following year.

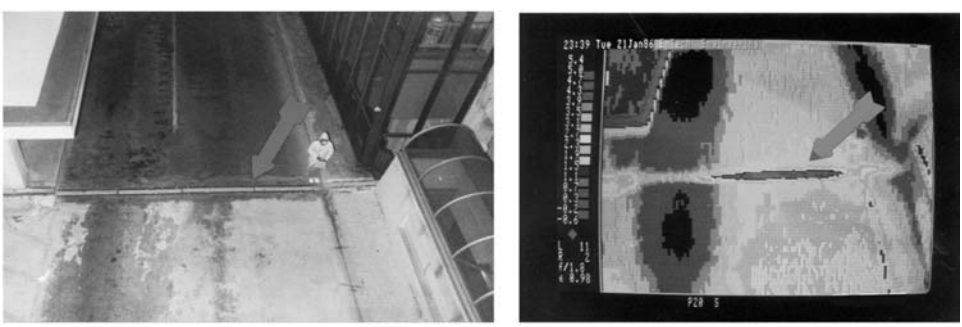

FIGURE 15.7 **(Color figure follows p. 15-10.)** Visual and thermal images illustrating a good roadway expansion joint located at Lambert St. Louis International Airport.

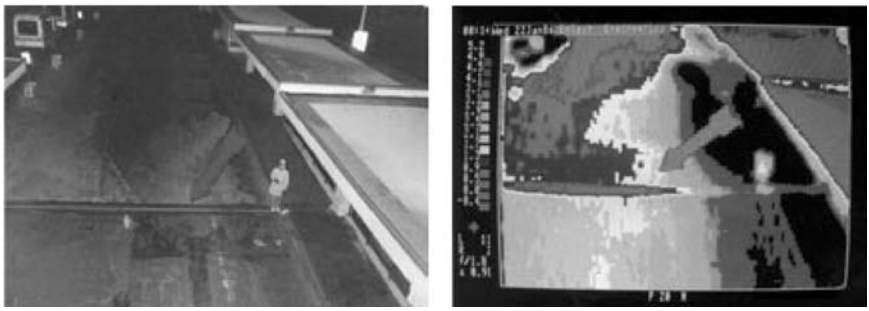

FIGURE 15.8 **(Color figure follows p. 15-10.)** Visual and thermal images illustrating a deteriorated roadway expansion joint containing both voids and water located at Lambert St. Louis International Airport.

A fourth case history involved the investigation of approximately 20,000 ft^2 (1860 m^2) of reinforced concrete in a municipal in-ground swimming pool. The investigation was performed during the night from 8:00 to 11:00 P.M. in September, and it involved the use of an infrared thermographic, wideband, 3- to 12-μm radiometric imager. The purpose of the investigation was to locate subsurface water supply pipeline leaks and water migration and erosion voids beneath the pool bottom. The detection and analysis process involved the use of the infrared thermographic radiometric imager to measure, display, and store a temperature image, or map, of the concrete surface temperatures in various areas of the pool, including the deep pool, shallow pool, and surrounding deck areas. Cooler concrete surface areas would represent subsurface areas containing either voids or moisture from leaking pipes or moisture movement through poor concrete joints and microcracks.

The deep pool walls and floor were investigated and no significant signs of leaks or voids were detected. The shallow pool floor contained a significant number of signatures indicative of subsurface water-saturated areas and their resulting erosion voids (Figure 15.9.). As a result of the large portion of the shallow pool floor that exhibited these signatures, approximately 60 to 70%, it was decided not to try to map each of the individual anomaly areas. Instead, it was recommended that the entire floor of the shallow pool be rehabilitated. During the investigation, verification, in the form of using a small hammer to sound the areas that exhibited thermal signatures indicative of subsurface voids, was performed, along with a control check of areas that exhibited no anomalies. These tests showed a 100% correlation.

The fifth case history involved an investigation on whether a patented system based on infrared thermography and ground-penetrating radar could be used to locate subsurface concrete voids and water leaks in the concrete lining of the immersed tubes (approximately 1 mile, or 1.6 km, long, 3 ft, or 900 mm, thick, and 29 ft, or 8.8 m, in diameter) of the Hung Hom Cross-Harbour Tunnel in Hong Kong.

The initial tunnel investigation occurred in the southbound tunnel during May. No interruption to traffic flow or to use of the facilities occurred because of the investigation process. The vertical walls of the main traffic portion of the tunnel were investigated using the infrared sensors on the system while the van carrying the sensors and associated electronics moved forward at 5 to 10 mph (8 to 16 km/h) in each outer lane (Figure 15.10A). One pass was required in each lane direction in order to image 100% of each vertical side wall. When this portion of the data collection was completed, the infrared thermography and ground-penetrating radar equipment was taken from the van and installed on small, wheeled carts, which were lifted into the upper and lower ventilation chambers to investigate concrete conditions in the normally inaccessible sections of the tunnel. Both ventilation ducts contained airflows greater than 30 mph, or 50 km/h) at more than 65% relative humidity.

Multiple areas of the upper and lower ventilation areas of the submerged tunnel crown walls were imaged by the infrared-based system and then confirmed by the bulkier and less efficient ground-penetrating radar system (Figure 15.10B).

The infrared thermographic system detected thermal anomalies indicative of conditions not normal to a concrete liner. The thermal signatures (surface temperature differences) were much less intense,

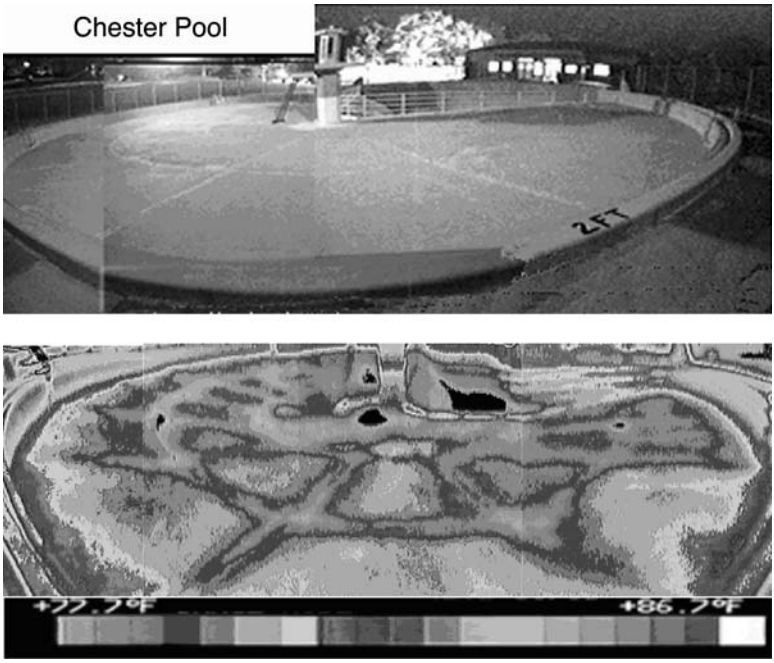

FIGURE 15.9 **(Color figure follows p. 15-10.)** Visual and thermal images of shallow pool floor. Purple and dark blue colors denote void and water migration areas.

0.1 to 0.2°C as opposed to typical expected values of 1 to 2°C. These reduced temperature signatures were believed to be due to the high airflow and high humidity in the ventilation ducts, which increased the heat transfer effects of the concrete surfaces dramatically. One of the anomalous areas detected first by the infrared sensors and then confirmed by the ground-penetrating radar system was located at station 23 + 15 ft (Figure 15.10B and C). This area contained a concrete void with a volume of about 3 ft^3 (0.08 m^3). On closer, invasive examinations, it was obvious that the defect had been previously detected and covered over without actually structurally repairing the concrete liner, a very dangerous practice.

The infrared-based investigation system proved to be very effective in detecting hidden concrete voids and leaks, even though the heat transfer effects of the high humidity and high airflow reduced the temperature signatures. For this type of application, it was recommended that future investigations be performed during tunnel-cleaning operations when traffic is reduced to a minimum and ventilation flow can be likewise reduced.

15.7 Advantages and Limitations

Infrared thermographic testing techniques for determining concrete subsurface voids, delaminations, pooled moisture, and other anomalies have advantages over invasive tests such as coring and other nondestructive testing techniques such as radioactive/nuclear, electrical/magnetic, acoustic, and ground-penetrating radar.

The obvious advantage of remote-sensing infrared thermographic data collection over invasive testing methods is that major concrete areas need not be destroyed during the testing. Only small calibration corings are used. This results in major savings in time, labor, equipment, traffic control, and scheduling problems. In addition, when aesthetics are important, no disfiguring occurs on the concrete to be tested. Rapid setup and takedown are also advantages when vandalism is possible. Finally, no concrete dust or debris is generated that could cause environmental problems.

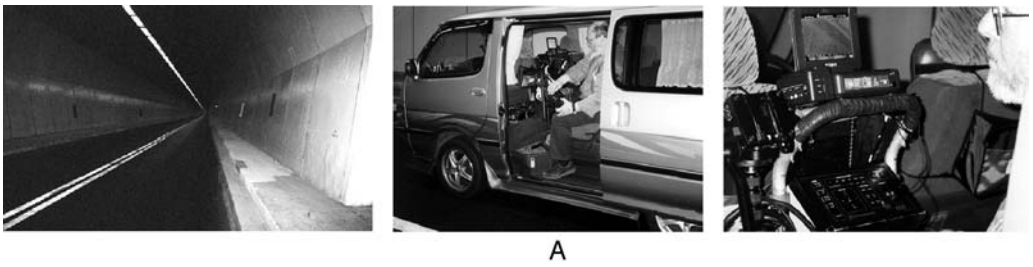

A

B

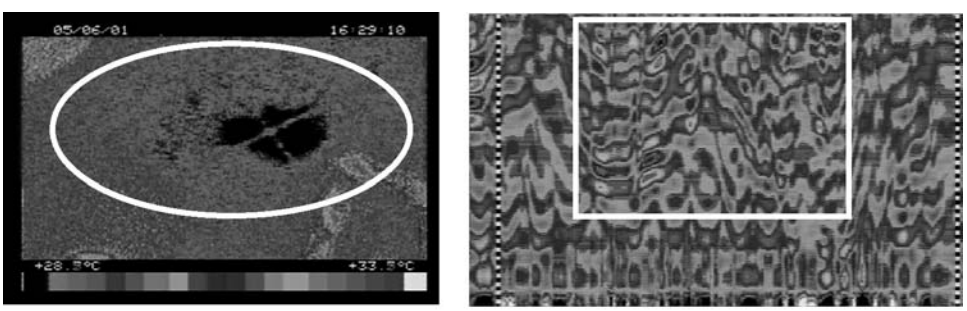

C

FIGURE 15.10 (Color figure for (C) follows p. 15-10.) (A) Hong Kong Cross-Harbour Tunnel showing walls adjacent to traffic lanes along with van-mounted infrared thermographic equipment used to investigate tunnel walls for voids and leaks. (B) Hong Kong Cross-Harbour Tunnel showing walls in top and bottom ventilation cavities with portable infrared thermography and ground-penetrating radar equipment used to investigate tunnel walls for voids and leaks. (C) Infrared thermogram (left) showing hidden wall cavity covered by painted plywood and confirming ground-penetrating radar profile (right).

There are other advantages of infrared thermographic methods over other nondestructive methods. Infrared thermographic equipment is safe, as it emits no radiation. It only records thermal radiation that is naturally emitted from the concrete, as well as from all other objects. It is similar in function to an ordinary thermometer, only much more efficient.

The final and main advantage of infrared thermography is that it is an area-testing technique, whereas the other nondestructive and destructive methods are point-testing or line-testing methods. Thus, infrared thermography is capable of forming a two-dimensional image of the test surface showing the extent of subsurface anomalies.

The other methods including radioactive/nuclear, electrical/magnetic, acoustic, and ground-penetrating radar are all point tests. They depend on a signal propagating downward through the concrete at a discrete point. This gives an indication of the concrete condition at that point. If an area is to be tested, then multiple readings must be taken.

Ground-penetrating radar has the advantage over the other point-testing techniques in that the sensor may be mounted on a vehicle and moved in a straight line over the test area. This improves efficiency somewhat, but if an area is wide, many line passes have to be made.

There is one disadvantage to infrared thermographic testing. At this stage of development, the depth or thickness of a void cannot be determined, although its outer dimensions are easily derived. It cannot be determined if a subsurface void is near the surface or farther down at the level of the reinforcing bars, although the temperatures of the surfaces above the anomalies are relative to their depth below the top surface. Techniques such as ground-penetrating radar or stress wave propagation methods can determine the depth of the void, but again these methods cannot determine the other dimensions in a single measurement.

In most testing instances, the thickness of the anomaly is not nearly as important as its other dimensions. But in those cases where information on a specific anomaly thickness or depth is needed, it is recommended that infrared thermography be used to survey the large areas for problems. Once specific problem locations are established, ground-penetrating radar can be used to spot-check the anomaly for its depth and thickness. This combined technique would give the best combination of accuracy, efficiency, economy, and safety.

15.8 Summary

1. Infrared thermographic testing techniques are based on the principle that various subsurface defects change the rate at which heat flows through a structure.
2. Infrared thermographic testing may be performed during both day- and nighttime hours depending on environmental conditions.
3. Infrared thermographic techniques can distinguish various types and depths of anomalies when combined with proper calibration techniques utilizing corings or ground-penetrating radar.
4. Infrared thermographic imaging techniques are more efficient than other invasive and nondestructive, manual and electronic, methods when testing large concrete areas.
5. Computer analysis of thermal images greatly improves the accuracy and speed of test interpretation.
6. Infrared thermographic techniques can determine subsurface anomaly locations and horizontal dimensions, and with new methods of data analysis it may be possible to estimate the depth of a void.

References

1. Moore, W.M., Swift, G., and Milberger, L.J. An instrument for detecting delamination of concrete bridge decks, *Highway Res. Rec.,* 451, 44, 1973.
2. Holt, F.B. and Manning, D.G., Infrared thermography for the detection of delaminations in concrete bridge decks, in *Proc. Fourth Biennial Infrared Information Exchange*, 1978, A61–A71.
3. Weil, G.J., Infrared thermal sensing of sewer voids, *Proc. Thermosense* VI, 446, 116, 1983.
4. Weil, G.J., Computer-aided infrared analysis of bridge deck delaminations, in *Proc. 5th Infrared Information Exchange,* 1985, A85–A93.

5. Weil, G.J., Infrared thermal sensing of sewer voids — 4-year update, *Proc. Thermosense X,* 934, 155, 1988.
6. ASTM D 4788, Test Method for Detecting Delaminations in Bridge Decks Using Infrared Thermography, *Annual Book of ASTM Standards*, Vol. 04.03, West Conshohocken, PA, 2002.
7. Weil, G.J., Toward an integrated non-destructive pavement testing management information system using infrared thermography, in *Proc. U.S. Transp. Res. Board,* June 22, Washington, D.C., 1989.
8. Weil, G.J., Remote sensing of land based voids using computer enhanced infrared thermography, in *Proc. Int. Cong. Optical Sci. and Eng.,* April 14, Paris, 1989.
9. Weil, G.J., Detecting the defects, *Civ. Eng. Mag.,* 59(9), 74, 1989.
10. Weil, G.J., Non-destructive remote sensing of subsurface utility distribution pipe problems using infrared thermography, in *Proc. 2nd Int. Conf. on Pipeline Constr. Cong.,* Centrum Hamburg, Oct. 26, 1989.

16

Acoustic Emission Methods

16.1 Introduction
16.2 Historical Background
16.3 Theoretical Considerations
16.4 Evaluation of Acoustic Emission Signals
16.5 Instrumentation and Test Procedures
16.6 Parameters Affecting Acoustic Emissions from Concrete
The Kaiser Effect · Effect of Loading Devices · Signal Attenuation · Specimen Geometry · Type of Aggregate · Concrete Strength
16.7 Laboratory Studies of Acoustic Emission
Fracture Mechanics Studies · Type of Cracks · Fracture Process Zone (Crack Source) Location · Strength vs. Acoustic Emission Relationships · Drying Shrinkage · Fiber Reinforced Cements and Concretes · High Alumina Cement · Thermal Cracking · Bond in Reinforced Concrete · Corrosion of Reinforcing Steel in Concrete
16.8 Field Studies of Acoustic Emission
16.9 Conclusions

Sidney Mindess
University of British Columbia

Acoustic emission refers to the sounds, both audible and subaudible, that are generated when a material undergoes irreversible changes, such as those due to cracking. Acoustic emissions (AE) from concrete have been studied for the past 30 years, and can provide useful information on concrete properties. This review deals with the parameters affecting acoustic emissions from concrete, including discussions of the Kaiser effect, specimen geometry, and concrete properties. There follows an extensive discussion of the use of AE to monitor cracking in concrete, whether due to externally applied loads, drying shrinkage, or thermal stresses. AE studies on reinforced concrete are also described. While AE is very useful laboratory technique for the study of concrete properties, its use in the field remains problematic.

16.1 Introduction

It is common experience that the failure of a concrete specimen under load is accompanied by a considerable amount of audible noise. In certain circumstances, some audible noise is generated even before ultimate failure occurs. With very simple equipment — a microphone placed against the specimen, an amplifier, and an oscillograph — subaudible sounds can be detected at stress levels of perhaps 50% of the ultimate strength; with the sophisticated equipment available today, sound can be detected at much lower loads, in some cases below 10% of the ultimate strength. These sounds, both audible and subaudible, are referred to as *acoustic emission*.

In general, acoustic emissions are defined as "the class of phenomena whereby transient elastic waves are generated by the rapid release of energy from localized sources within a material."[1] These waves propagate through the material, and their arrival at the surfaces can be detected by piezoelectric transducers. Acoustic emissions, which occur in most materials, are caused by irreversible changes, such as dislocation movement, twinning, phase transformations, crack initiation, and propagation, debonding between continuous and dispersed phases in composite materials, and so on. In concrete, since the first three of these mechanisms do not occur, acoustic emission is due primarily to:

1. Cracking processes
2. Slip between concrete and steel reinforcement
3. Fracture or debonding of fibers in fiber-reinforced concrete

16.2 Historical Background

The initial published studies of acoustic emission phenomena, in the early 1940s, dealt with the problem of predicting rockbursts in mines; this technique is still very widely used in the field of rock mechanics, in both field and laboratory studies. The first significant investigation of acoustic emission from metals (steel, zinc, aluminum, copper, and lead) was carried out by Kaiser.[2] Among many other things, he observed what has since become known as the Kaiser effect: "the absence of detectable acoustic emission at a fixed sensitivity level, until previously applied stress levels are exceeded."[1] While this effect is not present in all materials, it is a very important observation, and it will be referred to again later in this review.

The first study of acoustic emission from concrete specimens under stress appears to have been carried out by Rüsch,[3] who noted that during cycles of loading and unloading below about 70 to 85% of the ultimate failure load, acoustic emissions were produced only when the previous maximum load was reached (the Kaiser effect). At about the same time, but independently, L'Hermite[4,5] also measured acoustic emission from concrete, finding that a sharp increase in acoustic emission coincided with the point at which Poisson's ratio also began to increase (i.e., at the onset of significant matrix cracking in the concrete). In 1965, however, Robinson[6] used more sensitive equipment to show that acoustic emission occurred at much lower load levels than had been reported earlier, and hence, could be used to monitor earlier microcracking (such as that involved in the growth of bond cracks in the interfacial region between cement and aggregate). In 1970, Wells[7] built a still more sensitive apparatus, with which he could monitor acoustic emissions in the frequency range from about 2 to 20 kHz. However, he was unable to obtain truly reproducible records for the various specimen types that he tested, probably due to the difficulties in eliminating external noise from the testing machine. Also in 1970, Green[8] reported a much more extensive series of tests, recording acoustic emission frequencies up to 100 kHz. Green was the first to show clearly that acoustic emissions from concrete are related to failure processes within the material; using source location techniques, he was also able to determine the locations of defects. It was this work that indicated that acoustic emissions could be used as an early warning of failure. Green also noted the Kaiser effect, which suggested to him that acoustic emission techniques could be used to indicate the previous maximum stress to which the concrete had been subjected. As we will see below, however, a true Kaiser effect appears not to exist for concrete.

Nevertheless, even after this pioneering work, progress in applying acoustic emission techniques remains slow. An extensive review by Diederichs et al.[9] covers the literature on acoustic emissions from concrete up to 1983. However, as late as 1976, Malhotra[10] noted that there was little published data in this area, and that "acoustic emission methods are in their infancy." Even in January, 1988, a thorough computer-aided search of the literature found only some 90 papers dealing with acoustic emissions from concrete over about the previous 10 years; while this is almost certainly not a complete list, it does indicate that there is much work to be carried out before acoustic emission monitoring becomes a common technique for testing concrete. Indeed, there are still no standard test methods which have even been suggested for this purpose.

16.3 Theoretical Considerations

When an acoustic emission event occurs at a source with the material, due to inelastic deformation or to cracking, the stress waves travel directly from the source to the receiver as body waves. Surface waves may then arise from mode conversion. When the stress waves arrive at the receiver, the transducer responds to the surface motions that occur. It should be noted that the signal captured by the recording device may be affected by the nature of the stress pulse generated by the source, the geometry of the test specimen, and the characteristics of the receiver, making it difficult to interpret the recorded waveforms. Two basic types of acoustic emission signals can be generated (Figure 16.1):

Continuous emission is "a qualitative description of the sustained signal level produced by rapidly occurring acoustic emission events."[1] These are generated by events such as plastic deformations in metals, which occur in a reasonably continuous manner.

Burt emission is "a qualitative description of the discrete signal related to an individual emission event occurring within the matrial,"[1] such as that which may occur during crack growth or fracture in brittle materials. These burst signals are characteristic of the acoustic emission events resulting from the loading of cementitious materials.

Acoustic emissions from concrete occur over a very wide range of frequencies. The earliest work concentrated on rather low frequencies. Robinson[6] recorded acoustic emissions mainly at two frequencies: 2 kHz and 13 to 14 kHz; Wells[7] worked in the frequency range of 2 to 20 kHz; and Green[8] recorded emissions only up to 100 kHz. More modern instrumentation, however, can record much higher frequencies, typically in the range of 50 kHz to about 2 MHz. At lower frequencies, extraneous background noises from the test equipment of the laboratory environment become a problem; this was the difficulty faced in the earlier investigations referred to above. On the other hand, at very high frequencies, the attenuation of the signals is too severe, and thus, the distance from the piezoelectric transducer to the acoustic emission source must be reduced. The precise frequency range that is monitored does not appear to be very important for concrete. Detailed studies by Tanigawa et al.[11] in the frequency range up to 400 kHz showed that at low stresses, emissions tended to be in the frequency range below 150 kHz; at higher stresses, the higher frequency components become more significant. However, the relative shapes of the acoustic emission output vs. load curves were much the same for all of the frequency ranges studied.

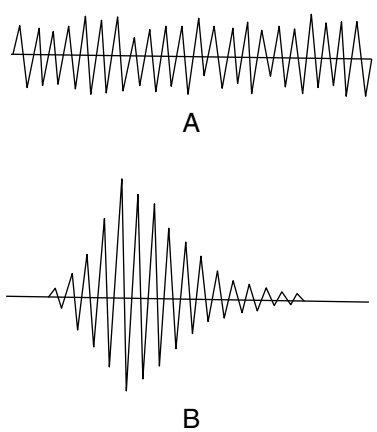

FIGURE 16.1 The two basic types of acoustic emission signals. (A) Continuous emission. (B) Burst emission.

16.4 Evaluation of Acoustic Emission Signals

A typical acoustic emission signal from concrete is shown in Figure 16.2.[12] However, when such acoustic events are examined in much greater detail, as shown in Figure 16.3,[13] the complexity of the signal becomes even more apparent; the scatter in noise, shown in Figure 16.3, makes it difficult to determine exactly the time of arrival of the signal; this means that very sophisticated equipment must be used to get the most information out of the acoustic emission signals. In addition, to obtain reasonable sensitivity, the acoustic emission signals must be amplified. In concrete, typically, system gains in the range of 80 to 100 decibels (dB) are used.

There are a number of different ways in which acoustic emission signals may be evaluated.

Acoustic Emission Counting (ring-down counting) — This is the simplest way in which an acoustic emission event may be characterized. It is "the number of times the acoustic emission signal exceeds a preset threshold during any selected portion of a test,"[1] and is illustrated in Figure 16.4. A monitoring system may record:

1. The *total number of counts* (e.g., 13 counts in Figure 16.4). Since the shape of a burst emission is generally a damped sinusoid, pulses of higher amplitude will generate more counts.
2. The *count rate*. This is the number of counts per unit of time; it is particularly useful when very large numbers of counts are recorded.
3. The *mean pulse amplitude*. This may be determined by using a root-mean square meter, and is an indication of the amount of energy being dissipated.

Clearly, the information obtained using this method of analysis depends upon both the gain and the threshold setting. Ring-down counting is affected greatly by the characteristics of the transducer, and the geometry of the test specimen (which may cause internal reflections) and may not be indicative of the nature of the acoustic emission event. In addition, there is no obvious way of determining the amount of energy released by a single event, or the total number of separate acoustic events giving rise to the counts.

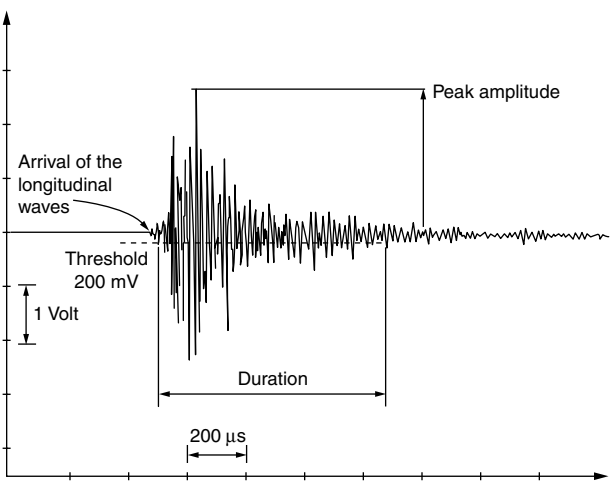

FIGURE 16.2 A typical acoustic emission signal from concrete. (From Berthelot, J.M. et al., private communication, 1987. With permission.)

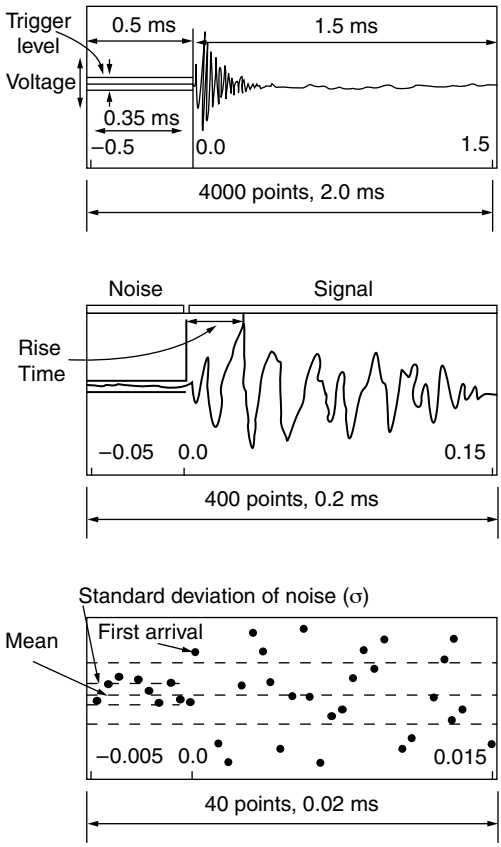

FIGURE 16.3 Typical view of an acoustic emission event as displayed in an oscilloscope screen. (Adapted from Maji, A. and Shah, S.P., *Exp. Mech.*, 26, 1, 1988, p. 27.)

Event counting — Circuitry is available which counts each acoustic emission event only once, by recognizing the end of each burst emission in terms of a predetermined length of time since the last count (i.e., since the most recent crossing of the threshold). In Figure 16.4, for instance, the number of events is three. This method records the number of events, which may be very important, but provides no information about the amplitudes involved.

Rise time — This is the interval between the time of first occurrence of signals above the level of the background noise and the time at which the maximum amplitude is reached. This may assist in determining the type of damage mechanism.

Signal duration — This is the duration of a single acoustic emission event; this too may be related to the type of damage mechanism.

Amplitude distribution — This provides the distribution of peak amplitudes. This may assist in identifying the sources of the emission events that are occurring.

Frequency analysis — This refers to the frequency spectrum of individual acoustic emission events. This technique, generally requiring a fast Fourier transformation analysis of the acoustic emission waves, may help discriminate between different types of events. Unfortunately, a frequency analysis may sometimes simply be a function of the response of the transducer, and thus reveal little of the true nature of the pulse.

Energy analysis — This is an indication of the energy released by an acoustic emission event; it may be measured in a number of ways, depending on the equipment, but it is essentially the area under the amplitude vs. time curve (Figure 16.4) for each burst. Alternatively, the area under the envelope of the amplitude vs. time curve may be measured for each burst.

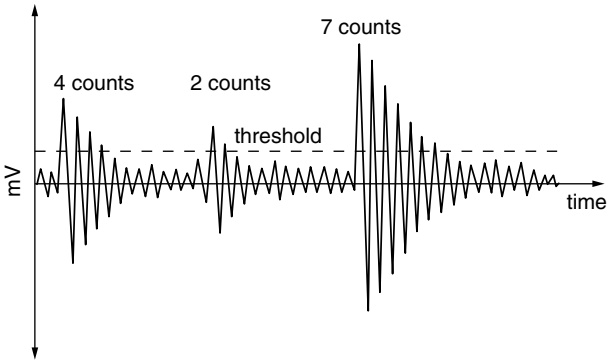

FIGURE 16.4 The principle of acoustic emission counting (ring-down counting).

Defect location — By using a number of transducers to monitor acoustic emission events, and determining the time differences between the detection of each event at different transducer positions, the location of the acoustic emission event may be determined by using triangulation techniques. Work by Maji and Shah,[13] for instance, has indicated that this technique may be accurate to within about 5 mm.
Analysis of the wave-form — Most recently, it has been suggested[14,15] that an elaborate signals processing technique (deconvolution) applied to the wave-form of an acoustic emission event can provide information regarding the volume, orientation, and type of microcrack.

Ideally, since all of these methods of data analysis provide different information, one would wish to measure them all. However, this is neither necessary nor economically feasible. In the discussion that follows, it will become clear that the more elaborate methods of analysis are useful in fundamental laboratory investigations, but may be inappropriate for practical applications.

16.5 Instrumentation and Test Procedures

Instrumentation (and, where necessary, the associated computer software) is available, from a number of different manufacturers, to carry out all of the methods of signal analysis described above. It might be added that advances in instrumentation have outpaced our understanding of the nature of the elastic waves resulting from microcracking in concrete. The main elements of a modern acoustic emission detection system are shown schematically in Figure 16.5. A brief description of the most important parts of this system is as follows:

1. *Transducers*: Piezoelectric transducers (generally made of lead zirconate titanate, PZT) are used to convert the surface displacements into electric signals. The voltage output from the transducers is directly proportional to the strain in the PZT, which depends in turn on the amplitude of the surface waves. Since these transducers are high impedance devices, they yield relatively low signals, typically less than 100 μV. There are basically two types of transducers. *Wide-band* transducers are sensitive to acoustic events with frequency responses covering a wide range, often several hundred kHz. *Narrow-band* transducers are restricted to a much narrower range of frequencies, using bandpass filters. Of course, the transducers must be properly coupled to the specimen, often using some form of silicone grease as the coupling medium.
2. *Preamplifier*: Because of the low voltage output, the leads from the transducer to the preamplifier must be as short as possible; often, the preamplifier is integrated within the transducer itself. Typically, the gain in the preamplifier is in the range 40 to 60 dB. (Note: The decibel scale measures only *relative* amplitudes. Using this scale:

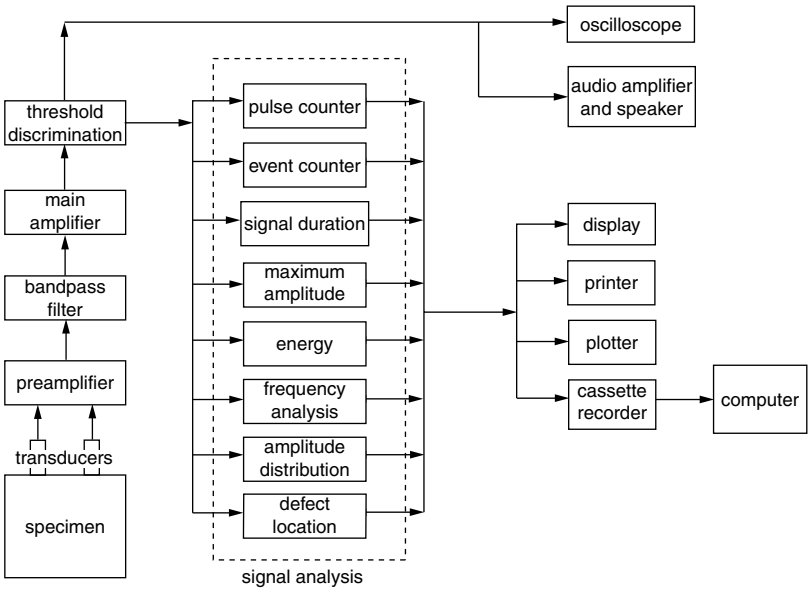

FIGURE 16.5 The main elements of a modern acoustic emission detection system.

$$\text{Gain}\left(\text{dB}\right) = 20\log\frac{V}{V_i}$$

where V is the output amplitude and V_i is the input amplitude. That is, a gain of 40 dB will increase the input amplitude by a factor of 100; a gain of 60 dB will increase the input amplitude by a factor of 1000, and so on.)

3. *Passband filters* are used to suppress the acoustic emission signals that lie outside of the frequency range of interest.
4. The *main amplifier* further amplifies the signals, typically with a gain of an additional 20 to 60 dB.
5. The *discriminator* is used to set the threshold voltage above which signals are counted.

The remainder of the electronic equipment depends upon the way in which the acoustic emission data are to be recorded, analyzed, and displayed.

Acoustic emission testing may be carried out in the laboratory or in the field. Basically, one or more acoustic emission transducers are attached to the specimen. The specimen is then loaded slowly, and the resulting acoustic emissions are recorded. There are generally two categories of tests:

1. To use the acoustic emission signals to learn something about the internal structure of the material, and how structural changes (i.e., damage) occur during the process of loading. In this case, the specimens are generally loaded to failure.
2. To establish whether the material or the structure meet certain design or fabrication criteria. In this case, the load is increased only to some predetermined level ("proof" loading). The amount and nature of the acoustic emissions may be used to establish the integrity of the specimen or structure, and may also sometimes be used to predict the service life.

16.6 Parameters Affecting Acoustic Emissions from Concrete

16.6.1 The Kaiser Effect

The earliest acoustic emission studies of concrete, such as the work of Rüsch,[3] indicated that a true Kaiser effect (see above) exists for concrete; that is, acoustic emissions were found not to occur in concrete that had been unloaded until the previously applied maximum stress had been exceeded on reloading. This was true, however, only for stress levels below about 75 to 85% of the ultimate strength of the material; for higher stresses, acoustic emissions began again at stresses somewhat lower than the previous maximum stress. Subsequently, a number of other investigators have also concluded that concrete exhibits a Kaiser effect, at least for stresses below the peak stress of the material.[10,13,16–18] Spooner and Dougill[16] confirmed that this effect did not occur beyond the peak of the stress-strain curve (i.e., in the descending portion of the stress-strain curve), where acoustic emissions occurred again before the previous maximum strain was reached. It has also been suggested that a form of the Kaiser effect occurs as well for cyclic thermal stresses in concrete,[19] and for drying and wetting cycles.[20] On the other hand, Nielsen and Griffin[21] have reported that the Kaiser effect is only a very *temporary* effect in concrete; with only a few hours of rest between loading cycles, acoustic emissions are again recorded during reloading to the previous maximum stress. They therefore concluded "that the Kaiser effect is not a reliable indicator of the loading history for plain concrete." Thus, it is unlikely that the Kaiser effect could be used in practice to determine the previous maximum stress that a structural member has been subjected to.

16.6.2 Effect of Loading Devices

As is well known, the end restraint of a compression specimen of concrete due to the friction between the ends of the specimen and the loading platens can have a considerable effect on the apparent strength of the concrete. These differences are also reflected in the acoustic emissions measured when different types of loading devices are used.[22] For instance, in compression testing with stiff steel platens, most of the acoustic emission appears at stresses beyond about half of the ultimate stress; with more flexible platens, such as brush platens, significant acoustic emission appears at about 20% of the ultimate stress. This undoubtedly reflects the different crack patterns that develop with different types of platens, but it nonetheless makes interlaboratory comparisons, and indeed even studies on different specimen geometries within the same laboratory, very difficult.

16.6.3 Signal Attenuation

The elastic stress waves that are generated by cracking attenuate as they propagate through the concrete. Thus, large acoustic emission events that take place in the concrete far from a pick-up transducer may not exceed the threshold excitation voltage due to this attenuation, while much smaller events may be recorded if they occur close to the transducer. Very little information is available on acoustic emission attenuation rates in concrete. It has been shown that more mature cements show an increasing capacity to transmit acoustic emissions.[20] Related to this, Mindess[23] has suggested that the total counts to failure for concrete specimens in compression are much higher for older specimens, which may also be explained by the better transmission through older concretes.

As a practical matter, the maximum distance between piezoelectric transducers, or between the transducers and the source of the acoustic emission event, should not be very large. Berthelot and Robert[24] required an array of transducers arranged in a 40-cm square mesh to locate acoustic emission events reasonably accurately. They found that for ordinary concrete, with a fifth transducer placed in the center of the 40 × 40-cm square mesh, only about 40% of the events detected by the central transducer were also detected by the four transducers at the corners; with high strength concrete, this proportion increased to 60 to 70%. Rossi[25] also found that a 40-cm square mesh was needed for a proper determination of

acoustic emission events. Although more distant events can, of course, be recorded, there is no way of knowing how many events are "lost" due to attenuation. This is an area that requires much more study.

16.6.4 Specimen Geometry

It has been shown that smaller specimens appear to give rise to greater levels of acoustic emission than do larger ones.[17] The reasons for this are not clear, although the observation may be related to the attenuation effect described above. After an acoustic emission event occurs, the stress waves not only travel from the source to the sensor, but also undergo reflection, diffraction, and mode conversions within the material. The basic problem of wave propagation within a bounded solid certainly requires further study, but there have apparently been no comparative tests on different specimen geometries.

16.6.5 Type of Aggregate

It is not certain whether the mineralogy of the aggregate has any effect on acoustic emission. It has been reported that concretes with a smaller maximum aggregate size produce a greater number of acoustic emission counts than those with a larger aggregate size;[10] however, the total energy released by the finer aggregate concrete is reduced. This is attributed to the observation that concretes made with smaller aggregates start to crack at lower stresses; in concretes with larger aggregate particles, on the other hand, individual acoustic events emit higher energies. For concretes made with lightweight aggregates, the total number of counts is also greater than for normal weight concrete, perhaps because of cracking occurring in the aggregates themselves.

16.6.6 Concrete Strength

It has been shown that the total number of counts to the maximum load is greater for higher strength concretes.[23] However, as was mentioned earlier,[23] for similar strength levels the total counts to failure appears to be much higher for older concretes.

16.7 Laboratory Studies of Acoustic Emission

By far the greatest number of acoustic emission studies of concrete have been carried out in the laboratory, and have been largely "theoretical" in nature:

1. To determine whether acoustic emission analysis could be applied to cementitious systems
2. To learn something about crack propagation in concrete

16.7.1 Fracture Mechanics Studies

A number of studies have shown that acoustic emission can be related to crack growth or fracture mechanics parameters in cements, mortars, and concretes. Evans et al.[26] showed that acoustic emission could be correlated with crack velocity in mortars. Morita and Kato[27,28] and Nadeau, Bennett, and Mindess[20] were able to relate total acoustic emission counts to K_c (the fracture toughness). In addition, Lenain and Bunsell[29] found that the number of emissions could be related to the sixth power of the stress intensity factor, K. Izumi et al.[30] showed that acoustic emissions could also be related to the strain energy release rate, G. In all cases, however, these correlations are purely empirical; no one has yet developed a fundamental relationship between acoustic emission events and fracture parameters, and it is unlikely that such a relationship exists.

16.7.2 Type of Cracks

A number of attempts have been made to relate acoustic events of different frequencies, or of different energies, to different types of cracking in concrete. For instance, Saeki et al.,[31] by looking at the energy

levels of the acoustic emissions at different levels of loading, concluded that the first stage of cracking, due to the development of bond cracks between the cement paste and the aggregate, emitted high energy signals; the second stage, which they termed "crack arrest," emitted low energy signals; the final stage, in which cracks extended through the mortar, was again associated with high energy acoustic events. Similarly, Tanigawa and Kobayashi[32] used acoustic energies to distinguish the onset of "the proportional limit, the initiation stress and the critical stress." On the other hand, Tanigawa et al.[11] tried to relate the fracture type (pore closure, tensile cracking, and shear slip) to the power spectra and frequency components of the acoustic events. The difficulty with these and similar approaches is that they tried to relate differences in the recorded acoustic events to preconceived notions of the nature of cracking in concrete; direct cause and effect relationships were never observed.

16.7.3 Fracture Process Zone (Crack Source) Location

Perhaps the greatest current interest in acoustic emission analysis is its use in *locating* fracture processes, and in monitoring the damage that concrete undergoes as cracks progress. Okada et al.[33,34] showed that the location of crack sources obtained from differences in the arrival times of acoustic emissions was in good agreement with the observed fracture surface. At about the same time, Chhuy et al.[35] and Lenain and Bunsell[29] were able to determine the length of the damaged zone ahead of the tip of a propagating crack using one-dimensional acoustic emission location techniques. In subsequent work, Chhuy et al.,[36] using more elaborate equipment and analytical techniques, were able to determine damage both before the initiation of a visible crack and after subsequent crack extension.

Berthelot and Robert[24,37] and Rossi[25] used acoustic emission to monitor concrete damage as well. They found that, while the number of acoustic events showed the progression of damage both ahead and behind the crack front, this technique alone could not provide a *quantitative* description of the cracking. However, using more elaborate techniques, including amplitude analysis and measurements of signal duration, Berthelot and Robert[24] concluded that "acoustic emission testing is practically the only technique which can provide a quantitative description of the progression in real time of concrete damage within test specimens."

Later, much more sophisticated signals processing techniques were applied to acoustic emission analysis. In 1981, Michaels et al.[15] and Niwa et al.[38] developed deconvolution techniques to analyze acoustic waveforms, in order to provide a stress-time history of the source of an acoustic event. Similar deconvolution techniques were subsequently used by Maji and Shah[13,39] to determine the volume, orientation and type of microcrack, as well as the source of the acoustic events. Such sophisticated techniques have the potential eventually to be used to provide a detailed picture of the fracture processes occurring within concrete specimens.

16.7.4 Strength vs. Acoustic Emission Relationships

Since concrete quality is most frequently characterized by its strength, many studies have been directed towards determining a relationship between acoustic emission activity and strength. For instance, Tanigawa and Kobayashi[32] concluded that "the compressive strength of concrete can be approximately estimated by the accumulated AE counts at relatively low stress level." Indeed, they suggested that acoustic emission techniques might provide a useful nondestructive test method for concrete strength. Earlier, Fertis[40] had concluded that acoustic emissions could be used to determine not only strength, but also static and dynamic material behavior. Rebic,[41] too, found that there is a relationship between the "critical" load at which the concrete begins to be damaged, which can be determined from acoustic emission measurements, and the ultimate strength; thus, acoustic emission analysis might be used as a predictor of concrete strength. Sadowska-Boczar et al.[42] tried to quantify the strength vs. acoustic emission relationship using the equation

$$F_r = aF_p + b$$

where F_r is the rupture strength, F_p is the stress corresponding to the first acoustic emission signal, and a and b are constants for a given material and loading conditions. Using this linear relationship, which they found to fit their data reasonably well, they suggested that the observation of acoustic emissions at low stresses would permit an estimation of strength, as well as providing some characterization of porosity and critical flaw size.

Unfortunately, the routine use of acoustic emissions as an estimator of strength seems to be an unlikely prospect, in large part because of the scatter in the data, as has been noted by Fertis.[40] As an example of the scatter in data. Figure 16.6[23] indicates the variability in the strength vs. total acoustic emission counts relationship; the within-batch variability is even more severe, as shown in Figure 16.7.[23]

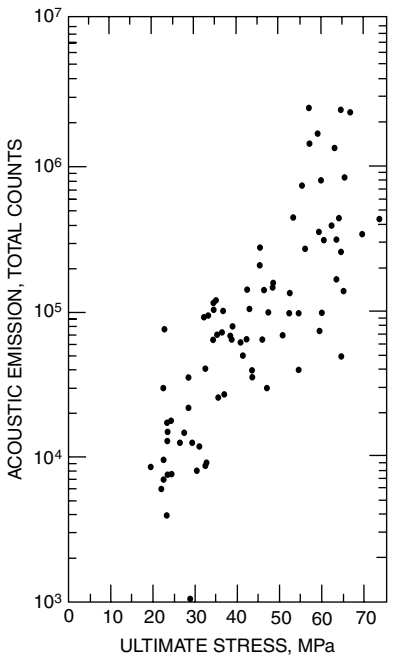

FIGURE 16.6 Logarithm of total acoustic emission counts vs. compressive strength of concrete cubes. (From Mindess, S., *Int. J. Cem. Comp. Lightweight Concr.*, 4, 173, 1982. With permission.)

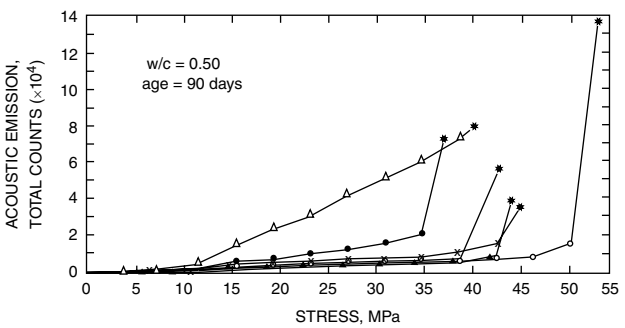

FIGURE 16.7 Within-batch variability of total acoustic emission counts vs. applied compressive stress on concrete-cubes. (From Mindess, S., *Int. J. Cem. Comp. Lightweight Concr.*, 4, 173, 1982. With permission.)

16.7.5 Drying Shrinkage

Acoustic emission has been used to try to monitor shrinkage in cement pastes and mortars. Nadeau et al.[20] found that, in hardened pastes, the acoustic emission resulted from cracking due to the unequal shrinkage of the hydration products. Mortar gave less acoustic emission than hardened paste, suggesting that the fracture processes at the sand/cement paste interface are not an important source of acoustic emission. Jeong et al.[43] also suggested that, in autoclaved aerated concrete, the acoustic emissions during drying could be related to microcracking. Again, however, it is unlikely that acoustic emission measurements will be able to be used as a means of predicting the shrinkage as a function of time.

16.7.6 Fiber Reinforced Cements and Concretes

A number of acoustic emission studies have been carried out on fiber reinforced cements and concretes. Lenain and Bunsell,[29] in a study of asbestos cement, found that acoustic emissions resulted both from cracking of the matrix and fiber pullout. They noted that the Kaiser effect was not found for this type of fiber-reinforced composite, since on unloading of a specimen the partially pulled out fibers were damaged, and particles of cement attached to them were crushed, giving rise to acoustic emissions on unloading. Because these damaged fibers were then less able to resist crack growth, on subsequent reloading cracks started to propagate at lower stress levels than on the previous cycle, thus, giving off acoustic emissions below the previously achieved maximum load. Akers and Garrett[44] also studied asbestos cement; they found that acoustic emission monitoring could be used to detect the onset and development of prefailure cracking. However, they concluded that "there is no basis whatsoever for using amplitude discrimination in acoustic emission monitoring for distinguishing between the various failure modes which occur in this material." On the other hand, Faninger et al.[45] argued that in fiber-reinforced concrete the amplitude pattern of the acoustic emission signals did make it possible to distinguish whether fracture had occurred in the fibers or between them. Similarly, Jeong et al.[43] stated that acoustic emission frequency analysis could distinguish between different micro-fracture mechanisms in fiber-reinforced autoclaved aerated concrete.

16.7.7 High Alumina Cement

In concretes made with high alumina (calcium aluminate) cement, the conversion from CAH_{10}* to C_3AH_6* on prolonged aging can lead to a large increase in porosity and therefore a large decrease in strength. There has thus been considerable interest in finding a nondestructive technique to monitor high alumina cement concrete (HAC) members. Parkinson and Peters[46] concluded that the conversion process itself is not a source of acoustic emission activity, since no acoustic emissions were generated during the accelerated conversion of pastes at the critical w/c ratio of 0.35. However, at the high *w/c* ratio of 0.65, conversion was accompanied by a high level of acoustic emission activity, due to the fracture processes taking place during conversion, associated perhaps with the liberation of excess water. Arrington and Evans[47] suggested that the structural integrity of HAC could be evaluated from the shape of the acoustic emission vs. load plot, the emissions recorded while the specimens were held under a constant load, and the decay of emission activity with time.

Perhaps the most extensive series of tests on HAC, carried out at the Fulmer Research Institute in the U.K., was reported by Williams.[48] Apart from observing that the Kaiser effect existed up to the point at which the beams cracked, some tentative suggestions were made for monitoring HAC beams with acoustic emissions:

1. If, on loading a beam, no acoustic emission is noted, then the applied load is still less than about 60% of the ultimate load; if acoustic emission occurs, then this percentage of the ultimate load has been exceeded. If, upon unloading such a beam, further acoustic emission activity is recorded,

*Note that cement chemistry notation is being used: C = CaO; A = Al_2O_3; H = H_2O.

then the beam is cracked. The amount of acoustic emission during this unloading could indicate the degree to which the cracking load had been exceeded.
2. If a beam is under its service load, it would behave similarly on application of a superimposed load. The presence or absence of acoustic emissions during this further loading and unloading might indicate the condition of the beam.
3. If a beam under service load showed no acoustic emission activity during further loading, but did so at a later date when loaded to the same level, then the strength must have decreased during that time interval.

As well, Williams[48] noted similar behavior on testing of ordinary prestressed concrete beams, and suggested that these techniques could be used to evaluate any type of concrete structure, as long as acoustic emissions not connected with beam damage could be eliminated.

16.7.8 Thermal Cracking

Relatively little work has been carried out on acoustic activity when concrete is subjected to high temperatures, such as those that may be encountered in fires. However, Hinrichsmeyher et al.[19] carried out tests up to temperatures of 900°C. They claimed that acoustic emission analysis during heating enabled them to distinguish the different types of thermally induced cracking that occurred. They noted a thermal Kaiser effect in the temperature range 300 to 600°C, which might help in determining the maximum temperature reached in a previous heating cycle. The technique was even sensitive enough to record the acoustic emissions from the quartz inversion at 573°C.

16.7.9 Bond in Reinforced Concrete

A number of acoustic emission studies of debonding of reinforcing bars in reinforced concrete have been carried out. Kobayashi et al.[49] tested simulated beam-column connections with a 90° hooked reinforcing bar subjected to various cyclic loading histories. They found that the penetration of a surface crack down to the level of the bar gave rise to only one or two acoustic events; most acoustic emission signals were generated by the internal cracking around the bar due to fracture at the lugs (ribs) of the bars. Acoustic emission signals were able to indicate, with reasonable accuracy, the degree of debonding. They suggested that acoustic emission techniques could be used to determine the amount of bond deterioration in concrete structures during proof testing, or due to overloads.

In addition, several studies of bond degradation at elevated temperatures have been carried out. Royles et al.[50] studied simple pullout specimens at temperatures up to 800°C. They found that acoustic emissions were associated with the adhesive failure at the steel-concrete interface, followed by local crushing under the ribs of the reinforcing bars. They suggested that acoustic emissions could be used to identify the point of critical slip. In further work, Royles and Morley[51] suggested that acoustic emission techniques might be useful in estimating the quality of the bond in reinforced concrete structures that had been subjected to fires.

16.7.10 Corrosion of Reinforcing Steel in Concrete

The deterioration of concrete due to corrosion of the reinforcing steel is a major problem, which is usually detected only after extreme cracking has already taken place. Weng et al.[52] found that measurable levels of acoustic emission occurred even during the corrosion of unstressed reinforced concrete. They suggested that, at least in the laboratory, acoustic emission monitoring would assist in characterizing corrosion damage. In subsequent work, Dunn et al.[53] developed a relationship between the observed damage and the resulting acoustic emissions. Damage could be detected in its early stages, and by a combination of total counts and amplitude measurements, the nature of the corrosion damage could be determined.

16.8 Field Studies of Acoustic Emission

As shown in the previous section, acoustic emission analysis has been used in the laboratory to study a wide range of problems. Unfortunately, its use in the field has been severely limited; only a very few papers on field application have appeared, and these are largely speculation on future possibilities. The way in which acoustic emission data might be used to provide information about the condition of a specimen or a structure has been described by Cole;[54] his analysis may be summarized as follows:

1. Is there any acoustic emission at a certain load level? If *no*, then no damage is occurring under these conditions; if *yes*, then damage is occurring.
2. Is acoustic emission continuing while the load is held constant at the maximum load level? If *no*, no damage due to creep is occurring; if *yes*, creep damage is occurring. Further, if the count rate is increasing, then failure may occur fairly soon.
3. Have high amplitude acoustic emissions events occurred? If *no*, individual fracture events have been relatively minor; if *yes*, major fracture events have occurred.
4. Does acoustic emission occur if the structure has been unloaded and is then reloaded to the previous maximum load? If *no*, there is no damage or crack propagation under low cycle fatigue; if *yes*, internal damage exists and the damage sites continue to spread even under low loads.
5. Does the acoustic emission occur only from a particular area? If *no*, the entire structure is being damaged; if *yes*, the damage is localized.
6. Is the acoustic emission in a local area *very* localized? if *no*, damage is dispersed over a significant area; if *yes*, there is a highly localized stress concentration causing the damage.

Naus[55] used acoustic emissions to monitor intermediate pressure vessels and simple concrete structures and determine whether this technique could be applied to primary nuclear containment structures. He concluded that, for monitoring prestressed concrete members, acoustic emission results correlated with beam behavior and could be used to locate cracks in simple concrete structures. Robert and Brachet-Rolland[56] also suggested that acoustic emission surveys could be used to detect the presence of active cracks in prestressed concrete structures and to help provide an estimate of the load-carrying capacity of such structures.

Perhaps the first real field application was carried out by Woodward,[57] who used acoustic emission to monitor cracks in the anchor block of a prestressed concrete bridge. The signals were characterized by bursts of activity, followed by periods of inactivity. Since the bridge was subjected to dead-weight loading, longitudinal and vertical prestress, and environmentally induced loads, it was not clear which of these effects gave rise to the acoustic emissions. At least three different sources of acoustic emission were identified; direct crack propagation, cracking due to the redistribution of strains within the concrete, and cracking due to thermal expansions and contractions, but no quantitative results could be obtained.

16.9 Conclusions

From the discussion above, it appears that acoustic emission techniques may be very useful in the laboratory to supplement other measurements of concrete properties. However, their use in the field remains problematic. Many of the earlier studies held out high hopes for acoustic emission monitoring of structures. For instance, McCabe et al.[17] suggested that, if a structure was loaded, the absence of acoustic emissions would indicate that it was safe under the existing load conditions; a low level of acoustic emissions would indicate that the structure should be monitored carefully, while a high level of acoustic emission could indicate that the structure was unsafe. But this is hardly a satisfactory approach, since it does not provide any help with quantitative analysis. In any event, even the sophisticated (and expensive) equipment now available still provides uncertain results when applied to structures, because of our lack of knowledge about the characteristics of acoustic emissions due to different causes, and because of the possibility of extraneous noise (vibration, loading devices, and so on). Another serious drawback is that acoustic emissions are only generated when the loads on a structure are increased, and this poses

considerable practical problems. Thus, one must still conclude, with regret, that "acoustic emission analysis has not yet been well developed as a technique for the evaluation of phenomena taking place in concrete in structures."[18]

References

1. ASTM E 1316-02a, Standard Terminology for Nondestructive Examinations, Section B: Acoustic Emission, *Annual Book of ASTM Standards*, ASTM, West Conshohocken, PA, 2003.
2. Kaiser, J., Untersuchungen über dem auftreten Geräuschen beim Zugversuch, Ph.D. thesis, Technische Hochschule, Munich, 1950.
3. Rüsch, H., Physical problems in the testing of concrete, *Zement-Kalk-Gips*, 12, 1, 1959.
4. L'Hermite, R.G., What we know about the plastic deformation and creep of concrete? *RILEM Bull.*, 1, 21, 1959.
5. L'Hermite, R.G., Volume changes of concrete, in *Proc. 4th Int. Symp. on Chemistry of Cement*, Vol. II, Washington, National Bureau of Standards, Washington, D.C., NBS, Monograph, No. 32, 1960, 659.
6. Robinson, G.S., Methods of detecting the formation and propagation of microcracks in concrete, in *Proc. Int. Symp. on the Structure of Concrete*, Brooks, A.E. and Newman, K., Eds., London, 1965, Cement and Concrete Association, London, 1968, 131.
7. Wells, D., An acoustic apparatus to record emissions from concrete under strain, *Nuclear Engineering and Design*, 12, 80, 1970.
8. Green, A.T., Stress wave emission and fracture of prestressed concrete reactor vessel materials, in *Proc. 2nd Interamerican Conf. on Materials Technology*, American Society of Mechanical Engineers, Vol. I, 1970, 635.
9. Malhotra, V.M., Testing hardened concrete: non-destructive methods, Monogr. No. 9, American Concrete Institute, Detroit, MI, 1976, chap. 12.
10. Diederichs, U., Schneider, U., and Terrien, M., Formation and propagation of cracks and acoustic emission, in *Fracture Mechanics of Concrete*, Wittmann, F.H., Ed., Elsevier, Amsterdam, 1983, chap. 3.5.
11. Tanigawa, Y., Yamada, K., and Kiriyama, S.-L., Power spectra analysis of acoustic emission wave of concrete, in *Proc. 2nd Austr. Conf. on Engineering Materials*, Sydney, 1981, 97.
12. Berthelot, J.M., Robert, J.L., Bruhat, D., and Gervais, J.P., Damage evaluation of concrete test specimens related to failure analysis, private communications, 1987.
13. Maji, A. and Shah, S.P., Process zone and acoustic emission measurements in concrete, *Exp. Mech.*, 1, 27, 1988.
14. Seruby, C.B., Baldwin, G.R., and Stacey, K.A., Characterization of fatigue crack extension by quantitative acoustic emission, *Int. J. Fracture*, 28, 201, 1985.
15. Michaels, J.E., Michaels, T.E., and Sachse, W., Applications of deconvolution to acoustic emission signal analysis, *Mater. Eval.*, 39, 1032, 1981.
16. Spooner, D.C. and Dougill, J.W., A quantitative assessment of damage sustained in concrete during compressive loading, *Mag. Conc. Res.*, 27, 151, 1975.
17. McCabe, W.M., Koerner, R.M., and Lord, A.E., Jr., Acoustic emission behaviour of concrete laboratory specimens, *Am. Concr. Inst. J.*, 73, 367, 1976.
18. Mlaker, P.F., Walker, R.E., Sullivan, B.R., and Chiarito, V.P., Acoustic emission behaviour of concrete, in *In Situ/Nondestructive Testing of Concrete*, Malhotra, V.M., Ed., ACI SP-82, American Concrete Institute, Detroit, MI, 1984, 619.
19. Hinrichsmeyer, K., Diederichs, U., and Schneider, U., Thermal induced cracks and acoustic emission in cement paste, mortar and concrete, *Sci. Ceram.*, 12, 1984, 667.
20. Nadeau, J.S., Bennett, R., and Mindess, S., Acoustic emission in the drying of hardened cement paste and mortar, *J. Am. Ceram. Soc.*, 64, 410, 1981.
21. Nielsen, J. and Griffin, D.F., Acoustic emission of plain concrete, *J. Test. Eval.*, 5, 476, 1977.

22. Schickert, G., Critical reflection on non-destructive testing of concrete, *Mater. Construct.*, 17, 217,1984.
23. Mindess, S., Acoustic emission and ultrasonic pulse velocity of concrete, *Int. J. Cement Composites Lightweight Concr.*, 4, 173, 1982.
24. Berthelot, J.-M. and Robert, J.-L., Modeling concrete damage by acoustic emission, *J. Acoust. Emission*, 6, 43, 1987.
25. Rossi, P., Fissuration du Beton: Du Materiaux a la Structure, Application de la Mechanique Lineaire de la Rupture, Ph.D. thesis, Ecole National des Ponts et Chausées, Paris, 1986.
26. Evans, A.G., Clifton, J.R., and Anderson, E., The fracture mechanics of mortars, *Cement Conc. Res.*, 6, 535, 1976.
27. Morita, K. and Kato, K., Fundamental study on fracture toughness and evaluation by acoustic emission technique of concrete, in *Rev. 32nd General Meet.*, Cement Association of Japan, Tokyo, 1978, 138.
28. Morita, K. and Kato, K., Fundamental study on evaluation of fracture toughness of artificial lightweight aggregate concrete, in *Rev. 33rd General Meet.*, Cement Association of Japan, Tokyo, 1979, 175.
29. Lenain, J.C. and Bunsell, A.R., The resistance to crack growth of asbestos cement, *J. Mater. Sci.*, 14, 321, 1979.
30. Izumi, M., Mihashi, H., and Nomura, N., Acoustic emission technique to evaluate fracture mechanics parameters of concrete, in *Fracture Toughness and Fracture Energy of Concrete*, Wittmann, F.H., Ed., Elsevier, Amsterdam, 1986, 259.
31. Saeki, N., Takada, N., and Hataya, S., On studies for cracking and failure of concrete by acoustic emission techniques, in *Rev. 33rd General Meet.*, Cement Association of Japan, Tokyo, 1979, 234.
32. Tanigawa, Y. and Kobayashi, H., A study on acoustic emission of concrete, in *Rev. 33rd General Meet.*, Cement Association of Japan, Tokyo, 1979, 159.
33. Okada, K., Koyanagi, W., and Rokugo, K., Energy transformation in the fracture process of concrete, in *Memoirs of the Faculty of Engineering*, Kyoto University, Kyoto, Japan, 34(3), 1977, 389.
34. Okada, K., Koyanagi, W., and Rokugo, K., Energy approach to flexural fracture process of concrete, *Trans. Jpn. Soc. Civil Eng.*, 11, 301, 1979.
35. Chhuy, S., Baron, J., and Francois, D., Mecanique de la rupture appliquée au beton hydraulique, *Cement Conc. Res.*, 9, 641, 1979.
36. Chhuy, S., Cannard, G., Robert, J.L., and Acker, P., Experimental investigations on the damage of cement concrete with natural aggregates, personal communication, 1987.
37. Berthelot, J.-M. and Robert, J.-L., Application de l'emission acoustique aux mecanismes d'endommagement du beton, *Bull. Liasion Ponts Chaussees*, 140, 101, 1985.
38. Niwa, Y., Ohtsu, M., and Shiomi, H., Waveform analysis of acoustic emission in concrete, in *Memoirs of the Faculty of Engineering*, Kyoto University, 43(4), 319, 1981.
39. Maji, A. and Shah, S.P., Initiation and propagation of bond cracks as detected by laser holography acoustic emission, in *Bonding in Cementitous Materials*, Mindess, S. and Shah, S.P., Eds., Materials Research Society Symposium Proceedings, Vol. 114, Materials Research Society, Pittsburgh, 1988, 55.
40. Fertis, D.G., Concrete material response by acoustic spectra analysis, *J. Struct. Div.*, ASCE, 102, 387, 1976.
41. Rebic, M.P., The distribution of critical and rupture loads and determination of the factor of crackability, in *In Situ/Nondestructive Testing of Concrete*, Malhotra, V.M., ed., ACI SP-82, American Concrete Institute, Detroit, 1984, 721.
42. Sadowskia-Boczar, E., Librant, Z., Ranachowski, J., and Ciesla, Z., Application of acoustic emission to investigate the mechanical strength of ceramic materials, *Sci. Ceram.*, 12, 1984, 639.
43. Jeong, H.D., Takahashi, H., and Teramura, S., Low temperature fracture behaviour and AE characteristics of autoclaved aerated concrete (AAC), *Cement Concr. Res.*, 17, 743, 1987.

44. Akers, S.A.S. and Garrett, G.G., Acoustic emission monitoring of flexural failure in asbestos cement composites, *Int. J. Cement Composites Lightweight Concrete*, 5, 97, 1983.
45. Faninger, Von G., Grünthaler, K.H., and Schwalbe, J.H., Faserverstärkter Beton und Schallemission [Fibre-reinforced concrete and acoustic emission], *Betonwerk Fertigteil-Technik*, 2, 82, 1977.
46. Parkinson, R.W. and Peters, C.T., Acoustic emission activity during accelerated conversion of high alumina cement pastes, *J. Mater. Sci.* (*Letters*), 12, 848, 1977.
47. Arrington, M. and Evans, B.M., Acoustic emission testing of high alumina cement concrete, *Non-Destructive Testing Int.*, 10, 81, 1977.
48. Williams, R.V., *Acoustic Emission*, Adam Hilger, Bristol, 1980, 110.
49. Kobayashi, A.S., Hawkins, N.M., Chan, Y.-L.A., and Jin, I.-J., A feasibility study of detecting reinforcing-bar debonding by acoustic-emission technique, *Exp. Mech.*, 20, 301, 1980.
50. Royles, R., Morley, P.D., and Khan, M.R., The behaviour of reinforced concrete at elevated temperatures with particular reference to bond strength, in *Bond in Concrete*, Bartos, P., Ed., Applied Science Publishers, London, 1982, 217.
51. Royles, R. and Morley, P.D., Acoustic emission and bond degradation in reinforced concrete due to elevated temperatures, *Mater. Construct.*, 17, 185, 1984.
52. Weng, M.S., Dunn, S.E., Hartt, W.H., and Brown, R.P., Application of acoustic emission to detection of reinforcing steel corrosion in concrete, *Corrosion*, 38, 9, 1982.
53. Dunn, S.E., Young, J.D., Hartt, W.H., and Brown, R.P., Acoustic emission characterization of corrosion induced damage in reinforced concrete, *Corrosion*, 40, 339, 1984.
54. Cole, P.T., Using acoustic emission (AE) to locate and identify defects in composite structures, *Compos. Struct.*, 3, 259, 1985.
55. Naus, D.J., Acoustic emission monitoring of steel and concrete structural elements with particular reference to primary nuclear containment structures, in *Advances in Acoustic Emission*, Dunhart, 1981, 249.
56. Robert, J.L. and Brachet-Rolland, N.M., Survey of structures by using acoustic emission monitoring, in *IABSE Symposium: Maintenance, Repair and Rehabilitation of Bridges, Final Report*, International Association for Bridge and Structural Engineering, Washington, D.C., 1982, 33.
57. Woodward, R.J., Cracks in a concrete bridge, *Concrete*, 17, 40, 1983.